frontiers | Research Topics

Emerging concepts for respiratory viruses after the pandemic

Edited by
Chrysanthi Skevaki, Paraskevi C. Fragkou, Florence Morfin, Fusun Can and Dimitra Dimopoulou

Published in
Frontiers in Cellular and Infection Microbiology

ISSN 1664-8714
ISBN 978-2-8325-7343-3
DOI 10.3389/978-2-8325-7343-3

Generative AI statement
Any alternative text (Alt text) provided alongside figures in the articles in this ebook has been generated by Frontiers with the support of artificial intelligence and reasonable efforts have been made to ensure accuracy, including review by the authors wherever possible. If you identify any issues, please contact us.

About Frontiers

Frontiers is more than just an open access publisher of scholarly articles: it is a pioneering approach to the world of academia, radically improving the way scholarly research is managed. The grand vision of Frontiers is a world where all people have an equal opportunity to seek, share and generate knowledge. Frontiers provides immediate and permanent online open access to all its publications, but this alone is not enough to realize our grand goals.

Frontiers journal series

The Frontiers journal series is a multi-tier and interdisciplinary set of open-access, online journals, promising a paradigm shift from the current review, selection and dissemination processes in academic publishing. All Frontiers journals are driven by researchers for researchers; therefore, they constitute a service to the scholarly community. At the same time, the *Frontiers journal series* operates on a revolutionary invention, the tiered publishing system, initially addressing specific communities of scholars, and gradually climbing up to broader public understanding, thus serving the interests of the lay society, too.

Dedication to quality

Each Frontiers article is a landmark of the highest quality, thanks to genuinely collaborative interactions between authors and review editors, who include some of the world's best academicians. Research must be certified by peers before entering a stream of knowledge that may eventually reach the public - and shape society; therefore, Frontiers only applies the most rigorous and unbiased reviews. Frontiers revolutionizes research publishing by freely delivering the most outstanding research, evaluated with no bias from both the academic and social point of view. By applying the most advanced information technologies, Frontiers is catapulting scholarly publishing into a new generation.

What are Frontiers Research Topics?

Frontiers Research Topics are very popular trademarks of the *Frontiers journals series*: they are collections of at least ten articles, all centered on a particular subject. With their unique mix of varied contributions from Original Research to Review Articles, Frontiers Research Topics unify the most influential researchers, the latest key findings and historical advances in a hot research area.

Find out more on how to host your own Frontiers Research Topic or contribute to one as an author by contacting the Frontiers editorial office: frontiersin.org/about/contact

Emerging concepts for respiratory viruses after the pandemic

Topic editors

Chrysanthi Skevaki — Universities of Giessen and Marburg Lung Center, Germany
Paraskevi C. Fragkou — Evaggelismos General Hospital, Greece
Florence Morfin — Université Claude Bernard Lyon 1, France
Fusun Can — Koç University, Türkiye
Dimitra Dimopoulou — Panagiotis & Aglaia Kyriakou Children's Hospital, Greece

Citation

Skevaki, C., Fragkou, P. C., Morfin, F., Can, F., Dimopoulou, D., eds. (2026). *Emerging concepts for respiratory viruses after the pandemic*. Lausanne: Frontiers Media SA. doi: 10.3389/978-2-8325-7343-3

Table of contents

frontiers | Frontiers in Cellular and Infection Microbiology

TYPE Editorial
PUBLISHED 16 December 2025
DOI 10.3389/fcimb.2025.1758434

OPEN ACCESS

EDITED AND REVIEWED BY
Yuxian He,
Institute of Pathogen Biology (CAMS), China

*CORRESPONDENCE
Paraskevi C. Fragkou
evita.fragou@gmail.com

RECEIVED 01 December 2025
ACCEPTED 08 December 2025
PUBLISHED 16 December 2025

CITATION
Dimopoulou D, Skevaki C, Can F, Morfin-Sherpa F, Fragkou PC and the ESCMID Study Group for Respiratory Viruses (ESGREV) (2025) Editorial: Emerging concepts for respiratory viruses after the pandemic. *Front. Cell. Infect. Microbiol.* 15:1758434. doi: 10.3389/fcimb.2025.1758434

Editorial: Emerging concepts for respiratory viruses after the pandemic

Dimitra Dimopoulou[1,2], Chrysanthi Skevaki[2,3,4,5,6], Fusun Can[2,7,8], Florence Morfin-Sherpa[9,10], Paraskevi C. Fragkou[2,6,11]* and the ESCMID Study Group for Respiratory Viruses (ESGREV)

[1]Second Department of Pediatrics, "P. & A. Kyriakou" Children's Hospital, National and Kapodistrian University of Athens, School of Medicine, Athens, Greece, [2]European Society of Clinical Microbiology and Infectious Diseases (ESCMID) Study Group for Respiratory Viruses (ESGREV), Basel, Switzerland, [3]Department of Environmental Health, Harvard T.H. Chan School of Public Health, Boston, MA, United States, [4]Institute of Laboratory Medicine and Pathobiochemistry, Molecular Diagnostics, University of Marburg, Marburg, Germany, [5]German Centre for Lung Research - Deutsches Zentrum für Lungenforschung (DZL), The Universities of Giessen and Marburg Lung Center (UGMLC), Giessen, Germany, [6]Centre for Public Health Research and Education (CPHRE), Academy of Athens, Athens, Greece, [7]Department of Medical Microbiology, School of Medicine, Koç University, Istanbul, Türkiye, [8]Koç University İşBank Center for Infectious Diseases, Koç University Hospital (KUISCID), Istanbul, Türkiye, [9]Laboratory of Virology, Institut des Agents Infectieux, Hospices Civils de Lyon, Lyon, France, [10]CIRI (Centre International de Recherche en Infectiologie), Team VirPatH, Univ Lyon, Institut national de la santé et de la recherche médicale (INSERM) U1111, Centre national de la recherche scientifique (CNRS) UMR5308, Université Claude Bernard Lyon 1, École Normale Supérieure (ENS) de Lyon, Lyon, France, [11]Internal Medicine Department, Aegli Medical Clinic, Athens, Greece

KEYWORDS

artificial intelligence - AI, diagnostics, epidemiology, long-term sequelae, pathogenesis, research tools and models, respiratory viruses

Editorial on the Research Topic
Emerging concepts for respiratory viruses after the pandemic

Respiratory virus research has been reshaped by the COVID-19 pandemic and the effects of climate change, both of which contributed to a shift in the epidemiology of respiratory viruses and highlighted gaps in our understanding about the plasticity and long-term consequences of these changes (Chow et al., 2023; He et al., 2023). The pandemic also accelerated advances in research models and methods, underscoring evolving seasonality patterns, viral pathogenesis, and host interactions (Chow et al., 2023; He et al., 2023). This Research Topic explored the changing epidemiology and pathogenesis of respiratory viruses, focusing on seasonality, long-term outcomes, and host responses. It also emphasized advances in diagnostics and therapeutics and the use of artificial intelligence for predictive modeling, aiming to inform public health strategies in the post-pandemic era.

Epidemiology and seasonality of respiratory infections in the post-COVID-19 era

The COVID-19 pandemic has significantly impacted the epidemiology of respiratory viruses due to widespread public health interventions such as lockdowns, masking, social distancing and school closures that resulted in the interruption of the SARS-CoV-2 transmission and the seasonal dynamics of other respiratory viruses (Chen and Er, 2022; Principi et al., 2023). Alzahrani et al. reported the prominence of rhinovirus/enterovirus, SARS-CoV-2, respiratory syncytial virus (RSV), and adenovirus in respiratory infections in Saudi Arabia, with clear winter peaks and age-specific susceptibility, highlighting the significant burden of respiratory infections, particularly among pediatric populations, the impact of public health interventions, such as COVID-19 restrictions, on the transmission of respiratory viruses and the need for targeted interventions. Similarly, in Mexico, De Arcos-Jimenez et al. found that influenza experienced a sharp decline during the pandemic but rebounded post-pandemic, RSV demonstrated a delayed resurgence, while other respiratory viruses exhibited heterogeneous rebound patterns. Importantly, advanced age, male sex, cardiovascular disease, obesity, and immunosuppression were major risk factors for severe acute respiratory infection (SARI), with vaccination offering consistent protection, reinforcing its crucial role in respiratory infection mitigation strategies. Thus, the dynamic interplay between viral competition, public health interventions, and human behavior likely contributed to the observed changes in SARI trends, emphasizing the need for ongoing surveillance and adaptive public health responses. Data from China further reinforce this pattern; Yue et al. showed that non-pharmaceutical interventions against COVID-19 markedly restricted the spread of influenza, adenovirus, and Mycoplasma pneumoniae in children, while also reduced bacterial co-infections. Following the end of China's "Zero-COVID" policy, atypical seasonal patterns and rising co-infections were observed, with respiratory viruses resuming circulation. These findings reflect the dual impact of population immunity gaps and viral re-emergence. Furthermore, Li et al. highlighted that in China, SARS-CoV-2 and influenza dominated respiratory infections in adults, while RSV remained predominant in children and influenza in school-aged children, underscoring shifting age distributions. These findings underscore the need for continuous multi-pathogen surveillance and vaccination strategies to prevent future epidemic surges.

In addition to the shifts in viral seasonality, important pathogen-specific and clinical insights that inform pediatric health policy are also highlighted. Lu et al. provide evidence that despite a global 76.8% reduction in childhood mortality due to lower respiratory tract infection (LRTI) since 1990, LRTIs remain a leading cause of death in children from low- and middle-income countries, with Streptococcus pneumoniae, Staphylococcus aureus, and *Klebsiella pneumoniae* remaining dominant pathogens, while among newborns, the leading pathogens were Klebsiella pneumoniae, Group B Streptococcus, and *Acinetobacter baumannii*. This study further predicts rising influenza-related mortality by 2031, reinforcing the urgency of expanding vaccine coverage, improving sanitary conditions and early interventions for high-risk children in order to reduce LRTI burden. Fang et al. provides molecular insights, demonstrating that specific adenovirus (HAdV) genotypes, such as HAdV-3, HAdV-7, HAdV-2, and HAdV-1 were the predominant HAdV types in children hospitalized with respiratory infections in China, and particularly HAdV-7 is linked to severe pediatric pneumonia, highlighting the role of viral genetic variability in determining disease severity and clinical outcome and the need to differentiate HAdV types for both epidemiological surveillance and clinical management. Finally, Fu et al. report high reinfection rates of nearly 30% within five months among primary healthcare workers in China during the Omicron wave, particularly among women, nurses, those with fever clinic experience and working over 8 hours per day, underscoring occupational risks and the need for targeted protective measures, including appropriate work arrangements, regular health monitoring, and the promotion of healthy lifestyle habits.

To conclude, these studies demonstrate that the pandemic reshaped the epidemiology, seasonality, and clinical impact of respiratory viruses, and they highlight the ongoing vulnerabilities across pediatric and healthcare populations, as well as the need for continuous enhanced surveillance, vaccination, and targeted protective strategies to address future respiratory viral infection threats in the post-pandemic era.

Immunology, pathogenesis, and therapeutic advances in COVID-19

While a huge body of data on COVID-19 pathogenesis is currently available, many aspects of the complex host-pathogen interplay remain still unknown. Bugatti et al. showed that SARS-CoV-2 can infect ACE2-negative primary human lung microvascular endothelial cells (HL-mECs) through an alternative entry mechanism that relies on the Arg-Gly-Asp (RGD) motif expressed in the receptor binding domain (RBD) of the spike protein in the viral spike protein. Viral entry into endothelial cells triggers phenotypic remodeling and angiogenic responses, contributing to vascular dysfunction observed in COVID-19. As RGD motif is not naturally exposed on the spike protein, heparan sulfate proteoglycans (HSPGs) function as essential cofactors that expose the RGD site, enabling spike interaction with αvβ3 integrin, thus HSPGs are central to SARS-CoV-2 infection of endothelial cells and its associated dysfunction, signifying them as a potential therapeutic target to mitigate endothelial involvement in COVID-19.

Understanding the pathogenetic mechanisms underlying respiratory viral infections requires the use of advanced single-cell

technologies. Mass cytometry or cytometry by time-of-flight (CyTOF) offers this possibility by enabling simultaneous measurement of more than 50 markers per cell, allowing comprehensive phenotypic and functional profiling of immune populations (Zunder et al., 2022). In this setting, Balz et al. introduced a novel CyTOF protocol optimized for the immunophenotyping of low-frequency antigen-specific T cells. Using this enhanced workflow, they assessed virus-specific T-cell responses in SARS-CoV-2–vaccinated, SARS-CoV-2–infected, and non-exposed healthy individuals through high-parameter mass cytometry. Their analysis revealed a marked phenotypic heterogeneity among antigen-responsive $CD4^+$, $CD8^+$, and γδ T-cell subsets following antigen-specific stimulation, highlighting the protocol's ability to resolve diverse functional T-cell states even within rare populations. Overall, this paper establishes a dual-barcoding, debris-free CyTOF protocol for reliable detection of extremely rare antigen-specific T cells; this protocol allows robust, high-content immunophenotyping of scarce T-cell responses in both mouse and human samples.

Regarding the treatment of COVID-19, the effectiveness of several therapeutic interventions patients has been evaluated since the onset of the pandemic. While evidence-based guidelines are now in place for both community dwellers and hospitalized patients, research in potential new or repurposed molecules remains ongoing. Xu et al., found in their retrospective study among 264 hospitalized COVID-19 patients, that azvudine significantly reduced both composite disease progression and all-cause mortality compared to standard care alone. Patients receiving azvudine also showed better improvement in oxygen saturation during hospitalization. These results highlight a potential therapeutic benefit of azvudine among COVID-19 hospitalized patients which should be further investigated and validated in randomized controlled trials.

Besides treatment, identifying predictive tools which stratify patients according to their risk for increased disease severity and adverse outcomes is crucial for the optimal management of COVID-19 patients. Tang et al. conducted a retrospective study among 137 Intensive Care Unit (ICU) patients with critical COVID-19 during the Omicron period; they found that lactate levels and the weekly lymphocyte change rate are strong predictors of mortality in ICU patients with severe COVID-19. A lactate threshold of 1.75 mmol/L effectively identified high-risk patients with significantly poorer survival. Combining lactate with lymphocyte dynamics improved prognostic accuracy. The neutrophil-to-lymphocyte ratio partially mediated lactate's effect on mortality, indicating an interaction between inflammation and metabolic stress. Respiratory parameters did not predict outcomes, suggesting that elevated lactate reflects microcirculatory dysfunction rather than ventilation failure. Although these biomarkers should be further evaluated in prospective studies, it may represent a useful tool for critical COVID-19.

Vaccination against respiratory viruses (when available) remains the cornerstone of prevention, particularly among high-risk populations. However, data on long-term immunity in immunocompromised children who received SARS-CoV-2 vaccines remain limited. Russo et al. conducted a prospective observational study that demonstrated Vaccinated children maintained immune memory up to 17 months after receiving COVID-19 vaccines, but immunocompromised children showed significantly weaker immunity than healthy children. Immunocompromised children had lower anti-spike IgG levels and markedly reduced neutralizing antibodies, especially against Omicron BA.5 and after BBIBP-CorV vaccination. While $CD4^+$ T-cell memory was similar between groups, $CD8^+$ T-cell responses and IFN-γ production were notably diminished in immunocompromised children. These findings denote the need for updated vaccines and improved booster coverage.

From a public health perspective, important insights were gained during the COVID-19 pandemic regarding optimal policies to control viral transmission. Policymakers and stakeholders implemented measures often without solid evidence of their effectiveness. In this context, Artificial Intelligence (AI) proves extremely valuable, as it can generate predictive models to evaluate the impact of public health interventions. To this end, Dong et al. developed a detailed agent-based COVID-19 simulation model for a Chinese town (Xi'an) using real geographic, census, and mobility data. The model accurately reproduced the city's 2021–2022 outbreak, with simulated case numbers closely matching official reports. By integrating individual behaviors and government measures such as testing, lockdowns, and mask use, it assessed how interventions affected disease spread. Scenario analyses, including a 100% mask-wearing simulation, showed modest reductions in cases. Overall, the model provides a powerful tool for predicting epidemic trends and supporting public health decision-making.

Conclusions

Taken together, the studies featured in this Research Topic offer a broad, yet detailed picture of how the pandemic has reshaped our understanding of respiratory viruses—from shifting in their circulation patterns to the emergence of new clinical and immunological insights. As we move forward, these observations emphasize the importance of flexible surveillance systems, thoughtful public health planning, and continued scientific investment to anticipate and respond to future challenges.

Author contributions

DD: Conceptualization, Writing – original draft, Writing – review & editing. CS: Supervision, Writing – review & editing, Methodology. FC: Methodology, Investigation, Writing – review & editing. FM-S: Writing – review & editing, Investigation, Methodology. PCF: Conceptualization, Data curation, Writing – review & editing, Supervision, Writing – original draft.

Conflict of interest

The authors declared that this work was conducted in the absence of any commercial or financial relationships that could be construed as a potential conflict of interest.

Generative AI statement

The author(s) declared that generative AI was used in the creation of this manuscript. The authors declare that Generative AI was used for language editing purposes for this manuscript.

Any alternative text (alt text) provided alongside figures in this article has been generated by Frontiers with the support of artificial intelligence and reasonable efforts have been made to ensure accuracy, including review by the authors wherever possible. If you identify any issues, please contact us.

Publisher's note

References

Chen, Y. J., and Er, T. K. (2022). Distribution of viral respiratory infections during the COVID-19 pandemic using the filmArray respiratory panel. *Biomedicines* 10, 2734. doi: 10.3390/biomedicines10112734

Chow, E. J., Uyeki, T. M., and Chu, H. Y. (2023). The effects of the COVID-19 pandemic on community respiratory virus activity. *Nat. Rev. Microbiol.* 21, 195–210. doi: 10.1038/s41579-022-00807-9

He, Y., Liu, W. J., Jia, N., Richardson, S., and Huang, C. (2023). Viral respiratory infections in a rapidly changing climate: the need to prepare for the next pandemic. *EBioMedicine* 93, 104593. doi: 10.1016/j.ebiom.2023.104593

Principi, N., Autore, G., Ramundo, G., and Esposito, S. (2023). Eidemiology of respiratory infections during the COVID-19 pandemic. *Viruses* 15, 1160.

Zunder, E. R., Finck, R., Behbehani, G. K., Amir, E.-A. D., Krishnaswamy, S., Gonzalez, V. D., et al. (2022). CyTOF® for the masses. *Front. Immunol.* 13. doi: 10.3389/fimmu.2022.815828

frontiers | Frontiers in Cellular and Infection Microbiology

TYPE Methods
PUBLISHED 15 January 2024
DOI 10.3389/fcimb.2023.1336489

OPEN ACCESS

EDITED BY
Michael H. Lehmann,
Ludwig Maximilian University of Munich, Germany

REVIEWED BY
Helen Marie McGuire,
The University of Sydney, Australia
Antonio Cosma,
Luxembourg Institute of Health, Luxembourg

*CORRESPONDENCE
Chrysanthi Skevaki
Chrysanthi.Skevaki@uk-gm.de

†These authors have contributed equally to this work and share first authorship

‡These authors have contributed equally to this work and share last authorship

RECEIVED 10 November 2023
ACCEPTED 20 December 2023
PUBLISHED 15 January 2024

CITATION
Balz K, Grange M, Pegel U, Karamya ZA, Mello M, Zhou X, Berger T, Bloch K, Dunham D, Chinthrajah S, Nadeau K, Luche H and Skevaki C (2024) A novel mass cytometry protocol optimized for immunophenotyping of low-frequency antigen-specific T cells. *Front. Cell. Infect. Microbiol.* 13:1336489. doi: 10.3389/fcimb.2023.1336489

A novel mass cytometry protocol optimized for immunophenotyping of low-frequency antigen-specific T cells

Kathrin Balz[1†], Magali Grange[2†], Uta Pegel[1], Zain A. Karamya[1], Marielle Mello[2], Xiaoying Zhou[3], Thilo Berger[1], Konstantin Bloch[1], Diane Dunham[4], Sharon Chinthrajah[4], Kari Nadeau[3‡], Hervé Luche[2‡] and Chrysanthi Skevaki[1*‡]

[1]Institute of Laboratory Medicine, Universities of Giessen and Marburg Lung Center (UGMLC), Philipps University Marburg, German Center for Lung Research (DZL), Marburg, Germany, [2]Centre d'Immunophénomique Centre d'Immunophénomique (CIPHE), Aix Marseille Université, INSERM, CNRS Philipps-Universität Marburg (UMR), Marseille, France, [3]Department of Environmental Health, Harvard T.H. Chan School of Public Health, Boston, MA, United States, [4]Sean N Parker Center for Allergy and Asthma Research at Stanford University, Stanford, CA, United States

Understanding antigen-specific T-cell responses, for example, following virus infections or allergen exposure, is of high relevance for the development of vaccines and therapeutics. We aimed on optimizing immunophenotyping of T cells after antigen stimulation by improving staining procedures for flow and mass cytometry. Our method can be used for primary cells of both mouse and human origin for the detection of low-frequency T-cell response using a dual-barcoding system for individual samples and conditions. First, live-cell barcoding was performed using anti-CD45 antibodies prior to an *in vitro* T-cell stimulation assay. Second, to discriminate between stimulation conditions and prevent cell loss, sample barcoding was combined with a commercial barcoding solution. This dual-barcoding approach is cell sparing and, therefore, particularly relevant for samples with low cell numbers. To further reduce cell loss and to increase debarcoding efficiency of multiplexed samples, we combined our dual-barcoding approach with a new centrifugation-free washing system by laminar flow (Curiox™). Finally, to demonstrate the benefits of our established protocol, we assayed virus-specific T-cell response in SARS-CoV-2–vaccinated and SARS-CoV-2–infected patients and compared with healthy non-exposed individuals by a high-parameter CyTOF analysis. We could reveal a heterogeneity of phenotypes among responding CD4, CD8, and gd-T cells following antigen-specific stimulations. Our protocol allows to assay antigen-specific responses of minute populations of T cells to virus-derived peptides, allergens, or other antigens from the same donor sample, in order to investigate qualitative and quantitative differences.

KEYWORDS

T-cell activation, CyTOF, sample barcoding, T-cell stimulation assay, method

1 Introduction

Mass cytometry or cytometry by time-of-flight (CyTOF) is a single-cell technology, which allows multiparametric phenotyping with the use of metal-tagged antibodies (Bendall et al., 2011). The advantage of CyTOF when compared to conventional flow cytometry is that the use of heavy metal ion conjugation of antibodies overcomes challenges associated to spectral overlap of fluorescently labeled antibodies. In this way, more than 50 markers per cell can be captured, which, in turn, enables massive phenotypic and functional assessment of cells of interest. Both CyTOF and spectral cytometry overcome technical limitations associated to autofluorescence related to specific cell types. However, for functional studies requiring detection of multiple cytokines or transcription factors, CyTOF appears superior (Smith et al., 2023). During the last years, CyTOF has significantly advanced scientific fields related to cancer (Levine et al., 2015; Spitzer et al., 2015; Krieg et al., 2018), allergy, autoimmunity (Hartmann et al., 2016; Rao et al., 2017; Mrdjen et al., 2018), and infection and hematopoiesis (Bendall et al., 2011; Bendall et al., 2014) by providing detailed insights into several research questions.

Often, explorative studies utilizing CyTOF involve a multitude of samples, also potentially containing relatively low cell numbers and considerable cell debris. Because of mechanical limitations, CyTOF has a cell transmission rate of 70% (Olsen et al., 2019) and, hence, requires a large number of cells per run in order to collect meaningful results. In recent years, there has been significant effort in terms of standardization and quality control of related experiments. One way of reducing technical variance across assays is barcoding individual samples, combining and subsequently processing as one single sample in one test tube. Certainly, the multitude of CyTOF channels available for assaying enables to assign specific ones for barcoding of samples and hence batched data acquisition. At the end, individual cells can be *in silico* assigned to their initial sample origin based on the utilized barcode. In the recent past, the CD45 antigen has been targeted by metal-tagged anti-CD45 antibodies for live-cell barcoding in cell types expressing this marker, such as peripheral blood mononuclear cells (PBMCs) (Mei et al., 2015). Barcoding approaches help reduce the number of cells required in one run, the consistency of staining, technical bias, and experimental costs.

Experiments involving *ex vivo* antigen stimulation assays for the identification and phenotyping of antigen-specific cells may pose additional challenges. First, depending on the number of stimuli/epitopes applied and the biological background/antigen exposure history of the sample's donor, the frequency of antigen-responding cells may be in the range of 0.01%–0.1% of stimulated T cells, the latter being only a fraction of seeded PBMCs. Second, *ex vivo* stimulation requires dual-barcoding systems, which would allow to barcode both donors/samples and stimulation conditions. Third, samples may contain a limited number of cells and a quite high level of debris. In the current study, we aimed to develop a flow and mass cytometry protocol involving dual barcoding for samples and stimuli, as well as a washing approach, which reduces cell loss and debris (Krutzik et al., 2011; Zivanovic et al., 2014). During the establishment of our protocol, we chose to barcode cells before stimulation and subsequent mixing to reduce early-stage cell loss and to enhance data quality, particularly in the context of surface staining for pooled samples. We further assessed barcode-induced artifacts and individual sample debarcoding efficiency among other parameters. In order to reach our objective, we utilized PBMC samples from donors with varying SARS-CoV-2 exposure (infection/vaccination), stimulated these *ex vivo* with relevant peptide pools and evaluated T-cell activation and phenotype of antigen-responsive cells. Experimental results were assessed in combination with dimensionality reduction and automated clustering approaches.

2 Materials and equipment

2.1 Mice

We employed naïve female C57BL/6N mice, sourced from Janvier Labs. Mice were sacrificed for further analysis at 13 weeks of age.

2.2 Human donors

All donors shown in our manuscript including Supplementary Figure 1 are listed in Table 1. The table includes the SARS-CoV-2 infection history, as well as the number of SARS-CoV-2 vaccinations in terms of immunization history and allergen sensitization, whenever applicable. Allergen sensitization tests involving the detection of allergen Specific Immunoglobulin E (sIgE) were performed by means of ImmunoCAP ISAC or ImmunoCAP (allergen mixes sx1 and fx5).

2.3 Buffer preparation

1. Buffer for organ collection/cell preparation: Iscove's Modified Dulbecco's Medium (IMDM) GlutaMAX; 2% Fetal Calf Serum (FCS) (Life Technologies, #10270-106) (collection) or 10% FCS (preparation), heat-inactivated (v/v); 10 mM Hepes (ThermoFisher Scientific, #15630056); 1 mM sodium pyruvate (ThermoFisher Scientific, #11360039); 1× MEM non-essential amino acids (ThermoFisher Scientific, #11140-035); 1× penicillin/streptomycin (ThermoFisher Scientific, #15140122); 0.05 mM 2-mercaptoethanol (ThermoFisher Scientific, #31350010).
2. Enzyme cocktail: Deoxyribonuclease I (DNAse I) (1 mg/mL) (Merck Chemicals, #DN25-1G) and collagenase II (7 mg/mL) (Serlabo, #WOLS04176) into IMDM with 2% FCS.
3. Stop reaction buffer: 1× PBS and 0.1 M EDTA
4. Isolation buffer: 1× PBS (no calcium and no magnesium) (ThermoFisher Scientific, #14200-067); 2 mM EDTA; 2% FCS (v/v) (Life Technologies, #10270-106).

10.3389/fcimb.2023.1336489

TABLE 1 List of donors.

Donor project ID	Sample-ID	SARS-CoV-2 Infection	Number of SARS-CoV-2 vaccinations	Allergy status
Figure 2				
1a	1 (HD)	no	0 x	not applicable
2a	2 (Vacc)	no	3 x	not applicable
3	3 (Vacc + Inf)	yes	3 x	not applicable
Figure 3				
4	1	yes	0 x	not sensitized against allergens
5	2	yes	0 x	not sensitized against allergens
6	3	yes	0 x	not sensitized against allergens
7	4	yes	0 x	sensitized against allergens
8	5	yes	0 x	sensitized against allergens
9	6	yes	0 x	sensitized against allergens
10	7	no	0 x	not sensitized against allergens
11	8	no	0 x	not sensitized against allergens
12	9	no	0 x	not sensitized against allergens
13	10	no	2 x	not sensitized against allergens
14	11 (HD)	no	0 x	not sensitized against allergens
Figure 4				
14	1 (HD)	no	0 x	not applicable
13	2 (Vacc)	no	3 x	not applicable
15	3	no	0 x	not applicable
16	4	yes	0 x	not applicable
Figure 5				
14	1 (HD 1)	no	0 x	not sensitized against allergens
17	2 (HD 2)	no	0 x	sensitized against allergens
13	3 (Vacc 1)	no	2 x	not known
2b	4 (Vacc 2)	no	3 x	not sensitized against allergens
18	5 (Inf)	yes	1 x	sensitized against allergens
19	6 (Vacc + Inf 1)	yes	3 x	not sensitized against allergens
1b	7 (Vacc + Inf 2)	yes	3 x	sensitized against allergens
20	8 (Vacc + Inf 3)	yes	3 x	not sensitized against allergens
Supplementary Figure 1				
21	1			
22	2			
23	3	not applicable	not applicable	not applicable
24	4			
25	5			

a,b: different time of blood draw for any given donor.

5. Hank's Balanced Salt Solution (HBSS) buffer (for counting/fluorescence-activated cell sorting (FACS) staining/wash steps/cytometer aquisition): 1× HBSS (no calcium and no magnesium) (ThermoFisher Scientific, #14185-045), EDTA 5mM; 2%FCS (v/v).
6. Sytox Green solution: Sytox Green (Life Technologies, #S7020) diluted in HBSS buffer at working concentration.
7. 4,6-diamidino-2-phenylindole (DAPI) solution: DAPI diluted in HBSS buffer at working concentration.

2.4 Peptides

Major histocompatibility complex (MHC) class I peptides (9-mer and 10-mer) with an high-performance liquid chromatography (HPLC)-measured purity of >95% were purchased from ProImmune. Lyophilized peptides were stored at −80°C until dissolving in sterile H_2O. Aliquots were prepared in order to avoid freeze/thawing cycles and stored at −20°C or −80°C. Peptide sequences are listed in Table 2.

3 Methods

3.1 Live-cell barcoding in flow cytometry with human or mouse cells

3.1.1 Mouse T-cell isolation

Popliteal, inguinal, axillary, mandibular, and parotid lymph nodes (LNs) were harvested and put in a 1.5-mL Eppendorf tube with 300 µL of IMDM with 2% FCS and enzyme cocktail. LNs were disrupted with scissors and put in a thermomixer (room temperature (RT), 20 min, 350 rpm) with pipette

TABLE 2 Allergen list.

Allergen source	Allergen protein	Allergen peptide
Aspergillus fumigatus	Asp f 5	MLYEVLWNL
	Asp f 10	SIFGDIFLK
	Asp f 22	ESDPSKWLTY
	Asp f 17	AGGTVYEDLKAQYTA
Dermatophagoides farinae	Der f 14	REYKSDVEL
	Der f 1	NYCQIYPPDVKQIREALTQ
	Der f 5	LIDGVRGVLNRLMKR
Dermatophagoides pteronyssinus	Der p 14	YENEFLFNL
	Der p 4	SIYSRLHNLNKEFFP
Phleum pratense	Phl p 4	SSCEVALSYY
	Phl p 5	KYKTFVATF
	Phl p	KNPLKFDNTYFTELL

homogenization at half-time. Stop reaction buffer (30 µL) was added. and cellular suspension was filtered on a 70-µm cell strainer.

Cellular extraction was counted with Attune NXT Cytometer using an aliquot diluted at 1:200 in Sytox Green solution.

Live T cells were isolated using a Dynabeads® Untouched™ Mouse T Cells kit (Life Technologies, #11413D) according to the manufacturer's protocol.

3.1.2 PBMC isolation and freezing/thawing

3.1.2.1 Human peripheral blood mononuclear cell isolation

Human PBMCs were isolated by means of Ficoll density gradient centrifugation (Cytiva, 17144003). Freshly taken blood (40 mL to 60 mL) was mixed 1:1 with PBS (Capricorn Scientific, Cat No: PBS-1A) before layering it slowly on an equal amount of Ficoll (density of 1,077 g/mL) in a 50-mL centrifugation tube. The samples were centrifuged for 20 min at room temperature, 1,300 rpm, with the break turned off. Afterward, the PBMC fraction was isolated and washed twice with 50 mL of PBS before resuspending the pellet in an appropriate amount of Roswell Park Memorial Institute (RPMI) medium, 10% human serum, L-glutamine (2 mmol/L), and penicillin and streptomycin (100 U/mL; RPMI: Anprotec, AC-LM-0060; Antibiotic Antimycotic: Capricorn, Cat No: ASS-B; Human Serum: Capricorn, HUM-3B; L-Glutamine: Capricorn, GLN-B).

3.1.2.2 Freezing and thawing of PBMCs

Cells (5×10^6 to 10×10^6) were frozen in RPMI medium with 10% DMSO at −80°C, using a Mr. Frosty system (gradual freezing of −1°C/min). After 24 h, cells were transferred to liquid nitrogen for long-term storage. For thawing, cells were put into a water bath at 37°C until they were almost thawed and subsequently transferred into 9 mL of RPMI medium, 10% human serum, L-glutamine (2 mmol/L), and penicillin and streptomycin (100 U/mL; same as above). After centrifugation for 8 min at (1,500 rpm, room temperature), the pellet was resuspended in cell culture medium with Benzonase (25 U/mL; Life Technologies, #88701) and incubated for 30 min at room temperature. Cells were centrifuged again and resuspended in an appropriate amount of cell culture medium and counted with an automated Luna-FL™ Dual Fluorescence Cell Counter (Logos Biosystems) or Attune NxT (Thermo Scientific). Cells (1×10^6 to 5×10^6) were seeded in a 96-well plate or 24-well plate and rested for 3 h at 37°C before counting again.

3.1.3 Live-cell barcoding (flow cytometry experiments)

Cells (2×10^6) were transferred to a V-bottom plate (Falcon, #353263) and incubated with 1 µg of Fc block per well [human Fc block (BD Pharmigen, #564220) or mouse CD16/32, clone 24G2 (#553142)] for 10 min at 4°C. Then, cells were centrifuged at 1,700 rpm for 3min at 4°C.

3.1.3.1 Mouse barcoding

Cell pellets were stained with anti-mouse CD45.2 antibodies for 20 min at 4°C, protected from light. These antibodies were coupled to three different fluorochromes: BC1 = CD45.2-BV421; BC2 = CD45.2-APC; BC3 = CD45.2-BV510; and BC 4 = CD45.2-BV421 + CD45.2APC.

3.1.3.2 Human barcoding

Cell pellets were stained with anti-human CD45 antibodies for 20 min at 4°C, protected from light. These antibodies were coupled to three different fluorochromes: BC1 = hCD45.BUV395; BC2 = hCD45.BUV805; and BC3 = hCD45 BV421.

After incubation, three washes in HBSS buffer were made before resuspending the cells in IMDM with 10% FCS. Cells were counted and later distributed for *ex vivo* stimulation.

3.1.4 *Ex vivo* stimulation

3.1.4.1 *Ex vivo* stimulation for mouse T cells

Cells (1×10^6) were seeded and stimulated with four conditions: unstimulated (NS), anti-mouse CD3ε (plate-bound, 10 µg/mL), anti-mouse CD3ε (plate-bound, 10 µg/mL; BIOXCELL, #BE0001-1, clone 145-2C11) + anti-mouse CD28 (soluble, 1 µg/mL; Exbio, #12-597-BULK, clone 37.51), or anti-mouse CD3ε (plate-bound, 10 µg/mL) + anti-mouse BTLA (plate-bound, 20 µg/mL).

Wells were coated with anti-mouse CD3 and anti-mouse B- and T-lymphocyte attenuator (BTLA) for overnight at 4°C. Coated wells were then washed with 1× PBS three times before adding barcoded or non-barcoded T cells.

The same conditions of stimulation were applied for non-barcoded T cells. Final medium volume in all wells was 200 µL. Plates were incubated for 6 h (T = 6 H) or 16 h (T = 16 H) at 37°C in a CO_2 incubator. The remaining cells after dispensing corresponded to the starting point (T = 0 H).

3.1.4.2 *Ex vivo* stimulation for human cells

Cells (1×10^6) were seeded and stimulated with three conditions: unstimulated as negative control, anti-human CD3 (5

μg/mL; BioLegend, 300438) (coated at 37°C for 3 h, washed twice with PBS before adding cells) + anti-CD28 (3 μg/mL, BioLegend, 302934) as positive control, and SARS Peptivators (1 μg/mL; see Table 3) as specific positive stimulation. All conditions were costimulated with αCD28 (1 μg/mL) and αCD40 (1 μg/mL; BioLegend, 334302). Cells were stimulated for 16 h at 37°C.

3.1.5 Flow staining

3.1.5.1 Flow cytometry staining

After stimulation, cells were transferred to a 96-well V-bottom plate and centrifuged at 1,500 rpm for 5 min at 4°C. The pellet was washed with 200 μL of PBS, centrifuged again and incubated with 1 μg of Fc block per well [human Fc block (BD Pharmigen, #564220) or 1 μg of mouse CD16/32, clone 24G2 (#553142)] for 10 min at 4°C. After centrifugation, cell pellets were stained with antibodies according to Table 4 (including Zombie Red dye for viability assessment in the case of human PBMCs) for 20 min at 4°C.

Mouse T cells were washed three times with HBSS buffer and resuspended in a DAPI solution (Thermo Fisher, #D1306) used for the staining of dead cells and were acquired on a BD Fortessa LSRII Cytometer.

Human cells were washed three times with HBSS buffer and resuspended in 4% PFA in H_2O for 30 min at 4°C. Afterward, cells were centrifuged for 5 min at 1500 rpm, 4°C, then washed once with HBSS buffer, and resuspended in 150 μL of HBSS buffer for acquisition on a CytoFLEX LX cytometer (Beckman Coulter).

Flow cytometry data were analyzed using FlowJo™ and FACSDiva™ software. Representative gating strategy for $CD4^+$, $CD8^+$, $CD25^+CD69^+$, $CD25^+CD137^+$, $CD69^+CD137^+$ is depicted in Supplementary Figure 2.

3.1.5.2 Flow cytometry staining with Curiox

After stimulation, cells were transferred to a 96-well V-bottom plate and centrifuged at 1,700 rpm for 3 min at 4°C. The pellet was washed with 200 μL of PBS and centrifuged again before resuspending in 50 μL of FACS buffer with human αCD16/αCD32 Fc block (1 μg/mL). Cells were transferred to a 96-well laminar wash plate (Curiox™) and incubated at 4°C for 20 min to 30 min until cells were settled on the plate. The Curiox Laminar Wash™ MINI 1000) was prepared with the following settings: input initial volume, 50 μL; 12× washes; flow rate, 5 μL/s; vortex plate for 20 s. These settings were used for all following washing steps. Cells were washed with PBS with the laminar flow device before adding 25 μL of the antibody mix with a two-fold concentration due to a residual volume of 25 μL per well after washing. Cells were mixed gently with a pipette and incubated for 45 min at 4°C. Afterward, the plate was washed with a FACS buffer using the laminar flow device, and cells were resuspended in 25 μL per well of 4% PFA in H_2O and incubated for 30 min at 4°C. The cells were washed once more before adding 115 μL of FACS buffer and transferring to a 96-well V-bottom plate for measurement. Cells were stored at 4°C until acquisition on a CytoFLEX LX cytometer (Beckman Coulter).

TABLE 3 SARS-CoV-2 peptivator pool.

Name	Catalog no.	Manufacturer
PepTivator® SARS-CoV-2 Prot_S	130-126-701	Miltenyi Biotec
PepTivator® SARS-CoV-2 Prot_S+	130-127-311	Miltenyi Biotec
PepTivator® SARS-CoV-2 Prot_S1	130-127-041	Miltenyi Biotec
PepTivator® SARS-CoV-2 Prot_M	130-126-703	Miltenyi Biotec
PepTivator® SARS-CoV-2 Prot_N	130-126-698	Miltenyi Biotec

3.2 Double barcoding in mass cytometry with human cells

3.2.1 Debris/dead cell removal with Laminar Wash, MINI 232 System (Curiox™)

After thawing and resting for 3 h, cells from each patient were pooled, centrifuged, and resuspended in Cell Staining Buffer (CSB)

TABLE 4 Flow cytometry panel for human and mouse cells.

Sample	Marker	Fluorochrome	Clone	Manufacturer	Dilution
Human	CD4	PerCP-Cy5	REA623	Miltenyi Biotec	1/250
	CD8	APC	SK1	BioLegend	1/250
	CD25	PE-Cy7	M-A251	BioLegend	1/250
	CD69	FITC	FN50	BioLegend	1/250
	CD137	PE	4B4-1	BD Biosciences	1/250
	Zombie Red™	–	–	Biolegend 423110	1/1,000
Mouse	CD8a	BUV737	53-6.7	BD Biosciences	1/200
	CD25	BB700	PC61	BD Biosciences	1/200
	CD69	PE	H1.2F3	BD Biosciences	1/100
	CD4	PE-Cy7	RM4-5	BD Biosciences	1/200
	Live/dead: DAPI	BUV496	–	Thermo Fisher #D1306	1/1,000,000

at a concentration of 1×10^6 to 1.5×10^6 cells in 25 µL. Twenty-five microliters per well was added on Curiox plate, left for 25 min at RT, and checked under microscope to ensure that cells were settled. Curiox program: 12 cycles; the flow rate of CSB buffer at 5 µL/s for washing debris was used. CSB (50 µL) was added in each well and gently pipetted especially around edges, and all cells were pooled from each sample and then counted before CD45 barcoding step.

3.2.2 Live-cell barcoding (mass cytometry experiment)

Patients were barcoded with different combinations of αCD45 antibodies labeled with variable metals tag (see Tables 5, 6).

A maximum of 2×10^6 to 2.5×10^6 cells were distributed in V-bottom plate (Falcon, #353263) and incubated with 1 µg of Fc block per well (human Fc block; BD Pharmigen, #564220) for 10 min 4°C. After one centrifugation at 1,700 rpm for 3min at 4°C, the pellets were resuspended in 100 µL of CSB (Standard Biotools, #201068) containing the respective barcoding antibodies combination. After 20 min of incubation at 4°C, cells were washed three times in CSB. The pellet was resuspended in medium, and cells were distributed for *ex vivo* stimulation.

3.2.3 *Ex vivo* stimulation in mass cytometry experiment

For mass cytometry experiment, we used the same protocol as for flow cytometry with human cells (see Section 3.1.4.2) except that we stimulated the cells for 16 h at 37°C with a pool of allergen peptides (100 µg/mL) (Table 2).

3.2.4 Mass cytometry staining (with Standard Biotools intracellular barcoding)

After stimulation, cells were transferred to a 96-well V-bottom plate and centrifuged at 1,700 rpm for 3 min at 4°C. The pellet was resuspended in 150 µL of Maxpar-PBS (Standard Biotools, #201058), and all wells from one stimulus were pooled in a 1.5-mL reaction tube. After centrifugation at 1,300 rpm for 7 min at 4°C, cells were stained with 100 µL of CisPt198 (1:5,000) (Standard Biotools, #201198) in Maxpar-PBS for 10 min at room temperature. Afterward, cells were washed twice with each 500 µL of CSB (Standard Biotools, #201068) and resuspended in 50 µL of human αCD16/αCD32 Fc block (BD Pharmigen, #564220) at 1 µg/mL in CSB. Cells were incubated for 10 min at 4°C and washed again with CSB, and a 100-µL mass cytometry antibody mix was added per 2×10^6 cells. After incubation for 45 min at 4°C, the cells were washed twice with CSB, and 100 µL of CytoFix (BD Pharmigen, #554714) was added and incubated for 30 min at 4°C. For subsequent barcoding of the stimuli, cells were washed twice with 1× Maxpar-Barcoding buffer (Standard Biotools, #201057), and 1×10^6 to 3×10^6 cells for each stimulus were resuspended in a 100-µL Pd Barcoding kit (Standard Biotools, #201060) following the Cell-ID™ 20-Plex Pd Barcoding Kit protocol. Cells were incubated for 30 min at room temperature and washed three times with CSB + 5% BSA. Afterward, all cells were pooled into one reaction tube, centrifuged at 1,300 rpm for 10 min and washed once with CSB, and the pellet was resuspended in 200 µL of iridium (1:1,000) (Standard Biotools, #201192) in a CytoFix buffer (BD Pharmigen, #554714). After incubation overnight at 4°C, the cells were washed twice with each 1 mL of CSB, and the pellet was resuspended in 100 µL of FCS + 10% DMSO and stored at −80°C until acquisition on a Helios Mass cytometer. We conducted mass cytometry analysis using the HT injector #107018, whereas the acquisition was performed in Standard Biotools water (#201069).

3.3 Mass cytometry analysis tools

Mass cytometry analysis was performed as previously described (Levine et al., 2015). Briefly, the FCS files generated from mass

TABLE 5 Barcoding scheme for human and mouse cells.

Experiment	Sample	Marker	Fluorochrome	Clone	Manufacturer	Dilution
Flow cytometry	Human	CD45	BV421	HI30	BD Biosciences	1/250
		CD45	BUV395	HI30	BD Biosciences	1/250
		CD45	BUV805	HI30	BD Biosciences	1/250
	Mouse	CD45.2	BV421	104	BD Biosciences	1/200
		CD45.2	APC	104	BioLegend	1/200
		CD45.2	BV510	104	BioLegend	1/100
Experiment	**Sample**	**Marker**	**Metal**	**Clone**	**Manufacturer**	**Dilution**
Mass cytometry	Human	CD45	89y	HI30	Standard Biotools	1/100
		CD45	111Cd	HI30	Standard Biotools	1/100
		CD45	112Cd	HI30	Standard Biotools	1/100
		CD45	113Cd	HI30	Standard Biotools	1/100
		CD45	114Cd	HI30	Standard Biotools	1/100
		CD45	116Cd	HI30	Standard Biotools	1/100

10.3389/fcimb.2023.1336489

TABLE 6 Barcoding scheme for donor samples for mass cytometry.

	111 Cd	112 Cd	113 Cd	114 Cd	116 Cd
Figure 2					
BC1					
BC2					
BC3					
BC4					
BC5					
BC6					
BC7					
BC8					
BC9					
BC10					
Figure 3					
Vacc					
HD					
Sample 3					
Sample 4					
Figure 4					
Vacc1					
Vacc2					
HD1					
HD2					
Inf					
Vacc + Inf1					
Vacc + Inf2					
Vacc + Inf3					

cytometry were manually gated to live CD45+ cells using Cytobank. Samples were debarcoded on Cytobank by manual gating (see Supplementary Figure 3). Representative gating strategy for mass cytometry is shown in Supplementary Figure 4. Pre-processing of the raw data was followed by dimensionality reduction and visualization. This work was done by t-Distributed Stochastic Neighbor Embedding (t-SNE) using the default parameters (perplexity = 30 and iterations = 1,000) or with the use of UMAP (Uniform Manifold Approximation and Projection) in Cytobank software. To obain unsupervised debarcoding, UMAP dimensional reduction was followed by the use of FlowSom (five-metacluster parameter) in Cytobank. t-SNE dimensional reduction was followed by PhenoGraph (Levine et al., 2015) using in-house developed R-shiny interface "CIPHEBox" to classify and visualize the subpopulations of cells based on their cell surface marker expression. PhenoGraph first identified the k-nearest neighbors (k = 30) using Euclidean distance and calculated the similarities using the Jaccard coefficient. Subsequently, the Louvain algorithm was used to partition the network for detecting communities with optimal modularity, generating 31 metaclusters. Median expression of marker intensities for each cluster were used for expert-guided manual annotation. Heatmaps and hierarchical clustering were generated using Morpheus (https://software.broadinstitute.org/morpheus). Cluster data were visualized in Cytobank to generate density plot and cluster overlays.

4 Results

4.1 Anti-CD45 fluorescent barcoding of purified mouse T cells does not alter their functional response

To determine whether live anti-CD45 barcoding of cells was compatible with *in vitro* T-cell stimulation protocols, mouse T

cells purified from the spleen and LNs from three mice were pooled to generate a homogenous cell suspension and then split into five different fractions. Four fractions were stained using different combinations of anti-CD45 conjugates and one remained unstained (Figure 1A). Barcoded and unbarcoded fractions were either acquired on the cytometer (t = 0) or distributed in two to four wells with different stimulation conditions respectively: unstimulated, aCD3/aCD28, aCD3 alone, or aCD3 and aBTLA. After 6 h or 16 h of incubation, cells were collected by sample barcodes. Half of each cell suspension was pooled in a multiplexed sample. Other half was kept separate to assert for the proportion of each cell phenotype in each stimulation condition before sample multiplexing. Individual fractions and multiplexed sample were then stained with a minimal surface staining panel containing T-cell lineage markers CD4 and CD8 as well as activation markers (CD69 and CD25). First, we could see that the staining intensity of each individual aCD45 conjugates remained stable over 6 h to 16 h of stimulation (Figure 1B). The stability of CD45 marker expression allowed for correct deconvolution of each sample from the multiplexed pool (Figures 1A, B) indifferently of the stimulation condition. Next, in order to evaluate the impact of live sample barcoding on T-cell activation, we analyzed the proportion of lineages as well as the upregulation of activation markers in barcoded and non-barcoded T cells (Figure 1C). As demonstrated in Figure 1C, no differences in CD4/CD8 proportion (83% and 84%) or CD69/CD25 upregulation (88% and 89%), respectively, were seen between barcoded and non-barcoded cells. On the basis of these readouts, we can conclude that live fluorescent cell barcoding of murine T cells does not prevent their normal activation kinetic of activation in different stimulation conditions.

4.2 Anti-CD45 barcoding of human PBMC is compatible with *in vitro* T-cell restimulation assay

Next, we wanted to test whether a similar live-cell barcoding approach would be compatible with human PBMCs in an antigen-specific T-cell restimulation assay. Similar to Figure 1A, PBMCs from three different donors (healthy donor, vaccinated, or infected and vaccinated against SARS-Cov2) were barcoded using different combination of anti-human CD45 antibodies. Barcoded cells were then set into different stimulation conditions for 16 h at 37°C. After stimulation, cells were pooled by stimulation conditions, stained with a minimal panel containing activation markers (CD69, CD25, and CD137), and acquired on a flow cytometer. Barcode expression intensity was used to drive a UMAP unsupervised data analysis (Figure 2A) and FLOWSOM clustering. As seen in Figure 2A, no difference in metacluster (MC) distribution was observed across stimulation conditions, indicating that the fluorescence intensity level of each samples remains comparable across stimulation conditions. Four MCs were identified among which three majors (MC3, MC4, and MC5) corresponding each to a barcoded patient and one minor (MC1 and MC2) containing illegitimate barcode combinations (doublets or debris). We then analyzed the upregulation of activation markers in specific stimulation conditions (Figure 2B). As expected, we could see that, upon aCD3/aCD28 non-specific stimulation, all patient samples showed that early activation markers CD69 and CD25 were strongly upregulated in both $CD4^+$ and $CD8^+$ T cells, whereas this was not the case with the costimulation only condition (Figure 2B). This highlights that patient cell barcoding before stimulation does not alter the capacity of the cells to modulate the intensity of their response to different stimuli. In response to a more physiological stimulation with SARS-Cov2 peptivator, we observed that every donor had a different level of baseline reaction considering CD25, CD69, and CD137 marker expression. Because the peptivator condition also contains the "co-stimulus" (αCD28 and αCD40), we normalized the response to the costimulation results to ease the evaluation of the global response to peptivator stimulation. We could detect an increase in proportion of $CD4^+CD69^+CD137^+$ and of $CD8^+CD69^+CD137^+$ minor T-cell populations in vaccinated + infected samples after stimulation with peptivator antigen pool (Figure 2B). This result is expected as it is conceivable that the proportion of T-cell clonotype reacting against SARS-Cov2 peptides would increase among the total T-cell population after vaccination and infection. It confirms that antigen-specific T-cell response can be studied reliably on samples after anti-CD45 live-cell barcoding by flow cytometry.

4.3 Cell viability of PBMC samples impact overall debarcoding efficiency of dual-barcoding scheme

In order to increase the phenotypic characterization of T cells responding to specific antigen stimulation, we adopted the assay to mass cytometry. We therefore developed a high-content mass cytometry panel aiming 37 surface markers that are important in T-cell function (Table 7). We performed sample barcoding of 10 individual PBMC samples using the barcoding scheme in Tables 5, 6, distributed equal number (500,000 cells) of encoded cells over three stimulation conditions (costimulation only, peptivator, or allergen + costimulation). Of note, donors 1–9 (BC1–BC9) came from one single COVID-19 cohort, whereas donor 10 (BC10) is a cohort-independent vaccinated donor (see Table 1, Figure 3, Sample ID 10). Because of the constraints in the numbers of cells recovered after thawing, only two samples (barcodes 7 and 10) were stimulated with a fourth stimulation using anti-CD3/anti-CD28 in order to determine the general activation pattern of marker expression induced after non-specific antigen stimulation using this panel. Cells from each stimulation conditions were stained using mass cytometry antibody panel and encoded with Standard Biotools barcoding kit. All fractions were then mixed in one multiplexed tube for acquisition on Helios instrument. As shown on sunburst plot of Figure 3A, stimulation conditions could be identified and yielded expected numbers of barcodes (2 for non-

10.3389/fcimb.2023.1336489

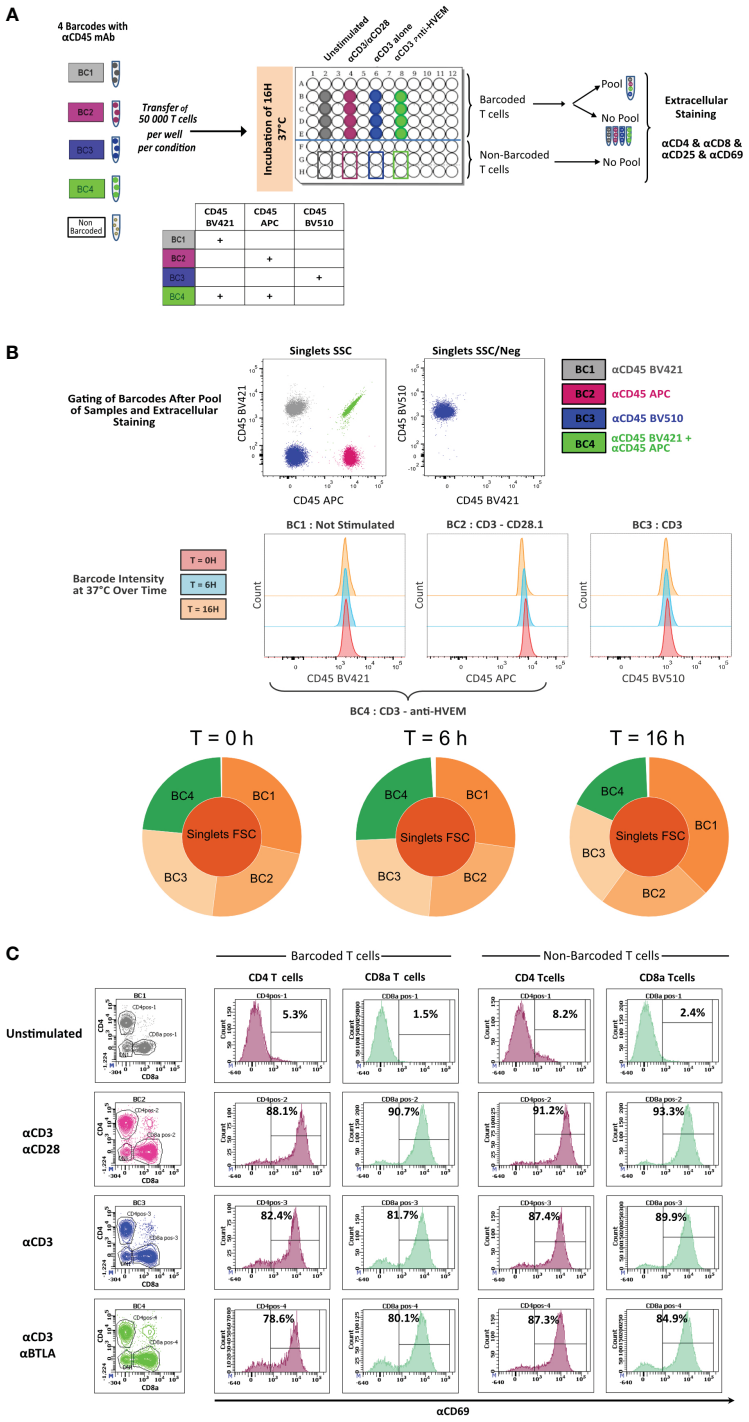

FIGURE 1
In vitro activation of CD45.2 barcoded mouse T cells. **(A)** Schematic drawing of the experiment. T cells isolated from LNs of a C57Bl/6 mouse were either not barcoded or barcoded with CD45.2 antibodies tagged with different fluorochromes. Barcoded and non-barcoded T cells were kept unstimulated or were stimulated with αCD3/αCD28, αCD3 alone, or αCD3/anti-HVEM during 6 h or 16 h and subsequently stained with a mix of antibodies containing CD4/CD8/CD25/CD69 antibodies. **(B)** Stained T cells were analyzed on a BD LSR Fortessa flow cytometer, and dot plot representation allowed to recover the four different barcodes. The histogram representation is gated on three different barcodes to analyze CD45.2 fluorescence intensity at time point 0 h, 6 h, and 16h. Sunburst representation of debarcoded samples done with Cytobank. **(C)** Analysis of $CD69^+$ level of expression in $CD4^+$ and $CD8^+$ T cells for barcoded and non-barcoded conditions.

10.3389/fcimb.2023.1336489

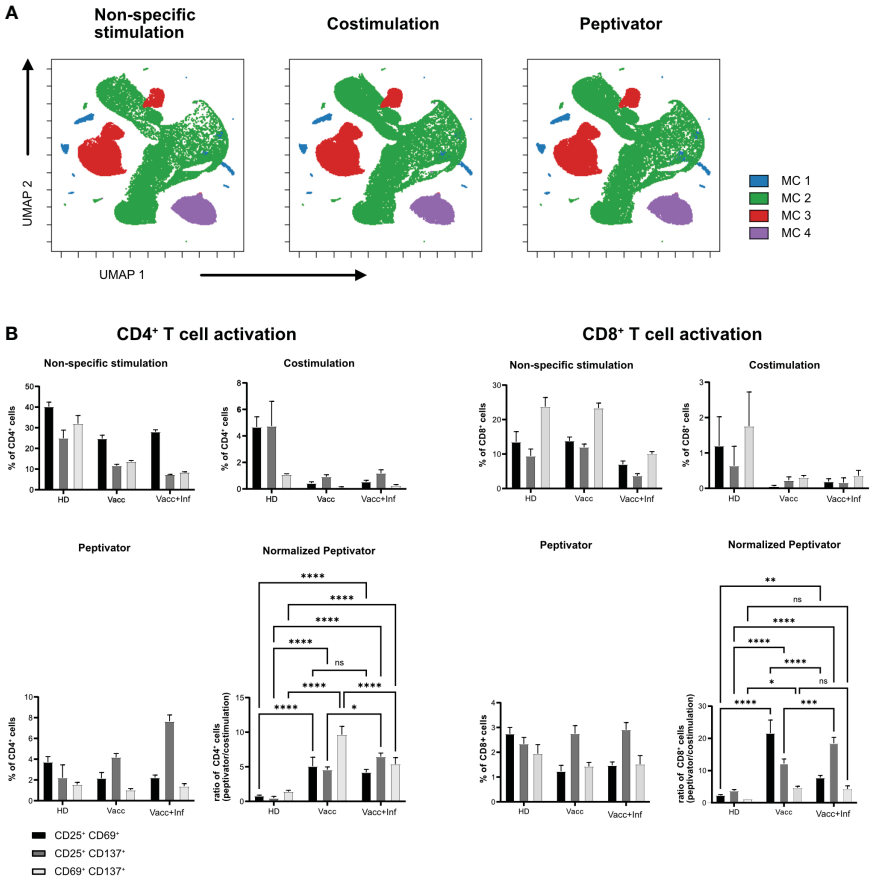

FIGURE 2
In vitro activation of human barcoded T cells. T cells were isolated from three different donors (see Table 1 for detailed donor information); HD, pre-pandemic PBMC donor; Vacc, vaccinated donor; and Vacc + Inf, vaccinated donor recovered from subsequent SARS-CoV-2 infection. **(A)** UMAP representation showing FlowSOM clusters of debarcoded human PBMCs after 16 h with non-specific stimulation (stimulation with αCD3/αCD28), costimulation (stimulation with αCD28/αCD40) and peptivator stimulation (stimulation with αCD28/αCD40 and a set of SARS peptide pools). **(B)** T cells were stimulated in three groups (non-specific, costimulation, and peptivator, as described above). Panels show the three stimulation groups and the normalization of the peptivator stimulation to the costimulation. Graphs show the frequency of activated $CD4^+$ T cells and $CD8^+$ T for each donor. Bars show a mean of three technical replicates; whiskers indicate standard deviation. Mean values of the groups were compared using a two-way ANOVA. *p < 0.05; **p < 0.01; ***p < 0.001; ****p < 0,0001. Statistical analysis for normalized peptivator is only shown.

specific stimulation and 10 for costimulation only, peptivator, and allergen). However, after sample debarcoding using live anti-CD45 barcodes, a high proportion of cells (40%) could not be attributed to any legitimate barcode (BC) combinations (Figure 3A). Corollary to this observation, very few cells for BC4 and BC6 could be retrieved in all stimulation conditions. As shown in Figure 3B, most of the cells for BC4 and BC6 were dead as indicated by the high proportion of cells stained by cisplatin (>80%). In general, most of the samples retrieved showed a high proportion (30%–90%) of cisplatin+ dead cells in this experiment. In addition to the potential generation of staining artifacts that could be attributed to dead cells, we recovered very low number of cells per stimulation condition for each sample. As the aim of our assay is to study rare activation phenotypes of CD4 and CD8 T-cell populations that are expected to be at low frequency (0.5% to 2% of total T cells), the added detrimental effects of low cell viability and inefficient sample debarcoding precluded any further meaningful analysis of the data.

4.4 Dual-barcoding scheme is improved after debris removal and allows for the detection of rare T-cell subset responding to peptide stimulation

By releasing anti-CD45–stained debris that would stick to live cells of other samples in the multiplexed pool, dead cells present in the dual-barcoding assay could lead to illegitimate barcode combination, resulting in low debarcoding efficiency as observed in Figure 3A. In order to test this hypothesis, we introduced a debris removal step after thawing the samples before the live-cell barcoding step (Figure 4A) either using a density gradient (Supplementary Figure 1) to remove debris (Figures 4B–D) or a laminar flow device (Figure 5). A new vial of PBMCs from vaccinated donor used in previous experiment (BC10) was thawed and treated with debris removal solution before live-cell barcoding step. After antigen stimulation, recovered samples showed a higher proportion of live cells compared to previous experiment

10.3389/fcimb.2023.1336489

TABLE 7 Mass cytometry panel.

Marker	Metal	Clone	Manufacturer	Dilution
CD45	089Y	HI30	Standard Biotools	1/100
CLA	115In	HECA-452	Homemade	1/100
CD3	141Pr	UCHT1	Homemade	1/400
CD134	142Nd	ACT35	Standard Biotools	1/100
CD45RA	143Nd	HI100	Standard Biotools	1/100
CD270	144Nd	122	Homemade	1/100
CD4	145Nd	RPA-T4	Standard Biotools	1/100
CD8	146Nd	RPA-T8	Standard Biotools	1/100
CD154	147Sm	24-31	Homemade	1/100
CD278	148Nd	C398.4A	Standard Biotools	1/100
CD25	149Sm	2A3	Standard Biotools	1/100
CD11a	150Nd	HI111	Homemade	1/100
CD107a	151Eu	H4A3	Standard Biotools	1/200
TCRgt	152Sm	11F2	Standard Biotools	1/100
CD62L	153Eu	DREG56	Standard Biotools	1/100
Gpr15	154Sm	SA302A10	Homemade	1/100
CD279	155Gd	EH12.2H7	Standard Biotools	1/100
CD272	156Gd	8.2	Homemade	1/100
CD137	158Gd	4B41	Standard Biotools	1/100
CD197	159Tb	G043H7	Standard Biotools	1/100
CD357	160Gd	621	Homemade	1/100
CD5	161Dy	UCHT2	Homemade	1/400
CD69	162Dy	FN50	Standard Biotools	1/100
CXCR3	163Dy	G025H7	Standard Biotools	1/200
CD95	164Dy	DX2	Standard Biotools	1/100
CD45RO	165Ho	UCHL1	Standard Biotools	1/100
CD44	166Er	BJ18	Standard Biotools	1/100
CD27	167Er	O323	Standard Biotools	1/100
CD366	169Tm	F38-2E2	Standard Biotools	1/100
CD152	170Er	14D3	Standard Biotools	1/100
CD185	171Yb	RF8B2	Standard Biotools	1/100
CD38	172Yb	HIT2	Standard Biotools	1/100
KLRG1	173Yb	REA261	Homemade	1/100
HLA-DR	174Yb	L243	Standard Biotools	1/100
CD49d	175Lu	9F10	Homemade	1/100
CD127	176Yb	A019D5	Standard Biotools	1/100
CD223	209Bi	7H2C65	Homemade	1/100
Cell-ID cisplatin	198Pt	201198	Standard Biotools	1/5000
Cell-ID intercalator	191/193Ir	201192	Standard Biotools	1/1,000

10.3389/fcimb.2023.1336489

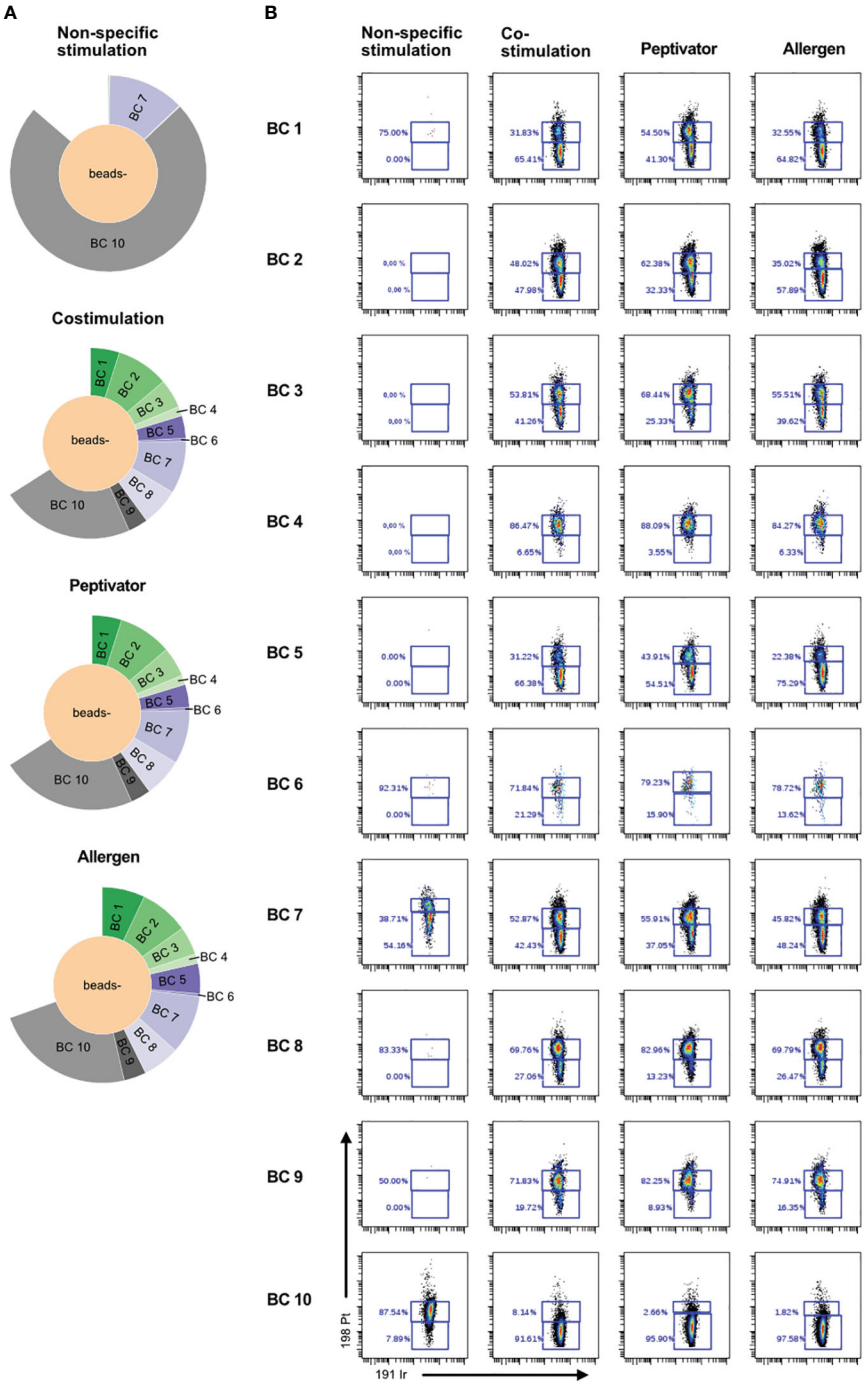

FIGURE 3
Poor cell viability after thawing is correlated to inefficient debarcoding. Patient cells from 11 donors were thawed and identified using 10 different barcode combinations. Note that samples 7 and 11 were mixed and are shown as BC7. **(A)** Sunburst representation of debarcoded samples wherein each color segment is proportionate to the percentage of cells within the combined barcoded pool, analyzed in Cytobank. **(B)** Viability of the cells after 16 h of stimulation with CD3/CD28, CD28/CD40, the peptivator pool, or the allergen. Analysis was done in Cytobank. Live PBMCs are 198 Pt-negative/191 Ir-negative.

(Figure 3) as low (<15%) cisplatin labeling was detected on cells for all stimulation conditions tested. Concomitantly, the sample debarcoding efficiency was improved to an average of 80% (Figure 4C). Both healthy donor (HD) and vaccinated samples produced a high proportion of CD25+CD69+ activated T cells (>20%) after non-specific TCR stimulation by anti-CD3/anti-CD28 treatment (Figure 4D) as opposed to <2% T cells in the costimulation only condition. CD25+CD69+ activated T cells were 0.78% and 2.14% in the HD and vaccinated donors respectively, after antigen specific stimulation. Therefore, debris removal before sample barcoding enhances debarcoding efficiency in our dual-barcoding assay and allows the detection of rare T-cell subsets after antigenic stimulation.

10.3389/fcimb.2023.1336489

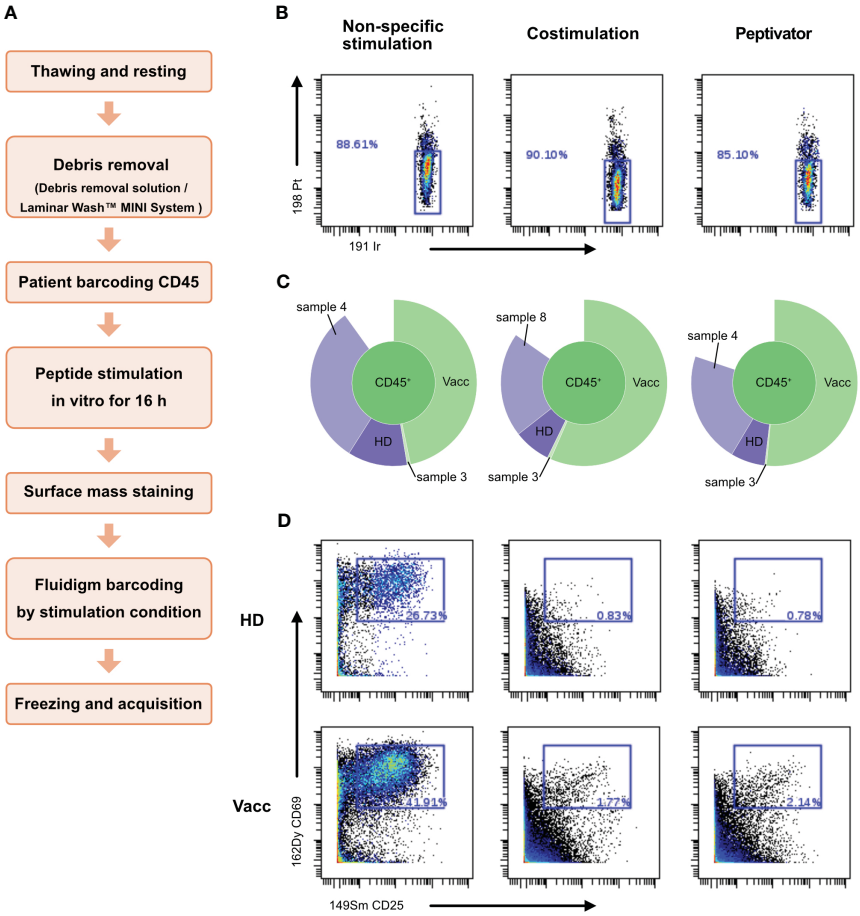

FIGURE 4
Use of debris removal solution (DRS) from Miltenyi allows to eliminate debris and subsequent analysis. Patient PBMCs were thawed and identified with the help of different barcode combinations. **(A)** Flowchart of the optimized CyTOF protocol to analyze low-frequency responding T cells after stimulation. **(B)** After 16 h of stimulation with CD3/CD28, CD28/CD40, the peptivator pool, or the allergen peptide pool, viability of the cells is analyzed on Cytobank. Live PBMCs are 198 Pt-negative/191 Ir-negative. **(C)** Sunburst representation of debarcoded samples, done with Cytobank. **(D)** T-cell activation status after stimulation. Event count of activated T cells is shown in the blue box inside the graphs.

4.5 High-content immunophenotyping of activated T cells reveals functional heterogeneity between vaccinated and non-vaccinated heathy donor

In order to maximize the number of cells available from each sample for the three stimulation conditions, we wished to study on all of our samples while preserving a high efficiency of sample debarcoding, the density gradient step introduced in Figure 4 to remove debris was replaced by several washes performed by laminar flow on a Curiox device (Figure 4A). PBMCs from two HD, two vaccinated, one infected and 3 vaccinated and infected donors for a total of eight samples were then barcoded following barcoding key described in Tables 5, 6 and set into costimulation only, peptivator, or allergen stimulation conditions. Only two samples (HD1 and Vacc1) were subjected to non-specific anti-CD3/anti-CD28 T-cell stimulation. After mass cytometry acquisition, acquired data on the multiplex pooled were normalized using eQBeads and debarcoded. Similar to the results observed using debris removal solution (Figure 4), laminar flow washes of samples after thawing and resting led to efficient sample debarcoding (Figure 5A) and correct representation of each barcodes in respective stimulation conditions. This is most probably due to the already described beneficial effect of laminar flow washes on the elimination of cell debris (Lye et al., 2022). In addition, we observed approximately 2%–8% $CD4^+$ or $CD8^+CD25^+CD69^+$ T cells after stimulation with peptivator or allergen (Figure 5B). Further unsupervised analysis using PhenoGraph clustering of all samples and conditions yielded to 31 clusters among which 23 were present in costimulation, peptivator, and allergen conditions only. In order to reduce the complexity of data interpretation in this paper, these clusters were regrouped in five metaclusters (MC) after hierarchical clustering using expression of all markers available in the panel (Figure 5C) and projected onto Opt-SNE manifold (Figure 5D). In order to visualize the change in the relative proportion of each MC, the density distribution of each sample in all stimulation conditions was projected onto the same Opt-SNE manifold (Figure 5E). We could observe very distinct patterns between HD and vaccinated samples in the costimulation, peptivator and allergen conditions. However, due to the low number of samples processed in each group in this preliminary experiment, it

10.3389/fcimb.2023.1336489

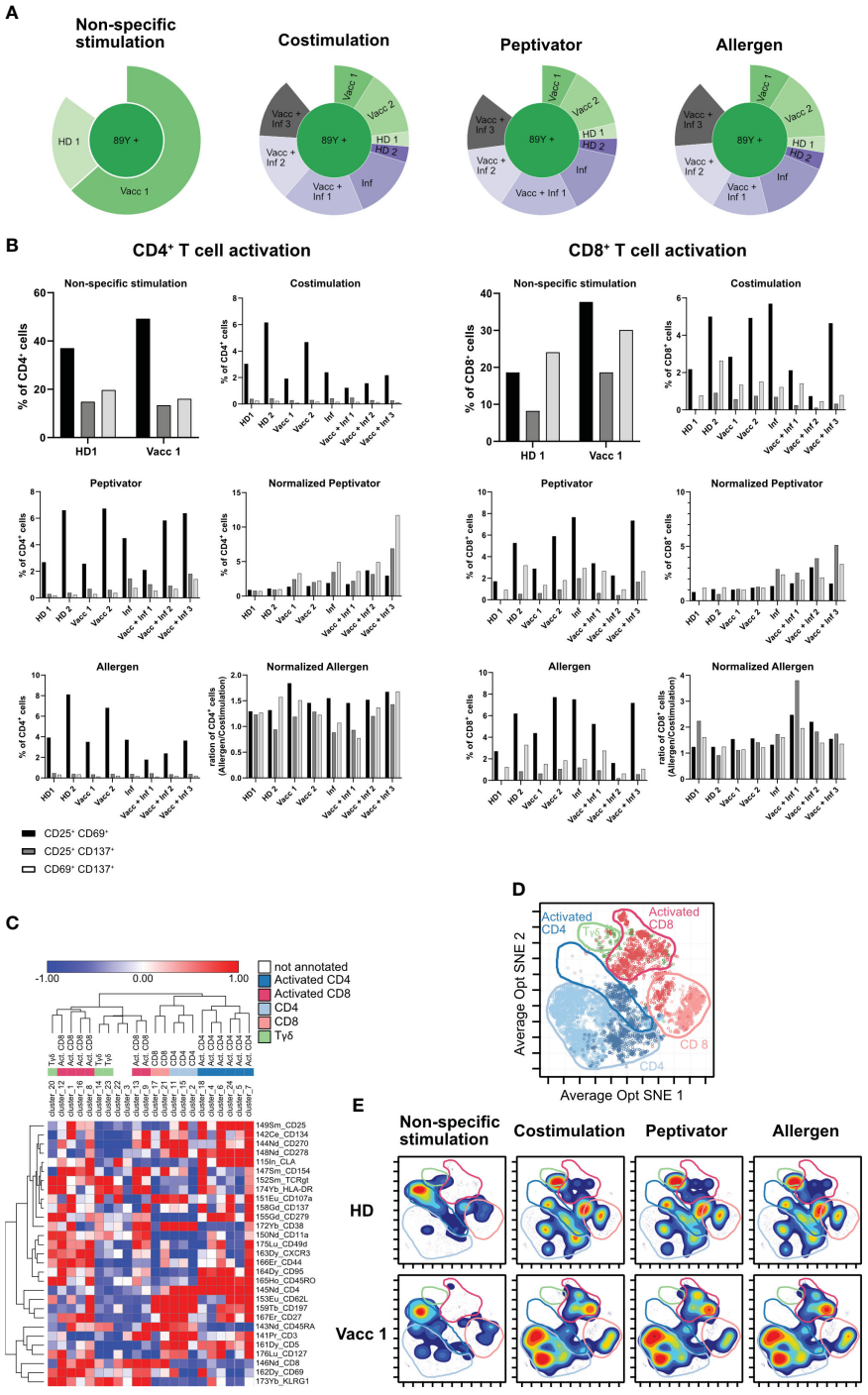

FIGURE 5
Final optimized CyTOF protocol for low-frequency PBMC stimulation analysis. **(A)** Sunburst representation to verify debarcoding efficiency after the use of Curiox. **(B)** PBMCs of eight different donors were stimulated with αCD3/αCD28 (non-specific stimulation), αCD28/αCD40 (costimulation), with a peptivator stimulus (stimulation with αCD28/αCD40 and a set of SARS peptide pools), and with an allergen stimulus (stimulation with αCD28/αCD40 and a set of allergen peptides). Panels show the four stimulation groups and the normalization of the peptivator/allergen stimulation to the costimulation. Graphs show the frequency of activated $CD4^+$ T cells and $CD8^+$ T for each donor. **(C)** Heat map representation based on the variation of marker expression to the mean expression in each Rphenograph clusters. Clusters and markers are arrayed by hierarchical clustering (Euclidian distance, complete linkage). Colors correspond to metaclusters regrouped by common biological annotation. **(D)** Projection of cells from vaccinated sample after costimulation only is shown. Same color code as in **(C)** was applied to defined area occupied by five metaclusters on the Opt SNE manifold. **(E)** Density plot of cell phenotypes observed across stimulation conditions. A manual delimitation of the space occupied by a same biological annotation determined in **(D)** on the Opt SNE manifold is shown.

is impossible to conclude whether the difference in the relative proportion of each MC and cluster is due to the individual variability of the donor or whether this is related to the differential activation of specific T-cell clone in the vaccinated group.

5 Discussion

Our study aimed at optimization of flow cytometry– and mass cytometry–based T-cell immunophenotyping in the context of ex vivo antigen stimulation assays. For this purpose, we stimulated PBMC samples derived from donors of variable relevant exposure history with SARS-CoV-2– and allergen-derived peptides and utilized dual-barcoding approaches for simultaneous acquisition of individual donor and stimulation conditions. We applied mouse and human live-cell CD45 barcoding of individual donor samples and showed that this is compatible with antigen stimulation assays by means of flow cytometry-based assessment of T-cell activation markers. We then combined with a commercially available barcoding system, which further attenuates cell loss but also technical bias by allowing simultaneous data acquisition of samples representing all stimulation conditions. Removal of dead cells and debris enhanced debarcoding efficiency in this dual-barcoding approach. Additional cell sparing was achieved by introducing a laminar flow-based cell washing system in our protocol, which avoids cell loss associated with multiple centrifugation steps (Lye et al., 2022). Our improved method was connected to reduced cell loss, as well as efficient debarcoding and immunophenotyping of low-frequency antigen-specific T cells by means of mass cytometry. The latter technology is advantageous over spectral cytometry when it comes to assessment of multiple cytokines and/or transcription factors as part of the assay's marker panel (Smith et al., 2023).

Live-cell barcoding of fresh or thawed cells is compatible with both short-term and long-term T-cell activation assays in mouse (Akkaya et al., 2016) and human cells, as it does not require fixation (our work) (Junker and Camillo Teixeira, 2022). This is a commonly used strategy in immunological research to mark individual donors and thus assess pooled samples simultaneously in a high-throughput manner. The kinetic of expression of activation markers upon relevant cell stimulation is not impacted as revealed by surface marker expression in our work. Initial/prior live-cell barcoding of sample is therefore not only reducing technical variance but is also fully compatible with T-cell functional assays and can be used for pooled immunophenotyping. Anti-CD45 live-cell barcoding signal was stable over at least 16 h of culture most probably due to the absence of receptor internalization, similar to the observations of (Junker and Camillo Teixeira, 2022) and (Palchaudhuri et al., 2016).

We observed that our dual-barcoding approach was compromised with poor cell viability upon thawing and following *ex vivo* cell stimulation. Indeed, cell membrane debris is released by apoptotic cells and is encoded with barcodes along with viable cells. Close adherence of debris to intact cells leads to non-meaningful barcode combinations and exclusion of involved cells from sample deconvolution. Removal of dead cells and cell debris before the live barcoding step proved to be essential for maximising debarcoding efficiency.

To further support debris removal and in order to reduce cell loss, we washed samples by means of laminar flow technology instead of centrifugation prior to live-cell barcoding and cell plating for stimulation. Laminar flow technology enabled efficient deconvolution of 32 experimental conditions in one single experiment. Corollary to this benefit, we achieved better cell retention at each step (our observations on several projects, data not shown). Laminar flow technology is therefore particularly suited for the investigation of rare cell types in low cell number samples.

Of note, a protentional alternative/complementary explanation for the low cell viability observed among dual barcoded samples, particularly in the context of non-specific stimulation, could be the lack of supplementary exogenous Interleukin-2 (IL-2) during the duration of stimulation. Further experimentation would help to shed light on the role of this factor.

Our established protocol allowed high-content characterization of $CD4^+$, $CD8^+$, and gd-T–cell response following activation in the context of functional assays. We observed biologically meaningful T-cell activation, which correlated with exposure history of individual donors. Multiple clusters of T-cell subsets could be identified, some encompassing minute cell populations in response to peptide stimulation. Additional complexity reduction pinpointed five metaclusters based on expression of all panel markers, and these showed specific shifts across stimulation conditions. Further studies with a larger number of samples are required to evaluate the relevance of these phenotypes in regards to the biological question.

Availability and dissemination of protocols, which are customized for specific sample types (e.g., human vs. mouse, high vs. low cell numbers, and high vs. low cell debris), type of assays (e.g., with or without ex vivo stimulation), target cells, and marker panels, will promote use of mass cytometry, single-cell analysis, and immunomics to further advance respective scientific fields. Our developed mass cytometry protocol is optimized for mouse and human samples with relatively low cell numbers and high debris, which are stimulated *ex vivo* with the goal of immunophenotyping scarce antigen-specific T cells, which has been hitherto a challenge.

Data availability statement

The datasets presented in this study can be found in online repositories. The names of the repository/repositories and accession number(s) can be found below: http://flowrepository.org/ (Repository ID: FR-FCM-Z72J).

Ethics statement

The studies involving humans were approved by Ethics Committee of the Philipps University of Marburg (AZ135/20 and AZ 136/20) as well as INSERM/EFS convention (N°2018-00099). The studies were conducted in accordance with the local legislation and institutional requirements. The participants provided their written informed consent to participate in this study. The animal study was approved by CIPHE animal facilities (agreement number:

B1301407). The study was conducted in accordance with the local legislation and institutional requirements.

Author contributions

KBa: Formal analysis, Investigation, Methodology, Visualization, Writing – original draft, Writing – review & editing. MG: Formal analysis, Investigation, Methodology, Visualization, Writing – original draft, Writing – review & editing. UP: Visualization, Writing – review & editing. ZK: Visualization, Writing – review & editing. MM: Formal analysis, Writing – review & editing. XZ: Methodology, Writing – review & editing. TB: Writing – review & editing. KBl: Formal analysis, Investigation, Visualization, Writing – review & editing. DD: Methodology, Writing – review & editing. SC: Writing – review & editing. KN: Writing – review & editing. HL: Conceptualization, Formal analysis, Investigation, Methodology, Project administration, Resources, Supervision, Visualization, Writing – original draft, Writing – review & editing. CS: Conceptualization, Funding acquisition, Methodology, Project administration, Resources, Supervision, Writing – original draft, Writing – review & editing.

Funding

The author(s) declare financial support was received for the research, authorship, and/or publication of this article. CS is supported by the Universities Giessen and Marburg Lung Center (UGMLC), the German Center for Lung Research (DZL), University Hospital Giessen and Marburg (UKGM) research funding according to article 2, section 3 cooperation agreement, and the Deutsche Forschungsgemeinschaft (DFG)- funded SFB 1021 (C04, Project number: 197785619), KFO 309 (P10, Project number: 284237345), and SK 317/1-1 (Project number 428518790) as well as by the Foundation for Pathobiochemistry and Molecular Diagnostics.

Acknowledgments

We are grateful for the FACS core facility of the University of Marburg (especially Hartmann Raifer and Heinke Lucks), enabling the usage of the cytoflex flow cytometer as well as the usage of the flow cytometry analysis tool FlowJo.

Conflict of interest

For CS: Consultancy and research funding, Bencard Allergie and Thermo Fisher Scientific; Research Funding, Mead Johnson Nutrition MJN.

Publisher's note

Supplementary material

The Supplementary Material for this article can be found online at: https://www.frontiersin.org/articles/10.3389/fcimb.2023.1336489/full#supplementary-material

SUPPLEMENTARY FIGURE 1
Pretesting of debris removal solution. The debris removal solution from Miltenyi was tested with PBMCs of 5 donors (Table 1, ID 1-5) depicted with different dot colors. Boxplots show the percentage of viable cells/debris with ("DRS") or without ("None") the use of debris removal solution. Light grey is the upper quartile of the boxplot, dark grey the lower quartile.

SUPPLEMENTARY FIGURE 2
Flow cytometry gating strategy for investigated cell populations. Gating strategy used in to analyze the subpopulations of activated T cells in one donor after one stimulation condition (non-specific stimulation), starting from CD45-based debarcoding of the multiplexed pool.

SUPPLEMENTARY FIGURE 3
Representative manual debarcoding gates. **(A)** Barcoding key used to encode samples in . **(B)** Marker Expression profiles of Cadnium isotopes on each debarcoded samples resulting of manual debarcoding using barcoding key described in **(A)**.

SUPPLEMENTARY FIGURE 4
Supervised gating strategy used to select relevant events for unsupervised analysis. **(A)** the data is corresponded to . Step 1-6 correspond to the Environmental background and doublets exclusion using Gaussian parameters (Center, Offset, Width) that are generated in the Helios Time-Of-Flight chamber. Step7: dead cell exclusion gating step with live cells (CisPt-198-/lo) and dead cells (CisPt-198+). Step8, Exclusion of normalization beads. Step 9: Identification of $CD45^+$ leukocytes. **(B)** the data here corresponds to , donor: Vacc2. Representative dot plots across stimulation showing the gating of CD69, CD25 and CD137 marker combinations and their corresponding frequencies.

References

Akkaya, B., Miozzo, P., Holstein, A. H., Shevach, E. M., Pierce, S. K., and Akkaya, M. (2016). A simple, versatile antibody-based barcoding method for flow cytometry. *J. Immunol.* 197, 2027–2038. doi: 10.4049/jimmunol.1600727

Bendall, S. C., Davis, K. L., Amir, El Ad D., Tadmor, M. D., Simonds, E. F., Chen, T. J., et al. (2014). Single-cell trajectory detection uncovers progression and regulatory coordination in human B cell development. *Cell* 157, 714–725. doi: 10.1016/J.CELL.2014.04.005

Bendall, S. C., Simonds, E. F., Qiu, P., Amir, El Ad D., Krutzik, P. O., Finck, R., et al. (2011). Single-cell mass cytometry of differential immune and drug responses across a human hematopoietic continuum. *Sci. (New York N.Y.)* 332, 687–696. doi: 10.1126/SCIENCE.1198704

Hartmann, F. J., Bernard-Valnet, R., Quériault, C., Mrdjen, D., Weber, L. M., Galli, E., et al. (2016). High-dimensional single-cell analysis reveals the immune signature of narcolepsy. *J. Exp. Med.* 213, 2621–2633. doi: 10.1084/JEM.20160897

Junker, F., and Camillo Teixeira, P. (2022). Barcoding of live peripheral blood mononuclear cells to assess immune cell phenotypes using full spectrum flow cytometry. *Cytometry A* 101, 909–921. doi: 10.1002/cyto.a.24543

Krieg, C., Nowicka, M., Guglietta, S., Schindler, S., Hartmann, F. J., Weber, L. M., et al. (2018). High-dimensional single-cell analysis predicts response to anti-PD-1 immunotherapy. *Nat. Med.* 24, 144–153. doi: 10.1038/NM.4466

Krutzik, P. O., Clutter, M. R., Trejo, A., and Nolan, G. P. (2011). Fluorescent cell barcoding for multiplex flow cytometry. *Curr. Protoc. cytometry*. doi: 10.1002/0471142956.CY0631S55

Levine, J. H., Simonds, E. F., Bendall, S. C., Davis, K. L., Amir, El Ad D., Tadmor, M. D., et al. (2015). Data-driven phenotypic dissection of AML reveals progenitor-like cells that correlate with prognosis. *Cell* 162, 184–197. doi: 10.1016/J.CELL.2015.05.047

Lye, M., Eberle, C., Wang, A., Feld, G. K., and Kim, N. (2022). Abstract 1885: Semi and fully automated immunostaining sample preparation platforms improve live leukocyte recovery, reproducibility, and cytometry data quality. *Cancer Res.* 82, 1885. doi: 10.1158/1538-7445.AM2022-1885

Mei, H. E., Leipold, M. D., Schulz, A. R., Chester, C., and Maecker, H. T. (2015). Barcoding of live human PBMC for multiplexed mass cytometry*. *J. Immunol.* 194, 2022–2031. doi: 10.4049/jimmunol.1402661

Mrdjen, D., Pavlovic, A., Hartmann, F. J., Schreiner, B., Utz, S. G., Leung, B. P., et al. (2018). High-dimensional single-cell mapping of central nervous system immune cells reveals distinct myeloid subsets in health, aging, and disease. *Immunity* 48, 380–395.e6. doi: 10.1016/J.IMMUNI.2018.01.011

Olsen, L. R., Leipold, M. D., Pedersen, C. B., and Maecker, H. T. (2019). The anatomy of single cell mass cytometry data. *Cytometry A* 95, 156–172. doi: 10.1002/cyto.a.23621

Palchaudhuri, R., Saez, B., Hoggatt, J., Schajnovitz, A., Sykes, D. B., Tate, T. A., et al. (2016). Non-genotoxic conditioning for hematopoietic stem cell transplantation using a hematopoietic-cell-specific internalizing immunotoxin. *Nat. Biotechnol.* 34, 738–745. doi: 10.1038/nbt.3584

Rao, D. A., Gurish, M. F., Marshall, J. L., Slowikowski, K., Fonseka, C. Y., Liu, Y., et al. (2017). Pathologically expanded peripheral T helper cell subset drives B cells in rheumatoid arthritis. *Nature* 542, 110–114. doi: 10.1038/NATURE20810

Smith, E. L., Cohen, M. J., Xu, W., Zhong, J., Selvanantham, T., King, D., et al. (2023). *30+ Color Intracellular Full Spectrum Flow Cytometry (FSFC) and Cytometry by Time of Flight (CyTOF): A comparison of two highdimensional*. ISAC - CYTO: Montréal, Québec, Canada.

Spitzer, M. H., Gherardini, P. F., Fragiadakis, G. K., Bhattacharya, N., Yuan, R. T., Hotson, A. N., et al. (2015). IMMUNOLOGY. An interactive reference framework for modeling a dynamic immune system. *Sci. (New York N.Y.)* 349. doi: 10.1126/SCIENCE.1259425

Zivanovic, N., Jacobs, A., and Bodenmiller, B. (2014). A practical guide to multiplexed mass cytometry. *Curr. topics Microbiol. Immunol.* 377, 95–109. doi: 10.1007/82_2013_335

frontiers | Frontiers in Cellular and Infection Microbiology

TYPE Original Research
PUBLISHED 07 November 2024
DOI 10.3389/fcimb.2024.1453234

OPEN ACCESS

EDITED BY
Dimitra Dimopoulou,
Panagiotis & Aglaia Kyriakou Children's Hospital, Greece

REVIEWED BY
Charalampos D. Moschopoulos,
University General Hospital Attikon, Greece
Petros Ioannou,
University Hospital of Heraklion, Greece

*CORRESPONDENCE
Lei Liu
liulei890207@163.com
Li Wang
wangli851217@163.com

†These authors have contributed equally to this work

RECEIVED 22 June 2024
ACCEPTED 22 October 2024
PUBLISHED 07 November 2024

CITATION
Xu Y, Huang Y, Yuan Z, Liu W, Wang L and Liu L (2024) Systematic evaluation of therapeutic effectiveness of Azvudine in treating COVID-19 hospitalized patients: a retrospective cohort study.
Front. Cell. Infect. Microbiol. 14:1453234.
doi: 10.3389/fcimb.2024.1453234

Systematic evaluation of therapeutic effectiveness of Azvudine in treating COVID-19 hospitalized patients: a retrospective cohort study

Yingkai Xu[1,2†], Yuan Huang[3†], Zihan Yuan[1,2], Wanbing Liu[2], Li Wang[4*] and Lei Liu[2*]

[1]Medical College, Wuhan University of Science and Technology, Wuhan, Hubei, China, [2]Department of Transfusion Medicine; General Hospital of Central Theater Command, Wuhan, Hubei, China, [3]Department of Gynaecology and Obstetrics; General Hospital of Central Theater Command, Wuhan, Hubei, China, [4]Department of Clinical Laboratory, The First Affiliated Hospital of Henan University, Kaifeng, Henan, China

Background: Azvudine, a repurposed oral small molecule antiviral drug, has potential effects in combating the SARS-CoV-2 virus. However, studies on its clinical efficacy in patients with COVID-19 are still limited and controversial, and further research and validation are necessary.

Methods: A retrospective cohort study was conducted on COVID-19 patients who were hospitalized in the General Hospital of Central Theater Command from 1 December 2022 to 31 January 2023. We included 132 patients treated with Azvudine and 132 controls after screening and propensity score matching. The primary outcomes including all-cause mortality and a composite outcome of disease progression such as non-invasive respiratory support, invasive respiratory support, admission to intensive care unit (ICU), and death were compared.

Results: Azvudine recipients had a much lower incidence rate of composite disease progression outcome than controls (13.9075/1000 person-days versus 25.7731/1000 person-days, $P<0.05$). Azvudine recipients also possessed a lower all-cause mortality rate than controls (2.6797/1000 person-days versus 8.5910/1000 person-days, $P<0.01$). Azvudine treatment significantly reduced the risk of composite disease progression (HR: 0.37, 95% CI: 0.16-0.84, $P=0.017$) and all-cause death (HR: 0.25, 95% CI: 0.08-0.81, $P=0.021$) after adjusting potential confounding factors such as age, sex, severity of COVID-19, complications, concomitant therapy, time from symptoms to treatment, and important laboratory indicators. The subgroup analyses of composite disease progression outcome and all-cause death indicated robustness of Azvudine's in treating COVID-19 patients in general.

Conclusion: Our study demonstrates that Azvudine has a significant positive impact on the clinical recovery of hospitalized patients with COVID-19. These findings provide important support for the use of Azvudine as a therapeutic option for COVID-19, given the current divergent views on its therapeutic efficacy and its importance in public health and medical care.

KEYWORDS

COVID-19, Azvudine, composite disease progression outcome, all-cause death, retrospective cohort study

Introduction

Since its emergence in late 2019, the novel coronavirus disease (COVID-19) has rapidly developed into a global pandemic, posing a significant threat to human health and causing negative impacts on the lives and health of hundreds of millions of people worldwide (Chakraborty and Maity, 2020). This unprecedented global health crisis has prompted scientists, medical experts, and research institutions around the world to urgently explore and develop effective means of prevention and treatment, as well as drugs, to meet this challenge. Several therapeutic agents such as Nirmatrelvir/Ritonavir, Molnupiravir, and Azvudine have been authorized for the treatment of COVID-19 (Hammond et al., 2022; Jayk Bernal et al., 2022; Yu and Chang, 2022). Azvudine is the first homegrown oral anti-COVID-19 drug, and it was approved by the National Medical Products Administration on July 25, 2022. Azvudine's approval has garnered significant attention from the medical community and provided a new weapon in the global to fight against the COVID-19 epidemic. Azvudine is a nucleoside analog that specifically acts on RNA-dependent RNA polymerase (RdRp) and that is efficiently embedded in the SARS-CoV-2 RNA synthesis process to inhibit virus replication (Zhang et al., 2021). Azvudine rapidly metabolizes *in vivo* into a 5'-triphosphate metabolite (Azvudine triphosphate) with potent antiviral activity.

In the monkey experiment, Azvudine is preliminarily demonstrated to be effective for fighting SARS-CoV-2 infection by improving lymphocyte profile, reducing viral loads, organ damage and inflammation, and protecting immune function of thymus (Zhang et al., 2021). However, the clinical therapeutic efficacy of Azvudine in fighting against COVID-19 is currently a subject of controversy in the academic community. Some studies suggest that Azvudine has significant advantages such as faster viral load reduction and higher recovery rates compared to other treatments in treating COVID-19 patients (Zhang et al., 2021; Qi et al., 2023; Ren et al., 2020; Yu and Chang, 2020). However, some studies also suggest limitations to its therapeutic efficacy are objectively existed, and further validations of Azvudine's efficacy are urgently needed (Gao et al., 2023; Han et al., 2023; Zhu, 2023). These varying findings and differing opinions among experts highlight the necessity for additional evaluation of the clinical effectiveness of Azvudine in patients with COVID-19. The purpose of this study was to retrospectively analyze the efficacy of Azvudine in treating COVID-19 patients hospitalized in the General Hospital of Central Theater Command and to establish a solid and adequate scientific basis for clinical practice, which will better guide the therapeutic strategy of COVID-19 and improve prognosis.

Methods

Study design and patients

A single-center retrospective cohort study was conducted in the General Hospital of Central Theater Command from December 1, 2022 to January 31, 2023. Initially, 546 patients consecutively admitted for COVID-19 pneumonia were screened from the medical record system. Among them, 495 patients (including 132 patients with Azvudine plus standard treatment and 363 controls with standard treatment) were enrolled and met the corresponding inclusion criteria. In order to minimize the impact of confounding factors on the analysis results, we finally included 264 patients by using 132 Azvudine recipients as a benchmark and 1:1 propensity score matching (Figure 1). Inclusion criteria: 1) had a confirmed diagnosis of SARS-CoV-2 infection (with positive RT-PCR results or positive SARS-CoV-2 antigen detection results, or both); 2) had CT imaging findings met the standard of COVID-19 pneumonia; 3) obtained standard treatment or standard treatment plus Azvudine. The standard treatment is based on the Chinese Diagnosis and Treatment Program for COVID-19 (Trial 10th Edition). Exclusion criteria: 1) age under 18 years; 2) received antiviral medications other than Azvudine; 3) received non-invasive or invasive respiratory support on the date of admission. A patient was categorized as severe COVID-19 case on admission if any of the below clinical scenes additionally appeared: 1) respiratory rate ≥ 30/min; 2) oxygen saturation ≤ 93%; 3) arterial partial pressure of oxygen (PaO_2)/fraction of inspired oxygen (FiO_2) ≤ 300 mmHg (1 mmHg=0.133 kPa); 4) >50% lesions progression within 24 to 48 hours in pulmonary imaging (Chen et al., 2023).

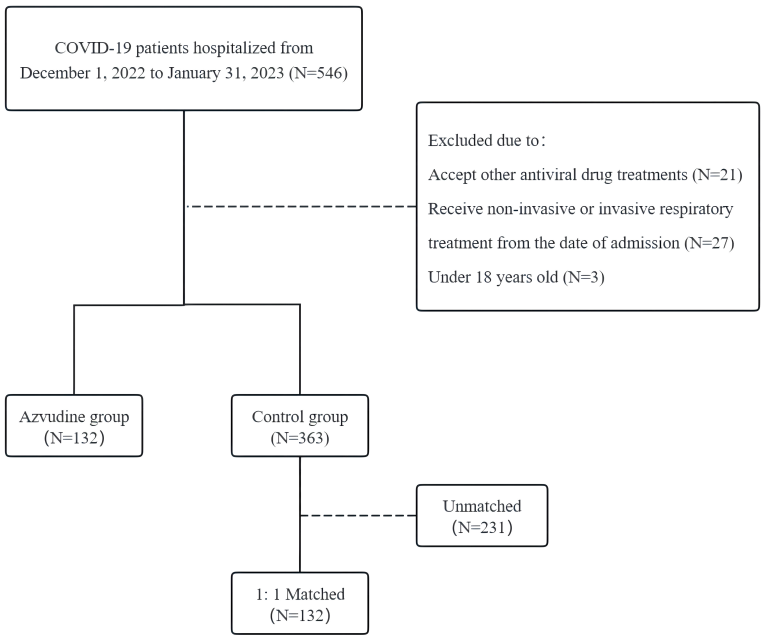

FIGURE 1
Flowchart of patient selection.

This study was approved by the medical ethics review committee of General Hospital of Central Theater Command ([2023]004-01). All enrolled patients in this retrospective cohort study were anonymous, and the requirement for informed consent was waived.

Data collection

The comprehensive data on COVID-19 patients were collected from electronic medical information system by two investigators, including demographic characteristics, dates of admission, intervals from symptom onset to hospital admission, and initial clinical presentations. Upon admission, the disease condition of each case was evaluated based on specific criteria including respiratory rates, oxygen saturation levels, PaO2/FiO2 ratios, and the extent of pulmonary infiltrates. The past medical histories, medical orders, key laboratory test results (such as blood counts, interleukins, and calcitonin), records of ICU admissions, and dates of discharge or death were also collected. All obtained data were checked by another researcher to confirm integrity and accuracy.

Treatment

The control group patients received the standard care outlined in the Chinese Diagnosis and Treatment Program for COVID-19 trial version 10 guidelines, mainly including 1) supportive treatments such as nutritional support, rest, maintenance of water, electrolyte balance, and acid-base balance; 2) symptomatic treatments such as oxygen therapy, fever reduction, cough and phlegm relief; 3) immunotherapy treatments such as systemic steroids and immunomodulators; 4) anti-infective treatments such as rational use of antibiotics. The patients in the Azvudine treatment group received 5 mg tablets of Azvudine orally once daily for up to 14 days on the basis of standard care. This ensured that all of these patients received the best clinical care practices at that time. The dosage and administration period were chosen based on initial evidence indicating Azvudine's potential benefits in mitigating the effects of COVID-19. The treatment exposure period was strategically defined to commence within the first 2 days following admission to ensure the integrity of the study's outcomes. Nasal cannula oxygen therapy was generally used to treat patients with oxygen saturation ≤ 92% or significant hypoxia symptoms. The patients who can maintain the target oxygen saturation (usually 93% -96%) in indoor air without symptoms such as difficulty breathing were often considered to stop oxygen therapy. The study carefully chose this approach to mitigate potential time bias associated with treatment initiation and admission, facilitating a more accurate assessment of Azvudine's effectiveness. By standardizing the initiation of treatment relative to the point of hospital admission, the study aimed to reduce variability in patients' outcomes that could arise from differences in disease progression at the time of treatment commencement.

Outcome events

The primary outcomes were composite metrics of disease progression including non-invasive respiratory support, invasive respiratory support, admission to intensive care unit (ICU), and all-cause death. The secondary outcomes were individual disease progression related clinical manifestations such as oxygen situation. We analyzed and compared the changes in oxygen saturation between the two groups patients who did not receive oxygen therapy within 12 days after admission. We recorded the

oxygen saturation of these patients every 3 days after admission. We collected data of patients from the date of admission to occurrence of any of the primary outcome events (non-invasive respiratory support, invasive respiratory support, ICU admission, or all-cause death), and discharge, whichever came first. Using this data, we were able to calculate the incidence of primary outcomes per 1,000 person-days. This allowed for a quantitative analysis of the rate of disease progression and treatment outcomes.

Statistical analyses

This study employed a propensity score matching (PSM) approach, which incorporated several key covariates including age, sex, time from symptom onset to treatment initiation and COVID-19 severity, to achieve accurate matching. A non-release matching strategy with a caliper width of 0.2 was used. Covariate balance between groups before and after matching was assessed by calculating the Standardized Mean Difference (SMD). Covariates were considered unbalanced if the SMD value exceeded 0.1 (Austin, 2009). Furthermore, we estimated the Hazard Ratio (HR) and 95% confidence intervals (CI) for disease progression outcomes between the two groups using multifactor Cox regression models. To ensure the stability of the results across subgroups, we conducted subgroup analyses on various levels of the aforementioned covariates. Continuous variables were described as the means and standard deviations or medians and interquartile ranges (IQR) values. Categorical variables were expressed as the counts and percentages. Independent group *t* tests were applied to continuous variables that were normally distributed; otherwise, the Mann-Whitney test was used. Categorical variables were compared using the chi-square tests, while the Fisher exact test was used when the data were limited. All statistical analyses were performed using Windrush software v1.9, employing two-tailed tests with a significance level of 0.05.

Results

Patients' demographics and clinical characteristics

We matched some important baseline characteristics such as age, gender, time from symptom onset to treatment exposure, illness severity, and concomitant treatments initiated on admission between two groups patients. After 1:1 propensity score matching, we finally included and identified 132 Azvudine recipients and 132 controls. Table 1 displayed the baseline characteristics of two groups patients before and after matching. The SMD value of each of matching baseline characteristics between two groups patients was less than 0.1, indicating a better balance between them. In addition, we examined a number of comorbidities and pathophysiological indicators related to disease progression, and the results showed that no statistically significant differences were observed between two groups patients for any of these parameters. Based on these data, we concluded that these potential confounding variables did not significantly affect the study results and conclusions.

Associations between Azvudine treatment and clinical outcomes

The proportion of patients who did not receive oxygen therapy in the Azvudine medication group and the control group was respectively 62.1% (82/132) and 58.3% (77/132), with no statistical differences (P=0.615). We compared the oxygen saturation situations of two groups patients and found that the patients treated with Azvudine overall possessed a higher oxygen saturation performance than the patients with standard treatment within 12 days after starting treatment (Figure 2). The oxygen saturation curve of Azvudine group patients showed a gradually increasing trend during hospitalization, while the oxygen saturation curve of controls showed a fluctuating downward and then upward trend. The oxygen saturation of Azvudine recipients was especially and significantly better within 6-12 days after treatment than controls, indicating a potential and quick improvement in respiratory function. These findings suggest that Azvudine may have a positive impact on the respiratory status and function of COVID-19 patients.

We found that the patients treated with Azvudine plus standard scheme had a significantly lower incidence of compound disease progression compared to the control group patients only receiving standard treatment (*P*=0.021, Figure 3A). The incidence rate of adverse outcome events in the Azvudine group was 13.9075/1000 person-days, while in the control group it was 25.7731/1000 person-days. Additionally, the mortality rate was significantly lower in the Azvudine group than that in the control group, with rates of 2.6797/1000 person-days and 8.5910/1000 person-days, respectively (*P*=0.0072, Figure 3B).

The Cox proportional hazard model was used to further assess the association between Azvudine treatment and composite metrics of disease progression and separate all-cause death (Table 2). The results indicated that Azvudine treatment significantly reduced the risk of all-cause mortality (HR: 0.28, 95% CI: 0.11-0.75, *P*=0.011) and compound disease progression (HR: 0.44, 95% CI: 0.22-0.90, *P*=0.024), after adjusting for age, sex, and severity of COVID-19 (HR: 0.32, 95% CI: 0.12-0.86, *P*=0.024 and HR: 0.46, 95% CI: 0.23-0.94, *P*=0.033; respectively), or additionally adjusting for complications, concomitant therapy, and time from symptoms to treatment (HR: 0.32, 95% CI: 0.12-0.88, *P*=0.028 and HR: 0.45, 95% CI: 0.21-0.93, *P*=0.032; respectively), or further additionally adjusting for interleukin-6, procalcitonin, lymphocyte count, and D-dimer (HR: 0.25, 95% CI: 0.08-0.81, *P*=0.021 and HR: 0.37, 95% CI: 0.16-0.84, *P*=0.017; respectively). In addition, the subgroup analyses showed that use of Azvudine was significantly associated with a reduced risk of all-cause death (Figure 4A) and composite disease progression (Figure 4B) in almost all subgroups of key variables except for pulmonary complications. This result was

10.3389/fcimb.2024.1453234

TABLE 1 Baseline characteristics before and after 1:1 propensity score matching.

Baseline characteristics	Before matching			After 1:1 propensity-score matching		
	Azvudine (n = 132)	Controls (n = 363)	SMD/P	Azvudine (n = 132)	Matched controls (n = 132)	SMD/P
Age (years), mean (SD)	71.23 (13.72)	70.95 (14.85)	SMD=0.019	71.23 (13.72)	71.45 (16.03)	SMD=0.015
Gender, n (%)			SMD=0.025			SMD<0.001
Male	87 (65.9)	235 (64.7)		87 (65.9)	87 (65.9)	
Female	45 (34.1)	128 (35.3)		45 (34.1)	45 (34.1)	
Time from symptoms onset to treatment exposure, n (%)			SMD=0.122			SMD=0.017
>5 days	94 (71.2)	238 (65.6)		94 (71.2)	93 (70.5)	
0–5 days	38 (28.8)	125 (34.4)		38 (28.8)	39 (29.5)	
Severity on admission, n (%)			SMD=0.059			SMD=0.068
Severe	35 (26.5)	87 (24.0)		35 (26.5)	39 (29.5)	
Non-severe	97 (73.5)	276 (76)		97 (73.5)	93 (70.5)	
Standard treatments, n (%)						
Supportive treatments	130 (98.4)	361 (99.4)	P =0.623	130 (98.4)	131 (99.2)	P >0.99
Symptomatic treatments	125 (94.6)	273 (75.2)	P <0.05	125 (94.6)	129 (97.7)	P =0.333
Immunotherapy treatments	122 (92.4)	268 (73.8)	P <0.05	122 (92.4)	125 (94.6)	P =0.616
Anti-infective treatments	118 (89.4)	308 (84.8)	P =0.252	118 (89.4)	115 (87.1)	P =0.702
Pulmonary complications, n (%)	49 (37.1)	137 (37.7)	P =0.888	49 (37.1)	60 (45.5)	P =0.950
Liver comorbidities, n (%)	17 (12.8)	68 (18.7)	P =0.206	17 (12.8)	25 (18.9)	P =0.136
Renal complications, n (%)	19 (14.3)	73 (20.1)	P =0.146	19 (14.3)	31 (23.4)	P =0.159
Diabetes, n (%)	37 (28.0)	118 (32.5)	P =0.458	37 (28.0)	48 (36.3)	P =0.370
Hypertension, n (%)	64 (48.5)	172 (47.3)	P =0.844	64 (48.5)	64 (48.5)	P =0.769
Lymphocyte count,10^9/L, median (IQR)	0.8 (0.5,1.2)	0.9 (0.6,1.3)	P =0.724	0.8 (0.5, 1.2)	0.9 (0.5, 1.2)	P =0.101
Procalcitonin, ng/ml, median (IQR)	0.1 (0.0,0.3)	0.1 (0.1,0.4)	P =0.803	0.1 (0.0, 0.3)	0.2 (0.1, 0.4)	P =0.359
interleukin-6, pg/ml, median (IQR)	25.2 (6.9,57.1)	25.6 (8.4,74.6)	P =0.141	25.2 (6.9, 57.1)	28.6 (8.7, 100.0)	P =0.302
D-Dimer, μg/ml, median (IQR)	0.3 (0.2,0.6)	0.3 (0.2,0.8)	P =0.365	0.3 (0.2, 0.6)	0.4 (0.2, 0.7)	P =0.536

SMD, Standard Mean Difference; SD, Standard Deviation; IQR, Interquartile Range.

highly consistent among the subgroups. It was also observed that Azvudine had a more pronounced therapeutic effect on patients with following characteristics such as male, severe, time from onset to treatment more than 5 days, combined hypertension, and taking accompanying treatment including systemic steroid, immunomodulators and antibiotics.

Discussion

The research on Azvudine's effectiveness in treating COVID-19 has yielded promising initial results, as demonstrated by some key studies in this field. A notable study by Ren et al. utilized a randomized, open-label, controlled trial design and showed that Azvudine significantly accelerates the transition to a nucleic acid-negative state in patients with mild to moderate COVID-19 and is demonstrated to be a significant advancement in therapeutic options in comparison to standard antiviral treatments (Ren et al., 2020). A randomized clinical trial corroborated these findings and showed that Azvudine can not only reduce the time to nucleic acid-negative conversion but also effectively decreases viral load and facilitates more rapid viral clearance comparing with a placebo group (da Silva et al., 2023). However, the promising results' scope and applicability are somewhat limited by the small sample sizes used in these studies. It is important to note that the past investigations primarily focus on the timing of nucleic acid conversion, which is an important metric but does not encompass all aspects of the impact of COVID-19. These limitations raise

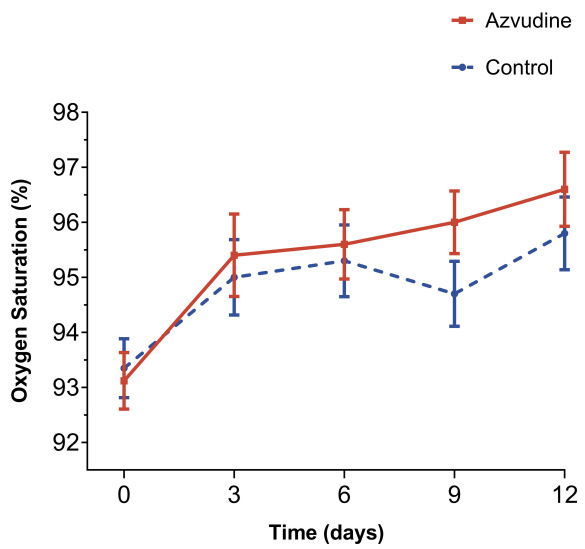

FIGURE 2
Oxygen saturation levels of Azvudine recipients and controls during hospitalization treatment. The Oxygen saturation levels of patients received standard treatment and Azvudine plus standard treatment on the 0, 3, 6, 9, and 12 days after admission for treatment were shown and compared. Day 0 (baseline) represents the first day of admission to hospital.

questions about the generalizability and reliability of the observed outcomes, which underscores the need for further research involving larger cohorts to validate these preliminary findings.

Our study conducted a comprehensive examination of Azvudine's clinical efficacy in treating hospitalized COVID-19 patients. We analyzed the impact of Azvudine on critical outcome events such as non-invasive respiratory support, invasive respiratory support, ICU admissions, and all-cause death, in addition to nucleic acid conversion times. We defined non-invasive respiratory support, invasive respiratory support, ICU admission, and death as composite disease progression outcomes. The results indicated that Azvudine significantly reduced the risk of composite disease progression outcomes and all-cause death in hospitalized patients with COVID-19. The effectiveness of Azvudine was further confirmed by adjusting several potential factors such as age, sex, disease severity, complications, concomitant therapy, time from symptoms to treatment, and some laboratory indicators. The results of subgroup analysis also showed that most of point estimates of HRs for baseline covariates and comorbidities fell to the left of 1, which demonstrates that Azvudine has stable and positive impacts on reducing mortality rate and slowing down disease progression. Thus, we may consider that Azvudine has a positive influence on the clinical recovery of hospitalized patients with COVID-19 on the basis of adopting the current standard COVID-19 treatment plan in China. Additionally, we found that Azvudine exhibited a more pronounced protective effect in male and critically ill patients with COVID-19. This observation is quite consistent with the conclusion from the retrospective cohort study by Yuming Sun et al. (Sun et al., 2023). The thymus gland, located in the human chest, is the major immune organ and is responsible for circulating T lymphocytes that play a crucial role in host immunity (Kellogg and Equils, 2021). One of the major blood abnormalities in severe COVID-19 is SARS-CoV-2-induced lymphopenia, indicating a compromised immune system (Rizk et al., 2020; Yang et al., 2020). In addition to its antiviral effects, Azvudine has immune-targeting properties and is unique among known RdRp inhibitors. It simultaneously inhibits SARS-

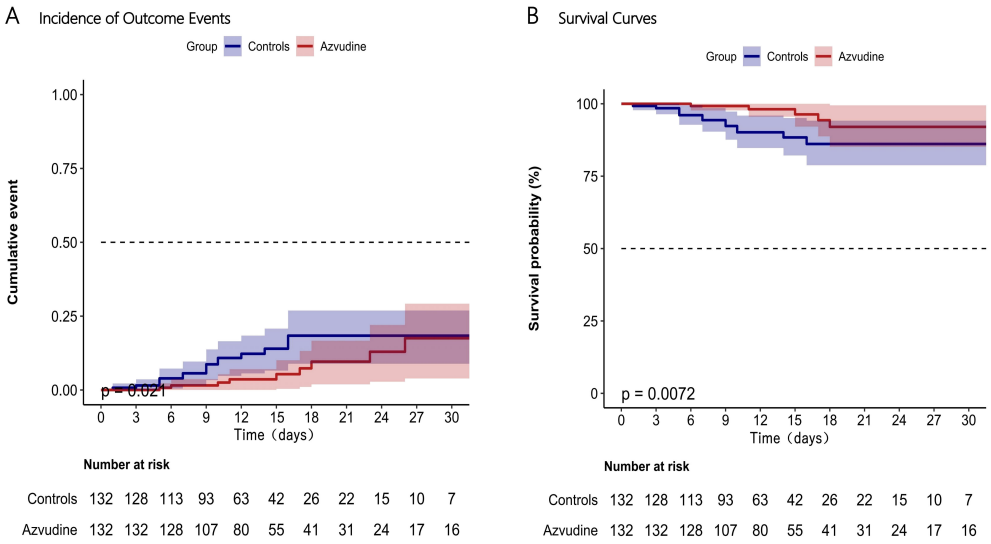

FIGURE 3
Incidence of composite disease progression outcome events **(A)** and separate all-cause death **(B)** in Azvudine recipients and controls. Day 0 (baseline) represents the first day of admission to hospital.

TABLE 2 Hazard analysis of Azvudine treatment on the all-cause death and composite disease progression outcomes.

Variable	Model 1[a]		Model 2[b]		Model 3[c]		Model 4[d]	
	HR (95% CI)	P	HR (95% CI)	P	HR (95% CI)	P	HR (95% CI)	P
All-cause death	0.28 (0.11~0.75)	0.011	0.32 (0.12~0.86)	0.024	0.32 (0.12~0.88)	0.028	0.25 (0.08~0.81)	0.021
Composite disease progression outcomes	0.44 (0.22~0.90)	0.024	0.46 (0.23~0.94)	0.033	0.45 (0.21~0.93)	0.032	0.37 (0.16~0.84)	0.017

[a]Model 1 was unadjusted.
[b]Model 2 was adjusted for age, sex, and severity of COVID-19.
[c]Model 3 was adjusted for complications (diabetes, hypertension, cardiovascular comorbidities, and other comorbidities), concomitant therapy (steroids, Immune preparations, antibiotics), and time from symptoms to treatment plus model 2.
[d]Model 4 was adjusted for interleukin-6, procalcitonin, lymphocyte count, and D-dimer plus model 3.
HR, Hazard Ratio; CI, Confidence Interval.

CoV-2 replication in the thymus and promotes host T-cell immunity against the virus, a mode of action that is considered to be a dual-phase chemo-immune antiviral therapy that may be applicable to viruses that target the immune system (Zhang et al., 2021). This might explain the strong protective efficiency of Azvudine in treating severe hospitalized patients with COVID-19 and preexisting conditions. However, the potential mechanism by which male patients with COVID-19 and benefit better from Azvudine requires further investigation. Our research presented evidence indicating that Azvudine may have a significant role in the treatment of COVID-19, particularly for critically ill patients. The insights from our study can assist healthcare professionals in refining their therapeutic strategies to meet the specific needs of severely affected individuals. Additionally, our findings reveal a noteworthy variation in the effectiveness of Azvudine based on gender. This highlights the need for further investigation into how biological differences may impact the drug's pharmacodynamics. Such research is crucial for advancing personalized medicine and ensuring that diverse patient groups receive tailored and effective treatment based on their unique physiological makeup.

The World Health Organization recommends the use of Nirmatrelvir/Ritonavir for the treatment of non-critically ill COVID-19 patients at high risk of severe illness and hospitalization, such as unvaccinated, elderly or immunosuppressed patients in its guidelines for the management of COVID-19. A number of existing studies also support the efficacy of Nirmatrelvir/Ritonavir in patients with COVID-19 (Hammond et al., 2022; Bai et al., 2024; Najjar-Debbiny et al., 2023; Reis et al., 2023; Yan et al., 2022). However, significant drug-drug interactions (DDIs) may occur when used in combination with other drugs due to the complex pharmacological mechanism of Nirmatrelvir/Ritonavir (Dresser et al., 2000). A study by Aurélie Grandvuillemin et al. showed a significant association is existed between Nirmatrelvir/Ritonavir use and the risk of drug-induced liver injury (DILI) in patients with COVID-19 (Grandvuillemin et al., 2023). Liver injury is common in COVID-19 patients (Vujčić, 2023; Yu et al., 2021). When making treatment decisions, clinicians should be aware of the potential impact on liver function, especially in patients with pre-existing liver disease. In the study by Mei-Ping Chen et al., Azvudine is the only drug to show a significant reduction in ALT and AST levels from baseline (Chen et al., 2024). Furthermore, our study also displayed that Azvudine has good therapeutic effects in the COVID-19 patients with underlying diseases.

Despite the promising outcomes, our study acknowledges several limitations that warrant caution. Firstly, this single-center cohort analysis was conducted exclusively in the General Hospital of Central Theater, and therefore the findings may not be broadly applicable. The characteristics of the specific patient demographics in this study may not be representative of the wider population encountered in various geographic locations and healthcare settings. Secondly, our research design's retrospective nature introduces additional complexities, such as the potential for selection and information biases, despite efforts to mitigate these through techniques like propensity score matching. The absence of data on critical socio-economic, lifestyle, and patient adherence factors limits our comprehensive understanding of the myriad influences on disease progression and response to treatment. Thirdly, our study did not address the long-term efficacy and safety profile of Azvudine, including potential delayed adverse effects. This is an important area for future research endeavors. Furthermore, literature such as the study by Rui Jiang et al. has highlighted concerns about the emergence of viral resistance to Azvudine, which is a challenge faced by many antiviral therapies (Jiang et al., 2023). This issue is driven by the rapid mutation capabilities of SARS-CoV-2 and selective drug pressure, emphasizing the critical need for ongoing surveillance and investigation to maintain the effectiveness of our antiviral strategies over time.

In summary, our findings contribute valuable knowledge to the battle against COVID-19 and support the potential utility of Azvudine in treating this global health threat. Since its emergence in late 2019, the SARS-CoV-2 virus has undergone significant mutations, leading to the development of several notable strains such as Alpha, Beta, Delta, and Omicron. Each of these strains exhibits distinct characteristics regarding their transmission, potential impact on disease severity, and the effectiveness of various treatment options. Our research focused specifically on the Omicron variant. However, it is important to acknowledge that the applicability of our findings to other strains may be limited due to the unique attributes of each variant. Our study provides strong support for the use of Azvudine in treating COVID-19, despite its limitations. However, further research is needed to fully understand its effectiveness against the evolving landscape of SARS-CoV-2

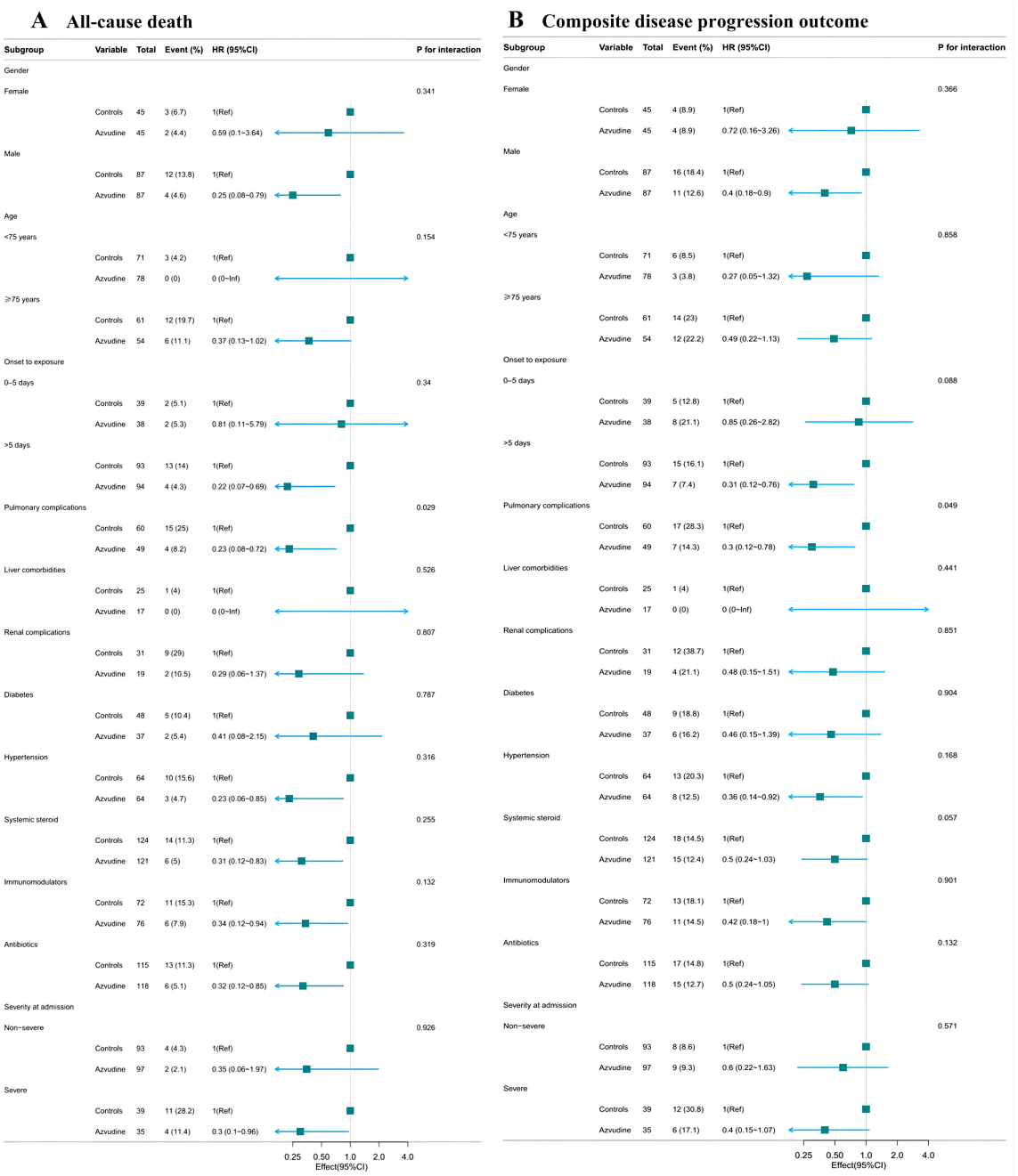

FIGURE 4
Subgroups analysis of Azvudine's effectiveness in reducing risk of all-cause death **(A)** and composite disease progression outcome events **(B)** in patients with COVID-19.

mutations. Subsequent research should aim to cover a broader geographic area, include a larger number of participants, and adopt a prospective study design to evaluate Azvudine's efficacy in diverse populations and various clinical scenarios. This approach will validate the initial promising results and contribute to refining and optimizing treatment protocols, particularly for critically ill patients. It is increasingly likely that SARS-CoV-2 will continue to circulate among humans for a considerable duration. Experts increasingly agree that COVID-19 may become endemic, meaning it will remain present in the global population. This suggests that individuals with significant risk factors may continue to be vulnerable to severe outcomes from COVID-19 infections. Therefore, it is crucial to develop more effective strategies to manage the epidemic and mitigate its public health impact. To overcome these challenges, a collaborative effort from the global scientific community is necessary. This requires emphasizing the need for collaborative research, data sharing, and innovative solutions to pave the way for more effective treatments.

Data availability statement

The data are available from the authors on reasonable request. Requests to access these datasets should be directed to LL, liulei890207@163.com.

Ethics statement

The studies involving humans were approved by Research Ethics Committee of General Hospital of Central Theater Command. The studies were conducted in accordance with the local legislation and institutional requirements. Written informed consent for participation was not required from the participants or the participants' legal guardians/next of kin in accordance with the national legislation and institutional requirements.

Author contributions

YX: Conceptualization, Data curation, Formal Analysis, Investigation, Methodology, Writing – original draft, Writing – review & editing. YH: Investigation, Methodology, Writing – original draft, Writing – review & editing. ZY: Formal Analysis, Resources, Writing – original draft, Writing – review & editing. WL: Investigation, Methodology, Writing – original draft, Writing – review & editing. LW: Formal Analysis, Funding acquisition, Supervision, Writing – original draft, Writing – review & editing. LL: Conceptualization, Data curation, Supervision, Writing – original draft, Writing – review & editing.

Funding

The author(s) declare that financial support was received for the research, authorship, and/or publication of this article. This work was supported by the Medical Youth Top Talents of Hubei Province (Eweitong [2023] 65th) and the Open Foundation of Hubei Province Key Laboratory (ZZYKF202201).

Conflict of interest

The authors declare that the research was conducted in the absence of any commercial or financial relationships that could be construed as a potential conflict of interest.

Publisher's note

References

Austin, P. C. (2009). Some methods of propensity-score matching had superior performance to others: Results of an empirical investigation and monte carlo simulations. *Biom J.* 51, 171–184. doi: 10.1002/bimj.200810488

Bai, Y., Du, Z., Wang, L., Lau, E. H. Y., Fung, I. C.-H., Holme, P., et al. (2024). Public health impact of paxlovid as treatment for covid-19, United States. *Emerging Infect. Dis. J.* 30, 262. doi: 10.3201/eid3002.230835

Chakraborty, I., and Maity, P. (2020). Covid-19 outbreak: Migration, effects on society, global environment and prevention. *Sci. Total Environ.* 728, 138882. doi: 10.1016/j.scitotenv.2020.138882

Chen, R., Guo, Y., Deng, S., Wang, J., Gao, M., Han, H., et al. (2023). All-cause mortality in moderate and severe covid-19 patients with myocardial injury receiving versus not receiving azvudine: A propensity score-matched analysis. *Cardiol. Plus* 8, 103–110. doi: 10.1097/CP9.0000000000000049

Chen, M. P., Jiang, D. X., Rang, J. X., Zhuo, H. B., and Zhou, Z. G. (2024). Comparison of azvudine, molnupiravir, and nirmatrelvir/ritonavir in adult patients with mild-to-moderate covid-19: A retrospective cohort study. *Sci. Rep.* 14, 3318. doi: 10.1038/s41598-024-53862-y

da Silva, R. M., Gebe Abreu Cabral, P., de Souza, S. B., Arruda, R. F., Cabral, S. P. F., de Assis, A., et al. (2023). Serial viral load analysis by ddpcr to evaluate fnc efficacy and safety in the treatment of mild cases of covid-19. *Front. Med. (Lausanne)* 10, 1143485. doi: 10.37247/PAMED5ED.5.23.7

Dresser, G. K., Spence, J. D., and Bailey, D. G. (2000). Pharmacokinetic-pharmacodynamic consequences and clinical relevance of cytochrome p450 3a4 inhibition. *Clin. Pharmacokinet.* 38, 41–57. doi: 10.2165/00003088-200038010-00003

Gao, Y., Luo, Z., Ren, S., Duan, Z., Han, Y., Liu, H., et al. (2023). Antiviral effect of azvudine and nirmatrelvir-ritonavir among hospitalized patients with covid-19. *J. Infect.* 86, e158–ee60. doi: 10.1016/j.jinf.2023.03.023

Grandvuillemin, A., Rocher, F., Valnet-Rabier, M. B., Drici, M. D., and Dautriche, A. (2023). Pharmacovigilance follow-up of patients in the context of the covid-19 pandemic. *Therapie* 78, 523–529. doi: 10.1016/j.therap.2023.01.004

Hammond, J., Leister-Tebbe, H., Gardner, A., Abreu, P., Bao, W., Wisemandle, W., et al. (2022). Oral nirmatrelvir for high-risk, nonhospitalized adults with covid-19. *N Engl. J. Med.* 386, 1397–1408. doi: 10.1056/NEJMoa2118542

Han, X., Han, X., Wang, Y., Wang, Z., Cui, J., Zhao, W., et al. (2023). *Effectiveness and Optimal timing of Azvudine in COVID-19 Patients: A Multi-center Retrospective Study in Beijing, China*. doi: 10.21203/rs.3.rs-3145554/v1

Jayk Bernal, A., Gomes da Silva, M. M., Musungaie, D. B., Kovalchuk, E., Gonzalez, A., Delos Reyes, V., et al. (2022). Molnupiravir for oral treatment of covid-19 in nonhospitalized patients. *N Engl. J. Med.* 386, 509–520. doi: 10.1056/NEJMoa2116044

Jiang, R., Sun, J., Zhao, B., Zhang, R., Liu, L., and Chen, J. (2023). Presence of the m184i mutation after short-term exposure to azvudine for covid-19 in people living with hiv. *AIDS* 37 (8), 1341–1342. doi: 10.1097/QAD.0000000000003564

Kellogg, C., and Equils, O. (2021). The role of the thymus in covid-19 disease severity: Implications for antibody treatment and immunization. *Hum. Vaccines Immunotherapeutics* 17, 638–643. doi: 10.1080/21645515.2020.1818519

Najjar-Debbiny, R., Gronich, N., Weber, G., Khoury, J., Amar, M., Stein, N., et al. (2023). Effectiveness of paxlovid in reducing severe coronavirus disease 2019 and mortality in high-risk patients. *Clin. Infect. Dis.* 76, e342–e3e9. doi: 10.1093/cid/ciac443

Qi, X., Yang, Y., Gong, B., Li, Z., and Liang, D. (2023). Real-world effectiveness of azvudine for patients infected with the sars-cov-2 omicron subvariant ba.5 in an intensive care unit. *J. Thorac. Dis.* 15, 4925–4937. doi: 10.21037/jtd-23-1093

Reis, S., Metzendorf, M. I., Kuehn, R., Popp, M., Gagyor, I., Kranke, P., et al. (2023). Nirmatrelvir combined with ritonavir for preventing and treating covid-19. *Cochrane Database Syst. Rev.* 11, Cd015395. doi: 10.1097/QAD.0000000000003564

Ren, Z., Luo, H., Yu, Z., Song, J., Liang, L., Wang, L., et al. (2020). A randomized, open-label, controlled clinical trial of azvudine tablets in the treatment of mild and common covid-19, a pilot study. *Adv. Sci. (Weinh)* 7, e2001435. doi: 10.1002/advs.202001435

Rizk, J. G., Kalantar-Zadeh, K., Mehra, M. R., Lavie, C. J., Rizk, Y., and Forthal, D. N. (2020). Pharmaco-immunomodulatory therapy in covid-19. *Drugs* 80, 1267–1292. doi: 10.1007/s40265-020-01367-z

Sun, Y., Jin, L., Dian, Y., Shen, M., Zeng, F., Chen, X., et al. (2023). Oral azvudine for hospitalised patients with covid-19 and pre-existing conditions: A retrospective cohort study. *EClinicalMedicine* 59, 101981. doi: 10.1016/j.eclinm.2023.101981

Vujčić, I. (2023). Outcomes of covid-19 among patients with liver disease. *World J. Gastroenterol.* 29, 815–824. doi: 10.3748/wjg.v29.i5.815

Yan, G., Zhou, J., Zhu, H., Chen, Y., Lu, Y., Zhang, T., et al. (2022). The feasibility, safety, and efficacy of paxlovid treatment in sars-cov-2-infected children aged 6-14 years: A cohort study. *Ann. Transl. Med.* 10, 619. doi: 10.21037/atm-22-2791

Yang, L., Liu, S., Liu, J., Zhang, Z., Wan, X., Huang, B., et al. (2020). Covid-19: immunopathogenesis and immunotherapeutics. *Signal Transduction Targeted Ther.* 5, 128. doi: 10.1038/s41392-020-00243-2

Yu, B., and Chang, J. (2020). Azvudine (fnc): A promising clinical candidate for covid-19 treatment. *Signal Transduct Target Ther.* 5, 236. doi: 10.1038/s41392-020-00351-z

Yu, B., and Chang, J. (2022). The first chinese oral anti-covid-19 drug azvudine launched. *Innovation (Camb)* 3, 100321. doi: 10.1016/j.xinn.2022.100321

Yu, D., Du, Q., Yan, S., Guo, X. G., He, Y., Zhu, G., et al. (2021). Liver injury in covid-19: Clinical features and treatment management. *Virol. J.* 18, 121. doi: 10.1186/s12985-021-01593-1

Zhang, J. L., Li, Y. H., Wang, L. L., Liu, H. Q., Lu, S. Y., Liu, Y., et al. (2021). Azvudine is a thymus-homing anti-sars-cov-2 drug effective in treating covid-19 patients. *Signal Transduct Target Ther.* 6, 414. doi: 10.1038/s41392-021-00835-6

Zhu, K. W. (2023). Efficacy and safety evaluation of azvudine in the prospective treatment of covid-19 based on four phase iii clinical trials. *Front. Pharmacol.* 14, 1228548. doi: 10.3389/fphar.2023.1228548

frontiers | Frontiers in Cellular and Infection Microbiology

TYPE Brief Research Report
PUBLISHED 17 February 2025
DOI 10.3389/fcimb.2025.1527573

OPEN ACCESS

EDITED BY
Chrysanthi Skevaki,
Universities of Giessen and Marburg Lung Center, Germany

REVIEWED BY
Kai Qin,
Yale University, United States
Katia Faliti,
Emory University, United States

*CORRESPONDENCE
Lourdes Arruvito
larruvito@fmed.uba.ar;
arruvitol@gmail.com

†These authors have contributed equally to this work

RECEIVED 13 November 2024
ACCEPTED 21 January 2025
PUBLISHED 17 February 2025

CITATION
Russo C, Otero A, Uranga M, Seery V, Raiden S, Algieri S, De Carli N, Borda M, Albistur MF, Heinitz L, Marcó del Pont M, Pardini M, Budano G, Alvarez L, Simaz N, Merhar C, Quintana MC, Garbini C, Portela LA, Pereira MS, Ferrero F, Geffner J and Arruvito L (2025) Immunological memory to COVID-19 vaccines in immunocompromised and immunocompetent children. *Front. Cell. Infect. Microbiol.* 15:1527573. doi: 10.3389/fcimb.2025.1527573

Immunological memory to COVID-19 vaccines in immunocompromised and immunocompetent children

Constanza Russo[1†], Adrián Otero[1†], Macarena Uranga[2], Vanesa Seery[1], Silvina Raiden[3], Silvia Algieri[4], Norberto De Carli[5], Mauricio Borda[6], María F. Albistur[2], Lourdes Heinitz[2], María Marcó del Pont[2], Martina Pardini[2], Guillermina Budano[2], Laura Alvarez[2], Nancy Simaz[4], Claudia Merhar[4], María C. Quintana[4], Cecilia Garbini[4], Luisa Aedo Portela[5], Misael Salcedo Pereira[5], Fernando Ferrero[3], Jorge Geffner[1] and Lourdes Arruvito[1*]

[1]Instituto de Investigaciones Biomédicas en Retrovirus y SIDA (INBIRS), Facultad de Medicina, UBA-CONICET, Buenos Aires, Argentina, [2]Departamento de Medicina, Hospital Universitario Austral, Buenos Aires, Argentina, [3]Departamento de Medicina, Hospital General de Niños Pedro de Elizalde, Buenos Aires, Argentina, [4]Servicio de Pediatria, Hospital Nacional Profesor Alejandro Posadas, Buenos Aires, Argentina, [5]Servicio de Pediatria, Clínica del Niño de Quilmes, Buenos Aires, Argentina, [6]Servicio de Pediatria, Hospital Pediátrico Juan Pablo II, Corrientes, Argentina

Background: Most children in Argentina received only the initial COVID-19 vaccine series, with presumed hybrid immunity after multiple Omicron waves. However, the durability of immune memory, particularly in immunocompromised (IC) children, remains poorly studied.

Methods: A cohort of IC (n=45) and healthy children (HC, n=79) was assessed between 13 to 17 months after receiving two or three doses of BBIBP-CorV and/or BNT162b2. Plasma anti-spike IgG, neutralizing activity and antigen-specific CD4+ and CD8+ T cells against Wuhan and Omicron BA.5 variants were assessed.

Results: Most children remained seropositive after two vaccine doses, but compared with HC, IC exhibited lower neutralizing titers against both Wuhan and Omicron BA.5, particularly those vaccinated with BBIBP-CorV. Even after three vaccine doses, IC showed weaker neutralizing antibody response, CD8+ T cell responses and lower IFN-γ production compared with HC. Integrated analysis of neutralizing antibodies, memory $CD4^+$, and $CD8^+$ T cells revealed a weak immune memory among IC with an important compromise in memory $CD8^+$ T cell responses.

Conclusions: Immunity can last up to 17 months, but reduced effectiveness against new variants highlights the need for updated COVID-19 vaccines, especially for IC children. Additional efforts are essential to enhance vaccination coverage and protect this vulnerable population.

KEYWORDS

children, SARS-CoV-2, variants, vaccines, antibodies, T cells

1 Introduction

Pediatric vaccination against severe acute respiratory syndrome coronavirus 2 (SARS-CoV-2) has effectively prevented Coronavirus Disease 2019 (COVID-19)-related hospitalizations (Head et al., 2024). However, our understanding of the durability of the immune memory induced by the original monovalent vaccines targeting the Wuhan-Hu-1 strain remains limited, particularly due to low and unequal booster coverage worldwide (Eccleston-Turner and Upton, 2021; Ferranna, 2024).

According to the latest data from Argentina's Nominalized Federal Vaccination Registry, as of August 4, 2023 (prior to the introduction of bivalent vaccines), 9.6 million children (73%) had received a first vaccine dose, 8 million (61%) a second dose, 2.6 million (20%) a first booster, and only 200,000 children (2%) a second booster. Since then, booster uptake among children has remained very low, with no updated official statistics available. Thus, it can be concluded that the majority of children in Argentina have not received any booster doses.

Given the emergence of the Omicron variant (Karim and Karim, 2021), which triggered multiple waves of infection, population immunity arises from both vaccination and Omicron breakthrough infections, resulting in hybrid immunity. Although most of the population is believed to have substantial immunity against SARS-CoV-2, immunocompromised patients remain at increased risk for severe outcomes (Petrelli et al., 2022; Meyerowitz et al., 2024).

There is limited information on the immune memory response to SARS-CoV-2 in immunocompromised children (IC), particularly those who received the whole-cell inactivated vaccine (BBIBP-CorV) (Peng et al., 2023) as their primary vaccine regimen a long time ago. This study analyzed humoral and cellular responses in immunocompromised children with various medical conditions, as well as in healthy children (HC), after receiving two or three doses of BBIBP-CorV and/or the mRNA vaccine BNT162b2 up to 17 months following the final vaccine dose.

2 Methods

2.1 Ethics statement

This study adhered to the Declaration of Helsinki and received IRB approval from participating institutions (Hospital General de Niños Pedro de Elizalde #8771/23 and Hospital Universitario Austral #P22-063). Parents or legal guardians from children under 8 years provided written, informed consent. Children older than 8 years old provided written, informed consent and their parents or legal guardians also provided written, informed consent. All samples were deidentified prior to processing.

Abbreviations: SARS-CoV-2, severe acute respiratory syndrome coronavirus 2; COVID-19, Coronavirus Disease 2019; IC, immunocompromised children; HC, healthy children; PBMCs, Peripheral blood mononuclear cells; PHA, Phytohemagglutinin; AIM, activation-induced markers.

2.2 Study population

This observational study was conducted at the Hospital General de Niños Pedro de Elizalde, Hospital Universitario Austral, Hospital Alejandro Posadas, Hospital Pediátrico Juan Pablo II, and Clínica del Niño de Quilmes. Two cohorts of children were enrolled, all of whom had received two or three doses of monovalent anti-SARS-CoV-2 vaccines targeting the Wuhan-Hu-1 strain. Blood samples were collected between 13 to 17 months after their last vaccine dose. The first cohort included 45 IC whose immunocompromised status was determined according to CDC criteria, including: recipients of solid organ transplants under immunosuppressive therapy; patients undergoing active cancer treatment (for tumor or blood cancers); those who had received a stem cell transplant within the past two years; children on chronic immunosuppressive therapy; and individuals with moderate to severe inborn errors of immunity (https://www.cdc.gov/covid/vaccines/immunocompromised-people.html). The second cohort included 79 HC who were vaccinated with two or three doses of COVID-19 vaccines. All children suffered SARS-CoV-2 infection between 22 and 24 months prior to obtaining blood samples. None of the participants were hospitalized or experiencing any acute active infections at the time of sampling. The characteristics of both cohorts are detailed in Table 1. Detailed clinical data of each immunocompromised children is presented in Supplementary Table 1. This study followed The Strengthening the Reporting of Observational studies in Epidemiology (STROBE) guidelines.

2.3 Blood sample processing

Approximately 0.5-1 mL of whole blood samples were obtained. After centrifugation for 10 min at 1000 rpm, plasma was separated and stored at -80°C until use. Peripheral blood mononuclear cells (PBMCs) were isolated using Ficoll-Paque gradient (Cytiva) and cryopreserved in liquid nitrogen until use.

2.4 Cells and virus

VERO C1008 (clone E6, ATCC, RRID: CVCL_0574) cells were used as described (Seery et al., 2022). Wuhan variant (GISAID ID: EPI_ISL-499083) was provided by InViV group, UNC, Argentina. Omicron BA.5 variant (GISAID ID: EPI_ISL-16297058) was provided by IIB group, UNSAM, Argentina.

2.5 Quantitation of plasma SARS-CoV-2–specific IgG antibodies

IgG antibodies to the SARS-CoV-2 spike protein were detected using an ELISA kit (COVIDAR, Lemos lab). Anti-spike IgG antibody titers were determined by endpoint titration, defined as the reciprocal of the highest dilution of serum that gives a reading above the cut-off (Ojeda et al., 2021).

10.3389/fcimb.2025.1527573

TABLE 1 Characteristics of study cohorts.

	Children	
	Healthy (n=79)	Immunocompromised (n=45)
Age, years, median (range)	9 (4-16)	11 (5-17)
Female, n (%)	22 (28)	15 (33)
Medical history		
Transplant	-	9 (20)
Cancer	-	15 (33)
Inborn Innate Error	-	14 (31)
Autoimmunity	-	7 (16)
COVID-19 history, n (%)	79 (100)	45 (100)
Immunosuppressive medications, n (%)	-	32 (71)
Gammaglobuline, n (%)	-	8 (18)
Doses of vaccines at sampling, n (%)		
#2	43 (54)	23 (51)
#3	36 (46)	22 (49)
Vaccination regimen, n (%)		
BBIBP-CorV (2 doses)	34 (43)	14 (33)
BNT162b2 (2 doses)	9 (12)	9 (18)
BBIBP-CorV (3 doses)	1 (1)	0 (0)
BNT162b2 (3 doses)	16 (20)	13 (27)
BBIBP-CorV (2 doses) plus BNT162b2 (1 dose)	19 (24)	9 (22)
Months post second dose, median (range)	480 (289-684)	504 (264-711)
Months post third dose, median (range)	395 (296-545)	382 (290-602)

2.6 Neutralization assay

Neutralization assays were performed as we previously described (Seery et al., 2022). Briefly, deidentified plasma samples were heat-inactivated at 56°C for 20 min. Two-fold serial dilutions were incubated at 37°C for 1 h with Wuhan and Omicron BA.5 variants (MOI=0.01) in DMEM with 2% FBS. Fifty µL of the mixtures were added to Vero E6 cell monolayers for 1 h at 37°C in 96-well plates. After removing the infectious media, DMEM with 2% FBS was added. Cells were cultured for 72 h, fixed with 4% paraformaldehyde, and stained with crystal violet. Inhibitory concentrations of 50% (IC50) values were calculated.

2.7 Expression of activation-induced markers in T cells

The activation of antigen-specific T cells was assessed by measuring the percentage of AIM+ cells: ($OX40^+CD137^+$) for $CD4^+$ T cells and ($CD69^+CD137^+$) for $CD8^+$ T cells. Peripheral blood mononuclear cells (PBMCs) were stimulated with overlapping peptide megapools corresponding to the Wuhan and/or Omicron BA.5 sequences, provided by the Sette Lab (La Jolla Institute of Immunology, CA, USA) (Grifoni et al., 2020; Dan et al., 2021; Grifoni et al., 2021). Thawed PBMCs were rested for 2 hours at 37°C in RPMI 1640 medium (Sigma-Aldrich) supplemented with 10% heat-inactivated human AB serum, 2 mM L-glutamine, and penicillin-streptomycin (all from Sigma-Aldrich). A total of 1×10^6 cells per well were seeded in U-bottom 96-well plates and stimulated with 1 µg/mL of SARS-CoV-2 peptide megapools for 24 hours. Phytohemagglutinin (PHA, 5 µg/mL; Sigma-Aldrich) were used as a positive control, and an equimolar amount of DMSO (Sigma-Aldrich) as a negative control. Supernatants were collected at 24 hours post-stimulation for IFN-γ detection. Cells were washed and stained with Zombie NIR Live/Dead Stain and the following antibody panel: CD19 PE, CD4 BV605, CD8 FITC, CD137 BV421, CD69 AF647, and OX40 PerCP-Cy5.5 (BioLegend). Data were acquired using a Northern Lights flow cytometer and analyzed with SpectroFlo software (Cytek). T-cell data were calculated either as background-subtracted values or as a stimulation index. Background-subtracted values were obtained by subtracting the percentage of AIM+ cells following DMSO stimulation from those observed after peptide-stimulation. Stimulation index was calculated as the ratio between the percentage of AIM+ cells after stimulation with SARS-CoV-2 peptides and the percentage of AIM+ cells cultures without stimulating peptides. An index >2 fold change was considered positive.

2.8 Measurement of IFN-γ by ELISA

It was performed in cell supernatants following manufacturer´s instructions (BD Biosciences).

2.9 Statistics

Clinical characteristics were summarized using descriptive statistics. Categorical variables are reported as numbers and percentages. Quantitative variables are reported as medians and interquartile ranges and presented as medians and minimum to maximum in the figures. Two groups were compared using the Mann-Whitney U test. Two groups' proportions were compared using the Chi-square test and Fisher exact test. Data were calculated using GraphPad Prism V.9. A p-value <0.05 was considered statistically significant.

3 Results

3.1 Vaccinated immunocompromised children exhibit lower levels of neutralizing antibodies against SARS-CoV-2 compared with healthy children

We analyzed serum antibody levels against SARS-CoV-2 in IC and HC following vaccination with two doses of either BBIBP-CorV or BNT162b2 vaccines. Blood samples were collected 13 to 17 months post-vaccination. Detailed participant information is provided in Table 1; Supplementary Table 1. Titers of anti-SARS-CoV-2 IgG and neutralizing antibodies across the study cohorts are shown in Supplementary Table 2. Four children receiving EV gammaglobulin were excluded from this analysis. Results showed that IC (n=19) had significantly lower IgG titers against the SARS-CoV-2 spike protein compared to HC (n=43, $p<0.05$; Figure 1A). Most children in both groups exhibited neutralizing antibodies against both, Wuhan and Omicron BA.5 variants long time after vaccination. However, IC demonstrated lower seropositivity for the Omicron BA.5 variant (84%, 16/19) compared to HC (100%, 43/43; $p<0.01$, Figure 1B left). Neutralizing antibody titers against SARS-CoV-2 were significantly reduced in IC for both variants ($p<0.05$, Figure 1B right). When comparing vaccine types, IC receiving BBIBP-CorV had lower neutralizing antibody levels for both variants than HC ($p<0.01$ for both Wuhan and Omicron BA.5). No significant differences were found between IC and HC who received the BNT162b2 vaccine (Figure 1C).

The lower antibody response in IC was also observed after three vaccine doses. Four children receiving EV gammaglobulin were excluded from this analysis. IC (n=18) had lower anti-SARS-CoV-2 IgG titers compared to HC (n=36, $p<0.05$; Figure 1D). Seropositivity for Omicron BA.5 was lower in IC (83%, 15/18) compared to HC (100%, 40/40; $p<0.01$, Figure 1E left). Neutralizing titers in IC were significantly decreased for both variants ($p<0.05$ for Wuhan and $p<0.01$ for Omicron BA.5; Figure 1E right). When analyzing vaccine regimens, a lower response in IC was observed overall ($p<0.05$), except for neutralizing antibodies against Omicron BA.5 in those receiving two doses of BBIBP-CorV followed by a third dose of BNT162b2, where no differences were found between IC and HC (Figure 1F). When grouping immunocompromised children based on their underlying conditions, among those vaccinated with two doses, 8 had cancer, 4 had undergone transplantation, 2 had autoimmunity and 9 had IIE. In the cohort receiving three doses, 7 had cancer, 5 had autoimmune diseases, 5 had undergone transplantation, and 5 had IIE. For the analysis, only subgroups with a minimum of three children were included, and those children receiving EV gammaglobulin were excluded. As shown in Supplementary Figure S1, we observed a lower neutralizing antibody response in IC compared to HC across all subgroups. However, statistically significant differences were only found between HC and the transplanted subgroup ($p<0.05$ for Wuhan and Omicron BA.5; $p<0.01$ for Omicron BA.5 in the two- and three-dose groups, respectively). Finally, as expected, we found a significant reduction in neutralizing titers against the Omicron variant compared to the Wuhan variant by analyzing paired samples in both HC ($p< 0.0001$ for Wuhan vs. Omicron BA.5 after 2 and 3 doses) and IC groups ($p< 0.01$ and $p< 0.001$ for Wuhan vs. Omicron BA.5 after 2 and 3 doses, respectively; Supplementary Figures S2A, B).

3.2 Vaccinated immunocompromised children display a decreased CD8+T cell memory response compared with healthy children

The memory response to SARS-CoV-2, mediated by either CD4+ and CD8+ T cells, was analyzed by flow cytometry following overnight stimulation of PBMCs with peptide megapools derived from the Wuhan and Omicron BA.5 variants. These peptide pools specifically stimulated CD4+ and CD8+ T cells. The gating strategy used for analysis is illustrated in Figure 2A. Approximately 50% of IC and HC showed a significant CD4+ T cell response to both variants after receiving two vaccine doses, while less than 20% displayed a significant CD8+ T cell response (IC, n=16 and n=20, HC, n=17 and n=26 for Wuhan and Omicron BA.5 response respectively; Figure 2B left). To quantify this response, we calculated the fold change in CD4+ and CD8+ T cell activity as the ratio of positive T cells for stimulated and unstimulated cells for each donor. No significant differences in this stimulation index were found between the HC and IC groups for either CD4+ or CD8+ T cells (Figure 2B right). A similar analysis was performed in children who received three vaccine doses. Over 40% of children in both cohorts showed a positive CD4+ T cell response to Wuhan and Omicron BA.5 variants, with no significant differences between the cohorts. For CD8+ T cells, IC had a lower response than HC, but a significant difference ($p<0.05$) was only observed in response to Omicron BA.5-derived peptides (IC, n=8 and n=22, HC, n=16 and n=21 for Wuhan and Omicron BA.5 respectively; Figure 2C left). Consistent with these findings, the CD4+ T cell stimulation index was similar across cohorts, while CD8+ T cells in IC showed a lower response to Wuhan and Omicron BA.5 peptides ($p<0.05$; Figure 2C right). Similar conclusions were obtained using DMSO-subtracted values as metrics for both specific CD4+ and CD8+ T cell response following two or three vaccine doses (Supplementary Figure S3).

Moreover, we observed a comparable T cell memory response against both the Wuhan and Omicron BA.5 variants in both HC and IC (Supplementary Figures S2C, D). We finally analyzed IFN-γ levels in supernatants of PBMCs from children who received two or three vaccine doses, stimulated with Wuhan and BA.5 peptides for 24 hours. In all cases, IFN-γ levels were lower in PBMCs from IC compared to HC ($p<0.001$ and $p<0.01$ for two doses against Wuhan and Omicron BA.5; $p<0.05$ for three doses against both variants; Figure 2D).

3.3 Integrated analysis of memory B and T cell responses

It was valuable to explore different relationships between the B and T memory compartments and analyze combinations of positive or negative responses by reexamining the data of neutralizing

10.3389/fcimb.2025.1527573

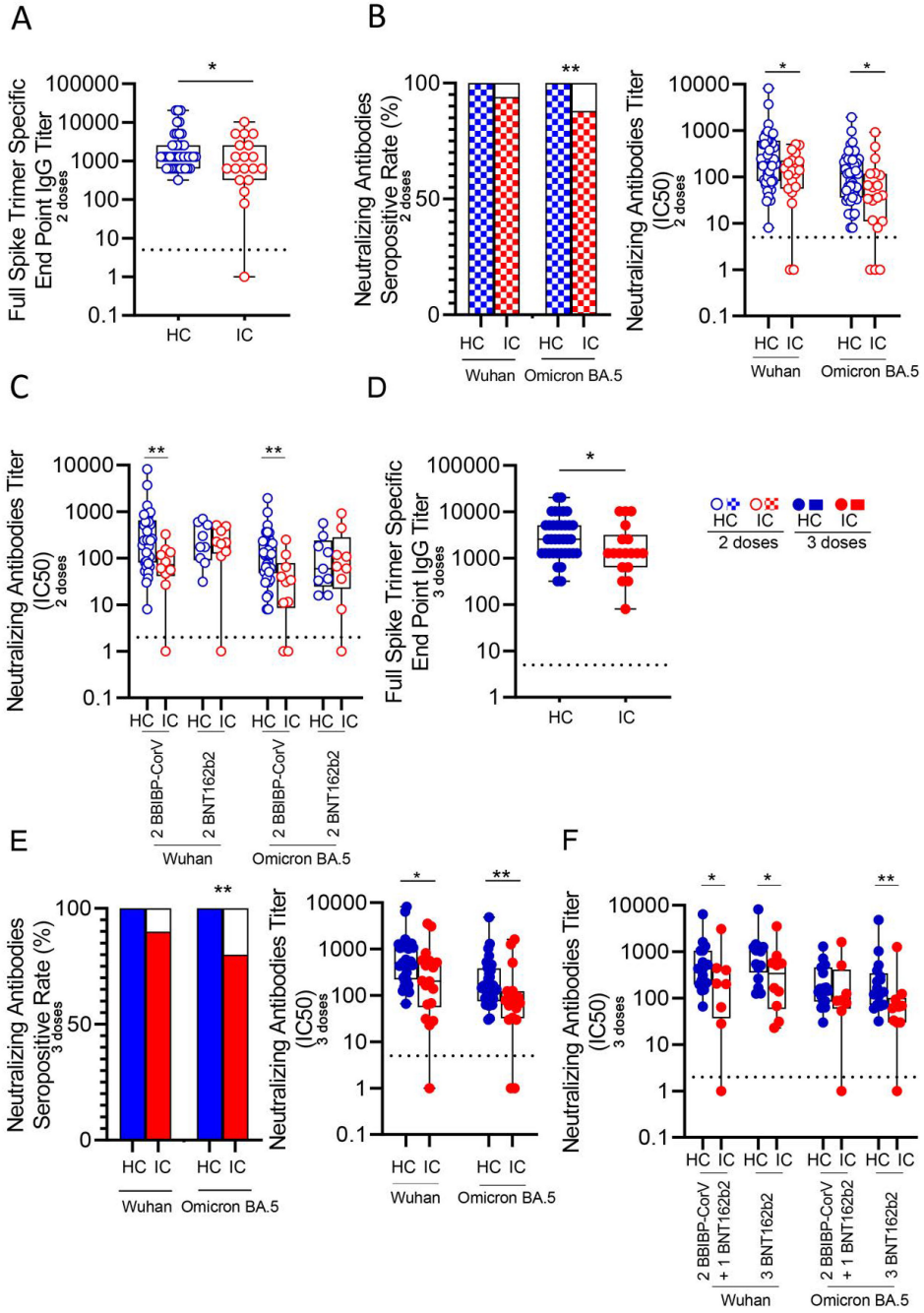

FIGURE 1
Antibody response against Wuhan and Omicron BA.5 variants in vaccinated IC and HC. **(A)** Titers of IgG anti-spike antibodies defined by end point dilution in plasma from IC (n=19) and HC (n=43) receiving two-doses of COVID-19 vaccines. **(B)** Neutralizing activity against Wuhan and Omicron BA.5 variants in plasma from IC and HC receiving two-doses of COVID-19 vaccines. Left: Bars show the percentage of positive samples for neutralizing activity. Right: Neutralization antibody titers determined by the reciprocal IC50. **(C)** Neutralizing activity against Wuhan and Omicron BA.5 variants in plasma from children receiving two-doses of BBIBP-CorV (IC, n=10 and HC, n=34) or BNT162b2 (IC, n=9 and HC, n=9) vaccines. **(D)** Titers of IgG anti-spike antibodies defined by end point dilution in plasma from IC (n=18) and HC (n=36) receiving three-doses of COVID-19 vaccines. **(E)** Neutralizing activity against Wuhan and Omicron BA.5 variants in plasma from IC and HC receiving three-doses of COVID-19 vaccines. Left: Bars show the percentage of positive samples for neutralizing activity. Right: Neutralization antibody titers determined by the reciprocal IC50. **(F)** Neutralizing activity against Wuhan and Omicron BA.5 variants in plasma from children receiving three-doses of COVID-19 vaccines: 2 doses BBIBP-CorV plus 1 dose BNT162b2 (IC, n=8 and HC, n=19) or 3 doses of BNT162b2 (IC, n=10 and HC, n=17). Dotted line indicates the limit of detection value. Median and min to max of n donors are shown in **(A, B)** right, **(C–E)** right and **(F)** P values were determined by Pearson's Chi square test (B left and E left) and Mann-Whitney U test **(A, B)** right, **(C–E)** right and **(F)**. *p<0.05, **p<0.01. HC (blue circle), IC (red circle), two-doses (open circle), three-doses (filled circle), negative (white square), positive two-doses (dotted square), positive three-doses (filled square).

10.3389/fcimb.2025.1527573

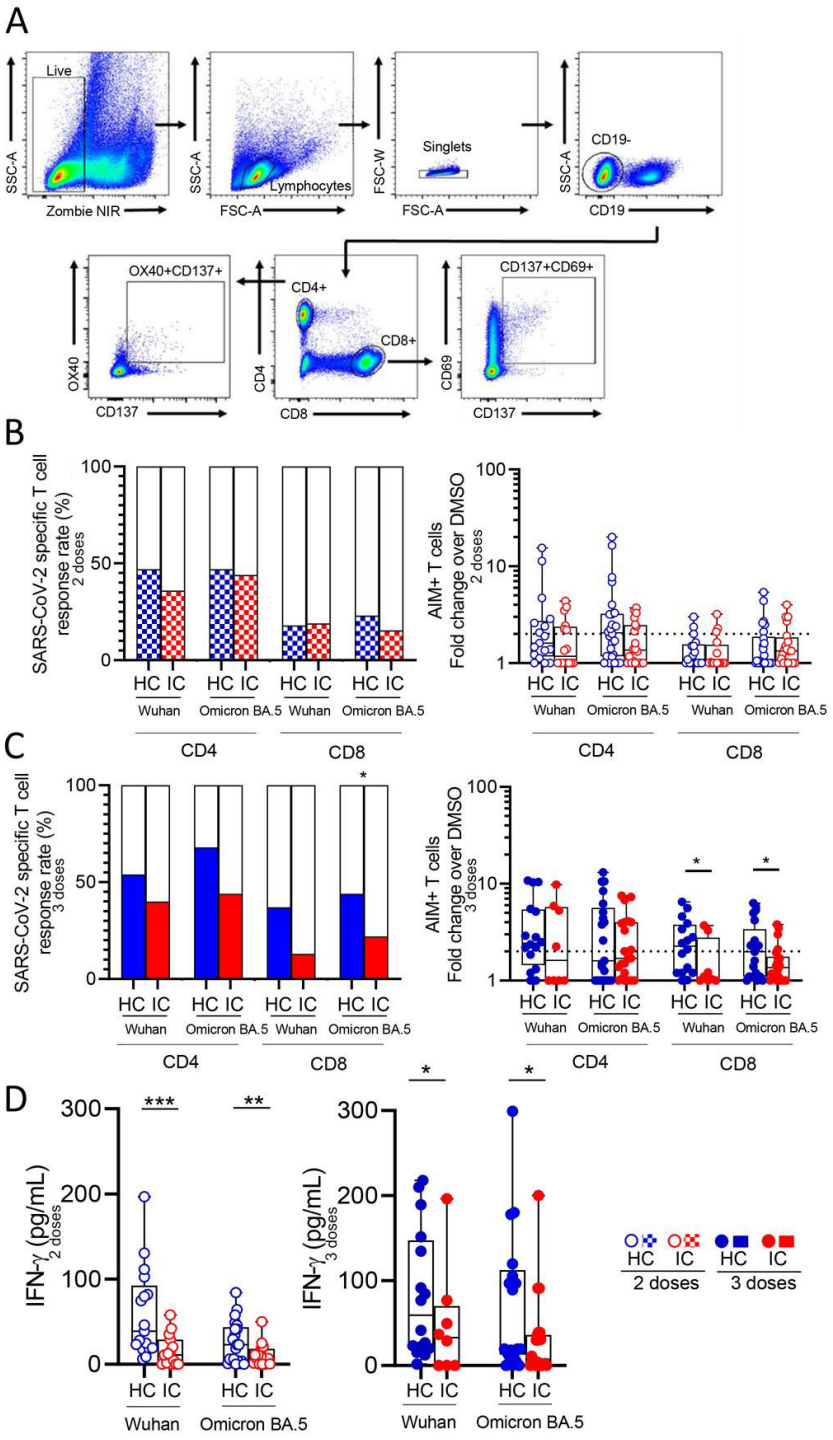

FIGURE 2
SARS-CoV-2 specific T cell response in vaccinated IC and HC. Antigen-specific T cells were measured as a percentage of CD4+OX40+CD137+ and CD8+CD69+CD137+ T cells after stimulation of PBMCs from children receiving two or three doses of COVID-19 vaccines with CD4_S and CD8_S peptide megapools of Wuhan and Omicron BA.5 compared to negative control (DMSO) analyzed by flow cytometry. **(A)** Gating strategies to define SARS-CoV-2-specific CD4+ and CD8+ T cells by flow cytometry. **(B)** Left: Bars show the percentage of IC and HC vaccinated with 2 doses that presented circulating specific CD4+ and CD8+ T cell response against Wuhan (IC, n=16 and HC, n=17) and Omicron BA.5 (IC, n=20 and HC, n=26). Right: Stimulation index quantitation of AIM+ T cells (fold change over the DMSO condition). **(C)** Left: Bars show the percentage of IC and HC vaccinated with 3 doses that presented circulating specific CD4+ and CD8+ T cell response against Wuhan (IC, n=8 and HC, n=16) and Omicron BA.5 (IC, n=22 and HC, n=21). Right: Stimulation index quantitation of AIM+ T cells (fold change over the DMSO condition). **(D)** Levels of IFN-γ in the supernatant culture of PBMCs from IC and HC stimulated with peptide megapools of Wuhan and Omicron BA.5 determined by ELISA. Dotted line indicates the fold change ≥ 2. Median and min to max of n donors are shown in **(B)** right, **(C)** right and **(D)** P values were determined by Pearson's Chi square test **(B)** left and **(C)** left] and Mann-Whitney U test **(B)** right, **(C)** right and **(D)**]. *p<0.05, **p<0.01, ***p<0.01. HC (blue circle), IC (red circle), two-doses (open circle), three-doses (filled circle), negative (white square), positive two-doses (dotted square), positive three-doses (filled square).

antibodies against the Wuhan and/or Omicron BA.5 variants ("N"), as well as antigen-specific $CD4^+$ ("4") and $CD8^+$ ("8") T cell responses targeting the Spike protein variants. This analysis was conducted exclusively in children who received three doses of the vaccine, and only in those children for whom both antibody memory and T cell memory could be assessed.

In the HC group (n=25), all children exhibited an immune response: 40% were positive across all three immune compartments, 28% had neutralizing antibodies along with either a CD4+ or CD8+ T cell response, and the remaining 32% showed only neutralizing antibodies. Although all IC (n=18) children also exhibited some kind of immune response, the pattern was different. While most of children had only neutralizing antibodies (61%), 17% of them were positive across all three immune compartments, 11% had neutralizing antibodies along with CD4+ T cell response, and the remaining 11% had only positive CD4+ T cell response. Comparison of children with positive responses in more than one of the parameters analyzed (antibodies, CD4+ T cell response and CD8+ T cell response) revealed that the IC group had a more restricted response than the HC group ($p < 0.01$, Figure 3).

4 Discussion

Vaccination has played a crucial role in addressing the pandemic (Watson et al., 2022), with memory B and T cell responses being key contributors to long-term protection (Sette and Crotty, 2021). During the Omicron period, two or more doses of the original monovalent COVID-19 vaccine prevented hospitalizations in children aged 5–18 (Price et al., 2022). However, optimal immunity requires a fully functional immune system, which IC often lack. Treatments such as B-cell depletion therapies, high-dose glucocorticoids, tacrolimus and mycophenolate mofetil among others, weaken the response to vaccines (Deepak et al., 2021; Friedman et al., 2021; Lee et al., 2022). This highlights the importance of booster doses, especially for immunocompromised individuals. However, the administration of boosters has significantly decreased both in Argentina and worldwide (Lazarus et al., 2023), and this decrease includes IC patients (Zheng et al., 2023). It's concerning that few studies have examined how the memory immune response against SARS-CoV-2 lasts over time in IC.

For instance, children with pediatric inflammatory bowel disease showed an antibody response to monovalent mRNA vaccines similar to HC. However, those on anti-TNF-α therapy, but not Infliximab or Adalimumab, had a weaker response (Cotugno et al., 2022). A study lacking a HC cohort found that most children with solid organ transplants, stem cell transplants, and rheumatologic diseases had detectable antibody and T cell responses after the second dose of mRNA vaccines, which improved after the third dose. Notably, while all children showed a CD4+ T cell response after the third dose, only 44% had a CD8+ T cell response (Morgans et al., 2023). Additionally, marked differences in immune responses were observed between liver transplant and IgA nephropathy patients following a standard two-dose mRNA regimen being these differences only partially explained by the different immunosuppressive treatments used (Lu et al., 2023). Two additional studies also reported substantial differences in the immune response induced by mRNA vaccines in IC according the underlying condition or treatment, being kidney transplant recipients who showed a significant reduction in both, the humoral and cellular response (Haskin et al., 2021; Lalia et al., 2023). Furthermore, a recent study found that while children with different immunocompromising conditions developed immune responses comparable to healthy children, solid organ transplant recipients had lower levels of neutralizing antibodies and reduced frequencies of Tregs and Bregs six months post-mRNA vaccination (Di Chiara et al., 2024). Data on inactivated COVID-19 vaccines in immunocompromised children are limited. One study reported that administering inactivated vaccines followed by an Ad5-nCoV booster in pediatric liver transplant recipients elicited a strong humoral response but a weak T-cell response (Zheng et al., 2024).

While previous studies primarily examined the short-term B and T cell responses to SARS-CoV-2 vaccination, we focused on the durability of the memory response 13 to 17 months post-vaccination. In our cohorts, we observed that IC who received two vaccine doses of BBIBP-CorV showed a lower neutralizing

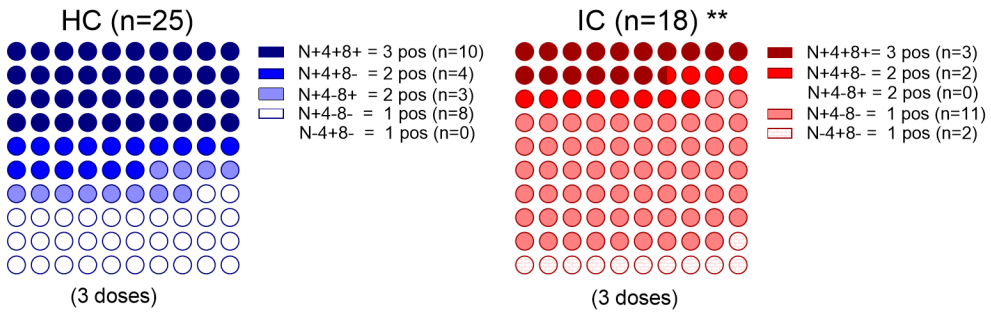

FIGURE 3
Immune memory components relationship. Percentage dot plots showing frequencies (normalized to 100%) of IC (n=18) and HC (n=25) participants who received 3 doses with indicated immune memory components evaluated. Comparison of positive responses in more than one of the parameters analyzed (antibodies, CD4+ T cell response and CD8+ T cell response) is shown. **p<0.01. Pearson's Chi square test. HC has no cases in the category N-4+8- and IC has no cases in the category N+4-8+. N, neutralizing antibodies, 4, SARS-CoV-2–specific CD4+ T cells; 8, SARS-CoV-2–specific CD8+ T cells. P values were determined by Pearson's Chi square test, **p<0.01.

antibody response against both Wuhan and Omicron BA.5 variants, compare with HC. The lower immunogenicity of the inactivated BBIBP-CorV vaccine may explain this observation. Even with three doses, IC had lower neutralizing antibody levels against both variants compared to HC. As expected, we found that the titers of neutralizing antibodies against Omicron were lower than those directed against the Wuhan variant, both in HC and IC.

When examining the T cell response, our findings revealed three key observations. First, fewer than 25% of children in both cohorts exhibited a specific CD8+ T cell response after two doses, with IC showing a more pronounced reduction after three doses compared to HC. Second, and consistent with previous observations (Tarke et al., 2022),we observed that first-generation COVID-19 vaccines induced a similar T-cell response against both, Omicron and Wuhan variants, in both cohorts. Third, IC showed a decreased production of IFN-γ by stimulated PBMCs, reinforcing the notion of a suboptimal T cell memory response. This is consistent with Rosnik et al, which demonstrated a skewed T cell response in IC patients, favoring IL-2 and TNF-α production over IFN-γ, even after receiving updated vaccines (Roznik et al., 2024). Finally, by analyzing the two compartments of the adaptive immune response in an integrated manner, we observed that while there is a decreased proportion of immune memory components in the IC group, our findings also underscore the heterogeneity of immune memory, revealing distinct patterns among different individuals.

This study has several limitations. The small sample size of the IC cohort means that our observations, particularly those related to the stratification of patients into different subgroups based on their underlying pathology and/or treatment regimens, should be validated in a study with a larger cohort. We were unable to conduct a longitudinal analysis of the immune response over time in our cohorts, as we did not have successive samples from each child at baseline and after the second and third vaccine doses. We also could not perform assays to analyze T cell responses using seasonal coronavirus antigens as control stimuli. Furthermore, all participants received monovalent vaccines rather than the bivalent vaccines targeting the predominant Omicron variants.

Given the ongoing threat of COVID-19 and other respiratory viruses, updated vaccines and boosters are critical to preventing severe disease, especially for children with immunocompromising conditions as well as in developing regions where booster coverage remains low and unevenly distributed. Ensuring access to boosters in these areas is essential to mitigating health disparities and controlling viral spread post-pandemic.

Data availability statement

The raw data supporting the conclusions of this article will be made available by the authors, without undue reservation.

Ethics statement

The studies involving humans were approved by Hospital General de Niños Pedro de Elizalde #8771/23 and Hospital Universitario Austral #P22-063. The studies were conducted in accordance with the local legislation and institutional requirements. Written informed consent for participation in this study was provided by the participants' legal guardians/next of kin.

Author contributions

CR: Formal analysis, Methodology, Writing – original draft. AO: Formal analysis, Methodology, Writing – original draft. MU: Conceptualization, Data curation, Writing – review & editing. VS: Formal analysis, Methodology, Writing – original draft. SR: Conceptualization, Data curation, Writing – review & editing. SA: Investigation, Supervision, Writing – review & editing. ND: Investigation, Writing – review & editing. MB: Investigation, Writing – review & editing. MA: Investigation, Writing – review & editing. LH: Investigation, Writing – review & editing. MM: Investigation, Writing – review & editing. MP: Investigation, Writing – review & editing. GB: Investigation, Writing – review & editing. LAL: Investigation, Writing – review & editing. NS: Investigation, Writing – review & editing. CM: Conceptualization, Data curation, Writing – review & editing. MQ: Investigation, Writing – review & editing. CG: Conceptualization, Data curation, Writing – review & editing. LP: Investigation, Writing – review & editing. MP: Investigation, Writing – review & editing. FF: Conceptualization, Data curation, Writing – review & editing. JG: Investigation, Writing – original draft, Conceptualization, Funding acquisition. LAR: Conceptualization, Funding acquisition, Investigation, Writing – original draft.

Funding

The author(s) declare financial support was received for the research, authorship, and/or publication of this article. This work was supported by grants from the National Agency for Promotion of Science and Technology, Argentina (PICTO-2021-0007 and PICT-2020-0261 to LA; PICT-2021-I-A-01186 to JG).

Acknowledgments

We sincerely thanks to the physicians and nurses for their contribution. Most of all, we are indebted to all the participating children and their families. We are grateful to the Dr Alessandro Sette lab for providing the SARS-CoV-2 megapools peptides and for their guidance in AIM T cell assays.

Conflict of interest

The authors declare that the research was conducted in the absence of any commercial or financial relationships that could be constructed as a potential conflict of interest.

Generative AI statement

The author(s) declare that no Generative AI was used in the creation of this manuscript.

Publisher's note

Supplementary material

The Supplementary Material for this article can be found online at: https://www.frontiersin.org/articles/10.3389/fcimb.2025.1527573/full#supplementary-material

References

Cotugno, N., Franzese, E., Angelino, G., Amodio, D., Romeo, E. F., Rea, F., et al. (2022). Evaluation of safety and immunogenicity of bnt162b2 mrna covid-19 vaccine in ibd pediatric population with distinct immune suppressive regimens. *Vaccines (Basel)* 10 (7), 1109. doi: 10.3390/vaccines10071109

Dan, J. M., Mateus, J., Kato, Y., Hastie, K. M., Yu, E. D., Faliti, C. E., et al. (2021). Immunological Memory to Sars-Cov-2 Assessed for up to 8 Months after Infection. *Science* 371, eabf4063. doi: 10.1126/science.abf4063

Deepak, P., Kim, W., Paley, M. A., Yang, M., Carvidi, A. B., Demissie, E. G., et al. (2021). Effect of immunosuppression on the immunogenicity of mrna vaccines to sars-cov-2: A prospective cohort study. *Ann. Intern. Med.* 174, 1572–1585. doi: 10.7326/M21-1757

Di Chiara, C., Cantarutti, A., Raffaella Petrara, M., Bonfante, F., Benetti, E., Boracchini, R., et al. (2024). Stronger and durable sars-cov-2 immune response to mrna vaccines in 5-11 years old children with prior covid-19. *Vaccine* 42, 263–270. doi: 10.1016/j.vaccine.2023.12.006

Eccleston-Turner, M., and Upton, H. (2021). International collaboration to ensure equitable access to vaccines for covid-19: the act-accelerator and the covax facility. *Milbank Q.* 99, 426–449. doi: 10.1111/1468-0009.12503

Ferranna, M. (2024). Causes and costs of global covid-19 vaccine inequity. *Semin. Immunopathology* 45, 469–480. doi: 10.1007/s00281-023-00998-0

Friedman, M. A., Curtis, J. R., and Winthrop, K. L. (2021). Impact of disease-modifying antirheumatic drugs on vaccine immunogenicity in patients with inflammatory rheumatic and musculoskeletal diseases. *Ann. Rheum Dis.* 80, 1255–1265. doi: 10.1136/annrheumdis-2021-221244

Grifoni, A., Sidney, J., Vita, R., Peters, B., Crotty, S., Weiskopf, D., et al. (2021). Sars-cov-2 human T cell epitopes: adaptive immune response against covid-19. *Cell Host Microbe* 29, 1076–1092. doi: 10.1016/j.chom.2021.05.010

Grifoni, A., Weiskopf, D., Ramirez, S. I., Mateus, J., Dan, J. M., Moderbacher, C. R., et al. (2020). Targets of T cell responses to sars-cov-2 coronavirus in humans with covid-19 disease and unexposed individuals. *Cell* 181, 1489–501.e15. doi: 10.1016/j.cell.2020.05.015

Haskin, O., Ashkenazi-Hoffnung, L., Ziv, N., Borovitz, Y., Dagan, A., Levi, S., et al. (2021). Serological response to the bnt162b2 covid-19 mrna vaccine in adolescent and young adult kidney transplant recipients. *Transplantation* 105, e226–ee33. doi: 10.1097/TP.0000000000003922

Head, J. R., Collender, P. A., León, T. M., White, L. A., Sud, S. R., Camponuri, S. K., et al. (2024). Covid-19 vaccination and incidence of pediatric sars-cov-2 infection and hospitalization. *JAMA Network Open* 7, e247822–e. doi: 10.1001/jamanetworkopen.2024.7822

Karim, S. S. A., and Karim, Q. A. (2021). Omicron sars-cov-2 variant: A new chapter in the covid-19 pandemic. *Lancet* 398, 2126–2128. doi: 10.1016/S0140-6736(21)02758-6

Lalia, J. K., Schild, R., Lutgehetmann, M., Dunay, G. A., Kallinich, T., Kobbe, R., et al. (2023). Reduced humoral and cellular immune response to primary covid-19 mrna vaccination in kidney transplanted children aged 5-11 years. *Viruses* 15 (7), 1553. doi: 10.3390/v15071553

Lazarus, J. V., Wyka, K., White, T. M., Picchio, C. A., Gostin, L. O., Larson, H. J., et al. (2023). A survey of covid-19 vaccine acceptance across 23 countries in 2022. *Nat. Med.* 29, 366–375. doi: 10.1038/s41591-022-02185-4

Lee, A., Wong, S. Y., Chai, L. Y. A., Lee, S. C., Lee, M. X., Muthiah, M. D., et al. (2022). Efficacy of covid-19 vaccines in immunocompromised patients: systematic review and meta-analysis. *BMJ* 376, e068632. doi: 10.1136/bmj-2021-068632

Lu, L., Chan, C. Y., Chan-Ng, P. P. L., Than, M., Tan, P. S. Y., Lim, L. K., et al. (2023). Heterogenous antibody and T-cell responses to sars-cov-2 mrna vaccines among immunocompromised young people. *Clin. Transl. Med.* 13, e1183. doi: 10.1002/ctm2.1183

Meyerowitz, E. A., Scott, J., Richterman, A., Male, V., and Cevik, M. (2024). Clinical course and management of covid-19 in the era of widespread population immunity. *Nat. Rev. Microbiol.* 22, 75–88. doi: 10.1038/s41579-023-01001-1

Morgans, H. A., Bradley, T., Flebbe-Rehwaldt, L., Selvarangan, R., Bagherian, A., Barnes, A. P., et al. (2023). Humoral and cellular response to the covid-19 vaccine in immunocompromised children. *Pediatr. Res.* 94, 200–205. doi: 10.1038/s41390-022-02374-4

Ojeda, D. S., Gonzalez Lopez Ledesma, M. M., Pallares, H. M., Costa Navarro, G. S., Sanchez, L., Perazzi, B., et al. (2021). Emergency response for evaluating sars-cov-2 immune status, seroprevalence and convalescent plasma in Argentina. *PloS Pathog.* 17, e1009161. doi: 10.1371/journal.ppat.1009161

Peng, W., Ma, X., Tan, K., Wang, H., Cong, M., Zhang, Y., et al. (2023). Evaluation of cross-neutralizing antibodies in children infected with omicron sub-variants. *Lancet Regional Health – Western Pacific* 40, 100939. doi: 10.1016/j.lanwpc.2023.100939

Petrelli, F., Luciani, A., Borgonovo, K., Ghilardi, M., Parati, M. C., Petro, D., et al. (2022). Third dose of sars-cov-2 vaccine: A systematic review of 30 published studies. *J. Med. Virol.* 94, 2837–2844. doi: 10.1002/jmv.27644

Price, A. M., Olson, S. M., Newhams, M. M., Halasa, N. B., Boom, J. A., Sahni, L. C., et al. (2022). Bnt162b2 protection against the omicron variant in children and adolescents. *N Engl. J. Med.* 386, 1899–1909. doi: 10.1056/NEJMoa2202826

Roznik, K., Xue, J., Stavrakis, G., Johnston, T. S., Kalluri, D., Ohsie, R., et al. (2024). Covid-19 vaccination induces distinct T-cell responses in pediatric solid organ transplant recipients and immunocompetent children. *NPJ Vaccines* 9, 73. doi: 10.1038/s41541-024-00866-4

Seery, V., Raiden, S., Russo, C., Borda, M., Herrera, L., Uranga, M., et al. (2022). Antibody response against sars-cov-2 variants of concern in children infected with pre-omicron variants: an observational cohort study. *EBioMedicine* 83, 104230. doi: 10.1016/j.ebiom.2022.104230

Sette, A., and Crotty, S. (2021). Adaptive immunity to sars-cov-2 and covid-19. *Cell* 184, 861–880. doi: 10.1016/j.cell.2021.01.007

Tarke, A., Coelho, C. H., Zhang, Z., Dan, J. M., Yu, E. D., Methot, N., et al. (2022). Sars-cov-2 vaccination induces immunological T cell memory able to cross-recognize variants from alpha to omicron. *Cell* 185, 847–59 e11. doi: 10.1016/j.cell.2022.01.015

Watson, O. J., Barnsley, G., Toor, J., Hogan, A. B., Winskill, P., and Ghani, A. C. (2022). Global impact of the first year of covid-19 vaccination: A mathematical modelling study. *Lancet Infect. Dis.* 22, 1293–1302. doi: 10.1016/S1473-3099(22)00320-6

Zheng, Z., Lu, Y., Wang, M., Luo, Y., Wan, P., Zhou, T., et al. (2023). Low covid-19 vaccine coverage and guardian acceptance among pediatric transplant recipients. *J. Med. Virol.* 95, e28377. doi: 10.1002/jmv.28377

Zheng, Z., Wu, H., Sun, X., Lu, Y., Song, Y., Luo, Y., et al. (2024). Evaluation of the effectiveness and safety of sequential vaccination with inactivated sars-cov-2 vaccine and ad5-ncov booster in pediatric liver transplant recipients. *J. Med. Virol.* 96, e29543. doi: 10.1002/jmv.29543

frontiers | Frontiers in Public Health

TYPE Original Research
PUBLISHED 28 March 2025
DOI 10.3389/fpubh.2025.1494463

OPEN ACCESS

EDITED BY
Paraskevi C. Fragkou,
Evaggelismos General Hospital, Greece

REVIEWED BY
Sumit Bhardwaj,
National Institute of Virology (ICMR), India
Juan Du,
Peking University, China

*CORRESPONDENCE
Jaime Briseno-Ramirez
✉ jaime.briseno@academicos.udg.mx

RECEIVED 10 September 2024
ACCEPTED 11 March 2025
PUBLISHED 28 March 2025

CITATION
De Arcos-Jiménez JC, Martinez-Ayala P, Quintero-Salgado E, Lopez-Romo R and Briseno-Ramirez J (2025) Trends of respiratory viruses and factors associated with severe acute respiratory infection in patients presenting at a university hospital: a 6-year retrospective study across the COVID-19 pandemic.
Front. Public Health 13:1494463.
doi: 10.3389/fpubh.2025.1494463

Trends of respiratory viruses and factors associated with severe acute respiratory infection in patients presenting at a university hospital: a 6-year retrospective study across the COVID-19 pandemic

Judith Carolina De Arcos-Jiménez[1,2], Pedro Martinez-Ayala[3,4], Ernestina Quintero-Salgado[2], Rosendo Lopez-Romo[2] and Jaime Briseno-Ramirez[3,4]*

[1]Laboratory of Microbiological, Molecular, and Biochemical Diagnostics (LaDiMMB), CUTlajomulco, University of Guadalajara, Tlajomulco de Zuñiga, Jalisco, Mexico, [2]State Public Health Laboratory, Guadalajara, Mexico, [3]Hospital Civil de Guadalajara "Fray Antonio Alcalde", Guadalajara, Mexico, [4]Division of Health, CUTlajomulco, University of Guadalajara, Tlajomulco de Zuñiga, Jalisco, Mexico

Background: The COVID-19 pandemic significantly disrupted the epidemiology of respiratory viruses, altering seasonal patterns and reducing circulation. While recovery trends have been observed, factors associated with severe acute respiratory infections (SARIs) during pre- and post-pandemic periods remain underexplored in middle-income countries.

Objective: This study aimed to analyze the trends in respiratory virus circulation and identify factors associated with SARI in patients attending a tertiary care university hospital in western Mexico over a six-year period spanning the pre-pandemic, pandemic, and post-pandemic phases.

Methods: A retrospective study was conducted using data from 19,088 symptomatic patients tested for respiratory viruses between 2018 and 2024. Viral trends were analyzed through interrupted time series (ITS) modeling, incorporating locally estimated scatterplot smoothing (LOESS) and raw positivity rates. Additionally, ITS analysis was performed to evaluate temporal changes in SARI proportions across different phases of the pandemic. Multivariate logistic regression models were applied to determine independent risk factors for SARI across different time periods.

Results: During the pandemic (2020–2021), respiratory virus positivity rates significantly declined, particularly for influenza, which experienced a sharp reduction but rebounded post-2022. Respiratory syncytial virus (RSV) demonstrated a delayed resurgence, whereas other respiratory viruses exhibited heterogeneous rebound patterns. ITS modeling of SARI proportions revealed a significant pre-pandemic increasing trend, followed by a slower rise during the pandemic, and a sharp post-pandemic drop in early 2022, before resuming an upward trajectory. Among older adults (>65 years), a marked increase in SARI was observed at the beginning of the pandemic, while younger groups showed more stable patterns. Logistic regression identified advanced age, male sex, cardiovascular disease, obesity, and immunosuppression as major risk factors

for SARI, while vaccination consistently showed a protective effect across all periods and subgroups.

Conclusion: The COVID-19 pandemic induced persistent shifts in respiratory virus circulation, disrupting seasonal dynamics and modifying the burden of SARI. The findings underscore the importance of continuous surveillance, targeted vaccination programs, and early diagnostics to mitigate severe outcomes. These results highlight the need for adaptive public health strategies in middle-income countries to address evolving respiratory disease threats.

KEYWORDS

COVID-19, respiratory viruses, influenza, severe acute respiratory infection (SARI), respiratory virus trends, respiratory syncytial virus (RSV), epidemiology

1 Introduction

The dynamics of respiratory viruses, including influenza, respiratory syncytial virus (RSV), parainfluenza virus (HPIV), and metapneumovirus (hMPV), have exhibited substantial variations across the pre-pandemic, pandemic, and post-pandemic periods of COVID-19 (1). Before the COVID-19 pandemic, respiratory viruses followed well-defined seasonal patterns, and influenza was the primary public health concern among respiratory infections (2). The COVID-19 pandemic profoundly disrupted the epidemiology of respiratory viruses (3). Public health measures implemented to curb the spread of severe acute respiratory syndrome coronavirus 2 (SARS-CoV-2), including mask-wearing, social distancing, and travel restrictions, drastically reduced the circulation of other respiratory viruses (3). For instance, positivity rates for influenza A, influenza B, and RSV dropped to nearly undetectable levels in many regions during the first year of the pandemic, as demonstrated by both hospital-based studies and population-level data analyses (2–4). With the relaxation of COVID-19 control measures, some respiratory viruses have resurged, although not all have returned to their pre-pandemic patterns (5–7). The detection of influenza and RSV has begun to rise again; however, their seasonality and epidemic magnitude initially appear to have shifted (7, 8). Additionally, the frequency of severe acute respiratory infections (SARI) and its role as a cause of hospitalization may have also been affected (5, 6, 8).

The 2009 influenza A H1N1 pandemic influenced the seasonality and age distribution of other respiratory viruses, highlighting the potential for pandemics to induce lasting shifts in respiratory virus epidemiology (9). Changes in the frequency and prevalence of respiratory viruses during and after the COVID-19 pandemic can be attributed to a combination of factors, primarily due to public health measures and shifts in human behavior (10–12). Interventions such as mask-wearing and social distancing played a critical role in significantly reducing the transmission of respiratory viruses (10, 13, 14). Although the presence of a dominant virus like SARS-CoV-2 may have influenced the spread of other viruses through competition for ecological niches, these patterns were likely driven by changes in human behavior, such as improved personal hygiene and altered healthcare-seeking practices (12, 15–18).

Viral interference between SARS-CoV-2 and other respiratory viruses has been a subject of significant interest (11). Specifically, interactions between SARS-CoV-2 and viruses such as influenza A and RSV are influenced by multiple immune and molecular mechanisms (19). Influenza A and RSV can elicit a strong interferon (IFN) response that inhibits SARS-CoV-2 replication, particularly when these infections occur prior to or concurrently with SARS-CoV-2 (11, 19). Conversely, SARS-CoV-2 induces a weaker IFN response, limiting its ability to interfere with influenza virus replication (11, 19, 20). Additionally, the SARS-CoV-2 ORF3a protein modulates ion channels and triggers pro-inflammatory responses, potentially altering viral replication dynamics (21). The nucleocapsid protein enhances viral RNA transcription and may influence the cellular environment, affecting co-infecting viruses (22). Furthermore, SARS-CoV-2's broad receptor usage, including ACE2 and neuropilin-1, may create competition for cellular entry, impacting co-infections (23). Its dysregulated inflammatory response, characterized by cytokine storms and autoimmune activation, can further suppress or exacerbate other viral infections (24, 25). These interactions highlight the complex interplay between SARS-CoV-2 and other respiratory viruses during the COVID-19 pandemic.

SARI, caused by various respiratory viruses, is a leading cause of hospitalizations, posing a significant health concern, especially among vulnerable populations, and placing substantial strain on healthcare systems during peak seasons or outbreaks (8, 26, 27). These vulnerable groups include pediatric patients under 2 years of age, older individuals, immunocompromised patients, and individuals with underlying health conditions (28–30). The presence of comorbidities such as cardiovascular disease, chronic pulmonary disease, chronic neurologic disease, and asthma significantly increases the risk of severe respiratory infections and poor outcomes (31–34). Immunocompromised patients are especially susceptible to severe respiratory infections, and respiratory viruses are known to exacerbate chronic respiratory conditions (34, 35). These infections can result in severe outcomes such as acute respiratory distress syndrome (ARDS) and pneumonia and are frequently complicated by bacterial coinfections (36, 37). Respiratory viruses commonly associated with severe pneumonia—whether community-acquired, hospital-acquired, or ventilator-associated—include influenza virus, human rhinovirus, parainfluenza, adenovirus, human metapneumovirus, respiratory syncytial virus, and coronaviruses (34, 38). Multiple respiratory viruses can infect the respiratory tract concurrently or sequentially, leading to interactions that may either enhance or suppress the infection and replication dynamics of other viruses (12, 15, 16, 37, 39, 40).

This study aimed to assess trends in respiratory virus circulation among symptomatic individuals presenting to triage areas at our institution and to identify factors associated with the development of

severe acute respiratory infections before and after the COVID-19 pandemic.

2 Materials and methods

2.1 Ethics statement

The study was evaluated and approved by the Research Committee of the Ministry of Health of Jalisco and registered in the State Research Registry under identifier 73/LESP/JAL/2024. Additionally, it was reviewed and approved by the "Comité de Ética en Investigación en Ciencias de la Salud del Centro Universitario de Tlajomulco, Universidad de Guadalajara" (ethical approval number CUTLAJO/DS/CEICS/017/24). This study, involving human participants, was conducted in accordance with the principles of the Declaration of Helsinki (1964) and its subsequent amendments, as well as applicable national legislation and institutional guidelines. As the research was retrospective and exclusively used de-identified data, the requirement for informed consent was waived.

2.2 Setting

This study was conducted at OPD Hospitales Civiles de Guadalajara, a tertiary referral and teaching institution affiliated with the University of Guadalajara, located in Jalisco, Mexico. The institution encompasses two referral hospitals that primarily serve an uninsured population from western Mexico, providing specialized care for both adults and children. As major regional centers, these hospitals receive patients from diverse urban and rural areas. During the COVID-19 pandemic, they played a pivotal role in the region by delivering comprehensive general and critical care services while managing a substantial portion of COVID-19 cases.

2.3 Population and eligibility criteria

The study population comprised symptomatic patients presenting with influenza-like illness (ILI) to the triage areas of our institution, who were tested for respiratory viruses between January 2018 and March 2024. A suspected case of ILI was defined according to local guidelines as the sudden onset of symptoms accompanied by at least one systemic symptom—fever, feverishness, cough, or headache—and at least one localized symptom, such as dyspnea, myalgias, arthralgias, odynophagia, chills, chest pain, rhinorrhea, tachypnea, anosmia, dysgeusia, or conjunctivitis (41).

Medical and state laboratory records were cross-referenced with the epidemiological surveillance platform to ensure data consistency. Demographic information, comorbidities, and severe acute respiratory infection (SARI) status—defined per local guidelines as a respiratory tract infection accompanied by severe symptoms such as dyspnea, chest pain, acute respiratory distress syndrome, or the need for hospitalization—were systematically recorded (42). Additional variables collected included the number of days from symptom onset to the date of specimen collection for RT-PCR testing, vaccination status, RT-PCR Ct values of detected viruses, and other relevant clinical parameters.

Patients were excluded if their tests did not correspond to symptomatic cases, such as those performed for contact tracing, or if discrepancies were identified between the state surveillance platform and hospital records. Cases requiring subsequent testing to confirm negativity for ending isolation were also excluded. Additionally, records with more than 10% missing sociodemographic or clinical data were omitted.

2.4 Viral testing

Nasopharyngeal swabs were collected in viral transport media and transported to the State Public Health Laboratory of Jalisco (SPHLJ) under strict cold chain conditions. Upon arrival, laboratory procedures included viral inactivation, nucleic acid extraction, and viral gene amplification using RT-PCR. The viral genetic material was extracted using automated platforms that employed magnetic bead-based technology to selectively bind viral RNA, followed by sequential washing steps for isolation. Two different extraction kits and systems were utilized for this process: the ExiPrep™ Plus Viral DNA/RNA Kit, designed for 96 reactions and operated on the ExiPrep™ 96 platform (Bioneer®, Daejeon, South Korea), and the MagNA Pure 96 Small Volume Kit, used on the MagNA Pure 96 System (Roche®, Basel, Switzerland). Viral detection was carried out using Health Mexico-approved single and multiplex RT-qPCR assays. These assays targeted key SARS-CoV-2 genes, including *E, N*, *RdRP*, and *ORF1ab*. Detection platforms and assays employed included the COBAS 6800 System (Roche®), the Logix Smart RT–PCR Kit (Co-Diagnostics®), the Flu-COVID Vitro Kit (Master Diagnóstica®), and the BioFire FilmArray Respiratory Panel (BioFire Diagnostics®). The respiratory viruses of interest included SARS-CoV-2, Influenza A virus, Influenza B virus, Respiratory syncytial virus (RSV), Human parainfluenza viruses 1–4 (HPIV1, HPIV2, HPIV3, HPIV4), Human metapneumovirus (hMPV), seasonal Human coronaviruses (HCoV-229E, HCoV-OC43, HCoV-NL63, and HCoV-HKU1), Human adenovirus (HAdV), Human enterovirus/rhinovirus (HEV/HRV), and Human Bocavirus (HBoV). A case was defined as laboratory-confirmed for each symptomatic case with a respiratory virus RT-PCR positive test.

2.5 Testing restrictions

In Mexico, prior to the COVID-19 pandemic, respiratory virus surveillance primarily focused on influenza, but it was significantly enhanced with the onset of COVID-19. According to pre-pandemic local guidelines, only 10% of suspected influenza cases among outpatients and 100% of hospitalized cases were tested for Influenza A and Influenza B viruses. Furthermore, 10% of severe cases that tested negative for influenza were evaluated for other respiratory viruses (43). The COVID-19 health emergency in 2020 prompted expanded monitoring and the implementation of new testing strategies. Comprehensive sampling and testing for SARS-CoV-2, Influenza A, and Influenza B were conducted on all suspected ILI and SARI cases using multiplex RT-PCR. Other respiratory viruses were tested in 10% of severe cases (44).

2.6 Definition of time periods

Based on the observed pandemic dynamics in western Mexico, we defined three distinct periods to analyze the frequency and positivity rates of respiratory viruses other than SARS-CoV-2: the pre-pandemic period (January 2018 to February 2020), the pandemic period (March 2020 to December 2021), and the post-pandemic period (January 2022 onward). These periods were designed to capture contrasting trends influenced by the implementation and subsequent relaxation of non-pharmaceutical interventions (NPIs). The pre-pandemic period served as a baseline to evaluate respiratory virus circulation under typical conditions. The pandemic period captured the significant decline in positivity rates driven by the emergence of SARS-CoV-2 and widespread NPIs, while the post-pandemic period documented recovery trends as SARS-CoV-2 cases declined and NPIs were progressively lifted. This framework allowed for a detailed analysis of the disruptions caused by the pandemic and the subsequent recovery in respiratory virus activity.

2.7 Statistical analysis

Demographic data were reported as simple relative frequencies. The percentage of positive values was calculated as the number of tests that yielded positive results divided by the total number of tests performed for a given period of time expressed as a percentage for each virus. The normality of the data distribution was assessed using the Shapiro–Wilk test. Pearson's chi-square test and Fisher's exact test were used to compare proportions, as appropriate. For comparisons of quantitative variables, Student's t test and the Wilcoxon–Mann–Whitney test were used for normally and nonnormally distributed data, respectively.

To analyze the temporal trends in viral positivity rates, we applied locally estimated scatterplot smoothing (LOESS) to weekly aggregated data for each respiratory virus. LOESS is a non-parametric regression technique that fits localized polynomial curves to the data, enabling the detection of trends and patterns without assuming a specific functional form. Weekly positivity rates for each virus were calculated as the ratio of positive cases to the total number of tests conducted during each week. To represent the uncertainty in trend estimates, 95% confidence intervals were calculated around the LOESS-adjusted curves. Both LOESS-derived positivity rates and raw, unadjusted positivity rates were subsequently used in interrupted time series (ITS) analyses, providing a robust assessment of the immediate and sustained impacts of the COVID-19 pandemic on viral circulation patterns.

To evaluate the impact of the COVID-19 pandemic on respiratory viruses circulation from 2017 to 2023 we use ITS analysis. Segmented linear regression models were used to assess changes in virus activity, with predictors including time, level changes, and trend changes for each period. The analysis was conducted on two distinct datasets: one containing raw weekly positivity rates and another with weekly LOESS-adjusted positivity rates. Both datasets represented positivity trends for influenza, RSV, HEV/HRV, HPIV, HCoV, HAdV, hMPV, and HBoV, aggregated by epidemiological week.

For both approaches, three temporal periods were defined:

1. Pre-pandemic period: Weeks before March 2020.
2. Pandemic period: Weeks between March 2020 and December 2021.
3. Post-pandemic period: Weeks from January 2022 onwards.

The ITS models included the following parameters:

- Constant (β_0): Baseline positivity rate at the start of the pre-pandemic period.
- Time (β_1): Trend in positivity rates during the pre-pandemic period.
- Level (β_2):
  - o Immediate change in positivity rates during the pandemic (2020–2021).
  - o Immediate change in positivity rates during the post-pandemic period (2022).
- Trend (β_3):
  - o Change in trend during the pandemic (2020–2021).
  - o Change in trend during the post-pandemic period (2022).

Separate linear regression models were fitted for each virus using the formula:

$$\boldsymbol{Y}_t = \beta_0 + \beta_1 \text{Time}_t + \beta_2 \text{Level}_t + \beta_3 \text{Trend}_t + \varepsilon_t$$

where $\boldsymbol{Y}_t$ represents the positivity rate (raw or LOESS-adjusted) for a given virus at time t.

The LOESS-adjusted dataset was used to reduce week-to-week variability and better capture long-term trends, while the raw dataset allowed for the analysis of unprocessed data to ensure robustness of findings. Statistical significance for all model parameters (β coefficients) was assessed, and results were presented with corresponding 95% confidence intervals, standard errors, and p-values.

Given the predominant impact of certain viruses on pediatric populations, the ITS analysis was also stratified by age into two primary groups: <18 years and < 5 years. These cutoffs were chosen to ensure an adequate number of observations in each subgroup, allowing for a reliable model fit. Additionally, ITS analyses of raw SARI proportions were conducted for the general population as well as for four specific age-stratified groups: <5 years, 5–18 years, 18–65 years, and > 65 years. This approach enabled the assessment of pre- and post-pandemic changes in SARI proportions and the detection of potential shifts across different age cohorts. The LOESS-adjusted dataset was primarily used to reduce week-to-week variability and better capture long-term trends, whereas the raw dataset was analyzed to preserve unprocessed data, ensuring the robustness of the findings. Statistical significance for all model parameters (β coefficients) was evaluated, with results presented alongside 95% confidence intervals, standard errors, and p-values.

Finally, multivariate logistic regression was performed to determine independent factors associated with SARI. Variables were included in the model if they met a significance threshold of $p < 0.1$ in univariate analysis and were considered biologically plausible. A stepwise selection method was applied to optimize the model. Model fit was assessed using the Hosmer–Lemeshow test, with p-values >0.1 indicating an adequate fit. Confidence

intervals were set at 95% (CI = 95%). The final models for each analyzed period were selected based on their goodness of fit, as determined by the Hosmer–Lemeshow test, and explanatory power, as indicated by McFadden's R^2 values. The results reflect the best-fitting models for each period and population group studied.

Statistical analyses were conducted using R version 4.3.1 and Python version 3.10. In R, *lm* and *segmented* packages were used for ITS analyses, while LOESS adjusting was applied with *ggplot2* and *stats*. Logistic regression models were implemented using *glm*, supported by *broom* and *ResourceSelection* for model evaluation. In Python, ITS analyses utilized the *statsmodels* library (version 0.14.0) for time-series modeling, with *scipy* (version 1.10.1) aiding hypothesis testing and diagnostics. These tools enabled comprehensive evaluation of virus circulation, positivity trends, and associations with SARI across time periods.

3 Results

From the records reviewed, a total of 21,134 patients were identified, of whom 19,088 met the selection criteria and were included in the analysis, as depicted in Figure 1.

The median age of the included patients was 36 years (IQR 26–51), with 56.74% (n = 10,831) being women. Among patients who tested positive for respiratory viruses, the median age was 38 years (IQR 27–52). The age and sex distributions by detected virus are presented in Figure 2, while additional sociodemographic data and characteristics of the study population are detailed in Table 1.

Among the positive tests for respiratory viruses, 36.44% corresponded to SARS-CoV-2 (n = 6,783), 12.20% corresponded to influenza virus (n = 1,187), and 11.33% to other respiratory viruses distinct from SARS-CoV-2 and influenza (n = 175). Regarding influenza subtypes, Influenza A H3 was the most prevalent (n = 737), followed by the Influenza B Victoria lineage (n = 285) and Influenza A H1N1 (n = 111). Among other respiratory viruses (OVRs), Human enterovirus/rhinovirus was the most frequently isolated (n = 73), followed by respiratory syncytial virus (n = 46). The remaining viral isolates are summarized in Table 2.

A total of 116 respiratory virus coinfections were identified. Among these, 94 cases involved coinfections between SARS-CoV-2 and influenza, 14 cases were coinfections among respiratory viruses other than SARS-CoV-2 and influenza, 5 cases were coinfections between SARS-CoV-2 and other respiratory viruses distinct from influenza, and 3 cases involved coinfections between influenza and other respiratory viruses distinct from SARS-CoV-2. Notably,

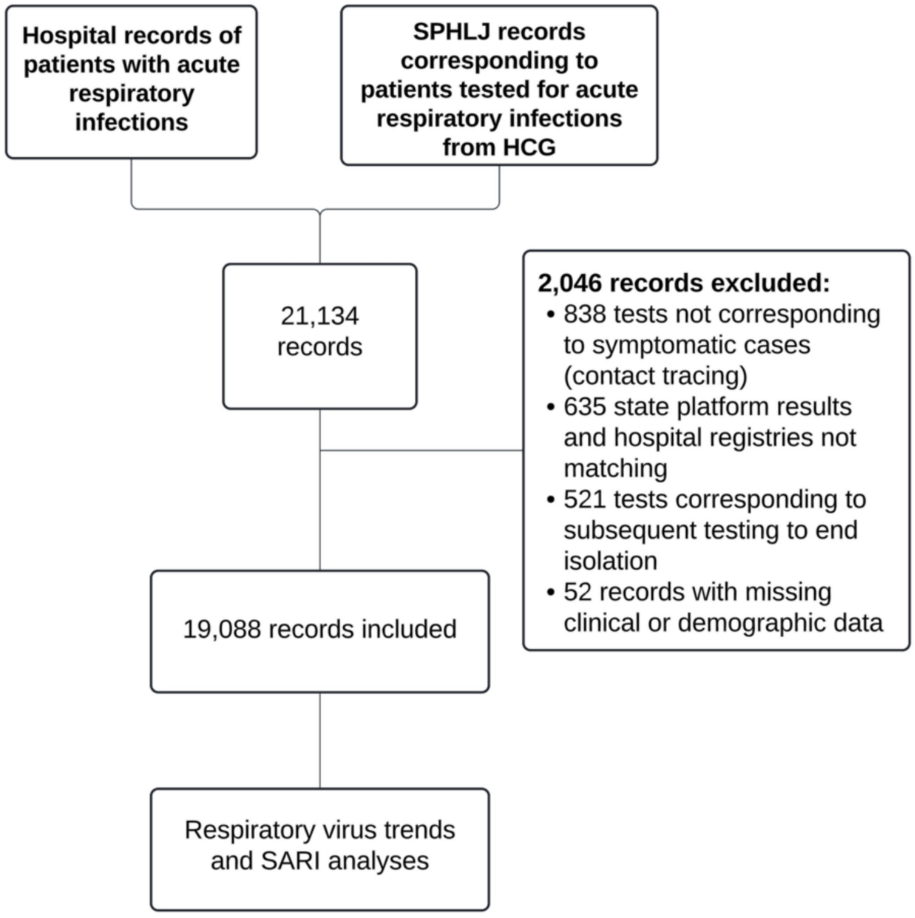

FIGURE 1
Flowchart of case selection.

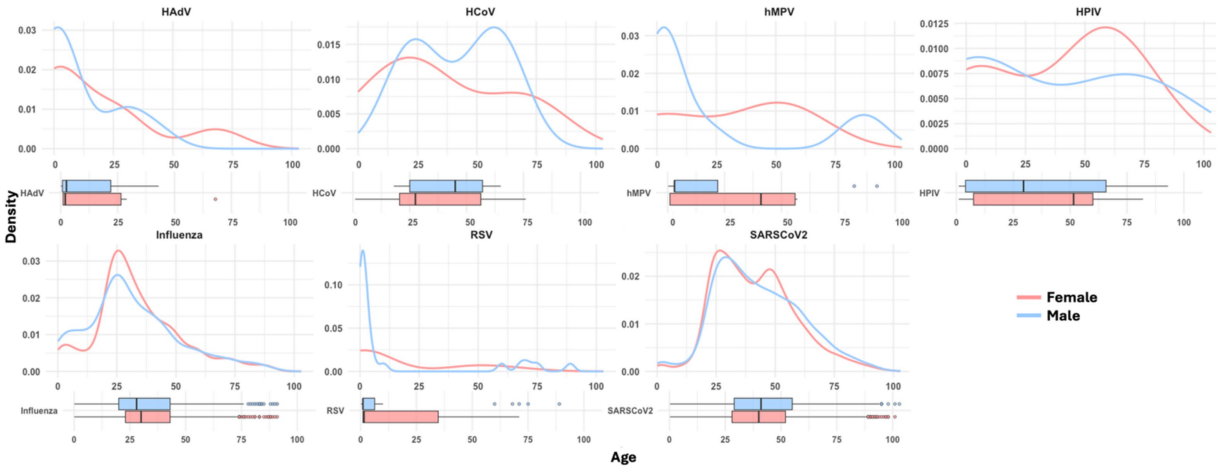

FIGURE 2
Age and sex distributions of patients by detected respiratory virus.

TABLE 1 Sociodemographic and clinical characteristics of patients tested for respiratory viruses during the study period.

Variable	Total (*n* = 19,088)	Women (*n* = 10,831)	Men (*n* = 8,256)	*p* value
Age—median, (IQR)	36.0 (26.0–51.0)	36.0 (26.0–50.0)	36.0 (25.0–52.0)	0.210
Days of symptoms to test -median, (IQR)	2.0 (1.0–3.0)	2.0 (1.0–3.0)	2.0 (1.0–3.0)	<0.001
Severe acute respiratory infection (SARI)—n, (%)	3,750 (19.65)	1721 (45.89)	2029 (54.11)	<0.001
Comorbidities—n, (%)	6,713 (35.17)	3,604 (33.27)	3,109 (37.66)	<0.001
Diabetes	1859 (9.74)	1,021 (9.43)	838 (10.15)	0.027
Cardiovascular disease	411 (2.15)	219 (2.02)	192 (2.33)	0.092
Obesity	1,377 (7.21)	768 (7.09)	609 (7.38)	0.218
Asthma	716 (3.75)	483 (4.46)	233 (2.82)	<0.001
COPD	368 (1.93)	190 (1.75)	178 (2.16)	0.025
Smoking	1,067 (5.59)	378 (3.49)	689 (8.35)	<0.001
Hypertension	2,316 (12.13)	1,259 (11.62)	1,057 (12.80)	0.002
Immunosuppression status	821 (4.30)	345 (3.19)	475 (5.75)	<0.001
Chronic kidney disease	447 (2.34)	187 (1.73)	260 (3.15)	<0.001
Pregnancy	66 (0.35)	66 (0.61)	0 (0.00)	-

SARS-CoV-2 Ct values were higher (indicating lower viral loads) in patients with influenza coinfection (SARS-CoV-2 Ct median: 35.5, IQR 30–37) compared to those without influenza coinfection (SARS-CoV-2 Ct median: 22, IQR 19–30), $p < 0.001$. No significant differences were observed in influenza Ct values between patients with and without SARS-CoV-2 coinfection, with median values of 27 (IQR 23–31) in coinfected patients versus 28 (IQR 23–32) in non-coinfected patients. The detailed distribution of these coinfections is described in Table 2 and illustrated in Figure 3, as well as the distributions of influenza and SARS-CoV-2 Ct values in both coinfected and non-coinfected patients, which are depicted in Figure 4.

Figure 5 illustrates the positivity rates of influenza, other respiratory viruses, and SARS-CoV-2 cases across pandemic years. Regarding influenza viruses, a significant reduction in positivity rates was observed during the first year of the COVID-19 pandemic. However, following 2020, and particularly after 2021, a marked increase in the positivity rates of influenza viruses and their subtypes was documented (Figures 5A,B). Notably, in 2023, after the rise in positivity rates for influenza A during 2022, an increase in the positivity rate of the influenza B Victoria lineage was observed (Figure 5B). Conversely, the Influenza B Yamagata lineage remained completely undetected during and after the pandemic.

For other respiratory viruses, positivity rates as a group declined to historically low levels during the 3 years following the onset of the pandemic (Figure 5A). Individually, however, certain viruses such as HEV/HRV and HPIV continued to be detected, and a slight increase in RSV positivity was noted in the last quarter of 2021 (Figure 5B). Despite this, all these viruses remained at historically low levels and had not returned to pre-pandemic rates as of the time of this report.

TABLE 2 Proportions of viruses detected among patients tested during the study period.

Virus	Total (*n* = 18,616)	Women (*n* = 10,601)	Men (*n* = 8,015)	*p* value
SARSCoV2 infection—n, (%)	6,783 (36.44)	3,915 (36.93)	2,868 (35.78)	0.111
	Total (*n* = 9,726)	Women (*n* = 5,546)	Men (*n* = 4,180)	*p* value
Influenza viruses—n, (%)	1,187 (12.20)	707 (12.75)	480 (11.48)	0.059
Influenza A	879 (9.04)	535 (9.65)	344 (8.23)	0.016
Influenza A H3	737 (7.58)	453 (8.17)	284 (6.79)	0.011
Influenza A H1N1	111 (1.14)	61 (1.10)	50 (1.20)	0.658
Influenza A nonsubtyped	31 (0.32)	21 (0.38)	10 (0.24)	0.227
Influenza B	308 (3.17)	172 (3.10)	136 (3.25)	0671
Influenza B Victoria lineage	285 (2.93)	156 (2.81)	129 (3.09)	0.429
Influenza B Yamagata lineage	15 (0.15)	13 (0.23)	2 (0.05)	0.020
Influenza B nonsubtyped	8 (0.08)	3 (0.05)	5 (0.12)	0.302
	Total (*n* = 1,545)	Women (*n* = 735)	Men (*n* = 810)	*p* value
Other respiratory viruses (ORVs)—n, (%)	175 (11.33)	78 (0.72)	97 (11.98)	0.399
Human adenovirus	17 (1.10)	7 (0.95)	10 (1.23)	0.595
Human metapneumovirus	14 (0.91)	5 (0.68)	9 (1.11)	0.372
Human enterovirus/rhinovirus	73 (4.72)	32 (4.35)	41 (5.06)	0.512
Human parainfluenza virus 1	3 (0.19)	2 (0.27)	1 (0.12)	0.607
Human parainfluenza virus 2	1 (0.06)	1 (0.14)	0 (0.00)	0.961
Human parainfluenza virus 3	11 (0.71)	5 (0.68)	6 (0.74)	0.888
Human parainfluenza virus 4	3 (0.19)	2 (0.27)	1 (0.12)	0.607
Respiratory syncytial virus	46 (2.98)	22 (2.99)	24 (2.96)	0.972
Human bocavirus	2 (0.13)	1 (0.14)	1 (0.12)	1
Human coronavirus 229E	2 (0.13)	1 (0.14)	1 (0.12)	1
Human coronavirus HKU1	3 (0.19)	1 (0.14)	2 (0.25)	1
Human coronavirus NL63	5 (0.32)	1 (0.14)	4 (0.49)	0.377
Human coronavirus OC43	5 (0.32)	3 (0.41)	2 (0.25)	0.673
Viral Coinfections—n, (%)	116 (7.51)	75 (10.20)	41 (5.06)	0.011
Coinfections between SARS-CoV-2 and Influenza	94 (6.08)	63 (8.57)	31 (3.83)	0.059
Coinfections between ORVs (excluding SARS-CoV-2 and Influenza)	14 (0.91)	7 (0.95)	7 (0.86)	0.855
Coinfections between SARS-CoV-2 and ORVs	5 (0.32)	3 (0.41)	2 (0.25)	0.679
Coinfections between Influenza and ORVs	3 (0.19)	2 (0.27)	1 (0.12)	0.607

Utilizing LOESS-adjusted positivity rates, the ITS analysis revealed significant disruptions in the positivity rates of respiratory viruses during the COVID-19 pandemic (2020–2021), with varied recovery patterns post-2022. Influenza experienced a sharp and significant immediate decline in positivity during 2020–2021 (Level β2 2020–2021: −44.166, $p < 0.001$), followed by a further reduction in 2022 (Level β2 2022: −51.761, $p < 0.001$), despite a slight upward recovery trend post-2022 (Trend β3 2022: 0.1061, $p < 0.001$). RSV showed a significant immediate increase during the pandemic (Level β2 2020–2021: 1.198, $p = 0.020$), with a non-significant decrease in 2022 (Level β2 2022: −0.0842, $p = 0.900$) but a significant upward trend post-2022 (Trend β3 2022: 0.0072, $p = 0.031$). HEV/HRV exhibited a substantial increase during the pandemic (Level β2 2020–2021: 5.5102, $p < 0.001$), followed by a significant downward trend (Trend β3 2020–2021: −0.0455, $p < 0.001$). HCoV and HAdV also showed significant increases during the pandemic (Level β2 2020–2021: 1.4338 and 0.4478, respectively, both $p < 0.001$), with HCoV demonstrating a declining trend post-pandemic (Trend β3 2020–2021: −0.0108, $p < 0.001$) and HAdV exhibiting a reduction post-2022. hMPV had significant increases during 2020–2021 (Level β2

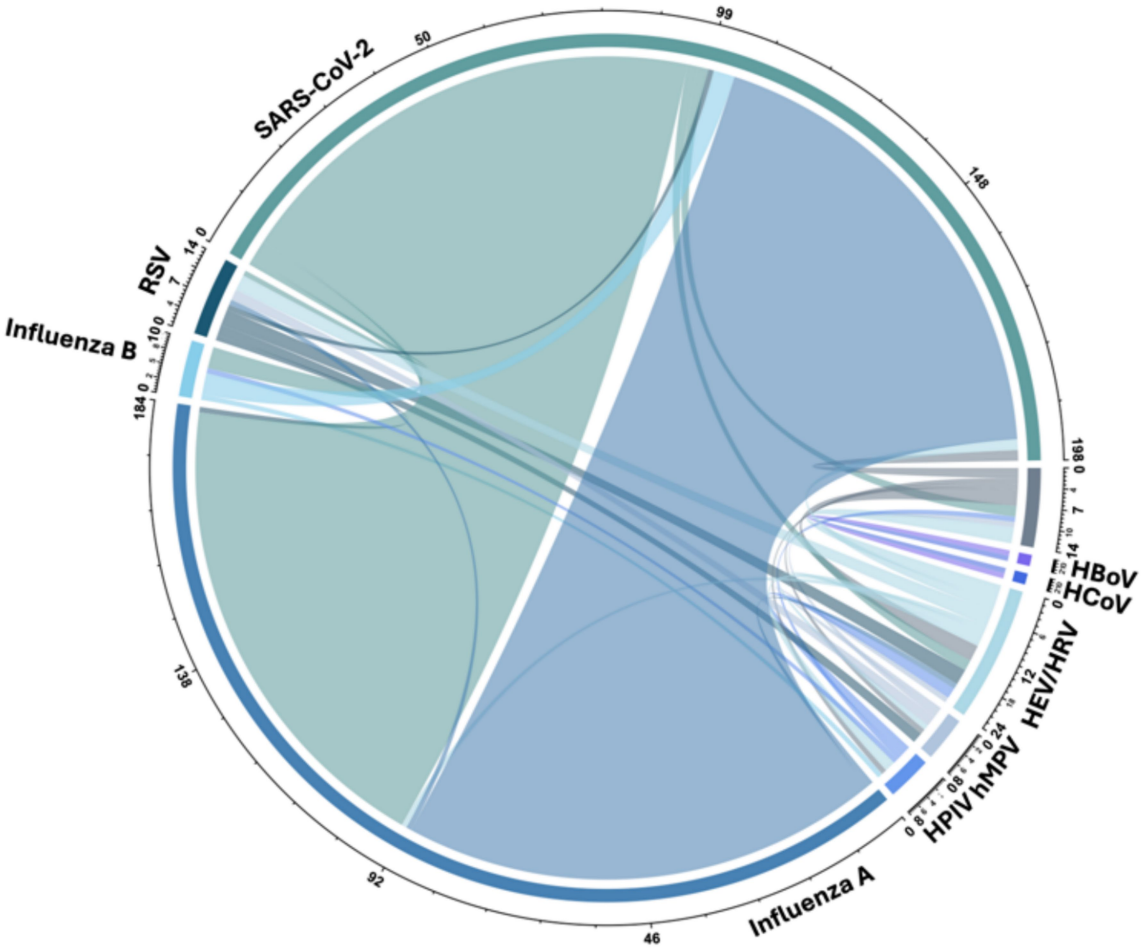

FIGURE 3
Coinfections among detected respiratory viruses.

2020–2021: 1.1036, $p < 0.001$) but showed limited recovery post-pandemic. Conversely, HPIV and HBoV exhibited minimal changes during the pandemic and subsequent periods, with trends remaining stable. A summary of the ITS results for both LOESS-adjusted positivity rates and raw positivity rates is provided in Table 3, while an extended version can be found in Supplementary Table S1.

The ITS analysis utilizing the raw positivity rates revealed noticeable differences in the significance and magnitude of the trends and levels observed during the pandemic (2020–2021) and post-pandemic periods (2022 onwards). For influenza, raw positivity rates only indicated a smaller and non-significant decline during 2020–2021 (β2: −3.63, $p = 0.513$) and a significant increase in 2022 (β2: 14.81, $p = 0.033$). For RSV, raw positivity rates highlighted a sharper initial decline during 2020–2021 (β2: −0.85, $p = 0.004$) and no significant trend post-2022 (β3: 0.00, $p = 0.771$). HEV/HRV displayed a substantial increase during 2020–2021 in both analyses. Other viruses, such as HCoV and HAdV, also showed marked differences. For HBoV, the ITS analysis could not be performed using raw positivity rates due to insufficient data points. LOESS-adjusted rates captured more pronounced shifts, particularly in post-pandemic recovery trends, which were less evident or not significant in the raw data. The complete ITS analyses utilizing LOESS-adjusted and raw positivity rates can be found in Supplementary Table S1.

In children under 5 years of age, influenza initially presented at a high baseline (~28.8%, $p = 0.003$) and exhibited two significant declines: one at the onset of the pandemic (Level $\beta_2 = -23.23$, $p = 0.045$) and another in early 2022 (−24.18, $p = 0.020$). In contrast, HEV/HRV demonstrated a positive pre-pandemic trend (+0.19 per week, $p = 0.041$) but remained largely unaffected during the pandemic and in 2022. RSV, however, showed a significant increase in slope following the pandemic's onset (+0.26 per week, $p < 0.001$) without subsequent shifts. Other respiratory viruses (ORVs), including HPIV and HCoV, displayed minimal or no significant changes in children under five, aside from a borderline increase in the pandemic slope for ORVs ($p = 0.057$). Among older children and adolescents (<18 years), influenza—despite its notable decline in younger children—did not exhibit clear changes, while RSV accelerated an already increasing trend ($p = 0.001$). HEV/HRV, ORVs as a group, and HPIV demonstrated limited or no immediate pandemic-related alterations, although some displayed positive slopes before and/or during the pandemic. Overall, RSV experienced the most pronounced increase in both pediatric subgroups, whereas influenza reductions were primarily observed in children under five. The complete ITS analysis with LOESS-adjusted trends stratified by age in non-adult populations is available in Supplementary Table S2.

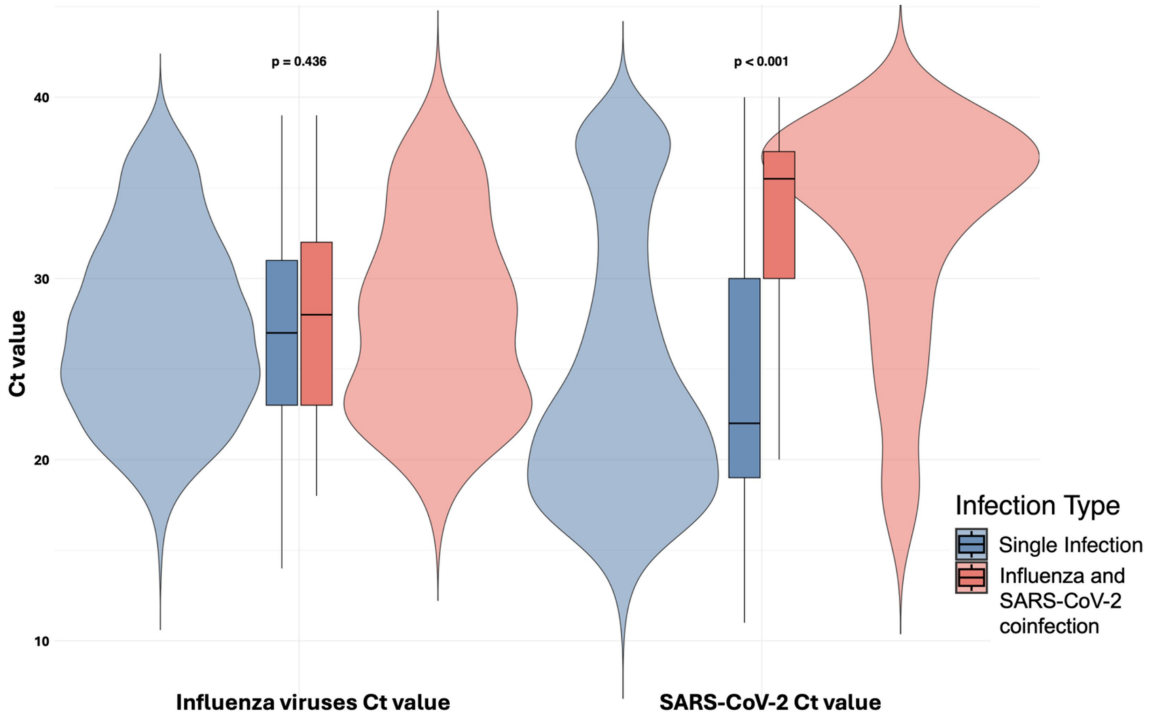

FIGURE 4
Comparison of Ct values in single infections versus influenza and SARS-CoV-2 coinfections.

In the overall population, our interrupted time series (ITS) analysis of SARI proportions demonstrated a high baseline at the study's outset, coupled with a progressive pre-pandemic increase. Specifically, during the pre-pandemic phase (before March 2020), the baseline (β_0) was approximately 43% ($p < 0.001$) and the weekly slope (Time, β_1) rose by +0.49 points ($p < 0.001$), indicating a steady, moderate growth in SARI prior to the pandemic. Upon entering the pandemic period (March 2020–December 2021), no significant immediate change (Level, β_2) was detected ($p = 0.789$), suggesting that the pandemic did not produce a sharp, abrupt shift in SARI at its onset. Nonetheless, there was a statistically significant reduction in the slope (Trend, $\beta_3 \approx -0.21$, $p = 0.008$), implying that, although SARI continued to rise, it did so at a slower rate compared to pre-pandemic levels. In January 2022, marking the post-pandemic phase, SARI exhibited a pronounced drop of approximately 37 percentage points ($p < 0.001$), followed by a renewed weekly uptick of +0.33 points ($p < 0.001$). Thus, after an abrupt decline at the onset of 2022, SARI subsequently rebounded with a positive trend in the post-pandemic period. Overall, these findings suggest that while SARI was already climbing in the months leading up to COVID-19, the pandemic brought about a significant slowing of that trajectory. Despite no immediate "jump" at pandemic onset, a sharp decrease occurred as public health measures and viral circulation patterns evolved at the start of 2022. Notably, this decline was then followed by an upswing, reflecting the dynamic interplay of shifting viral landscapes, evolving interventions, and possible changes in healthcare-seeking or diagnostic practices post-pandemic. The detailed ITS analysis of SARI proportions, including trend estimates and statistical findings, is presented in Table 4.

Across the four age-stratified groups, SARI proportions displayed distinct patterns. In children under 5 years (<5), the baseline was notably high at nearly 78% ($p < 0.001$), yet neither the onset of the pandemic nor the post-pandemic period revealed significant immediate or trend-related changes. By contrast, in older children (5–18 years), the estimated intercept was about 52% ($p < 0.001$) but likewise showed no meaningful shifts during or after the pandemic; any modest tendencies did not reach statistical significance. Among adults aged 18–65 years, a baseline of approximately 34% ($p < 0.001$) was accompanied by a strong pre-pandemic slope (+1.28/week, $p < 0.001$), followed by a slight (and non-significant) level change during the pandemic but a pronounced drop (−35 points, $p < 0.001$) and subsequent rebound (+0.31/week, $p < 0.001$) at the start of 2022. Lastly, in older adults (>65 years), the model indicated a lower initial estimate (~30%, $p < 0.001$) but with a marked immediate jump of +45 points when the pandemic began ($p < 0.001$), coupled with a mild negative slope thereafter (−0.26/week, $p = 0.012$); however, the post-2022 level could not be estimated due to insufficient data, even though the trend in that phase became significantly positive (+0.43/week, $p < 0.001$). These age-specific findings suggest that while younger individuals had either persistently high SARI or inconclusive changes, middle-aged adults experienced a sharp 2022 downturn and rebound, and older adults saw the largest pandemic-era surge but a partial tapering over time. The detailed ITS analysis of SARI proportions, including trend estimates and statistical findings across age stratified groups, is also presented in Table 4.

The univariate analysis of factors associated with SARI revealed significant associations in both the pre-pandemic and post-pandemic periods. Predictors such as age, sex, and the presence of comorbidities consistently demonstrated strong

10.3389/fpubh.2025.1494463

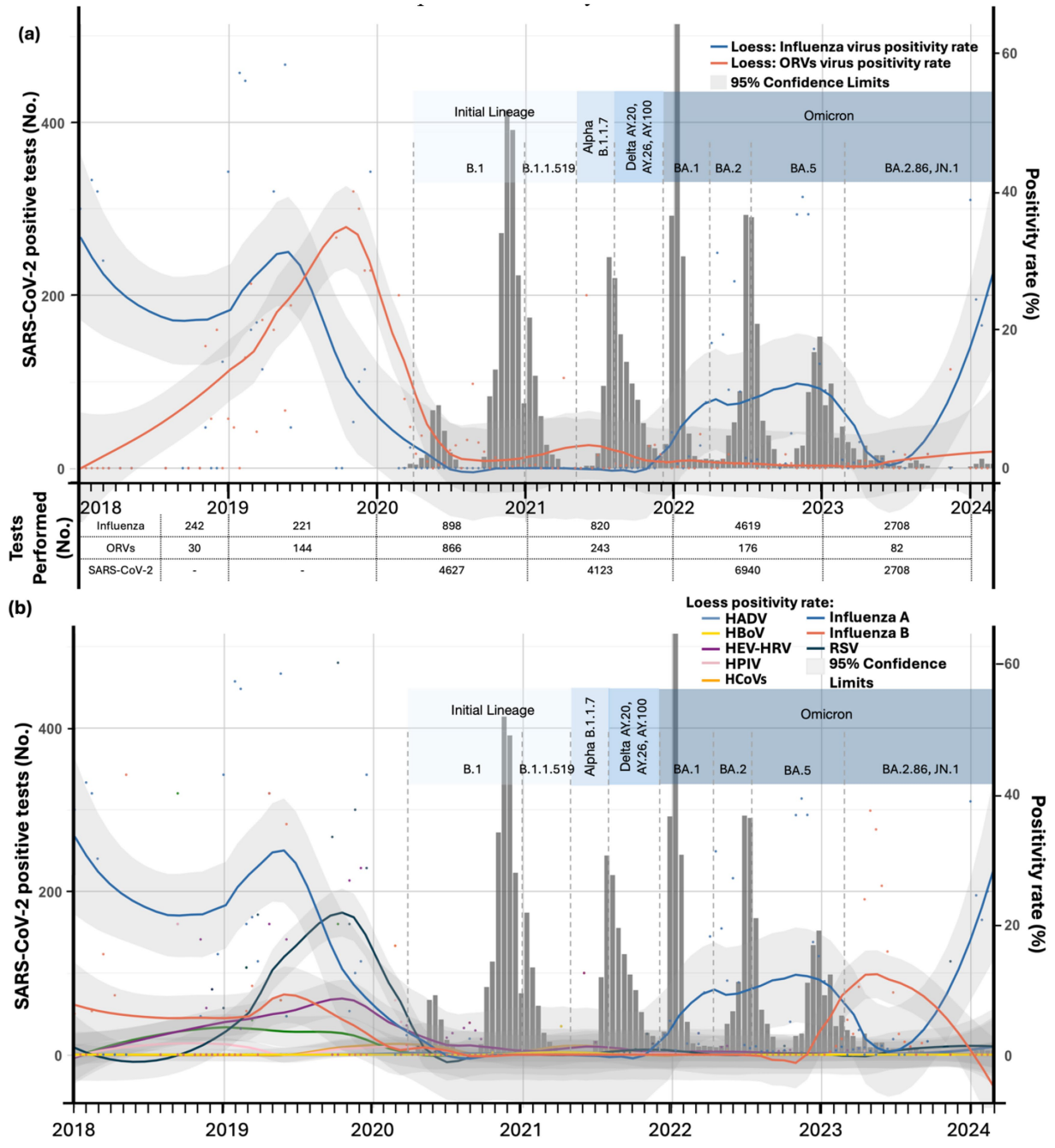

FIGURE 5
Positivity rates of influenza, other respiratory viruses (ORVs), and SARS-CoV-2 cases across pandemic years. **(A)** Positivity rates of influenza viruses and other respiratory viruses as a group, in relation to SARS-CoV-2 positive cases. **(B)** Positivity rates of influenza virus subtypes and individual respiratory viruses, in relation to SARS-CoV-2 positive cases. Dots represent raw positivity rates, while lines represent LOESS-adjusted positivity rates with 95% confidence intervals. The figure includes key SARS-CoV-2 variants detected during the timeline, contextualized with the number of tests performed each year.

associations with SARI across various subgroups. Among these, comorbidities exhibited a particularly robust relationship, with higher proportions of SARI cases observed in patients with pre-existing conditions during both periods. Notably, in the post-pandemic period, the influence of comorbidities was further accentuated, with a markedly higher proportion of SARI cases attributable to these factors. Comprehensive results from the univariate analyses, including stratifications by virus groups for both periods and by age for the post-pandemic period, are presented in Supplementary Table S3.

Figure 6A presents the adjusted odds ratios (ORs) for factors associated with SARI from the logistic regression analyses conducted during the pre-pandemic period. The analysis identified distinct risk patterns among patients with positive test results for any respiratory virus. Significant associations with SARI were observed for age, male sex, and days from symptom onset to testing ($p < 0.05$), with age

TABLE 3 Interrupted time series analysis using LOESS positivity rates for influenza, respiratory syncytial virus, human enterovirus/rhinovirus, and human adenovirus during the pre-pandemic, pandemic (2020–2021), and post-pandemic periods (2022–2023).

Variable	Influenza			Respiratory syncytial virus			Human enterovirus/ rhinovirus			Human adenovirus		
	β	SE	*p* value	*β*	SE	*p* value	*β*	SE	*p* value	*β*	SE	*p* value
Constant (β0)	45.32	1.04	<0.001	−0.96	0.29	<0.001	−0.28	0.17	0.098	−0.05	0.03	0.0840
Time (β1)	−0.60	0.04	<0.001	0.20	0.01	<0.001	0.16	0.01	<0.001	0.01	0.01	0.0030
Level												
2020–2021 (β2)	−44.16	1.860	<0.001	1.20	0.51	0.020	5.51	0.31	<0.001	0.45	0.05	<0.001
2022 (β2)	−51.76	2.44	<0.001	−0.08	0.67	0.900	0.87	0.40	0.030	−0.25	0.07	<0.001
Trend												
2020–2021 (β3)	−0.01	0.02	0.566	0.01	0.01	0.840	−0.05	0.01	<0.001	−0.01	0.01	<0.001
2022 (β3)	0.11	0.01	<0.001	0.01	0.01	0.031	−0.01	0.01	0.448	0.01	0.01	<0.001

TABLE 4 Interrupted time series analysis of SARI proportions, during the pre-pandemic, pandemic (2020–2021), and post-pandemic periods (2022–2023).

Variable	General population			Age group < 5 years			Age group 5–18 years			Age group 18–65 years			Age group > 65 years		
	β	SE	*p* value	*β*	SE	*p* value	*β*	SE	*p* value	*β*	SE	*p* value	*β*	SE	*p* value
Constant (β0)	43.26	5.83	<0.01	77.8	18.65	<0.01	52.03	11.36	<0.01	33.96	8.00	<0.01	29.85	5.48	<0.01
Time (β1)	0.49	0.12	<0.01	−0.12	0.80	0.88	0.21	0.28	0.45	1.28	0.32	<0.01	–	–	–
Level															
2020–2021 (β2)	1.93	7.19	0.79	−31.17	22.60	0.17	−15.98	14.04	0.26	5.29	9.04	0.56	45.30	7.72	<0.01
2022 (β2)	−37.45	7.09	<0.01	−27.35	20.26	0.18	−14.40	12.96	0.27	−34.73	8.90	<0.01	–	–	–
Trend															
2020–2021 (β3)	−0.21	0.08	0.01	0.00	0.34	0.99	0.08	0.17	0.65	−0.21	0.08	0.01	−0.26	0.10	<0.01
2022 (β3)	0.33	0.07	<0.01	−0.09	0.19	0.64	0.04	0.15	0.80	0.31	0.07	<0.01	0.43	0.10	<0.01

– Parameters were not estimable due to insufficient data points or collinearity during those time segments. For older adults (>65 years), the number of weekly observations in the pre-pandemic and post-2022 periods was limited, thus preventing stable estimation of the slope (Time) and level shift (Level) parameters in those intervals.

(OR = 1.04, CI: 1.02–1.06) and male sex (OR = 3.18, CI: 1.25–8.51) emerging as notable risk factors. In the influenza-specific model, Ct values from influenza RT-PCR tests demonstrated a protective effect (OR = 0.786, CI: 0.649–0.916), while obesity was strongly associated with an increased SARI risk (OR = 13.7, CI: 2.03–147.0). Conversely, the analysis of other respiratory viruses (OVRs) revealed no significant associations, with limited case numbers contributing to a low model fit (McFadden's $R^2 = 0.05$), highlighting challenges in assessing ORV-related outcomes. The complete data from the logistic regression models of the pre-pandemic period are detailed in Supplementary Table S4.

Figure 6B presents the adjusted odds ratios (ORs) from the logistic regression analyses of factors associated with SARI during the post-pandemic period. Risk factors for SARI varied significantly across age groups among patients with positive test results for any virus. Among individuals aged 0–18 years, immunosuppression emerged as a significant risk factor (OR = 3.8, CI: 1.38–11.2, $p = 0.011$), while vaccination demonstrated a robust protective effect (OR = 0.172, CI: 0.038–0.554, $p = 0.008$). In adults aged 18–65 years, key risk factors included cardiovascular disease (OR = 3.26, CI: 1.74–6.11, $p < 0.001$), diabetes (OR = 1.77, CI: 1.38–2.27, $p < 0.001$), and obesity (OR = 1.38, CI: 1.06–1.78, $p = 0.015$), while vaccination continued to demonstrate a protective association (OR = 0.291, CI: 0.221–0.381, $p < 0.001$). For individuals aged >65 years, cardiovascular disease (OR = 2.29, CI: 1.17–4.73, $p = 0.019$), obesity (OR = 2.23, CI: 1.30–3.93, $p = 0.004$), and chronic obstructive pulmonary disease (COPD; OR = 1.99, CI: 1.13–3.57, $p = 0.019$) emerged as significant risk factors, while vaccination showed a protective effect (OR = 0.594, CI: 0.377–0.927, $p = 0.023$).

The post-pandemic analysis of specific viral infections revealed further associations with SARI. For SARS-CoV-2, age (OR = 1.03, CI: 1.02–1.03, $p < 0.001$), days from symptom onset to testing (OR = 1.26, CI: 1.20–1.32, $p < 0.001$), cardiovascular disease (OR = 2.88, CI: 1.75–4.79, $p < 0.001$), and immunosuppression (OR = 2.79, CI: 1.93–4.00, $p < 0.001$) were significant risk factors, while vaccination provided robust protection (OR = 0.259, CI: 0.199–0.337, $p < 0.001$). For post-pandemic influenza, days from symptom onset to testing (OR = 1.48,

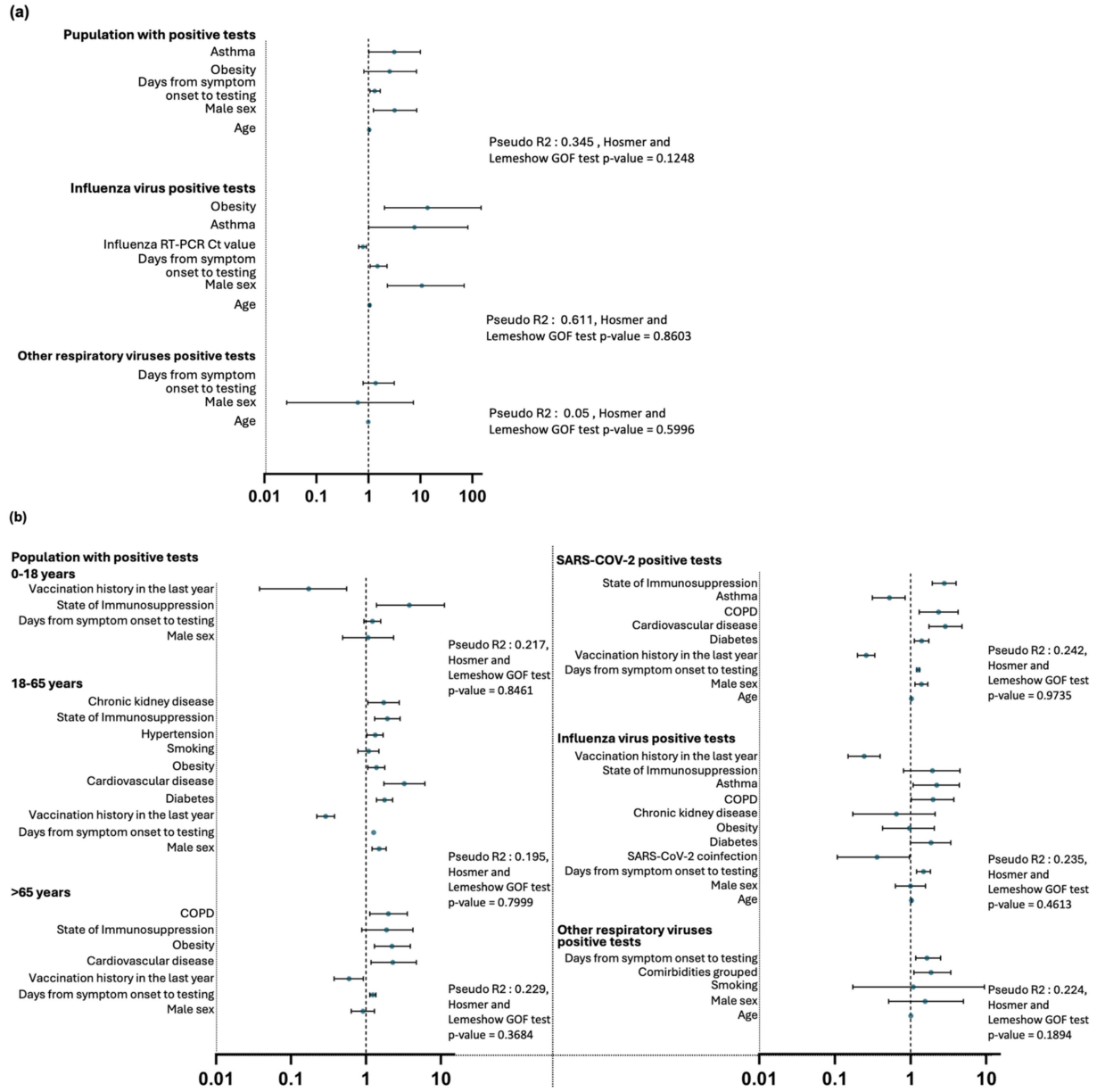

FIGURE 6
Logistic regression analyses for factors associated with SARI by time periods and virus types. **(a)** Pre-pandemic period analyses. **(b)** Post-pandemic period analyses. *GOF, Goodness-of-Fit.

CI: 1.20–1.83, $p < 0.001$) and asthma (OR = 2.22, CI: 1.08–4.42, $p = 0.026$) were associated with SARI, with vaccination again showing a protective effect (OR = 0.244, CI: 0.150–0.397, $p < 0.001$). For OVRs, days from symptom onset to testing (OR = 1.65, CI: 1.17–2.50, $p = 0.009$) and the presence of comorbidities as a group (OR = 1.86, CI: 1.11–3.41, $p = 0.027$) were significant risk factors for SARI. The complete data from the logistic regression models of the post-pandemic period are detailed in Supplementary Table S5.

4 Discussion

In our analysis, we observed significant decreases in the circulation of respiratory viruses other than SARS-CoV-2 during the pandemic period, which were tested in our institution, followed by a marked increase in influenza circulation. Additionally, we identified that the main variables associated with an increased risk of developing SARI were sociodemographic factors and comorbidities. This study enhances the limited body of knowledge on respiratory virus trends across pre-pandemic and post-pandemic periods in reference healthcare institutions, while also examining factors associated with SARI development in patients seeking care in a middle-income Latin American country.

Currently, some studies addressing this issue in reference hospitals in middle-income Latin American countries are available in the literature. A report conducted in Brazil in 2021 (45), documented a very low frequency of influenza A among hospitalized patients with ARDS during the COVID-19 pandemic, likely due to preventive

measures and high influenza vaccination coverage. Another study, conducted in a pediatric hospital in Argentina (46), reported a decrease in hospitalization rates due to acute lower respiratory tract infections in children, with no seasonal respiratory virus circulation observed during the first year of the pandemic. A third report, also from Brazil (47), examined seasonal respiratory virus trends in pediatric patients, showing a significant increase in the circulation of non-SARS-CoV-2 viruses following the relaxation of pandemic response measures. Other studies conducted in hospital units in developed countries have documented similar trends in respiratory virus circulation, showing significant decreases in positivity and diversity during the pandemic, followed by a gradual resumption of activity in the post-pandemic period. However, these studies did not perform an interrupted time series analysis on the frequency of SARI before, during, and after the COVID-19 pandemic (45–48).

Based on data obtained from our institution, we observed significant reductions in respiratory virus circulation during the pandemic period, with influenza viruses and their subtypes being particularly affected. This was followed by a notable resurgence beginning in 2022. Similarly, other respiratory viruses, distinct from influenza and SARS-CoV-2, experienced marked declines during the pandemic, primarily driven by reductions in respiratory syncytial virus (RSV) and human rhinovirus (HRV) circulation. After 2 years of historically low influenza positivity rates, a significant rebound in influenza viruses and their subtypes was documented. Likewise, other respiratory viruses showed an increase as a group after the first year of the pandemic (Figure 5A), predominantly driven by increases in rhinovirus and respiratory syncytial virus (Figure 5B). Notably, an alternating non-seasonal pattern in influenza virus subtypes emerged from 2022 onward, characterized by fluctuations between Influenza A H3 and Influenza B Victoria lineage.

These findings in our institution also align with population-based studies conducted in other regions of Latin America. For instance, countries like Chile reported historically low influenza activity during the pandemic, characterized by atypical timing and altered duration of influenza seasons (49). For instance, Chile's influenza season in 2022 began earlier than usual, predominantly with influenza A (H3N2) virus, reflecting a disruption in typical seasonal patterns (49). This disruption was also observed in other Southern Hemisphere countries, where influenza activity decreased significantly in 2020 compared to previous years (50, 51). In Europe, similar trends were noted, with a resurgence of respiratory viruses like influenza and RSV following the relaxation of NPIs (52). In Catalonia, Spain, for example, a resurgence of non-SARS-CoV-2 respiratory viruses was observed during the de-escalation of COVID-19 measures, indicating a shift in the epidemiological patterns of these viruses (52). Asia also experienced changes in respiratory virus activity, with reductions in influenza and RSV infections noted during the pandemic (53). A global analysis of respiratory viral circulation indicated that the pandemic altered the typical patterns of these viruses, leading to earlier peaks and extended durations in some regions (53).

Although post-pandemic increases were observed for both influenza and, to a lesser extent, other respiratory viruses distinct from influenza and SARS-CoV-2, positivity rates recorded at our center have not yet returned to their pre-pandemic levels or seasonal patterns at the time of this report. This phenomenon has been previously documented in a study conducted 6 years after the 2009 H1N1 pandemic in China. In that study, by comparing pre-pandemic, pandemic, and post-pandemic periods, the authors reported that the 2009 H1N1 pandemic influenced the age distribution, seasonal patterns, and peak timing of other respiratory viruses, likely due to immune interference and changes in health-seeking behavior (9).

These findings may reflect mainly the impact of public health measures implemented for infection control and changes in human behavior during the pandemic periods (54). The widespread adoption of NPIs, such as mask-wearing, social distancing, hand hygiene, travel restrictions, and school closures, played a significant role in reducing the transmission of respiratory viruses (55). These measures were initially implemented to control the spread of SARS-CoV-2 but also effectively reduced the transmission of other respiratory pathogens, including influenza and RSV (6). However, viral circulation patterns may not have been solely driven by NPIs; changes in human behavior, such as reduced mobility and increased time spent at home, may have also contributed to the decline in respiratory virus transmission (56). For example, in Hong Kong, a significant reduction in close contacts was observed, which correlated with a decrease in the effective reproduction number of influenza (56). Similar behavioral changes were noted in other regions, further supporting the role of reduced interpersonal interactions in limiting virus spread (57). There is evidence suggesting that viral interference, particularly the presence of SARS-CoV-2, may have contributed to the suppression of other respiratory viruses (57). This interference could be mediated by the host's immune response, such as the induction of interferons, and immune-mediated interference, modulation of viral replication, competition for cellular entry via ACE2 and neuropilin-1, and dysregulation of the inflammatory response, which can either suppress or enhance the replication of co-circulating viruses (21–25, 57).

The resurgence of respiratory viruses following the COVID-19 pandemic can be attributed to several factors, including the relaxation of NPIs, a decline in natural immunity due to reduced viral circulation during strict public health measures, and a resulting increase in the pool of susceptible individuals (58). Changes in human behavior and testing practices, coupled with heightened public awareness and surveillance, may have also contributed to the increased detection of infections after the most intense phases of the pandemic (59). Additionally, the overall reduction in respiratory virus transmission during the pandemic led to decreased genetic diversity in several viruses, potentially altering their evolutionary dynamics and increasing the likelihood of larger outbreaks once restrictions were lifted (60).

Furthermore, beyond the role of NPIs and behavioral changes, the interplay between host immunity, antigenic drift, and evolutionary pressures on viral strains may have contributed to post-pandemic shifts in viral circulation (61). The limited circulation of certain respiratory viruses during the pandemic likely imposed selective pressures that favored the emergence of antigenic variants, potentially influencing their post-pandemic resurgence (62). Similarly, adaptive immune responses generated by prior infections or vaccinations could have shaped susceptibility patterns and viral competition dynamics (63). Vaccination strategies may have also played a role in shaping viral interactions, as cross-protection and trained immunity from influenza and other vaccines could have temporarily influenced susceptibility patterns and viral competition (64).

Interestingly, our analysis suggested that during both the pre-pandemic and post-pandemic periods, most SARI cases were associated with male sex, the presence of various types of

comorbidities, older age, and an increase in the number of days from symptom onset to testing, which may reflect delayed diagnosis. Among these, some associations with SARI are worth highlighting, such as the presence of obesity in influenza cases during the pre-pandemic period; the association with male sex in populations testing positive for any virus, including influenza; immunosuppression status in the 0–18-year age group during the post-pandemic period; the higher association of cardiovascular disease in individuals older than 18 years; the protective effect of vaccination across subgroups; and the association between prolonged symptom duration before testing and SARI in various subgroups. These findings are consistent with previous studies that have highlighted risk factors for the development of SARI, including older age, male sex, comorbidities such as hypertension, diabetes, cardiovascular diseases, chronic respiratory diseases, and immunosuppression status (65–71).

Regarding the increase in days from symptom onset to testing and its relationship with SARI, we believe this finding should be interpreted with caution, as it may not indicate a direct causal relationship. Instead, it could reflect logistical or systemic barriers, such as delays in transportation to healthcare facilities, referral processes from other centers, or internal delays in testing and laboratory processing. This association may serve as a proxy for unmeasured factors, such as disparities in healthcare access or the severity of illness contributing to these delays. Socioeconomic disparities have been shown to affect COVID-19 screening and hospitalization rates. For instance, non-Hispanic Black patients and those from low-income neighborhoods were more likely to test positive for SARS-CoV-2 and were more frequently tested in emergency departments, which is associated with higher hospitalization rate (72). Testing accessibility is another critical factor. Disparities in access to testing can lead to underdiagnosis and delayed treatment of respiratory infections, exacerbating their severity. For example, communities with lower socioeconomic status often face barriers to testing, which can result in higher rates of undiagnosed infections and subsequent severe outcomes (73). Healthcare-seeking behavior is also shaped by socioeconomic factors. Individuals from lower socioeconomic backgrounds may delay seeking care due to financial constraints or lack of access to healthcare facilities, leading to more severe disease presentations when they do seek care (74). Further research is needed to better elucidate the potential implications of this association and the underlying mechanisms driving these delays, particularly in the context of healthcare access disparities, testing availability, and systemic barriers that may contribute to more severe disease presentations.

Although not statistically significant according to the multivariate models with the highest level of adjustment possible, co-infection with SARS-CoV-2 exhibited a trend toward a negative association in cases of influenza during the post-pandemic period. This finding contrasts with studies suggesting that co-infection with SARS-CoV-2 and influenza may increase disease severity (75). Conversely, other studies propose that co-infection does not exacerbate severity and may even mitigate it through mechanisms involving viral or immunological interference (11, 20, 76–78). However, it is important to acknowledge the inherent limitations of our study, which relies on data from a single institution rather than systematic, community-level surveillance. The study population comprises patients who sought care, and as such, it does not represent the broader community. The higher Ct values observed in SARS-CoV-2 among patients co-infected with influenza, indicating lower viral loads, could be due to competitive interactions between the two viruses. The presence of influenza virus might limit SARS-CoV-2 replication, either through direct viral interference or by triggering innate immune responses that modulate viral load dynamics (11). Previous studies have suggested that influenza virus infection may induce robust interferon-mediated antiviral responses, which could suppress SARS-CoV-2 replication in co-infected individuals (11). However, the specific mechanisms underlying this interaction remain unclear and warrant further investigation. Additionally, the testing volume from our institution alone is insufficient to draw definitive conclusions about viral interference, and this potential phenomenon was not studied at the individual level, falling beyond the scope of this study. Nevertheless, these findings underscore the need for further research to better understand the potential implications and mechanisms of viral interactions.

Another noteworthy observation was the behavior of asthma as a factor associated with SARI in patients with influenza during the post-pandemic period, which, in contrast, demonstrated a negative association with SARI in cases of confirmed SARS-CoV-2. While chronic pulmonary diseases have traditionally been linked to poor outcomes in patients with viral respiratory infections, the current consensus in the medical literature suggests that asthma does not significantly increase the risk of severe outcomes from COVID-19 for most patients (79, 80). Certain aspects of asthma may influence the course of SARS-CoV-2 infections. For example, research has shown that specific asthma phenotypes, such as allergic asthma, may have a protective effect, with allergic asthmatics being less likely to require hospitalization compared to non-allergic asthmatics (81). Additionally, some studies suggest that certain asthma treatments, such as inhaled corticosteroids, may confer a protective effect against severe COVID-19 outcomes (82). However, a systematic review indicated that adults with severe asthma, particularly those requiring high-dose inhaled corticosteroids or oral corticosteroids, face a higher risk of hospitalization from COVID-19 compared to individuals with mild asthma or no asthma (83). Further research is needed to fully elucidate the complex relationship between asthma and COVID-19.

The limitations of our study primarily stem from its retrospective design. First, while data were collected, some variables were incomplete and had to be excluded from the analyses. Additionally, certain variables intended for inclusion could not be retrieved from hospital or testing platform records. Finally, due to local guidelines prioritizing testing for respiratory viruses such as SARS-CoV-2 and influenza, the number of tests conducted for other respiratory viruses was significantly lower. This limitation restricted the scope of analyses for these subgroups. Furthermore, our study was unable to precisely differentiate between the effects of influenza and COVID-19 vaccines on SARI risk, as the vaccination history recorded in our platform did not specify the type of vaccine received. Although the registry primarily captured COVID-19 vaccination data, influenza vaccination campaigns were reinforced during the study period, preventing a stratified analysis to assess the independent contribution of each vaccine type. Additionally, our dataset did not include exact vaccination dates, limiting our ability to evaluate the potential waning of immunity over time. Similarly, we lacked complete data on the timing of prior infections, whether caused by SARS-CoV-2 or other respiratory viruses, which restricts our capacity to fully explore the interplay between previous infections, vaccination, and SARI risk.

To ensure accurate and reliable results, additional studies should be conducted prospectively in diverse regions worldwide, either at the

hospital or population level. Such studies would provide opportunities to include larger datasets and better control for confounding variables. Importantly, the findings of this study are limited to a single institution, which may constrain the generalizability of the results. Furthermore, more targeted testing strategies should be developed to explore associations with greater effect sizes, particularly in relation to respiratory virus infections other than influenza and SARS-CoV-2. Expanding on these findings requires further research within the same population and region, especially in this post-pandemic period, through prospective multicentric cohort studies. Additionally, future studies should focus on the genetic changes in RSV and influenza to assess their adaptation to reduced host exposure during the pandemic. Such research could provide valuable insights into viral evolution, inform public health strategies, and guide the development of vaccines and treatments.

In conclusion, the COVID-19 pandemic induced profound disruptions in the circulation patterns of respiratory viruses, significantly altering seasonal trends and reducing overall viral positivity rates. While post-pandemic recovery has been observed, influenza and other respiratory viruses have not fully reverted to their pre-pandemic seasonal dynamics, suggesting lasting epidemiological shifts. This study provides evidence that SARI remains strongly associated with key demographic factors and comorbidities, including advanced age, male sex, cardiovascular disease, obesity, and immunosuppression. Importantly, vaccination was consistently identified as a protective factor against SARI, reinforcing its crucial role in respiratory infection mitigation strategies. The dynamic interplay between viral competition, public health interventions, and human behavior likely contributed to the observed changes in SARI trends, emphasizing the need for ongoing surveillance and adaptive public health responses. As respiratory virus epidemiology continues to evolve in the post-pandemic era, it is imperative to sustain high-resolution surveillance efforts and refine public health policies to anticipate and mitigate future outbreaks. Strengthening vaccination programs, ensuring equitable access to diagnostic testing, and developing predictive models for respiratory virus resurgence will be critical in reducing morbidity and mortality associated with these infections. Further longitudinal studies are required to assess the long-term implications of these epidemiological shifts and to guide data-driven decision-making in infectious disease control.

Data availability statement

The raw data supporting the conclusions of this article will be made available by the authors, without undue reservation.

Ethics statement

The studies involving humans were approved by the Research Committee of the Ministry of Health of Jalisco (State Research Registry identifier: 73/LESP/JAL/2024) and the "Comité de Ética en Investigación en Ciencias de la Salud del Centro Universitario de Tlajomulco, Universidad de Guadalajara" (ethical approval number: CUTLAJO/DS/CEICS/017/24). The studies were conducted in accordance with the local legislation and institutional requirements. The ethics committee/institutional review board waived the requirement of written informed consent for participation from the participants or the participants' legal guardians/next of kin because the study was performed retrospectively and only deidentified data were used.

Author contributions

JA-J: Conceptualization, Data curation, Investigation, Writing – original draft. PM-A: Data curation, Investigation, Methodology, Writing – original draft. EQ-S: Data curation, Investigation, Writing – original draft. RL-R: Data curation, Investigation, Writing – original draft. JB-R: Formal analysis, Methodology, Software, Supervision, Visualization, Writing – review & editing.

Funding

The author(s) declare that no financial support was received for the research and/or publication of this article.

Conflict of interest

The authors declare that the research was conducted in the absence of any commercial or financial relationships that could be construed as potential conflicts of interest.

Publisher's note

Supplementary material

The Supplementary material for this article can be found online at: https://www.frontiersin.org/articles/10.3389/fpubh.2025.1494463/full#supplementary-material

References

1. Heiskanen A, Galipeau Y, Little J, Mortimer L, Ramotar K, Langlois MA, et al. Seasonal respiratory virus circulation was diminished during the COVID-19 pandemic. *Influenza Other Respir Viruses*. (2023) 17:17. doi: 10.1111/IRV.13065

2. Li Y, Reeves RM, Wang X, Bassat Q, Brooks WA, Cohen C, et al. Global patterns in monthly activity of influenza virus, respiratory syncytial virus, parainfluenza virus, and metapneumovirus: a systematic analysis. *Lancet Glob Health*. (2019) 7:e1031–45. doi: 10.1016/S2214-109X(19)30264-5

3. Agca H, Akalin H, Saglik I, Hacimustafaoglu M, Celebi S, Ener B. Changing epidemiology of influenza and other respiratory viruses in the first year of COVID-19 pandemic. *J Infect Public Health*. (2021) 14:1186–90. doi: 10.1016/j.jiph.2021.08.004

4. Stamm P, Sagoschen I, Weise K, Plachter B, Münzel T, Gori T, et al. Influenza and RSV incidence during COVID-19 pandemic—an observational study from in-hospital point-of-care testing. *Med Microbiol Immunol*. (2021) 210:277–82. doi: 10.1007/s00430-021-00720-7

5. Liu P, Xu M, Lu L, Ma A, Cao L, Su L, et al. The changing pattern of common respiratory and enteric viruses among outpatient children in Shanghai, China: two years of the COVID-19 pandemic. *J Med Virol*. (2022) 94:4696–703. doi: 10.1002/jmv.27896

6. Olsen SJ, Winn AK, Budd AP, Prill MM, Steel J, Midgley CM, et al. Changes in influenza and other respiratory virus activity during the COVID-19 pandemic - United States, 2020-2021. *MMWR Morb Mortal Wkly Rep*. (2021) 70:1013–9. doi: 10.15585/MMWR.MM7029A1

7. Treggiari D, Piubelli C, Formenti F, Silva R, Perandin F. Resurgence of respiratory virus after relaxation of COVID-19 containment measures: a real-world data study from a regional Hospital of Italy. *Int J Microbiol*. (2022) 2022:1–5. doi: 10.1155/2022/4915678

8. Weinberger Opek M, Yeshayahu Y, Glatman-Freedman A, Kaufman Z, Sorek N, Brosh-Nissimov T. Delayed respiratory syncytial virus epidemic in children after relaxation of COVID-19 physical distancing measures, Ashdod, Israel, 2021. *Euro Surveill*. (2021) 26, 1–5. doi: 10.2807/1560-7917.ES.2021.26.29.2100706

9. Yang L, Chan KH, Suen LKP, Chan KP, Wang X, Cao P, et al. Impact of the 2009 H1N1 pandemic on age-specific epidemic curves of other respiratory viruses: a comparison of pre-pandemic, pandemic and post-pandemic periods in a subtropical city. *PLoS One*. (2015) 10:1–11. doi: 10.1371/journal.pone.0125447

10. Cheng Y, Ma N, Witt C, Rapp S, Wild PS, Andreae MO, et al. Face masks effectively limit the probability of SARS-CoV-2 transmission. *Science*. (2021) 372:1439–43. doi: 10.1126/SCIENCE.ABG6296

11. Gilbert-Girard S, Piret J, Carbonneau J, Hénaut M, Goyette N, Boivin G. Viral interference between severe acute respiratory syndrome coronavirus 2 and influenza a viruses. *PLoS Pathog*. (2024) 20:e1012017. doi: 10.1371/JOURNAL.PPAT.1012017

12. Nickbakhsh S, Mair C, Matthews L, Reeve R, Johnson PCD, Thorburn F, et al. Virus-virus interactions impact the population dynamics of influenza and the common cold. *Proc Natl Acad Sci USA*. (2019) 116:27142–50. doi: 10.1073/PNAS.1911083116

13. Yeoh DK, Foley DA, Minney-Smith CA, Martin AC, MacE AO, Sikazwe CT, et al. Impact of coronavirus disease 2019 public health measures on detections of influenza and respiratory syncytial virus in children during the 2020 Australian winter. *Clin Infect Dis*. (2021) 72:2199–202. doi: 10.1093/CID/CIAA1475

14. Yang B, Huang AT, Garcia-Carreras B, Hart WE, Staid A, Hitchings MDT, et al. Effect of specific non-pharmaceutical intervention policies on SARS-CoV-2 transmission in the counties of the United States. *Nat Commun*. (2021) 12:1–10. doi: 10.1038/s41467-021-23865-8

15. Piret J, Boivin G. Viral interference between respiratory viruses. *Emerg Infect Dis*. (2022) 28:273–81. doi: 10.3201/EID2802.211727

16. Fage C, Hénaut M, Carbonneau J, Piret J, Boivin G. Influenza a(H1N1)pdm09 virus but not respiratory syncytial virus interferes with SARS-CoV-2 replication during sequential infections in human nasal epithelial cells. *Viruses*. (2022) 14:1–11. doi: 10.3390/V14020395

17. Zhang J, Tan S, Peng C, Xu X, Wang M, Lu W, et al. Heterogeneous changes in mobility in response to the SARS-CoV-2 omicron BA.2 outbreak in Shanghai. *Proc Natl Acad Sci USA*. (2023) 120:1–8. doi: 10.1073/pnas.2306710120

18. Komarova NL, Azizi A, Wodarz D. Network models and the interpretation of prolonged infection plateaus in the COVID19 pandemic. *Epidemics*. (2021) 35:100463. doi: 10.1016/J.EPIDEM.2021.100463

19. Dee K, Schultz V, Haney J, Bissett LA, Magill C, Murcia PR. Influenza a and respiratory syncytial virus trigger a cellular response that blocks severe acute respiratory syndrome virus 2 infection in the respiratory tract. *J Infect Dis*. (2023) 227:1396–406. doi: 10.1093/INFDIS/JIAC494

20. Cheemarla NR, Watkins TA, Mihaylova VT, Foxman EF. Viral interference during influenza A-SARS-CoV-2 coinfection of the human airway epithelium and reversal by oseltamivir. *J Infect Dis*. (2024) 229:1430–4. doi: 10.1093/INFDIS/JIAD402

21. Zhang J, Ejikemeuwa A, Gerzanich V, Nasr M, Tang Q, Simard JM, et al. Understanding the role of SARS-CoV-2 ORF3a in viral pathogenesis and COVID-19. *Front Microbiol*. (2022) 13:13. doi: 10.3389/FMICB.2022.854567

22. Savastano A, Ibáñez de Opakua A, Rankovic M, Zweckstetter M. Nucleocapsid protein of SARS-CoV-2 phase separates into RNA-rich polymerase-containing condensates. *Nat Commun*. (2020) 11:1–10. doi: 10.1038/s41467-020-19843-1

23. Zhang Q, Xiang R, Huo S, Zhou Y, Jiang S, Wang Q, et al. Molecular mechanism of interaction between SARS-CoV-2 and host cells and interventional therapy. *Signal Transduct Target Ther*. (2021) 6:233. doi: 10.1038/S41392-021-00653-W

24. Boechat JL, Chora I, Morais A, Delgado L. The immune response to SARS-CoV-2 and COVID-19 immunopathology – current perspectives. *Pulmonol*. (2021) 27:423–37. doi: 10.1016/J.PULMOE.2021.03.008

25. Gusev E, Sarapultsev A, Solomatina L, Chereshnev V. SARS-CoV-2-specific immune response and the pathogenesis of COVID-19. *Int J Mol Sci*. (2022) 23:23. doi: 10.3390/IJMS23031716

26. Boussarsar M, Ennouri E, Habbachi N, Bouguezzi N, Meddeb K, Gallas S, et al. Epidemiology and burden of severe acute respiratory infections (SARI) in the aftermath of COVID-19 pandemic: a prospective sentinel surveillance study in a Tunisian medical ICU, 2022/2023. *PLoS One*. (2023) 18:e0294960. doi: 10.1371/JOURNAL.PONE.0294960

27. Orosz N, Gömöri G, Battamir U, Nagy AC. Hospital-based cross-sectional study on the clinical characteristics of children with severe acute respiratory infections in Hungary. *BMC Infect Dis*. (2024) 24:1268. doi: 10.1186/S12879-024-10186-6/TABLES/3

28. Nguyen-Van-tam JS, O'leary M, Martin ET, Heijnen E, Callendret B, Fleischhackl R, et al. Burden of respiratory syncytial virus infection in older and high-risk adults: a systematic review and meta-analysis of the evidence from developed countries. *Eur Respir Rev*. (2022) 31:220105. doi: 10.1183/16000617.0105-2022

29. Pijls BG, Jolani S, Atherley A, Derckx RT, Dijkstra JIR, Franssen GHL, et al. Demographic risk factors for COVID-19 infection, severity, ICU admission and death: a meta-analysis of 59 studies. *BMJ Open*. (2021) 11:e044640. doi: 10.1136/bmjopen-2020-044640

30. van Kerkhove MD, Vandemaele KAH, Shinde V, Jaramillo-Gutierrez G, Koukounari A, Donnelly CA, et al. Risk factors for severe outcomes following 2009 influenza a (H1N1) infection: a global pooled analysis. *PLoS Med*. (2011) 8:1–12. doi: 10.1371/JOURNAL.PMED.1001053

31. Matera L, Manti S, Petrarca L, Pierangeli A, Conti MG, Mancino E, et al. An overview on viral interference during SARS-CoV-2 pandemic. *Front Pediatr*. (2023) 11:1308105. doi: 10.3389/fped.2023.1308105

32. Desforges M, Le Coupanec A, Dubeau P, Bourgouin A, Lajoie L, Dubé M, et al. Human coronaviruses and other respiratory viruses: underestimated opportunistic pathogens of the central nervous system? *Viruses*. (2019) 12:1–28. doi: 10.3390/v12010014

33. Gabutti G, De Motoli F, Sandri F, Toffoletto MV, Stefanati A. Viral respiratory infections in hematological patients. *Infect Dis Ther*. (2020) 9:495–510. doi: 10.1007/s40121-020-00313-6

34. Azoulay E, Russell L, Van de Louw A, Metaxa V, Bauer P, Povoa P, et al. Diagnosis of severe respiratory infections in immunocompromised patients. *Intensive Care Med*. (2020) 46:298–314. doi: 10.1007/s00134-019-05906-5

35. Seemungal T, Harper-Owen R, Bhowmik A, Moric I, Sanderson G, Message S, et al. Respiratory viruses, symptoms, and inflammatory markers in acute exacerbations and stable chronic obstructive pulmonary disease. *Am J Respir Crit Care Med*. (2001) 164:1618–23. doi: 10.1164/ajrccm.164.9.2105011

36. Cillóniz C, Pericàs JM, Rojas JR, Torres A. Severe infections due to respiratory viruses. *Semin Respir Crit Care Med*. (2022) 43:060–74. doi: 10.1055/s-0041-1740982

37. Zhang AJ, Lee ACY, Chan JFW, Liu F, Li C, Chen Y, et al. Coinfection by severe acute respiratory syndrome coronavirus 2 and influenza a(H1N1)pdm09 virus enhances the severity of pneumonia in Golden Syrian hamsters. *Clin Infect Dis*. (2021) 72:E978–92. doi: 10.1093/cid/ciaa1747

38. Ciotti M, Maurici M, Santoro V, Coppola L, Sarmati L, De Carolis G, et al. Viruses of respiratory tract: an observational retrospective study on hospitalized patients in Rome, Italy. *Microorganisms*. (2020) 8:1–13. doi: 10.3390/MICROORGANISMS8040501

39. Laurie KL, Horman W, Carolan LA, Chan KF, Layton D, Bean A, et al. Evidence for viral interference and cross-reactive protective immunity between influenza B virus lineages. *J Infect Dis*. (2018) 217:548–59. doi: 10.1093/infdis/jix509

40. Achangwa C, Park H, Ryu S, Lee MS. Collateral impact of public health and social measures on respiratory virus activity during the COVID-19 pandemic 2020–2021. *Viruses*. (2022) 14:1–10. doi: 10.3390/v14051071

41. Instituto de Diagnóstico y Referencia Epidemiológicos. Lineamientos para la vigilancia por laboratorio de virus respiratorios (Versión 2). Ciudad de México.: Secretaría de Salud (2024).

42. Secretaría de Salud, Subsecretaría de Prevención y Promoción de la Salud. Lineamiento Estandarizado para la Vigilancia Epidemiológica y por Laboratorio de la Enfermedad Respiratoria Viral. México: Dirección General de Epidemiología (2023).

43. Instituto de Diagnóstico y Referencia Epidemiológicos. Lineamientos para la vigilancia de Influenza por laboratorio (Versión 1). Ciudad de México, México: Secretaría de Salud (2015, 2024).

44. Secretaría de Salud, Subsecretaría de Prevención y Promoción de la Salud. Lineamiento Estandarizado para la Vigilancia Epidemiológica y por Laboratorio de la Enfermedad Respiratoria Viral. Ciudad de México: Dirección General de Epidemiología (2020).

45. Eisen AKA, Gularte JS, Demoliner M, De Abreu Goés Pereira VM, Heldt FH, Filippi M, et al. Low circulation of influenza a and coinfection with SARS-CoV-2 among other respiratory viruses during the COVID-19 pandemic in a region of southern Brazil. *J Med Virol*. (2021) 93:4392–8. doi: 10.1002/JMV.26975

46. Orqueda AS, Bollón LR, Mistchenko AS. Impact of COVID-19 on the circulation of respiratory viruses in a children's hospital: an expected absence. *Arch Argent Pediatr*. (2022) 120:99–105. doi: 10.5546/AAP.2022.ENG.99

47. Lima AKS, Banho CA, Sacchetto L, de Carvalho MB, dos Santos MG, Ribeiro MR, et al. Seasonal respiratory virus trends in pediatric patients during the COVID-19 pandemic in Brazil. *Braz J Microbiol*. (2023) 54:1827–34. doi: 10.1007/S42770-023-01087-Y

48. Brañas P, Muñoz-Gallego I, Espartosa E, Moral N, Abellán G, Folgueira L. Dynamics of respiratory viruses other than SARS-CoV-2 during the COVID-19 pandemic in Madrid, Spain. *Influenza Other Respir Viruses*. (2023) 17:17. doi: 10.1111/IRV.13199

49. Olivares Barraza MF, Fasce RA, Nogareda F, Marcenac P, Vergara Mallegas N, Bustos Alister P, et al. Influenza incidence and vaccine effectiveness during the Southern hemisphere influenza season - Chile, 2022. *MMWR Morb Mortal Wkly Rep*. (2022) 71:1353–8. doi: 10.15585/MMWR.MM7143A1

50. Kim J, Gómez Gómez RE, Hong K, Yum S, Jang J, Chun BC. Changing influenza activity in the Southern hemisphere countries during the COVID-19 pandemic. *Int J Infect Dis*. (2021) 108:109–11. doi: 10.1016/J.IJID.2021.05.039

51. Olsen SJ, Azziz-Baumgartner E, Budd AP, Brammer L, Sullivan S, Pineda RF, et al. Decreased influenza activity during the COVID-19 pandemic - United States, Australia, Chile, and South Africa, 2020. *MMWR Morb Mortal Wkly Rep*. (2020) 69:1305–9. doi: 10.15585/MMWR.MM6937A6

52. Guadalupe-Fernández V, Martínez-Solanas E, Sabrià-Sunyé A, Ferrer-Mikoly C, Martínez-Mateo A, Ciruela-Navas P, et al. Investigating epidemiological distribution (temporality and intensity) of respiratory pathogens following COVID-19 de-escalation process in Catalonia, September 2016-June 2021: analysis of regional surveillance data. *PLoS One*. (2024) 19:e0285892. doi: 10.1371/journal.pone.0285892

53. Del Riccio M, Caini S, Bonaccorsi G, Lorini C, Paget J, van der Velden K, et al. Global analysis of respiratory viral circulation and timing of epidemics in the pre-COVID-19 and COVID-19 pandemic eras, based on data from the global influenza surveillance and response system (GISRS). *Int J Infect Dis*. (2024) 144:107052. doi: 10.1016/j.ijid.2024.107052

54. Qi Y, Shaman J, Pei S. Quantifying the impact of COVID-19 nonpharmaceutical interventions on influenza transmission in the United States. *J Infect Dis*. (2021) 224:1500–8. doi: 10.1093/INFDIS/JIAB485

55. Li ZJ, Yu LJ, Zhang HY, Shan CX, Bin LQ, Zhang XA, et al. (COVID-19) pandemic on acute respiratory infections in China: an observational study. *Clin Infect Dis*. (2019) 75:E1054–62. doi: 10.1093/CID/CIAB942

56. Zhang N, Jia W, Lei H, Wang P, Zhao P, Guo Y, et al. Effects of human behavior changes during the coronavirus disease 2019 (COVID-19) pandemic on influenza spread in Hong Kong. *Clin Infect Dis*. (2021) 73:E1142–50. doi: 10.1093/CID/CIAA1818

57. Han S, Zhang T, Lyu Y, Lai S, Dai P, Zheng J, et al. Influenza's plummeting during the COVID-19 pandemic: the roles of mask-wearing, mobility change, and SARS-CoV-2 interference. *Engineering (Beijing)*. (2023) 21:195–202. doi: 10.1016/J.ENG.2021.12.011

58. Munro APS, House T. Cycles of susceptibility: immunity debt explains altered infectious disease dynamics post -pandemic. *Clin Infect Dis*. (2024). doi: 10.1093/CID/CIAE493

59. Petros BA, Milliren CE, Sabeti PC, Ozonoff A. Increased pediatric respiratory syncytial virus case counts following the emergence of SARS-CoV-2 can be attributed to changes in testing. *Clin Infect Dis*. (2024) 78:1707–17. doi: 10.1093/CID/CIAE140

60. Chow EJ, Uyeki TM, Chu HY. The effects of the COVID-19 pandemic on community respiratory virus activity. *Nat Rev Microbiol*. (2023) 21:195–210. doi: 10.1038/S41579-022-00807-9

61. Perofsky AC, Huddleston J, Hansen CL, Barnes JR, Rowe T, Xu X, et al. Antigenic drift and subtype interference shape a(H3N2) epidemic dynamics in the United States. *eLife*. (2024) 13:13. doi: 10.7554/ELIFE.91849

62. Xu C, Zhang N, Yang Y, Liang W, Zhang Y, Wang J, et al. Immune escape adaptive mutations in hemagglutinin are responsible for the antigenic drift of Eurasian avian-like H1N1 swine influenza viruses. *J Virol*. (2022) 96:e0097122. doi: 10.1128/jvi.00971-22

63. Marchi J, Lässig M, Walczak AM, Mora T. Antigenic waves of virus-immune coevolution. *Proc Natl Acad Sci USA*. (2021) 118:1–8. doi: 10.1073/PNAS.2103398118

64. Domnich A, Orsi A, Sticchi L, Panatto D, Dini G, Ferrari A, et al. Effect of the 2020/21 season influenza vaccine on SARS-CoV-2 infection in a cohort of Italian healthcare workers. *Vaccine*. (2022) 40:1755–60. doi: 10.1016/J.VACCINE.2022.02.013

65. Cilloniz C, Torres A, Luna CM, Hurtado JC, Marcos MÁ. Respiratory viruses: their importance and lessons learned from COVID-19. *Eur Respir Rev*. (2022) 31:220051. doi: 10.1183/16000617.0051-2022

66. Sliedrecht A, Den Elzen WPJ, Verheij TJM, Westendorp RGJ, Gussekloo J. Incidence and predictive factors of lower respiratory tract infections among the very elderly in the general population. The Leiden 85-plus study. *Thorax*. (2008) 63:817–22. doi: 10.1136/THX.2007.093013

67. Kim YJ, Guthrie KA, Waghmare A, Walsh EE, Falsey AR, Kuypers J, et al. Respiratory syncytial virus in hematopoietic cell transplant recipients: factors determining progression to lower respiratory tract disease. *J Infect Dis*. (2014) 209:1195–204. doi: 10.1093/INFDIS/JIT832

68. Lu L, Zhong W, Bian Z, Li Z, Zhang K, Liang B, et al. A comparison of mortality-related risk factors of COVID-19, SARS, and MERS: a systematic review and meta-analysis. *J Inf Secur*. (2020) 81:e18–25. doi: 10.1016/J.JINF.2020.07.002

69. Zhou F, Yu T, Du R, Fan G, Liu Y, Liu Z, et al. Clinical course and risk factors for mortality of adult inpatients with COVID-19 in Wuhan, China: a retrospective cohort study. *Lancet*. (2020) 395:1054–62. doi: 10.1016/S0140-6736(20)30566-3

70. Kojima N, Taylor CA, Tenforde MW, Ujamaa D, O'Halloran A, Patel K, et al. Clinical outcomes of US adults hospitalized for COVID-19 and influenza in the respiratory virus hospitalization surveillance network, October 2021-September 2022. *Open Forum Infect Dis*. (2023) 11:1–4. doi: 10.1093/OFID/OFAD702

71. Kuypers J. Impact of rapid molecular detection of respiratory viruses on clinical outcomes and patient management. *J Clin Microbiol*. (2019) 57:57. doi: 10.1128/JCM.01890-18

72. Dalton JE, Gunzler DD, Jain V, Perzynski AT, Dawson NV, Einstadter D, et al. Mechanisms of socioeconomic differences in COVID-19 screening and hospitalizations. *PLoS One*. (2021) 16:e0255343. doi: 10.1371/JOURNAL.PONE.0255343

73. Wei R, Zhang Y, Gao S, Brown BJ, Hu S, Link BG. Health disparity in the spread of COVID-19: evidence from social distancing, risk of interactions, and access to testing. *Health Place*. (2023) 82:103031. doi: 10.1016/J.HEALTHPLACE.2023.103031

74. Zheng W, Kämpfen F, Huang Z. Health-seeking and diagnosis delay and its associated factors: a case study on COVID-19 infections in Shaanxi Province, China. *Sci Rep*. (2021) 11:17331. doi: 10.1038/S41598-021-96888-2

75. Yan X, Li K, Lei Z, Luo J, Wang Q, Wei S. Prevalence and associated outcomes of coinfection between SARS-CoV-2 and influenza: a systematic review and meta-analysis. *Int J Infect Dis*. (2023) 136:29–36. doi: 10.1016/J.IJID.2023.08.021

76. Dao TL, Hoang VT, Colson P, Million M, Gautret P. Co-infection of SARS-CoV-2 and influenza viruses: a systematic review and meta-analysis. *J Clin Virology Plus*. (2021) 1:100036. doi: 10.1016/J.JCVP.2021.100036

77. Guan Z, Chen C, Li Y, Yan D, Zhang X, Jiang D, et al. Impact of coinfection with SARS-CoV-2 and influenza on disease severity: a systematic review and Meta-analysis. *Front Public Health*. (2021) 9:9. doi: 10.3389/FPUBH.2021.773130

78. Chekuri S, Szymczak WA, Goldstein DY, Nori P, Marrero Rolon R, Spund B, et al. SARS-CoV-2 coinfection with additional respiratory virus does not predict severe disease: a retrospective cohort study. *J Antimicrob Chemother*. (2021) 76:iii12–9. doi: 10.1093/JAC/DKAB244

79. Aggarwal AN, Agarwal R, Dhooria S, Prasad KT, Sehgal IS, Muthu V. Impact of asthma on severity and outcomes in COVID-19. *Respir Care*. (2021) 66:1912–23. doi: 10.4187/RESPCARE.09113

80. Terry PD, Heidel RE, Dhand R. Asthma in adult patients with COVID-19. Prevalence and risk of severe disease. *Am J Respir Crit Care Med*. (2021) 203:893–905. doi: 10.1164/RCCM.202008-3266OC

81. Eggert LE, He Z, Collins W, Lee AS, Dhondalay G, Jiang SY, et al. Asthma phenotypes, associated comorbidities, and long-term symptoms in COVID-19. *Allergy*. (2022) 77:173–85. doi: 10.1111/ALL.14972

82. Izquierdo JL, Almonacid C, González Y, Del Rio-Bermudez C, Ancochea J, Cárdenas R, et al. The impact of COVID-19 on patients with asthma. *Eur Respir J*. (2021) 57:2003142. doi: 10.1183/13993003.03142-2020

83. Lee B, Lewis G, Agyei-Manu E, Atkins N, Bhattacharyya U, Dozier M, et al. Risk of serious COVID-19 outcomes among adults and children with moderate-to-severe asthma: a systematic review and meta-analysis. *Eur Respir Rev*. (2022) 31:220066. doi: 10.1183/16000617.0066-2022

10.3389/fpubh.2025.1494463

Glossary

ARDS - Acute respiratory distress syndrome

COPD - Chronic obstructive pulmonary disease

GOF - Goodness-of-Fit

HAdV - Human adenovirus

HBoV - Human bocavirus

HCoV-229E - Human coronavirus 229E

HCoV-HKU1 - Human coronavirus HKU1

HCoV-OC43 - Human coronavirus OC43

HCoV-NL63 - Human coronavirus NL63

HEV/HRV - Human enterovirus/rhinovirus

hMPV - Human metapneumovirus

HPIV - Human parainfluenza virus

HPIV1 - Human parainfluenza virus 1

HPIV2 - Human parainfluenza virus 2

HPIV3 - Human parainfluenza virus 3

HPIV4 - Human parainfluenza virus 4

ILI - Influenza-like illness

INFAH3 - Influenza A virus H3

INFAH1N1 - Influenza A virus H1N1

INFBVIC - Influenza B Victoria lineage

INFBYAM - Influenza B Yamagata lineage

ORVs. Other respiratory viruses (distinct from SARS-CoV-2 and influenza virus)

RSV - Respiratory syncytial virus

RT–PCR - Real-time polymerase chain reaction

SARIs - Severe acute respiratory infections

SARS-CoV-2 - Severe acute respiratory syndrome coronavirus 2

frontiers | Frontiers in Public Health

TYPE Original Research
PUBLISHED 02 April 2025
DOI 10.3389/fpubh.2025.1492653

OPEN ACCESS

EDITED BY
Paraskevi C. Fragkou,
Evangelismos General Hospital, Greece

REVIEWED BY
Nadim Sharif,
Jahangirnagar University, Bangladesh
Muhammad Masroor Alam,
National Institute of Health, Pakistan

*CORRESPONDENCE
Nabeel Alzahrani
✉ Alzahranin@ksau-hs.edu.sa

RECEIVED 07 September 2024
ACCEPTED 17 March 2025
PUBLISHED 02 April 2025

CITATION
Alzahrani N, Alshehri A, Alshehri A and Al Johani S (2025) Epidemiology, co-infection, and seasonal patterns of respiratory tract infections in a tertiary care center in Saudi Arabia between 2021 and 2022.
Front. Public Health 13:1492653.
doi: 10.3389/fpubh.2025.1492653

Epidemiology, co-infection, and seasonal patterns of respiratory tract infections in a tertiary care center in Saudi Arabia between 2021 and 2022

Nabeel Alzahrani[1,2,3]*, Ahmed Alshehri[3], Ali Alshehri[3] and Sameera Al Johani[2,3]

[1]Department of Clinical Laboratory Sciences, College of Applied Medical Sciences, King Saud bin Abdulaziz University for Health Sciences, Riyadh, Saudi Arabia, [2]King Abdullah International Medical Research Center, Riyadh, Saudi Arabia, [3]Division of Microbiology, Department of Pathology and Laboratory Medicine, Ministry of the National Guard-Health Affairs, Riyadh, Saudi Arabia

Objectives: To investigate the etiology and epidemiological trends of respiratory tract infections (RTIs) during the COVID-19 pandemic in Saudi Arabia, focusing on age and seasonality.

Methods: We conducted a retrospective analysis of 19,509 respiratory specimens collected from January 2021 to December 2022 at King Abdulaziz Medical City, Riyadh, using the BioFire Filmarray Respiratory Panel 2.1 plus kit.

Results: Of the analyzed specimens, 53.3% (10,406) tested positive for at least one pathogen. Pediatric patients represented 72.5% of positive cases. Rhinovirus/enterovirus (32%) was the most prevalent, followed by SARS-CoV-2 (16%), respiratory syncytial virus (RSV; 13%), and adenovirus (10%).

Conclusions: The study underscores the significant seasonality and age-specific prevalence of RTIs, with winter peaks and a high incidence of rhinovirus/enterovirus, SARS-CoV-2, RSV, and adenovirus. These results emphasize the necessity of ongoing surveillance and targeted public health interventions to manage RTIs effectively.

KEYWORDS

infectious disease epidemiology, multiplex PCR, respiratory viruses, seasonality, Saudi Arabia

1 Background

Respiratory tract infections (RTIs) are one of the most common infections and are a leading cause of morbidity and mortality worldwide. They can cause disease in all age groups; nonetheless, children <5 years old, older adults, and individuals with underlying morbidities are among the most vulnerable. Acute respiratory failure and acute respiratory distress syndrome are serious conditions that can be brought on by respiratory infections. While respiratory viruses such as rhinovirus, parainfluenza viruses, adenovirus, human bocavirus, and seasonal coronaviruses are known to cause mild upper respiratory tract infections, influenza A and B viruses and respiratory syncytial virus (RSV) account for the majority of deaths and hospitalizations.

The COVID-19 pandemic has profoundly impacted the epidemiology of respiratory viruses due to widespread public health interventions such as lockdowns, mask mandates,

and social distancing (1–5). Several international studies have examined RTI patterns during the COVID-19 era. Reports from Taiwan and Switzerland found that, in addition to SARS-CoV-2, rhinovirus/enterovirus remained the dominant pathogen despite extensive public health measures, whereas influenza detection declined significantly (1, 3). In contrast, a study conducted in Turkey observed a sharp drop in influenza cases during the pandemic, indicating regional variability in RTI trends (6). A systematic review of global RTI prevalence also highlighted the sustained circulation of rhinoviruses and enteroviruses, which were less affected by pandemic interventions than other respiratory viruses (7). In the Middle East, RTI epidemiological data remain scarce. Studies from Lebanon and Qatar have reported high rates of rhinovirus, influenza, and adenovirus infections among hospitalized patients (8, 9).

Previous research from Saudi Arabia has focused primarily on pediatric RTI cases, with findings indicating that RSV and adenovirus were the most commonly detected pathogens in children (10–12). However, few studies have comprehensively analyzed RTI epidemiology across all age groups in the region, particularly during the COVID-19 era.

The seasonality of respiratory infections is a well-documented phenomenon and is impacted by a number of variables, such as human behavior, virus features, and environmental influences (10). In temperate regions, infections like influenza and the common cold peak in winter, while in tropical areas, patterns vary, often aligning with rainy seasons (11, 12). Cold temperatures and low humidity enhance viral stability and transmission, while increased indoor activity facilitates spread. Additionally, viruses like influenza and RSV undergo genetic drift and shift, driving seasonal outbreaks as immunity wanes (13).

In Saudi Arabia, respiratory infection seasonality is shaped by its unique climate and cultural events, such as the annual Hajj pilgrimage. A study of children with respiratory tract infections in Riyadh (2013–2014) found viral pathogens in 24% of cases, with RSV being most common and peaking in winter.

This study demonstrated the importance of viral pathogens in RTIs, noting a peak in virus detection during the winter months (14).

This emphasizes the need for continuous surveillance and tailored public health interventions, especially considering the country's role as a host for large-scale religious gatherings, which poses unique challenges for disease control and prevention.

In this study, the etiology and epidemiological parameters of RTIs, including age and seasonality, in all patients tested using multiplex polymerase chain reaction (PCR) in King Abdulaziz Medical City in Riyadh, Saudi Arabia, between January 2021 and December 2022 were investigated. We aimed to evaluate the age, gender, pathogen distribution, and seasonality of respiratory pathogens during the COVID-19 pandemic.

2 Materials and methods

King Abdulaziz Medical City (KAMC) is part of the Ministry of National Guard Health Affairs and is an advanced 2,500-bed tertiary health facility located in Riyadh, Saudi Arabia. Respiratory specimens, including nasopharyngeal swabs, bronchoalveolar lavage, sputum, and tracheal aspirates, were collected from patients presenting to our hospital with respiratory illness from January 2021 to December 2022 and tested using the BioFire Filmarray Respiratory Panel 2.1 plus (RP2.1 plus) kit (BioFire®Diagnostics, Salt Lake City, UT, USA) run on the BioFire Torch System instrument as per the manufacturer's instructions. The RP2.1 plus kit is intended for the detection and differentiation of nucleic acid from the following organisms: Adenovirus, coronavirus 229E, coronavirus HKU1, coronavirus NL63, coronavirus OC43, Middle East respiratory syndrome coronavirus (MERS-CoV), severe acute respiratory syndrome coronavirus 2 (SARS-CoV-2), human metapneumovirus, human rhinovirus/enterovirus, influenza A virus, influenza A virus A/H1, influenza A virus A/H3, influenza A virus A/H1-2009, influenza B virus, parainfluenza virus 1, parainfluenza virus 2, parainfluenza virus 3, parainfluenza virus 4, respiratory syncytial virus, *Bordetella parapertussis, Bordetella pertussis, Chlamydia pneumoniae*, and *Mycoplasma pneumoniae*. The BioFire RP2.1 Plus assay utilizes a nested set multiplex PCR to amplify and detect nucleic acid sequences from multiple respiratory pathogens in a single test. This method integrates sample preparation, nested amplification, and detection into a streamlined process, enabling rapid and accurate identification of viral and bacterial targets directly from patient specimens. The BioFire RP2.1 Plus assay has demonstrated high sensitivity and specificity across multiple studies (15–18). According to a study by Leber et al., the assay shows a sensitivity range of 95–100% and specificity exceeding 99% for most of the pathogens it tests (17). In terms of cross-reactivity, the design of the BioFire RP2.1 Plus assay minimizes this risk by using unique primer and probe sets that are highly specific to target pathogens. Independent evaluations, such as those conducted by Poritz et al., have shown minimal cross-reactivity, confirming the assay's robustness against potential diagnostic errors (15).

In this retrospective study, we reviewed our laboratory records from KAMC for samples that were tested during the period from January 2021 to December 2022. The study employed a convenience sampling approach, as respiratory specimens were included based on their availability in the hospital's records and their alignment with the study's inclusion criteria. The etiology and epidemiological parameters that were examined, were age, gender, pathogen detected. and seasonality.

A total of 19,509 (7,484 in 2021 and 12,019 in 2022) respiratory specimens were included in this study. To address potential biases from repeat testing, samples collected from the same patient within a 30-day period were excluded to ensure each data point represented a unique infection event. The study was approved by the King Abdullah International Medical Research Center's (KAIMRC) institutional review board (IRB) (Approval No: IRB/0945/23). The study employed descriptive statistical methods to elucidate the frequency and distribution of respiratory pathogens identified in the specimens. Data were tabulated and visualized using Microsoft Excel (Microsoft Corporation. Redmond, Washington, United States) and PowerBI (Microsoft Corporation. Redmond, Washington, United States)., which facilitated the generation of pie and rainbow charts to

illustrate the distribution of pathogens across different times and demographic groups.

3 Results

A total of 19,509 respiratory samples across 2021 and 2022 were tested. The demographic distribution of the patients, detailed in Table 1, revealed a predominance of pediatric patients, comprising 72.5% of the study population. Regarding gender distribution, males represented 53.9% (5,612) and females 46.1% (4,794) of the cases. Of the specimens, 53.3% (10,406) tested positive for at least one pathogen. Most of the samples were positive for one pathogen (78.2%), while co-infections were seen in the remainder of the samples (21.8%), where 18.3% had two pathogens, 3% had three pathogens, and <1% had four or more pathogens (Figure 1). The data on co-infections revealed layered complexity within respiratory infections. While most patients had mono-infections, the presence of multiple pathogens in over a fifth of the positive cases presents a challenge for treatment due to potential interactions between pathogens and their cumulative effect on the patient's condition.

TABLE 1 Demographic characteristics and frequency of viral respiratory infections by age group.

Demographic	Number/frequency
Males	5,612 (53.9%)
Females	4,794 (46.1%)
Age group (in years)	
0 to < 6 months	1,693 (16.2%)
6 months to 2 years	3,137 (30.1%)
3 to 7 years	1,944(18.6%)
8 to 17 years	795 (7.6%)
18 to 64 years	1,380 (13.2%)
≥ 65 years	1,457 (14%)

3.1 Etiology of respiratory infections

Over the 2-year period in which this study was conducted, rhinovirus/enterovirus were the predominant pathogens throughout, comprising 32% (4,199) of all positive samples, followed by SARS-CoV-2 (2097, 16%), respiratory syncytial virus (RSV) (1,782, 13%), and adenovirus (1,358, 10%; Figure 2). There were 931 (7%) cases of influenza A virus, 549 of which were caused by the influenza A h3 variant, while 309 cases were caused by the influenza A h1-2009 variant, and 73 cases were attributed to non-typeable influenza A (Figure 2). There were 1,126 (8.5%) parainfluenza virus cases. Parainfluenza 3 was the most common parainfluenza (620, 55%) of all parainfluenza cases, followed by parainfluenza 4 and 1 [231 (20.5%) and 212 (18.8%), respectively], and there were only 63 cases (5.5%) of parainfluenza 2 (Figure 2).

3.2 Distribution of respiratory infections by age group

The highest positivity rates were observed in pediatric patients (72.5%), with the age group from 6 months to 2 years old presenting the highest positivity rate (30.1%; Figure 3). This suggests a higher vulnerability or exposure within this demographic. Conversely, the

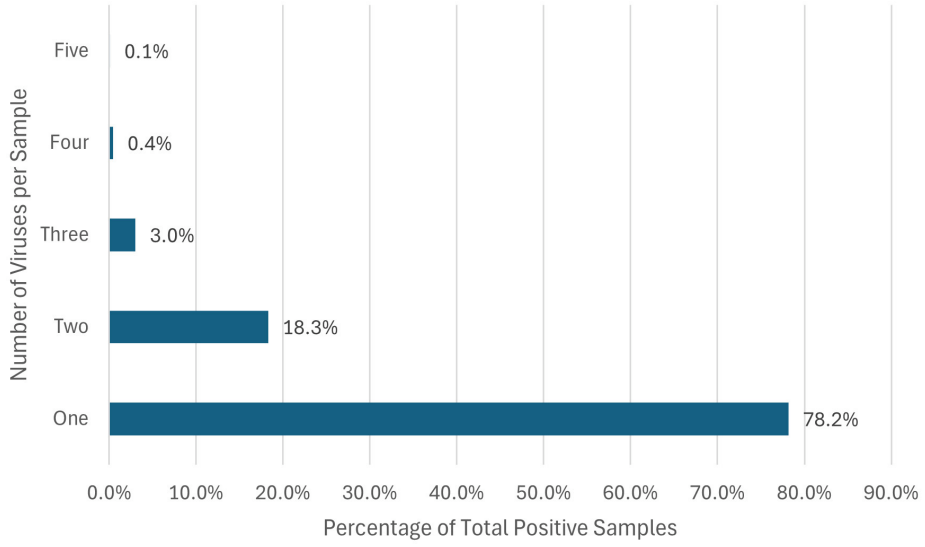

FIGURE 1
Percentage of respiratory co-infections. This horizontal bar chart represents the distribution of the percentage of different organisms identified per positive sample.

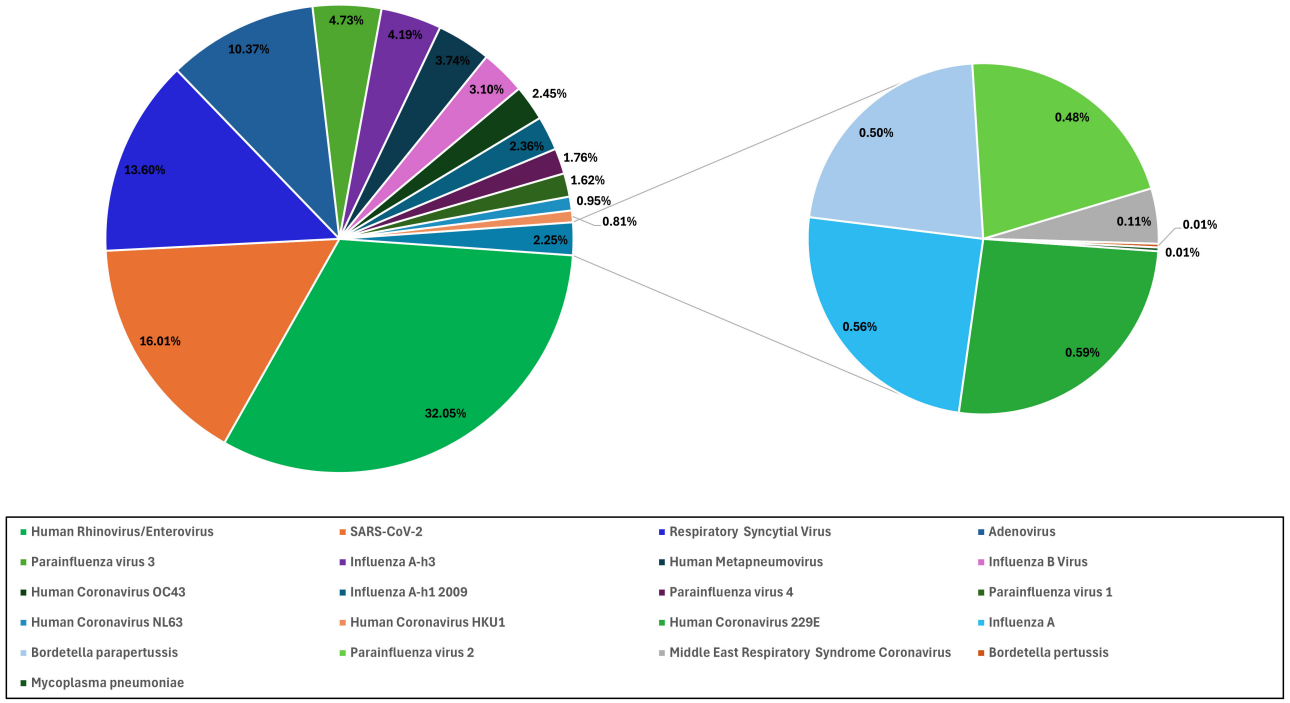

FIGURE 2
The percentage of different respiratory viruses. The proportional distribution of positive samples for various respiratory pathogens.

8–17-year-old age group showed the lowest positivity rates among all age groups (7.6%; Figure 3). This could be partially explained by the completion of childhood vaccinations.

When clustered by age groups, rhinovirus/enterovirus remained the most prevalent pathogen among the pediatric groups (<6 months, 6 months to 2 years, 3–7 years, and 8–17 years). In the <6 months demographic, RSV was the second most prevalent pathogen (522, 23.5%), followed by SARS-CoV-2 (238, 10%; Figure 3). Despite a large difference in their positivity rate, those aged 6 months to 2 years and 3–7 years followed a similar pattern, where adenovirus infections were the second most common etiological agent of respiratory disease, trailed closely by RSV. The majority of infections in the adult (18–64 years) and older adult (≥65 years) populations were caused by SARS-CoV-2 (572, 39%) and then rhinovirus/enterovirus and influenza A infections. Notably, all 15 MERS-CoV cases occurred in adult patients (Figure 3).

3.3 Seasonal distribution

The monthly number of positive cases for each respiratory pathogen is illustrated in Figure 4. Starting in October, there was a sharp increase in the number of cases, with rhinovirus/enterovirus, RSV, and SARS-CoV-2 being the dominant etiologies during these months (Figure 4). During the month of November, SARS-CoV-2 was overtaken by influenza and adenovirus infections, with influenza B being the predominant influenza subtype, followed by influenza A H1-2009, and then adenovirus. Rhinovirus/enterovirus and SARS-CoV-2 consistently exhibited a constant presence, showing the highest number of cases from January to September, with SARS-CoV-2 peaking at its highest levels in January and February and peaking again in June and July (Figure 4). The differences in seasonal distribution and number of infections between 2021 and 2022 could be partially explained by COVID-19 restrictions in Saudi Arabia. COVID-19 restrictions, including mandatory mask-wearing, were officially lifted on June 13, 2022. This explains the increase in respiratory infections following this restriction lift (Figure 4).

4 Discussion

This study provides a comprehensive analysis of the epidemiology and seasonal patterns of respiratory infections in Saudi Arabia during the COVID-19 era, utilizing multiplex PCR technology. By examining data from 19,509 respiratory samples collected between 2021 and 2022, we identified key trends in pathogen prevalence, age-specific susceptibility, and seasonal dynamics. The findings underscore the significant burden of respiratory infections, particularly among pediatric populations, and underscore the impact of public health interventions, such as COVID-19 restrictions, on the transmission of respiratory viruses.

Our study revealed a pediatric predominance, with 72.5% of samples coming from children, and a slight male majority (53.9%). Overall, 53.3% of samples tested positive for at least one pathogen, with single infections accounting for 78.2% of cases and co-infections for 21.8%. These findings align with global trends observed during the COVID-19 pandemic, particularly

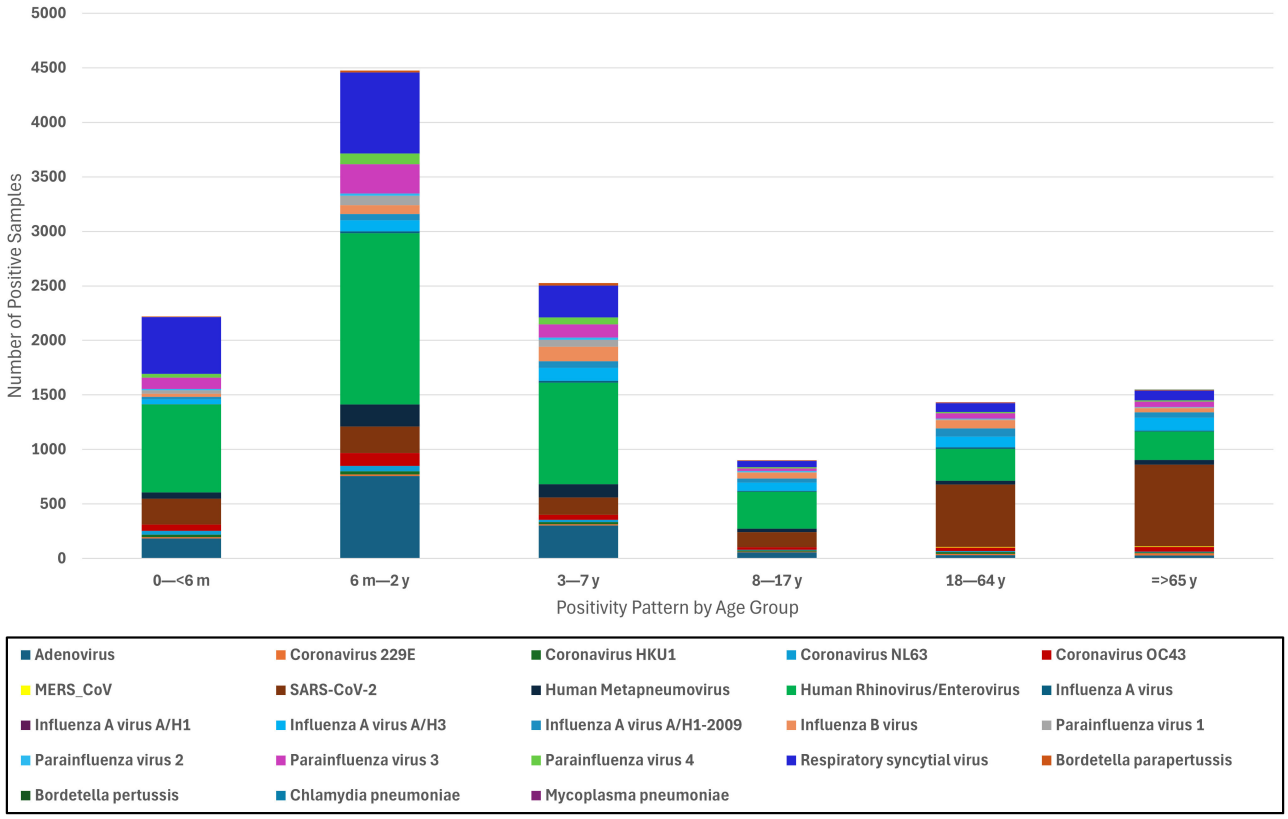

FIGURE 3
Distribution of respiratory pathogens by age group. This stacked bar chart presents the distribution of positive samples for various respiratory pathogens across different age groups.

the increased prevalence of co-infections following the easing of pandemic restrictions. For instance, Maison et al. reported a rise in co-infections among pediatric patients post-lockdown, with single infections remaining predominant but multiple viral detections becoming more common in 2021 and 2022 compared to pre-pandemic levels (19). This similarity in findings underscores the broader epidemiological shifts during the pandemic where increased interactions and subsequent viral exposures may have facilitated higher rates of co-infections.

The most frequently detected pathogens in our study were rhinovirus/enterovirus (32%), SARS-CoV-2 (16%), RSV (13.6%), and adenovirus (10.3%). Rhinovirus/enterovirus was particularly prevalent in pediatric patients, especially those aged 6 months to 2 years, while SARS-CoV-2 was more common in adults and the adults aged 65 years and older. These findings are consistent with global patterns reported during the pandemic, where rhinoviruses/enteroviruses remained highly prevalent despite public health measures aimed at curbing respiratory virus transmission. Schüz et al. noted similar trends in their meta-analysis, emphasizing the resilience of these viruses in the face of widespread interventions (7). Furthermore, the systematic review and meta-analysis by Dallmeyer et al. revealed that rhinovirus/enterovirus and RSV were the most frequent pathogens detected in pediatric patients, particularly among younger age groups, underscoring the significant burden of these infections even during a period dominated by SARS-CoV-2 (20). The presence of these viruses in younger pediatric cohorts illustrates the significant burden of these infections, even during a period characterized by widespread public health interventions aimed at reducing the spread of SARS-CoV-2.

Our findings are consistent with global observations, though regional variations exist. For instance, a study from Qatar, reported influenza as the leading cause of influenza-like illnesses (ILIs) among adults, followed by rhinovirus and seasonal coronaviruses, with RSV and human metapneumovirus (HMPV) showing strong winter peaks (8). Similarly, Chen et al. found that rhinovirus/enterovirus was the most common pathogen in Taiwan during the pandemic, followed by adenovirus and SARS-CoV-2, with co-infections accounting for 5.3% of cases (1). A report from a tertiary hospital in Singapore during the early phase of the COVID-19 outbreak identified rhinovirus as the leading cause of community-acquired respiratory infections requiring hospitalization, followed by influenza and seasonal coronaviruses (5). These results underscore differences in etiological distribution and detection methods across regions, while also aligning with our observations and highlighting the global predominance of rhinoviruses, even during a pandemic dominated by SARS-CoV-2.

The COVID-19 pandemic significantly altered the epidemiology of respiratory infections. In Saudi Arabia, comprehensive restrictions were implemented early in the

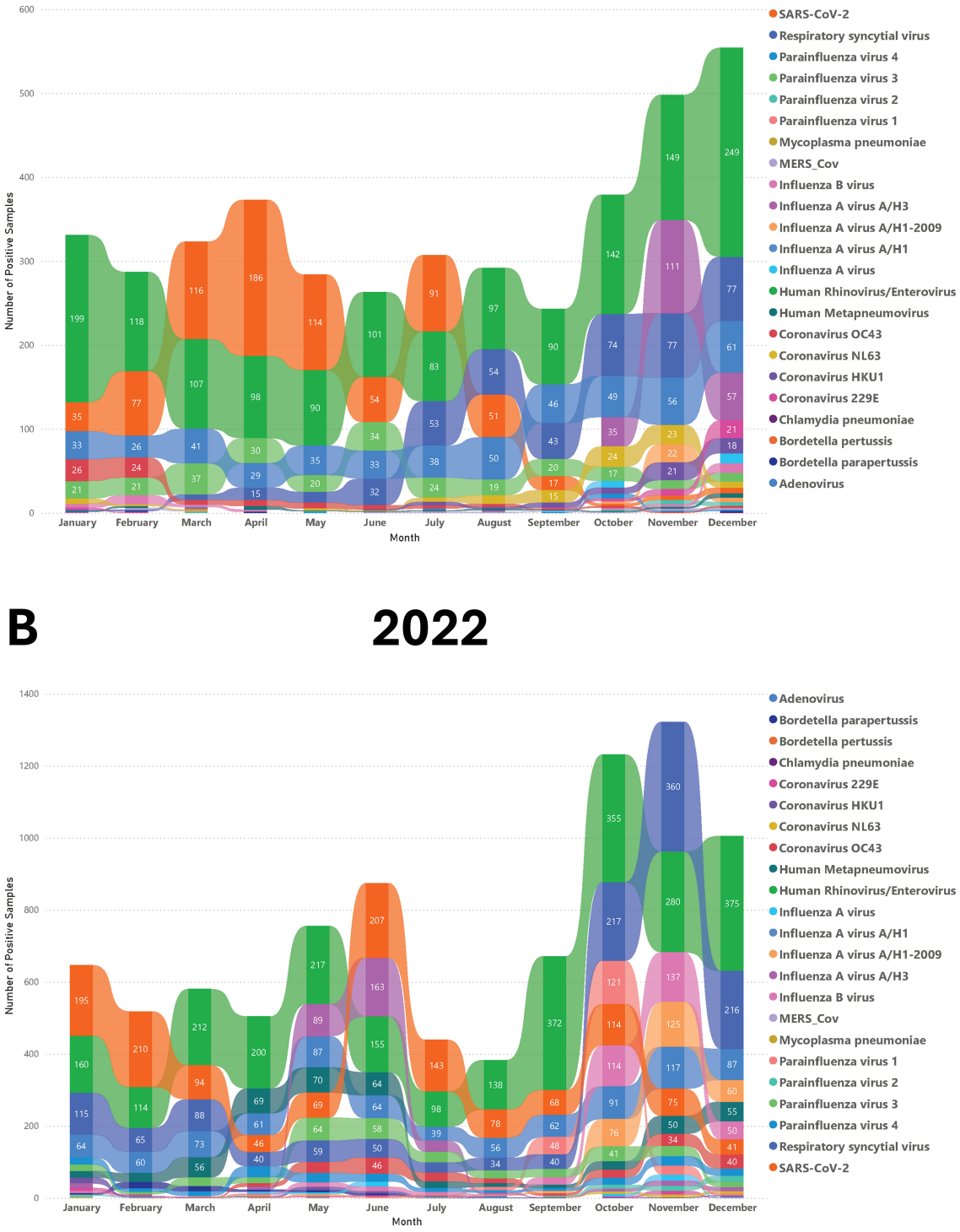

FIGURE 4
The seasonal pattern of different respiratory viruses in 2021 and 2022. The rainbow chart shows monthly positive samples for various respiratory pathogens in 2021 **(A)** and 2022 **(B)**.

pandemic and gradually lifted by June 2022. Our study period (2021–2022) captured both the height of these measures and their subsequent relaxation. Notably, we observed a marked increase in respiratory tract infections (RTIs) following the easing of restrictions, particularly in the latter half of 2022. This rise in RTIs, driven by pathogens such as rhinovirus/enterovirus, RSV, and adenovirus, underscores the impact of public health policies on disease transmission dynamics. Reduced social distancing and preventive measures likely facilitated increased viral spread, a trend mirrored globally as countries relaxed COVID-19 restrictions. Pre-pandemic studies in Saudi Arabia pointed out the significant burden of respiratory infections, particularly among children. A 2017 study reported over five million cases of acute respiratory infections from 2012 to 2013, with more than 60% occurring in infants under 1 year old. Similarly, our study found that 46% of infections occurred in children under 2 years old, with rhinovirus/enterovirus and RSV being the most common pathogens. These findings suggest a persistent epidemiological profile for these viruses over the years (21). More recent studies from Saudi Arabia and neighboring regions have corroborated these trends. For example, a study from Riyadh involving 503 pediatric patients under 5 years old identified RSV and influenza as the most prevalent viruses, consistent with our findings. However, the limited scope of PCR assays used in some studies, which excluded pathogens like rhinovirus, may have underestimated their prevalence (22). Farrag et al. also emphasized the impact of mass gatherings, such as the Hajj pilgrimage, on respiratory virus transmission, with rhinoviruses and influenza viruses being the most common pathogens detected in Hajj returnees (23). These findings align with global trends, where similar rises in RTIs were documented post-COVID-19 restrictions, shedding light on the dual impact of pandemic policies on both COVID-19 and other respiratory infections.

Seasonal patterns were also evident, with respiratory infections peaking in the colder months. Influenza and adenovirus cases surged in November, while RSV activity increased from October, peaking in winter. These observations align with studies from other regions, such as Rousogianni et al., who reported similar winter peaks for influenza A and adenovirus in Greece (24). The U.S. CDC reported that RSV epidemics typically peak during winter, a pattern initially disrupted by the COVID-19 pandemic but later returning to its usual seasonal regularity (25). Similarly, a report from the United Kingdom noted an increase in RSV cases during winter, further corroborating our findings (26). A review by Moriyama et al. highlighted that influenza, human coronaviruses, and RSV are typically winter viruses, while rhinoviruses, adenoviruses, and human metapneumoviruses circulate year-round (10). These findings correlate with our study, where rhinovirus/enterovirus was detected throughout the year, and influenza and RSV peaked in winter. However, our observation that RSV activity began earlier (October) and declined by February differs from a 2013–2014 Saudi Arabian study, which reported RSV peaks from December to March. This discrepancy may stem from differences in detection methods (multiplex PCR vs. DFA) and factors such as enhanced surveillance, increased public awareness, and improved healthcare access, all of which can influence epidemic timing and intensity (14). Nonetheless, these consistent observations across different regions underscore the robust seasonal dynamics of respiratory viruses, particularly RSV, and validate the winter peaks identified in our study. Saudi Arabia's arid climate, characterized by extreme temperatures and low humidity, may contribute to the observed winter peaks. Lower humidity in colder months could enhance viral stability and airborne transmission, while increased indoor crowding during winter likely facilitates spread. Future studies might further our understanding by incorporating meteorological data with infection rates to give a fuller analysis of the factors affecting respiratory virus transmission.

The significance of this research lies in its examination of the distribution and seasonality of respiratory pathogens at a time when global health systems were predominantly oriented toward managing COVID-19. Particularly novel is the study's illumination of the seasonal distribution of these pathogens, and to our knowledge the first and largest study from the middle east to report the frequency and distribution of respiratory pathogens using the Filmarray multiplex PCR technology, providing critical data that diverge from the patterns noted in previous research conducted prior to the pandemic (8, 9, 21, 23). This study has several limitations. As a retrospective analysis using a single multiplex PCR assay, it does not capture co-infections with pathogens outside the Filmarray respiratory panel. Additionally, the study was conducted at a single center, although the large sample size (over 19,000 samples) strengthens its validity. The lack of clinical severity markers, such as ICU admissions or mortality rates, limits our ability to assess the disease burden associated with detected pathogens. Future prospective studies integrating laboratory data with clinical outcomes are essential to fully understand the public health impact of respiratory infections.

Our findings have significant implications for public health strategies in Saudi Arabia. The observed winter peaks of RSV, influenza, and adenovirus suggest that vaccination campaigns should be prioritized in early autumn, particularly for high-risk groups such as infants, older adults, and immunocompromised individuals. Enhanced surveillance during mass gatherings, such as the Hajj pilgrimage, could further mitigate transmission risks. Additionally, understanding seasonal trends can help health systems optimize resource allocation, staff levels, and medical supplies during peak transmission periods.

The prominence of rhinovirus/enterovirus and RSV in pediatric populations underscores the need for targeted interventions, such as earlier and more frequent vaccinations for young children. Public health communications should also emphasize the importance of preventive measures, especially during peak seasons, to reduce the burden of respiratory infections.

This study provides critical insights into the epidemiology of respiratory viruses in Saudi Arabia during the COVID-19 era, delineating the prevalence, seasonality, and demographic distribution of key pathogens. By leveraging multiplex PCR technology, we have identified patterns that diverge from pre-pandemic studies, reflecting the unique impact of COVID-19 on respiratory virus transmission. These findings fill important knowledge gaps and offer a foundation for refining public health strategies, improving disease surveillance, and enhancing clinical management of respiratory infections in Saudi Arabia. Future

research integrating environmental and clinical data will further advance our understanding of respiratory virus dynamics and inform more effective interventions.

Data availability statement

The data supporting the findings of this study are not publicly available due to restrictions imposed by the King Abdullah International Medical Research Center (KAIMRC). According to KAIMRC policies, patient data and related clinical information cannot be shared publicly to protect patient privacy and confidentiality. However, specific data details may be available from the corresponding author upon reasonable request and with permission from KAIMRC, subject to institutional and ethical guidelines. Requests to access the datasets should be directed to Alzahranin@ksau-hs.edu.sa.

Ethics statement

The studies involving humans were approved by Institutional Review Board of King Abdullah International Medical Research Center (KAIMRC), Riyadh, Saudi Arabia. The studies were conducted in accordance with the local legislation and institutional requirements. The human samples used in this study were acquired from a by-product of routine care or industry. Written informed consent for participation was not required from the participants or the participants' legal guardians/next of kin in accordance with the national legislation and institutional requirements.

Author contributions

NA: Conceptualization, Data curation, Formal analysis, Investigation, Methodology, Project administration, Writing – original draft, Writing – review & editing. AhA: Data curation, Formal analysis, Methodology, Writing – review & editing. AlA: Data curation, Formal analysis, Methodology, Writing – review & editing. SA: Supervision, Writing – review & editing.

Funding

The author(s) declare that no financial support was received for the research and/or publication of this article.

Conflict of interest

The authors declare that the research was conducted in the absence of any commercial or financial relationships that could be construed as a potential conflict of interest.

Publisher's note

All claims expressed in this article are solely those of the authors and do not necessarily represent those of their affiliated organizations, or those of the publisher, the editors and the reviewers. Any product that may be evaluated in this article, or claim that may be made by its manufacturer, is not guaranteed or endorsed by the publisher.

References

1. Chen YJ, Er, TK. Distribution of viral respiratory infections during the COVID-19 pandemic using the filmarray respiratory panel. *Biomedicines.* (2022) 10:2734. doi: 10.3390/biomedicines10112734

2. Huang CP, Tsai CS, Su PL, Huang TH, Ko WC, Lee NY. Respiratory etiological surveillance among quarantined patients with suspected lower respiratory tract infection at a medical center in southern Taiwan during COVID-19 pandemic. *J Microbiol Immunol Infect.* (2022) 55:428–35. doi: 10.1016/j.jmii.2021.07.009

3. Leuzinger K, Roloff T, Gosert R, Sogaard K, Naegele K, Rentsch K, et al. Epidemiology of severe acute respiratory syndrome coronavirus 2 emergence amidst community-acquired respiratory viruses. *J Infect Dis.* (2020) 222:1270–9. doi: 10.1093/infdis/jiaa464

4. Principi N, Autore G, Ramundo G, Esposito S. Epidemiology of respiratory infections during the COVID-19 pandemic. *Viruses.* (2023) 15:1160. doi: 10.3390/v15051160

5. Wee LE, Ko KK, Ho WQ, Kwek GT, Tan TT, Wijaya L. Community-acquired viral respiratory infections amongst hospitalized inpatients during a COVID-19 outbreak in Singapore: co-infection and clinical outcomes. *J Clin Virol.* (2020) 128:104436. doi: 10.1016/j.jcv.2020.104436

6. Agca H, Akalin H, Saglik I, Hacimustafaoglu M, Celebi S, Ener B. Changing epidemiology of influenza and other respiratory viruses in the first year of COVID-19 pandemic. *J Infect Public Health.* (2021) 14:1186–90. doi: 10.1016/j.jiph.2021.08.004

7. Schuz ML, Dallmeyer L, Fragkou PC, Omony J, Krumbein H, Hünerbein BL, et al. Global prevalence of respiratory virus infections in adults and adolescents during the COVID-19 pandemic: a systematic review and meta-analysis. *Int J Infect Dis.* (2023) 137:16–24. doi: 10.1016/j.ijid.2023.10.001

8. Al-Romaihi HE, Smatti MK, Ganesan N, Nadeem S, Farag E, Coyle PV, et al. Epidemiology of respiratory infections among adults in Qatar (2012–2017). *PLoS ONE.* (2019) 14:e0218097. doi: 10.1371/journal.pone.0218097

9. Helou M, Mahdi A, Daoud Z, Mokhbat J, Farra A, Nassar E, et al. Epidemiology of community-acquired respiratory tract infections in patients admitted at the emergency departments. *Trop Med Infect Dis.* (2022) 7:233. doi: 10.3390/tropicalmed7090233

10. Moriyama M, Hugentobler WJ, Iwasaki A. Seasonality of respiratory viral infections. *Annu Rev Virol.* (2020) 7:83–101. doi: 10.1146/annurev-virology-012420-022445

11. Dowell SF. Seasonal variation in host susceptibility and cycles of certain infectious diseases. *Emerg Infect Dis.* (2001) 7:369–74. doi: 10.3201/eid0703.017301

12. Lowen AC, Mubareka S, Steel J, Palese P. Influenza virus transmission is dependent on relative humidity and temperature. *PLoS Pathog.* (2007) 3:1470–6. doi: 10.1371/journal.ppat.0030151

13. Lofgren E, Fefferman NH, Naumov YN, Gorski J, Naumova EN. Influenza seasonality: underlying causes and modeling theories. *J Virol.* (2007) 81:5429–36. doi: 10.1128/JVI.01680-06

14. Albogami SS, Alotaibi MR, Alsahli SA, Masuadi E, Alshaalan M. Seasonal variations of respiratory viruses detected from children with respiratory tract infections in Riyadh, Saudi Arabia. *J Infect Public Health.* (2018) 11:183–6. doi: 10.1016/j.jiph.2017.06.001

15. Poritz MA, Blaschke AJ, Byington CL, Allen L, Nilsson K, Jones DE, et al. FilmArray, an automated nested multiplex PCR system for multi-pathogen detection: development and application to respiratory tract infection. *PLoS ONE.* (2011) 6:e26047. doi: 10.1371/journal.pone.0026047

16. Ramirez MM, Zarate MN, Rodriguez LA, Aquino VH. Performance evaluation of biofire film array respiratory panel 21 for SARS-CoV-2 detection in a pediatric hospital setting. *PLoS ONE.* (2023) 18:e0292314. doi: 10.1371/journal.pone.0292314

17. Leber AL, Everhart K, Daly JA, Hopper A, Harrington A, Schreckenberger P, et al. Multicenter evaluation of biofire filmarray respiratory panel 2 for detection

of viruses and bacteria in nasopharyngeal swab samples. *J Clin Microbiol.* (2018) 56:10–128. doi: 10.1128/JCM.01945-17

18. Popowitch EB, O'Neill SS, Miller MB. Comparison of the biofire filmarray RP, genmark eSensor RVP, luminex xTAG RVPv1, and luminex xTAG RVP fast multiplex assays for detection of respiratory viruses. *J Clin Microbiol.* (2013) 51:1528–33. doi: 10.1128/JCM.03368-12

19. Maison N, Omony J, Rinderknecht S, Kolberg L, Meyer-Bühn M, von Mutius E, et al. Old foes following news ways?-Pandemic-related changes in the epidemiology of viral respiratory tract infections. *Infection.* (2024) 52:209–18. doi: 10.1007/s15010-023-02085-w

20. Dallmeyer LK, Schüz ML, Fragkou PC, Omony J, Krumbein H, Dimopoulou D, et al. Epidemiology of respiratory viruses among children during the SARS-CoV-2 pandemic: a systematic review and meta-analysis. *Int J Infect Dis.* (2024) 138:10–8. doi: 10.1016/j.ijid.2023.10.023

21. Fagbo SF, Garbati MA, Hasan R, AlShahrani D, Al-Shehri M, AlFawaz T, et al. Acute viral respiratory infections among children in MERS-endemic Riyadh, Saudi Arabia, 2012-2013. *J Med Virol.* (2017) 89:195–201. doi: 10.1002/jmv.24632

22. Ahmed A, Alsenaidy AM, Mobaireek KF, AlSaadi MM. Viral etiology of acute respiratory infections during 2014–2016 in Riyadh, Saudi Arabia. *Future Virology.* (2022) 17:269–80. doi: 10.2217/fvl-2020-0071

23. Farrag MA, Hamed ME, Amer HM, Almajhdi FN. Epidemiology of respiratory viruses in Saudi Arabia: toward a complete picture. *Arch Virol.* (2019) 164:1981–96. doi: 10.1007/s00705-019-04300-2

24. Rousogianni E, Perlepe G, Boutlas S, Rapti GG, Gouta E, Mpaltopoulou E, et al. Proportions and seasonal patterns of respiratory viruses via rapid tests in adults at a greek hospital (Oct. 2023-Mar. 2024). *J Pers Med.* (2024) 14:824. doi: 10.3390/jpm14080824

25. Hamid S. Seasonality of respiratory syncytial virus - United States, 2017-2023. *MMWR Morb Mortal Wkly Rep.* (2023) 72:355–61. doi: 10.15585/mmwr.mm7214a1

26. Purcell M, Morelli T, Cox O, Lee P, Thorne K, Roberts CA, et al. Seasonality of respiratory viruses and viral co-infection across two winter seasons in the UK. *Eur Respir J.* 64:PA3299. doi: 10.1183/13993003.congress-2024.PA3299

frontiers | Frontiers in Cellular and Infection Microbiology

TYPE Original Research
PUBLISHED 03 April 2025
DOI 10.3389/fcimb.2025.1552116

OPEN ACCESS

EDITED BY
Dimitra Dimopoulou,
Panagiotis & Aglaia Kyriakou Children's Hospital, Greece

REVIEWED BY
Venkateswarlu Kanamarlapudi,
Swansea University Medical School, United Kingdom
Juan Pablo Robles,
National Autonomous University of Mexico, Mexico

*CORRESPONDENCE
Francesca Caccuri
francesca.caccuri@unibs.it

†These authors have contributed equally to this work and share first authorship

RECEIVED 27 December 2024
ACCEPTED 17 March 2025
PUBLISHED 03 April 2025

CITATION
Bugatti A, Zani A, Bardelli M, Giovanetti M, Ravelli C, Ciccozzi M, Caruso A and Caccuri F (2025) Heparan sulfate proteoglycans remodel SARS-CoV-2 spike conformation to allow integrin interaction and infection of endothelial cells.
Front. Cell. Infect. Microbiol. 15:1552116.
doi: 10.3389/fcimb.2025.1552116

Heparan sulfate proteoglycans remodel SARS-CoV-2 spike conformation to allow integrin interaction and infection of endothelial cells

Antonella Bugatti[1†], Alberto Zani[1†], Marta Bardelli[1], Marta Giovanetti[2], Cosetta Ravelli[3], Massimo Ciccozzi[2], Arnaldo Caruso[1,4] and Francesca Caccuri[1,4*]

[1]Section of Microbiology, Department of Molecular and Translational Medicine, University of Brescia, Brescia, Italy, [2]Unit of Medical Statistics and Molecular Epidemiology, University Campus Bio-Medico of Rome, Rome, Italy, [3]Section of General Pathology, Department of Molecular and Translational Medicine, University of Brescia, Brescia, Italy, [4]Centre for Advanced Medical and Pharmaceutical Research, "George Emil Palade" University of Medicine, Pharmacy, Science and Technology, Targu Mures, Romania

SARS-CoV-2 infects ACE2-negative primary HL-mECs through the interaction of an RGD motif, included in all spike proteins, up to the Omicron BA.1 subvariant, with $\alpha_v\beta_3$ integrin. Following its entry, SARS-CoV-2 remodels ECs phenotype and promotes angiogenesis in the absence of productive viral replication. Moreover, lack of spike/$\alpha_v\beta_3$ interaction, occurring in Omicron BA.5 which contains the D405N mutation in the RGD motif, inhibits HL-mECs infection and dysfunction. It is worth noting that anti-spike antibodies do not impact SARS-CoV-2 entry into HL-mECs. This data highlights the fact that i) the RGD motif is not exposed in the entire spike protein and ii) the need of a cofactor favoring spike/$\alpha_v\beta_3$ interaction. HSPGs are used by different viruses as receptors and coreceptors for their entry into host cells. Here, we use different approaches to scrutinize the role exerted by HSPGs in favoring SARS-CoV-2 infection of ECs. We highlight HSPGs as key molecules responsible for RGD exposure allowing its binding to the $\alpha_v\beta_3$ integrin as the first step toward viral entry by endocytosis. Indeed, SPR analysis showed lack of spike/$\alpha_v\beta_3$ interaction in the absence of heparin. This data was further corroborated by immunofluorescence and infectivity assays. Interestingly, the use of Heparinase III or sodium chlorate counteracts the release of proangiogenic molecules and inhibits signaling pathways induced by SARS-CoV-2 infection. Thus, HSPGs may represent a target for preventing SARS-CoV-2 infection of ECs and EC dysfunction-related COVID-19 severity.

KEYWORDS

SARS-CoV-2, heparan sulphates, integrins, angiogenesis, von Willebrand factor, FAK-Src and Erk signaling pathway

Introduction

Severe acute respiratory syndrome coronavirus 2 (SARS-CoV-2) infections have been mainly associated with local bronchopulmonary symptoms (Su et al., 2021; Rabaan et al., 2023). However, 20% of these infections leads to life-threatening respiratory, cardiac, renal, and cerebral injury (Odilov et al., 2021; Rabaan et al., 2023). These severe forms of disease induce an inflammatory status with a strong microvascular involvement driven by the endothelial cells (ECs) response to the infection (Canale et al., 2022). EC activation results in elevated levels of pro-inflammatory cytokines, chemokines, pro-angiogenic and anti-thrombotic factors in critical patients (Oxford et al., 2020). Indeed, it has been shown that the disruption of vascular homeostasis, secondary to EC damage, contributes to systemic proinflammatory state and multiorgan involvement observed in COVID-19 disease (Giordo et al., 2021).

Several studies demonstrated that SARS-CoV-2 infects lung ECs both *in vivo* and *in vitro* (Liu F. et al., 2021). We proved that SARS-CoV-2 infects primary human lung microvascular ECs (HL-mECs), which do not express ACE2, by using an endocytic pathway (Bugatti et al., 2022). In particular, we showed that the Arg-Gly-Asp (RGD) motif expressed in the receptor binding domain (RBD) of the spike protein, at amino acid (aa) position 403-405, is responsible for SARS-CoV-2 entry into HL-mECs through a specific $\alpha_v\beta_3$ integrin interaction, giving rise to inflammatory and angiogenic responses (Bugatti et al., 2022). It is worth noting that the latest Omicron sublineages were found to differ from all previous SARS-CoV-2 VOCs for displaying a D405N mutation in their spike protein (Tuekprakhon et al., 2022; Bugatti et al., 2023), which impairs SARS-CoV-2/$\alpha_v\beta_3$ integrin interaction, thus impeding EC infection and dysfunction (Bugatti et al., 2023).

Antibodies recognizing the epitope containing the RGD motif, even those evocated by BNT162b2 vaccination, demonstrated a negligible effect in neutralizing the live virus (Nitahara et al., 2021; Bugatti et al., 2022). This is due to the knowledge that the RGD motif is not exposed on the surface of the RBD neither in its "up" nor "down" conformation (Nitahara et al., 2021). Moreover, microscale accelerated molecular dynamic (MD) simulations showed that neither the RGD motif nor its microenvironment exhibit any significant conformational shift in the RBD structure able to acquire an optimal geometry for its interaction with integrins (Othman et al., 2022). These data lead to the hypothesis that, in order to expose and obtain the optimal geometry of the RGD motif in its spike, SARS-CoV-2 needs a cofactor.

Heparan sulfates (HSs) are linear polysaccharide chains found on the surface of cells and play a critical role in several biological processes (Sarrazin et al., 2011), including viral attachment (Madu et al., 2007; Cagno et al., 2019; Koganti et al., 2021). Viruses use HS interaction to improve their chances of binding to specific receptors expressed on the surface of host cells (Cagno et al., 2019). In particular, in the context of coronavirus, it has been demonstrated that SARS-CoV-2 attachment and infection involves HS-dependent enhancement of binding to ACE2 (de Haan et al., 2005; Clausen et al., 2020; Zhang et al., 2020; Liu L. et al., 2021), through conformational changes leading to RBD better exposure, thus serving as coreceptors in facilitating viral infection (Milewska et al., 2014; Clausen et al., 2020; Kim et al., 2020; Mycroft-West et al., 2020; Kalra and Kandimalla, 2021; Tandon et al., 2021; Kearns et al., 2022). These data indicate that molecules disrupting HSs/spike interaction may represent novel therapeutics against COVID-19 (Yu et al., 2021). Interestingly, it has also been suggested that SARS-CoV-2 variants evolve to be more dependent on HSs for viral attachment and infection (Kim et al., 2023).

Here, we scrutinize the role played by heparan sulfate proteoglycans (HSPGs) in promoting $\alpha_v\beta_3$ integrin-mediated entry of SARS-CoV-2 into HL-mECs. We highlight HSPGs as key molecules for the first step toward viral entry by integrin-mediated endocytosis. Moreover, inhibition of HSPGs/spike interaction was sufficient to inhibit the SARS-CoV-2-sustained ECs dysfunction and related signaling pathways.

Materials and methods

Reagents

Recombinant trimeric Omicron BA.1 and Omicron XBB.1.5 spike proteins were purchased from BPS Bioscience (San Diego, CA, USA). The proteins were purified from HEK293 cells with a purity ≥ 90% and run at a higher molecular weight by SDS-PAGE due to glycosylation; anti-phospho-extracellular signal-regulated kinase 1/2 (pERK) and anti-total $ERK_{1/2}$ (tERK) antibodies were purchased from Santa Cruz Biotechnology (Santa Cruz, CA, USA); anti-phospho-focal adhesion kinase (pFAK), anti phospho-Src (pSrc), anti-Glyceraldehyde-3-phosphate dehydrogenase (GAPDH) and anti-total Src (tSrc) were purchased from Cell Signaling Technology (Danvers, MA, USA); recombinant human integrin alphaV beta3 ($\alpha_v\beta_3$), sodium chlorate, Heparinase III and heparin sodium salt from porcine intestinal mucosa were purchased from Merck (Darmstadt, Germany). Human $\alpha_v\beta_3$ integrin antibody was purchased from Bio-Techne (Minneapolis, MN, USA).

Cells

African green monkey kidney Vero E6 cell line was obtained from Istituto Zooprofilattico Sperimentale della Lombardia e dell'Emilia Romagna (Brescia, Italy) and maintained in Dulbecco's Modified Eagle Medium (DMEM; Gibco, Thermo Fisher Scientific, Waltham, MA, USA) supplemented with 10% fetal bovine serum (FBS; Gibco, Thermo Fisher Scientific). Human lung microvascular endothelial cells (HL-mECs) were purchased from Lonza (Basel, Switzerland) and cultured in EGM-2 (Lonza), containing 10% FBS.

Abbreviations: SARS-CoV-2, Severe Acute Respiratory Syndrome Coronavirus 2; HSPGs, Heparan sulfate proteoglycans; SPR, Surface plasmon resonance; ECs, endothelial cells; COVID-19, Coronavirus disease 2019; RBD, receptor binding domain; RGD, Arg-Gly-Asp.

Biacore

Surface Plasmon Resonance (SPR) measurements were conducted on a Biacore X100 (Cytiva, MN, USA) at 25°C. For the study of spike proteins/heparin interaction, biotinylated heparin was immobilized onto a SA sensor chip containing pre-immobilized streptavidin, allowing the immobilization of 186 resonance units (RU). A sensor chip pre-coated with streptavidin alone was used to evaluate nonspecific binding and for blank subtraction (Bugatti et al., 2007). Increasing concentrations of trimeric SARS-CoV-2 spike proteins belonging to Omicron BA.1 or Omicron XBB.1.5 sublineages in 10 mM HEPES, pH 7.4 containing 150 mM NaCl, 3 mM EDTA, and 0.005% surfactant P20 (HBS-EP$^+$, running buffer) were injected over the heparin or streptavidin surfaces for 4 min and then washed until dissociation. After each run, the sensor chip was regenerated by injection of 2.0 M NaCl in HBS-EP$^+$. Kinetic parameters of the interactions were calculated from the sensorgram overlays by using the nonlinear fitting single-site model software package BIAevaluation (version 3.2 [Cytiva]). For spike proteins/$\alpha_v\beta_3$ interaction, 20 µg/ml of recombinant integrin was immobilized onto a CM5 sensor chip using standard amine-coupling chemistry allowing the immobilization of 996 resonance units, equal to 5,24 x 10^{-9} pmol/mm^2 of $\alpha_v\beta_3$. A sensor chip alone was used to evaluate nonspecific binding and for blank subtraction (Rusnati et al., 2001). Trimeric SARS-CoV-2 Omicron BA.1 or Omicron XBB.1.5 spike proteins, were diluted in running buffer and injected alone or in the presence of free heparin (10 µg/ml) over the surface for 4 min and then washed until dissociation.

Viral infection

Infections were carried out as previously described (Bugatti et al., 2023), using the clinical SARS-CoV-2 isolates belonging to Omicron BA.1 (GISAID accession number: EPI_ISL_15700833), or Omicron XBB.1.5 (GISAID accession number: EPI_ISL_19500251) sublineages. The viruses were propagated in Vero E6 cells and the viral titer was determined by a standard plaque assay. All the experiments were performed with a single viral inoculum. Mock-infected cell cultures were obtained from uninfected cells (NI), processed exactly as the SARS-CoV-2-infected ones. All the infection experiments were carried out in a biosafety level-3 (BSL-3) laboratory at a Multiplicity of Infection (MOI) of 1. Where indicated, to inhibit the sulfation of cell-associated HS chains, HL-mECs cells were grown for 48 h in presence of sodium chlorate (50 mM). Alternatively, cells were incubated for 1 h at 37°C with Heparinase III (15 mU/ml in phosphate-buffered saline [PBS], Merck) before experimentation.

Viral RNA extraction and qRT–PCR

RNA was extracted from infected cells using the RNeasy Plus mini kit (Qiagen, Hilden, Germany), according to the manufacturer's instructions. RNA was eluted in 30 µl of RNase-free water and stored at -80°C until use. The qRT-PCR was carried out following previously described procedures (Bugatti et al., 2023). Each quantification was run in triplicates.

Immunofluorescence assay

For the evaluation of spike-$\alpha_v\beta_3$ localization, HL-mECs were seeded (5 x 10^4 cells per well) on collagen-coated 8-well chamber slides (Thermo Fisher Scientific) in complete medium. After 24 h, cells were incubated at 4°C for 1 h in complete media containing 100 ng/ml of recombinant Omicron BA.1 and XBB.1.5 spike proteins. After incubation, cells were washed, fixed with 4% PFA in PBS for 10 min and saturated with 3% BSA in PBS. For staining, the cells were incubated for 1 h at 4°C with a human serum (1:1000 dilution) containing IgG against SARS-CoV-2 spike protein and with mAb against $\alpha_v\beta_3$ integrin (1 µg/ml; Bio-techne) followed by Alexa Fluor 488-conjugated anti-human IgG or Alexa Fluor 594-conjugated anti-mouse IgG (Thermo Fisher Scientific). Nuclei were counterstained with DAPI (Merck). To evaluate the viral antigen in HL-mECs after infection, the cells were seeded (5 x 10^4 cells per well) on collagen-coated 8-well chamber slides (Thermo Fisher Scientific) and infected with SARS-CoV-2 isolates belonging to Omicron BA.1 or Omicron XBB.1.5 sublineages, as previously described. After infection, cells were fixed with 4% paraformaldehyde in PBS for 10 min and stained with an anti-spike protein antibody as previously described (Bugatti et al., 2022). Cells were photographed under a Zeiss Axiovert 200 M epifluorescence microscope equipped with a Plan-Apochromat 63x/1.4 NA oil objective (Zeiss Axiovert 200M system).

Spheroids

Spheroids were generated by mixing HL-mECs (1 x 10^5 cells/ml) with 5 mg/mL of methylcellulose (Merck) in EGM-2 medium containing 10% FBS, making the final volume to 10 ml. The cells (100 µl/well) were then added to 96-well plates (Greiner Bio-one, Kremsmünster, Austria) and incubated at 37°C and 5% CO_2 for 24 h. Separately, the collagen I gel solution (Rat tail, Corning, NY, USA) was maintained on ice and neutralized by adding NaOH 0.1 N and PBS 10X to a final pH of 7.4. Then, 24-well plates were coated with neutralized collagen (150 µl/well) and incubated in a humidified 5% CO_2 incubator for 1 h at 37°C. The spheroids from 96-well plates were collected in eppendorf tubes and centrifuged at 2,000 x rpm for 10 s. When a clear pellet was distinguished, the supernatant was removed, and the pellet was kept in a volume of about 150 µl collagen I-neutralized solution. Each collagen-spheroid mixture was rapidly added to the pre-coated 24-well plates (200 µl/well) and incubated for 1 h. After 1 h, 500 µl of EGM-2 containing 10% FBS, was added to the wells to completely cover the surface and plates were further incubated for 24 h. Where indicated, HL-mECs cells were grown for 48 h in presence of sodium chlorate or alternatively, ECs were incubated for 1 h at 37°C with Heparinase III before experimentation. Sprouting occurred from the spheroid core, photographed with a Hitachi KP-

D50 camera (Hitachi Ltd., Tokyo, Japan), and the number of sprouts was counted with the spheroids of similar sizes from three different wells of the plate.

Microarray analysis

Supernatants from infected treated and not treated HL-mECs were collected at 3 days post infection (p.i.), clarified and analyzed for the expression of 55 different angiogenesis-related proteins by Human Angiogenesis Array Kit (Proteome Profiler, R&D systems, Minneapolis, USA) according to the manufacturer's instructions.

Fluorescent vWF expression and quantification

HL-mECs were nucleofected with a mCherry-vWF expressing plasmid (Bugatti et al., 2020) by using the Amaxa Nucleofector Technology (Lonza). Twenty-four h after nucleofection, HL-mECs were infected with SARS-CoV-2 belonging to Omicron BA.1 lineage and the fluorescence was analyzed at different time points (1, 3, 6 and 24 h p.i.). When reported, HL-mECs were treated with sodium chlorate and Heparinase III, for 48 h or 1 h respectively, before the SARS-CoV-2 infection. Nuclei were counterstained with DAPI (Merck). Fluorescence was analyzed using a Zeiss Axiovert 200 M epifluorescence microscope equipped with a Plan-Apochromat 63x/1.4 NA oil objective (Zeiss Axiovert 200M system). The number of puncta per cell was quantified using Image J software (Fiji, NIH, Bethesda, USA), by counting vWF-positive puncta in 20 cells/experiment. Error bars represent the standard deviation calculated as the mean of 3 independent experiments with similar results.

Human vWF ELISA array

Supernatants from mCherry-vWF expressing plasmid nucleofected and SARS-CoV-2 infected HL-mECs were collected at different time points (1, 3, 6 and 24 h p.i.), clarified and analyzed for the level of secreted vWF by Human vWF ELISA Kit (Merck) according to the manufacturer's instructions.

Signaling pathways activation assay

HL-mECs were infected with SARS-CoV-2 belonging to Omicron BA.1 or XBB.1.5 sublineages as previously described and 1 h p.i. the cells were lysed in 50 mM Tris-HCl pH 7.4 containing 150 mM NaCl, 1% Triton X-100, 1 mM Phenylmethylsulfonyl fluoride (PMSF) and Protease Inhibitor Cocktail (Merck) and centrifuged. Twenty μg of total proteins were analyzed on SDS-12% PAGE followed by Western blotting with anti-pFAK, anti-p-Src and anti-pERK antibodies. Equal loading of the lanes was confirmed by immunoblotting with anti-tSrc, anti-tERK or anti-GAPDH antibodies. The intensity of the pSrc, pERK and pFAk signal was quantified and normalized to the intensity of the corresponding tSrc, tERK and GAPDH band using Image J software.

Monitoring of recent SARS-CoV-2 strains with reverse mutation S405D and phylogenetic analysis

A total of 1083 SARS-CoV-2 whole-genome sequences, carrying all four mutations of interest (D405D, D405N, N405S), as well as recent strains with the reverse mutation S405D, selected based on the availability of comprehensive associated metadata, were analyzed in this study. Each sequence was aligned using the ViralMSA tool (Moshiri, 2021). For phylogenetic analysis, we employed IQ-TREE2 (Minh et al., 2020) with a maximum likelihood approach. To provide a temporal framework, we then used TreeTime (Sagulenko et al., 2018) to transform the raw maximum likelihood tree into a dated tree, applying a constant mean substitution rate of 8.0×10^{-4} nucleotide substitutions per site per year. This temporal calibration, after excluding outlier sequences, allowed us to place each sample in a chronological context, enhancing our understanding of the timing and dynamics of viral spread.

Statistical analysis

Data were analyzed for statistical significance using the Student's two-tailed t-test or one-way ANOVA when appropriate. Bonferroni post-test was used to compare data. Differences were considered significant when $P < 0.05$. Statistical tests were performed using Prism 8 software (GraphPad Software, La Jolla, CA, USA).

Results

HSPGs mediate spike/$\alpha_v\beta_3$ interaction

The RGD motif is not exposed on the surface of the RBD domain of the entire spike protein (Nitahara et al., 2021). It is worth noting that the optimal RBD conformation for ACE2 binding is promoted by HSPGs/spike interaction (Clausen et al., 2020). Previously, we demonstrated that the RBD domain of Omicron BA.1 endowing the RGD motif, but not the one belonging to Omicron BA.5 carrying the D405N mutation, directly interacts with $\alpha_v\beta_3$ (Bugatti et al., 2023). To assess whether a correct three-dimensional configuration of the entire trimeric spike protein of SARS-CoV-2 is required to bind the $\alpha_v\beta_3$ integrin, the latter was immobilized on a CM5 sensor chip. Two recombinant trimeric SARS-CoV-2 spike proteins were used; one belonging to Omicron

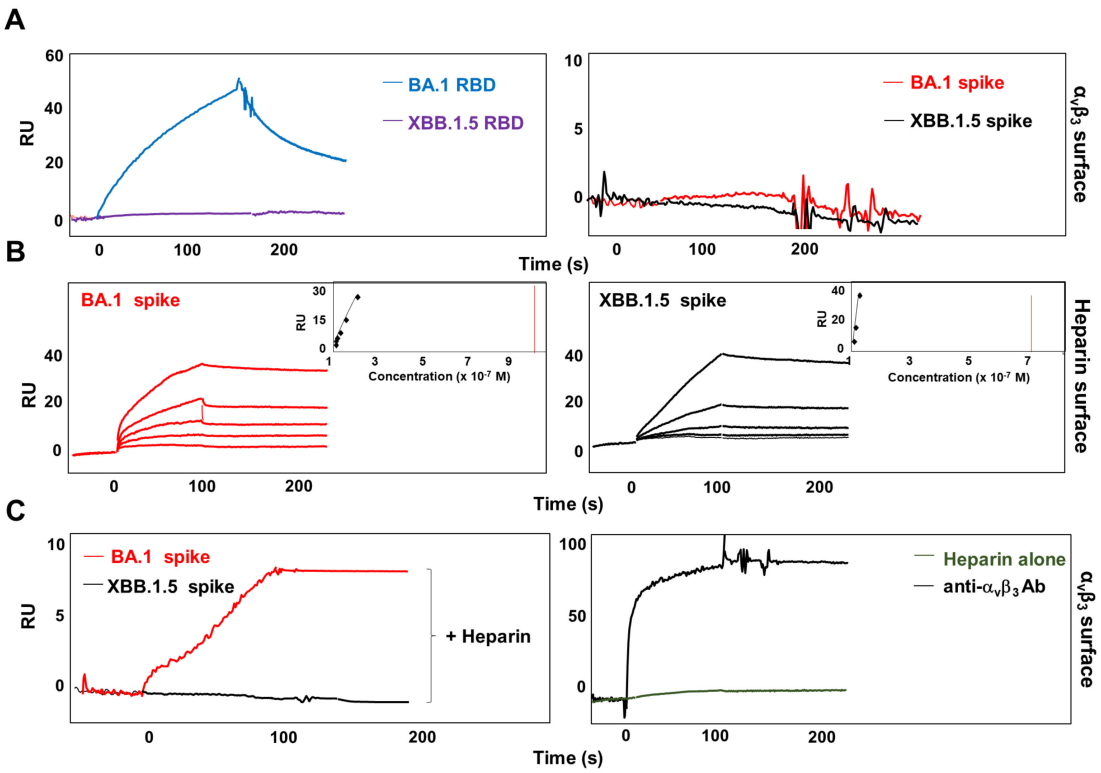

FIGURE 1
Heparin mediates SARS-CoV-2 Omicron BA.1 interaction with $\alpha_v\beta_3$ integrin. **(A)** BA.1 (blue line) and XBB.1.5 (purple line) RBDs or BA.1 (red line) and XBB.1.5 (black line) spike proteins were injected onto $\alpha_v\beta_3$ surface at a single concentration. **(B)** Sensogram overlay showing the binding of increasing amounts of BA.1 (range from 6.25 to 100 nM, left panel) and XBB.1.5 (range from 1.56 to 25 nM, right panel) spike proteins to heparin surface. The response, in resonance units (RU), was recorded as a function of time. Inset of left and right panels: equilibrium binding data generate the saturation curve and scatchard plot regression. **(C)** BA.1 (red line, left panel) and XBB.1.5 (black line, left panel) spikes were co-injected with heparin onto the $\alpha_v\beta_3$ surface. Antibody against $\alpha_v\beta_3$ (black line, right panel) and soluble heparin alone (green line, right panel) were injected as control.

BA.1, displaying the RGD motif, (BA.1 spike) and the other belonging to Omicron XBB.1.5, displaying the mutated RGN domain, (XBB.1.5 spike). The RBD domains of Omicron BA.1 and XBB.1.5 (BA.1 RBD and XBB.1.5 RBD, respectively) were used as control of interaction. Interestingly, as shown in Figure 1A, right panel, the trimeric SARS-CoV-2 spike protein belonging to the Omicron BA.1 lineage, differently from its RBD counterpart (Figure 1A, left panel), did not show any interaction with immobilized $\alpha_v\beta_3$ integrin. As expected, trimeric Omicron XBB.1.5 spike protein (Figure 1A, right panel), as well as its RBD domain (Figure 1A, left panel), is not capable of binding $\alpha_v\beta_3$ integrin. Based on this evidence, we hypothesized that to convert the RBD from inaccessible to accessible conformation and to expose the RGD motif, SARS-CoV-2 spike protein needs a cofactor. Past work shows that HSPGs, abundant components of the extracellular matrix (ECM) (Hassan et al., 2021), binds to spike proteins and increase the number of spike RBDs in the up conformation (Zhang et al., 2024). Thus, we speculate that HSPGs may act as cofactors favoring spike/$\alpha_v\beta_3$ interaction. To test this hypothesis, we used an SPR model that mimics the binding of proteins to cell surface-associated HSPGs immobilizing biotinylated heparin on the sensor chip. As shown in Figure 1B, both BA.1 and XBB.1.5 spike proteins interact with immobilized heparin (left panel and right panel, respectively), in a dose-dependent manner. The sensorgram overlay allowed the calculation of association (k_{on}) and dissociation (k_{off}) rates and of *Kd* (as k_{off}/k_{on} ratio) value. Kinetic parameters of spike proteins/heparin interaction are reported in Table 1. Equilibrium binding data were used to generate the saturation curve and scatchard plot regression (inset panels in Figure 1B) and to calculate a *Kd* value independent from kinetic parameters (Table 1). This evidence prompted us to deeply scrutinize whether spike/heparin interaction could induce the exposure of the RGD motif thus allowing its interaction with $\alpha_v\beta_3$ integrin. Interestingly, as shown in Figure 1C, BA.1 spike protein (left panel, red line) acquired the capacity to bind the immobilized $\alpha_v\beta_3$ when injected in the presence of soluble heparin. On the contrary, no interaction was observed between immobilized $\alpha_v\beta_3$ and XBB.1.5 spike (left panel, black line), carrying the mutated RGD motif, in the presence of heparin (Figure 1C). Antibody against $\alpha_v\beta_3$ (black line) was used as positive control of surface specificity while soluble heparin alone (green line) was used as negative control of interaction (Figure 1C, right panel). This result confirmed the hypothesis that HSPGs act as a cofactor that promote the RBD open conformation and the exposure of the RGD motif in SARS-CoV-2 Omicron BA.1 spike protein allowing its interaction with $\alpha_v\beta_3$ integrin.

TABLE 1 Kinetic and affinity parameters of SARS-CoV-2 Omicron BA.1 and XBB.1.5 spike proteins on immobilized Heparin.

	K_{on} (1/Ms)	K_{off} (1/s)	Kd (M)	Kd_{eq} (M)
Omicron BA.1	3.137×10^{5}	0.5616	1.790×10^{-6}	8.807×10^{-7}
Omicron XBB.1.5	2.425×10^{5}	0.02681	1.105×10^{-7}	6.022×10^{-7}

To further confirm the SPR experiments, an immunofluorescence (IF) assay was performed. For this purpose, HL-mECs were incubated for 1 h at 4°C with recombinant SARS-CoV-2 Omicron BA.1 and Omicron XBB.1.5 spike proteins and then fixed before being stained with antibodies against the spike proteins (green signal) and $\alpha_v\beta_3$ integrin (red signal). As shown in Figure 2A, BA.1 spike protein localized on the surface and along the contour of the cell at the integrin signal (left panel), whereas the XBB.1.5 spike protein localized on the surface of the HL-mECs only, and was not localize along the integrin signal (Figure 2B, left panel). This result demonstrates that both BA.1 and XBB.1.5 proteins bind to HSPGs, but only the BA.1 spike protein is also able to interact with $\alpha_v\beta_3$ integrin via its RGD motif. When HL-mECs were pretreated with sodium chlorate, no surface signal was observed for both BA.1 and XBB.1.5 spike proteins (Figures 2A, B, middle panel, respectively), thus confirming that HSPGs are involved in the attachment of SARS-CoV-2 spikes to the ECs. To assess whether soluble heparin was able to rescue the ability of the spike proteins to bind $\alpha_v\beta_3$ integrin in HL-mECs pretreated with sodium chlorate, BA.1 and XBB.1.5 spike proteins were pre-incubated with soluble heparin (10 µg/ml) at 37°C for 1 h and then incubated for 1 h at 4°C on HL-mECs. As shown in Figure 2A (right panel), the localization of BA.1 spike protein was overlapping with that observed in untreated HL-mECs, indicating an interaction between BA.1 and $\alpha_v\beta_3$ integrin. As expected, XBB.1.5 spike protein was not observed on the surface of HL-mECs not expressing HSPGs (Figure 2B, right panel). Taken together, our data confirmed the ability of heparin/HSPGs to promote the exposure of the RGD motif in the BA.1 spike protein, allowing its subsequent binding to the $\alpha_v\beta_3$ integrin.

HSPGs mediate Omicron BA.1-HL-mECs infection

SPR and IF experiments demonstrated that the trimeric spike/integrin interaction depends on the presence of HSPGs. To verify *in vitro* that HSPGs are indispensable to promote SARS-CoV-2 attachment and infection of HL-mECs, Heparinase III or sodium chlorate pretreated-HL-mECs were infected with 1 MOI of authentic SARS-CoV-2 belonging to Omicron BA.1 lineage. SARS-CoV-2 Omicron XBB.1.5 lineage, carrying the D405N mutation, was used as a negative control of infection.

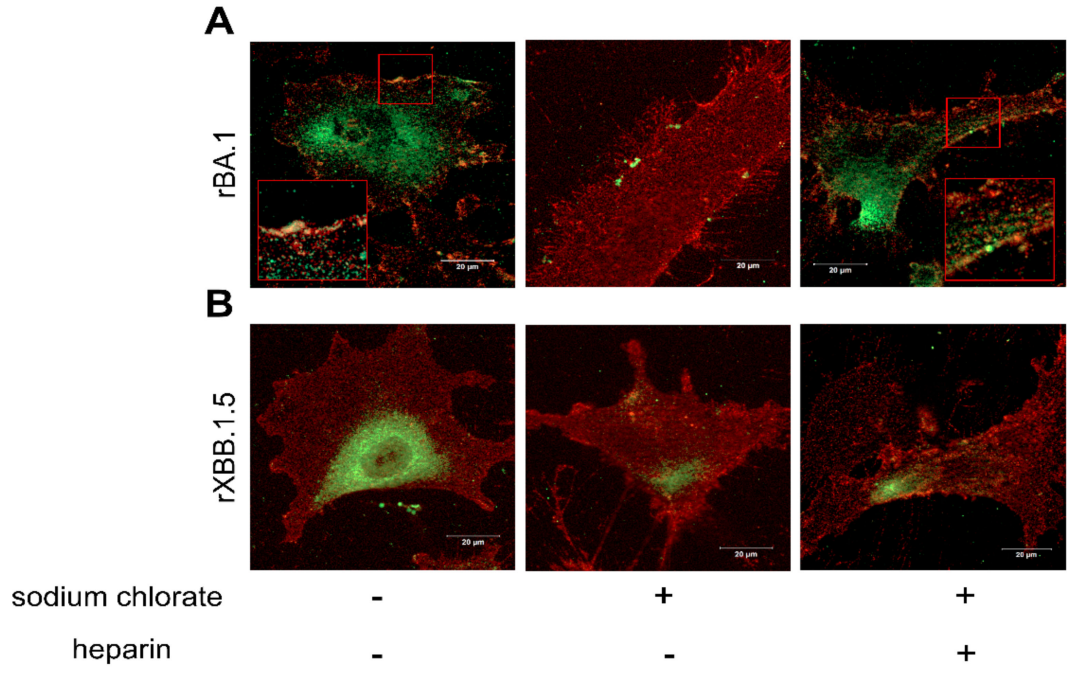

FIGURE 2
HSPGs mediate SARS-CoV-2 Omicron BA.1 interaction with $\alpha_v\beta_3$ integrin on HL-mECs. HL-mECs were incubated with recombinant Omicron SARS-CoV-2 BA.1 (**A,** left panel) or XBB.1.5 (**B,** left panel) spike proteins (rBA.1 and rXBB.1.5, respectively) for 2 h at 4°C, then washed and fixed with 4% PFA in PBS. For staining, cells were incubated for 1 h at 4°C with a human serum containing IgG to SARS-CoV-2 or anti-$\alpha_v\beta_3$ antibody followed by Alexa Fluor 488-conjugated anti-human IgG or Alexa Fluor 594-conjugated anti-mouse IgG, respectively. Nuclei were counterstained with DAPI. Images display SARS-CoV-2 spike signal in green, $\alpha_v\beta_3$ signal in red and cell nuclei in blue. HL-mECs were pretreated with sodium chlorate, incubated with rBA.1 (**A,** middle panel) and rXBB.1.5 (**B,** middle panel) and decorated as described above. After all, pretreated sodium chlorate-HL-mECs were incubated with a mix solution of rBA.1 (**A,** right panel) or rXBB.1.5 (**B,** right panel) spike proteins and soluble heparin (preincubation at 37°C for 1 h) and decorated as above. Scale bar, 20 µm.

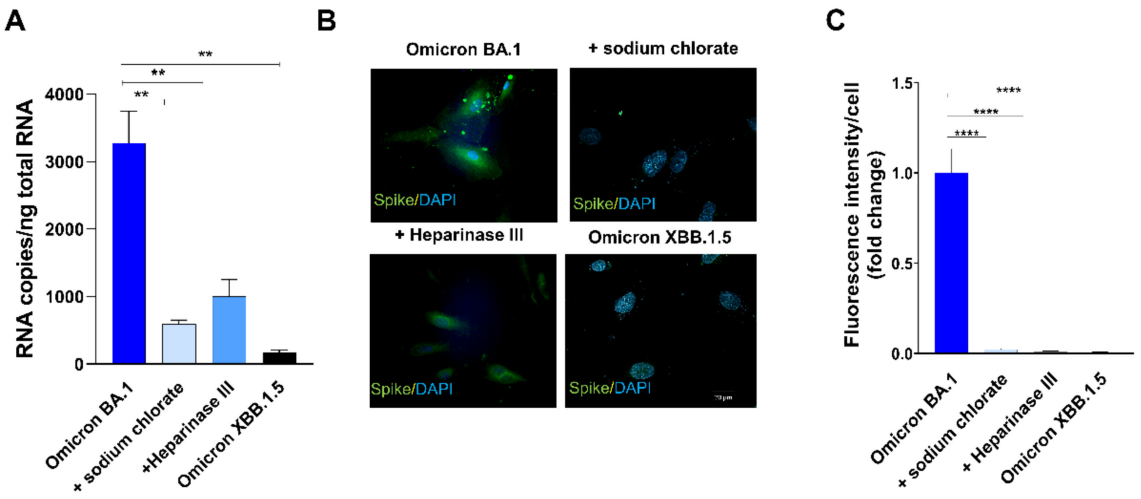

FIGURE 3
HSPGs are indispensable to mediate Omicron BA.1-HL-mECs infection. HL-mECs were pretreated with Heparinase III and sodium chlorate for 1 h and 48 h at 37°C, respectively. After treatment, the cells were infected with Omicron BA.1 and Omicron XBB.1.5 at a MOI of 1 for 1 h at 37°C, then washed and cultured until day 1 p.i. **(A)** The graph shows quantification of SARS-CoV-2 genomes at the intracellular level by qRT-PCR. At least three replicates were performed. Data are representative of two independent experiments with similar results. Statistical analysis was performed by one-way ANOVA (**p = 0.0023). **(B)** HL-mECs were fixed, permeabilized, and saturated with BSA. For staining, cells were incubated for 1 h at 37°C with a human serum containing IgG to SARS-CoV-2 and followed by Alexa Fluor 488-conjugated anti-human IgG. Nuclei were counterstained with DAPI. Images display SARS-CoV-2 signal in green and cell nuclei in blue (scale bar, 20 μm). **(C)** Spike-related fluorescent area was quantified in 20-30 Omicron BA.1-infected cells pretreated or not with sodium chlorate or Heparinase III and subtracted from not-infected cells fluorescence signal. Decrease of spike-related fluorescence in pretreated cells with sodium chlorate or Heparinase III Omicron BA.1 infected-cells was related to Omicron BA.1 signal and was expressed as fold change. Statistical analysis was performed by unpaired t-test (****p < 0.0001).

Twenty-four h p.i., SARS-CoV-2 viral genome and protein expression were evaluated by quantitative real-time PCR and indirect IF assay, respectively. As shown in Figure 3A, quantification of intracellular SARS-CoV-2 RNA showed a significant reduction of viral RNA in Heparinase III- and sodium chlorate-pretreated HL-mECs as compared to SARS-CoV-2 Omicron BA.1-infected ones. As expected, Omicron XBB.1.5 did not infect HL-mECs. Similar results were obtained by evaluating viral protein expression in HL-mECs by IF. As shown in Figure 3B, the presence of SARS-CoV-2 spike protein was observed in Omicron BA.1-infected HL-mECs, whereas viral protein expression was not observed in Heparinase III and sodium chlorate pretreated-cells, as well as in Omicron XBB.1.5 infected-ones. Quantification of the spike-related fluorescence in Omicron BA.1-infected cells pretreated with HSPGs inhibitors confirmed the absence of viral proteins (Figure 3C). Taken together, these findings demonstrate that the binding of SARS-CoV-2 spike protein to HSPGs on the cell surface is indispensable to expose the RGD motif thus allowing its interaction with ECs and promoting virus infection.

HSPGs are favor Omicron BA.1-induced angiogenic phenotype

To scrutinize the role of HSPGs in Omicron BA.1-induced angiogenesis, we took advantage of the spheroid assay, a three-dimensional (3D) cell model that mimics *in vivo* sprouting angiogenesis (Caccuri et al., 2021). To this end, 3 days p.i., HL-mECs infected with SARS-CoV-2 belonging to Omicron BA.1 and Omicron XBB.1.5 sublineages, pretreated or not with sodium chlorate or Heparinase III, were collected to generate spheroids (Chiodelli et al., 2011). As shown in Figure 4A, after 24 h of observation, non-infected spheroids (NI) did not develop any sprout while in SARS-CoV-2 Omicron BA.1-infected spheroids (Omicron BA.1) a consistent outgrowth of sprouts was observed. The effect of Omicron BA.1 infection on sprouting angiogenesis was found to be superimposable to that observed upon FGF-2 treatment, representing the positive control. Interestingly, spheroids generated by using HSPGs inhibitors-pretreated cells infected with Omicron BA.1, showed a dramatic reduction of vessel outgrowth (Figure 4A). Once again, the Omicron XBB.1.5 virus, carrying the RGN motif, was not able to gain access into ECs and to induce pro-angiogenic activity.

In order to understand whether HSPGs inhibition was impacting ECs pro-angiogenic functions upon Omicron BA.1 infection, we analyzed the infected-HL-mECs secretome at day 3 p.i., by using a human angiogenic array. As expected, SARS-CoV-2 Omicron BA.1 triggered the secretion of different pro-angiogenic molecules, in particular Interleukin-8 (IL-8), Fibroblast growth factor-2 (FGF-2), Angiopoietin-2 (Ang2), Endothelin-1 (ET-1) and dipeptidyl-peptidase IV (DPPIV) (Figure 4B, dark blue bars). The release of these factors was strongly inhibited by sodium chlorate or Heparinase III pretreatment of HL-mECs (Figure 4B, light blue and azul bars, respectively) confirming that lack of HSPGs on HL-mECs inhibits viral infection and the release of angiogenic factors in the microenvironment.

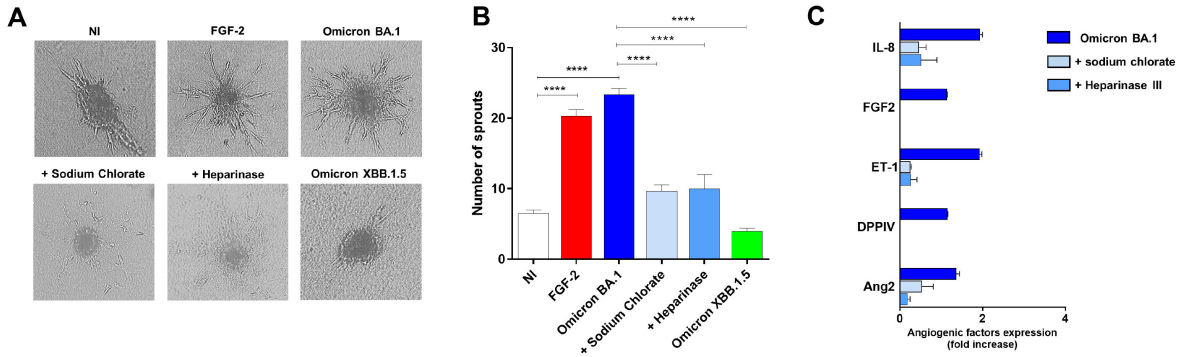

FIGURE 4
HSPGs inhibitors-treated HL-mECs do not acquire an angiogenic phenotype and do not release angiogenic factors upon Omicron BA.1 infection. HL-mECs were not-infected (NI) or infected with SARS-CoV-2 belonging to Omicron BA.1 or XBB.1.5 sublineages at MOI 1, for 1 h at 37°C and then washed and cultured until day 3 p.i. When indicated HL-mECs were pretreated with sodium chlorate (50 mM) or Heparinase III (5 mU/ml). **(A)** Sprouting of spheroids generated with NI, Omicron BA.1, and HSPGs inhibitors pretreated-HL-mECs. Pictures are representative of one out of three independent experiments with similar results (scale bar, 10 µm). FGF-2 was used as a positive control. **(B)** Values reported in the graph are the mean ± SD of one representative experiment out of three independent experiments with similar results performed in triplicate. Statistical analysis was performed by one-way ANOVA and Bonferroni's post-test was used to compare data (****$p < 0.0001$). **(C)** Sodium chlorate and Heparinase III pretreated- or not HL-mECs, were infected with SARS-CoV-2 Omicron BA.1 lineage at MOI 1, for 1 h at 37°C and then washed and cultured until day 3 p.i. Clarified supernatants were evaluated for the presence of angiogenic molecules by a human proteome array. The results are expressed as mean values ± SD of duplicates given as fold increase as compared to NI cells. Data are representative of one out of two independent experiments with similar results.

SARS-CoV-2 induces accumulation and degradation of von Willebrand factor into ECs

Some viruses, such as Kaposi sarcoma-associated herpesvirus (KSHV) induce the release of IL-8, Ang2, ET-1, and von Willebrand factor (vWF) in ECs (Ye et al., 2013). Furthermore, it has been shown that SARS-CoV-2 spike protein induces the release of vWF from ECs (Li et al., 2022). Interestingly, we found the presence of IL-8, Ang2 and ET-1 in SARS-CoV-2-infected HL-mECs secretome. This finding led us to investigate whether the authentic virus was able to induce the storage and the release of vWF which is known to exert multiple vascular roles in ECs including angiogenesis (Starke et al., 2011). To this aim, a mCherry-vWF-expressing plasmid was used to nucleofect ECs and to monitor vWF accumulation in Weibel Palade Bodies (WPBs) in Omicron BA.1 infected-HL-mECs at different time points (1, 3, 6, and 24 h p.i.). As shown in Figure 5A, upon SARS-CoV-2 infection, Omicron BA.1 infected-HL-mECs (Omicron BA.1) showed an increase of vWF accumulation until 6 h p.i. and a decrease at 24 h p.i., as compared to NI cells. To evaluate if the amount of vWF observed in infected HL-mECs was secreted in the extracellular environment or degraded upon time, we quantified the amount of vWF in cell supernatants by an ELISA array. As shown in Figure 5B, there was no difference in the quantity of vWF found in infected or NI cells at 1, 3 and 6 h p.i. Interestingly at 24 h p.i., a significant amount of secreted vWF was observed in the supernatants of NI cells as compared to the infected ones. These data suggest that the accumulated vWF, observed in infected-HL-mECs, is not released into the extracellular environment, but it is likely to be degraded within cells. As expected, in NI cells after its accumulation vWf is released within 24 h of observation (Figure 5B). vWF decrease observed in our results could be related to the strong expression of the angiogenic factors previously described in HL-mECs secretome, as already shown for Ang2 (Randi et al., 2018).

To further scrutinize the direct involvement of virus entry in vWF accumulation and degradation, we pretreated HL-mECs with HSPGs inhibitors before SARS-CoV-2 infection. As shown in Figure 5C, pretreatment with sodium chlorate or Heparinase III strongly inhibited (78% and 71%, respectively) vWF accumulation into infected HL-mECs demonstrating that the block of viral binding to HSPGs and subsequently to integrin, directly correlates with vWF presence in WPBs. Taken together, our data demonstrate that cytoplasmic vWF increase upon SARS-CoV-2 infection is specific and depends on the virus entry.

SARS-CoV-2 promotes angiogenesis through the activation of FAK/Src/ERK signaling pathways

The binding to integrin receptors activates tyrosine kinase signaling pathways, leading to phosphorylation of FAK, and Src (Ye et al., 2013). In particular, $\alpha_v\beta_3$ integrin promotes signaling events necessary for vascular cell survival, thereby facilitating the induction and/or maintenance of the angiogenic phenotype (Eliceiri et al., 1998). This knowledge prompted us to investigate the ability of SARS-CoV-2 to induce a productive cross-talk between spike and $\alpha_v\beta_3$ integrin to trigger FAK/Src signaling in infected HL-mECs. To this aim, the cells were infected with Omicron BA.1 and Omicron XBB.1.5, as previously described. At 1 h p.i., HL-mECs were lysed and 20 µg of total proteins were analyzed by western blotting with anti-p-FAK and anti-p-Src

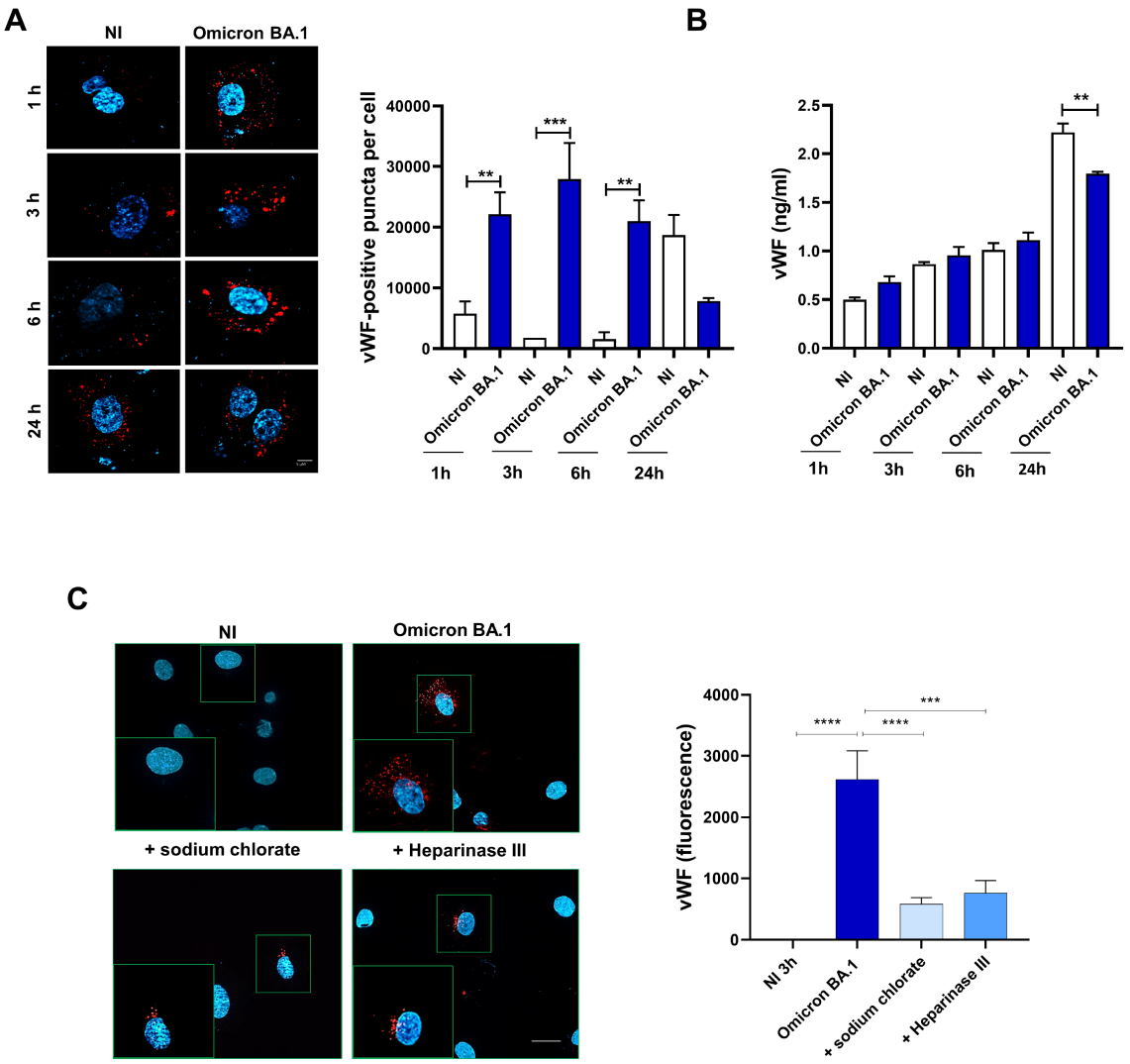

FIGURE 5
SARS-CoV-2 induces vWF accumulation in WPBs and subsequently degradation in ECs. HL-mECs were nucleofected with a mCherry-vWF-expressing plasmid and 24 h after nucleofection, cells were infected with Omicron BA.1 virus and analyzed at different time points (1, 3, 6 and 24 h). (**A,** left panel) The images display vWF signals in red and cell nuclei in blue (scale bar, 10 µm). Red-positive punctate structures were counted in order to quantify the levels of WPBs. (**A,** right panel) Values reported for vWF positive structures are the mean ± SD of 3 independent experiments with similar results. **(B)** Amount of vWF in SARS-CoV-2 infected HL-mECs supernatants are the mean ± SD of 3 independent experiments with similar results. Statistical analysis was performed by one-way ANOVA, and the Bonferroni post-test was used to compare data (**p = 0.022, ***p = 0.0008). **(C)** Infected HL-mECs pretreated or not with HSPGs inhibitors were analyzed at 3 h p.i. Values reported for vWF positive structures are the mean ± SD of 3 independent experiments with similar results. Statistical analysis was performed by one-way ANOVA, and the Bonferroni post-test was used to compare data (***p = 0.0008, ****p < 0.0001).

antibodies. As shown in Figures 6A, B, Omicron BA.1 induced the phosphorylation of FAK and Src (2.3 ± 0.7 and 1.8 ± 0.5-fold increase, respectively). On the contrary, Omicron XBB.1.5, carrying the D405N mutation, does not activate FAK/Src signaling pathways (Figures 6A, B), thus supporting the direct role exerted by $\alpha_v\beta_3$ in promoting FAK/Src phosphorylation in ECs. This data also indicates that spike/HSPGs interaction is not sufficient to direct HL-mECs toward a pro-angiogenic phenotype.

To further confirm the role played spike/$\alpha_v\beta_3$ interaction in inducing an angiogenic signaling activation, HL-mECs were pretreated with a neutralizing monoclonal antibody against $\alpha_v\beta_3$ integrin (mAb anti-$\alpha_v\beta_3$), Heparinase III or sodium chlorate, then infected with Omicron BA.1 and analyzed for FAK/Src signaling activation. As shown in Figures 6D, E, Omicron BA.1 was able to induce an increase of FAK and Src phosphorylation as compared to NI-HL-mECs while mAb anti-$\alpha_v\beta_3$, Heparinase III and sodium chlorate treatment induced a significant inhibition of FAK (54%, 48% and 48% respectively) and pSrc (56%, 66% and 65%, respectively) activation.

Since pERK signal transduction pathway in ECs is required for angiogenesis and correlates with FAK/Src activation (Murphy et al., 2006), we investigated ERK phosphorylation upon SARS-CoV-2 infection. To this end, HL-mEC were infected with SARS-CoV-2 Omicron BA.1 or Omicron XBB.1.5 in the presence or

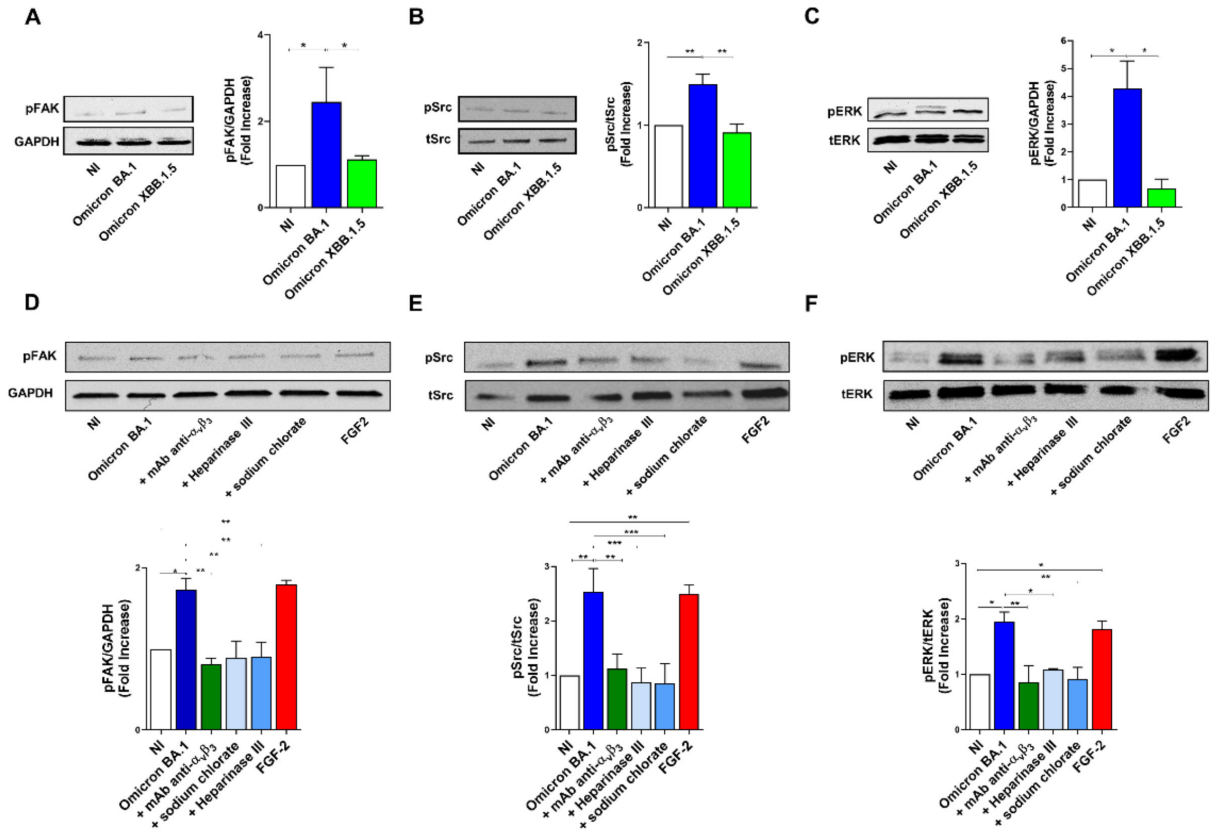

FIGURE 6
SARS-CoV-2 Omicron BA.1 induces FAK/Src and ERK signaling after $\alpha_v\beta_3$ interaction. HL-mECs were not infected (NI) or infected with Omicron SARS-CoV-2 belonging to BA.1 and only XBB.1.5 sublineages (Omicron BA.1 and Omicron XBB.1.5, respectively) at a MOI of 1 for 1 h at 37°C. After 1 h p.i., cell lysates were analyzed by western blotting with anti-pFAK, anti-pSRC and anti-pERK antibodies (**A-C**, respectively). Blots are representative of three independent experiments with similar results. Quantification was carried out by densitometric analysis and plotting of the pFAK, pSrc and pERK normalized on GAPDH, tSrc or tERK as indicated in the graph. Values reported are the means ± the SD of three independent experiments. Statistical analysis was performed by one-way ANOVA, and the Bonferroni post-test was used to compare data (*p = 0.05, **p = 0.022, ***p = 0.0008). When indicated HL-mECs were pretreated with a mAb against $\alpha_v\beta_3$ integrin (mAb anti- $\alpha_v\beta_3$) or HSPGs inhibitors and analyzed for FAK/Src and ERK phosphorylation status **(D-F)**.

absence of the mAb anti-$\alpha_v\beta_3$ or HSPGs inhibitors. As shown in Figure 6C, Omicron BA.1, but not Omicron XBB.1.5, was able to induce a strong increase (3.5 ± 1.5-fold increase) in ERK phosphorylation as compared to NI cells. As expected, ERK activation was inhibited when HL-mECs were pretreated with the mAb anti-$\alpha_v\beta_3$ or HPSGs inhibitors, in particular sodium chlorate treatment inhibited SARS-CoV-2-ERK phosphorylation of about 53%, while mAb anti-$\alpha_v\beta_3$ and Heparinase III treated-HL-mECs showed an inhibition of ERK activation equal to 44% and 56%, respectively (Figure 6F). Our data highlight that the docking of spike protein to HSPGs allows its interaction with $\alpha_v\beta_3$, thus promoting the angiogenic signaling pathway in SARS-CoV-2-infected HL-mECs.

Recent SARS-CoV-2 strains carry the reverse mutation S405D

Phylogenetic analysis, based on 1,083 SARS-CoV-2 whole-genome sequences, revealed distinct evolutionary patterns among the four mutations of interest: D405D, D405N, N405S, and the reverse mutation S405D (Figure 7A). D405D was the predominant substitution from 2020 to 2022. The emergence of D405N and N405S suggests transient evolutionary shifts, potentially representing intermediate states. Notably, S405D reappeared in 2024 within a distinct clade, indicating a possible adaptive event. High support values at key nodes reinforce the reliability of these phylogenetic relationships. As shown in Figure B, temporal analysis further confirms that D405D remained dominant from 2020 to 2022, while D405N and N405S gradually increased in prevalence, particularly in 2022. A distinct shift was observed in 2024, marked by the re-emergence of S405D, suggesting a potential selective advantage or convergent evolution (Figure 7B).

Discussion

SARS-CoV-2 infects primary ACE2-negative HL-mECs, by using $\alpha_v\beta_3$ integrin as an alternate receptor to ACE2 (Caccuri et al., 2021; Bugatti et al., 2022). Specifically, SARS-CoV-2 binding

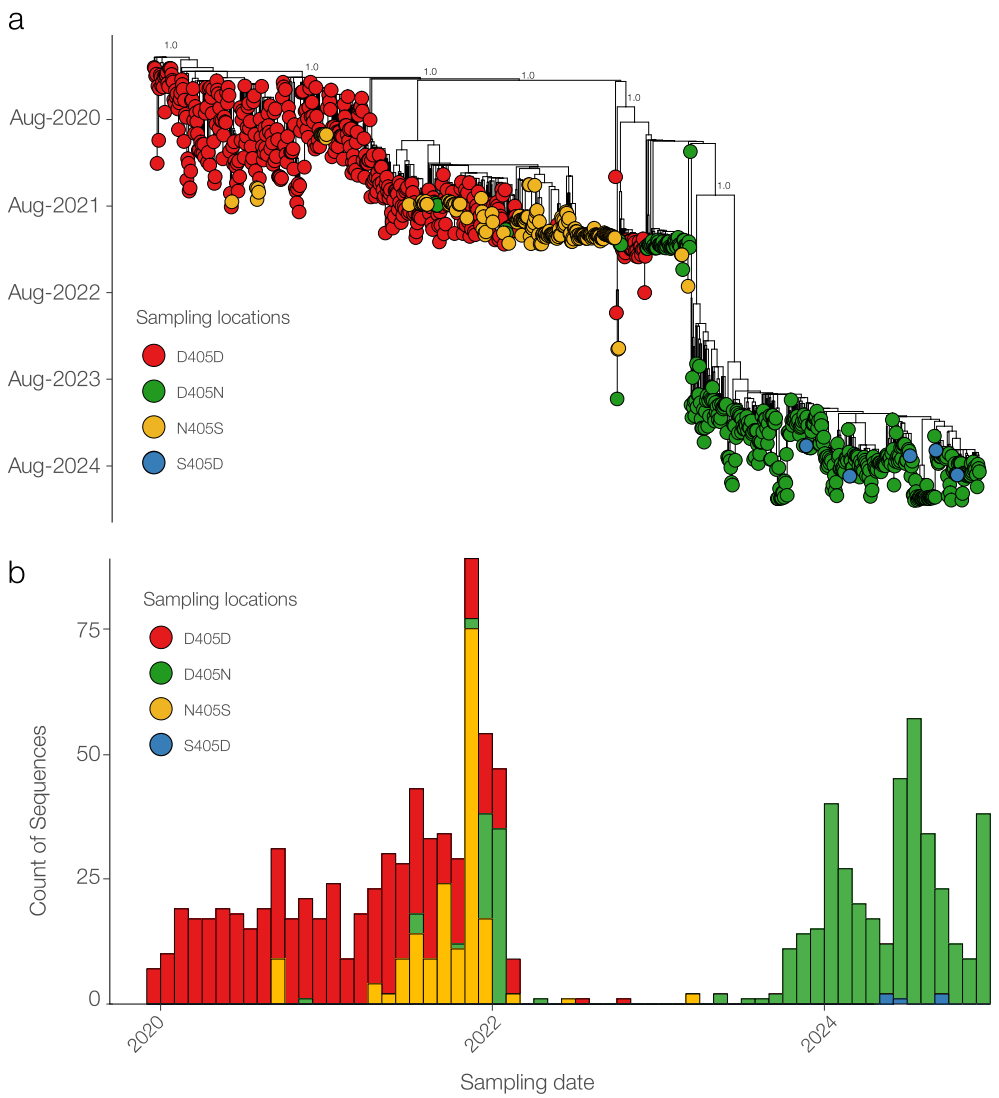

FIGURE 7
Phylogenetic and temporal analysis of SARS-CoV-2 sequences carrying D405D and its mutations. **(A)** Maximum likelihood phylogenetic tree showing the distribution of sequences with D405D (red) and its alternative substitutions: D405N (green), N405S (yellow), and S405D (blue). **(B)** Temporal distribution of SARS-CoV-2 sequences by substitution type.

to $\alpha_v\beta_3$ integrin occurs through an RGD (403–405: Arg-Gly-Asp) motif included in the RBD of the viral spike protein. Even if HL-mECs do not support virus replication, the presence of viral RNA and/or newly synthesized viral proteins into ECs induce the release of pro-inflammatory and pro-angiogenic molecules thus promoting an angiogenic phenotype (Caccuri et al., 2021; Bugatti et al., 2022).

It has been demonstrated that neither antibodies binding the epitope containing the RGD motif (Koehler et al., 2020) nor neutralizing antibodies evoked by BNT162b2 vaccination against the spike protein (Caccuri et al., 2021; Bugatti et al., 2022) are able to counteract virus infection on ECs, highlighting that they do not interfere with the integrins recognition site. These results suggest that the RGD motif is not accessible to antibodies and that conformational changes induced by a cofactor may favor its exposure and interaction with $\alpha_v\beta_3$ integrin.

HSPGs are highly sulfated glycosaminoglycan ubiquitously distributed on cell surfaces. They are used by different viruses including herpes simplex virus (Bacsa et al., 2011), dengue virus (Chen et al., 1997), and human papillomavirus (Richards et al., 2013) for attachment and entry into host cells. It has been recently shown that HSPGs act as coreceptors also for SARS-CoV-2 infection (Clausen et al., 2020). In particular, SARS-CoV-2 spike protein interacts with HSPGs on cell surface and undergoes conformational leading to a better interaction with ACE2 (Milewska et al., 2014). In this view HSPGs may be also involved in conformational changes conducting to RGD exposure.

Here we show by SPR analysis that heparin, a structural analogue of HS, interacts with the spike protein and induces conformational changes, a *conditio sine qua non* for triggering RGD/$\alpha_v\beta_3$ interaction. Moreover, we show that Heparinase III and sodium chlorate, catalyzing HSPGs degradation and

undersulfation respectively, significantly inhibit integrin-mediated SARS-CoV-2 entry into ACE2-negative ECs. Interestingly, the altered bioavailability and activity of HSPGs not only impact SARS-CoV-2 entry into ECs, but also modify critical cellular signaling pathways and microenvironmental responses usually occurring after viral infection. Indeed, SARS-CoV-2 activates FAK-Src and ERK signaling pathways, which are mainly involved in $\alpha_v\beta_3$-related angiogenesis (Pang et al., 2023). Interestingly, impairment of HSPGs interaction with the spike protein, by specific inhibitors, completely abrogates angiogenesis-related pathways, as previously demonstrated by using cilengitide, an $\alpha_v\beta_3$ antagonist (Nader et al., 2021). HSPGs inhibitors also block SARS-CoV-2-induced release of pro-angiogenic molecules, in particular IL-8, FGF-2, Ang2, ET-1 and DPPIV, which have been previously shown to be secreted in the microenvironment of SARS-CoV-2-infected HL-mECs (Caccuri et al., 2021; Bugatti et al., 2022).

$\alpha_v\beta_3$ is known to play a complex role in angiogenesis, as both pro- or anti-angiogenic molecules, mostly depending on the local extracellular environment and/or the specific ligand(s) (Somanath et al., 2009). One of such ligands is vWF, a multimeric plasma glycoprotein that mediates platelet adhesion to both the subendothelial matrix and the endothelial surface. It acts as a carrier for coagulation factor VIII in the circulation and is essential for the hemostasis involved in inflammation (Casari et al., 2013). Besides its well-characterized role in hemostasis, vWF has increasingly been implicated in angiogenic processes (Randi and Laffan, 2017). vWF regulates angiogenesis through multiple cross-talking pathways involving $\alpha_v\beta_3$, VEGFR-2 and Ang2 (Starke et al., 2011) and is essential for the formation of WPBs, which contain vasoactive molecules mediating angiogenesis (Mojzisch and Brehm, 2021). Dysfunctional vWF may result in constitutive release of WPB components such as Ang2. It is known that vWF controls Ang2 levels by promoting its storage and inhibiting its synthesis (Randi et al., 2013). Indeed, inhibition of vWF induces angiogenesis on ECs and is coupled with increased release of Ang2 (Randi et al., 2018). Thus, it can be hypothesized that vWF modulates angiogenesis by regulating Ang2 storage in ECs. The latter is known to promote angiogenesis by destabilizing blood vessels and acting synergistically with VEGF-A (Randi et al., 2013). Here we demonstrate that upon SARS-CoV-2 infection, vWF accumulates within – but is not secreted by – ECs leading to the hypothesis that this factor is degraded in WPBs thus allowing Ang2 release. Taken together, our findings support the hypothesis that dysfunctional vWF metabolism coupled with Ang2 signaling accompanied to a dysregulated anti-angiogenic and inflammatory environment contribute to promoting angiogenesis during SARS-CoV-2 infection (Figure 8). Additional studies may lead to insight into whether targeting the vWF-Ang2 axis may prevent aberrant angiogenesis observed in the lung of SARS-CoV-2 infected patients.

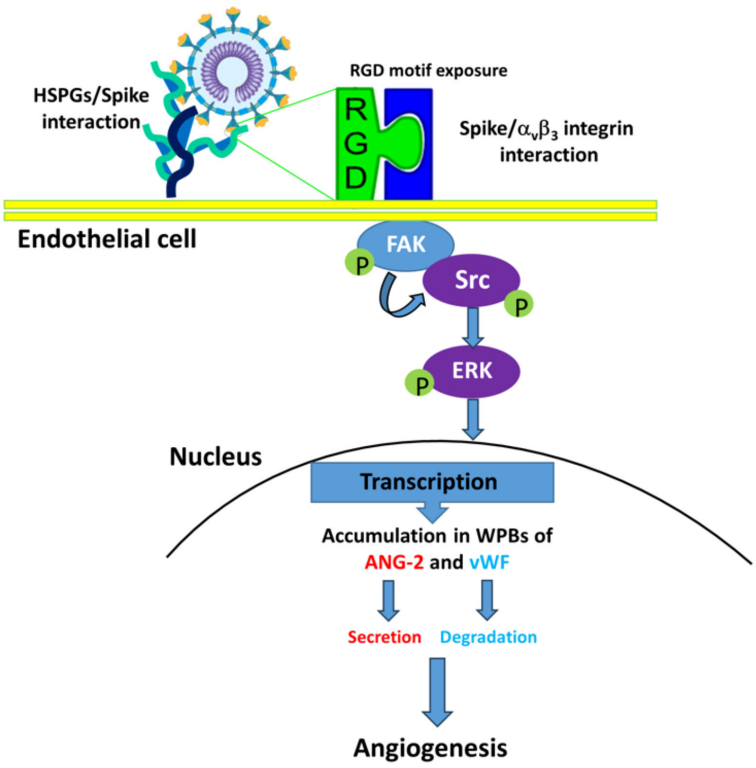

FIGURE 8
Proposed mechanisms for SARS-CoV-2-induced angiogenesis on ACE2-negative HL-mECs. HSPGs mediate spike/$\alpha_v\beta_3$ interaction enhancing phosphorylation of FAK, Src and ERK, which mediates Ang-2 and vWF accumulation in WPBs of SARS-CoV-2-infected HL-mECs. Then, Ang-2 secretion and vWF degradation induces infected-HL-mECs toward an angiogenic phenotype.

SARS-CoV-2 underwent mutagenesis over time and some mutations are considered to be part of its adaptive evolution process leading to changes in disease severity and immunological responses including antigenic properties, immune evasion and sensitivity to therapeutics. The viral fitness, which influences the virus ability to infect, replicate and spread, is highly dynamic and depends on a variety of factors such as virus properties and escape of immunity. Thus, it is of extreme importance to understand the drivers of SARS-CoV-2 fitness and the prediction of the mutational pathways by which the virus will evolve. Among the multiple variations, the virus switched the RGD to RGN motif thus acquiring two loss of function, fitness to infect ECs and capability to promote EC dysfunction (Caccuri et al., 2021; Bugatti et al., 2022). In particular, this event occurred with Omicron subvariants that emerged upon time (Cao et al., 2022). Virus evolution is unpredictable, however, it is more likely that future variants will be derived from prior or contemporary VOCs, most recently exemplified by the spate of 'second-generation' Omicron variants derived from BA.2 (Carabelli et al., 2023). Of interest, our phylogenetic analysis revealed that after the mutation D405N/S, in recent clades appeared sequences carrying the back-mutation S405D, indicating a reversion that suggests potential selective pressures influencing these substitutions as an adaptation to environmental or host-related factors. Moreover, the fact that sequences carrying S405D were sampled across diverse regions underscores the global circulation and evolutionary adaptation of SARS-CoV-2. The homoplastic back mutation S405D brings back the ability of SARS-CoV-2 to infect ECs, allowing endothelium dysfunction, thus highlighting the need of a vigilant oversight correlated with clinical data that may be of interest for patient treatment. Tracking the emergence of SARS-CoV-2 variants as potentially more virulent or antigenically significant will help to guide the implementation of targeted control measures and further characterization.

In conclusion, HSPGs represent an attractive target molecule for potential antiviral therapeutics, since they serve as a critical player in the infection of a wide range of viruses, either directly or indirectly (Cagno et al., 2015; Rusnati and Lembo, 2016). Different studies have evaluated a variety of approaches for this purpose (i.e. nanoparticle or peptides) (Donalisio et al., 2012). Data on the interactions between the RBD and HSs, revealed several low-specificity binding modes and potential interaction sites (Parafioriti et al., 2023; Yang et al., 2024). These evidences suggest that HSPGs-targeted therapies can efficiently control SARS-CoV-2 infection being effective intervention strategies (Yang et al., 2024).

COVID-19 is frequently associated with coagulopathy and inflammation, which are clinical targets of heparin (Zhang et al., 2022). Indeed, heparin and its derivatives have been proven to be also useful anti-coagulant and anti-inflammatory molecules (Banik et al., 2021). Thus they may represent a winning therapeutic approach, to not only prevent SARS-CoV-2 infection of ECs, but also to impede endothelial dysfunctions related to viral infection.

Data availability statement

The original contributions presented in the study are included in the article/supplementary material. Further inquiries can be directed to the corresponding author.

Author contributions

AB: Data curation, Investigation, Methodology, Writing – original draft. AZ: Data curation, Investigation, Methodology, Writing – review & editing. MB: Investigation, Methodology, Writing – review & editing. MG: Investigation, Methodology, Writing – review & editing. CR: Investigation, Writing – review & editing. MC: Writing – review & editing. AC: Conceptualization, Funding acquisition, Writing – review & editing. FC: Conceptualization, Funding acquisition, Project administration, Writing – review & editing.

Funding

The author(s) declare that financial support was received for the research and/or publication of this article. This research was funded by PRIN 2022 CUP: F53D23000980006 2023-PRIN-BD_002 to CF and RIPREI 2023–0b6c6c2dcd-cb to CA.

Conflict of interest

The authors declare that the research was conducted in the absence of any commercial or financial relationships that could be construed as a potential conflict of interest.

The author(s) declared that they were an editorial board member of Frontiers, at the time of submission. This had no impact on the peer review process and the final decision.

Generative AI statement

The author(s) declare that no Generative AI was used in the creation of this manuscript.

Publisher's note

References

Bacsa, S., Karasneh, G., Dosa, S., Liu, J., Valyi-Nagy, T., and Shukla, D. (2011). Syndecan-1 and syndecan-2 play key roles in herpes simplex virus type-1 infection. *J. Gen. Virol.* 92, 733–743. doi: 10.1099/vir.0.027052-0

Banik, N., Yang, S. B., Kang, T. B., Lim, J. H., and Park, J. (2021). Heparin and its derivatives: challenges and advances in therapeutic biomolecules. *Int. J. Mol. Sci.* 22, 10524. doi: 10.3390/ijms221910524

Bugatti, A., Filippini, F., Bardelli, M., Zani, A., Chiodelli, P., Messali, S., et al. (2022). SARS-CoV-2 infects human ACE2-negative endothelial cells through an integrin-mediated endocytosis even in the presence of vaccine-elicited neutralizing antibodies. *Viruses* 14, 705. doi: 10.3390/v14040705

Bugatti, A., Filippini, F., Messali, S., Giovanetti, M., Ravelli, C., Zani, A., et al. (2023). The D405N Mutation in the spike Protein of SARS-CoV-2 Omicron BA.5 Inhibits spike/Integrins Interaction and Viral Infection of Human Lung Microvascular Endothelial Cells. *Viruses* 15, 332. doi: 10.3390/v15020332

Bugatti, A., Marsico, S., Mazzuca, P., Schulze, K., Ebensen, T., Giagulli, C., et al. (2020). Role of autophagy in von willebrand factor secretion by endothelial cells and in the *in vivo* thrombin-antithrombin complex formation promoted by the HIV-1 matrix protein p17. *Int. J. Mol. Sci.* 21, 2022. doi: 10.3390/ijms21062022

Bugatti, A., Urbinati, C., Ravelli, C., De Clercq, E., Liekens, S., and Rusnati, M. (2007). Heparin mimicking sulfonic acid polymers as multitarget inhibitors of human immunodeficiency virus type 1 Tat and gp120 proteins. *Antimicrob. Agents Chemother.* 51, 2337–2345. doi: 10.1128/AAC.01362-06

Caccuri, F., Bugatti, A., Zani, A., De Palma, A., Di Silvestre, D., Manocha, E., et al. (2021). SARS-CoV-2 infection remodels the phenotype and promotes angiogenesis of primary human lung endothelial cells. *Microorganisms* 9, 1438. doi: 10.3390/microorganisms9071438

Cagno, V., Donalisio, M., Bugatti, A., Civra, A., Cavalli, R., Ranucci, E., et al. (2015). The agmatine-containing poly(amidoamine) polymer AGMA1 binds cell surface heparan sulfates and prevents attachment of mucosal human papillomaviruses. *Antimicrob. Agents Chemother.* 59, 5250–5259. doi: 10.1128/AAC.00443-15

Cagno, V., Tseligka, E. D., Jones, S. T., and Tapparel, C. (2019). Heparan sulfate proteoglycans and viral attachment: true receptors or adaptation bias? *Viruses* 11, 596. doi: 10.3390/v11070596

Canale, M. P., Menghini, R., Martelli, E., and Federici, M. (2022). COVID-19-associated endothelial dysfunction and microvascular injury: from pathophysiology to clinical manifestations. *Card Electrophysiol. Clin.* 14, 21–28. doi: 10.1016/j.ccep.2021.10.003

Cao, Y., Yisimayi, A., Jian, F., Song, W., Xiao, T., Wang, L., et al (2022). BA.2.12.1, BA.4 and BA.5 escape antibodies elicited by Omicron infection. *Nature.* 608 (7923), 593–602. doi: 10.1038/s41586-022-04980-y

Carabelli, A. M., Peacock, T. P., Thorne, L. G., Harvey, W. T., and Hughes, J. (2023). COVID-19 Genomics UK Consortium. (2023) SARS-CoV-2 variant biology: immune escape, transmission and fitness. *Nat. Rev. Microbiol.* 21, 162–177. doi: 10.1038/s41579-022-00841-7

Casari, C., Lenting, P. J., Wohner, N., Christophe, O. D., and Denis, C. V. (2013). Clearance of von Willebrand factor. *J. Thromb. Haemost.* 11 Suppl 1, 202–211. doi: 10.1111/jth.12226

Chen, Y., Maguire, T., Hileman, R., Fromm, J. R., Esko, J. D., Linhardt, R. J., et al. (1997). Dengue virus infectivity depends on envelope protein binding to target cell heparan sulfate. *Nat. Med.* 3, 866–871. doi: 10.1038/nm0897-866

Chiodelli, P., Mitola, S., Ravelli, C., Oreste, P., Rusnati, M., and Presta, M. (2011). Heparan sulfate proteoglycans mediate the angiogenic activity of the vascular endothelial growth factor receptor-2 agonist gremlin. *Arterioscler. Thromb. Vasc. Biol.* 31, e116–e127. doi: 10.1161/ATVBAHA.111.235184

Clausen, T. M., Sandoval, D. R., Spliid, C. B., Pihl, J., Perrett, H. R., Painter, C. D., et al. (2020). SARS-CoV-2 infection depends on cellular heparan sulfate and ACE2. *Cell* 183, 1043–1057.e15. doi: 10.1016/j.cell.2020.09.033

de Haan, C. A. M., Li, Z., te Lintelo, E., Bosch, B. J., Haijema, B. J., et al. (2005). Murine coronavirus with an extended host range uses heparan sulfate as an entry receptor. *J. Virol.* 79 (22), 14451–14456. doi: 10.1128/JVI.79.22.14451-14456.2005

Donalisio, M., Rusnati, M., Cagno, V., Civra, A., Bugatti, A., Giuliani, A., et al. (2012). Inhibition of human respiratory syncytial virus infectivity by a dendrimeric heparan sulfate-binding peptide. *Antimicrob. Agents Chemother.* 56, 5278–5288. doi: 10.1128/AAC.00771-12

Eliceiri, B. P., Klemke, R., Strömblad, S., and Cheresh, D. A. (1998). Integrin alphavbeta3 requirement for sustained mitogen-activated protein kinase activity during angiogenesis. *J. Cell Biol.* 140, 1255–1263. doi: 10.1083/jcb.140.5.1255

Giordo, R., Paliogiannis, P., Mangoni, A. A., and Pintus, G. (2021). SARS-CoV-2 and endothelial cell interaction in COVID-19: molecular perspectives. *Vasc. Biol.* 3 (1), R15–R23. doi: 10.1530/VB-20-0017

Hassan, N., Greve, B., Espinoza-Sánchez, N. A., and Götte, M. (2021). Cell-surface heparan sulfate proteoglycans as multifunctional integrators of signaling in cancer. *Cell Signal.* 77, 109822. doi: 10.1016/j.cellsig.2020.109822

Kalra, R. S., and Kandimalla, R. (2021). Engaging the spikes: heparanSulfate facilitates SARS-CoV-2 spike protein binding to ACE2 and potentiates viral infection. *Signal Transduct Target Ther.* 6, 39. doi: 10.1038/s41392-021-00470-1

Kearns, F. L., Sandoval, D. R., Casalino, L., Clausen, T. M., Rosenfeld, M. A., Spliid, C. B., et al. (2022). Spike-heparan sulfate interactions in SARS-CoV-2 infection. *Curr. Opin. Struct.* 76, 102439. doi: 10.1016/j.sbi.2022.102439

Kim, S. Y., Jin, W., Sood, A., Montgomery, D. W., Grant, O. C., Fuster, M. M., et al. (2020). Characterization of heparin and severe acute respiratory syndrome-related coronavirus 2 (SARS-CoV-2) spike glycoprotein binding interactions. *Antiviral Res.* 181, 104873. doi: 10.1016/j.antiviral.2020.104873

Kim, S. H., Kearns, F. L., Rosenfeld, M. A., Votapka, L., Casalino, L., and Papanikolas, M. (2023). SARS-CoV-2 evolved variants optimize binding to cellular glycocalyx. *Cell Rep. Phys. Sci.* 4, 101346. doi: 10.1016/j.xcrp.2023.101346

Koehler, M., Delguste, M., Sieben, C., Gillet, L., and Alsteens, D. (2020). Initial step of virus entry: virion binding to cell-surface glycans. *Annu. Rev. Virol.* 7, 143–165. doi: 10.1146/annurev-virology-122019-070025

Koganti, R., Memon, A., and Shukla, D. (2021). Emerging roles of heparan sulfate proteoglycans in viral pathogenesis. *Semin. Thromb. Hemost* 47, 283–294. doi: 10.1055/s-0041-1725068

Li, K., Yao, L., Wang, J., Song, H., Zhang, Y. H., Bai, X., et al. (2022). SARS-CoV-2 spike protein promotes vWF secretion and thrombosis via endothelial cytoskeleton-associated protein 4 (CKAP4). *Signal Transduct Target Ther.* 7, 332. doi: 10.1038/s41392-022-01183-9

Liu, L., Chopra, P., Li, X., Bouwman, K. M., Tompkins, S. M., Wolfert, M. A., et al. (2021). Heparan sulfate proteoglycans as attachment factor for SARS-CoV-2. *ACS Cent Sci.* 7, 1009–1018. doi: 10.1021/acscentsci.1c00010

Liu, F., Han, K., Blair, R., Kenst, K., Qin, Z., Upcin, B., et al. (2021). SARS-CoV-2 infects endothelial cells *in vivo* and *in vitro*. *Front. Cell Infect. Microbiol.* 6. doi: 10.3389/fcimb.2021.701278

Madu, I. G., Chu, V. C., Lee, H., Regan, A. D., Bauman, B. E., and Whittaker, G. R. (2007). Heparan sulfate is a selective attachment factor for the avian coronavirus infectious bronchitis virus beaudette. *Avian Dis.* 51, 45–51. doi: 10.1637/0005-2086(2007)051[0045:HSIASA]2.0.CO;2

Milewska, A., Zarebski, M., Nowak, P., Stozek, K., Potempa, J., and Pyrc, K. (2014). Human coronavirus NL63 utilizes heparan sulfate proteoglycans for attachment to target cells. *J. Virol.* 88, 13221–13230. doi: 10.1128/JVI.02078-14

Minh, B. Q., Schmidt, H. A., Chernomor, O., Schrempf, D., Woodhams, M. D., von Haeseler, A., et al. (2020). IQ-TREE 2: new models and efficient methods for phylogenetic inference in the genomic era. *Mol. Biol. Evol.* 37, 1530–1534. doi: 10.1093/molbev/msaa015

Mojzisch, A., and Brehm, M. A. (2021). The manifold cellular functions of von willebrand factor. *Cells* 10, 2351. doi: 10.3390/cells10092351

Moshiri, N. (2021). ViralMSA: massively scalable reference-guided multiple sequence alignment of viral genomes. *Bioinformatics* 37, 714–716. doi: 10.1093/bioinformatics/btaa743

Murphy, D. A., Makonnen, S., Lassoued, W., Feldman, M. D., Carter, C., and Lee, W. M. (2006). Inhibition of tumor endothelial ERK activation, angiogenesis, and tumor growth by sorafenib (BAY43-9006). *Am. J. Pathol.* 169, 1875–1885. doi: 10.2353/ajpath.2006.050711

Mycroft-West, C. J., Su, D., Pagani, I., Rudd, T. R., Elli, S., Gandhi, N. S., et al. (2020). Heparin inhibits cellular invasion by SARS-CoV-2: structural dependence of the interaction of the spike S1 receptor-binding domain with heparin. *Thromb. Haemostasis* 120 (12), 1700–1715. doi: 10.1055/s-0040-1721319

Nader, D., Fletcher, N., Curley, G. F., and Kerrigan, S. W. (2021). SARS-CoV-2 uses major endothelial integrin αvβ3 to cause vascular dysregulation *in-vitro* during COVID-19. *PloS One* 23, 16(6). doi: 10.1371/journal.pone.0253347

Nitahara, Y., Nakagama, Y., Kaku, N., Candray, K., Michimuko, Y., Tshibangu-Kabamba, E., et al. (2021). High-Resolution Linear Epitope Mapping of the Receptor Binding Domain of SARS-CoV-2 spike Protein in COVID-19 mRNA Vaccine Recipients. *Microbiol. Spectr.* 9, e0096521. doi: 10.1128/Spectrum.00965-21

Odilov, A., Volkov, A., Abdullaev, A., Gasanova, T., Lipina, T., and Babichenko, I. (2021). COVID-19: multiorgan dissemination of SARS-CoV-2 is driven by pulmonary factors. *Viruses* 14, 39. doi: 10.3390/v14010039

Othman, H., Messaoud, H. B., Khamessi, O., Ben-Mabrouk, H., Ghedira, K., Bharuthram, A., et al. (2022). SARS-CoV-2 spike Protein Unlikely to Bind to Integrins *via* the Arg-Gly-Asp (RGD) Motif of the Receptor Binding Domain: Evidence From Structural Analysis and Microscale Accelerated Molecular Dynamics. *Front. Mol. Biosci.* 14. doi: 10.3389/fmolb.2022.834857

Oxford, A. E., Halla, F., Robertson, E. B., and Morrison, B. E. (2020). Endothelial cell contributions to COVID-19. *Pathogens* 9, 785. doi: 10.3390/pathogens9100785

Pang, X., He, X., Qiu, Z., Zhang, H., Xie, R., Liu, Z., et al. (2023). Targeting integrin pathways: mechanisms and advances in therapy. *Sig. Transduct Target Ther.* 8, 1. doi: 10.1038/s41392-022-01259-6

Parafioriti, M., Ni, M., Petitou, M., Mycroft-West, C. J., Rudd, T. R., Gandhi, N. S., et al. (2023). Evidence for multiple binding modes in the initial contact between SARS-coV-2 spike S1 protein and cell surface glycans. *Chemistry* 29, e202202599. doi: 10.1002/chem.202202599

Rabaan, A. A., Smajlović, S., Tombuloglu, H., Ćordić, S., Hajdarević, A., Kudić, N., et al. (2023). SARS-CoV-2 infection and multi-organ system damage: A review. *Biomol. Biomed.* 23, 37–52. doi: 10.17305/bjbms.2022.7762

Randi, A. M., and Laffan, M. A. (2017). Von Willebrand factor and angiogenesis: basic and applied issues. *J. Thromb. Haemost.* 15, 13–20. doi: 10.1111/jth.13551

Randi, A. M., Laffan, M. A., and Starke, R. D. (2013). Von Willebrand factor, angiodysplasia and angiogenesis. *Mediterr. J. Hematol. Infect. Dis.* 5, e2013060. doi: 10.4084/MJHID.2013.060

Randi, A. M., Smith, K. E., and Castaman, G. (2018). von Willebrand factor regulation of blood vessel formation. *Blood* 132, 132–140. doi: 10.1182/blood-2018-01-769018

Richards, K. F., Bienkowska-Haba, M., Dasgupta, J., Chen, X. S., and Sapp, M. (2013). Multiple heparan sulfate binding site engagements are required for the infectious entry of human papillomavirus type 16. *J. Virol.* 87, 11426–11437. doi: 10.1128/JVI.01721-13

Rusnati, M., and Lembo, D. (2016). Heparan sulfate proteoglycans: A multifaceted target for novel approaches in antiviral drug discovery. *J. Bioengineer Biomed. Sci.* 6, 177. doi: 10.4172/2155-9538.1000177

Rusnati, M., Urbinati, C., Caputo, A., Possati, L., Lortat-Jacob, H., Giacca, M., et al. (2001). Pentosan polysulfate as an inhibitor of extracellular HIV-1 Tat. *J. Biol. Chem.* 276, 22420–22425. doi: 10.1074/jbc.M010779200

Sagulenko, P., Puller, V., and Neher, R. A. (2018). TreeTime: Maximum-likelihood phylodynamic analysis. *Virus Evol.* 4, vex042. doi: 10.1093/ve/vex042.34

Sarrazin, S., Lamanna, W. C., and Esko, J. D. (2011). Heparan sulfate proteoglycans. *Cold Spring Harb. Perspect. Biol.* 1, 3(7). doi: 10.1101/cshperspect.a004952

Somanath, P. R., Malinin, N. L., and Byzova, T. V. (2009). Cooperation between integrin alphavbeta3 and VEGFR2 in angiogenesis. *Angiogenesis* 12, 177–185. doi: 10.1007/s10456-009-9141-9

Starke, R. D., Ferraro, F., Paschalaki, K. E., Dryden, N. H., McKinnon, T. A., Sutton, R. E., et al. (2011). Endothelial von Willebrand factor regulates angiogenesis. *Blood* 117, 1071–1080. doi: 10.1182/blood-2010-01-264507

Su, W. L., Lu, K. C., Chan, C. Y., and Chao, Y. C. (2021). COVID-19 and the lungs: A review. *J. Infect. Public Health* 14, 1708–1714. doi: 10.1016/j.jiph.2021.09.024

Tandon, R., Sharp, J. S., Zhang, F., Pomin, V. H., Ashpole, N. M., Mitra, D., et al. (2021). Effective inhibition of SARS-CoV-2 entry by heparin and enoxaparin derivatives. *J. Virol.* 95 (3), e01987-20. doi: 10.1128/JVI.01987-20

Tuekprakhon, A., Nutalai, R., Dijokaite-Guraliuc, A., Zhou, D., Ginn, H. M., Selvaraj, M., et al. (2022). Antibody escape of SARS-CoV-2 Omicron BA.4 and BA.5 from vaccine and BA.1 serum. *Cell* 185, 2422–2433.e13. doi: 10.1016/j.cell.2022.06.005

Yang, Z. S., Li, T. S., Huang, Y. S., Chang, C. C., and Chien, C. M. (2024). Targeting the receptor binding domain and heparan sulfate binding for antiviral drug development against SARS-CoV-2 variants. *Sci. Rep.* 14, 2753. doi: 10.1038/s41598-024-53111-2

Ye, F. C., Zhou, F. C., Nithianantham, S., Chandran, B., Yu, X. L., Weinberg, A., et al. (2013). Kaposi's sarcoma-associated herpesvirus induces rapid release of angiopoietin-2 from endothelial cells. *J. Virol.* 87, 6326–6335. doi: 10.1128/JVI.03303-12

Yu, M., Zhang, T., Zhang, W., Sun, Q., Li, H., and Li, J. (2021). Elucidating the interactions between heparin/heparan sulfate and SARS-CoV-2-related proteins-an important strategy for developing novel therapeutics for the COVID-19 pandemic. *Front. Mol. Biosci.* 490. doi: 10.3389/fmolb.2020.628551

Zhang, Q., Chen, C. Z., Swaroop, M., Xu, M., Wang, L., Lee, J., et al. (2020). Heparan sulfate assists SARS-CoV-2 in cell entry and can be targeted by approved drugs *in vitro*. *Cell Discovery* 6, 80. doi: 10.1038/s41421-020-00222-5

Zhang, H., Lao, Q., Zhang, J., and Zhu, J. (2022). Coagulopathy in COVID-19 and anticoagulation clinical trials. *Best Pract. Res. Clin. Haematol.* 35, 101377. doi: 10.1016/j.beha.2022.101377

Zhang, Q., Pavlinov, I., Ye, Y., and Zheng, W. (2024). Therapeutic development targeting host heparan sulfate proteoglycan in SARS-CoV-2 infection. *Front. Med. (Lausanne)* 11. doi: 10.3389/fmed.2024.1364657

frontiers | Frontiers in Cellular and Infection Microbiology

TYPE Original Research
PUBLISHED 07 April 2025
DOI 10.3389/fcimb.2025.1549497

OPEN ACCESS

EDITED BY
Dimitra Dimopoulou,
Panagiotis & Aglaia Kyriakou Children's Hospital, Greece

REVIEWED BY
José J. Leija-Martínez,
Autonomous University of San Luis Potosí, Mexico
Sumit Bhardwaj,
National Institute of Virology (ICMR), India

*CORRESPONDENCE
Xin Lv
etyyjyklvxin@163.com
Ling Wang
Wlingetyy@163.com

†These authors have contributed equally to this work and share first authorship

RECEIVED 21 December 2024
ACCEPTED 10 March 2025
PUBLISHED 07 April 2025
CORRECTED 27 June 2025

CITATION
Yue Y, Wu D, Zeng Q, Li Y, Yang C, Lv X and Wang L (2025) Changes in children respiratory infections pre and post COVID-19 pandemic.
Front. Cell. Infect. Microbiol. 15:1549497.
doi: 10.3389/fcimb.2025.1549497

Changes in children respiratory infections pre and post COVID-19 pandemic

Yuanyuan Yue[1,2†], Dan Wu[1,2†], Qian Zeng[1,2], Yurong Li[1,2], Chun Yang[1,2], Xin Lv[1,2*] and Ling Wang[1,2*]

[1]Clinical Laboratory, Children's Hospital Affiliated to Shandong University, Jinan, China, [2]Clinical Laboratory, Jinan Children's Hospital, Jinan, China

Background: Non-pharmaceutical interventions (NPIs) implemented during the COVID-19 pandemic had a significant impact on the prevalence of various acute respiratory infections (ARIs) pathogens.

Methods: We collected 337,310 real-time PCR results for 13 pathogens from clinical samples between January 2018 and January 2024 to assess the changes of ARIs among children before and after the COVID-19 pandemic.

Results: A variety of ARIs pathogens, including Influenza A (Flu A), Influenza B (Flu B), Adenovirus (ADV), Rhinovirus (RhV), and Respiratory Syncytial Virus (RSV), as well as co-infecting bacterial such as Klebsiella pneumoniae (KPN), Pseudomonas aeruginosa (PAE), Streptococcus pneumoniae (SP), Haemophilus influenzae (HI), and Legionella pneumophila (LP), reached a peak positive rate at the age of 3. The susceptible age of Mycoplasma pneumoniae (MP) was from 3 to 7 years old. Compared to the pre-COVID pandemic period, the positive rates of Flu A, MP, ADV, SP, HI, *Staphylococcus aureus* (SA) and KPN decreased during the COVID-19 pandemic. And the positive rates of Flu B and PAE increased. Compared to the period during the COVID-19 pandemic, the positive rates of Flu A, ADV, RSV, RhV, SP, HI, KPN, PAE and SA were increased after the pandemic. Conversely, the positive rates of MP, Flu B, and Parainfluenza virus (PIV) decreased.

Conclusions: The implementation of NPIs interrupted the circulation of ARIs pathogens. However, release of NPIs and the reduced baseline of population immunity, may contribute to a resurgence of ARIs pathogens among children.

KEYWORDS

COVID-19, respiratory infection, non-pharmaceutical interventions, children, qPCR

1 Introduction

Influenza virus, RSV and RhV are the three leading viral pathogens and SP, MP and KPN are the three leading bacterial pathogens in China between 2009eenns (Li et al., 2021). Common childhood respiratory pathogens, including MP, Flu A, Flu B, ADV, RSV, PIV and RhV through aerosol particles and respiratory droplets during close contact (Li et al., 2022; Meyer Sauteur et al., 2022). The general population is susceptible to these infections, which manifest epidemically every few years, often reaching their peak in winter around January or February (Olsen et al., 2021). Furthermore, many bacteria also cause of childhood respiratory invasive infections, include KPN, KPN, SA, SP, HI, LP. The rates of these respiratory bacterial diseases are influenced by the frequency of bacterial exposure and host susceptibility (Major et al., 2023). Epidemiological, clinical, and experimental evidence suggests that certain viruses can enhance susceptibility to bacterial respiratory infections (Tsang et al., 2020; Palani et al., 2023). Given that SARS-CoV-2 is a respiratory virus, the COVID-19 pandemic may increase susceptibility to respiratory bacterial infections (Danino et al., 2022; Lubkin et al., 2024).

Since the outbreak of COVID-19, Jinan city in Shandong province entered a stage of normalization epidemic prevention and control. These robust non-pharmaceutical interventions (NPIs) not only reduce the spread of COVID-19 but also influence the epidemiology of common respiratory pathogens in children to some extent (Spinelli et al., 2021; Cai et al., 2024). The spread and seasonality of these respiratory pathogens have been temporarily interrupted, and the incidence of childhood bacterial infectious respiratory disease also changed (Perra, 2021; Meyer Sauteur et al., 2022). On December 7, 2022, China ended its "Zero-COVID" policy (Zhou et al., 2023). This transition allowed for a restoration of normalcy in people's lives. Following this, a significant rise in Omicron cases emerged in China, accompanied by a sharp increase in influenza incidence in February 2023 (Chakraborty et al., 2023). Additionally, other pathogens causing respiratory tract infections appeared successively during this period. Although people still keep maintain certain NPI habits, such as maintaining social distance, washing hand frequently, and wearing face mask.

We gathered a total of 337,310 Real-time Quantitative polymerase chain reaction (qPCR) results for KPN, PAE, SA, SP, HI, LP, MP, Flu A, Flu B, ADV, RSV, PIV, and RhV from clinical samples collected between January 2018 and January 2024 in Children's Hospital Affiliated to Shandong University to investigate the epidemiological features of prevalent respiratory pathogens in children both prior to and following the COVID-19 pandemic.

2 Methods

2.1 Data collection

This study was approved by the Ethics Committee of Children's Hospital Affiliated to Shandong University (Ethical approval number: SDFE-IRB/P-202315). The requirement for informed consent was waived because this study was based on a retrospective analysis of electronic medical records (EMRs). Children with respiratory tract infections, either inpatient or outpatient, were enrolled between January 1, 2018, and January 31, 2024. Inclusion criteria were as follows: 1) diagnosed with respiratory infection; 2) PCR results are available. Exclusion criteria were as follows: 1) children with severe malformations, including large atrial or ventricular septal defects, bronchopulmonary dysplasia, dextrocardia, and neuromuscular diseases; 2) children diagnosed with malignant tumors or primary immunodeficiency diseases, or those who received immunosuppressive drugs during hospitalization.

2.2 Temporal segmentation

On January 20, 2020, the National Health Commission declared that COVID-19 pneumonia would be classified as a Category B infectious disease according to the law of the People's Republic of China regarding the Prevention and Treatment of Infectious Diseases, which had received approval from the State Council, and they implemented prevention and control strategies applicable to Category A infectious diseases. In response to the continuing COVID-19 pandemic, Shandong province implemented a first-level response for Major Public Health Emergency on January 24, 2020. The majority of these preventive measures were non-pharmaceutical in nature and comprised the blockade of areas affected by the outbreak, border closures, limitations on travel, restrictions on social and public activities, shutdowns of schools and businesses, stay-at-home directives, promotion of physical distancing, an emphasis on hand hygiene practices, and the use of face masks. On December 7, 2022, the State Council of China issued the "Notice on Further Optimizing the Implementation of COVID-19 prevention and control measures". Cancel mass nucleic acid testing and health code inspection (except in special places); allow mild and asymptomatic infections to be isolated at home; no longer delineate high-risk areas, narrow the scope of sealing and control. Those marking a major adjustment of the COVID-19 pandemic prevention and control policy from "dynamic Zero-COVID" to "scientific and precise prevention and control". Subsequently, on January 8, 2023, the Chinese government announced that COVID-19 would downgrading Class B diseases from enhanced to routine management. The focus has shifted to health resource preparation, vaccination and protection of vulnerable populations. Therefore, we period from January 1, 2018, to December 31, 2019, has been designated as the pre-COVID-19 pandemic phase, from January 1, 2020, to December 31, 2022, has been designated as during the COVID-19 pandemic phase; and from January 1, 2023, to January 31, 2024, has been designated as post-COVID-19 pandemic phase.

2.3 Specimens collection and detection

ARIs samples comprised nasopharyngeal swabs, pharyngeal swab, sputum, bronchoalveolar lavage fluid and pleural effusion,

were collected by trained nurses according to Standard Operating Procedures (SOP). These samples were promptly transported to the clinical laboratory, tested by the Respiratory Pathogen Nucleic Acid Diagnostic Detection Kit (Beijing Zhuocheng Huisheng Biotechnology Co. Ltd and SANSURE BIOTECH INC.), conducted by professional staff in adherence to established SOP. All test items were strictly subjected to quality control in accordance with the sample instructions. Thirteen ARIs pathogens were identified, including KPN, PAE, SA, SP, HI, LP, MP, Flu A, Flu B, ADV, RSV, PIV and RhV.

2.4 Statistical analysis

The overall detection rates of thirteen common pathogens, including KPN, PAE, SA, SP, HI, LP, MP, Flu A, Flu B, ADV, RSV, PIV, and RhV, were analyzed across three periods: prior to, during, and following the COVID-19 pandemic. To explore seasonal variations in viral activity and age-related differences in pathogen infections, the trends in detection rates from 2018.01 to 2024.01 and age-specific differences in pathogen infections were illustrated using GraphPad Prism 8.0. We performed chi-square analyses to assess changes in pathogen distribution across different phases of the COVID-19 pandemic in the Supplementary Tables ($P<0.05$).

3 Results

3.1 Study population

A total of 337,310 children were included, the male-to-female ratio was 1.43:1, males (58.85%) were 17% higher than females (58.85%) (Table 1; Figure 1A). The gender distribution among the 13 pathogens was different, PAE was the highest (2.05), LP was the lowest at 1.18, (Figure 1B). All children were divided into five age groups: 0~1 y (17.20%), 1~3 y (25.24%), 3~6 y (33.52%), and ≥6 y (24.04%) (Table 1). The positive rates of eight pathogens (KPN, PAE, SA, SP, HI, LP, RSV and PIV) were highest at age 0~1, gradually decreased with age. The positive rates of four pathogens (Flu A, Flu B, ADV and RhV) were highest at age 3 and MP's positive rate was highest at age 7 at 14.97% (Figure 2).

3.2 Monthly changes in PCR results for 7 infectious pathogens from 2018.01 to 2024.01

Before the COVID-19 pandemic, PCR was only used for MP testing, and we established PCR testing for Flu A, Flu B and ADV in June 2019, with the increased application of PCR testing during the COVID-19 pandemic, PCR testing for RSV in January 2020, PIV in July 2020 and RhV in December 2020 were established.

From January 31, 2018, to January 31, 2024, we collected a total of 314,648 respiratory tract infectious samples. These samples were not tested for all seven pathogens(MP, Flu A, Flu B, ADV, RSV, PIV and RhV) simultaneously. Some specimens were individually tested for single pathogen such as Mp, while others underwent combination tests (Flu A/Flu B/RSV, ADV/PIV/RhV, MP/Flu A/Flu B, or Flu A/Flu B/RSV/ADV/PIV).

From January 31, 2018, to January 31, 2024, We detected two peaks of MP epidemics (2019.07~2020.03, 2021.07~2022.02), with the monthly positive rate was greater than 11.52%, and the highest was 39.80%. Four peaks of Flu A epidemics (2019.12~2020.01, 2022.08~2022.11, 2023.02~2023.04, 2023.11~2023.12), with the monthly positive rate was greater than 11.07%, the highest was 48.44%. Two epidemic peaks of Flu B occurred in January 2020 and from December 2021 to February 2022, with the monthly positive rate was greater than 14.29% and the highest was 47.71%. Two epidemic peaks of AVD (2019.10~2020.02, 2023.10~2024.01), with the monthly positive rate was greater than 9.70%, and the highest was 18.94%. RSV had six epidemic peaks scattered from January 2020 to January 2024, with the monthly positive rate was greater than 10.27%, the highest positive rate was 40.98%. PIV had two epidemic peaks (2020.09~12, 2023.07~08), with the monthly positive rate was greater than 11.11% and the highest positive rate was 16.67%. The RhV epidemic peak was recorded from March to November 2021, with the monthly positive rate exceeding 26.67% and a maximum positive rate of 39.13%. (Figure 3A; Supplementary Table 1). However, the positive number for both PIV and RhV remained relatively low throughout the year.

3.3 Monthly changes in PCR results for 5 bacterial species from 2018.01 to 2024.01

From January 31, 2018, to January 31, 2024, we collected a total of 22,662 respiratory tract infection samples, each of these samples underwent PCR testing for six types of bacteria: KPN, PAE, SA, SP, HI, and LP. Since the positive rate of LP was too low (24/22662, 0.11%), we no longer analyze the data for this bacterium.

Before the COVID-19 pandemic, between January 2018 and December 2019, the positive number and positive rates for the five bacteria (KPN, PAE, SA, SP, and HI) remained relatively stable. The positive rates were 5.17% at KPN, 1.59% at PAE, 12.73% at SA, 29.23% at SP, and 28.01% at HI. With the outbreak of COVID-19 in 2020, the number of positive cases and the positive rates of five bacterial strains decreased significantly, however, the order of positive rates remained relatively consistent compared to the pre-COVID-19 period. From January to December 2020, the total number of respiratory tract specimens was 1,342, the positive rates were 2.76% at KPN, 2.01% at PAE, 8.87% at SA, 21.09% at SP, and 19.08% at HI. During the mid-to-late stages of the COVID-19 pandemic, particularly after December 2020, the number of respiratory tract specimens for five bacterial experienced a significant rise, surpassing pre-COVID-19 pandemic levels, while the positive rates of five bacterial still lower than in the pre-COVID-19 pandemic period. From January 2021 to December 2022, the total number of respiratory tract specimens was 14,104, the positive rates were 1.35% at KPN, 1.79% at PAE, 6.22% at SA, 16.36% at SP,

TABLE 1 The PCR results of 13 pathogens were summarized from January 31, 2018 to January 31, 2024.

year		2018 N=2761		2019 N=22785		2020 N=27337		2021 N=71093		2022 N=113049		2023 N=82332		2024 N=17953		Sum N=337310	
		n	%	n	%	n	%	n	%	n	%	n	%	n	%	n	%
sex	male	1684	60.99	13472	59.13	16224	59.35	41893	58.93	66679	58.98	48093	58.41	10446	58.19	198491	58.85
	female	1077	39.01	9313	40.87	11113	40.65	29200	41.07	46370	41.02	34239	41.59	7507	41.81	138819	41.15
age	0-1	1375	49.80	4511	19.80	5622	20.57	12526	17.62	20786	18.39	10809	13.13	2398	13.36	58027	17.20
	1-3	836	30.28	6577	28.87	8671	31.72	18814	26.46	27703	24.51	18517	22.49	4007	22.32	85125	25.24
	3-6	342	12.39	7304	32.06	8026	29.36	22293	31.36	41574	36.78	29202	35.47	4328	24.11	113069	33.52
	>6	208	7.53	4393	19.28	5018	18.36	17460	24.56	22986	20.33	23804	28.91	7220	40.22	81089	24.04
pathogen	KPN	83	6.01	83	4.53	37	2.76	99	1.24	91	1.49	320	8.84	21	5.48	734	3.24
	PAE	25	1.81	26	1.42	27	2.01	148	1.85	104	1.70	168	4.64	45	11.75	543	2.40
	SA	182	13.19	227	12.38	119	8.87	465	5.83	412	6.73	282	7.79	17	4.44	1704	7.52
	SP	414	30.00	525	28.64	283	21.09	1344	16.84	963	15.72	2205	60.91	290	75.72	6024	26.58
	HIB	354	25.65	546	29.79	256	19.08	1749	21.92	1164	19.00	1008	27.85	138	36.03	5215	23.01
	LP	1	0.07	2	0.11	7	0.52	4	0.05	5	0.08	5	0.14	0	0.00	24	0.11
	MP	62	4.49	1757	16.30	518	5.55	5269	19.93	1375	5.83	258	2.40	125	9.45	9364	11.20
	Flu A	-	-	777	22.14	966	20.69	7	0.13	1727	10.57	2587	18.72	116	3.70	6180	13.13
	Flu B	-	-	143	4.10	674	14.46	1399	25.05	1619	9.91	66	0.48	595	18.96	4496	9.56
	ADV	-	-	303	9.53	170	4.62	450	4.22	1191	7.13	987	7.31	580	18.94	3681	7.25
	RSV	-	-	-	-	298	10.70	868	18.38	1221	7.84	1842	13.41	805	25.65	5034	12.60
	PIV	-	-	-	-	45	5.72	405	4.78	309	5.78	107	2.67	14	0.57	880	4.18
	RhV	-	-	-	-	16	20.25	240	14.65	1474	11.28	1184	13.06	146	11.04	3060	12.16

"n": Number of positives; "%": Positive rate.

KPN, Klebsiella pneumoniae; PAE, Pseudomonas aeruginosa; SA, Staphylococcus aureus; SP, Streptococcus pneumoniae; HI, Haemophilus influenzae; LP, Legionella pneumophila; MP, Mycoplasma Pneumoniae; Flu A, Influenza A virus; Flu B, Influenza B virus; ADV, Adenoviridae; RSV, respiratory syncytial virus; PIV, parainfluenza virus; RhV, Rhinovirus; "-": The test was not performed in our laboratory."-"

10.3389/fcimb.2025.1549497

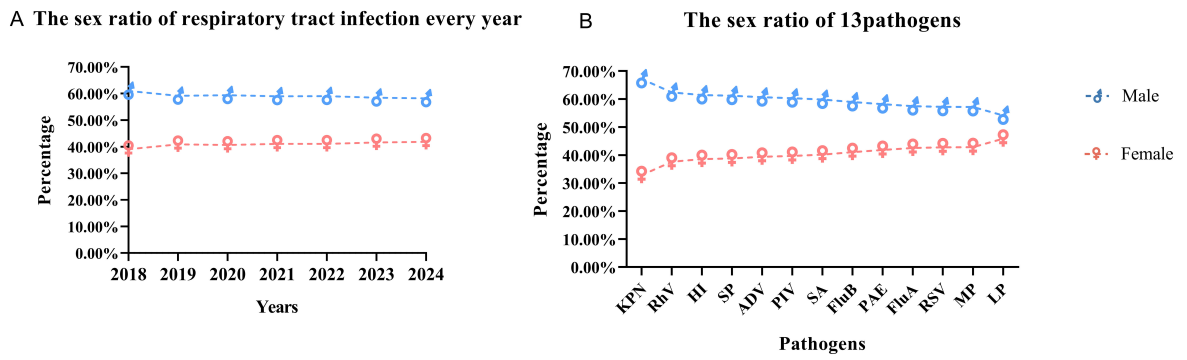

FIGURE 1
Sex distribution of pathogen positive results. **(A)**: The sex ratio of respiratory tract infection every year; **(B)**: The sex ratio of 13 pathogens.

and 20.65% at HI. Notably, an infectious peak was observed in December 2021, with the largest increases in positive samples occurring in SP (187/1,100) and HI (234/1,100). From February to May 2022, the number of respiratory tract specimens decreased, followed by an increase from June to August, where the most significant rise in positive samples was again noted in SP and HI. After the peak in August, the number of specimens declined until January 2023, which may be attributed to summer vacation activities. From January 8, 2023, the control measures for COVID-19 were lifted. Between January 2023 and January 2024, we collected 4,003 respiratory tract specimens, with the positive rates were recorded as 8.52% for KPN, 5.32% for PAE, 7.47% for SA, 62.33% for SP, and 28.63% for HI. The most significant increase was observed at SP, with a positive rate of 62.33% (Figure 3B; Supplementary Table 2).

3.4 Changes in the positive rate of pathogens before and after the COVID-19 epidemic

Before the COVID-19 pandemic, the positive rates of five bacteria in respiratory tract specimens from high to low were SP, HI, SA, KPN, PAE. During the COVID-19 pandemic, the positive rates of these five bacteria from high to low were HI, SP, SA, PAE, and KPN. Following the COVID-19 pandemic, the positive rates of five bacteria from high to low were SP, HI, KPN, SA, and PAE. In comparison to the pre-COVID pandemic period, the positive rates of the four bacteria, excluding PAE, showed a decline during the COVID-19 pandemic. Specifically, SP decreased by 12.48% (P=0.000), HI by 7.52% (P<0.001), SA by 6.29% (P<0.001), and KPN by 3.70% (P<0.001) (Supplementary Table 4). However, after the COVID-19 pandemic, the positive rates of all five bacteria increased compared to the COVID-19 pandemic period, with SP increased by 45.58% (P=0.000), HI by 8.14% (P<0.001), SA by 1.03% (P=0.021), KPN by 7.05% (P<0.001), and PAE by 3.52% (P<0.001) (Supplementary Table 4). Notably, the most significant change in positive rate was observed in SP (Figure 4).

Before the COVID-19 pandemic, the positive rates of infectious pathogens from high to low were Flu A, MP, ADV, Flu B. During the COVID-19 pandemic, the positive rates of infectious pathogens from high to low were Flu B, MP, RhV, RSV, Flu A, ADV and PIV. After COVID-19 pandemic, the positive rates for infectious pathogens from high to low were Flu A, RSV, RhV, ADV, Flu B, MP, and PIV. Compared to the pre-COVID-19 period, the positive rates of three infectious pathogens decreased: Flu A decreased by

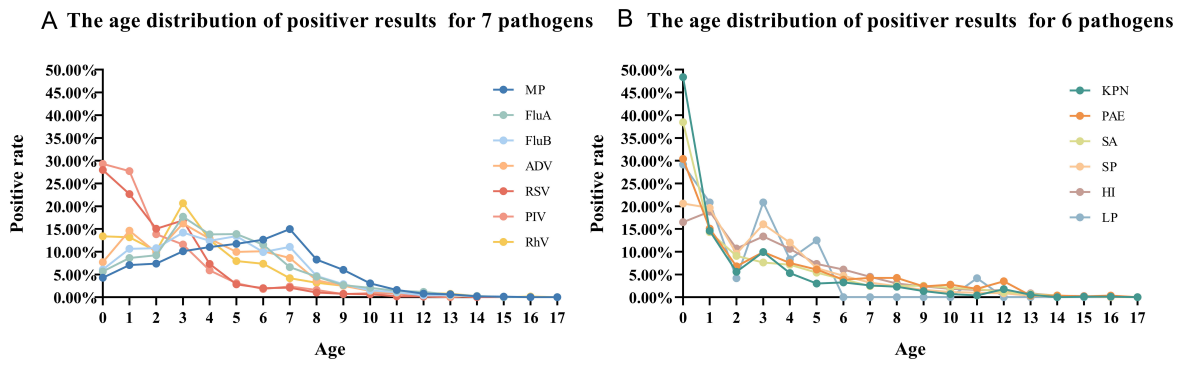

FIGURE 2
Age distribution of positive rates for 13 pathogens. **(A)**: The age distribution of positiver results for 7pathogens; **(B)**: The age distribution of positiver results for 6 pathogens.

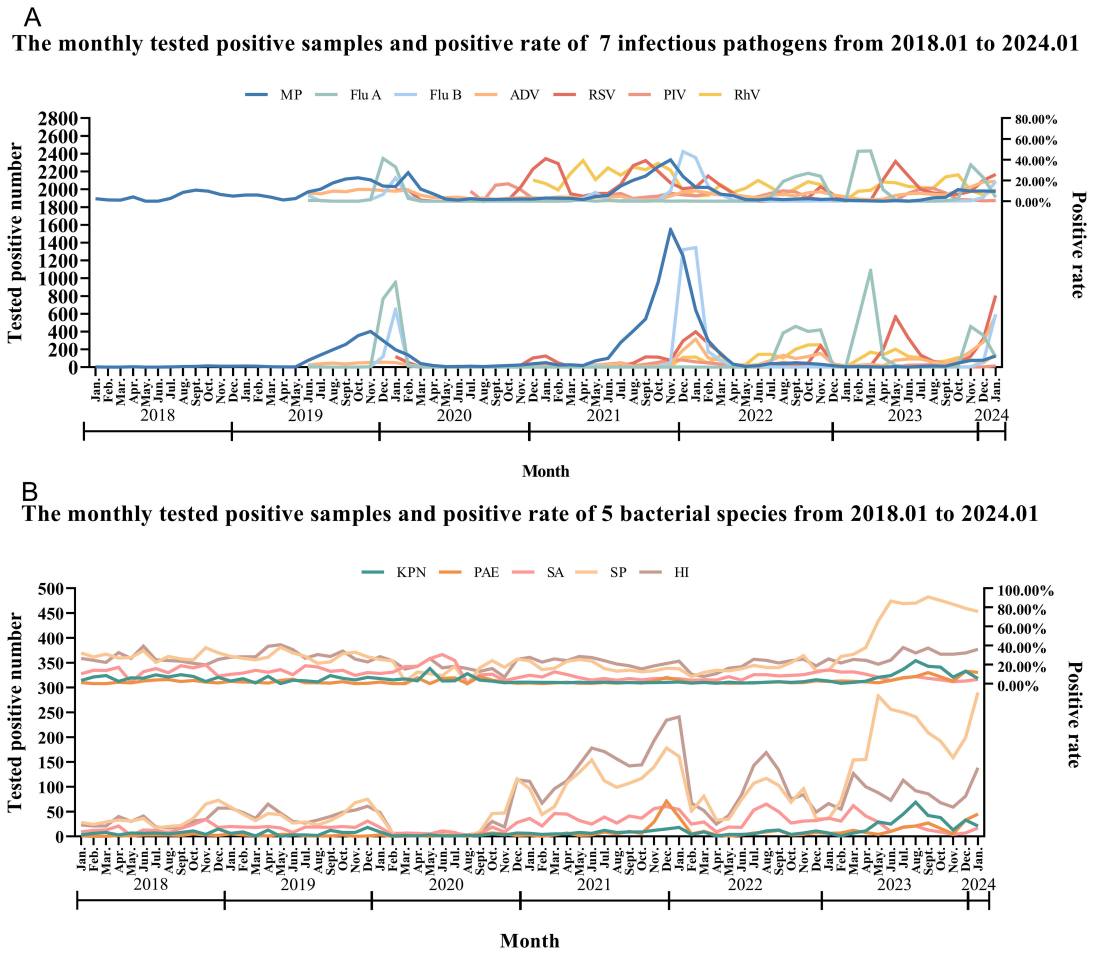

FIGURE 3
The monthly positive samples of testing systems and test positive rate of 12 infectious pathogens from 2018.01 to 2024.01. **(A)**: The monthly tested positive samples and positive rate of 7 infectious pathogens from 2018.01 to 2024.01; **(B)**: The monthly tested positive samples and positive rate of 5 bacterial species from 2018.01 to 2024.01

11.98%, MP decreased by 2.89%, ADV decreased by 3.69%, while Flu B increased by 9.78% during the COVID-19 pandemic. In comparison to the period during the COVID-19 pandemic, the positive rates of all four infectious pathogens increased after the COVID-19 pandemic: Flu A increased by 5.79% (P<0.001), ADV increased by 3.62% (P<0.001), RSV increased by 5.34% (P<0.001), RhV increased by 1.10% (P=0.009), however, the positive rates of the other three infectious pathogens decreased, as MP by 8.90% (P<0.001), Flu B by 9.99% (P<0.001), and PIV by 3.32% (P<0.001) (Figure 4) (Supplementary Table 3).

4 Discussion

Since the outbreak of SARS-CoV-2 in December 2019, China has implemented a series of NPIs to address this public health emergency (Yang et al., 2021; Leung et al., 2023). In February 2023, a sharp increase in Flu A activity, combined with the spread of the Omicron variant, posed a significant threat to the public healthcare system for children (Goldberg et al., 2023). To understand how the transmission dynamics of other respiratory viral infections co-evolve with those of SARS-CoV-2, we conducted a retrospective observation of the co-circulation of multiple respiratory pathogens at Children's Hospital Affiliated to Shandong University from January 31, 2018, to January 31, 2024.

The sex ratio (male to female) of children with respiratory tract infections was approximately 1.43, while the sex ratio for individuals aged 0-19 years was 1.15, according to data from the National Bureau of Statistics (NBS) of China over the past five years. This disparity may be attributed to regional differences; additionally, it could be related to boys being more active and thus more likely to come into contact with sources of infection. Furthermore, studies indicate that girls' immune systems develop earlier than boys', leading females to produce stronger immune responses and antibodies to combat infectious pathogens (Oertelt-Prigione, 2012; Moulton, 2018; Sparks et al., 2023). Among five bacterial species studied, the highest sex ratio (2.05) was observed in KPN, while the lowest sex ratio (1.18) was found in LP. Among the seven infectious pathogens examined, RhV exhibited the highest sex ratio (1.66), whereas Flu A, RSV, and MP showed similar sex ratios

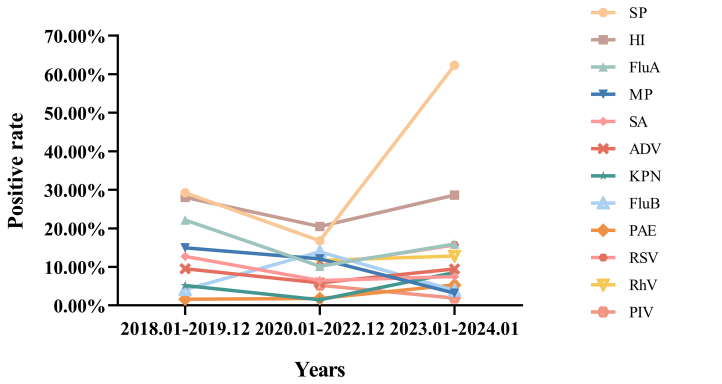

FIGURE 4
Changes in the positive rate of 12 pathogens before and after the COVID-19 epidemic.

of 1.34. Flu A, Flu B, ADV, RhV and RSV, as well as co-infecting bacterial pathogens such as KPN, PAE, SP, HI and LP, exhibit a peak positive rate at the age of 3. Children typically enter kindergarten at the age of 3, where close gatherings for learning and living can facilitate the spread of epidemic diseases. In contrast to viruses and bacteria, MP exhibits a broader age susceptibility, with positive rates exceeding 10% between the ages of 3 and 7, peaking at 14.97% at age 7.

In northern China, the period from November to February marks the peak season for epidemic respiratory diseases1. Prior to the COVID-19 pandemic, outbreaks of such diseases were identified from November 2019 to February 2020, including MP, Flu A, Flu B, ADV and RSV. With the NPIs implemented, from March 2020 to March 2021, many epidemic respiratory pathogens, including MP, Flu A, Flu B and ADV, circulated at low levels, and the incidence of various co-infecting bacteria, such as KPN, PAE, SA, SP and HI, was significantly reduced.3 However, during the winter of 2020, unusual epidemics of RSV and PIV emerged, which were not influenced by the NPIs11. On May 5, 2020, Jinan reduced its epidemic response level, leading to an increase in people's activities and the reopening of schools. From July 2021 to February 2022, a resurgence of multiple infectious respiratory pathogens, including RhV, RSV, Flu B, and MP. Concurrently, the positive rates of co-infecting bacteria, specifically SP and HI, also showed a slight increase3. From February 2023 to January 2024, outbreaks of Flu A, ADV, RSV, PIV, and RhV, with a notable increase in the prevalence of SP among coinfectious bacteria.

In comparison to the period prior to the COVID-19 pandemic (January 2018 to December 2019), the positive rates of various infectious respiratory pathogens decreased during the pandemic (January 2020 to December 2022). This includes pathogens such as MP, Flu A, and ADV (Data for RSV, PIV and RhV were not available before the COVID-19). Additionally, the positive rates of co-infecting bacteria, including KPN, SA, SP and HI, also declined. This reduction may be attributed to the sustained implementation of NPIs, such as personal protective measures and physical distancing. Conversely, the positive rates of Flu B and PAE increased. In comparison to the COVID-19 pandemic period (January 2020 to December 2022), the positive rates of various infectious respiratory pathogens increased following the conclusion of the COVID-19 pandemic (January 2023 to January 2024). This includes pathogens such as Flu A, ADV, RSV, RhV. The positive rates of coinfected bacteria also increased, including KPN, PAE, SA, SP and HI. Conversely, the positive rates of MP and Flu B decreased. These changes in the transmission dynamics of respiratory pathogens may be attributed to modifications in COVID-19 pandemic mitigation measures, as well as shifts in prevalence and immunity. Meanwhile, this increase is attributed to the "immunity debt" resulting from the relaxation of COVID-19 pandemic restrictions.

Notably, lower levels of population immunity, particularly among younger children, could signal the potential for more widespread disease and a possibly more severe epidemic when influenza virus circulation resumes (Cai et al., 2024; Li et al., 2024).Investigations revealed that this increase was primarily due to the relaxation of COVID-19 control measures, which coincided with the onset of the cold season (Burrell et al. 2023; Meyer Sauteur et al.; Parums, 2023). After the epidemic ended, many children who had been unexposed to these pathogens for an extended period became more vulnerable (Cheng et al. 2022; Fujita, 2021).

In our study, we acknowledge several limitations, including the use of a single-center design, lack of detailed symptom severity data, underreporting, and potential bias introduced by the development of testing methods. To address these limitations, we plan to conduct more in-depth research in the future. Specifically, we will:1)Multi-center Data Collection: Collaborate with other medical institutions or research centers to jointly collect and analyze a larger dataset.2) Symptom Severity Data: Perform a retrospective case review to gather detailed information about symptom severity, design additional questionnaires or interviews, and directly inquire with patients or their parents about symptoms.3)Reduce Underreporting: Conduct community surveys to better understand children's medical behaviors and health status during the epidemic. We will also explore other data sources (e.g., school absentee records, pharmacy sales data) to estimate the actual infection rate more accurately. Additionally, we will strengthen

public health education and encourage children with mild symptoms to seek medical attention promptly.4)Consider the Impact of Testing Policy Changes: During data analysis, we will clearly distinguish between different time periods, particularly at points when testing policies changed. Statistical methods (e.g., breakpoint regression analysis) will be applied to assess the effect of these changes on the results. These efforts will require additional manpower, resources, and funding, which are part of our future research goals, though they are beyond our current capacity.

5 Conclusion

The results of this study suggest that the implementation of NPIs against COVID-19 likely restricted the transmission of Flu A, Flu B ADV and MP in children, and the incidence of co-infection bacterial pathogens was substantially reduced too. As China fully exited its "Zero-COVID" policy, the co-circulation of multiple respiratory pathogens and increasing co-infection rates during the autumn and winter of 2023 indicate that respiratory viruses are not exhibiting typical seasonal circulation patterns, and a resumption of circulation of certain respiratory viruses is occurring. The retention of some NPIs post-COVID-19, such as improved hand hygiene, respiratory etiquette, physical distancing, and the use of masks in healthcare settings, may help mitigate the burden of infections caused by multiple respiratory pathogens. Increasing testing for multiple respiratory pathogens, promoting vaccine uptake, and enhancing non-pharmaceutical interventions can actively prevent the transmission of various respiratory pathogens in children.

Data availability statement

The original contributions presented in the study are included in the article/Supplementary Material. Further inquiries can be directed to the corresponding author.

Ethics statement

The studies involving humans were approved by the Ethics Committee of Children's Hospital Affiliated to Shandong University. The studies were conducted in accordance with the local legislation and institutional requirements. The human samples used in this study were acquired from a by-product of routine care or industry. Written informed consent for participation was not required from the participants or the participants' legal guardians/next of kin in accordance with the national legislation and institutional requirements.

Author contributions

YY: Data curation, Visualization, Writing – original draft, Writing – review & editing, Formal Analysis, Methodology, Software, Investigation. DW: Data curation, Formal Analysis, Methodology, Software, Visualization, Writing – original draft, Writing – review & editing, Investigation. QZ: Data curation, Writing – review & editing, Formal Analysis, Investigation, Methodology, Resources. YL: Investigation, Data curation, Formal Analysis, Resources, Supervision, Writing – review & editing. CY: Data curation, Investigation, Project administration, Resources, Supervision, Writing – review & editing. XL: Conceptualization, Formal Analysis, Funding acquisition, Methodology, Project administration, Resources, Writing – review & editing. LW: Conceptualization, Formal Analysis, Funding acquisition, Methodology, Project administration, Resources, Writing – review & editing.

Funding

The author(s) declare that financial support was received for the research and/or publication of this article. This research was funded by Science and Technology Development Program of Jinan Municipal Health Commission (No. 2023-1-60). All grant numbers and funding information are included in full and accurately.

Acknowledgments

We are very grateful to all those who helped with the study: all the subjects, their families, and collaborating clinicians for their participation.

Conflict of interest

The authors declare that the research was conducted in the absence of any commercial or financial relationships that could be construed as a potential conflict of interest.

Generative AI statement

The author(s) declare that no Generative AI was used in the creation of this manuscript.

Correction note

A correction has been made to this article. Details can be found at: 10.3389/fcimb.2025.1644555.

Publisher's note

All claims expressed in this article are solely those of the authors and do not necessarily represent those of their affiliated organizations, or those of the publisher, the editors and the reviewers. Any product that may be evaluated in this article, or claim that may be made by its manufacturer, is not guaranteed or endorsed by the publisher.

Supplementary material

The Supplementary Material for this article can be found online at: https://www.frontiersin.org/articles/10.3389/fcimb.2025.1549497/full#supplementary-material

SUPPLEMENTARY TABLE 1
Monthly results for 7 infectious pathogens from 2018.01 to 2024.01.

SUPPLEMENTARY TABLE 2
Monthly results for 5 bacterial species from 2018.01 to 2024.01.

SUPPLEMENTARY TABLE 3
Chi-square test for positive rate of 7 infectious pathogens before and after COVID-19 pandemic.

SUPPLEMENTARY TABLE 4
Chi-square test for positive rate of 6bacterial species before, during and after COVID-19 pandemic. P0 is before and during COVID-19, P1 is during and after COVID-19, P2 is before and after COVID-19.

References

Burrell, R., Saravanos, G., and Britton, P. N. (2023) Unintended impacts of COVID-19 on the epidemiology and burden of paediatric respiratory infections. *Paediatr. Respir. Rev*. 53, 3-13. doi: 10.1016/j.prrv.2023.07.004

Cai, W., Köndgen, S., Tolksdorf, K., Dürrwald, R., Schuler, E., and Biere, B.. (2024). Atypical age distribution and high disease severity in children with RSV infections during two irregular epidemic seasons throughout the COVID-19 pandemic, Germany, 2021 to 2023. *Euro Surveill.: Bull. Europeen sur les Maladies Transmissibles = Eur. Communicable Dis. Bull.* 29 (13), 2300465. doi: 10.2807/1560-7917.ES.2024.29.13.2300465

Chakraborty, C., Bhattacharya, M., Chopra, H., Bhattacharya, P., Islam, M. A., and Dhama, K. (2023). Recently emerged omicron subvariant BF.7 and its R346T mutation in the RBD region reveal increased transmissibility and higher resistance to neutralization antibodies: need to understand more under the current scenario of rising cases in China and fears of driving a new wave of the COVID-19 pandemic. *Int. J. Surg. (London England)* 109, 1037–1040. doi: 10.1097/JS9.0000000000000219

Cheng, Y., Cheng, Y., Dai, S., Hou, D., Ge, M., Zhang, Y., et al. (2022). Te prevalence of mycoplasma pneumoniae among children in beijing before and during the COVID-19 pandemic. *Front. Cell. Infect. Microbiol.* 12, 854505. doi: 10.3389/fcimb.2022.854505

Danino, D., Ben-Shimol, S., van der Beek, B. A., Givon-Lavi, N., Avni Shemer, Y., Greenberg, D., et al. (2022). Decline in pneumococcal disease in young children during the coronavirus disease 2019 (COVID-19) pandemic in Israel associated with suppression of seasonal respiratory viruses, despite persistent pneumococcal carriage: A prospective cohort study. *Clin. Infect. Dis: an Off. Publ. Infect. Dis. Soc. America* 75, e1154–e1164. doi: 10.1093/cid/ciab1014

Fujita, J. (2021). Mycoplasma pneumoniae pneumonia and respiratory syncytial virus infection in Japan during the severe acute respiratory syndrome coronavirus 2 pandemic. *Respir. Investig.* 59, 5–7. doi: 10.1016/j.resinv.2020.11.002

Goldberg, E. E., Lin, Q., Romero-Severson, E. O., and Ke, R. (2023). Swift and extensive Omicron outbreak in China after sudden exit from 'zero-COVID' policy. *Nat. Commun.* 14, 3888. doi: 10.1038/s41467-023-39638-4

Leung, K., Lau, E. H. Y., Wong, C. K. H., Leung, G. M., and Wu, J. T. (2023). Estimating the transmission dynamics of SARS-CoV-2 Omicron BF.7 in Beijing after adjustment of the zero-COVID policy in November-December 2022. *Nat. Med.* 29, 579–582. doi: 10.1038/s41591-023-02212-y

Li, Y., Yu, J., Wang, Y., Yi, J., Guo, L., Wang, Q., et al. (2024). Cocirculation and coinfection of multiple respiratory viruses during autumn and winter seasons of 2023 in Beijing, China: A retrospective study. *J. Med. Virol* 96, e29602. doi: 10.1002/jmv.29602

Li, Z. J., Yu, L. J., Zhang, H. Y., Shan, C. X., Lu, Q. B., Zhang, X. A., et al. (2022). Broad impacts of coronavirus disease 2019 (COVID-19) pandemic on acute respiratory infections in China: an observational study. *Clin. Infect. Dis: an Off. Publ. Infect. Dis. Soc. America* 75, e1054–e1062. doi: 10.1093/cid/ciab942

Li, Z. J., Zhang, H. Y., Ren, L. L., Lu, Q. B., Ren, X., Zhang, C. H., et al. (2021). Etiological and epidemiological features of acute respiratory infections in China. *Nat. Commun.* 12, 5026. doi: 10.1038/s41467-021-25120-6

Lubkin, A., Bernard-Raichon, L., DuMont, A. L., Jimenez Valero, A. M., Putzel, G. G., Gago, J., et al. (2024). SARS-CoV-2 infection predisposes patients to coinfection with *Staphylococcus aureus*. *mBio* 15, e0166724. doi: 10.1128/mbio.01667-24

Major, J., Crotta, S., Finsterbusch, K., Chakravarty, P., Shah, K., Frederico, B., et al. (2023). Endothelial AHR activity prevents lung barrier disruption in viral infection. *Nature* 621, 813–820. doi: 10.1038/s41586-023-06287-y

Meyer Sauteur, P. M., Beeton, M. L., Uldum, S. A., Bossuyt, N., Vermeulen, M., Loens, K., et al. (2022). Mycoplasma pneumoniae detections before and during the COVID-19 pandemic: results of a global survey, 2017 to 2021. *Euro Surveill.: Bull. Europeen sur les Maladies Transmissibles = Eur. Communicable Dis. Bull.* 27 (19), 2100746. doi: 10.2807/1560-7917.ES.2022.27.19.2100746

Meyer Sauteur, P. M., and Beeton, M. L. (2024). Mycoplasma pneumoniae: Delayed re-emergence afer COVID-19 pandemic restrictions. *Lancet Microbe* 5, 100–101. doi: 10.1016/s2666-5247(23)00344-0

Moulton, V. R. (2018). Sex hormones in acquired immunity and autoimmune disease. *Front. Immunol.* 9, 2279. doi: 10.3389/fimmu.2018.02279

Oertelt-Prigione, S. (2012). The influence of sex and gender on the immune response. *Autoimmun. Rev.* 11, A479–A485. doi: 10.1016/j.autrev.2011.11.022

Olsen, S. J., Winn, A. K., Budd, A. P., Prill, M. M., Steel, J., Midgley, C. M., et al. (2021). Changes in influenza and other respiratory virus activity during the COVID-19 pandemic - United States, 2020-2021. *MMWR Morbid. Mortal. Wkly. Rep.* 70, 1013–1019. doi: 10.15585/mmwr.mm7029a1

Palani, S., Uddin, M. B., McKelvey, M., Shao, S., and Sun, K. (2023). Immune predisposition drives susceptibility to pneumococcal pneumonia after mild influenza A virus infection in mice. *Front. Immunol.* 14, 1272920. doi: 10.3389/fimmu.2023.1272920

Parums, D. V. (2023). Editorial: Outbreaks of post-pandemic childhood pneumonia and the re-emergence of endemic respiratory infections. *Med. Sci. Monit.* 9, e943312. doi: 10.12659/MSM.943312

Perra, N. (2021). Non-pharmaceutical interventions during the COVID-19 pandemic: A review. *Phys. Rep.* 913, 1–52. doi: 10.1016/j.physrep.2021.02.001

Sparks, R., Lau, W. W., Liu, C., Han, K. L., Vrindten, K. L., Sun, G., et al. (2023). Influenza vaccination reveals sex dimorphic imprints of prior mild COVID-19. *Nature* 614, 752–761. doi: 10.1038/s41586-022-05670-5

Spinelli, M. A., Glidden, D. V., Gennatas, E. D., Bielecki, M., Beyrer, C., Rutherford, G., et al. (2021). Importance of non-pharmaceutical interventions in lowering the viral inoculum to reduce susceptibility to infection by SARS-CoV-2 and potentially disease severity. *Lancet Infect. Dis.* 21, e296–e301. doi: 10.1016/S1473-3099(20)30982-8

Tsang, T. K., Lee, K. H., Foxman, B., Balmaseda, A., Gresh, L., Sanchez, N., et al. (2020). Association between the respiratory microbiome and susceptibility to influenza virus infection. *Clin. Infect. Dis: an Off. Publ. Infect. Dis. Soc. America* 71, 1195–1203. doi: 10.1093/cid/ciz968

Yang, J., Marziano, V., Deng, X., Guzzetta, G., Zhang, J., Trentini, F., et al. (2021). Despite vaccination, China needs non-pharmaceutical interventions to prevent widespread outbreaks of COVID-19 in 2021. *Nat. Hum. Behav.* 5, 1009–1020. doi: 10.1038/s41562-021-01155-z

Zhou, Y. H., Xu, C., Tao, Y., Gu, M., Zhou, G., Zhou, W., et al. (2023). Incidence of SARS-CoV-2 infection in children shortly after ending zero-COVID-19 policy in China on December 7, 2022: a cross-sectional, multicenter, seroepidemiological study. *Front. Public Health* 11, 1283158. doi: 10.3389/fpubh.2023.1283158

frontiers | Frontiers in Cellular and Infection Microbiology

TYPE Correction
PUBLISHED 27 June 2025
DOI 10.3389/fcimb.2025.1644555

OPEN ACCESS

APPROVED BY
Frontiers Editorial Office,
Frontiers Media SA, Switzerland

*CORRESPONDENCE
Xin Lv
etyyjyklvxin@163.com
Ling Wang
Wlingetyy@163.com

†These authors have contributed equally to this work and share first authorship

RECEIVED 10 June 2025
ACCEPTED 11 June 2025
PUBLISHED 27 June 2025

CITATION
Yue Y, Wu D, Zeng Q, Li Y, Yang C, Lv X and Wang L (2025) Correction: Changes in children respiratory infections pre and post COVID-19 pandemic.
Front. Cell. Infect. Microbiol. 15:1644555.
doi: 10.3389/fcimb.2025.1644555

Correction: Changes in children respiratory infections pre and post COVID-19 pandemic

Yuanyuan Yue[1,2†], Dan Wu[1,2†], Qian Zeng[1,2], Yurong Li[1,2], Chun Yang[1,2], Xin Lv[1,2*] and Ling Wang[1,2*]

[1]Clinical Laboratory, Children's Hospital Affiliated to Shandong University, Jinan, China, [2]Clinical Laboratory, Jinan Children's Hospital, Jinan, China

KEYWORDS

COVID-19, respiratory infection, non-pharmaceutical interventions, children, qPCR

A Correction on

Changes in children respiratory infections pre and post COVID-19 pandemic

By Yue Y, Wu D, Zeng Q, Li Y, Yang C, Lv X and Wang L (2025). *Front. Cell. Infect. Microbiol.* 15:1549497. doi: 10.3389/fcimb.2025.1549497

In the published article, there was an error in Table 1 as published. The end date was not "January 31, 2014", it should be corrected to "January 31, 2024"; and in Table 1, Under the "Age" column, the category "01" lacks a hyphen. This should be revised to "0-1" for consistency with standard notation. The corrected Table 1 and its caption appear below.

In the published article, there was an error in the **Funding** statement. This research was funded by one Science and Technology Development Program of Jinan Municipal Health Commission, not two. The original text: "The author(s) declare that financial support was received for the research and/or publication of this article. This research was funded by two Science and Technology Development Program of Jinan Municipal Health Commission (No. 2023-1–60 and No. 2023-2-139). All grant numbers and funding information are included in full and accurately." The correct **Funding** statement appears below.

"The author(s) declare that financial support was received for the research and/or publication of this article. This research was funded by Science and Technology Development Program of Jinan Municipal Health Commission (No. 2023-1-60). All grant numbers and funding information are included in full and accurately."

In the published article, there was an error. The bacterial name "*Listeria monocytogenes* (abbreviated as LP)" is incorrect. It should be revised to "*Legionella pneumophila* (LP)."

A correction has been made to **Abstract**, *Results*:, From line 81 to line 86. This sentence previously stated:

"A variety of ARIs pathogens, including Influenza A (Flu A), Influenza B (Flu B), Adenovirus (ADV), Rhinovirus (RhV), and Respiratory Syncytial Virus (RSV), as well as co-infecting bacterial such as Klebsiella pneumoniae (KPN), Pseudomonas aeruginosa (PAE), Streptococcus pneumoniae (SP), Haemophilus influenzae (HI), and Listeria monocytogenes (LP), reached a peak positive rate at the age of 3."

The corrected sentence appears below:

"A variety of ARIs pathogens, including Influenza A (Flu A), Influenza B (Flu B), Adenovirus (ADV), Rhinovirus (RhV), and Respiratory Syncytial Virus (RSV), as well as

co-infecting bacterial such as Klebsiella pneumoniae (KPN), Pseudomonas aeruginosa (PAE), Streptococcus pneumoniae (SP), Haemophilus influenzae (HI), and Legionella pneumophila (LP), reached a peak positive rate at the age of 3."

The authors apologize for this error and state that this does not change the scientific conclusions of the article in any way. The original article has been updated.

Publisher's note

TABLE 1 The PCR results of 13 pathogens were summarized from January 31, 2018 to January 31, 2024.

year		2018 N=2761		2019 N=22785		2020 N=27337		2021 N=71093		2022 N=113049		2023 N=82332		2024 N=17953		Sum N=337310	
		n	%	n	%	n	%	n	%	n	%	n	%	n	%	n	%
sex	male	1684	60.99	13472	59.13	16224	59.35	41893	58.93	66679	58.98	48093	58.41	10446	58.19	198491	58.85
	female	1077	39.01	9313	40.87	11113	40.65	29200	41.07	46370	41.02	34239	41.59	7507	41.81	138819	41.15
age	0-1	1375	49.80	4511	19.80	5622	20.57	12526	17.62	20786	18.39	10809	13.13	2398	13.36	58027	17.20
	1-3	836	30.28	6577	28.87	8671	31.72	18814	26.46	27703	24.51	18517	22.49	4007	22.32	85125	25.24
	3-6	342	12.39	7304	32.06	8026	29.36	22293	31.36	41574	36.78	29202	35.47	4328	24.11	113069	33.52
	>6	208	7.53	4393	19.28	5018	18.36	17460	24.56	22986	20.33	23804	28.91	7220	40.22	81089	24.04
pathogen	KPN	83	6.01	83	4.53	37	2.76	99	1.24	91	1.49	320	8.84	21	5.48	734	3.24
	PAE	25	1.81	26	1.42	27	2.01	148	1.85	104	1.70	168	4.64	45	11.75	543	2.40
	SA	182	13.19	227	12.38	119	8.87	465	5.83	412	6.73	282	7.79	17	4.44	1704	7.52
	SP	414	30.00	525	28.64	283	21.09	1344	16.84	963	15.72	2205	60.91	290	75.72	6024	26.58
	HIB	354	25.65	546	29.79	256	19.08	1749	21.92	1164	19.00	1008	27.85	138	36.03	5215	23.01
	LP	1	0.07	2	0.11	7	0.52	4	0.05	5	0.08	5	0.14	0	0.00	24	0.11
	MP	62	4.49	1757	16.30	518	5.55	5269	19.93	1375	5.83	258	2.40	125	9.45	9364	11.20
	Flu A	-	-	777	22.14	966	20.69	7	0.13	1727	10.57	2587	18.72	116	3.70	6180	13.13
	Flu B	-	-	143	4.10	674	14.46	1399	25.05	1619	9.91	66	0.48	595	18.96	4496	9.56
	ADV	-	-	303	9.53	170	4.62	450	4.22	1191	7.13	987	7.31	580	18.94	3681	7.25
	RSV	-	-	-	-	298	10.70	868	18.38	1221	7.84	1842	13.41	805	25.65	5034	12.60
	PIV	-	-	-	-	45	5.72	405	4.78	309	5.78	107	2.67	14	0.57	880	4.18
	RhV	-	-	-	-	16	20.25	240	14.65	1474	11.28	1184	13.06	146	11.04	3060	12.16

"n": Number of positives; "%": Positive rate.

KPN, Klebsiella pneumoniae; PAE, Pseudomonas aeruginosa; SA, Staphylococcus aureus; SP, Streptococcus pneumoniae; HI, Haemophilus influenzae; LP, Legionella pneumophila; MP, Mycoplasma Pneumoniae; Flu A, Influenza A virus; Flu B, Influenza B virus; ADV, Adenoviridae; RSV, respiratory syncytial virus; PIV, parainfluenza virus; RhV, Rhinovirus; "-": The test was not performed in our laboratory."-"

10.3389/fcimb.2025.1644555

frontiers | Frontiers in Cellular and Infection Microbiology

TYPE Original Research
PUBLISHED 13 May 2025
DOI 10.3389/fcimb.2025.1547601

OPEN ACCESS

EDITED BY
Dimitra Dimopoulou,
Panagiotis & Aglaia Kyriakou Children's Hospital, Greece

REVIEWED BY
Patikiri Arachchige Don Shehan Nilmantha Wijesekara,
University of Ruhuna, Sri Lanka
Nuur Wachid Abdul Majid,
Indonesia University of Education, Indonesia

*CORRESPONDENCE
Henan Yao
kongxinlab@163.com yaohennan@163.com

RECEIVED 18 December 2024
ACCEPTED 31 March 2025
PUBLISHED 13 May 2025

CITATION
Dong W, Yao H and Wang W-N (2025) Study on the impact of COVID-19 epidemic and agent disease risk simulation model based on individual factors in Xi'an City. *Front. Cell. Infect. Microbiol.* 15:1547601. doi: 10.3389/fcimb.2025.1547601

Study on the impact of COVID-19 epidemic and agent disease risk simulation model based on individual factors in Xi'an City

Wen Dong[1,2], Henan Yao[1,2*] and Wei-Na Wang[3]

[1]Faculty of Geography, Yunnan Normal University, Kunming, China, [2]Geographic Information System (GIS) Technology Engineering Research Centre for West-China Resources and Environment of Educational Ministry, Yunnan Normal University, Kunming, China, [3]Network and Information Center, Yunnan Normal University, Kunming, China

Introduction: Since the first discovery and reporting of the COVID - 19 pandemic towards the end of 2019, the virus has rapidly propagated across the world. This has led to a remarkable spike in the number of infections. Even now, doubt lingers over whether it has completely disappeared. Moreover, the issue of restoring normal life while ensuring safety continues to be a crucial challenge that public health agencies and people globally are eager to tackle.

Methods: To thoroughly understand the epidemic's outbreak and transmission traits and formulate timely prevention measures to fully safeguard human lives and property, this paper presents an agent - based model incorporating individual - level factors.

Results: The model designates Xi'an—where a characteristic disease outbreak occurred—as the research area. The simulation results demonstrate substantial consistency with official records, effectively validating the model's applicability, adaptability, and generalizability. This validated capacity enables accurate prediction of epidemic trends and comprehensive assessment of disease risks.

Discussion: From late 2021 to early 2022, it employs a one - to - one population simulation approach and simulates epidemic impacts and disease risks. Initially, using building statistical data in the study area, the model reconstructs the local real - world geographical environment. Leveraging data from the seventh national population census, it also replicates the study area's population characteristics. Next, the model takes into account population mobility, contact tracing, patient treatment, and the diagnostic burden of COVID - 19 - like influenza symptoms. It integrates epidemic transmission impact parameters into the model framework. Eventually, the model's results are compared with official data for validation, and it's applied to hypothetical scenarios. It provides scientific theoretical tools to support the implementation of government - driven prevention and control measures. Additionally, it facilitates the adjustment of individual behavioral guidelines, promoting more effective epidemic management.

KEYWORDS

COVID-19, individual factor, agent model, government macro intervention policy, simulation and prediction

1 Introduction

The emergence of the severe acute respiratory syndrome coronavirus 2 (SARS-CoV-2) pandemic at the end of 2019 severely disrupted life globally, negatively affecting the mental and physical wellbeing of people around the world (Aldhawyan et al., 2024). The sudden emergence of coronavirus disease 2019 (COVID-19) as a global public health concern not only impacted the global economy but also led to social instability. This pandemic necessitates global unity (Dietz and Brondstater, 2024). Understanding the rapid progression of the COVID-19 epidemic and effectively translating this understanding into government policies has become an urgent requirement for governments worldwide. Rajagopal et al. (2020) developed a SEIRD model with fractional derivatives and validated it using epidemic data from Italy. The results demonstrated that the fractional model exhibited smaller prediction errors compared to the traditional SIR series model. Maier and Brockmann (2020) developed a concise susceptible-infected-recovered-X (SIR-X) model. This model aimed to explore the impacts of isolation measures, containment policies, and unidentified patients, including asymptomatic individuals, on epidemic progression. Truszkowska et al. (2021) constructed an agent-based model. They used it to examine the effects of different vaccination strategies on epidemic prevention and control in New Rochelle, a town in the United States. Beira and Sebastiao (2021) devised a comprehensive protected-susceptible-exposed-infectious-recovered-deceased (s) [PSEIRD(S)] model. They fitted the model using data on the number of infected individuals, deaths, and hospitalizations during the post-Christmas 2020 outbreak in Portugal. The fitting results showed that some model parameters underwent discrete temporal changes, reflecting the multi-phase nature of the epidemic. A comprehensive protected-susceptible-exposed-infectious-recovered-deceased (s) [PSEIRD(S)] model was devised. They fitted the model using data on the number of infected individuals, deaths, and hospitalizations during the post-Christmas 2020 outbreak in Portugal. The fitting results showed that some model parameters underwent discrete temporal changes, reflecting the multi-phase nature of the epidemic.

Building on the basic SIR model of COVID-19 transmission, Dehning et al. (2020) proposed a Bayesian framework based on Markov chain Monte Carlo (MCMC) sampling. This framework was used to characterize key epidemiological parameters, time-varying transmission rates, and potential change points. It also helped identify the optimal timing for intervention effectiveness. Bertrand and Pirch (2021) developed the susceptible-exposed-infectious-quarantined-recovered-deceased (SEIRQD) model. They explored the optimal control of the second-phase COVID-19 lockdown in Morocco and analyzed the impact of optimal control strategies on the pandemic in the country. Wijesekara and Wang (2022) employed the proposed susceptible, transmitted, quarantined, non-diagnosed infected, hospitalized diagnosed infected, recovered, dead, susceptible (SEQIJRDS) model. They predicted mortality rates under various lockdown procedures, vaccination scenarios, quarantine measures, and mask-usage cases. Additionally, they projected hospital resource utilization to identify the most effective interventions that would prevent over-straining hospital resources. Building on the SEIR model of disease transmission, they (Liu et al., 2021) put forward an adaptive model named SEAIRD, which incorporates internal sources and isolation interventions. This model simulates the evolving behavior of SARS-CoV-2 in the United States. Neural networks are applied to enhance the fit of the SEAIRD model. Schlosser et al. (2020) demonstrated that lockdown measures in Germany not only significantly reduced population mobility but also led to a substantial decrease in the long-term connectivity of the mobility network. The study revealed that these structural changes could flatten the epidemic curve and slow down disease transmission. Cacciapaglia et al. (2021) proposed a continuous waveform graph based on the epidemic severity normalizing group framework (eRG). They concluded that understanding the relaxation periods between different epidemic phases is crucial for controlling future major outbreaks. Aleta et al. (2020) constructed an agent-based COVID-19 epidemic dynamics model. By integrating anonymous mobile phone location data from the entire Boston area with census statistics, they found that agents adhered strictly to social distancing requirements for a specific period. Contact tracing, nucleic acid testing, and isolation measures effectively curbed the spread of COVID-19. These measures also alleviated the burden on the healthcare system, enabling it to handle current medical demands.

2 Materials and methods

2.1 Data collection

This study amassed diverse fundamental epidemiological parameters, including those of the COVID-19 virus. A Python web crawler was utilized to gather and analyze the most recent daily COVID-19 epidemic data publicized by the Xi'an Health Commission on its official website. These data encompasses the number of new cases, cumulative confirmed cases, and new deaths on each given day. The number of deaths are accumulated, and the missing data are further supplemented through the network platform. Through the API interface of AMAP (2022), the geographic coordinates, building categories, and population capacity of various buildings in Xi 'an, such as houses, schools, hospitals, nursing homes, workplaces, leisure, and entertainment venues, were collected and counted, and the above data were checked and corrected by manual collection on Google Map (Google, 2022). The population data were sourced from China's seventh national population census in 2020, along with relevant government-released macro-policy data. These were organized into datasets for use in the model. Transmission parameters of the COVID-19 virus, clinical parameters, and patient hospitalization parameters were drawn from research conducted by global scholars and official announcements of Xi'an. Parameters were adjusted in accordance with the actual situation in Xi'an.

2.2 Agent model

In this study, the classical SEIR epidemiological infection model underwent improvement. The model's states were both increased in

number and refined. Concurrently, it was integrated with the discrete-event simulation model and extended on the GIS platform, enabling the construction of a comprehensive agent-based model.

Within this study, agents are categorized into Sicken Individual Agent (SIA), Healthy Individual Agent (HIA), and Intervention Agent (VA). The attributes and behaviors of these agents are precisely defined in Table 1.

During each simulation step (Δs), agents switch locations among the six types of places generated by the model, guided by their own requirements. The model assigns distinct propagation parameters to different locations. For simulated travelers, the flow of various vehicles between different regions is factored in. Travel modes are interconnected through the Haversine equation—an algorithm calculating distances between two points using latitude and longitude data. This mimics real-world scenarios where people select travel modes based on distance and time constraints.

Six typical locations are denoted as Q={1,2,3,…., q}, while residents in the study area are C={1,2,3,….}, A transfer function fk: C → Q is defined using the semi-positive vector formula. Here, k∈{F, B, S, Rt, Hp} is used to allocate generated inhabitants to various locations. The function fk sends each agent i ∈C to its corresponding location q. Locations q include homes (F), public places (B), schools (S), nursing homes (Rt), and hospitals (Hp). Given that an agent may not be connected to all locations, when agent i has no connection with location q, we denote it as fk(i) = ∅, and Cq represents the total number of agents connected to location q.

The Haversine formula (Baskar and Anthony Xavior, 2021) is as follows:

$$d = 2\mathrm{Rarcsin}\left(\sqrt{\sin 2\left(\right) + \cos(\mathrm{lat2})\cos(\mathrm{lat1})\sin 2\left(\right)}\right) \quad (1)$$

This paper builds an Agent model across three dimensions: individuals, settings, and the epidemic itself. At the individual level, Agents represent real-world people as embodied entities. The setting dimension pertains to the environment where Agents interact and carry out actions. Regarding the epidemic, it encompasses the age distribution of hospitalized patients, the proportion of ICU hospitalizations, and the age-specific mortality ratio. This paper conducts research at three levels. At the city level, Xi'an is chosen as a representative city for epidemic outbreaks. At the community level, research focuses on family units. Using census data from the study area, data such as the total number of household accounts, age ratio, total population, age distribution of household heads, proportion of single-parent families, proportion of childless families, and proportion of families with the elderly are integrated with official data for model calculation, demonstrating local community structure characteristics. Building

TABLE 1 Agent attributes and behavior definition.

	Agent sort	Common attribute	Concrete attribute	Behavior	Infectious disease influencing factors
Individual agent	SIA HIA	Time attribute	Age	Flow in the location where the model is generated	Location migration
			Sex		
			Whether to become a close contact		
			Whether to become a close contact		
			Whether to become a close contact		Behavior trajectory
			No exposure history (no contact with confirmed patients, suspected cases)		
			Have a history of travel (i.e., have you ever traveled or lived in a place where a confirmed case has been reported)		Social travel
			Have fever, cough, and other symptoms		
	VA	Spatial attribute	When the model is started, an appropriate time attribute value is selected for initialization according to the start and end time of the local government intervention	The VA treats patients with fever and cough	Traffic control
				VA restricts the public activities of agents with a history of exposure and residence	Stay-at-home order
				VA observed and detected agents with exposure history and travel history	No workplace business
				VA controls the traffic of agents with a history of exposure and residence	No gathering, no public activities
				VA conducted standardized isolation therapy for SIA	

data in the study area is retrieved via the AMAP API interface to recreate the real-world environment. Starting from community characteristics and combining the total number of working people, working hours, and the proportion of different transportation methods, the local population mobility model is analyzed and simulated.

Relevant model parameters are integrated. Infection-related parameters, family size, and age-related proportions of agents after exposure are incorporated into the SEIR model as code. This enables their specific impact on the spread of infectious diseases. The model architecture is illustrated in Figure 1.

3 Result

3.1 Simulation and verification of agent model based on Xi'an City

The model amasses and organizes data including geographical latitude and longitude coordinates, building types, population capacities, and similar information for various buildings such as houses, schools, workplaces, hospitals, and leisure and entertainment venues in all districts of Xi'an, China. The population data come from Xi'an's 2020 seventh national census. With this data, a population-related model is established. The number of students and school employees is retrieved from statistical results publicized by the Xi'an Education Bureau. The number of hospital employees and hospitalized patients is sourced from statistical announcements by the Xi'an Health Bureau.

The model assigns housing to individual agents statistically. It bases this on data from the seventh national census, like the number of existing families, average family size, and housing vacancy rate in Xi'an. The model generates 13,078,200 agents and forms 5,577,852 households. At the start of model operation, the entire generated population of Xi'an is initialized as susceptible individuals. A specific number of agents are set in the exposed state. During subsequent simulations, agents change states. When the model is initialized, Figure 2 presents the relevant locations of the created buildings. Figure 3 shows the age distribution generated by the model using census data.

The study applies evenly distributed random sampling to perform nucleic acid testing on agents within the susceptible population. Agents can be in diverse states, such as the healthy state, undergoing testing, or receiving treatment. Both individuals with influenza-like symptoms similar to confirmed infection and exposed persons must undergo nucleic acid testing. The daily volume of nucleic acid testing is scheduled according to actual timelines. Once the test results are available, decisions on hospitalizing patients are made based on positive or negative outcomes, although there are also some false-negative and false-positive cases.

Specifically, nucleic acid detection is conducted on individuals who were within the same 800 m × 800 m spatio-temporal range as confirmed patients. The study does not involve explicit and specific tracking. Case detection is achieved on an average-significance basis, and nucleic acid detection for a particular agent is determined through even distributed random sampling.

According to test results, infected individuals are classified into two categories: asymptomatic carriers and confirmed cases. The model arranges routine hospitalization for ordinary confirmed cases. For agents with deteriorating conditions, the model assigns ICU treatment. For agents in centralized isolation, when they exhibit symptoms of COVID-19 infection, their status changes to routine hospitalization or ICU treatment. For agents requiring treatment, their treatment status can be adjusted based on clinical observations. Considering the patient's age and the probabilities of routine and ICU hospitalization, initial treatment plans are derived from clinical data (Eubank et al., 2020; Verity et al., 2020). For patients admitted to the ICU, their recovery status is recalculated based on ICU mortality (Verity et al., 2020). After diagnosis, the

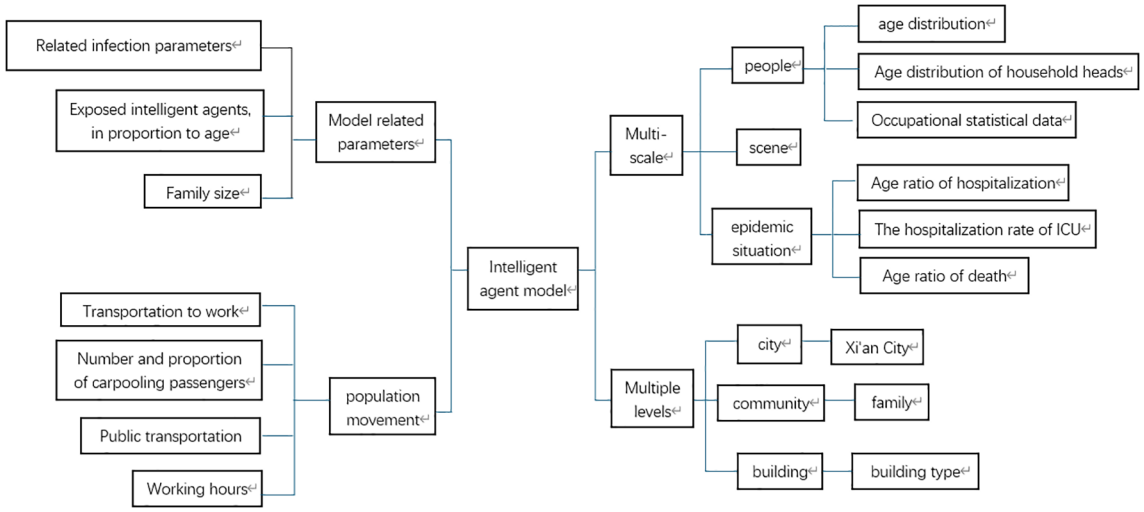

FIGURE 1
Model architecture diagram.

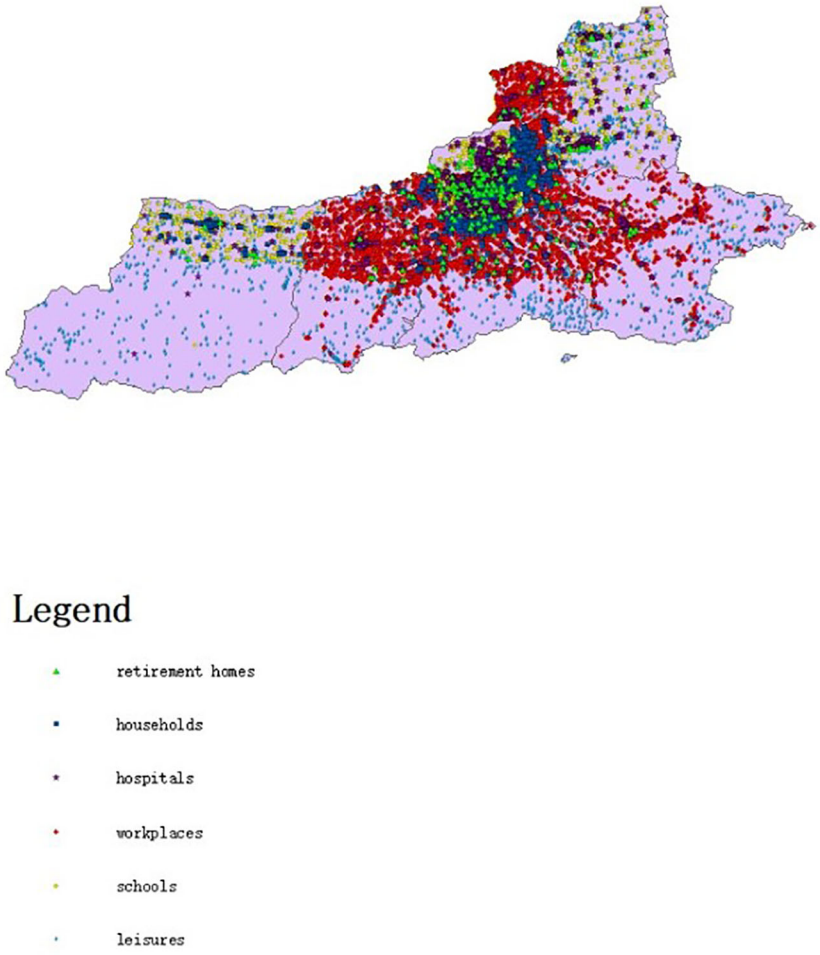

FIGURE 2
Map of different types of buildings in Xi'an.

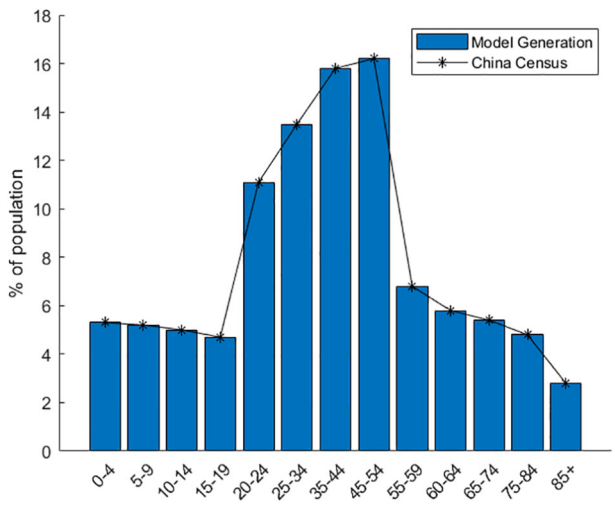

FIGURE 3
Distribution of population age characteristics created by the model.

treatment type of agents will be changed. Since cured and deceased patients no longer influence the spread of COVID-19, the model will remove them. The model also takes into account a category of agents with a high mortality rate: patients who have not undergone nucleic acid testing yet still require ICU treatment. In line with our policy, the number of such agents is set to zero in the model.

When susceptible agents contract the common cold or seasonal influenza, they are quarantined due to symptoms resembling those of COVID-19 (Verity et al., 2020). If the nucleic acid test result is negative, the quarantine is lifted (Verity et al., 2020).

The model simulated the spread of COVID-19 in Xi'an from 1 December 2021 to 29 January 2022—from the onset of the epidemic to the reopening of Xi'an. This aimed to demonstrate the model's practicality. In this study, three types of COVID-19-related data released by the Xi'an Municipal Health Commission were selected: the daily number of newly confirmed cases, the cumulative number of confirmed cases, and the total number of deaths. Using these data, weekly new cases and deaths in the study area were extracted to validate the model.

For instance, by altering the daily nucleic acid detection rate and the number of initially infected people in the model, it was observed

that the infection rate in public places decreased during Xi'an's complete lockdown. Conversely, the infection rate increased after Xi'an reopened. In line with the actual situation, the number of agents undergoing nucleic acid testing daily changed over time.

The model simulation was run 100 times. Figure 4 presents the model validation results. The model's output data were verified and compared with Xi'an's real-world data from four aspects: a) the total number of COVID-19 confirmed cases during the simulation period, b) the total number of deaths during the simulation period, c) the average weekly number of new cases during the simulation period, and d) the average weekly number of deaths during the simulation period. The total number of COVID-19 confirmed cases represents the sum of false positives detected during model operation and all positive agents. Some diseased agents died because they could not be admitted to the ICU due to medical resource constraints. Introducing weekly averages helps avoid spurious fluctuations caused by uneven data collection.

The model's output regarding the total number of COVID-19 confirmed cases, weekly new cases, and weekly deaths aligns closely with the actual data reported by the Xi'an Health Commission. This validates the model's effectiveness in predicting daily new cases. The simulated 95% confidence interval for the cumulative number of confirmed cases was (1526.059982, 1076.640018), while the actual 95% confidence interval was (1458.295568, 990.1377655). The 95% confidence interval for the simulated weekly new confirmed cases was (470.6553997, 117.5946003), compared to the actual 95% confidence interval of (464.8929787, 117.3570213). The simulation and prediction accuracy for the cumulative number of confirmed cases and mask-wearing rate reached 100%.

The model exhibits generality. To apply it to different cities, parameters need to be determined based on each city's specific circumstances, enabling city-specific simulation and prediction. During a certain period, the cumulative number of confirmed cases output by the model is slightly higher than the actual official data. This could be attributed to the frequency of official data reporting. It may also be due to the implementation of patient nucleic acid testing and active contact tracing at the start of model operation, corresponding to the early stage of the epidemic. Thus,

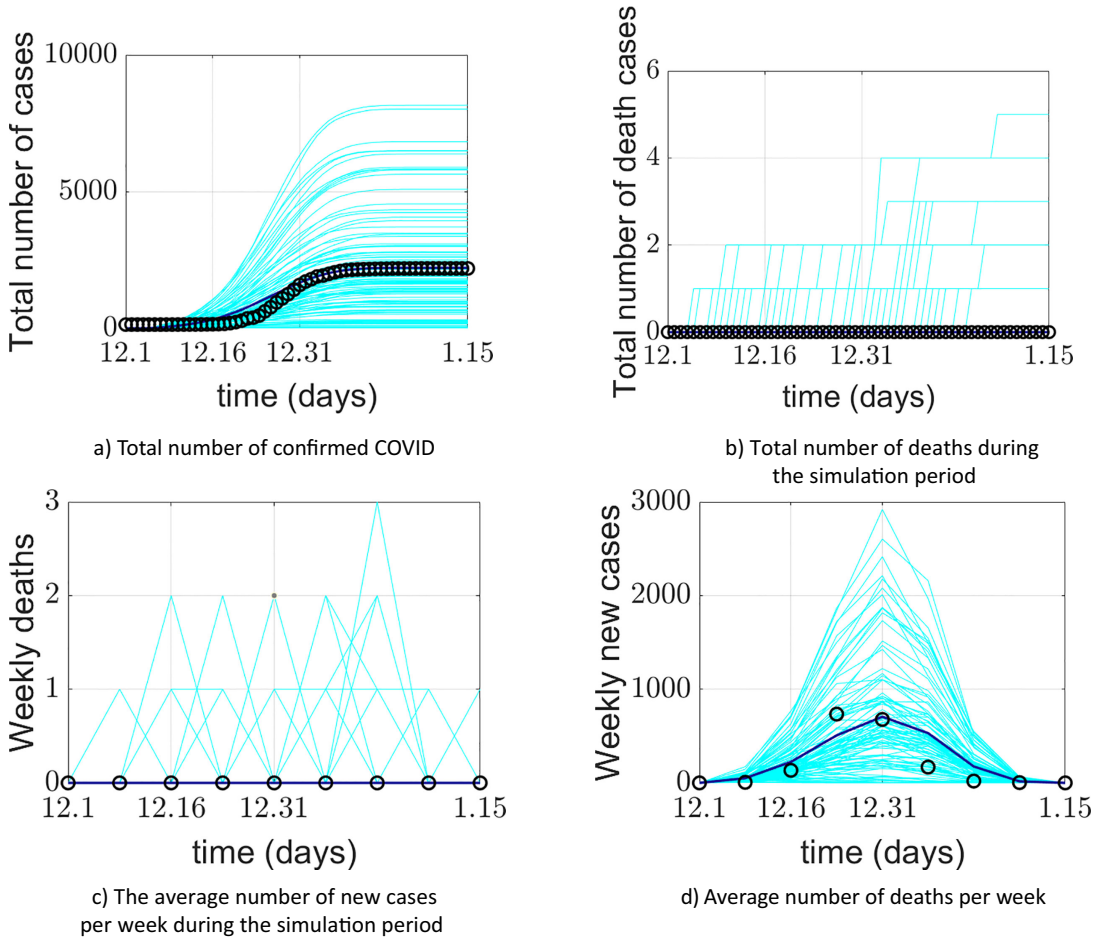

FIGURE 4
Comparison between the COVID-19 epidemic in Xi'an simulated by the model and the official reported data. **(a)** Comparison of cumulative confirmed cases; **(b)** comparison of cumulative deaths; **(c)** comparison of the average weekly number of new cases; **(d)** comparison of average weekly deaths. The cyan lines in the figure represent 100 implementations of the model, the blue lines represent the average of the model implementations, and the o represents the official reported data.

under the model-provided practical scenario of patient nucleic acid testing, discrepancies between simulated and actual data may occur. Regarding weekly new cases and simulations under a 100% mask-wearing rate scenario, spikes in real-world data may be associated with variations in hospital reporting frequency or delays.

3.2 Simulation and effect evaluation of agent epidemic prevention scenario

The virus exists in droplets or aerosols. When air carries and spreads particles contaminated with the virus, people can inhale them directly, resulting in infection. Infected individuals exhale virus-laden particles while breathing, communicating, coughing, sneezing, or singing. This easily infects those in their vicinity. Therefore, wearing masks stands as a crucial measure to prevent virus spread.

To demonstrate the model's value and the impact of mask wearing on the COVID-19 epidemic, the model simulated a scenario where all Xi'an residents wore masks in public places during the outbreak. This means that the mask-wearing rate was set at 100%, and a 1-m social distance was maintained. According to the health-behavior survey of Xi'an citizens, 90% of them wear masks when going out. Figures 5 and 6, respectively, display the simulated COVID-19 situation in Xi'an regarding the cumulative number of confirmed cases and the weekly new cases, compared with official data under a 100% mask-wearing rate.

Figures 5 and 6 depict the simulated COVID-19 situation and official reported figures in Xi'an during scenario simulations involving mask-wearing and social distancing: a) comparison of cumulative confirmed cases and b) comparison of cumulative deaths. In the figures, cyan lines denote 100 model simulations. The blue line represents the average of model implementations, while circles (o) represent officially reported data.

When the mask-wearing rate hits 100%, both the cumulative number of confirmed cases and the weekly increment in the model's output decline slightly although not substantially. This may stem from some individuals' casual approach to the epidemic, leading to imperfect execution of mask wearing.

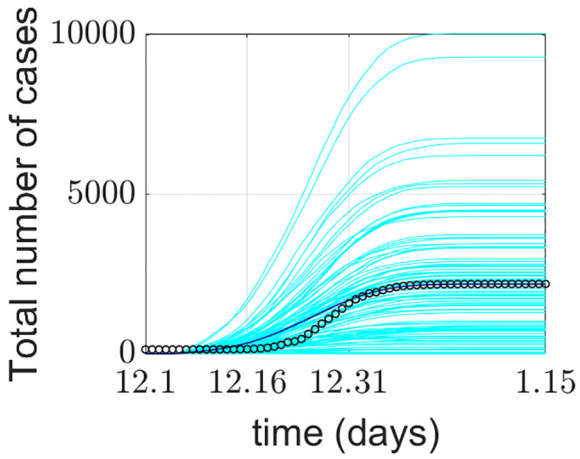

FIGURE 5
Cumulative number of confirmed cases in Xi'an with masks.

4 Discussion

In late December 2019, Wuhan, a city in Hubei Province, emerged as the first location where the COVID-19 virus was detected and reported. Shortly thereafter, the virus began to spread swiftly, reaching numerous countries worldwide (Marcel et al., 2020). This caused significant harm globally. To effectively contain the COVID-19 outbreak in China, it is essential to carry out efficient testing, promptly trace patient contacts, and identify related cases. Targeted prevention and control and rational public health intervention strategies will play a positive role in reducing the spread of COVID-19 (Aleta et al., 2020; Marcel et al., 2020; Unwin et al., 2020; Adriana et al., 2021). Identifying infected individuals and tracing their subsequent contacts represents a crucial aspect of the testing process. To address these challenges, it is necessary to gain a more in-depth understanding of community composition, the location and context of COVID-19 outbreaks, and people's daily habits (Singh et al., 2020; Heidarzadeh et al., 2021). To maximize the alignment between the experimental environment and the population characteristics and geographical environment of the study area, this research drew on relevant data from the seventh national population census of Xi'an. Data including the total number of permanent residents in Xi'an, the total number of household accounts, the age ratio, the age-distribution characteristics of household heads, the average family size, and the proportions of childless families, single-parent families, and families with the elderly were collected.

The population agents of Xi'an in the model were generated using data that reflect the local community structure. Based on these data, family units were created for the agents. Subsequently, family members were assigned to each family, with the granularity reaching individual level. This approach aimed to achieve one-to-

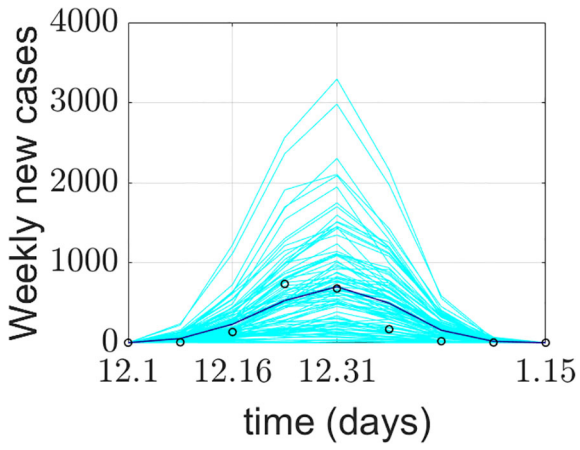

FIGURE 6
Number of new cases per week in Xi'an with masks.

one modeling of residents in the study area and reconstruct the community characteristics of the study area to the greatest extent possible. Accurate and comprehensive map data are essential for reconstructing the real-world geographical environment of the study area. On the one hand, the map data were sourced from the basic map data of the study area. On the other hand, leveraging AMAP and Baidu Map is crucial for acquiring detailed statistical data on all buildings in the study area. These data include building types, names, precise locations, and their latitudes and longitudes. The data are generated onto the study area's basic map using Point of Interest (POI) data, facilitating the creation of a comprehensive study area map. This, in turn, maximally restores the real-world geographical environment of the study area.

To conduct simulation research on the impact of macro-intervention behavior on epidemic transmission and disease risk, considering individual factors, it is essential to gather data on individual influencing factors and relevant government macro-policy data. Individual-factor data encompasses an individual's age, occupation, travel mode, history of traveling in areas with suspected cases, contact with confirmed patients, presence of symptoms like fever, cough, and fatigue, population density at their location, and implementation of traffic control and public-activity restrictions. Government macro-policy data cover containment and quarantine measures, promotion of mask-wearing and avoidance of social activities, and closure and reopening of schools and workplaces. Beginning with the unique community characteristics of the study area and integrating the total number of working individuals and the data on the proportion of different transportation modes that they select for commuting, the local population's movement patterns and behavior trends can be analyzed. When residents commute to work, attend school, or visit the hospital, their movements contribute to crowd mobility, thereby forming the crowd movement model. Given that infection rates vary across different settings, this paper primarily focuses on residents at home, during crowd movement, and in locations such as schools, hospitals, and workplaces. By integrating the infection rates specific to these relevant settings, the simulation of the epidemic transmission process is completed. For confirmed patients, the model classifies them into general hospitalization and ICU treatment categories based on predefined age parameters. Confirmed patients undergoing treatment in general hospital wards will experience improvement and recovery, influenced by factors such as the COVID-19 recovery time. For patients receiving ICU treatment, the model predicts the number of deaths among confirmed patients by considering relevant parameters like the ICU treatment mortality rate and patient age. The model no longer includes recovered and deceased confirmed patients in its calculations. Subsequently, a comprehensive agent model is constructed. In this study, a model is developed within a simulated spatial environment that closely resembles the real-world geographical landscape. This achieves a seamless integration of agent entities and the geospatial environment.

Building on existing research, Zhou et al. (2022)and his team effectively demonstrated the transmission process of COVID-19. They integrated data from mobile network operators with the space–time simulation technology of gravity models. Through this approach, they identified four primary transmission modes. These modes are constrained by the specific spatial layout and geographical location of the city. In this study, the simulation of human behavior is not only accurate at the individual level but also provides highly accurate spatiotemporal representation for each individual (Ferguson et al., 2005, 2006; Perez and Dragicevic, 2009; Ajelli et al., 2010; Perra and Gonçalves, 2015; Aleta et al., 2020), In the agent-based model, various physical locations are considered, including enterprises, hospitals, residences, nursing homes, and schools. Simultaneously, by integrating the unique attributes of the community, this research delves into the behavior patterns of local residents and population movement trends. This approach aims to overcome the limitations imposed by relying on specific spatial layouts and geographical locations. By integrating population density and spatial density across different regions to predict outbreak times, the corresponding mathematical model is developed to achieve epidemic early warning. An agent-simulation prediction model is designed and implemented, considering the unique spatial structures and community characteristics of Chinese cities and the interactions of government macro-intervention measures. In the control and prevention of disease spread, the construction and analysis of mathematical models are of crucial importance. The compartment model serves as the foundation for understanding the complex dynamics of epidemics (Jiao et al., 2020). This model can be employed to analyze the impact of influencing factors, transmission routes, and population susceptibility on disease progression. It offers scientific theoretical support for the rational formulation of prevention strategies. Koo et al. (2020) utilized a model simulating the influenza epidemic to explore the impact of four interventions on the transmission of the COVID-19 epidemic in Singapore under three scenarios with different basic reproductive numbers. Compared to previous studies, this paper's advantage lies in its straightforward coding approach. This enables more efficient presentation of the effects of various macro-interventions. It facilitates public health institutions in quickly and promptly evaluating current strategies and provides direction for subsequent policy adjustments. The compartment model is also an invaluable tool for understanding epidemics and evaluating pre-conceived strategies (Baldea, 2020; Della Rossa et al., 2020; Estrada, 2020; Gilbert et al., 2020; Vespignani et al., 2020). This research model builds upon the SEIR model. By incorporating the patient's death state, nucleic acid detection state, and treatment state, and integrating with the discrete-event simulation model, it expands based on GIS. This results in the formation of the entire agent model. Currently, many agent models focus on specific settings such as university campuses. For instance, Gressman and Peck (2020) investigated an agent model centered on a university campus. This model was used to explore small-scale micro-environments, like the strategies for universities to reopen during the epidemic, or to construct agents for simulating an entire country as the research context. This paper conducts numerical simulations in a medium-scale environment to explore interactions between agents themselves and between agents and their environment. Tatapudi et al. (2021) developed an agent model based on population and social data from an urban community in

the United States with 2.8 million residents. They used it to study the impact of vaccine prioritization strategies on curbing COVID-19. A large number of experimental studies have validated the advantages of agent models. These studies have demonstrated their technical feasibility and expandability in cross-scenario research (Adler et al., 2020; Gopalan and Tyagi, 2020; Keskinocak et al., 2020; Kuzdeuov et al., 2020; Kerr et al., 2021). By integrating relevant elements, this paper addresses the scarcity of medium-scale agent simulations in existing research. It also develops an agent model suitable for Chinese cities, incorporating the unique characteristics of Chinese community structures. This model can more accurately and comprehensively reflect the distinct lifestyles of Chinese residents. Moreover, it enables refined population representation when simulating large-scale activities, making it highly relevant to the epidemic outbreak, prevention, and control processes in China. Although this paper has certain limitations, its fitting results are generally consistent with official data. This provides scientific reference for public health departments to adopt more comprehensive, rigorous, and detailed measures to safeguard public health.

5 Conclusions

Acknowledging the complexity and uncertainties within human society, human behavior, and the continuous mutation of the COVID-19 virus, this paper gathered 60 days' worth of epidemic case data from Xi'an. The data collection period extended from late November 2020 to early 2021 and encompassed cumulative confirmed cases, cumulative deaths, daily new cases, and daily deaths. Taking Xi'an's epidemic situation as a case study, the research incorporated geographic information technology. It delved into the attributes and characteristics of typical clustered epidemic scenarios. This investigation relied on population census statistical data, which enabled one-to-one population modeling. It also made use of basic geographic data including longitude and latitude information of homes, schools, hospitals, public areas, nursing homes, Xi'an's basic map data, and epidemic big data. Spatial structures closely related to the COVID-19 transmission path, such as homes, schools, hospitals, nursing homes, public areas, and leisure and entertainment venues, were identified. One-to-one high-precision modeling of geographical buildings was carried out. This created a physical environment for simulating the "human" (agent) and "epidemic" (virus transmission process) scenarios of COVID-19. During the modeling process, the model offers two distinct nucleic acid detection methods based on residents' travel status: hospital-based detection and home-isolation detection. The model precisely tracks and performs nucleic acid testing on individuals who have had spatio-temporal intersections with patients. Patients are classified into general hospitalization, ICU hospitalization, and home isolation (after treatment completion) based on the severity of their symptoms and hospitalization requirements. Special scenarios, such as agents working in schools, hospitals, and nursing homes, are modeled separately. The daily number of nucleic acid tests varies over time. Moreover, accounting for the additional burden of nucleic acid testing imposed by influenza patients with virus-like symptoms, Xi'an was simulated to undergo complete lockdown, isolation, and reopening. This aimed to simulate the impact of different government policies and measures on virus transmission during the movement and interaction of urban residents. In addition, a prediction model for the spread of COVID-19 in urban space was proposed. This model incorporates individual factors, geospatial structures, and macro-intervention behaviors. The dynamic transmission patterns of the disease were explored within spatial distribution units, focusing on the interaction between agents and intervention agents. Finally, the model's results were compared with official epidemic data released by the Xi'an Health Commission.

This study effectively developed a COVID-19 agent-based disease risk prediction model. The model can capture the influence of individual factors on the epidemic and the impact of macro-intervention measures. It utilizes multi-source data, such as influenza statistics, building data, and population data. By comprehensively applying the agent-based model, it enables long-term and dynamic simulation and prediction of the COVID-19 epidemic transmission trend in Xi'an, the disease risk faced by residents, and the effectiveness of intervention strategies. This model serves as a reference for the government to anticipate epidemic development, optimize the allocation of prevention and control resources, and evaluate prevention and control measures.

Data availability statement

Publicly available datasets were analyzed in this study. This data can be found here: https://www.kingcounty.gov/depts/health/covid-19/data.aspx.

Author contributions

WD: Funding acquisition, Writing – review & editing. HY: Conceptualization, Data curation, Methodology, Validation, Visualization, Writing – original draft. W-NW: Resources, Supervision, Writing – review & editing.

Funding

The author(s) declare that financial support was received for the research and/or publication of this article. This research was supported by the National Natural Science Foundation of China (Grant nos. 42161071 and 41661087). This work was supported by the project funding of the "Support Program of Xingdian Talents".

Acknowledgments

Thanks to the National Nature Foundation for the financial support of the article and the teacher's advice and guidance in writing too much.

Conflict of interest

The authors declare that the research was conducted in the absence of any commercial or financial relationships that could be construed as a potential conflict of interest.

Generative AI statement

The author(s) declare that no Generative AI was used in the creation of this manuscript.

Publisher's note

All claims expressed in this article are solely those of the authors and do not necessarily represent those of their affiliated organizations, or those of the publisher, the editors and the reviewers. Any product that may be evaluated in this article, or claim that may be made by its manufacturer, is not guaranteed or endorsed by the publisher.

References

Adler, S., Bodeit, O., Bonn, L., Goldenbogen, B., Haffner, J., Karnetzki, M., et al. (2020). Geospatially referenced demographic agent-based modeling of SARS-CoV-2-infection (COVID-19) dynamics and mitigation effects in a real-world community[J]. *medRxiv*, 2020: 2020.05. 03.20089235.

Adriana, R. L., David, S. P., Sergio, G., Clara, G., Matamalas., J. T., Benjamin, S., et al. (2021). Virus spread versus contact tracing: Two competing contagion processes. *Phys. Rev. Res.* 3 (1), 013163.

Ajelli, M., Goncalves, B., Balcan, D., Colizza, V., Hu, H., Ramasco, J. J., et al. (2010). Comparing large-scale computational approaches to epidemic modeling: Agent-based versus structured metapopulation models. *BMC Infect. Dis.* 10, 1–13. doi: 10.1186/1471-2334-10-190

Aldhawyan, A. F., BuSaad, M. A., Almaghlouth, N. E., Alnasser, A. H., Alnasser, J. A., Almansour, A. H., et al. (2024). Understanding long COVID: prevalence, characteristics, and risk factors in the Eastern Province of Saudi Arabia. *Front. Med.* 11. doi: 10.3389/fmed.2024.1459583

Aleta, A., Martin-Corral, D., Pastore y Piontti, A., Ajelli, M., Litvinova, M., Chinazzi, M., et al. (2020). Modelling the impact of testing, contact tracing and household quarantine on second waves of COVID-19. *Nat. Hum. Behav.* 4, 964–96+. doi: 10.1038/s41562-020-0931-9

AMAP, N (2022). *NASDAQ: AMAP*. Available online at: https://mobile.amap.com/ (Accessed October 16, 2023).

Baldea, I. (2020). Suppression of Groups Intermingling as an Appealing Option for Flattening and Delaying the Epidemiological Curve While Allowing Economic and Social Life at a Bearable Level during the COVID-19 Pandemic. *Advanced Theory Simulations* 3 (12), 2000132.

Baskar, A., and Anthony Xavior, M. (2021). A four-point direction search heuristic algorithm applied to facility location on plane, sphere, and ellipsoid surfaces. *J. Operational Res. Soc.* 73, 2385–2394. doi: 10.1080/01605682.2021.1984185

Beira, M. J., and Sebastiao, P. J. (2021). A differential equations model-fitting analysis of COVID-19 epidemiological data to explain multi-wave dynamics. *Sci. Rep.* 11 (1), 16312.

Cacciapaglia, G., Cot, C., and Sannino, F. (2021). Multiwave pandemic dynamics explained: how to tame the next wave of infectious diseases. *Sci. Rep.* 11 (1), 6638.

Dehning, J., Zierenberg, J., Spitzner, F. P., Wibral, M., Neto, J. P., Wilczek, M., et al. (2020). Inferring change points in the spread of COVID-19 reveals the effectiveness of interventions. *Science* 369 (6500), eabb9789. doi: 10.1126/science.abb9789

Della Rossa, F., Salzano, D., Di Meglio, A., De Lellis, F., Coraggio, M., Calabrese, C., et al. (2020). A network model of Italy shows that intermittent regional strategies can alleviate the COVID-19 epidemic. *Nat. Commun.* 11 (1), 5106.

Dietz, T. K., and Brondstater, K. N. (2024). Long COVID management: a mini review of current recommendations and underutilized modalities. *Front. Med.* 11. doi: 10.3389/fmed.2024.1430444

Estrada, E. (2020). COVID-19 and SARS-CoV-2. Modeling the present, looking at the future. *Phys. Reports-Review Section Phys. Lett.* 869, 1–51.

Eubank, S., Eckstrand, I., Lewis, B., Venkatramanan, S., Marathe, M., and Barrett, C. L. (2020). Commentary on Ferguson, et al., "Impact of Non-pharmaceutical Interventions (NPIs) to Reduce COVID-19 Mortality and Healthcare Demand. *Bull. Math. Biol.* 82, 52.

Ferguson, N. M., Cummings, D. A. T., Cauchemez, S., Fraser, C., Riley, S., Meeyai, A., et al. (2005). Strategies for containing an emerging influenza pandemic in Southeast Asia. *Nature* 437, 209–214. doi: 10.1038/nature04017

Ferguson, N. M., Cummings, D. A. T., Fraser, C., Cajka, J. C., Cooley, P. C., and Burke, D. S. (2006). Strategies for mitigating an influenza pandemic. *Nature* 442, 448–452. doi: 10.1038/nature04795

Gilbert, M., Pullano, G., Pinotti, F., Valdano, E., Poletto, C., Boelle, P.-Y., et al. (2020). Preparedness and vulnerability of African countries against importations of COVID-19: a modelling study. *Lancet* 395, 871–877. doi: 10.1016/S0140-6736(20)30411-6

Google, G. m (2022). *Google maps*. Available online at: https://www.google.com/maps (Accessed October 16, 2023).

Gopalan, A., and Tyagi, H. (2020). How reliable are test numbers for revealing the COVID-19 ground truth and applying interventions? *J. Indian Institute Sci.* 100, 863–884. doi: 10.1007/s41745-020-00210-4

Gressman, P. T., and Peck, J. R. (2020). Simulating COVID-19 in a university environment. *Math. Biosci.* 328, 108436. doi: 10.1016/j.mbs.2020.108436

Heidarzadeh, A., Narayanan, K., and IEEE (2021). "Two-stage adaptive pooling with RT-QPCR for COVID-19 screening," in *2021-2021 IEEE International Conference on Acoustics, Speech and Signal Processing (ICASSP)*. (IEEE), 8148–8152.

Jiao, J., Liu, Z., and Cai, S. (2020). Dynamics of an SEIR model with infectivity in incubation period and homestead-isolation on the susceptible. *Appl. Mathematics Lett.* 107, 106442. doi: 10.1016/j.aml.2020.106442

Kerr, C. C., Stuart, R. M., Mistry, D., Abeysuriya, R. G., Rosenfeld, K., Hart, G. R., et al. (2021). Covasim: An agent-based model of COVID-19 dynamics and interventions. *PloS Comput. Biol.* 17 (7), e1009149. doi: 10.1371/journal.pcbi.1009149

Keskinocak, P., Oruc, B. E., Baxter, A., Asplund, J., and Serban, N. (2020). The impact of social distancing on COVID19 spread: State of Georgia case study. *PloS One* 15 (10), e0239798. doi: 10.1371/journal.pone.0239798

Koo, J. R., Cook, A. R., Park, M., Sun, Y., Sun, H., Lim, J. T., et al. (2020). Interventions to mitigate early spread of SARS-CoV-2 in Singapore: a modelling study. *Lancet Infect. Dis.* 20, 678–688. doi: 10.1016/S1473-3099(20)30162-6

Kuzdeuov, A., Baimukashev, D., Karabay, A., Ibragimov, B., Mirzakhmetov, A., Nurpeiissov, M., et al. (2020). A network-based stochastic epidemic simulator: controlling COVID-19 with region-specific policies. *IEEE J. Biomed. Health Inf.* 24, 2743–2754. doi: 10.1109/JBHI.6221020

Liu, X. X., Fong, S. J., Dey, N., González Crespo, R., and Herrera-Viedna, E. (2021). A new SEAIRD pandemic prediction model with clinical and epidemiological data analysis on COVID-19 outbreak. *Appl. Intell.* 51, 4162–4198. doi: 10.1007/s10489-020-01938-3

Maier, B. F., and Brockmann, D. (2020). Effective containment explains subexponential growth in recent confirmed COVID-19 cases in China. *Science* 368, 742–746. doi: 10.1126/science.abb4557

Marcel, S., Christian, A. L., Richard, N., Silvia, S., Emma, H., Jacques, F., et al. (2020). COVID-19 epidemic in Switzerland: on the importance of testing, contact tracing and isolation. *Swiss Med. Wkly* 150, w202205.

Perez, L., and Dragicevic, S. (2009). An agent-based approach for modeling dynamics of contagious disease spread. *Int. J. Health Geographics* 8, 50. doi: 10.1186/1476-072X-8-50

Perra, N., and Gonçalves, B. (2015). *Modeling and predicting human infectious diseases[M]//Social phenomena: From data analysis to models*. Cham: Springer International Publishing, 59–83.

Rajagopal, K., Hasanzadeh, N., Parastesh, F., Hamarash, I. I., Jafari, S., and Hussain, I. (2020). A fractional-order model for the novel coronavirus (COVID-19) outbreak. *Nonlinear Dynamics* 101, 711–718. doi: 10.1007/s11071-020-05757-6

Schlosser, F., Maier, B. F., Jack, O., Hinrichs, D., Zachariae, A., and Brockmann, D. (2020). COVID-19 lockdown induces disease-mitigating structural changes in mobility networks. *Proc. Natl. Acad. Sci. U. S. A.* 117, 32883–32890. doi: 10.1073/pnas.2012326117

Singh, R., Liu, F., and Shroff, N. (2020). A partially observable MDP approach for sequential testing for infectious diseases such as COVID-19. *arXiv preprint arXiv:2007.13023, 2020.*

Tatapudi, H., Das, R., and Das, T. K. (2021). Impact of vaccine prioritization strategies on mitigating COVID-19: an agent-based simulation study using an urban region in the United States. *BMC Med. Res. Method.* 21, 1–14. doi: 10.1186/s12874-021-01458-9

Truszkowska, A., Behring, B., Hasanyan, J., Zino, L., Butail, S., Caroppo, E., et al. (2021). High-resolution agent-based modeling of COVID-19 spreading in a small town. *Advanced Theory Simulations* 4 (3), 2000277. doi: 10.1002/adts.202000277

Unwin, H. J. T., Mishra, S., Bradley, V. C., Gandy, A., Mellan, T. A., Coupland, H., et al. (2020). State-level tracking of COVID-19 in the United States. *Nat. Commun.* 11 (1), 6189. doi: 10.1038/s41467-020-19652-6

Verity, R., Okell, L. C., and Dorigatti, I. (2020). Estimates of the severity of coronavirus disease 2019: a model-based analysis (vol 20, pg 669, 2020). *Lancet Infect. Dis.* 20, E116.

Vespignani, A., Tian, H., Dye, C., Lloyd-Smith, J. O., Eggo, R. M., Shrestha, M., et al. (2020). Modelling COVID-19. *Nat. Rev. Phys.* 2, 279–281. doi: 10.1038/s42254-020-0178-4

Wijesekara, P. A. D. S. N., and Wang, Y.-K. (2022). A mathematical epidemiological model (SEQIJRDS) to recommend public health interventions related to COVID-19 in Sri Lanka. *COVID* 2, 793–826. doi: 10.3390/covid2060059

Zhou, S., Zhou, S., Zheng, Z., Lu, J., and Song, T. (2022). Risk assessment for precise intervention of COVID-19 epidemic based on available big data and spatio-temporal simulation method: Empirical evidence from different public places in Guangzhou, China. *Appl. Geogr.* 143, 102702. doi: 10.1016/j.apgeog.2022.102702

frontiers | Frontiers in Public Health

TYPE Original Research
PUBLISHED 02 June 2025
DOI 10.3389/fpubh.2025.1521658

OPEN ACCESS

EDITED BY
Faris Lami,
University of Baghdad, Iraq

REVIEWED BY
Gamze Kalin Unuvar,
Erciyes University, Türkiye
Dmitry Bulaev,
Luxembourg Institute of Health, Luxembourg

*CORRESPONDENCE
Bingwei Chen
✉ drchenbw@126.com
Jinshui Xu
✉ 353112354@qq.com

RECEIVED 02 November 2024
ACCEPTED 19 May 2025
PUBLISHED 02 June 2025

CITATION
Fu M, Chen H, Qian Y, Zhang Y, Guo H, Shen Y, Xu B, Han W, Zhou H, Xu J and Chen B (2025) Analysis of COVID-19 reinfection and its influencing factors among primary healthcare workers in Jiangsu Province: a study based on the omicron variant epidemic.
Front. Public Health 13:1521658.
doi: 10.3389/fpubh.2025.1521658

Analysis of COVID-19 reinfection and its influencing factors among primary healthcare workers in Jiangsu Province: a study based on the omicron variant epidemic

Mingwang Fu[1], Hualing Chen[1], Yongkang Qian[1], Yongjie Zhang[2], Haijian Guo[2], Ya Shen[2], Biyun Xu[3], Wantong Han[1], Haoran Zhou[1], Jinshui Xu[2]* and Bingwei Chen[1,4]*

[1]Department of Epidemiology and Biostatistics, School of Public Health, Southeast University, Nanjing, China, [2]Jiangsu Provincial Center for Disease Control and Prevention, Nanjing, China, [3]Medical Statistics and Analysis Center, Nanjing Drum Tower Hospital, Nanjing University Medical School, Nanjing, China, [4]Key Laboratory of Environmental Medicine Engineering, Ministry of Education, School of Public Health, Southeast University, Nanjing, China

Objectives: Since the global outbreak of SARS-CoV-2 in 2019, COVID-19 reinfection has become an increasing concern, particularly during the spread of the Omicron variant. Despite numerous international studies on COVID-19 reinfection, research focusing on healthcare workers, particularly those in primary care settings in mainland China, remains limited. This study aims to evaluate COVID-19 reinfection rates among primary healthcare workers (PHWs) in Jiangsu Province and to explore potential risk factors contributing to reinfection.

Methods: This study utilized a combination of online questionnaires and on-site surveys to conduct two waves of investigation targeting PHWs after epidemic control policy adjustment in Jiangsu Province. Differences between the infection at the baseline visit and re-infection at the follow-up visit were analyzed, and multivariate logistic regression was used to assess the factors influencing reinfection.

Results: A total of 5,541 PHWs were included in the study. At the baseline visit, the initial infection rate was 85.85% [95% confidence interval (CI): 84.93–86.77%], and the self-reported reinfection rate was 40.05% (95% CI: 38.65–41.44%). After adjustment, the reinfection rate was 29.41% (95% CI: 28.12–30.71%). The median reinfection interval between the two infections was 146 days (Interquartile range: 129–164 days). Logistic regression model revealed that female sex [odds ratio (OR) = 1.376, 95% CI: 1.190–1.592], history of fever clinic work (OR = 1.179, 95% CI: 1.045–1.330), working over 8 h per day (OR = 1.178, 95% CI: 1.040–1.336), being a nurse (OR = 1.201, 95% CI: 1.029–1.402), and a "less meat, more vegetables" diet (OR = 1.206, 95% CI: 1.020–1.426) were significant risk factors for reinfection. Additionally, regular physical exercise was found to be a protective factor (OR = 0.861, 95% CI: 0.754–0.983).

Conclusion: COVID-19 reinfection rates were relatively high among PHWs in Jiangsu Province, particularly among women, nurses, those with fever clinic experience and working over 8 h per day. This study offers valuable insights for the prevention of COVID-19 reinfection and the development of protection strategies for PHWs. It is recommended that more targeted protective measures

be implemented for high-risk groups, including appropriate work arrangements, regular health monitoring, and the promotion of healthy lifestyle habits.

KEYWORDS

COVID-19, COVID-19 reinfection, SARS-CoV-2, primary healthcare workers, omicron variant

1 Introduction

Since December 2019, SARS-CoV-2 has caused widespread and sustained global transmission. As of the seven days leading up to 15 September 2024, more than 776 million COVID-19 cases have been reported globally, with over 7.06 million deaths, according to estimates from the World Health Organization (1). However, the actual number of infections and deaths is likely much higher than reported (2). With the continuous mutation of SARS-CoV-2, the immune evasion capabilities of the virus have significantly increased, while human immunity wanes over time (3). This has resulted in frequent reports of reinfections, even multiple infections (4–8). However, research on reinfection among healthcare workers in mainland China, particularly those in primary care settings, remains relatively limited.

Since its first detection in November 2021, the Omicron variant has demonstrated a high degree of immune evasion. By 2022, Omicron had become the dominant variant in many countries worldwide (9). Numerous studies have shown that Omicron has a higher transmission rate and greater capacity to cause reinfections, with its reinfection rate surpassing that of earlier variants (10–12). Although Omicron appears to cause milder clinical manifestations compared to earlier variants, its significantly higher re-infection rate presents new challenges for public health control efforts (13, 14).

Unlike many other regions, mainland China successfully avoided large-scale nationwide outbreaks during the early stages of the pandemic through stringent control measures. However, following the adjustment of COVID-19 control policies to "normalized management" in December 2022, China experienced a surge in COVID-19 cases, reaching its first peak by the end of that month (15). Between September 26, 2022, and July 31, 2023, all 80,531 reported domestic COVID-19 cases in mainland China were caused by the Omicron variant (16). Due to their close contact with COVID-19 patients, primary healthcare workers (PHWs) faced a significantly higher risk of infection compared to the general population (17). Studies also indicate that repeated infections may result in more severe symptoms, with the risk of severe outcomes potentially increasing with each successive infection. In the context of ongoing SARS-CoV-2 mutations and adjustments to pandemic control policies, it is crucial to track infection and reinfection risks among healthcare workers. Effective preventive measures are needed to mitigate the risk of reinfection among this vulnerable population (18, 19).

This study investigates the infection and reinfection patterns among PHWs in Jiangsu Province during two distinct infection peaks. It aims to assess the characteristics and differences between the infection at baseline visit and re-infection at follow-up visit, and seeks to identify factors that may increase the risk of reinfection.

2 Materials and methods

2.1 Study design

This study employed a combination of online questionnaires and on-site surveys to conduct two waves of investigation among PHWs in Jiangsu Province. The first wave of the survey, conducted from January 17 to February 2, 2023, involved 34,090 individuals and took place approximately 6 weeks after the adjustment of COVID-19 prevention policies. The second wave of on-site survey, conducted from July 4 to July 20, 2023, targeted 5,754 PHWs from five counties included in the first wave. Professional staff collected data on infections occurring between April 1, 2023, and the survey date. All data were collected through the Questionnaire Star platform.[1]

The study protocol was approved by the Ethics Committee of the Jiangsu Provincial Center for Disease Control and Prevention (JSJK2023-B010-01). All participants voluntarily participated in the study and provided informed consent before completing the questionnaire.

2.2 Definitions

Some variables used in this study were defined as follows:

Individuals who self-reported infection: Defined as those meeting any of the following criteria: (1) positive nucleic acid test for SARS-CoV-2; (2) positive antigen test; (3) both nucleic acid and antigen tests positive; (4) exhibiting COVID-19-related symptoms without undergoing nucleic acid or antigen testing.

Uninfected individuals: Defined as those meeting any of the following criteria: (1) negative nucleic acid and/or antigen test; (2) the absence of COVID-19-related symptoms and no nucleic acid or antigen testing performed.

Individuals who self-reported an infection at baseline visit: Defined as those self-reported being infected with SARS-CoV-2 during the first wave of the survey.

Individuals who self-reported reinfection: Defined as those self-reported being infected during both waves of the survey.

Non-reinfected individuals: Defined as those infected during the first survey period but not confirmed to have been infected during the second survey period.

Abbreviations: COVID-19, coronavirus disease 2019; SARS-CoV-2, severe acute respiratory syndrome coronavirus 2; PHWs, primary healthcare workers; RIs, reinfection intervals; CI, confidence interval; HCWs, healthcare workers; BMI, body mass index; OR, odds ratio; IQR, Interquartile range.

1 https://www.wjx.cn/

Reinfection interval (RI): The time interval between the self-reported infection at baseline visit and self-reported re-infection at the follow-up visit.

Body Mass Index (BMI): BMI was calculated by dividing weight (kg) by the square of height (m^2). According to classification standards (20), BMI was categorized as follows: underweight (<18.5 kg/m^2), normal weight (18.5–23.9 kg/m^2), overweight (24.0–27.9 kg/m^2), and obesity (≥28.0 kg/m^2).

2.3 Survey questionnaire

The questionnaire used in this study was adapted from the second-round COVID-19 pneumonia questionnaire issued by the Chinese Center for Disease Control and Prevention and the Peking Union Medical College, and modified with reference to the "Diagnosis and Treatment Protocol for COVID-19 (Trial Version 10)" (21). The information collected by the questionnaire included: (1) Basic information: Demographic characteristics, medical history, occupation, lifestyle behaviors, and habits; (2) Infection-related information: Infection dates, typical symptoms (e.g., fever, muscle aches, cough, sore throat, nasal congestion, runny nose), hospitalization status, and any newly diagnosed diseases following infection; (3) Vaccination status: Number of vaccine doses and vaccine type; (4) Work burden: Weekly working hours and whether the participant had worked in fever clinics.

2.4 Statistical analysis

The sample size calculations resulted in $n = 4{,}489$, based on a projected long COVID prevalence of 8.89% and a two-sided 95% Clopper-Pearson confidence interval (CI) with a margin of error of 0.01778 (22). Considering that the reinfection rate exceeds the prevalence of long COVID, this sample size is deemed sufficient.

Continuous variables were expressed as means (standard deviation, SD), while categorical variables were summarized as frequencies and percentages. The 95% CI for the reinfection rate was calculated using the Wald method. For some individuals who exhibited COVID-19 symptoms but lacked nucleic acid tests or antigen detection, the adjusted reinfection rate was estimated using a weighted approach based on data from China's National Influenza Surveillance System (16).

Statistical differences between groups were assessed by two-sample t-tests for continuous variables. For categorical variables, Pearson's chi-square test was applied when the expected frequency in each cell was at least 5; otherwise, Fisher's exact test was used. For the comparison of 14 symptom rates, the Bonferroni-Hochberg method was used for multiple comparisons. Both univariate and multivariate logistic regression analyses were conducted to identify factors associated with self-reported reinfection among PHWs. All variables were included in a multivariate logistic regression analysis using a stepwise selection method, with an entry criterion of $p < 0.05$ and a removal criterion of $p > 0.10$. Odds ratio (OR) and 95%CI quantified the risk associated with reinfection. A two-sided p-value < 0.05 was considered statistically significant.

Considering that some self-reported infected individuals had not undergone virus testing, resulting in potential ambiguity in the definitions, a sensitivity analysis was conducted. Nucleic acid or antigen-positive individuals were regarded as confirmed cases, while nucleic acid/antigen-negative or untested asymptomatic individuals were categorized as uninfected. Logistic regression was performed again using these groups.

All statistical analyses were performed using R software (version 4.3.3).

3 Results

3.1 Participants and self-reported reinfection rates

In the first wave of survey, a total of 34,090 questionnaires were collected between January 17 and February 2, 2023 in Jiangsu Province, the overall infection rate among PHWs was 81.05% (95% CI: 80.61–81.48%) from December 2022 to January 2023 (23). From these, five counties/districts were selected for second wave of on-site survey: Ganyu District in Lianyungang City, Funing County, Yandu District in Yancheng City, and the county-level cities of Kunshan and Changshu in Suzhou.

The second wave of the on-site survey included 5,754 PHWs across five counties. After data verification, questionnaires with inconsistent or illogical responses were excluded, resulting in the removal of 213 questionnaires. A total of 5,541 valid questionnaires remained for analysis.

Among the 5,541 participants included in this study, 67.30% were female, with a mean age of 39.80 years (SD = 10.80). Of the 4,757 participants who self-reported an infection at baseline visit, 1,905 were self-reported reinfected, and 2,852 did not experience reinfection. The self-reported infection at baseline visit rate was 85.85% (95% CI: 84.93–86.77%), and the self-reported reinfection rate was 40.05% (95% CI: 38.65–41.44%). Among those reporting an infection at baseline visit, 6.71% exhibited COVID-19-related symptoms without having undergone nucleic acid or antigen testing. In the second wave survey, 1,253 participants had a positive nucleic acid test, positive antigen test, or both, while 652 participants (34.23%) had COVID-19-related symptoms without testing. Based on the positivity rate among influenza-like illness patients from national sentinel hospitals, we assumed that a proportion of these 652 symptomatic participants were false positives. By adding the confirmed positives to the numerator and incorporating the estimated number of false positives into the denominator, we recalculated the positivity rate, yielding an adjusted reinfection rate of 29.41% (95% CI: 28.12–30.71%).

3.2 Analysis of infection at the baseline visit and follow-up visit

3.2.1 Infection dates and time intervals

The distribution of infection dates for both self-reported infections at baseline visit and reinfections is illustrated using histograms (Figure 1). Infections at baseline visit were concentrated in late December 2022, while reinfections exhibited a more dispersed pattern, peaking in May 2023, followed by a gradual decline in infection numbers. Figure 2 presents reinfection intervals (RIs), the median RI was 146 days [Interquartile Range (IQR): 129–164 days],

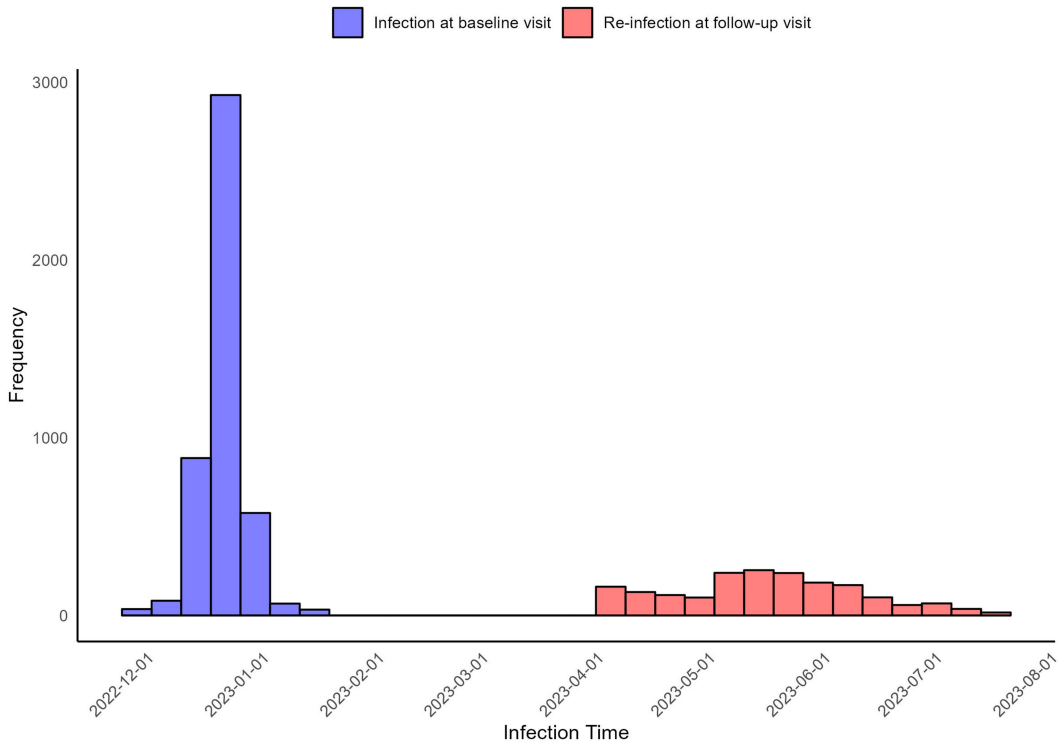

FIGURE 1
Distribution of infection dates.

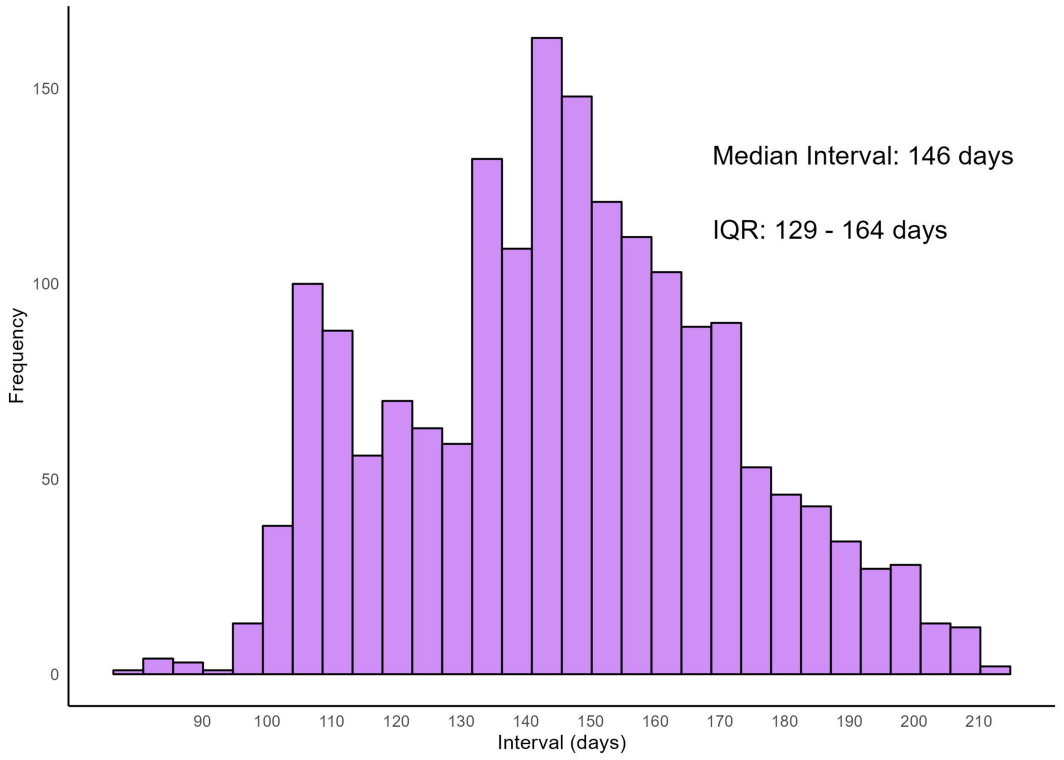

FIGURE 2
Distribution of reinfection intervals.

with the shortest and longest RIs being 77 days and 211 days, respectively.

3.2.2 Newly diagnosed diseases and symptom comparison between infection at baseline visit and re-infection at follow-up visit

As shown in Figure 3, 13.35% of participants who experienced an infection at baseline visit reported developing one or more newly diagnosed diseases afterward. The most frequently reported condition was allergic diseases, such as asthma and rhinitis, affecting 7.13% of participants. This was followed by cardiovascular disease (2.96%), lung disease (2.69%), immune system disorders (2.38%), diabetes (1.16%), mental health issues (0.42%), kidney disease (0.32%), and liver disease (0.21%).

When comparing symptom frequencies between the infection at baseline visit and re-infection at Follow-up Visit (Figure 4), the main symptoms during the infection at baseline visit were cough (87.81%), fatigue (82.83%), fever (82.38%), sore throat/dry throat (73.45%), muscle pain (72.73%), and nasal congestion/runny nose (69.77%). During the reinfection, the main symptoms included fatigue (80.37%), sore throat/dry throat (78.74%), nasal congestion/runny nose (72.60%), cough (71.23%), dizziness/headache (69.45%), and fever (67.14%). In comparison, cough, diarrhea, fatigue, fever, loss of taste/smell, muscle pain, and nausea/vomiting were significantly more frequent during the infection at baseline visit, while nasal congestion/runny nose, rash, eczema and other dermatological manifestations, and sore throat/dry throat were significantly more frequent during the reinfection. All comparisons among the symptoms were performed using chi-square tests.

3.2.3 Severity of infections

Among self-reported reinfected participants, 73.65% reported that their symptoms during the infection at baseline visit were more severe, 14.5% indicated that the severity of symptoms were similar between the two waves, and only 11.9% perceived that their symptoms were more severe during the reinfection. However, the hospitalization rate (1.10%) during reinfection was significantly higher compared to the hospitalization rate (0.48%) during the infection at baseline visit ($p < 0.05$, Chi-squared test). The ICU admission rates during the follow-up visit and at the baseline visit were 0.21 and 0.04%, respectively. The difference between the two groups was not statistically significant ($p = 0.059$, Fisher's exact test), as shown in Figure 5.

3.3 Comparison between reinfected and non-reinfected groups

3.3.1 Univariate analysis

Univariate analysis was performed to compare the baseline characteristics of 1,905 reinfected individuals and 2,852 non-reinfected individuals, as shown in Table 1. Females had a significantly higher reinfection rate (42.74%) compared to males (34.10%), indicating that females may face a higher risk of reinfection. In addition, nurses had the highest reinfection rate, followed by medical technicians and pharmacists. Regarding vaccination status, those who had received 0–1 doses of the vaccine had the highest reinfection rate (47.66%). The reinfection rate decreased as the number of vaccine doses increased, and the differences between the various dose groups were not

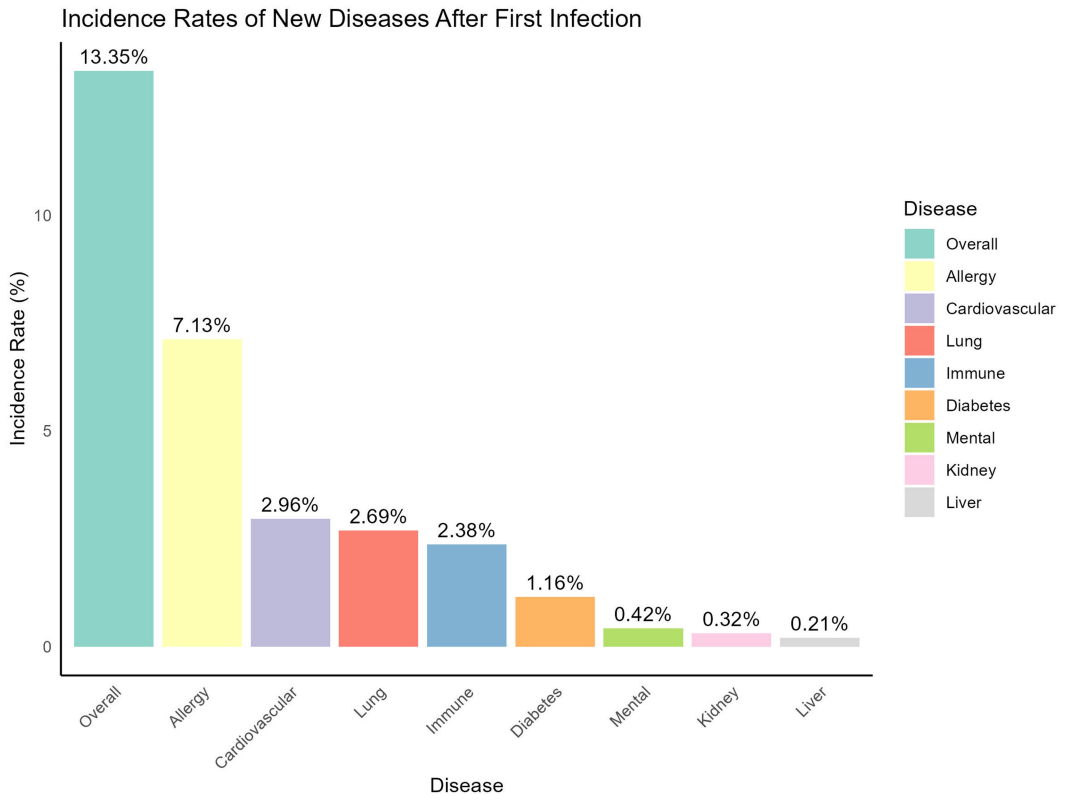

FIGURE 3
Newly diagnosed diseases after infection at baseline visit.

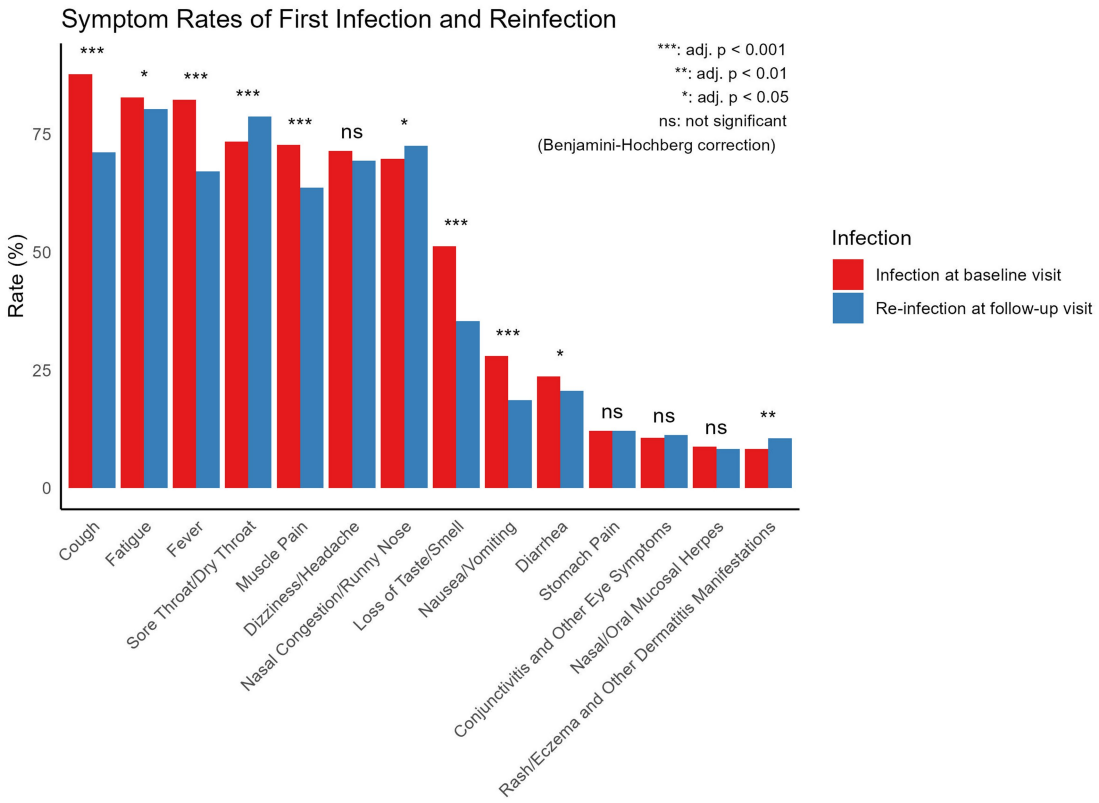

FIGURE 4
Comparison of symptom frequencies between infection at baseline visit and self-reported re-infection at follow-up visit. All symptom comparisons were performed using Chi-square tests.

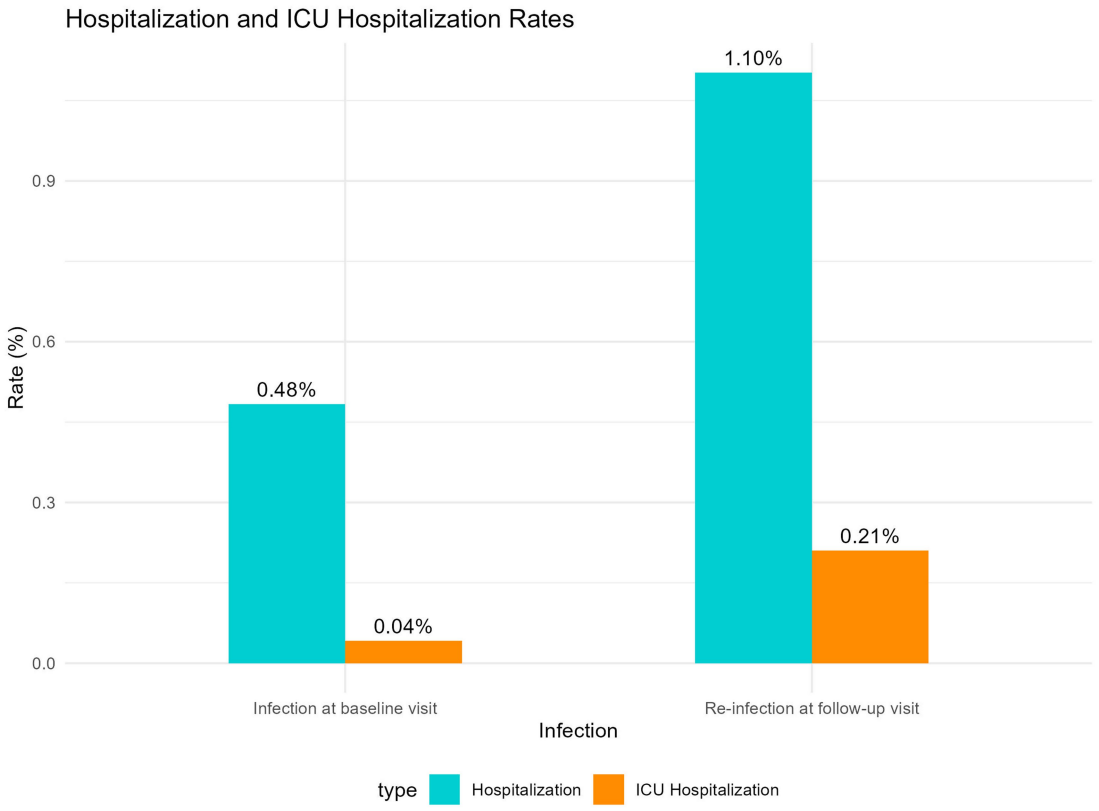

FIGURE 5
Comparison of hospitalization and ICU admission rates between infection at baseline visit and re-infection at follow-up visit.

10.3389/fpubh.2025.1521658

TABLE 1 Univariate analysis for factors associated with Self-reported reinfection.

Variables	Non-reinfected group	Reinfected group	Total	*P*-value
Age (mean ± SD)	39.71 ± 10.98	39.30 ± 10.02	39.55 ± 10.61	0.175
Gender				<0.001
Female	1,874(57.26%)	1,399(42.74%)	3,273	
Male	978(65.9%)	506(34.1%)	1,484	
BMI				0.695
Normal weight	1,468 (59.63%)	994 (40.37%)	2,462	
Obesity	348 (58.68%)	245 (41.32%)	593	
Overweight	882 (61.17%)	560 (38.83%)	1,442	
Underweight	154 (59.23%)	106 (40.77%)	260	
Smoking				0.006
No	2,576 (59.34%)	1,765 (40.66%)	4,341	
Yes	276 (66.35%)	140 (33.65%)	416	
Drinking				<0.001
No	2,358 (58.88%)	1,647 (41.12%)	4,005	
Yes	494 (65.69%)	258 (34.31%)	752	
Weekly exercise				0.004
No	746 (56.64%)	571 (43.36%)	1,317	
Yes	2,106 (61.22%)	1,334 (38.78%)	3,440	
Management				0.573
No	2,375 (59.76%)	1,599 (40.24%)	3,974	
Yes	477 (60.92%)	306 (39.08%)	783	
Daily working hours				0.122
≤8 h	1,850 (60.80%)	1,193 (39.20%)	3,043	
>8 h	1,002 (58.46%)	712 (41.54%)	1,714	
History of fever clinic				0.004
No	1,492 (61.99%)	915 (38.01%)	2,407	
Yes	1,360 (57.87%)	990 (42.13%)	2,350	
Diet structure				0.049
Balanced	2,100 (60.90%)	1,348 (39.10%)	3,448	
Less meat, more veg.	381 (55.95%)	300 (44.05%)	681	
More meat, less veg.	371 (59.08%)	257 (40.92%)	628	
Diabetic				0.380
No	2,778(59.84%)	1,864(40.16%)	4,642	
Yes	74(64.35%)	41(35.65%)	115	
History of cardiovascular disease				0.043
No	2,645(59.56%)	1,796(40.44%)	4,441	
Yes	207(65.51%)	109(34.49%)	316	
Vaccine doses				0.206
0 ~ 1	56(52.34%)	51(47.66%)	107	
2 ~ 3	1,520(60.61%)	988(39.39%)	2,508	
≥4	1,276(59.57%)	866(40.43%)	2,142	
Position				<0.001
Doctor	1,318(62.23%)	800(37.77%)	2,118	
Medical technician	333(59.57%)	226(40.43%)	559	
Nurse	733(54.74%)	606(45.26%)	1,339	
Other position	271(65.46%)	143(34.54%)	414	
Pharmacist	197(60.24%)	130(39.76%)	327	

statistically significant. Chi-square test was used in all univariate analyses, statistically significant differences were observed among the variables gender, smoking, drinking, weekly exercise, history of fever clinic, diet structure and position.

3.3.2 Multivariate logistic regression model

The final model (Table 2) indicated that female gender (OR = 1.376, 95% CI: 1.190–1.592), history of fever clinic work (OR = 1.179, 95% CI: 1.045–1.330), working over 8 h per day (OR = 1.178, 95% CI: 1.040–1.336), and a "less meat, more vegetables" diet (OR = 1.206, 95% CI: 1.020–1.426), along with being a nurse (OR = 1.201, 95% CI: 1.029–1.402), were significant risk factors for reinfection. Regular weekly exercise was identified as a protective factor (OR = 0.861, 95% CI: 0.754–0.983).

3.3.3 Sensitivity analysis

The sensitivity analysis results (Table 3) were highly consistent with the main analysis, with female gender (OR = 1.413, 95% CI: 1.190–1.679), a "less meat, more vegetables" diet (OR = 1.256, 95% CI: 1.031–1.529), fever clinic work (OR = 1.255, 95% CI: 1.089–1.447), and being a nurse (OR = 1.278, 95% CI: 1.067–1.530) remaining significant risk factors for reinfection. Medical technician (OR = 1.319, 95% CI:

TABLE 2 Factors associated with Self-reported reinfection in univariate and multivariate logistic regression.

Variable	Univariate analysis		Multivariate analysis	
	OR (95% CI)	*P*-value	OR (95% CI)	*P*-value
Age	0.996 (0.991–1.002)	0.182		
Gender				
Male	1.000		1.000	
Female	1.443 (1.270–1.639)	<0.001	1.376 (1.190–1.592)	<0.001
BMI				
Normal weight	1.000			
Overweight	0.938 (0.821–1.071)	0.343		
Obesity	1.04 (0.867–1.248)	0.675		
Under weight	1.017 (0.784–1.319)	0.902		
Weekly exercise	0.828 (0.728–0.941)	0.004	0.861 (0.754–0.983)	0.027
History of fever clinic work	1.187 (1.057–1.333)	0.004	1.179 (1.045–1.330)	0.007
Daily working hours				
≤8 h	1.000		1.000	
>8 h	1.102 (0.977–1.243)	0.115	1.178 (1.040–1.336)	0.010
Diet structure				
Balanced			1.000	
More meat, less veg.	1.079 (0.908–1.283)	0.388	1.09 (0.914–1.301)	0.337
Less meat, more veg.	1.227 (1.039–1.448)	0.016	1.206 (1.020–1.426)	0.028
Position				
Doctor	1.000		1.000	
Medical technician	1.118 (0.924–1.353)	0.25	1.149 (0.946–1.396)	0.160
Nurse	1.362 (1.185–1.565)	<0.001	1.201 (1.029–1.402)	0.021
Pharmacist	1.087 (0.857–1.380)	0.492	1.041 (0.816–1.328)	0.749
Other position	0.869 (0.697–1.084)	0.214	0.892 (0.711–1.118)	0.322
Vaccine doses				
0 ~ 1	1.000		1.000	
2 ~ 3	0.714 (0.484–1.052)	0.088	0.718 (0.486–1.062)	0.097
≥4	0.745 (0.505–1.100)	0.138	0.795 (0.537–1.178)	0.253
Management	0.953 (0.814–1.115)	0.546		
Smoking	0.74 (0.599–0.915)	0.005		
Drinking	0.748 (0.635–0.880)	<0.001		
Cardiovascular disease	0.775 (0.610–0.985)	0.038		
Diabetic	0.826 (0.561–1.215)	0.331		

OR, odds ratio; CI, confidence interval; Veg., vegetables.

10.3389/fpubh.2025.1521658

TABLE 3 Sensitivity analysis logistic regression results.

Variable	Univariate analysis		Multivariate analysis	
	OR (95% CI)	*P*-value	OR (95% CI)	*P*-value
Age	0.998 (0.992–1.004)	0.542		
Gender				
Male	1.000		1.000	
Female	1.478 (1.269–1.722)	<0.001	1.413 (1.190–1.679)	<0.001
BMI				
Normal weight	1.000			
Overweight	0.984 (0.842–1.151)	0.845		
Obesity	1.009 (0.814–1.252)	0.932		
Under weight	1.031 (0.758–1.401)	0.847		
Weekly exercise	0.883 (0.758–1.029)	0.110		
History of fever clinic work	1.241 (1.082–1.423)	0.002	1.255 (1.089–1.447)	0.002
Daily working hours				
≤8 h	1.000		1.000	
>8 h	1.072 (0.930–1.236)	0.338	1.144 (0.988–1.326)	0.073
Diet structure				
Balanced			1.000	
More meat, less veg.	1.085 (0.886–1.329)	0.431	1.120 (0.912–1.375)	0.279
Less meat, more veg.	1.276 (1.050–1.550)	0.014	1.256 (1.031–1.529)	0.023
Position				
Doctor	1.000		1.000	
Medical technician	1.259 (1.009–1.573)	0.042	1.319 (1.051–1.657)	0.017
Nurse	1.444 (1.228–1.698)	<0.001	1.278 (1.067–1.530)	0.008
Pharmacist	1.03 (0.774–1.371)	0.838	1.004 (0.750–1.345)	0.977
Other position	0.854 (0.653–1.116)	0.248	0.891 (0.678–1.172)	0.411
Vaccine doses				
0 ~ 1	1.000		1.000	
2 ~ 3	0.632 (0.410–0.976)	0.038	0.630 (0.406–0.977)	0.039
≥4	0.693 (0.449–1.070)	0.098	0.727 (0.469–1.129)	0.156
Management	0.92 (0.764–1.108)	0.38		
Smoking	0.691 (0.533–0.897)	0.005		
Drinking	0.738 (0.607–0.898)	0.002		
Cardiovascular disease	0.792 (0.597–1.051)	0.106		
Diabetic	1.048 (0.665–1.652)	0.840		

OR, odds ratio; CI, confidence interval; Veg., vegetables.

1.051–1.657) was identified as a risk factor only in the sensitivity analysis. Vaccine doses of 2 ~ 3 was identified as a protective factor (OR = 0.630, 95% CI: 0.406–0.977). These findings demonstrate that regardless of the infection definition used, certain risk factors consistently contribute to reinfection, further confirming the robustness of the results.

4 Discussion

In this study, we analyzed the reinfection characteristics and potential risk factors among PHWs during the Omicron variant wave. Female PHWs, nurses, and individuals with a history of fever clinic work were found to have a significantly higher risk of re-infection. Additionally, working more than 8 h per day and having a "less meat, more vegetables" diet were identified as risk factors, while regular weekly exercise was a protective factor. Vaccine doses of 2 ~ 3 was identified as a protective factor against reinfection in the sensitivity analysis. These findings highlight important occupational and behavioral factors associated with COVID-19 reinfection, underscoring the need for targeted protective measures for high-risk healthcare workers.

The results indicate that after adjustments to epidemic control policies, the two major waves of Omicron infections in Jiangsu

occurred at the end of 2022 and mid-2023, with a median reinfection interval of 146 days (IQR: 129–164 days). Moreover, first-time COVID-19 infections may be associated with the onset of various diseases, particularly allergic conditions (e.g., asthma, rhinitis), with 7.13% of patients reporting new allergic conditions after infection. Although these comorbidities may not be directly caused by COVID-19—such as the development of diabetes potentially due to natural aging—the higher rates of allergies, immune system, pulmonary, and cardiovascular conditions suggest that COVID-19 could have a broader impact on these systems, providing a direction for future research into long-COVID effects (24, 25). The study also observed that primary infections tended to present more systemic symptoms (e.g., fever, cough, fatigue), while reinfections predominantly involved upper respiratory symptoms (e.g., sore throat, nasal congestion). This pattern may reflect the immune system's response to reinfection. During the first infection, the immune system is in its initial response phase, resulting in a stronger systemic reaction.

In terms of reinfection rates, the study found that the primary infection rate among frontline healthcare workers in Jiangsu was 85.85% (95% CI: 84.93–86.77%), and the reinfection rate was 40.05% (95% CI: 38.65–41.44%). After adjusting for sentinel hospital influenza-like illness SARS-CoV-2 positivity rates, the recalculated reinfection rate was 29.41% (95% CI: 28.12–30.71%). Flacco et al.'s meta-analysis from June 2022 found that reinfection rates before the Omicron wave were 0.97%, rising to 3.31% in the first 3 months of Omicron's spread (26). Similarly, research by Fonseca et al. in Brazil found a reinfection rate of up to 8%, which increased over time (27). Wei et al., utilizing data from the UK Office for National Statistics (ONS) COVID-19 Infection Survey, reported that reinfection rates rose from 10–11% to 14–16% (28). In China, a retrospective study by Zhang et al. in Shanxi Province found that the reinfection rate could reach as high as 25.1% (29). Additionally, research by Cai et al. in Guangdong Province indicated a reinfection rate of 18.4% following an initial Omicron infection, with an overall reinfection rate of 28.3% (30). The reinfection rates observed in these studies are consistent with our findings on the Chinese population. The relatively high reinfection rates in our study may be attributed to concentrated infection clusters during the adjustment of national control policies, potentially resulting in a higher reinfection rate compared to other countries.

The severity of reinfection remains a contentious issue, with no clear consensus in the literature (31). Some studies suggest that reinfection leads to milder symptoms, with lower hospitalization and mortality rates (32). However, other studies report an increased risk of hospitalization and death during reinfection, with cumulative risks and burdens rising with each subsequent infection (33). Nguyen et al. found no significant difference in symptom severity between primary and secondary infections (19). In our study, most participants perceived their reinfection symptoms as milder than their initial infection, while the hospitalization and ICU admission rates for reinfection were significantly higher. This discrepancy may be related to strained healthcare resources during the first wave of infections, such as shortages of hospital bed, which led to lower hospitalization rates during primary infections. Hadley et al. found a statistically significant association between the severity of the first and subsequent infections, with individuals experiencing severe first infections showing a higher risk of hospitalization and death upon reinfection (34). These findings underscore the importance of studying the severity of COVID-19 reinfection, which is crucial for assessing disease burden and shaping future public health policies.

The multivariate logistic regression analysis indicated that being female, having a history of working in fever clinics, and being a nurse were significant risk factors for reinfection. The higher reinfection risks for females and nurses might be related to their higher occupational exposure frequency, particularly nurses who often work in high-risk environments on the frontlines of care. Furthermore, experience working in fever clinics increases exposure risks, highlighting the need for strengthened occupational protections for healthcare workers, particularly for high-risk groups. Only in the sensitivity analysis, Vaccine doses of 2~3 was identified as a protective factor against reinfection. Although the OR values for both 2~3 and ≥4 doses were less than 1.000, most of the *p*-values were greater than 0.05. This may be due to the small number of individuals with Vaccine doses of 0~1, as only 2.25% of PHWs received one or fewer doses. This may also suggest that maintaining high immunity levels through vaccine boosters is critical in the context of ongoing SARS-CoV-2 mutations. Future vaccination strategies should consider the waning efficacy of vaccines over time, and regular booster doses may be an effective way to reduce reinfection risks (35).

Increasing the supply of personal protective equipment, rationalizing work hours, implementing regular health monitoring, and prioritizing vaccination for these groups could effectively reduce infection risks.

However, this study has several limitations. First, data collection involved a combination of online and offline methods, with online questionnaires used during the first wave and on-site during the second. This discrepancy may have led to inconsistencies in the accuracy of responses. Second, due to the extensive scale of the outbreak, it was not feasible to test all participants for SARS-CoV-2 using nucleic acid or antigen tests. Consequently, individuals who were not tested but exhibited symptoms were classified as infected, which may have overestimated infection and reinfection rates. To mitigate these limitations, we adjusted the reinfection rate using data from sentinel hospitals, and conducted a sensitivity analysis to validate the robustness of the results. However, some residual errors may still remain.

In conclusion, this study identified higher reinfection risks for female healthcare workers, nurses, "less meat, more vegetables" diet and those with fever clinic experience. It also highlighted significant differences in the symptoms and severity of primary and secondary infections. These findings provide important insights into the risk factors for reinfection and strategies for its prevention.

5 Conclusion

This study examined the characteristics of COVID-19 primary infections and reinfections among PHWs during the Omicron wave in Jiangsu Province and identified potential risk factors for reinfection. The results showed a primary infection rate of 85.85% and a reinfection rate of 40.05%, with an adjusted reinfection rate of 29.41%. The study also highlighted differences in symptomatology and severity between primary infections and reinfections. While primary infections were more systemic in nature, reinfections predominantly involved upper respiratory symptoms. Although most participants perceived their reinfection symptoms as milder, the hospitalization and ICU admission rates were significantly higher during reinfection

compared to primary infections, possibly due to healthcare resource constraints during the first infection wave.

Female healthcare workers, nurses, and individuals with a history of working in fever clinics were found to have a significantly higher risk of reinfection. Additionally, working more than 8 h per day and following a "less meat, more vegetables" diet were associated with increased reinfection risk, while regular weekly exercise was identified as a protective factor. These findings underscore the need for targeted protective measures for high-risk healthcare workers, particularly females, nurses, and those with fever clinic experience. Enhancing personal protective equipment supplies, rationalizing work hours, and implementing regular health monitoring for these high-risk groups may effectively reduce the risk of reinfection. By improving workplace protections and health measures for healthcare workers, the risk of reinfection can be mitigated, further safeguarding this critical population.

Data availability statement

The raw data supporting the conclusions of this article will be made available by the authors, without undue reservation.

Ethics statement

The studies involving humans were approved by Ethics Committee of Jiangsu Provincial Center for Disease Prevention and Control. The studies were conducted in accordance with the local legislation and institutional requirements. The participants provided their written informed consent to participate in this study.

Author contributions

MF: Conceptualization, Data curation, Formal analysis, Investigation, Methodology, Resources, Software, Writing – original draft, Writing – review & editing. HC: Conceptualization, Data curation, Formal analysis, Investigation, Project administration, Resources, Writing – review & editing. YQ: Conceptualization, Investigation, Methodology, Project administration, Writing – review & editing. YZ: Conceptualization, Data curation, Formal analysis, Investigation, Methodology, Writing – review & editing. HG: Conceptualization, Data curation, Formal analysis, Investigation, Methodology, Writing – review & editing. YS: Conceptualization, Formal analysis, Investigation, Project administration, Writing – review & editing. BX: Conceptualization, Formal analysis, Methodology, Writing – review & editing. WH: Conceptualization, Data curation, Methodology, Writing – review & editing. HZ: Conceptualization, Data curation, Methodology, Writing – review & editing. JX: Conceptualization, Data curation, Formal analysis, Investigation, Methodology, Writing – review & editing. BC: Conceptualization, Data curation, Formal analysis, Investigation, Methodology, Project administration, Writing – review & editing.

Funding

The author(s) declare that financial support was received for the research and/or publication of this article. This research was supported by the Health Commission of Nanjing, China (ZKX22019) and the 2022 Annual Open Project of Jiangsu Provincial Primary Health Development and General Practice Medical Education Research Center (No. 2022A02).

Conflict of interest

The authors declare that the research was conducted in the absence of any commercial or financial relationships that could be construed as a potential conflict of interest.

Generative AI statement

The authors declare that Gen AI was used in the creation of this manuscript. Generative AI, ChatGPT (GPT-4, OpenAI, https://openai.com) was used to help polish this manuscript, followed by multiple rounds of human proofreading and revision to ensure accuracy and clarity.

Publisher's note

References

1. World Health Organization. WHO COVID-19 dashboard: global case data 2024. Available online at: https://data.who.int/dashboards/covid19/cases?m49=001&n=c.

2. Wang H, Paulson KR, Pease SA, Watson S, Comfort H, Zheng P, et al. Estimating excess mortality due to the COVID-19 pandemic: a systematic analysis of COVID-19-related mortality, 2020–21. *Lancet*. (2022) 399:1513–36. doi: 10.1016/S0140-6736(21)02796-3

3. Goldberg Y, Mandel M, Bar-On YM, Bodenheimer O, Freedman LS, Ash N, et al. Protection and waning of natural and hybrid immunity to SARS-CoV-2. *N Engl J Med*. (2022) 386:2201–12. doi: 10.1056/NEJMoa2118946

4. To KK-W, Hung IF-N, Ip JD, Chu AW-H, Chan W-M, Tam AR, et al. Coronavirus disease 2019 (COVID-19) re-infection by a phylogenetically distinct severe acute respiratory syndrome coronavirus 2 strain confirmed by whole genome sequencing. *Clin Infect Dis*. (2020) 73:e2946–51. doi: 10.1093/cid/ciaa1275

5. Sabino EC, Buss LF, Carvalho MPS, Prete CA Jr, Crispim MAE, Fraiji NA, et al. Resurgence of COVID-19 in Manaus, Brazil, despite high seroprevalence. *Lancet*. (2021) 397:452–5. doi: 10.1016/S0140-6736(21)00183-5

6. Falahi S, Kenarkoohi A. COVID-19 reinfection: prolonged shedding or true reinfection? *New Microb New Infect*. (2020) 38:100812. doi: 10.1016/j.nmni.2020.100812

7. Pinto LM, Nanda V, Sunavala A, Rodriques C. Reinfection in COVID-19: a scoping review. *Med J Armed Forces India*. (2021) 77:S257–63. doi: 10.1016/j.mjafi.2021.02.010

8. Hadley E, Yoo YJ, Patel S, Zhou A, Laraway B, Wong R, et al. Insights from an N3C RECOVER EHR-based cohort study characterizing SARS-CoV-2 reinfections and long COVID. *Commun Med*. (2024) 4:129. doi: 10.1038/s43856-024-00539-2

9. Rathinasamy M, Kandhasamy S. An exploratory study on the propagation of SARS-CoV-2 variants: omicron is the most predominant variant. *J Med Virol*. (2022) 94:2414–21. doi: 10.1002/jmv.27634

10. Chen Y, Zhu W, Han X, Chen M, Li X, Huang H, et al. How does the SARS-CoV-2 reinfection rate change over time? The global evidence from systematic review and meta-analysis. *BMC Infect Dis*. (2024) 24:339. doi: 10.1186/s12879-024-09225-z

11. Guedes AR, Oliveira MS, Tavares BM, Luna-Muschi A, Lazari CS, Montal AC, et al. Reinfection rate in a cohort of healthcare workers over 2 years of the COVID-19 pandemic. *Sci Rep*. (2023) 13:712. doi: 10.1038/s41598-022-25908-6

12. Bastard J, Taisne B, Figoni J, Mailles A, Durand J, Fayad M, et al. Impact of the omicron variant on SARS-CoV-2 reinfections in France, march 2021 to February 2022. *Euro Surveill*. (2022) 27:2200247. doi: 10.2807/1560-7917.ES.2022.27.13.2200247

13. Rana R, Kant R, Huirem RS, Bohra D, Ganguly NK. Omicron variant: current insights and future directions. *Microbiol Res*. (2022) 265:127204. doi: 10.1016/j.micres.2022.127204

14. Tian D, Sun Y, Xu H, Ye Q. The emergence and epidemic characteristics of the highly mutated SARS-CoV-2 omicron variant. *J Med Virol*. (2022) 94:2376–83. doi: 10.1002/jmv.27643

15. Luo M, Gong F, Sun J, Gong Z. For COVID-19, what are the priorities of normalized prevention and control strategies? *Biosci Trends*. (2023) 17:63–7. doi: 10.5582/bst.2023.01005

16. Prevention CCfDCa. National situation of novel coronavirus infection. (2024). Available online at https://www.chinacdc.cn/jkzt/crb/zl/szkb_11803/jszl_13141/202301/t20230125_263519.html (Accessed August 20, 2024).

17. van der Plaat DA, Madan I, Coggon D, van Tongeren M, Edge R, Muiry R, et al. Risks of COVID-19 by occupation in NHS workers in England. *Occup Environ Med*. (2022) 79:176–83. doi: 10.1136/oemed-2021-107628

18. Gholami M, Fawad I, Shadan S, Rowaiee R, Ghanem H, Hassan Khamis A, et al. COVID-19 and healthcare workers: a systematic review and meta-analysis. *Int J Infect Dis*. (2021) 104:335–46. doi: 10.1016/j.ijid.2021.01.013

19. Bowe B, Xie Y, Al-Aly Z. Acute and postacute sequelae associated with SARS-CoV-2 reinfection. *Nat Med*. (2022) 28:2398–405. doi: 10.1038/s41591-022-02051-3

20. Zhou BF. Predictive values of body mass index and waist circumference for risk factors of certain related diseases in Chinese adults--study on optimal cut-off points of body mass index and waist circumference in Chinese adults. *Biomed Environ Sci*. (2002) 15:83–96.

21. Commission GOotNH. Diagnosis and treatment protocol for novel coronavirus infection (trial version 10). (2023). Available online at: https://www.chinacdc.cn/jkzt/crb/zl/szkb_11803/jszl_11815/202301/t20230107_263257.html (Accessed August 24, 2024).

22. Chen H, Qian Y, Lu B, Ma R, Miao P, Fu M, et al. Prevalence and factors influencing long COVID among primary healthcare workers after epidemic control policy adjustment in Jiangsu, China. *BMC Infect Dis*. (2024) 24:964. doi: 10.1186/s12879-024-09764-5

23. Lu B, Ma R, Xu J, Zhang Y, Guo H, Chen H, et al. Primary healthcare workers' COVID-19 infection status following implementation of adjusted epidemic prevention and control strategies: a cross-sectional study in Jiangsu, China. *Front Public Health*. (2023) 11:1297770. doi: 10.3389/fpubh.2023.1297770

24. Boufidou F, Medić S, Lampropoulou V, Siafakas N, Tsakris A, Anastassopoulou C. SARS-CoV-2 reinfections and long COVID in the post-omicron phase of the pandemic (2023) 24:12962. doi: 10.3390/ijms241612962,

25. Lippi G, Sanchis-Gomar F, Henry BM. COVID-19 and its long-term sequelae: what do we know in 2023? *Polish Arch Internal Med*. (2023) 133:16402. doi: 10.20452/pamw.16402

26. Flacco ME, Acuti MC, Baccolini V, De Vito C, Renzi E, Villari P, et al. Risk of reinfection and disease after SARS-CoV-2 primary infection: Meta-analysis. *Eur J Clin Investig*. (2022) 52:e13845. doi: 10.1111/eci.13845

27. Fonseca PLC, Malta FSV, Braga-Paz I, do Prado Silva J, de Souza CSA, de Aguiar RS, et al. SARS-CoV-2 reinfection rate before and after VOC omicron emergence: a retrospective study in Brazil. *Braz J Microbiol*. (2024) 55:3959–64. doi: 10.1007/s42770-024-01467-y

28. Wei J, Stoesser N, Matthews PC, Khera T, Gethings O, Diamond I, et al. Risk of SARS-CoV-2 reinfection during multiple omicron variant waves in the UK general population. *Nat Commun*. (2024) 15:1008. doi: 10.1038/s41467-024-44973-1

29. Zhang M, Cao L, Zhang L, Li X, Chen S, Zhang Y. SARS-CoV-2 reinfection with omicron variant in Shaanxi Province, China: December 2022 to February 2023. *BMC Public Health*. (2024) 24:496. doi: 10.1186/s12889-024-17902-6

30. Chunsheng Cai YL, Hu T, Liang R, Wang K, Guo C, Li Y, et al. The associated factors of SARS-CoV-2 reinfection by omicron variant—Guangdong Province, China, December 2022 to January 2023. *China CDC Weekly*. (2023) 5:391–6. doi: 10.46234/ccdcw2023.075

31. Chen Y-H, Lee C-Y, Cheng H-Y, Chen C-M, Cheuh Y-N, Lee C-L, et al. Risk factors and mortality of SARS-CoV-2 reinfection during the omicron era in Taiwan: a nationwide population-based cohort study. *J Microbiol Immunol Infect*. (2024) 57:30–7. doi: 10.1016/j.jmii.2023.10.013

32. Medić S, Anastassopoulou C, Lozanov-Crvenković Z, Vuković V, Dragnić N, Petrović V, et al. Risk and severity of SARS-CoV-2 reinfections during 2020–2022 in Vojvodina, Serbia: a population-level observational study (2022) 20:100453. doi: 10.1016/j.lanepe.2022.100453,

33. Mensah AA, Lacy J, Stowe J, Seghezzo G, Sachdeva R, Simmons R, et al. Disease severity during SARS-COV-2 reinfection: a nationwide study. *J Infect*. (2022) 84:542–50. doi: 10.1016/j.jinf.2022.01.012

34. Nguyen NN, Houhamdi L, Hoang VT, Delerce J, Delorme L, Colson P, et al. SARS-CoV-2 reinfection and COVID-19 severity. *Emerg Microb Infect*. (2022) 11:894–901. doi: 10.1080/22221751.2022.2052358

35. Andrews N, Tessier E, Stowe J, Gower C, Kirsebom F, Simmons R, et al. Duration of protection against mild and severe disease by Covid-19 vaccines. *N Engl J Med*. (2022) 386:340–50. doi: 10.1056/NEJMoa2115481

frontiers | Frontiers in Cellular and Infection Microbiology

TYPE Original Research
PUBLISHED 23 June 2025
DOI 10.3389/fcimb.2025.1567341

OPEN ACCESS

EDITED BY
Paraskevi C. Fragkou,
Evaggelismos General Hospital, Greece

REVIEWED BY
Alpaslan Alp,
Hacettepe University, Türkiye
Char Leung,
University of Leicester, United Kingdom

*CORRESPONDENCE
Li Qi
qili19812012@126.com
Yanxia Sun
sunyanxiamay@163.com

†These authors have contributed equally to this work and share first authorship

RECEIVED 27 January 2025
ACCEPTED 05 June 2025
PUBLISHED 23 June 2025

CITATION
Li T, Long J, Li Z, Xiong Y, Feng L, Jiang M, Sun Y and Qi L (2025) Epidemiology of human respiratory tract infection in Chongqing, China after COVID-19–based on surveillance data encompassing 17 respiratory pathogens.
Front. Cell. Infect. Microbiol. 15:1567341.
doi: 10.3389/fcimb.2025.1567341

Epidemiology of human respiratory tract infection in Chongqing, China after COVID-19–based on surveillance data encompassing 17 respiratory pathogens

Tingting Li[1,2†], Jiang Long[1,2†], Zhourong Li[3†], Yu Xiong[1,2], Luzhao Feng[4], Mingyue Jiang[4], Yanxia Sun[4*] and Li Qi[1,2*]

[1]Chongqing Center for Disease Control and Prevention (Chongqing Academy of Preventive Medicine), Chongqing, China, [2]Chongqing Disease Prevention and Public Health Research Center Construction Program, Chongqing, China, [3]School of Public Health, Chongqing Medical University, Chongqing, China, [4]School of Population Medicine and Public Health, Chinese Academy of Medical Sciences & Peking Union Medical College, Beijing, China

Background: Respiratory tract infections (RTIs) are an important public health concern, and SARS-CoV-2 affects the epidemic pattern of RTIs globally. National multipathogenic surveillance for RTIs was conducted in mid-October 2023. However, baseline data on the pathogen spectrum of RTIs in Chongqing, China, before mid-October 2023 are limited.

Methods: A descriptive analysis was conducted to determine the epidemiology of RTIs in Chongqing, China, in 2023.Results A total of 1,894 individuals were included in 2023, with an overall positivity rate of 28.7%. The highest overall positivity rate was observed in May 2023 (53.0%). Different predominant respiratory pathogens were observed among different age groups. Among all single-infected individuals, SARS-CoV-2 accounted for 32.1%, followed by IFV, which accounted for 28.2%. In the children group, RSV ranked first, accounting for 15.7%. Among school-aged children, IFV ranked the top, accounting for 46.7%. SARS-CoV-2 ranked the top among adults and the elderly, accounting for 45.5% and 47.0%, respectively.

Conclusions: The local pathogen spectrum of RTIs one year after the onset of COVID-19 showed that SARS-CoV-2 was steady, and viral infection might be the main cause of RTIs. Both upper respiratory tract infections and lower respiratory tract infections (LRIs) showed high RTI positivity rates. The pathogen spectra of upper respiratory tract infections (URIs) and LRIs differ in adults. Holistic surveillance of RTIs is necessary to estimate the local disease burden. Vaccination against respiratory infections remains an important strategy to prevent and control RTIs.

KEYWORDS

respiratory tract infection, epidemiology, multiple respiratory pathogens, SARS-CoV-2, surveillance

Introduction

Respiratory tract infections (RTIs) are major global health problems that can be classified into upper respiratory tract infections (URIs) and lower respiratory tract infections (LRIs). LRIs are the fourth leading cause of death worldwide, accounting for 2.50 million deaths, and pose a significant global health challenge (Collaborators GL, 2022). Most RTIs are self-limiting but can lead to severe outcomes including hospitalization and death, especially in immunocompromised young children and the elderly (Echavarría et al., 2018). During the global COVID-19 pandemic, the epidemiology of respiratory pathogens such as influenza, mycoplasma pneumoniae (M. pneumonia) (Meyer Sauteur et al., 2022), and respiratory syncytial virus (RSV) (Chuang et al., 2023), appears to have changed dramatically, showing an obvious downward trend (Li et al., 2022; Yoshioka et al., 2023). The phenomenon could be attributed to the public health and social measures (PHSMs) that were implemented to curb the spread of SARS-CoV-2, such as social distancing, school closures, and mask mandates. However, studies conducted at home and abroad showed that these respiratory pathogens resurged as PHSMs lifted (Mott et al., 2021; Ujiie et al., 2021; Li et al., 2022).

The PHSMs implemented during the COVID-19 pandemic, while effective in containing SARS-CoV-2 transmission, also modulated the incidence of other respiratory infections (Shi et al., 2022; Yuan et al., 2022; Boehm et al., 2023). In late 2022 after Chinese government has shifted COVID-19 prevention and control policies, the long-term impact of pandemic-era measures on the resurgence patterns of other respiratory pathogens remained unclear (Li et al., 2022). Chongqing is the largest subtropical municipality in China, with a heavy burden of respiratory diseases (Qi et al., 2020a; Qi et al., 2020b; Li et al., 2023). Owing to COVID-19 pandemic, the activity of mutations in respiratory pathogens shifted significantly. Follow the WHO declaration of the pandemic's end in May 2023, PHSMs were gradually relaxed globally. In this context, evaluating the evolving spectrum of respiratory pathogens and monitoring their activity has become critical. Such assessments help guide localized prevention and control policies in response to shifting epidemiological trends.

Following the COVID-19 pandemic, the government realized it was essential to re-evaluate the activity of respiratory pathogens. This could help understand the updated circulation of these pathogens and their impact on the population. As a result, the government support to conduct multipathogen surveillance across most regions of China. Chongqing, an important city in southwestern China, is a key focus. These data will serve as a reference for southern China and even other parts of the country. The previous historical surveillance data of respiratory diseases in China, primarily focused on influenza (National surveillance protocol for influenza (version 2010): China National Influenza Center, 2010), underscore the significance of expanding research to encompass a broader spectrum of other respiratory pathogens. Meanwhile, there were limited data before the national multipathogenic surveillance for RTIs was conducted.

Therefore, our study first reported and analyzed the epidemiology of RTIs with seventeen respiratory pathogens in Chongqing, China, with the goal of revealing the dynamic epidemic characteristics of multiple pathogens after the COVID-19 pandemic (in 2023). Additionally, we aimed to identify the risk groups for severe disease in Chongqing, intending to offer practical references for preventing and controlling respiratory infectious diseases. Through our research, we can establish the baseline of the pathogen spectrum of local respiratory tract infections. Furthermore, it could provide a guidance for the allocation of medical resources (such as medications, hospital beds, medical staff, and vaccines). Beside, these data will serve as a reference for southern China and even other parts of the country.

Materials and methods

This is a multi-center research led by the Chinese Academy of Medical Sciences to analysis of the characteristics of multi-pathogen composition in cases of acute respiratory infection, with more than 14 joint institutions around China, including Chongqing. National multipathogenic surveillance for RTIs was conducted in mid-October 2023. However, baseline data on the pathogen spectrum of RTIs in Chongqing, China, before mid-October 2023 are limited. Based on the holistic protocol, our sample size was approximately 2000 individuals. According to different economic levels, this cross-sectional study was executed in four districts in Chongqing from 1 January to 31 December 2023, including Wanzhou District, Yongchuan District, Wulong District, and Nan'an District. This study randomly enrolled individuals with acute respiratory infection (Daoud Perez et al., 2022) from four districts in Chongqing, from 12 hospitals (Wulong District People's Hospital, Fukang Hospital, Wulong District Traditional Chinese Medicine Hospital, Wulong District Maternal and Child Health Hospital, Chongqing No. 5 People's Hospital, The First Affiliated Hospital of Chongqing Medical and Pharmaceutical College Chongqing Southeast Hospital, The Affiliated People's Hospital of Three Gorges Medical College, The Affiliated Hospital of Three Gorges Medical College, The Central Health Center of Fenshui Town, The Central Health Center of Longsha Town, and The Affiliated Yongchuan Hospital of Chongqing Medical University).

The criteria of enrollment were as follows: URIs, 1) Individuals of all age groups can be included; 2) Have clinical manifestations of acute infection, including any one of fever (with possible hypothermia considering age), abnormal white blood cells (increase, decrease, or abnormal distribution), and chills; 3) Have any one of the respiratory symptoms simultaneously, including pharyngeal discomfort, dry throat or sore throat, nasal congestion,

Abbreviations: RTIs, Respiratory tract infections; URIs, upper respiratory tract infections; LRIs, lower respiratory tract infections; M. pneumonia, mycoplasma pneumoniae; RSV, respiratory syncytial virus; IFV-A, influenza A virus; IFV-B, influenza B virus; HAdV, human adenovirus; HPIV, human parainfluenza virus; HMPV, human metapneumovirus; HCoV, human coronavirus; HRV, human rhinovirus; C. pneumonia, chlamydia pneumoniae.

runny nose, obvious congestion and edema of the nose/pharynx/larynx, cough (new onset or aggravated cough), expectoration, shortness of breath, abnormal auscultation of breath sounds (rales, rhonchi, wheezing, dullness), and chest pain; 4) Sign the informed consent form.

LRIs, 1) Inpatients whose illness onset was within 7 days; 2) Have respiratory symptoms such as fever, cough or sore throat; 3) Chest X - ray (or chest CT) examination shows pneumonia; 4) Sign the informed consent form.

A uniform questionnaire with information regarding demography, diagnosis and treatment, sample collection, and laboratory testing was obtained from all involved individuals. URIs samples (oropharyngeal swabs) were collected from both outpatients and inpatients. Lower respiratory tract samples such as bronchoalveolar lavage fluid, tracheal secretions, or deeply induced sputum are preferred by inpatients; however, oropharyngeal swabs can be collected if lower respiratory tract samples cannot be obtained. Seventeen respiratory pathogens which included SARS-CoV-2, influenza A virus (IFV-A), influenza B virus (IFV-B), RSV, human adenovirus (HAdV), human parainfluenza virus (HPIV) 1-4, human metapneumovirus (HMPV), human coronavirus (HCoV) 229E, NL63, OC43, HKU-1, human rhinovirus (HRV), *M.pneumonia, chlamydia pneumoniae (C. pneumonia)*, were identified by real-time fluorescent polymerase chain reaction testing.

Data analysis was performed by R software (version 4.2) and Microsoft Excel (version 2019; Redmond, WA, USA). Descriptive analysis was employed to illustrate the epidemiological characteristics. Line charts and percentage bar chart were used to show the monthly distribution of positive respiratory pathogens detection and the distribution of respiratory pathogens by age, respectively. Chi-square test was conducted to compare differences between subgroups. P values less (two-tail) than 0.05 were considered statistically significant.

Results

In total, 2,242 people participated in this research in Chongqing. After data cleaning, a total of 1,894 individuals were included in our study, with an overall positivity rate of 28.7%. The single infection and co-infection rates were 25.8% and 2.9%, respectively. Higher positivity rates were observed among school-aged children, outpatients, and patients with URIs. Table 1 shows the positive rates of respiratory pathogens in the different groups.

The highest overall positivity rate was observed in May 2023 (53.0%), with a higher number of outpatients than inpatients. Figure 1a shows the monthly distribution of positive rates among the RTI cases. Different predominant respiratory pathogens were observed among different age groups. The pathogens detection in URIs varied significantly across age groups (χ^2=34.79, P < 0.001), whereas no statistically differences were observed in LRIs (χ^2=7.54 P=0.581). In the three groups of all cases, the elderly, and the adults, viral monoinfection had a higher rate (27.0%–15.7%), followed by viral-viral coinfection, among both among LRIs and URIs. In the school-aged children group, the proportion bar charts displayed results from limited samples (two samples tested viral monoinfection out of twelve samples). In the children group, viral monoinfection was most frequently identified among the LRIs (20.3%), M. pneumonia, and C. pneumonia were not detected. Figure 1b shows the proportion of respiratory pathogens among the different age groups.

Among all single-infected individuals, SARS-CoV-2 accounted for 32.1%, followed by IFV, which accounted for 28.2%. In the children group, RSV, IFV, and HPIV ranked the first three, accounting for 15.7%, 14.7%, and 13.7%, respectively. Among school-aged children, IFV ranked the top, accounting for 46.7%, followed by SARS-CoV-2 and HRV, which accounted for 15.2%, respectively. SARS-CoV-2 ranked the top among adults, accounting for 45.5%, followed by IFV (32.1%) (Qi et al., 2020a). SARS-CoV-2 accounted for the majority (47.0%) of the elderly, followed by IFV (17.9%). Figure 2 illustrates the details of the viral and bacterial compositions of single infections.

Discussion

Chongqing, a megacity with a larger population than the capital Beijing, holds significant importance in China. Our previous studies have estimated that Chongqing has a substantial influenza- and pneumonia-related mortality burden (Qi et al., 2020a; Qi et al., 2020b; Li et al., 2023). Owing to mutations in respiratory pathogens and immunity debt during the COVID-19 period, people may exhibit increased susceptibility to respiratory pathogens (Zuurbier et al., 2023), which could lead to the recurrence of epidemic peaks of RTIs after the COVID-19 pandemic. Based on our surveillance, the findings revealed that school-aged children, outpatients, and patients with URIs suffered the most respiratory infections, with a higher overall positive rate. Similarly, a community-based cohort study revealed a positivity rate of > 70% among healthy children in New Zealand (Walker et al., 2022). The proportion of people infected with SARS-CoV-2 remains at a relatively high level locally, even PHSMs to curb the spread of SARS-CoV-2 were lifted. This also leading to the relatively low proportion of other pathogens (Oishi et al., 2022; Presti et al., 2024). But in different age groups, the predominant respiratory pathogens were differed; like in children and school-aged children group, the predominant respiratory pathogens were still those prevailed before COVID-19.

We observed that viral monoinfection was prevalent in all cases of respiratory infection in Chongqing, China, in 2023, including both URIs and LTIs. Besides, viral-viral co-infection was also observed in all age groups. Another community-acquired pneumonia study (Liu et al., 2023) conducted from 2009 to 2020 in China indicated that among adults and the elderly, bacterial monoinfection was the leading respiratory pathogen and viral-bacterial co-detection was rare in all age groups. Hence, persistent comprehensive monitoring of respiratory infections was necessary in the local area. Further analysis of the single infection revealed different pathogens among different age groups. In children and school-aged children, IFV, RSV, and HRV were responsible for the foremost respiratory tract infections in 2023. Conversely, in adults and elderly individuals, SARS-CoV-2 was

TABLE 1 Positive rates of respiratory pathogens among patients with respiratory infection in Chongqing, in 2023. (N=1,894).

Characteristics	All respiratory pathogens tested			
	No. specimens tested	No. laboratory-confirmed cases (%)		
		Total	Single infection	Co-infection
Sex				
Male	1,050 (55.4)	290 (27.6)	270 (25.7)	20 (1.9)
Female	844 (44.6)	253 (30.0)	219 (26.0)	34 (4.0)
Age group				
Children (≤5 years)	350 (18.5)	122 (34.9)	102 (29.1)	20 (5.7)
School-aged children (6–17 years)	303 (16.0)	117 (38.6)	105 (34.7)	12 (4.0)
Adults (18–59 years)	628 (33.2)	181 (28.8)	165 (26.3)	16 (2.5)
Older people (≥60 years)	613 (32.4)	123 (20.1)	117 (19.1)	6 (1.0)
Case type				
Inpatients	1,046 (55.2)	195 (18.6)	184 (17.6)	11 (1.0)
Outpatients	848 (44.8)	348 (41.0)	305 (36.0)	43 (5.1)
RTIs type				
URIs	1,438 (75.9)	459 (31.9)	412 (28.7)	47 (3.3)
LRIs	456 (24.1)	84 (18.4)	77 (16.9)	7 (1.5)
Total	1,894 (100.0)	543 (28.7)	489 (25.8)	54 (2.9)

superior to the other seventeen respiratory pathogens. However, before the COVID-19 pandemic, IFV was responsible for most respiratory infections in different age groups in China (Li et al., 2021). Also, our previous study found a resurgence of IFV during COVID-19 in Chongqing, China, implying the high prevalence of IFV locally, even though HCoV remained in a low-level epidemic (Li et al., 2023). There was another report indicating that RSV causes a considerable disease burden for older and high-risk adults (Nguyen-Van-Tam et al., 2022), so attention regarding the older, and adults should not be neglected even though many citations signify children are more vulnerable individuals to RSV (Li et al., 2022).

This study has a few limitations. Our tested pathogens were mostly viruses, common bacteria were not included tested. In addition, the LRI samples from school-aged children were limited compared to other age groups, and more data should be collected for in-depth analysis.

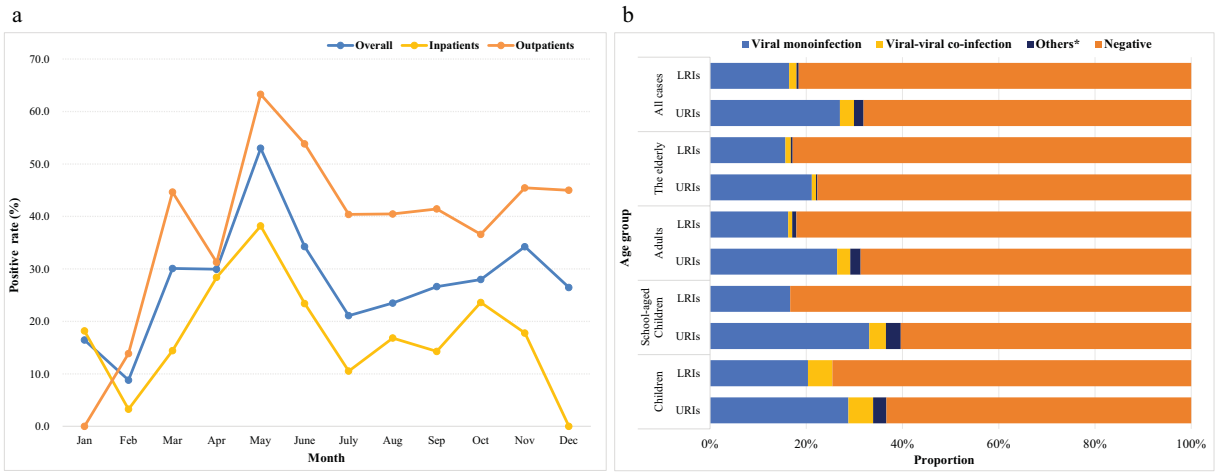

FIGURE 1
Positive rates **(a)** and respiratory pathogens detection **(b)** in Chongqing, China, in 2023. *Others indicate M. pneumonia, **(C)** pneumonia single infection and they co-infected with other viruses.

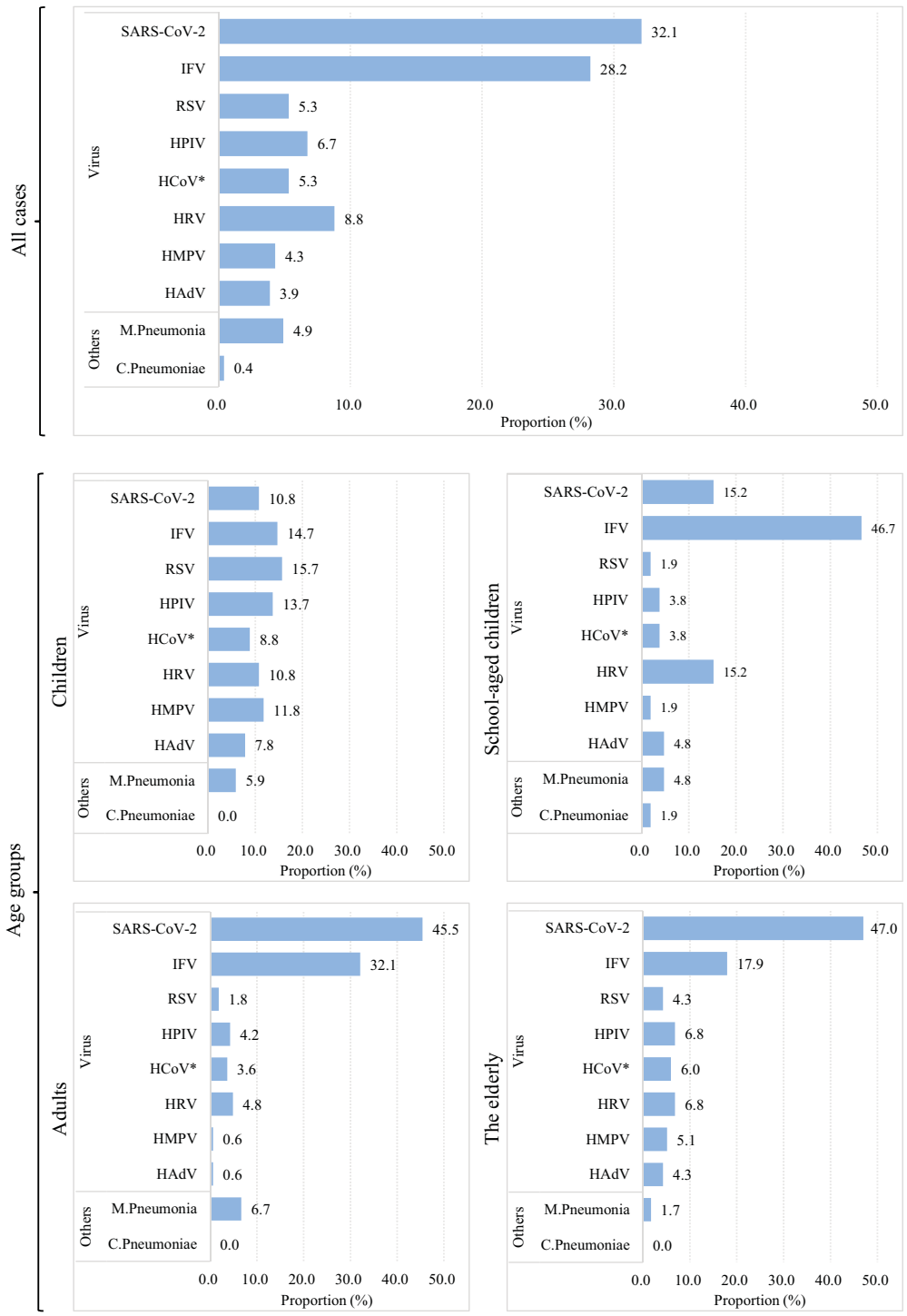

FIGURE 2
Viral composition of single infection patients in Chongqing China, in 2023. Note: The length of colored bars and the number behind indicate the proportion of each pathogen, calculated by its positive number used as the numerator and the total positive number of all pathogens used as the denominator. *HCoV includs 229E, NL63, OC43, HKU-1.

Conclusions

This descriptive analysis revealed the pathogen spectrum of respiratory infections according to age, URIs, and LRIs. RTIs are an important public health issue, especially in school-aged children. Viral infection may be the main cause of local RTIs, and the prevalence of SARS-CoV-2 remains at a certain level locally. These findings underscore the need to monitor the epidemiological trends in respiratory infections. A comprehensive surveillance of RTIs is necessary to estimate the disease burden, and

conducive to implement prevention and control measures such as health advisories for the public, vaccination, and the stockpiling of medical resources, locally.

Data availability statement

The raw data supporting the conclusions of this article will be made available by the corresponding author LQ on reasonable request, without undue reservation.

Ethics statement

The studies involving humans were approved by Chongqing Municipality Center for Disease Control and Prevention (KY-2023-010-1). The studies were conducted in accordance with the local legislation and institutional requirements. Written informed consent for participation in this study was provided by the participants' legal guardians/next of kin.

Author contributions

TL: Data curation, Formal analysis, Investigation, Writing – original draft, Writing – review & editing. JL: Conceptualization, Funding acquisition, Methodology, Project administration, Supervision, Writing – review & editing. ZL: Data curation, Formal analysis, Investigation, Validation, Visualization, Writing – original draft, Writing – review & editing. YX: Investigation, Resources, Validation, Writing – original draft, Writing – review & editing. LF: Conceptualization, Funding acquisition, Project administration, Resources, Supervision, Writing – review & editing. MJ: Data curation, Investigation, Resources, Writing – original draft, Writing – review & editing. YS: Data curation, Methodology, Validation, Visualization, Writing – original draft, Writing – review & editing. LQ: Conceptualization, Funding acquisition, Investigation, Project administration, Supervision, Writing – review & editing.

Funding

The author(s) declare that financial support was received for the research and/or publication of this article. This work was supported by the Chongqing Municipal Science and Technology Bureau (CSTC2021jscx-gksb-N0005, cstc2024ycjh-bgzxm0224), National Natural Science Foundation of China (12371503), and the Chinese Academy of Medical Sciences Innovation Fund for Medical Sciences (2022-I2M-CoV19-006). Chinese Preventive Medicine Association (CPMA2024CRBFK).

Acknowledgments

We sincerely thank colleagues and participants from four districts CDCs and hospitals in Chongqing.

Conflict of interest

The authors declare that the research was conducted in the absence of any commercial or financial relationships that could be construed as a potential conflict of interest.

Generative AI statement

The author(s) declare that no Generative AI was used in the creation of this manuscript.

Publisher's note

All claims expressed in this article are solely those of the authors and do not necessarily represent those of their affiliated organizations, or those of the publisher, the editors and the reviewers. Any product that may be evaluated in this article, or claim that may be made by its manufacturer, is not guaranteed or endorsed by the publisher.

References

(2010). *National surveillance protocol for influenza (version 2010): China National Influenza Center*. Available online at: https://ivdc.chinacdc.cn/cnic/fascc/201708/t20170809_149276.htm (Accessed December 11, 2022).

Boehm, A. B., Hughes, B., Duong, D., Chan-Herur, V., Buchman, A., Wolfe, M. K., et al. (2023). Wastewater concentrations of human influenza, metapneumovirus, parainfluenza, respiratory syncytial virus, rhinovirus, and seasonal coronavirus nucleic-acids during the COVID-19 pandemic: a surveillance study. *Lancet Microbe* 4, e340–e3e8. doi: 10.1016/S2666-5247(22)00386-X

Chuang, YA-OX, Lin, K. P., Wang, L. A., Yeh, T. A.-O., and Liu, P. A.-O. (2023). The impact of the COVID-19 pandemic on respiratory syncytial virus infection: A narrative review. *Infection Drug resistance* 16, 661–675. doi: 10.2147/IDR.S396434

Collaborators GL (2022). Age-sex differences in the global burden of lower respiratory infections and risk factors, 1990-2019: results from the Global Burden of Disease Study 2019. *Lancet Infect. diseases* 22, 1626–1647. doi: 10.1016/S1473-3099(22)00510-2

Daoud Perez, Z., Razquin Arias, M., Lopez-Escobar, A., Diaz-Conradi, A., Arce, A., Ruggeri, N., et al. (2022). The impact of COVID-19 lockdown on children with recurrent wheezing and asthma in Spain. *J. Paediatr. Child Health* 58, 1635–1641. doi: 10.1111/jpc.16068

Echavarría, M., Marcone, D. N., Querci, M., Seoane, A., Ypas, M., Videla, C., et al. (2018). Clinical impact of rapid molecular detection of respiratory pathogens in patients with acute respiratory infection. *J. Clin. virology* 108, 90–95. doi: 10.1016/j.jcv.2018.09.009

Li, Y., Wang, X., Blau, D. M., Caballero, M. T., Feikin, D. R., Gill, C. J., et al. (2022). Global, regional, and national disease burden estimates of acute lower respiratory infections due to respiratory syncytial virus in children younger than 5 years in 2019: a systematic analysis. *Lancet.* 399, 2047–2064. doi: 10.1016/S0140-6736(22)00478-0

Li, Z., Xiong, Y., Long, J., Li, T., Fu, X., Yang, S., et al. (2023). Resurgence of influenza during COVID-19 in Chongqing, China: A retrospective analysis. *J. Med. Virol.* 95, e29249. doi: 10.1002/jmv.v95.11

Li, Z. J., Yu, L. J., Zhang, H. Y., Shan, C. X., Lu, Q. B., Zhang, X. A., et al. (2022). Broad impacts of coronavirus disease 2019 (COVID-19) pandemic on acute respiratory infections in China: an observational study. *Clin. Infect. Dis.* 75, e1054–e1e62. doi: 10.1093/cid/ciab942

Li, Z. J., Zhang, H. Y., Ren, L. L., Lu, Q. A.-O., Ren, X., Zhang, C. H., et al. (2021). Etiological and epidemiological features of acute respiratory infections in China. *Nat. Commun.* 12, 5026. doi: 10.1038/s41467-021-25120-6

Liu, Y. N., Zhang, Y. F., Xu, Q., Qiu, Y., Lu, Q. B., Wang, T., et al. (2023). Infection and co-infection patterns of community-acquired pneumonia in patients of different ages in China from 2009 to 2020: a national surveillance study. *Lancet Microbe* 4, e330–e3e9. doi: 10.1016/S2666-5247(23)00031-9

Meyer Sauteur, P. M., Beeton, M. L., Uldum, S. A., Bossuyt, N., Vermeulen, M., Loens, K., et al. (2022). Mycoplasma pneumoniae detections before and during the COVID-19 pandemic: results of a global survey, 2017 to 2021. *Euro surveillance* 27, 2100746. doi: 10.2807/1560-7917.ES.2022.27.19.2100746

Mott, J. A., Fry, A. M., Kondor, R., Wentworth, D. E., and Olsen, S. J. (2021). Re-emergence of influenza virus circulation during 2020 in parts of tropical Asia: Implications for other countries. *Influenza Other Respir. Viruses* 15, 415–418. doi: 10.1111/irv.12844

Nguyen-Van-Tam, J. S., O'Leary, M., Martin, E. T., Heijnen, E., Callendret, B., Fleischhackl, R., et al. (2022). Burden of respiratory syncytial virus infection in older and high-risk adults: a systematic review and meta-analysis of the evidence from developed countries. *Eur. Respir. Rev.* 31, 220105. doi: 10.1183/16000617.0105-2022

Oishi, K., Horiuchi, S., Minkoff, J. M., and tenOever, B. R. (2022). The host response to influenza A virus interferes with SARS-coV-2 replication during coinfection. *J. Virol.* 96, e0076522. doi: 10.1128/jvi.00765-22

Presti, S., Manti, S., Gammeri, C., Parisi, G. F., Papale, M., and Leonardi, S. (2024). Epidemiological shifts in bronchiolitis patterns and impact of the COVID-19: A two-season comparative study. *Pediatr. Pulmonol* 59, 1298–1304. doi: 10.1002/ppul.26904

Qi, L., Gao, Y., Yang, J., Ding, X. B., Xiong, Y., Su, K., et al. (2020a). The burden of influenza and pneumonia mortality attributable to absolute humidity among elderly people in Chongqing, China, 2012-2018. *Sci. Total Environ.* 716, 136682. doi: 10.1016/j.scitotenv.2020.136682

Qi, L., Li, Q., Ding, X. B., Gao, Y., Ling, H., Liu, T., et al. (2020b). Mortality burden from seasonal influenza in Chongqing, China, 2012-2018. *Hum. Vaccin Immunother* 16, 1668–1674. doi: 10.1080/21645515.2019.1693721

Shi, H. J., Kim, N. Y., Eom, S. A., Kim-Jeon, M. D., Oh, S. S., Moon, B. S., et al. (2022). Effects of non-pharmacological interventions on respiratory viruses other than SARS-coV-2: analysis of laboratory surveillance and literature review from 2018 to 2021. *J. Korean Med. Sci.* 37, e172. doi: 10.3346/jkms.2022.37.e172

Ujiie, M., Tsuzuki, S., Nakamoto, T., and Iwamoto, N. (2021). Resurgence of respiratory syncytial virus infections during COVID-19 pandemic, tokyo, Japan. *Emerg. Infect. Dis.* 27, 2969–2970. doi: 10.3201/eid2711.211565

Walker, G. A.-O., Stelzer-Braid, S., Shorter, C., Honeywill, C., Wynn, M., Willenborg, C., et al. (2022). Viruses associated with acute respiratory infection in a community-based cohort of healthy New Zealand children. *J. Med. virology* 94 , 454–460. doi: 10.1002/jmv.25493

Yoshioka, S., Phyu, WA-OX, Wagatsuma, K., Nagai, T., Sano, Y., Taniguchi, K., et al. (2023). Molecular Epidemiology of Respiratory Syncytial Virus during 2019–2022 and Surviving Genotypes after the COVID-19 Pandemic in Japan. *Viruses.* 15, 2382. doi: 10.3390/v15122382

Yuan, H., Yeung, A., and Yang, W. (2022). Interactions among common non-SARS-CoV-2 respiratory viruses and influence of the COVID-19 pandemic on their circulation in New York City. *Influenza Other Respir. Viruses* 16, 653–661. doi: 10.1111/irv.12976

Zuurbier, R. A.-O., Bogaert, D. A.-O., de Steenhuijsen Piters, W. A.-O., Arp, K., Chu, M. A.-O., Sanders, E. A.-O., et al. (2023). Asymptomatic viral presence in early life precedes recurrence of respiratory tract infections. *Pediatr. Infect. Dis. J.* 42, 59–65. doi: 10.1097/INF.0000000000003732

frontiers | Frontiers in Cellular and Infection Microbiology

TYPE Original Research
PUBLISHED 14 July 2025
DOI 10.3389/fcimb.2025.1600990

OPEN ACCESS

EDITED BY
Paraskevi C. Fragkou,
Evaggelismos General Hospital, Greece

REVIEWED BY
Benjamin M. Liu,
George Washington University, United States
Arnold Lambisia,
KEMRI Wellcome Trust Research Program, Kenya

*CORRESPONDENCE
Chunquan Cai
cqcns6@126.com

†These authors have contributed equally to this work and share first authorship

RECEIVED 27 March 2025
ACCEPTED 17 June 2025
PUBLISHED 14 July 2025

CITATION
Fang Y, Lei M, Zhang L, Hou M, Wang N and Cai C (2025) Epidemiological, clinical, and molecular analysis of human adenovirus infections in hospitalized children with acute respiratory infections in Tianjin, China. *Front. Cell. Infect. Microbiol.* 15:1600990. doi: 10.3389/fcimb.2025.1600990

Epidemiological, clinical, and molecular analysis of human adenovirus infections in hospitalized children with acute respiratory infections in Tianjin, China

Yulian Fang[1,2†], Min Lei[1,2†], Lu Zhang[3†], Mengzhu Hou[1,2], Ning Wang[1,2] and Chunquan Cai[1,2*]

[1]Department of Pediatric Research Institute, Children's Hospital of Tianjin University/Tianjin Children's Hospital, Tianjin, China, [2]Tianjin Key Laboratory of Birth Defects for Prevention and Treatment, Children's Hospital of Tianjin University/Tianjin Children's Hospital, Tianjin, China, [3]Department of Respiratory, Children's Hospital of Tianjin University/Tianjin Children's Hospital, Tianjin, China

Background: Human Adenovirus (HAdV) is a significant pathogen for acute respiratory infections(ARIs) in children. However, its epidemiological patterns, serotype distribution changes, and molecular mechanisms associated with severe pneumonia during and after the COVID-19 pandemic require further elucidation through large-scale and molecular typing studies.

Methods: This study used a retrospective cohort design to analyze 28060 respiratory specimens from Tianjin Children's Hospital from March 2022 to March 2024. HAdV detection and typing were performed through targeted high-throughput sequencing and PCR-based amplification of Penton, Hexon, and Fiber genes for phylogenetic analysis. Additionally, clinical data were compared to assess differences in clinical presentations among pediatric patients infected with different HAdV types.

Results: The overall HAdV detection rate was 8.9% (2,484/28,060), with significant male predominance (9.2% *vs*. 8.4%, $P = 0.019$) and age-specific susceptibility peaking in school-aged children (10.4%, $P < 0.001$). Seasonal patterns demonstrated winter predominance (15.9%), contrasting with other seasons ($P < 0.001$). Genotyping of 1,914 positive specimens demonstrated HAdV-3 dominance (53.4%, 1,022), followed by HAdV-7 (17.7%, 338), HAdV-2 (8.4%, 160), HAdV-1 (7.9%, 152), and HAdV-21 (6.4%, 122). The diagnosis mainly included pneumonia, bronchitis, adenopharyngitis, and upper respiratory tract infections (URTIs). Genotype-clinical correlations showed distinct patterns: HAdV-3 (55.6%) and HAdV-7 (20.9%) predominated in pneumonia cases, with HAdV-7 linked to severe pneumonia ($P<0.001$). HAdV-3 (40.6%) and HAdV-2 (16.7%) were more common in adenopharyngitis, while HAdV-3 and HAdV-21 were more common in bronchitis (51.2% and 11.1%) and URTIs (31.9% and 19.1%). Molecular characterization revealed structural conservation in the Penton protein of HAdV-C and identified Hexon as the most polymorphic region with 85 variable sites, indicating divergent evolutionary pressures across viral domains.

Conclusion: HAdV-3, HAdV-7, HAdV-2, and HAdV-1 were the predominant HAdV types in children hospitalized with ARIs in Tianjin. Moreover, not only the epidemiological characteristics of different HAdV types vary, but there are also certain differences in the clinical symptoms and outcomes of children infected with different types of HAdV. Therefore, it is essential to differentiate HAdV types for epidemiological surveillance and clinical management purposes.

KEYWORDS

human adenovirus, acute respiratory infections, children, epidemiology, molecular types

1 Introduction

Human adenovirus (HAdV), a non-enveloped dsDNA virus of the genus *Mastadenovirus* (family Adenoviridae), represents a significant global pathogen causing heterogeneous clinical manifestations across age groups. Pediatric populations exhibit heightened susceptibility, with 80% of infections occurring in children under 4 years of age due to waning maternal antibodies and immature adaptive immunity (Lynch and Kajon, 2016). The International Committee on Taxonomy of Viruses (https://talk.ictvonline.org/taxonomy) classifies more than 120 genotypes into seven species (A-G), with distinct tissue tropisms dictating clinical outcomes. Acute respiratory infections (ARIs) are commonly linked to species B (B3, B7, B14, B16, B21), C (C1, C2, C5, C6, C57), and E (E4) (Lynch and Kajon, 2016; Tian et al., 2021), manifested as pneumonia, bronchitis, upper respiratory tract infections (URTIs), or tonsillitis (Wen et al., 2021). Notably, approximately one-third of HAdV-associated pneumonia progresses to severe adenoviral pneumonia, characterized by radiographic consolidation and extrapulmonary complications (Lu et al., 2013; Wang et al., 2021). Despite this clinical burden, evidence remains limited regarding genotype-specific virulence determinants. This emphasizes the importance of rapid and accurate HAdV genotyping in clinical diagnosis and epidemiological investigation.

Conventional HAdV serotype determination relies on neutralization assays and hemagglutination inhibition tests, which are time-consuming and reagent-limited. The emergence of novel recombinant strains through homologous recombination complicates traditional serological typing, as evidenced by circulating variants containing discordant antigenic determinants. Modern molecular approaches, particularly multiplex PCR and real-time quantitative PCR (qPCR), demonstrate superior diagnostic utility with higher sensitivity for established genotypes (Ison and Hayden, 2016). However, partial genome sequencing strategies (e.g., Hexon hypervariable region analysis) carry inherent misidentification risks, as critical recombination breakpoints frequently occur outside targeted loci. To ensure accurate molecular epidemiology, the WHO HAdV Working Group (http://hadvwg.gmu.edu) recommends integrated analysis of three capsid genes (Hexon, Penton base, and Fiber) (Wu et al., 2022).

During the last decade, outbreaks of respiratory tract infections caused by HAdV have occurred frequently in many countries including China (Barnadas et al., 2018; Zhao et al., 2020; Huang et al., 2021; Pscheidt et al., 2021; Huang et al., 2023). While genotype-specific virulence has been hypothesized, only a few published pediatric studies incorporate molecular subtyping data, and existing evidence suggests a correlation between genotypes and clinical outcomes (Lin et al., 2017; Wang et al., 2021). Thus, the genotyping of HAdV is crucial for understanding local epidemiology, tracking virulence variants, and guiding vaccine development. Notably, the widespread implementation of non-pharmaceutical interventions (NPI) during the COVID-19 pandemic significantly altered the transmission patterns of respiratory viruses, including HAdV (Huang et al., 2023). In the post-pandemic era, the epidemiological characteristics, predominant serotype distribution, and associations with disease severity of HAdV have exhibited new dynamics, urgently requiring continuous surveillance and in-depth investigation (Yan et al., 2024; Zhao et al., 2024; Contes and Liu, 2025; Han et al., 2025). The aim of this study was to investigate the epidemiological, clinical, and molecular characteristics of HAdV infections among hospitalized children with ARIs in Tianjin from March 2022 to March 2024, aiming to inform future prediction and intervention strategies for HAdV-related diseases. The findings provide scientific evidence for the prevention and control of HAdV-related diseases.

2 Materials and methods

2.1 Patients and specimens

This retrospective cohort study was conducted from March 2022 to March 2024 at Tianjin Children's Hospital in Tianjin. Clinical specimens (nasopharyngeal swabs, sputum, and bronchoalveolar lavage fluid) were collected from children with

ARIs within 24 hours after hospitalization. All specimens were stored at -80°C for further genotyping. Demographic and clinical data of HAdV-positive patients by targeted next-generation sequencing were obtained from their medical records. The inclusion criteria were as follows (1): presentation of typical ARIs symptoms (e.g., fever, cough, nasal congestion) (2); hospitalization during the specified period; (3) age range of 1 day to 18 years; (4) informed consent from patients or guardians. Exclusion criteria were as follows: (1) hospital-acquired infections; (2) patients with incomplete electronic medical records; (3) cause of hospitalization other than ARIs. Severe pneumonia was diagnosed according to the Chinese 2019 version of diagnosing and treating children's community-acquired pneumonia (National Health Commission of the People's Republic of China and State Administration of Traditional Chinese Medicine, 2019). This study protocol was approved by the ethics committee of the Tianjin Children's Hospital and conducted by the Declaration of Helsinki guidelines. The parents or guardians of all participants signed informed consent. Specimens for this study were collected in Tianjin, located in the North China region at approximately 39°N latitude in the Northern Hemisphere. The seasons were defined according to the Northern Hemisphere standards: spring (March to May), summer (June to August), autumn (September to November), and winter (December to February of the following year). A flow diagram of the study design is shown in Figure 1.

2.2 Detection of HAdV and molecular genotyping

HAdVs were detected and genotyped using a multiplex PCR-based targeted next-generation sequencing (tNGS) platform. This assay not only identified HAdV presence but also resolved 13 distinct genotypes (HAdV-1, 2, 3, 4, 5, 6, 7, 8, 21, 31, 55, 57, and 108). The diagnostic panel development and validation were conducted by JinYu Biotechnology. Viral DNA was randomly extracted from 100 HAdV-positive clinical specimens using the QIAamp MinElute Virus Spin Kit (QIAGEN, Germany) following the manufacturer's protocol. Target regions encompassing the Hexon, Penton base, and Fiber genes were amplified by conventional polymerase chain reaction (PCR) as previously described (Wu et al., 2022). Amplification products were analyzed by electrophoresis on 1.5% agarose gels, and positive amplification products were sequenced by GENEWIZ (Suzhou, China) using Sanger sequencing technology. Obtained sequences were aligned against the National Center for Biotechnology Information (NCBI, https://www.ncbi.nlm.nih.gov/) GenBank database using Basic Local Alignment Search Tool (BLAST). Genotype assignment was determined through maximum sequence identity matching across the Hexon, Penton base, and Fiber. Phylogenetic reconstruction and amino acid substitution analyses were subsequently performed to characterize viral evolution.

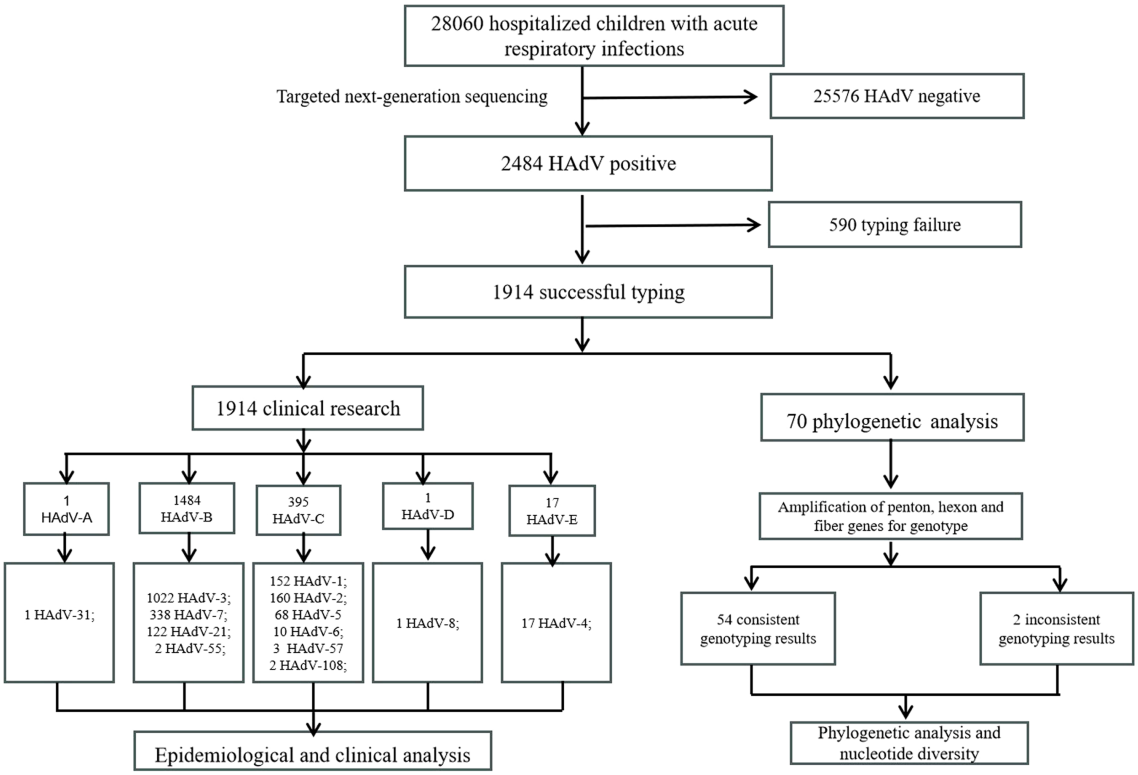

FIGURE 1
Flow diagram of study design.

2.3 Phylogenetic and amino acid mutation analysis

For preliminary genotyping analysis, the 188 successfully sequenced nucleotide fragments were aligned against the NCBI database (https://www.ncbi.nlm.nih.gov). Reference sequences comprising prototype strains with definitive genotypes and circulating strains exhibiting >99% nucleotide identity to study isolates were downloaded from GenBank. Sequences with length <1000 bp were excluded. Multiple sequence alignment was performed using ClustalW, followed by trimming all sequences to uniform length. Maximum likelihood trees were reconstructed in MEGA-X (v10.2.6) with branch support assessed by 1000 bootstrap replicates. Nucleotide and amino acid sequence homology analyses, along with mutational profiling, were performed using BioEdit v7.2.0 (https://www.mbio.ncsu.edu/BioEdit/page2.html). The sequences of the Hexon, Penton base, and Fiber genes characterized in this study have been deposited in the GenBank database under accession number PV106134-PV106159.

2.4 Recombination analysis

For strains exhibiting genotypic discordance across the Penton, Hexon, and Fiber genes (indicative of potential recombination), the trimmed nucleotide sequences of these three genes from each suspected recombinant strain were concatenated in-frame. Corresponding gene sequences from Human adenovirus C (HAdV-C) prototype strains and closely related, genotypically well-defined circulating strains retrieved from GenBank were similarly trimmed, aligned with the study sequences, and concatenated. Recombination events within the concatenated sequences were assessed using the RDP5 software package, employing seven detection algorithms: RDP, GENECONV, 3Seq, Chimaera, SiScan, MaxChi, and LARD. Recombination events detected by at least five methods with a p-value < 0.05 were considered statistically supported. Putative recombination breakpoints identified by RDP5 were further characterized and visualized using SimPlot software (version 3.5.1), with the suspected recombinant strain as the query sequence. BootScan analysis was performed using a window size of 200 nucleotides (nt), a step size of 20 nt, 100 replicates, gap stripping enabled, and the Kimura 2-parameter distance model.

2.5 Nucleotide diversity analysis

Nucleotide diversity plots were constructed using the DNA Sequence Polymorphism software (DnaSP v5.10.01; www.ub.edu/dnasp/). Sites with alignment gaps were excluded. The analysis was performed with a sliding window length of 100 bps and step size of 25 bps.

2.6 Statistical analysis

Statistical analysis was performed using IBM SPSS Statistics (version 23.0). Continuous variables were described as mean ± standard deviation for normally distributed data or median with interquartile range (IQR) for nonparametric distributions. Continuous variables were compared using the *t*-test or the Mann-Whitney U test. Categorical data were displayed as numbers and percentages, and were compared by chi-square test or Fisher's exact test, as appropriate. Each statistical test was two-sided, and *P* values of <0.05 were considered statistically significant.

3 Results

3.1 Characteristics of inpatient children with ARIs

Between March 2022 and March 2024, a total of 28,060 pediatric patients were hospitalized with ARIs. The cohort comprised 15,584 males (55.5%) and 12,476 females (44.5%), yielding a male-to-female ratio of 1.25:1. Notably, 45.1% of cases (12,655/28,060) involved children under 3 years of age.

3.2 Epidemiological characteristics of HAdV infection in children with ARIs

A total of 28,060 children with ARIs were enrolled in the study, and 2,484 cases (8.9%) were identified as positive for HAdV. Among these, 1,435 (57.8%) were male and 1,049 (42.2%) were female. The detection rate of HAdV was higher in males (9.2%, 1435/15584) than in females (8.4%, 1049/12476), and the difference was significant (χ^2 =5.496, P = 0.019). All cases were categorized into four age groups: infants (<1 year), toddlers (1–<3 years), preschoolers (3–<6 years), and school-aged children (6–<18 years). Among all age groups, the HAdV detection rate was highest in the 6–18 years age group (10.4%), and the difference was statistically significant (χ^2 =97.022, P < 0.001). HAdV infections were detected throughout the year, and a significant difference was observed in the HAdV detection rate across seasons (χ^2 =834.146, P < 0.001), with the highest detection rate of HAdV in winter (15.9%, 1315/8266). To investigate the temporal trends in HAdV prevalence, we analyzed the monthly distribution of positive samples. Notably, significant peaks in detection rates were observed during specific months: January 2023 (23.9%, 16/67), December 2023 (17.1%, 520/3046), and January 2024 (16.8%, 489/2914). In contrast, strikingly low HAdV positivity was detected in August 2022 (2.3%, 13/566) and March 2023 (2.3%, 8/355). The clinical and epidemiological data are shown in Table 1 and Figure 2.

TABLE 1 HAdV-positive in children of different ages and gender with ARIs.

Variable	Total ARIs (N (%))	HAdV-positive (N (%))	χ^2	*P*
Sex			5.496	**0.019**
Male	15584 (55.5)	1435 (9.2)		
Female	12476 (44.5)	1049 (8.4)		
Age group			97.022	< **0.001**
Infant (<1 Year)	7323 (26.1)	458 (6.3)		
Toddler (1 Year to <3 Year)	5332 (19.0)	456 (8.6)		
Preschool (3 Year to <6 Year)	7113 (25.3)	708 (10.0)		
School (6 Year to <18 Year)	8292 (29.6)	862 (10.4)		
Season			834.146	< **0.001**
Spring (Mar-May)	3981 (14.2)	393 (9.9)		
Summer (Jun-Aug)	7347 (26.2)	294 (4.0)		
Autumn (Sep-Nov)	8466 (30.2)	482 (5.7)		
Winter (Dec-Feb)	8266 (29.5)	1315 (15.9)		
Total	28060 (100.00)	2484 (8.9)		

Values showing statistically significant differences are indicated in bold (P < 0.05).

3.3 Distribution characteristics of HAdV genotypes

A total of 1914 specimens were successfully genotyped, revealing 13 distinct HAdV types spanning species B, C, D, and E (Figure 3A). The epidemiological profile demonstrated HAdV-3 as the predominant type (53.4%, 1022/1914), followed in descending order by HAdV-7 (17.7%, 338/1914), HAdV-2 (8.4%, 160/1914), HAdV-1 (7.9%, 152/1914), HAdV-21 (6.4%, 122/1914), and HAdV-5 (3.6%, 68/1914). Sporadic cases (<1% prevalence) included HAdV-4 (17/1914), HAdV-6 (10/1914), HAdV-57 (3/1914), HAdV-55 (2/1914), HAdV-108 (2/1914), HAdV-8 (1/1914), and HAdV-31 (1/1914). Notably, 16 co-infection cases were characterized, with HAdV-1/HAdV-2 (*n*=7) was the most frequent, followed by HAdV-1/HAdV-3 (n=2), HAdV-1/HAdV-5 (*n*=2), HAdV-2/HAdV-5 (*n*=2), with single occurrences of HAdV-3/HAdV-21, HAdV-3/HAdV-7, and HAdV-5/HAdV-7. Temporal analysis revealed that samples genotyped prior to August 2023

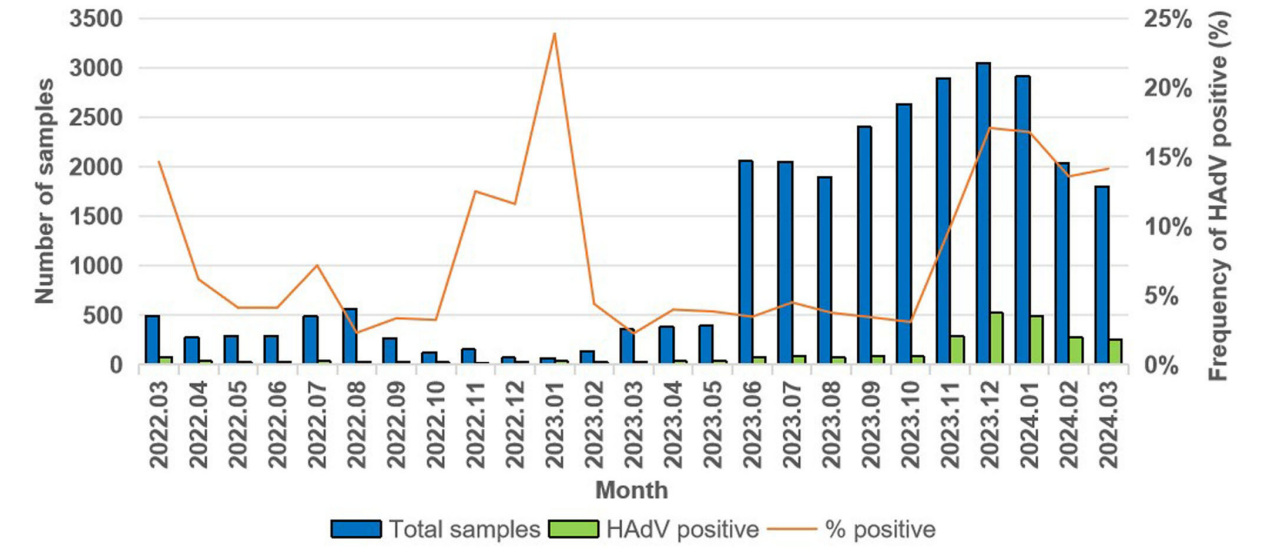

FIGURE 2
Monthly distribution of HAdV infection in children with ARIs in Tianjin from March 2022 to March 2024.

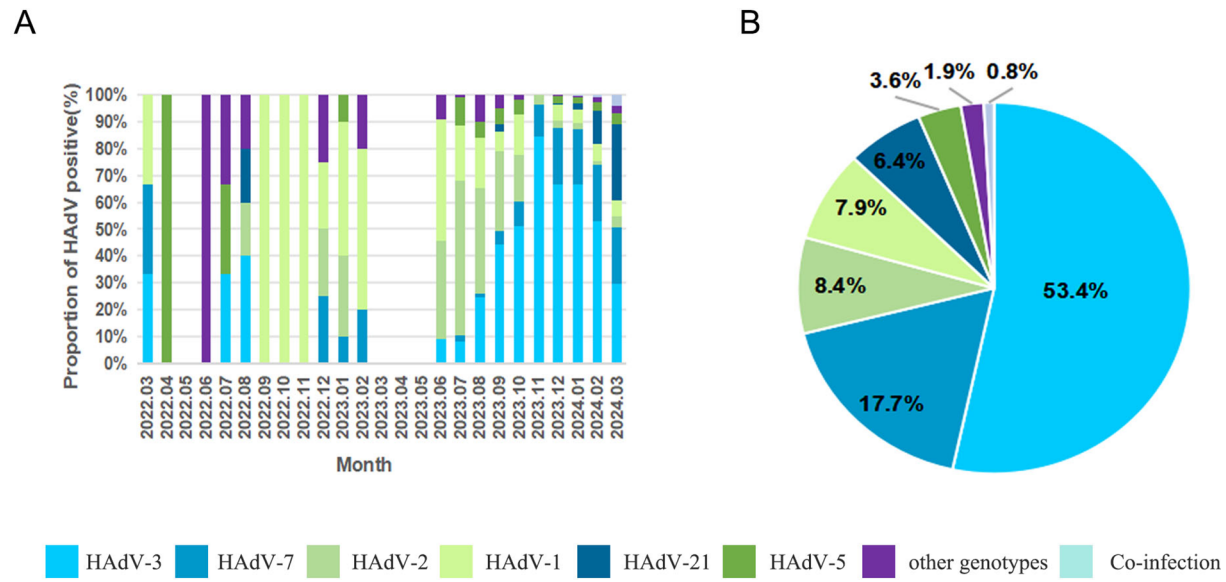

FIGURE 3
The distributions of human adenovirus types detected in children with acute respiratory infections. **(A)** HAdV genotype distribution of ARI in patients by month; **(B)** HAdV genotype distribution of ARI inpatients.

exhibited a higher prevalence of the HAdV-C species, whereas those genotyped after August 2023 showed a dominance of the HAdV-B species (Figure 3B).

3.4 Demographic and clinical characteristics of different HAdV genotypes

3.4.1 HAdV genotypes according to age

To investigate age-specific epidemiological patterns of HAdV infection in children, patients were stratified into four distinct age categories: infants (<1 year of age), toddlers (1–3 years), preschoolers (3–6 years), and school-aged children (6–18 years). Significant differences in HAdV type distribution were observed across age groups (χ^2=111.479, $P < 0.001$). The HAdV-3/HAdV-7 dominance pattern persisted across all age strata, particularly accentuated in school-aged children, where HAdV-3 accounted for 62.2% of cases, followed by HAdV-7 at 21.2%. Moreover, distinct age-specific prevalence peaks were observed. HAdV-2, -5, and -21 showed maximal detection during infancy (13.7%, 6.9%, 9.0%), while HAdV-1 demonstrated its highest infection rate in toddlers (12.2%) (Figure 4A).

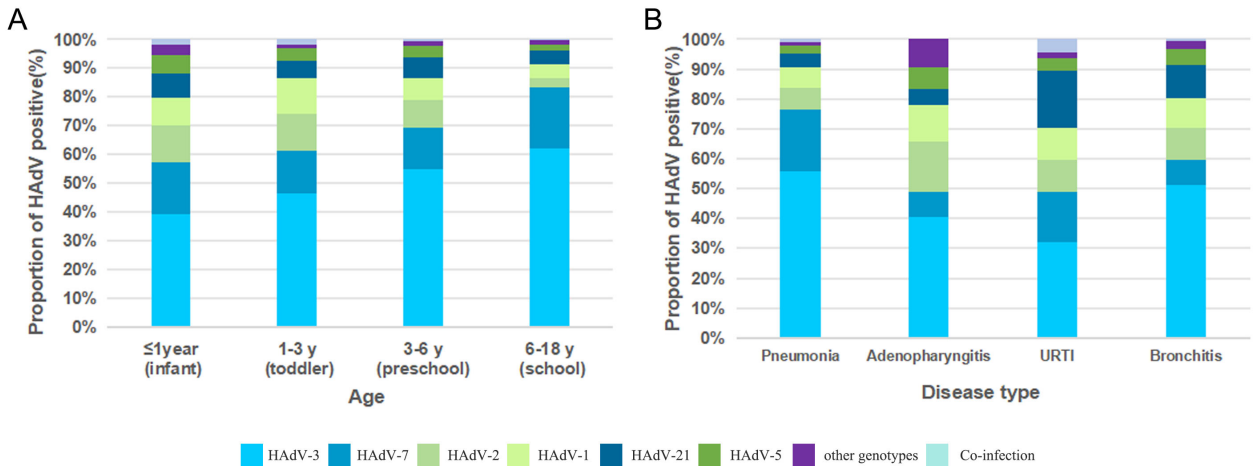

FIGURE 4
(A) HAdV genotype distribution of ARI inpatients by age; **(B)** HAdV genotype distribution of ARI inpatients by disease type.

3.4.2 HAdV genotypes according to the disease type

Significant differences in HAdV-type distribution were observed among various clinical diagnoses (χ^2 =104.385, P < 0.001). Analysis of 1,914 confirmed cases revealed pneumonia as the predominant diagnosis (72.2%, 1,382/1,914), followed by bronchitis (20.3%, 389/1,914). In contrast, adenopharyngitis (5.0%, 96/1,914) and URTIs (2.5%, 47/1,914) represented relatively smaller proportions of the total cases. Notably, HAdV-3 maintained predominance across all disease entities, particularly in pneumonia (55.6%, 769/1382) and bronchitis (51.2%, 199/389). Diagnosis-specific secondary genotypes emerged: HAdV-7 constituted 20.9% (289/1382) of pneumonia cases, while HAdV-2 accounted for 16.7% (16/96) of adenopharyngitis cases. Notably, HAdV-21 demonstrated dual clinical relevance, representing 11.1% (43/389) of bronchitis cases and 19.1% (9/47) of URTIs (Figure 4B).

3.4.3 Clinical characteristics of different HAdV types infections in children with pneumonia

Focusing on the predominant HAdV-3 (n=769) and HAdV-7 (n=289) pneumonia cases, we conducted comparative analyses with other HAdV types of pneumonia (n=324). No sex-based differences were observed across groups (χ^2 =1.469, P =0.480). Age stratification revealed a significant difference (χ^2 =106.821, P < 0.001), with school-aged children predominating in both HAdV-3 (62.4%, 337/540) and HAdV-7 (23.7%, 128/540). The clinical symptoms comprised fever (94.1%), cough (98.7%), and hyperpyrexia (74.0%), with frequent erythra and lymphadenopathy. Further analysis found that patients infected with HAdV-7 exhibited marked clinical severity, showing longer Duration of hospitalization, prolonged fever duration, and higher incidence of high fever than other groups (χ^2 =18.93, P < 0.001; χ^2 =24.369, P < 0.001; χ^2 =28.165, P < 0.001). These findings collectively indicated that HAdV-7 infections were more likely to develop severe pneumonia (χ^2 =42.434, P < 0.001). In addition, transcutaneous oxygen saturation levels in this group were significantly lower compared to other groups (χ^2 =11.585, P =0.003). Gastrointestinal symptoms were also observed in a subset of patients, including vomiting, diarrhea, abdominal pain. Wheezing demonstrated a higher prevalence in children infected with other types of HAdV (χ^2 =8.5, P =0.014).

Within the HAdV-7 cohort, a higher prevalence of underlying conditions was observed among patients, such as anemia (n=13), immunodeficiency (n=3), congenital heart disease (n=9), epilepsy (n=2), fatty liver (n=9), developmental delays (n=1), and growth retardation (n=1). Furthermore, intrapulmonary complications occurred more frequently in HAdV-7 infection cases compared to other types HAdV. Specifically, the incidence of pulmonary atelectasis (χ^2 =8.797, P =0.012), pleurisy (χ^2 =11.344, P =0.003), pleural effusion (χ^2 =19.629, P < 0.001), and plastic bronchitis (χ^2 =27.587, P < 0.001) was significantly higher in this group than other groups. Extrapulmonary complications also showed a higher incidence in cases of HAdV-7 infection, particularly abnormal coagulation function, liver injury, and gastrointestinal dysfunction. Statistical analysis found that there were significant differences among the three groups in terms of the incidence of myocardial injury (χ^2 =13.166, P <0.001), toxic encephalopathy, or encephalitis (χ^2 =10.236, P =0.004). Importantly, children infected with HAdV-7 have a higher probability of receiving immunoglobulin therapies and fiberoptic bronchoscopy procedures compared to other groups (χ^2 =24.333, P < 0.001; χ^2=93.644, P < 0.001) (Table 2).

3.5 Phylogenetic analysis

To further analyze the HAdV genotype, the Hexon, Penton base, and Fiber genes of 70 HAdV-positive samples were amplified using conventional PCR in this study. Finally, the three genes of 56 samples were successfully sequenced simultaneously. Comparative analysis of sequence homology between established HAdV genotypes and their prototype strains revealed consistently high nucleotide and amino acid conservation across all examined genetic lineages (Table 3). Phylogenetic analysis of HAdV Hexon, Penton base, and Fiber genes demonstrated the genotyping results of 54 samples were consistent, wherein the identified HAdV types were distributed as follows: HAdV-3 (25.9%, 14/54), HAdV-7 (13.0%, 7/54), HAdV-21 (42.6%, 23/54), HAdV-1 (7.4%, 4/54), HAdV-4 (3.7%, 2/54), HAdV-5 (3.7%, 2/54), HAdV-89 (1.9%, 1/54), and HAdV-14 (1.9%, 1/54). However, the Penton gene sequences from the remaining two cases (TJ2024-734, H5F5; TJ2023-142, H1F2) could not be definitively typed (Figure 5).

3.5.1 Phylogenetic tree of the Penton gene

In the Penton-based phylogenetic tree, the 13 HAdV-3 sequences obtained in this study, except for TJ2024-481, were completely identical and clustered with BJ2018 (MW748652.1) and SX2018 (OQ128172.1), with an average genetic distance of 0.0025 within the cluster. The 7 HAdV-7 sequences obtained in this study were entirely identical and clustered tightly with GZ2019 (MT895666.1) and JL2014 (MT019940.1), showing an average intra-cluster genetic distance of 0.0024. Interestingly, the Penton gene of the HAdV-3 isolate exhibited relatively high similarity to its prototype strain, reaching 98.1%-98.2%. However, it did not form a cluster with the prototype. Further nucleotide concordance analysis demonstrated that the HAdV-3 Penton sequences in this study showed even higher concordance with both the HAdV-7 prototype (99.2%-99.3%) and studied sequences (99.5%). The sole HAdV-14 clinical isolate clustered robustly with BJ2010 (JN032132.1) and GZ2010 (MF062484.1), presenting an average intra-cluster genetic distance of 0.0020. Additionally, all 22 HAdV-21 sequences, except TJ2024-749, were entirely identical and grouped into a clade with GZ2020 (MW151243.1) and USA2009 (OR753097.1), with an average intra-cluster genetic distance of 0.0017. For HAdV-4, the three Penton sequences obtained in this study were completely identical and clustered tightly with BJ2018 (OP715945.1) and USA2022 (OP785763.1), these sequences showed only 96.4% nucleotide identity with their prototype strain, and the average intra-cluster genetic distance was calculated as 0.0242. Phylogenetic analysis further revealed that HAdV-C strains could not be fully

TABLE 2 Clinical manifestations and outcomes among children hospitalized with adenovirus pneumonia.

Characteristics	Group				χ^2/Z	P
	HAdVs (n=1382)	HAdV-3 (n=769)	HAdV-7 (n=289)	Others (n=324)		
Gender					1.469	0.48
Male	796 (57.6)	437 (56.8)	163 (56.4)	196 (60.5)		
Female	586 (42.4)	332 (43.2)	126 (43.6)	128 (39.5)		
Age (year)					106.821	**<0.001**
≤1y (infant)	258 (18.7)	111 (14.4)	57 (19.7)	90 (27.8)		
1–3 y (toddler)	220 (15.9)	112 (14.6)	43 (14.9)	65 (20.1)		
3–6 y (preschool)	364 (26.3)	209 (27.2)	61 (21.1)	94 (29.0)		
6–18 y (school)	540 (39.1)	337 (43.8)	128 (44.3)	75 (23.1)		
Clinical manifestation						
Duration of hospitalization(d) [M (P25, P75)]	5 (4,7)	5 (4,7)	6 (4.5,7)	5 (4,6)	18.93	**<0.001**
Fever [n (%)]	1300 (94.1)	729 (94.8)	279 (96.5)	292 (90.1)	12.931	**0.002**
Hyperpyrexia (≥ 39°C) [n (%)]	1022 (74.0)	593 (77.1)	226 (78.2)	203 (62.7)	28.165	**<0.001**
Highest temperature (°C) [M (P25, P75)]	39.4 (38.9,40)	39.5 (39,40)	39.4 (39,40)	39 (38.5,39.6)	42.91	**<0.001**
Duration of fever(d) [M (P25, P75)]	4 (3,7)	5 (3,7)	5 (3,7)	3 (2,6)	24.369	**<0.001**
Breathe (times/min) [M (P25, P75)]	22 (24,27)	21 (24,26)	21 (24,27)	22 (24,28)	2.077	0.126
SpO2(%)	98 (97,98)	98 (97,98)	98 (96,98)	98 (96.25,98)	11.585	**0.003**
Cough [n (%)]	1364 (98.7)	760 (98.8)	286 (99)	318 (98.1)	1.059	0.589
Wheezing [n (%)]	109 (7.9)	48 (6.2)	24 (8.3)	37 (11.4)	8.5	**0.014**
Conjunctivitis [n (%)]	39 (2.8)	24 (3.1)	3 (1.0)	12 (3.7)	4.523	0.104
Vomiting [n (%)]	241 (17.4)	128 (16.6)	58 (20.1)	55 (17.0)	1.774	0.412
Chest pain [n (%)]	20 (1.4)	7 (0.9)	8 (2.8)	5 (1.5)	4.913	0.069
Stomachache [n (%)]	115 (8.3)	74 (9.6)	28 (9.7)	13 (4.0)	10.301	**0.006**
Diarrhea [n (%)]	60 (4.3)	25 (3.3)	15 (5.2)	20 (6.2)	5.32	0.07
Erythra [n (%)]	90 (6.5)	54 (7.0)	15 (5.2)	21 (6.5)	1.158	0.573
Headache [n (%)]	37 (2.7)	25 (3.3)	7 (2.4)	5 (1.5)	2.643	0.264
Lymphadenopathy [n (%)]	70 (5.1)	50 (6.5)	5 (1.7)	15 (4.6)	10.114	**0.006**
Comorbid disease [n (%)][a]	122 (8.8)	56 (7.3)	38 (13.1)	28 (8.6)	9.001	**0.011**
Pulmonary complications						
Emphysema [n (%)]	14 (1.0)	7 (0.9)	4 (1.4)	3 (0.9)	0.687	0.714
Pulmonary atelectasis [n (%)]	112 (8.1)	65 (8.5)	32 (11.1)	15 (4.6)	8.797	**0.012**
Pleurisy [n (%)]	373 (27.0)	204 (26.5)	98 (33.9)	71 (21.9)	11.344	**0.003**
Pleural effusion [n (%)]	74 (5.4)	35 (4.6)	30 (10.4)	9 (2.8)	19.629	**<0.001**
Respiratory failure [n (%)]	5 (0.4)	3 (0.4)	2 (0.7)	0	1.886	0.321
Necrotizing pneumonia [n (%)]	6 (0.4)	4 (0.5)	1 (0.3)	1 (0.3)	0.263	1
Plastic bronchitis [n (%)]	63 (4.6)	32 (4.2)	28 (9.7)	3 (0.9)	27.587	**<0.001**

(Continued)

TABLE 2 Continued

Characteristics	Group				χ^2/Z	P
	HAdVs (n=1382)	HAdV-3 (n=769)	HAdV-7 (n=289)	Others (n=324)		
Extrapulmonary complications						
Liver injury [n (%)]	65 (4.7)	36 (4.7)	19 (6.6)	9 (2.8)	4.148	0.126
Myocardial injury [n (%)]	19 (1.4)	7 (0.9)	11 (3.8)	1 (0.3)	13.166	**0.001**
Abnormal coagulation function [n (%)]	204 (14.8)	128 (16.6)	46 (15.9)	30 (9.3)	10.271	**0.006**
Gastrointestinal dysfunction [n (%)]	94 (6.8)	52 (6.8)	26 (9.0)	16 (4.9)	3.973	0.137
Toxic encephalopathy or encephalitis	21 (1.5)	7 (0.9)	11 (3.8)	3 (0.9)	10.236	**0.004**
Urinary system injury [n (%)]	17 (1.2)	11 (1.4)	2 (0.7)	4 (1.2)	0.771	0.755
Pyemia [n (%)]	17 (1.2)	13 (1.7)	3 (1.0)	1 (0.3)	3.52	0.156
Severe pneumonia [n (%)]	364 (26.3)	197 (25.6)	114 (39.4)	53 (16.4)	42.434	**<0.001**
Treatment						
Immunoglobulin therapy [n (%)]	132 (9.6)	70 (9.1)	47 (16.3)	15 (4.6)	24.333	**<0.001**
Bronchoscope [n (%)]	525 (38.0)	315 (41.0)	155 (53.6)	55 (17.0)	93.644	**<0.001**
Endotracheal intubation [n (%)]	9 (0.7)	6 (0.8)	3 (1.0)	0	2.99	0.23

Values showing statistically significant differences are indicated in bold ($P < 0.05$)
[a]Including anemia, immune deficiency, congenital heart disease, malnutrition, epilepsy, fatty liver, developmental delay, and underdevelopment.

differentiated based on Penton gene sequences alone, with an average intra-cluster genetic distance of 0.0146 (Figure 5A). A comparative analysis of nucleotide polymorphisms indicated that the Penton gene of HAdV-C exhibited a lower nucleotide diversity (1.4%) compared to Hexon (10.4%) and Fiber (18.9%). Furthermore, the Penton gene nucleotide diversity of HAdV-C species was lower than that of HAdV-B (8.8%) and HAdV-E (1.5%) (Figure 6).

3.5.2 Phylogenetic tree of the Hexon gene

Phylogenetic analysis of the Hexon gene indicated that three species of HAdV, including 11 different types, were identified throughout the study period (Figure 7). In this study, the HAdV-3 isolates clustered with BJ2018 (MW748652.1) and NMG2019 (MW767985.1), exhibiting an average genetic distance of 0.0022 within the group. The six HAdV-7 sequences were completely identical except for TJ2024-656. However, they did not cluster with the prototype strain, displaying a nucleotide sequence identity of only 95.7%, resulting in an average genetic distance of 0.0115 within the group. The HAdV-14 strain obtained clustered with GZ2010 (MF062484.1) and BJ2010 (JN032132.1), showing an average genetic distance of 0.0009. Additionally, the 23 HAdV-21 isolates exhibited a nucleotide similarity ranging from 99.9% to 100.0%, clustering with GZ2019 (MW151243.1) and presenting an average genetic distance of 0.0009 within the group. The 3 HAdV-4 sequences, with the exception of TJ2024-651, were identical and clustered with BJ2018 (OP715934.1) and GZ2013 (KF006344.1), with an average genetic distance of 0.0152 within the group.

TABLE 3 The nucleotide and amino acid identified of Penton, Hexon and Fiber.

Species	Genotypes	Percent identity of nucleotide (nt%)			Percent identity of amino acid (nt%)		
		Penton	Hexon	Fiber	Penton	Hexon	Fiber
HAdV-B	HAdV-3	98.1-98.2	98.6-98.7	98.3-98.4	98.7-98.9	98.6-98.7	96.3-96.6
	HAdV-7	99.1	95.7	99.3	99.1	96.8	98.5
	HAdV-14	99.8	99.8	99.9	99.0	99.3	98.8
	HAdV-21	99.3-99.4	98.9-99.1	99.3-99.4	93.7-94.2	97.2-98.0	98.8-99.1
HAdV-C	HAdV-1	99.6-99.8	99.8-99.9	98.9-99.8	99.7-99.8	99.5-99.8	98.3-99.5
	HAdV-89	99.4	99.9	99.9	99.7	99.6	100
	HAdV-5	98.4-98.5	95.5	99.5-99.6	98.2	98.5	99.5
HAdV-E	HAdV-4	96.4	97.6	98	96.1	97.5	97.9

10.3389/fcimb.2025.1600990

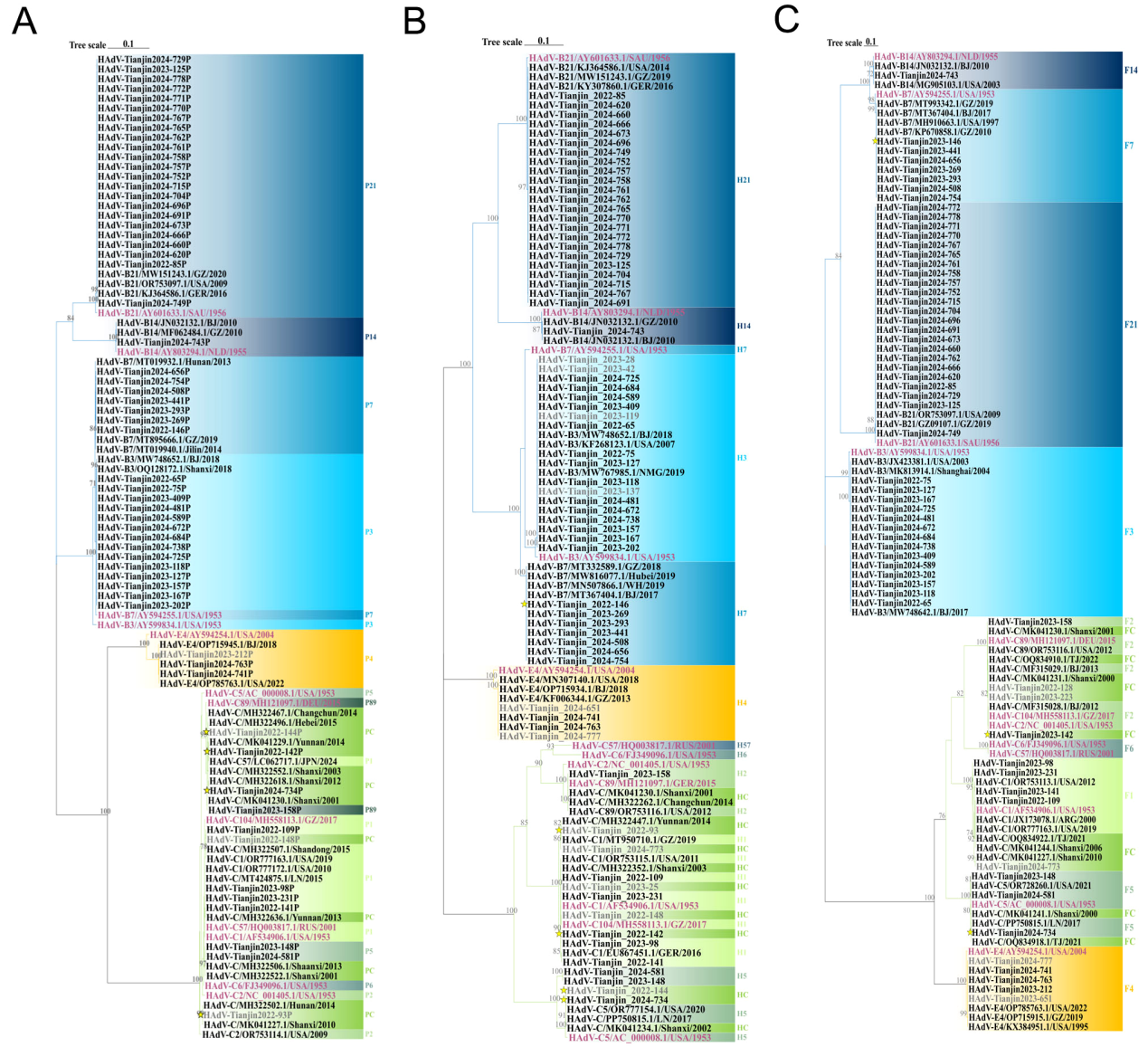

FIGURE 5
Phylogenetic tree constructed on the basis of the nucleotide sequences of the Penton base **(A)**, Hexon **(B)** and Fiber **(C)** gene sequences of the isolation. Additional reference sequences were retrieved from GenBank to provide context and reference. The original strains are marked in purple, strains that failed to successfully amplify three gene sequences simultaneously are marked in gray, strains with inconsistent gene sequence typing results are represented. by yellow stars. The phylogenetic tree is constructed using ML method, and the values at the branch nodes represent the Bootstrap support for 1000 repetitions (only displaying values ≥ 70%).

Furthermore, both HAdV-1 and 2 were found to be capable of being divided into two distinct branches. Interestingly, the HAdV-1 sequences obtained in this study primarily clustered with the prototype strains to form cluster 1. However, two samples, TJ2022–93 and TJ2024-773, grouped with YN2014 (MH322447.1) and GZ2019 (MT950710.1) to form cluster 2. The average genetic distances within the groups of cluster 1 and cluster 2 were 0.0043 and 0.0015, respectively, and the average genetic distances between groups was 0.0065. The HAdV-2 prototype strains formed a separate cluster, while the TJ2023–158 from our study and HAdV-89 prototype strains, along with SX2001 (MK041230.1), CC2014 (MH322262.1), and USA2012 (OR753116.1), were grouped into another cluster. The average genetic distance between this cluster and the HAdV-2 prototype strain was 0.0074. The 4 HAdV-5 sequences obtained were divided into two clusters. In the first cluster, the sequences of TJ2024–581 and TJ2023–148 were identical, showing 95.5% nucleotide sequence identity to the prototype strain. In the second cluster, TJ2024–734 and TJ2022–144 were identical and clustered with SX2002 (MK041234.1) and LN2017 (PP750815.1), displaying 99.2% nucleotide sequence identity with the prototype strain. The average genetic distance within this cluster was 0.0259 (Figure 5B).

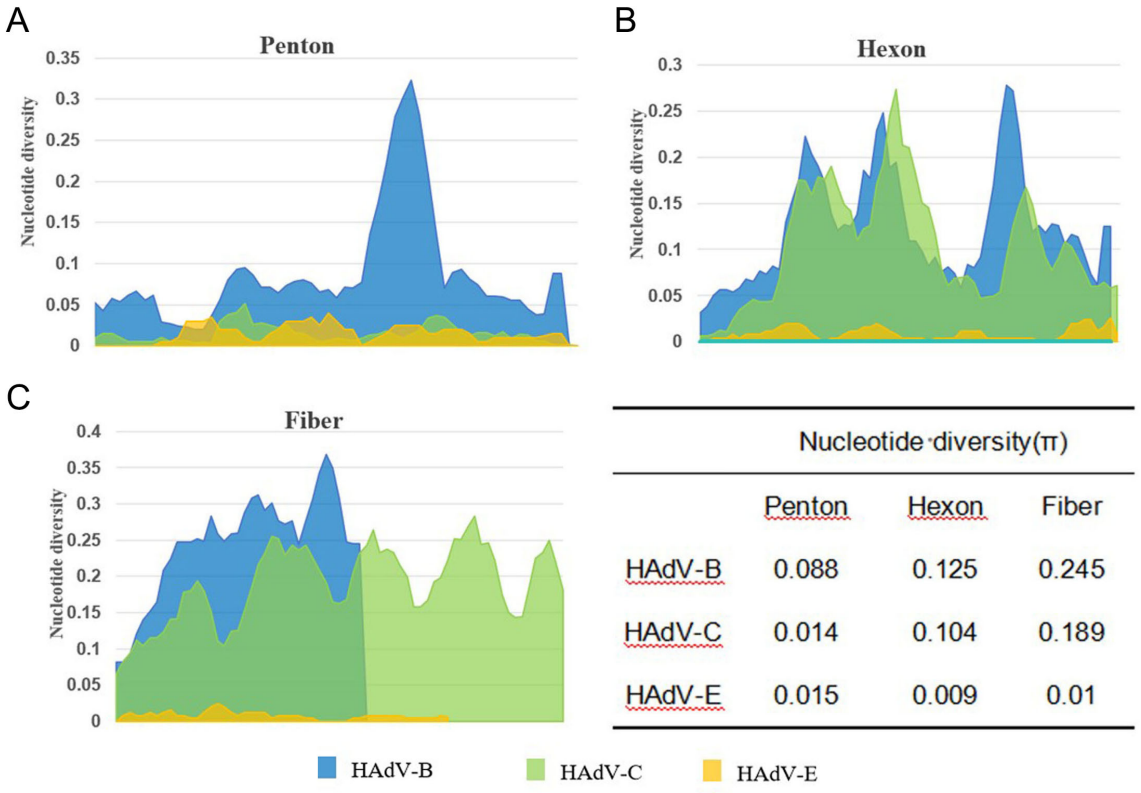

	Nucleotide diversity(π)		
	Penton	Hexon	Fiber
HAdV-B	0.088	0.125	0.245
HAdV-C	0.014	0.104	0.189
HAdV-E	0.015	0.009	0.01

FIGURE 6
Nucleotide diversity plots showing the average number of nucleotide differences per site along each gene for HAdV-B, C and E, calculated for Penton base **(A)**, Hexon **(B)**, and Fiber **(C)** prototype sequences.

3.5.3 Phylogenetic tree of the Fiber gene

In the phylogenetic analysis of the Fiber gene, a clear separation of genotypes was well-supported. Among the 14 HAdV-3 sequences obtained, a discrepancy was observed only at nucleotide position 214. These sequences clustered with SH2004 (MK813914.1) and BJ2017 (MW748642.1), with an average genetic distance of 0.0026 within the group. The 7 HAdV-7 sequences exhibited complete congruence and clustered with GZ2010 (KP670858.1) and BJ2017 (MT367404.1), showing an average genetic distance of 0.0020. The HAdV-14 sequence shared a cluster with BJ2010 (JN032132.1), displaying an average genetic distance of 0.0010. Excluding TJ2024-749, the 22 sequences of HAdV-21 were entirely consistent and clustered with GZ2019 (GZ09107.1) with an average genetic distance of 0.0006. The 5 HAdV-4 sequences were also found to be completely consistent, clustering alongside GZ2019 (OP715915.1), with an average genetic distance of 0.0078. Interestingly, HAdV-1 was categorized into two clusters, with the 4 HAdV-1 sequences showing a consistency of 98.1% to 99.9%, resulting in an average genetic distance of 0.0109 within the cluster. Additionally, TJ2023–158 clustered with the HAdV-89 prototype strain SX2001 (MK041230.1), while TJ2022-128, TJ2023-142, and TJ2023–223 clustered with the HAdV-2 prototype strains BJ2012 (MF315028.1) and GZ2017 (MH558113.1). The nucleotide identity among these four sequences ranged from 99.3% to 99.8%, with an average genetic distance of 0.0031 within the cluster. The three HAdV-5 sequences obtained were 99.3%-99.9% concordant and clustered with LN2017 (PP750815.1), TJ2021 (OQ834919.1), with an average genetic distance of 0.0042 within the cluster (Figure 5C).

3.6 Recombination analysis

For strains TJ2024–734 and TJ2023-142, multiple algorithms within RDP5 (≥5 algorithms) consistently and highly significantly ($p << 0.01$) detected identical recombination breakpoint positions and identical parental combinations (Figure 7).

SimPlot and BootScan analyses for TJ2024–734 revealed clear evidence of recombination within its concatenated Penton-Hexon-Fiber sequence relative to reference strains OR735212.1 and AC_000008.1. Upstream of approximately nt 1000, TJ2024–734 exhibited strong bootstrap support (>75%) with reference strain OR735212.1. Downstream of approximately nt 1300, high bootstrap support (>90%) shifted to reference strain AC_000008.1. This sharp transition around nt 1000–1300 indicates a recombination breakpoint, consistent with the RDP-predicted breakpoint location (nt 820-1141). The SimPlot profile clearly showed distinct peaks of sequence similarity to the different reference strains across the genomic regions, strongly indicating that TJ2024–734 is a recombinant strain.

For TJ2023-142, SimPlot and BootScan analyses revealed distinct phylogenetic patterns across different genomic regions:

10.3389/fcimb.2025.1600990

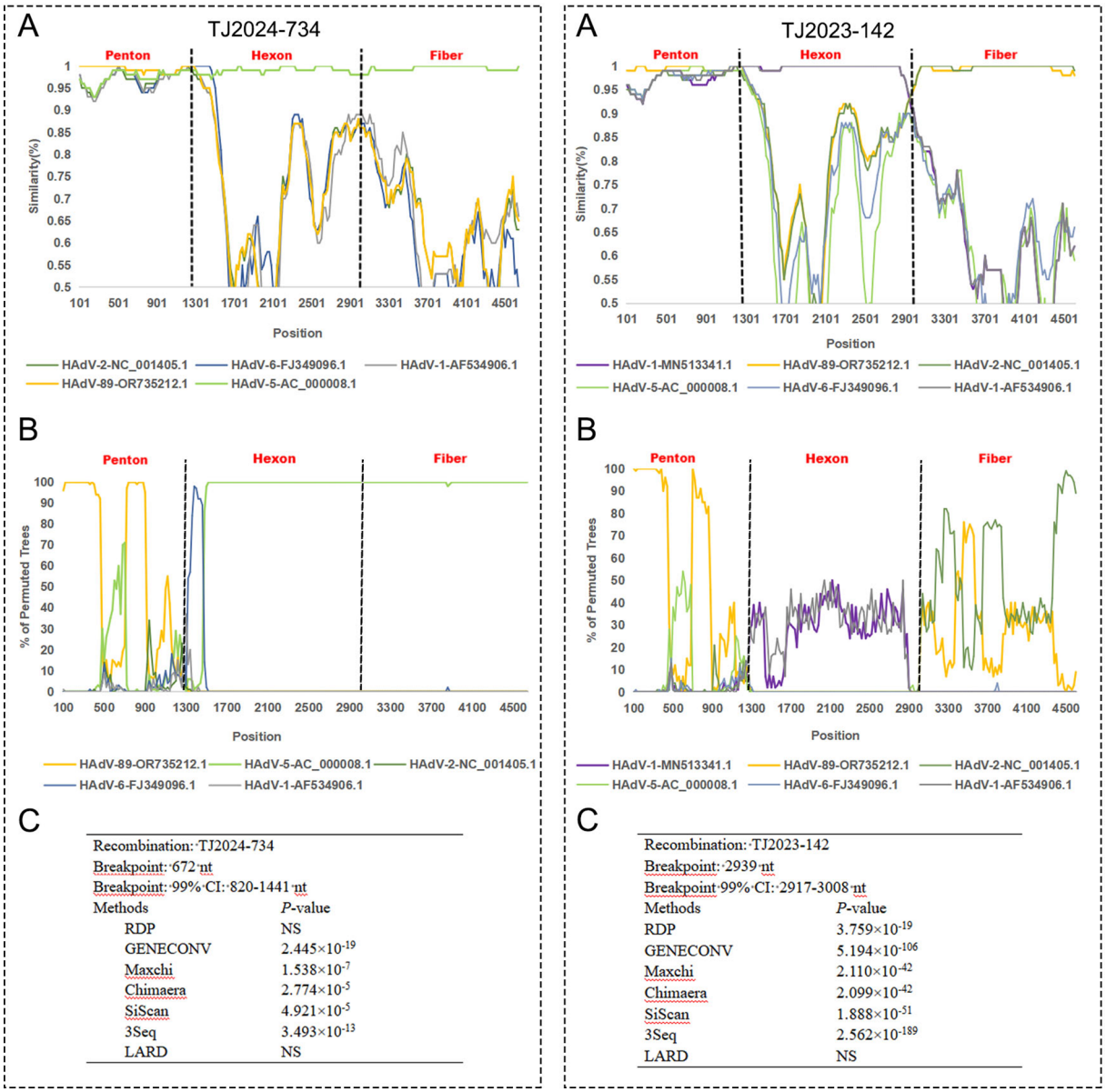

FIGURE 7
Recombination analysis of TJ2024–742 and TJ2023–142 with other HAdV-C species using SimPlot **(A)**, BootScan **(B)** and RDP **(C)**. The analysis supports TJ2024–742 as a recombinant strain.

the Penton region showed strong bootstrap support (>75%) for reference strain OR735212.1. The Hexon region exhibited consistently low bootstrap support (<50%) across all reference strains, although MN513341.1 displayed slightly higher affinity (~50%). The Fiber region showed moderate bootstrap support (40-75%) for OR735212.1. Despite the reduced bootstrap support in the Hexon region, several lines of evidence strongly suggest TJ2023–142 is a recombinant strain (1): RDP5 consistently detected a highly significant recombination breakpoint ($p < 0.01$) at nt 2917-3008 (Hexon-Fiber junction) (2); SimPlot analysis showed nearly 100% sequence identity between the TJ2023–142 Hexon region and MN513341.1; and (3) the Penton and Fiber regions maintained high sequence similarity (Bootstrap >75%) to OR735212.1.

3.7 Amino acid mutation analysis

Using prototype strains as references, we systematically characterized amino acid polymorphisms across the Penton base, Hexon, and Fiber genes of HAdV (Figure 8). Key findings revealed that Hexon protein exhibited the highest variability with 85 polymorphic sites. Penton protein showed intermediate diversity (55 polymorphic sites). Fiber protein demonstrated the lowest variation (46 polymorphic sites). Notably, amino acid substitutions predominated over deletions in all gene products except for the HAdV-21 Penton protein, where deletion events occurred more frequently. In addition, HAdV-21 and HAdV-7 displayed a higher polymorphism rates (41 and 34 variants,

respectively). But, HAdV-89 showed remarkable sequence conservation with only 4 variants detected.

3.7.1 Amino acid mutation analysis of Penton

The Penton protein contains the Arg-Gly-Asp (RGD) sequence, which interacts with cellular integrins and thereby mediates viral endocytosis. When compared to the prototype strain, HAdV- B species exhibited 32 polymorphic sites, HAdV-C species had 10 polymorphic sites, and HAdV-E species displayed 13 polymorphic sites. Importantly, all 23 cases of HAdV-21 obtained in this study had 15 consecutive amino acid deletions at positions 313–327 within the RGD loop and two amino acid insertions downstream of the RGD motif. Compared with the prototype, it maintains 99.3-99.4% nucleotide conservation while reducing amino acid identity to 93.7-94.2%.

3.7.2 Amino acid mutation analysis of Hexon

The Hexon protein serves as the major antigenic component of HAdV and forms the basis for typing in neutralization assays. In comparison to the prototypic strains, HAdV-B species exhibited 54 polymorphic sites, HAdV-C species had 20 polymorphic sites, and HAdV-E species displayed 11 polymorphic sites. Notably, HAdV-7 possessed the highest number of polymorphic sites with 28 sites, comprising 5 deletions and 23 substitutions. The amino acid identity of HAdV-7 is only 96.8% compared to the prototype strain.

3.7.3 Amino acid mutation analysis of Fiber

The Fiber protein serves as the foundation for typing in hemagglutination inhibition assays and contains type-specific antigenic epitopes that determine viral tropism. Variants in this region may result in different histophilicity. In comparison to the prototypic strains, HAdV-B species exhibited 22 polymorphic sites, HAdV-C species had 16 polymorphic sites, and HAdV-E species displayed 8 polymorphic sites. Notably, no amino acid deletions were found in any of the strains except for HAdV-14, which had three consecutive amino acid deletions at positions 251-253.

4 Discussion

HAdV infection represents a significant etiology of ARIs in children, accounting for approximately 4%-10% of global pediatric ARIs cases (Yu et al., 2021; Zhu et al., 2021). Our surveillance in Chinese cities revealed substantial spatiotemporal variation in HAdV detection. Among hospitalized pediatric ARIs patients in Tianjin, the HAdV positive rate was 8.9%, significantly higher than Beijing (2.89%, 2015-2021) but lower than Hangzhou (26.77%, 2020-2021) (Huang et al., 2023; Wang et al., 2024).Longitudinal analysis showed cyclical fluctuations in Tianjin, peaking at 12.22% in 2019, aligning with the national trend (Liu et al., 2022; Wang et al., 2024). The implementation of NPI measures from 2020 to 2022 substantially suppressed HAdV transmission (declining to 7.82% in 2020, 172/2199). However, a resurgence was observed in 2021 as social activities resumed (9.69%, 897/9253) (Supplementary Figure S1). Parallel trends were documented in other urban centers (Wang et al., 2024). During the NPI period, the HAdV positivity rate in Tianjin was 8.78% (1,270/1,4471). Following the lifting of the NPI, there was a significant increase in both the number of ARIs patients and the absolute number of HAdV cases. However, the HAdV positivity rate remained stable at 9.12% (2,283/25,041), in contrast to the upward trend observed in Beijing and Hebei (Zhao

FIGURE 8
Amino acid alignment view of the Hexon, Penton and Fiber proteins from the selected HAdV sequences representing different genotypes. The original strains are marked in purple, the mutated amino acids are highlighted in yellow.

et al., 2024; Han et al., 2025). This 'asynchronous change' highlights the complexity of transmission dynamics in the context of co-circulation of multiple pathogens (such as RSV) (Lyu Y and Zhang, 2024).

HAdV positivity exhibited significant differences by age, gender, and season in Tianjin. Infections peaked in autumn and winter (December-January), consistent with seasonal patterns in northern temperate regions (Huang et al., 2021; Yu et al., 2021), with HAdV-3 predominating (53.4%). Contrary to previous studies reporting higher prevalence in children under 5 (Barnadas et al., 2018; Zhao et al., 2020; Huang et al., 2021; Pscheidt et al., 2021), our study found the lowest rate in 0–1 year-olds (6.25%) and the highest in 6–18 year-olds (10.4%). This shift may relate to reduced intra-family transmission during NPIs (decreasing infant exposure) and increased transmission within schools post-reopening (Huang et al., 2023; Yan et al., 2024). Gender difference analysis showed that there were more hospitalized male ARIs patients in this study, which may be related to biological factors (boys with relatively narrower airway diameters are more prone to severe lung infections (Pagtakhan et al., 1984)) and behavioral factors (girls have higher compliance with mask wearing during NPI (Huang et al., 2023)). The HAdV positivity rate was significantly higher in males (9.2% *vs.* 8.4%; $\chi^2 = 5.496$, $P = 0.019$), consistent with some studies (Pscheidt et al., 2021; Huang et al., 2023) but not others (Wang et al., 2021; Liu et al., 2022). The reasons for gender differences warrant further investigation. Clinically, male HAdV patients may require heightened vigilance for severe symptoms and pneumonia progression. Molecular epidemiology showed a shift in predominant types: HAdV-C dominated during NPIs (typically milder), rapidly replaced by HAdV-B (78.2%) post-NPIs, often associated with more severe illness (Huang et al., 2023; Wang et al., 2024). This indicates NPIs not only affect transmission but also viral type composition and community disease severity, underscoring the need for long-term subtype surveillance and early warning.

HAdV-C infections were predominantly observed in children under 3 years old (206/395, 52.2%), whereas HAdV-B3/B7 infections were more prevalent among school-aged children. In addition to the age-specific distribution, adenovirus serotypes significantly influenced disease phenotypes and severity. HAdV-3 predominated across all disease categories, especially pneumonia and bronchitis. Previous study revealed that HAdV-C frequently resides latently in adenoid tissues (Alkhalaf et al., 2013); thus, it is the second most common serotype observed in tonsillitis patient samples. Although HAdV-3 displayed higher overall prevalence, children infected with HAdV-7 more commonly progressed to severe symptoms, which may be attributed to its replication advantages: *in vitro* experiments demonstrated that HAdV-7 exhibits a higher viral load compared to HAdV-3 and induces stronger cytokine responses. Additionally, infections with HAdV-7 were more frequently associated with complications such as myocardial injury and toxic encephalopathy or encephalitis. Patients infected with this serotype exhibited a higher requirement for bronchoscopic interventions and immunoglobulin therapy. These findings suggest that HAdV-7 infections should be incorporated into pediatric severe case warning systems, prioritizing the allocation of intensive care resources for such cases (Lin et al., 2017; Fu et al., 2019; Zhao et al., 2020; Liu et al., 2022).

We identified two HAdV-C suspected recombinant samples but found no evidence of recombination in the B/E subgroups. Previous studies have shown that HAdV-C establishes persistent infections after primary infection, characterized by intermittent shedding in the host (Alkhalaf et al., 2013). Such persistence creates conditions conducive to mixed infections with different serotypes within this subgroup, thereby promoting homologous recombination between distinct viral types (Wang et al., 2024). Notably, new recombinant HAdV strains may exhibit significant alterations in pathogenicity, tissue tropism, and clinical manifestations compared to their prototype strains (Wang et al., 2021; Wu et al., 2022), highlighting the importance of conducting continuous surveillance on emergent recombinant strains. Phylogenetic analysis revealed that all types exhibited complete segregation across the three gene fragments (Bootstrap >90%), except for HAdV-C in the Penton tree (Bootstrap <70%). The observed high heterozygosity in Hexon and Fiber gene sequences indicates that these proteins may be under significant immune pressure. The sequence diversity of the HAdV-C Penton gene is notably lower than that observed for HAdV-B and HAdV-E. However, Mao et al. 's (Mao et al., 2019) research demonstrated that the HAdV-C Penton phylogenetic tree could be divided into distinct clades with robust bootstrap support, implying a greater degree of genetic diversity in the Penton gene than previously recognized.

High nucleotide consistency across HAdV types was observed, clustering with strains circulating widely in China, reflecting the slow evolutionary rate of this DNA virus—a positive factor for vaccine development. Among the 14 HAdV-3 isolates analyzed, all exhibited >98.0% nucleotide identity across three core structural genes relative to the prototype strain. This is attributed to the combined effects of HAdV DNA polymerase's high-fidelity replication, which enables HAdV-3 to maintain genomic stability for at least 50 years (Mahadevan et al., 2010). Notably, The 7 HAdV-7 strains isolated in this study exhibited low nucleotide consistency in the Hexon gene fragment, which comprises 28 sites of amino acid mutation. Research has shown that Hexon gene fragments contain specific antigenic epitopes that can stimulate the production of neutralizing antibodies in the host. Mutations in this region may result in immune escape (Lee et al., 2025). While genomic variation in HAdV-7 shows a high correlation with enhanced pathogenicity, establishing the causative relationship between specific mutation sites and the high-virulence phenotype observed in contemporary pediatric HAdV-7 strains requires further experimental data support. There are few reports of sporadic infections with HAdV-14. The singular HAdV-14 isolate showed >99.0% genomic conservation across all three genes compared to the prototype strain, and the fiber fragment contained three amino acid deletions. Studies have indicated that the fiber fragment contains type-specific antigenic epitopes that determine viral tropism, and that mutations in this region may result in different tissue tropism (Wang et al., 2014). In the HAdV-21 cohort (n=23), all except TJ2024–749 exhibited complete Penton

sequence identity with GZ2019 (MW091531.1), classifying them as 21a subvariants. Due to the presence of 15 consecutive amino acid deletion variants on the Penton fragment (residues 287-301), the amino acid consistency is low, which may affect the RGD motif mediated viral endocytosis function on Penton. This deletion results in a truncated RGD loop, exhibiting structural homology to the naturally shorter loops found in HAdV-B3 and HAdV-B7. Research suggests that this conserved deletion pattern may compromise viral internalization mediated by the RGD motif and potentially contribute to the severe lower respiratory tract tropism associated with 21a infections (Hage et al., 2014).

Although our investigation provided crucial molecular insights into the epidemiological and clinical characteristics of HAdV infections in Tianjin, China, several limitations warrant consideration. Firstly, focusing solely on hospitalized pediatric ARIs patients may introduce selection bias, potentially underestimating HAdV-C prevalence (milder cases) and skewing subtype analysis towards more severe variants like HAdV-B7. Secondly, clinical manifestations could be influenced by co-infections. Thirdly, cost constraints limited Sanger sequencing to 100 randomly selected HAdV-positive samples, reducing statistical power for nucleotide diversity analysis of some serotypes. Fourthly, recombination analysis is based on partial gene fragments (Penton, Hexon, Fiber), and there may be additional recombination events in the unanalyzed regions, which may affect the precise localization of recombination breakpoints. Finally, sampling from a single institution may limit generalizability to the broader Tianjin population. These factors may lead to underestimation of HAdV prevalence and incomplete characterization of type distribution.

This two-year study systematically characterized HAdV epidemiology among pediatric inpatients with ARIs in Tianjin, revealing key insights into prevalence, age-specific susceptibility, seasonal dynamics, and evolving genotype distributions. Significant heterogeneity in genotype distributions across clinical phenotypes was observed. These findings are crucial for optimizing diagnosis, antiviral stewardship, and region-specific vaccine development.

Data availability statement

The datasets presented in this study can be found in online repositories. The names of the repository/repositories and accession number(s) can be found below: https://www.ncbi.nlm.nih.gov/, PV106134-PV106159.

Ethics statement

The study was approved by the ethics board of Tianjin Children's Hospital (No. 2023-LXKY-004). The studies were conducted in accordance with the local legislation and institutional requirements. Written informed consent for participation in this study was provided by the participants' legal guardians/next of kin.

Author contributions

YF: Funding acquisition, Writing – review & editing, Data curation, Project administration. ML: Validation, Writing – original draft, Software, Data curation. LZ: Investigation, Formal analysis, Writing – review & editing, Methodology. MH: Data curation, Methodology, Writing – review & editing. NW: Visualization, Resources, Conceptualization, Writing – review & editing. CC: Supervision, Conceptualization, Writing – review & editing.

Funding

The author(s) declare that financial support was received for the research and/or publication of this article. This study was funded by the Scientific Research Project of Tianjin Education Commission (grant number 2022YGYB16).

Conflict of interest

The authors declare that the research was conducted in the absence of any commercial or financial relationships that could be construed as a potential conflict of interest.

Generative AI statement

The author(s) declare that no Generative AI was used in the creation of this manuscript.

Publisher's note

Supplementary material

The Supplementary Material for this article can be found online at: https://www.frontiersin.org/articles/10.3389/fcimb.2025.1600990/full#supplementary-material

References

Alkhalaf, M. A., Guiver, M., and Cooper, R. J. (2013). Prevalence and quantitation of adenovirus DNA from human tonsil and adenoid tissues. *J. Med. Virol.* 85, 1947–1954. doi: 10.1002/jmv.23678

Barnadas, C., Schmidt, D. J., Fischer, T. K., and Fonager, J. (2018). Molecular epidemiology of human adenovirus infections in Denmark, 2011-2016. *J. Clin. Virol.* 104, 16–22. doi: 10.1016/j.jcv.2018.04.012

Contes, K. M., and Liu, B. M. (2025). Epidemiology, clinical significance, and diagnosis of respiratory viruses and their co-infections in the post-COVID era. *Pathogens.* 14. doi: 10.3390/pathogens14030262

Fu, Y., Tang, Z., Ye, Z., Mo, S., Tian, X., Ni, K., et al. (2019). Human adenovirus type 7 infection causes a more severe disease than type 3. *BMC Infect. Dis.* 19, 36. doi: 10.1186/s12879-018-3651-2

Hage, E., Huzly, D., Ganzenmueller, T., Beck, R., Schulz, T. F., and Heim, A. (2014). A human adenovirus species B subtype 21a associated with severe pneumonia. *J. Infect.* 69, 4909. doi: 10.1016/j.jinf.2014.06.015

Han, T., Wang, Y., Zhang, D., Li, Y., Zhang, L., Yan, J., et al. (2025). Changes in infant respiratory pathogens pre-, during, and post-COVID-19 non-pharmacological interventions in Beijing. *Ital J. Pediatr.* 51, 8. doi: 10.1186/s13052-025-01848-5

Huang, S., Wang, H., Li, L., Xiang, W., Song, Z., and Li, W. (2023). Molecular epidemiology and phylogenetic analyses of human adenovirus in pediatric patients with acute respiratory infections from Hangzhou during COVID-19 pandemic. *Front. Pediatr.* 11. doi: 10.3389/fped.2023.1237074

Huang, Y., Wang, C., Ma, F., Guo, Q., Yao, L., Chen, A., et al. (2021). Human adenoviruses in paediatric patients with respiratory tract infections in Beijing, China. *Virol. J.* 18, 191. doi: 10.1186/s12985-021-01661-6

Huang, D., Wang, Z., Zhang, G., and Sai, L. (2021). Molecular and epidemiological characterization of human adenoviruses infection among children with acute diarrhea in Shandong Province, China. *Virol. J.* 18, 195. doi: 10.1186/s12985-021-01666-1

Ison, M. G., and Hayden, R. T. (2016). Adenovirus. *Microbiol. Spectr.* 4. doi: 10.1128/microbiolspec.DMIH2-0020-2015

Lee, D. H., Kwon, Y., Um, K. H., Yoo, J. K., Ha, W., Kim, K. S., et al. (2025). Transferrin-binding domain inserted-adenovirus hexon engineering enables systemic immune evasion and intratumoral T-cell activation. *Theranostics.* 15, 1221–1237. doi: 10.7150/thno.105163

Lin, M. R., Yang, S. L., Gong, Y. N., Kuo, C. C., Chiu, C. H., Chen, C. J., et al. (2017). Clinical and molecular features of adenovirus type 2, 3, and 7 infections in children in an outbreak in Taiwan, 2011. *Clin. Microbiol. Infect.* 23, 110–116. doi: 10.1016/j.cmi.2016.11.004

Liu, W., Qiu, S., Zhang, L., Wu, H., Tian, X., Li, X., et al. (2022). Analysis of severe human adenovirus infection outbreak in Guangdong Province, southern China in 2019. *Virol. Sin.* 37, 331–340. doi: 10.1016/j.virs.2022.01.010

Lu, M. P., Ma, L. Y., Zheng, Q., Dong, L. L., and Chen, Z. M. (2013). Clinical characteristics of adenovirus associated lower respiratory tract infection in children. *World J. Pediatr.* 9, 346–349. doi: 10.1007/s12519-013-0431-3

Lynch, J. P. 3rd, and Kajon, A. E. (2016). Adenovirus: epidemiology, global spread of novel serotypes, and advances in treatment and prevention. *Semin. Respir. Crit. Care Med.* 37, 586–602. doi: 10.1055/s-0036-1584923

Lyu Y, X. J., and Zhang, H. (2024). Clinical epidemiological characteristics of respiratory syncytial virus infection in children in single center in Tianjin. *Chin. J. Microbiol. Immunol.*, 149–154.

Mahadevan, P., Seto, J., Tibbetts, C., and Seto, D. (2010). Natural variants of human adenovirus type 3 provide evidence for relative genome stability across time and geographic space. *Virology.* 397, 113–118. doi: 10.1016/j.virol.2009.10.052

Mao, N., Zhu, Z., Rivailler, P., Yang, J., Li, Q., Han, G., et al. (2019). Multiple divergent Human mastadenovirus C co-circulating in mainland of China. *Infect. Genet. Evol.* 76, 104035. doi: 10.1016/j.meegid.2019.104035

National Health Commission of the People's Republic of China and State Administration of Traditional Chinese Medicine (2019). Guideline for diagnosis and treatment of community-acquired pneumonia in Children (2019 version). *Chin. J. Clin. Infect. Dis.* 12, 6–13.

Pagtakhan, R. D., Bjelland, J. C., Landau, L. I., Loughlin, G., Kaltenborn, W., Seeley, G., et al. (1984). Sex differences in growth patterns of the airways and lung parenchyma in children. *J. Appl. Physiol. Respir. Environ. Exerc Physiol.* 56, 1204–1210. doi: 10.1152/jappl.1984.56.5.1204

Pscheidt, V. M., Gregianini, T. S., Martins, L. G., and Veiga, A. (2021). Epidemiology of human adenovirus associated with respiratory infection in southern Brazil. *Rev. Med. Virol.* 31, e2189. doi: 10.1002/rmv.2189

Tian, X., Fan, Y., Wang, C., Liu, Z., Liu, W., Xu, Y., et al. (2021). Seroprevalence of neutralizing antibodies against six human adenovirus types indicates the low level of herd immunity in young children from guangzhou, China. *Virol. Sin.* 36, 373–381. doi: 10.1007/s12250-020-00307-1

Wang, F., De, R., Han, Z., Xu, Y., Zhu, R., Sun, Y., et al. (2024). High-frequency recombination of human adenovirus in children with acute respiratory tract infections in beijing, China. *Viruses.* 16. doi: 10.3390/v16060828

Wang, N., Fang, Y., Dong, H., Wang, L., Hou, M., Wang, W., et al. (2024). Clinical features and prediction of risk factors for severe adenovirus pneumonia in children. *Transl. Pediatr.* 13, 63–71. doi: 10.21037/tp-23-312

Wang, C., Liu, J., Mi, Y., Chen, J., Bi, J., and Chen, Y. (2021). Clinical features and epidemiological analysis of respiratory human adenovirus infection in hospitalized children: a cross-sectional study in Zhejiang. *Virol. J.* 18, 234. doi: 10.1186/s12985-021-01705-x

Wang, Z., Wang, B., Lou, J., Yan, J., Gao, L., Geng, R., et al. (2014). Mutation in fiber of adenovirus serotype 5 gene therapy vector decreases liver tropism. *Int. J. Clin. Exp. Med.* 7, 4942–4950.

Wang, X., Wang, D., Umar, S., Qin, S., Ling, Q., Gray, G. C., et al. (2021). Molecular typing of human adenoviruses among hospitalized patients with respiratory tract infections in a tertiary Hospital in Guangzhou, China between 2017 and 2019. *BMC Infect. Dis.* 21, 748. doi: 10.1186/s12879-021-06412-0

Wen, S., Lin, Z., Zhang, Y., Lv, F., Li, H., Zhang, X., et al. (2021). The epidemiology, molecular, and clinical of human adenoviruses in children hospitalized with acute respiratory infections. *Front. Microbiol.* 12. doi: 10.3389/fmicb.2021.629971

Wu, X., Zhang, J., Lan, W., Quan, L., Ou, J., Zhao, W., et al. (2022). Molecular typing and rapid identification of human adenoviruses associated with respiratory diseases using universal PCR and sequencing primers for the three major capsid genes: penton base, hexon, and fiber. *Front. Microbiol.* 13. doi: 10.3389/fmicb.2022.911694

Yan, Y., Zeng, Z., Gao, H., Zeng, S., Duan, S., Jiang, J., et al. (2024). Comparative analysis of the epidemiological characteristics of adenovirus, rotavirus A, and coinfection in children during 2014–2023 in Guangzhou. *China. Virol. J.* 21, 292. doi: 10.1186/s12985-024-02537-1

Yu, X., Ma, Y., Gao, Y., and You, H. (2021). Epidemiology of adenovirus pneumonia and risk factors for bronchiolitis obliterans in children during an outbreak in jilin, China. *Front. Pediatr.* 9. doi: 10.3389/fped.2021.722885

Zhao, M. C., Guo, Y. H., Qiu, F. Z., Wang, L., Yang, S., Feng, Z. S., et al. (2020). Molecular and clinical characterization of human adenovirus associated with acute respiratory tract infection in hospitalized children. *J. Clin. Virol.* 123, 104254. doi: 10.1016/j.jcv.2019.104254

Zhao, P., Zhang, Y., Wang, J., Li, Y., Wang, Y., Gao, Y., et al. (2024). Epidemiology of respiratory pathogens in patients with acute respiratory infections during the COVID-19 pandemic and after easing of COVID-19 restrictions. *Microbiol. Spectr.* 12, e0116124. doi: 10.1128/spectrum.01161-24

Zhu, Y., Xu, B., Li, C., Chen, Z., Cao, L., Fu, Z., et al. (2021). A multicenter study of viral aetiology of community-acquired pneumonia in hospitalized children in chinese mainland. *Virol. Sin.* 36, 1543–1553. doi: 10.1007/s12250-021-00437-0

frontiers | Frontiers in Cellular and Infection Microbiology

TYPE Original Research
PUBLISHED 22 September 2025
DOI 10.3389/fcimb.2025.1582159

OPEN ACCESS

EDITED BY
Dimitra Dimopoulou,
Panagiotis & Aglaia Kyriakou Children's Hospital, Greece

REVIEWED BY
Larry Ellingsworth,
Novavax, Inc., United States
Tangtian He,
Hong Kong Polytechnic University, Hong Kong SAR, China

*CORRESPONDENCE
Xiangtao Wu
xiangtaowu131225@163.com
Nali Cai
cailinann9@outlook.com
Shujun Li
ruolin2223@126.com

RECEIVED 24 February 2025
ACCEPTED 13 August 2025
PUBLISHED 22 September 2025

CITATION
Lu W, Guo X, Ren Y, Wang L, Xu T, Xu Y, Li D, Cai N, Li S, Zhang X, Li H and Wu X (2025) Time trends in the burden of non-COVID-19 lower respiratory tract infections among children aged 0 to 14 years. *Front. Cell. Infect. Microbiol.* 15:1582159. doi: 10.3389/fcimb.2025.1582159

Time trends in the burden of non-COVID-19 lower respiratory tract infections among children aged 0 to 14 years

Weihong Lu[1], Xixia Guo[1], Yishuai Ren[1], Li Wang[1], Tingting Xu[1], Yali Xu[1], Duoduo Li[1], Nali Cai[2*], Shujun Li[1*], Xingliang Zhang[3], Haibin Li[4] and Xiangtao Wu[1*]

[1]Department of Pediatrics, The First Affiliated Hospital of Xinxiang Medical University, Xinxiang, Henan, China, [2]Department of Pediatrics, Guangdong Medical University, Zhanjiang, Guangdong, China, [3]Pneumology Department, Shenzhen Children's Hospital, Shenzhen, Guangdong, China, [4]School of Public Health, Xinxiang Medical University, Xinxiang, Henan, China

Objective: This study aims to analyze the global burden, temporal trends, and main pathogenic characteristics of pediatric lower respiratory tract infections (LRTIs) across different age groups.

Methods: This repeated cross-sectional study included children with LRTIs aged 0–14 years from 204 countries and regions from 1990 to 2021. The primary outcomes were cases and rates of incidence, disability-adjusted life years (DALYs), mortality, and their trends associated with LRTIs. Estimates were generated using the DisMod-MR 2.1 tool.

Results: In 2021, neonates had the highest incidence and mortality. From 1990 to 2021, the global mortality rate of LRTIs in children decreased by 76.8%, with the reduction primarily driven by a 79.1% decrease in children aged 2–4 years. However, in low-middle SDI regions, the mortality rate remained as high as 4502.003 per 100,000. The primary pathogens contributing to LRTI-related DALYs and deaths in most age groups were *Streptococcus pneumoniae, Staphylococcus aureus*, and *Klebsiella pneumoniae*, while among newborns, the leading pathogens were *Klebsiella pneumoniae, Group B Streptococcus*, and *Acinetobacter baumannii*. BAPC predicted a slight improvement in the mortality rates from 18 LRTI pathogens over the next decade; however, influenza may cause an increase in childhood mortality reaching 44,820 deaths per 100,000 by 2031.

Conclusions: The burden of LRTIs remains significant in low- and middle-income countries, as well as among neonates and females. While the burden of various pathogens is gradually declining, influenza warrants particular attention. Expanding vaccine coverage, improving sanitary conditions, and early interventions for high-risk children are crucial strategies to reduce LRTI burden.

KEYWORDS

lower respiratory tract infections, children, global burden of disease, mortality, incidence, pathogens, risk factors

Introduction

Lower respiratory tract infections (LRTIs) are a leading cause of morbidity and mortality among children globally, particularly those under the age of 5 (Infections GBDLR and Antimicrobial Resistance C, 2024). Despite advances in medical technology and public health improvements, the global burden of LRTIs remains substantial, particularly in low- and middle-income countries. These infections, primarily caused by bacteria, viruses, or other pathogens, often manifest as pneumonia or bronchitis, significantly impacting the health and survival of children (Infections GBDLR and Antimicrobial Resistance C, 2024). The 2021 Global Burden of Disease (GBD) study highlights that, while incidence and mortality rates have declined, LRTIs still exert a profound public health burden (Safiri et al., 2022).

From 1990 to 2019, global LRTI incidence and mortality rates decreased significantly, driven largely by advancements in high-income countries. However, in low- and middle-income regions, pediatric LRTIs continue to present alarmingly high rates, influenced by factors such as air pollution, malnutrition, and inadequate sanitation (Mrcela et al., 2022; Yigezu et al., 2023). In Sub-Saharan Africa and South Asia, LRTIs remain a leading cause of child mortality (Jia et al., 2022). Studies have shown that air pollution, particularly from the use of household solid fuels for cooking and heating, contributes significantly to the high incidence and mortality rates of LRTIs (Ruan et al., 2021; Shi et al., 2023). In the coming decades, trends in pediatric LRTIs may be further shaped by increasing antimicrobial resistance, shifts in vaccine coverage, and the effects of climate change (Antimicrobial Resistance, 2022). These ongoing challenges underscore the need for a comprehensive understanding of the global burden and temporal trends of pediatric LRTIs.

Streptococcus pneumoniae and respiratory syncytial virus (RSV) are the most common pathogens causing LRTIs in children under 5 years old. Before the COVID-19 pandemic, influenza viruses also played an important role (Safiri et al., 2022; Wu et al., 2023). Studies have shown that the rate of RSV infection was significantly higher in low- and middle-income countries than in other regions (Wang et al., 2021). Globally, RSV-related acute LRTIs cause over 13,000 deaths annually among children under 5 years old, with the disease burden being particularly significant in Africa and Asia (Sah et al., 2023). However, an in-depth understanding of the specific distribution and impact of these pathogens on pediatric LRTIs remains lacking at different age groups.

Therefore, the limited understanding of the LRTIs risk factors among children across different regions and age groups, especially neonates and infants, hinders the development of clinical intervention strategies and global public health policies. Therefore, further research on the pathogen distribution, incidence, and mortality burden of pediatric LRTIs can greatly contribute to further understanding of the long-term impact of the pandemic and optimization of intervention measures (Zhu et al., 2022).

The 2021 GBD study represents the first update following the COVID-19 pandemic, offering new insights into the burden of LRTIs in children under 5 years old. In this study, we aim to provide a detailed analysis of the global trends, pathogen distribution, and risk factors influencing pediatric LRTIs. We also assess the indirect effects of the COVID-19 pandemic, including the "immunity debt" phenomenon. Using the updated GBD 2021 data, we conducted a subgroup analysis based on geographical regions, social development indices (SDI), age groups, and gender. Furthermore, we employed the Bayesian Age-Period-Cohort (BAPC) model to predict future trends in the epidemiology of LRTIs caused by various pathogens.

Methods

Study population and data collection

This study was based on data from the estimates of the 2021 GBD study (https://vizhub.healthdata.org/gbd-results/), which aimed to systematically analyze the incidence and mortality rates of non-COVID-19 LRTIs among children under 14 years old at the global, regional, and national levels from 1990 to 2021. This study included children aged 0–14 years from 204 countries and regions worldwide. In the GBD study, LRTI are defined as pneumonia or bronchiolitis (Infections GBDLR and Antimicrobial Resistance C, 2024), corresponding to International Classification of Diseases (Shin et al., 2023).

The GBD project collected data through global and regional public health organizations; hospital admission, discharge, death, and health examination records; global epidemiological surveys; and other channels. These data included the incidence, prevalence, disability-adjusted life years (DALYs) and mortality rates of various diseases, as well as health-related influencing factors. To ensure data accuracy and consistency, the GBD implemented data validation and adjustment processes. Evaluation of the incidence and mortality trends of LRTIs on a global scale was made possible by aggregating LRTI data from different regions and countries.

Analytical methods

The GBD project used DisMod-MR 2.1, which is a Bayesian large-scale iterative hierarchical regression tool, to generate internally consistent estimates of incidence and prevalence rates. Based on estimates of DALYs and mortality rates of LRTIs, multiple stratified analyses based on age, sex, and region were performed to assess the role of different pathogens in the LRTI burden.

Analysis of Major Pathogens: The burden of multiple pathogens, including *S. pneumoniae*, *Staphylococcus aureus*, RSV, *H. influenzae*, and *Klebsiella pneumoniae*, among children in

Abbreviations: LRTIs, Lower respiratory tract infections; RSV, Respiratory syncytial virus; EAPC, Estimated annual percent change; BAPC, Bayesian age-period-cohort; UI, Unconfidence interval; CI, Confidence interval; DALY, Disability-adjusted life years; GBD, Global Burden Disease, Injuries, and Risk Factors Study; SDI, Sociodemographic index.

different age groups was evaluated. Determining the mortality rates associated with these pathogens across various age groups and the impact of each pathogen in different countries and regions can aid in the identification of key intervention targets.

Risk Factor Analysis: The extent and impact of 13 major LRTI risk factors, including child malnutrition, particulate matter pollution, and household solid fuel pollution, were systematically evaluated. The changes in these risk factors were assessed using historical data from 1990 to 2021.

Temporal Trend Analysis: Using historical data from 1990 to 2021, the temporal changes in LRTI burden before and after the pandemic were evaluated, taking into consideration the confounding effects of COVID-19.

Group Comparisons: Data were compared among patient groups of income level, sex, and geographic region. The study population was divided into different age groups, as follows: neonates (0–28 days), 1–5 months, 6–11 months, 1–4 years, 5–9 years, and 10–14 years. Based on the Socio-Demographic Index (SDI), 204 countries and regions are classified into different development categories: high SDI regions ($0.858 < SDI \leq 1$), high-middle SDI regions($0.812 < SDI \leq 0.858$), middle SDI regions ($0.670 < SDI \leq 0.812$), low-middle SDI regions ($0.570 < SDI \leq 0.670$), and low SDI regions($0 < SDI \leq 0.570$) (Jin et al., 2025).

Calculation of annual percentage changes

This study utilizes the Age-Period-Cohort (APC) model framework to analyze trends in mortality due to LRTI by age, period, and birth cohort. The APC model helps clarify the effects of age-related biological factors as well as technological and social factors on disease trends, offering advantages over traditional epidemiological analyses. It has been successfully applied to chronic diseases like cardiovascular diseases. The model fits a log-linear Poisson regression to the Lexis diagram of observed rates, quantifying the additive effects of age, period, and cohort. Given the linear relationship between age, period, and cohort (birth cohort = period − age), this study uses a Poisson-based APC model to explore LRI mortality trends. The model provides a unique perspective on how these factors interact, offering a deeper understanding of the dynamic trends in LRI mortality. For the data from 1992 to 2021, Poisson log-linear models are used to quantify and analyze LRI mortality trends.

The trends are assessed through the Estimated Annual Percentage Change (EAPC) for mortality rates and their corresponding Age-Standardized Rates (ASR). EAPC was calculated utilizing a regression model based on the natural logarithm of the ratio, expressed as: $y = \alpha + \beta x + \varepsilon$.The EAPC is calculated using the formula: $100 \times (\exp(\beta) - 1)$, where x represents the calendar year and y is the natural logarithm (ln) of ASR. The 95% Confidence Interval (CI) for the EAPC is also estimated. If the EAPC and its lower bound of the 95% UI are both greater than 0, it indicates an upward trend in ASR; if both the EAPC and its upper bound are less than 0, it suggests a downward trend in ASR. If the EAPC crosses 0, the ASR is considered stable.

In the Bayesian Age-Period-Cohort (BAPC) model, prior distributions are assigned to the model parameters (age, period, and cohort effects) based on existing literature or expert knowledge. The likelihood of the observed data is modeled using a Poisson distribution, suitable for incidence rates. The Markov Chain Monte Carlo (MCMC) method is used to estimate posterior distributions for the parameters, providing the most probable values based on both the data and prior information. The model is then used to predict LRTI incidence rates for 2022-2031 by projecting the estimated effects of age, period, and cohort into the future, incorporating uncertainties through credible intervals (CI). After fitting the model to historical data from 1990 to 2021, forecasts for LRI incidence are generated by extrapolating the trends. The model adjusts for future changes in healthcare, environmental conditions, and other factors, reflecting the potential impacts of policy changes, medical advancements, and socio-economic improvements. Uncertainty in the forecasts is captured by the credible intervals, providing a range of possible outcomes and reflecting the inherent uncertainty in long-term predictions.

Reporting standards

This study adheres to the relevant reporting standards for epidemiological research, particularly those concerning the analysis of temporal trends in disease burden. The data and methods used are consistent with the Strengthening the Reporting of Observational Studies in Epidemiology (STROBE) guidelines. Efforts were made to minimize bias in data collection, analysis, and interpretation. Any limitations inherent in the dataset or methodology, such as potential underreporting or misclassification of disease, are clearly stated. All rates are presented per 100,000 person-years, with 95% uncertainty intervals (UI) reported for all estimates. Uncertainty is propagated throughout each step of the burden estimation process, with the CI representing the 2.5th and 97.5th percentiles from 1,000 simulations at each stage.

By comprehensively analyzing GBD data and using the DisMod-MR 2.1 tool, this study generated global, regional, and national estimates of the incidence and mortality rates of LRTIs among children under 14 years old. The significance level was set at $\alpha = 0.05$ for statistical purposes. R software (version 4.2.0) was employed for all analyses and data processing.

Results

Incidence of lower respiratory tract infections in children aged 0–14 years in 2021

In 2021, 69.9 million LRTI cases occurred globally among children aged 0–14 years, with an incidence rate of 3,474.42 per

100,000 (95% UI: 3,088.43–3,965.51). Among the regions stratified by the Sociodemographic Index (SDI), the low–middle region had the highest incidence and number of LRTI cases at 26.1 million. Among the countries stratified by the World Bank income classification, low–middle-income countries had the highest number of LRTI cases at 45.78 million and incidence rate at 4,519.835 per 100,000 population (95% UI 4,014.096 to 5,154.413) for children aged 0–14 years. Among the GBD super regions, South Asia had the highest number of LRTI cases at 29.89 million and incidence rate at 5,996.088 per 100,000 population (95% UI 5,191.431 to 6,777.824) (Table 1).

Across 204 countries or regions in 2021, the incidence rate of LRTIs among children aged 0–14 years ranged from 227.885 per 100,000 population (95% UI 188.185 to 273.606) in the Netherlands to 7,531.439 per 100,000 population (95% UI 6,669.170 to 8,627.229) in Pakistan. Among children aged 0–14 years, the incidence rate was highest in newborns, at 14,740.851 per 100,000 population (95% UI 13,118.822 to 16,546.953) (Table 1), followed by children aged 1–5 months, with an incidence rate of 12,487.260 per 100,000 population (95% UI 11,243.756 to 13,810.984) (Table 1). The incidence rate decreased gradually with age, reaching 1,840.776 per 100,000 population (95% UI 1,445.697 to 2,329.717) among children aged 10–14 years (Table 1).

Since 1990, the global incidence of lower respiratory tract infections (LRTI) in children of all ages has decreased by 221.9% (95% UI: 199.5–244.3). When classified by SDI (Socio-Demographic Index) region, the incidence in children from low-middle SDI regions decreased by 195.7% (95% UI -178.2 to -213.5), while in high SDI regions, the decrease was 312.4% (95% UI -288.1 to -337.2). When categorized by age group, the incidence of LRTI in neonates (0–28 days) decreased by 183.2% (95% UI-162.4 to -204.7), in infants aged 1–5 months, it decreased by 201.5% (95% UI -180.3 to -222.9), and in children aged 10–14 years, the decrease was 68.4% (95% UI -61.5 to -75.4). For high-burden countries, the incidence in Pakistan decreased by 158.9% (95% UI -142.1 to -176.2), while in the Netherlands, it decreased by 401.2% (95% UI -375.8 to -427.1) (Table 1).

Mortality of lower respiratory tract infections in children aged 0–14 years in 2021

In 2019, before the COVID-19 pandemic, an estimated 745,080 (95% UI 624,870 to 871,680) children aged 0–14 years died because of LRTIs, with a mortality rate of 37.144 per 100,000 population (95% UI 31.151 to 43.455). Since 1990, the mortality rate per 100,000 population has increased by 76.8%, reaching 27.123 (95% UI: 22.238–32.570). Among children aged 0–14 years, the LRTI mortality rate in neonates (0–28 days) increased by 71.5%, with a rate of 1,560.637 (95% UI 1,308.891–1,835.706), while for children aged 10–14 years, the mortality rate increased to 2.492 (95% UI 2.183–2.774) (Table 2).

In 2021, there were 550 deaths due to LRTIs globally among children aged 0–14 years, with a mortality rate of 27.123 per 100,000 population (95% UI 22.238 to 32.570). Among the SDI regions, the low–middle SDI region had the highest number of LRTI deaths at 300 and mortality rate at 4,502.003 per 100,000 population (95% UI 4,004.209 to 5,137.527). Among income groups, the mortality rate in low-income countries increased by 63.1% since 1990, reaching 4,502.003 (95% UI: 4,004.209–5,137.527), while in high SDI regions, the increase was only 0.891 (95% UI: 0.752–1.042), despite a 92.7% rise. The highest number of LRTI deaths was attributed to Streptococcus pneumoniae, with 153.9 deaths and a mortality rate of 7.651 per 100,000 population (95% UI: 6.086–9.194). In contrast, Staphylococcus aureus accounted for 54.0 deaths, with a mortality rate of 2.684 per 100,000 population (95% UI: 2.163–3.247) (Table 2).

Across 204 countries or regions, the LRTI mortality rate among children aged 0–14 years in 2021 ranged from 151.794 per 100,000 population (95% UI 112.772 to 195.504) in Chad to 0.142 per 100,000 population (95% UI 0.097 to 0.194) in Andorra (Figure 1). The highest mortality rate was observed in newborns (1,560.637 per 100,000 population; 95% UI 1,308.891 to 1,835.706). In children aged 10–14 years, mortality rate decreased with age, reaching 2.492 per 100,000 population (95% UI 2.183 to 2.774) (Table 2).

TABLE 1 Number of cases, incidence rate, and annual percentage change in incidence rate of lower respiratory tract infections in children aged 0–14 years from 1990 to 2021.

Category	Subgroup	Cases (millions)	Incidence per 100,000 (95% UI)	% change since 1990 (95% UI)
Global	All ages	69.9	3,474.42 (3,088.43-3,965.51)	-221.9% (-199.5 to -244.3)
By SDI Region	Low-middle	26.1	4,502.003 (4,004.209-5,137.527)	-195.7% (-178.2 to -213.5)
	High	5.3	1,240.15 (1,102.84-1,410.26)	-312.4% (-288.1 to -337.2)
By Age Group	Neonates (0-28d)	/	14,740.851 (13,118.822-16,546.953)	-183.2% (-162.4 to -204.7)
	1-5 months	/	12,487.260 (11,243.756-13,810.984)	-201.5% (-180.3 to -222.9)
	10-14 years	/	1,840.776 (1,445.697-2,329.717)	-68.4% (-61.5 to -75.4)
High-Burden Countries	Pakistan	/	7,531.439 (6,669.170-8,627.229)	-158.9% (-142.1 to -176.2)
	Netherlands	/	227.885 (188.185-273.606)	-401.2% (-375.8 to -427.1)

Values in parentheses are 95% uncertainty intervals. Count data are presented to three significant figures.
GBD, Global Burden of Diseases, Injuries, and Risk Factors Study; SDI, Sociodemographic Index.

TABLE 2 Number of deaths, death rates, and annual percentage changes in death rate of lower respiratory infections in children aged 0–14 years in 1990, 2019, 2020, and 2021.

Stratification	Group	Deaths (thousands)	Mortality per 100,000 (95% UI)	% reduction since 1990
Global	Total	550.0	27.123 (22.238-32.570)	76.8% (72.2-80.5)
By SDI	Low-middle SDI	300.0	4,502.003 (4,004.209-5,137.527)	63.1% (58.7-67.4)
	High SDI	8.2	0.891 (0.752-1.042)	92.7% (90.1-94.8)
By Age	Neonates (0-28d)	156.1	1,560.637 (1,308.891-1,835.706)	71.5% (66.8-75.7)
	10-14 years	2.5	2.492 (2.183-2.774)	47.3% (40.6-52.8)
Pathogen Leaders (2021)	*S. pneumoniae*	153.9	7.651 (6.086-9.194)	/
	S. aureus	54.0	2.684 (2.163-3.247)	/

Values in parentheses are 95% uncertainty intervals. Count data are presented to three significant figures.
GBD, Global Burden of Diseases, Injuries, and Risk Factors Study; SDI, Sociodemographic Index.

In 2021, the number of LRTI deaths among newborns was mainly concentrated in low-SDI regions. Of the 204 countries or regions, 98 countries had mortality rates greater than 1,000 per 100,000 population (Table 2).

Mortality of lower respiratory tract infections in all children aged 0–14 years from 1990 to 2021

Globally, from 1990 to 2021, the all-age mortality rate of LRTIs among children aged 0–14 years decreased by 76.8% (95% UI 72.2–80.5), from 20.340 (95% UI 17.759 to 23.139) to 5.457 (95% UI 4.474 to 6.553) deaths per 100,000 population (Figure 2). Among boys, the mortality rate decreased by 76.0% (95% UI 71.0–80.1), from 10.539 (95% UI 9.069 to 12.189) to 2.941 (95% UI 2.372 to 3.573) deaths per 100,000 population (Figure 2). Among girls, the mortality rate decreased by 77.7% (95% UI 72.9–81.7), from 9.801 (95% UI 8.306 to 11.259) to 2.516 (95% UI 2.060 to 2.968) deaths per 100,000 population (Figure 2). Overall, the changes in LRTI mortality rates among children aged 0–14 years were not significantly different between sexes. The decline in the number of deaths was primarily driven by the reduction in LRTI mortality rates among children aged 1–4 years, decreasing by 77.5% (95% UI 71.8–82.0) among those aged 12–23 months and by 79.1% (95% UI 72.8–84.4) among those aged 2–4 years (Figure 2). Similar to the incidence rate, the smallest decline in LRTI mortality rate was observed among children aged 10–14 years (47.3%, 95% UI 40.6–52.8) (Figure 2).

Risk factors for LRTIs in children aged 0–14 years from 1990 to 2021

In 2019, before the COVID-19 pandemic, the total number of DALYs attributable to LRTI risk factors was 59.746 million (95% UI 49.011 to 71.078 million), representing a reduction of 376.7% (95% UI 365.3 to 387.8), compared with 168.373 million (95% UI 144.370 to 194.828) in 1990. According to the GBD framework, the 13 risk factors for LRTI burden among children aged 0–14 years include underweight children, particulate matter pollution, childhood stunting, household air pollution from solid fuels, child wasting, low birth weight, lack of access to handwashing facilities, ambient particulate matter pollution, short gestation, secondhand smoke, nonexclusive breastfeeding, high temperature, and low temperature. The leading risk factor was low birth weight (2.627 million DALYs, 95% UI 1.065 to 4.342 million), followed by particulate matter pollution (2.610 million DALYs, 95% UI 0.750 to 4.251 million); child stunting (1.941 million DALYs, 95% UI 1.315 to 2.564 million); household air pollution from solid fuels (1.824 million DALYs, 95% UI 0.563 to 3.200 million; and child wasting (1.493 million DALYs, 95% UI 0.956 to 2.054 million). High and low temperatures were found to have minimal correlation with LRTI DALYs (Figure 3).

Compared with the data in 2019, the LRTI burden among children aged 0–14 years in 2021 remained attributable to the same 13 risk factors, although the number of DALYs decreased by 74.2% (95% UI 69.0 to 78.6) at 4.345 million (95% UI 3.434 to 5.247 million). However, the leading risk factor became particulate matter pollution, accounting for 1.930 million DALYs (95% UI 0.573 to 3.218 million) and with 75.6% reduction (95% UI 69.8 to 80.2). The second leading risk factor was child underweight (1.845 million DALYs, 95% UI 0.071 to 3.116 million), which decreased by 77.2% (95% UI 72.3 to 82.5). Household air pollution from solid fuels was the third leading risk factor, with 1.371 million DALYs (95% UI 0.427 to 2.411 million) and a 78.5% reduction (95% UI 72.4 to 83.3). The fourth and fifth leading risk factors were child stunting (1.369 million DALYs, 95% UI 0.926 to 1.830 million) and child wasting (1.013 million DALYs, 95% UI 0.631 to 1.440 million), respectively. Notably, from 2019 to 2021, the ranking of particulate matter pollution and household air pollution from solid fuels increased, whereas high and low temperatures remained minimally associated with LRTI DALYs among children aged 0–14 years (Figure 3).

Analysis of the main pathogens and worldwide burden of lower respiratory tract infections among children aged 0–14 years in 2021

In 2021, influenza A/H3N2 was the dominant subtype globally, accounting for 58.3% (95% UI 52.1-64.5) of influenza-associated

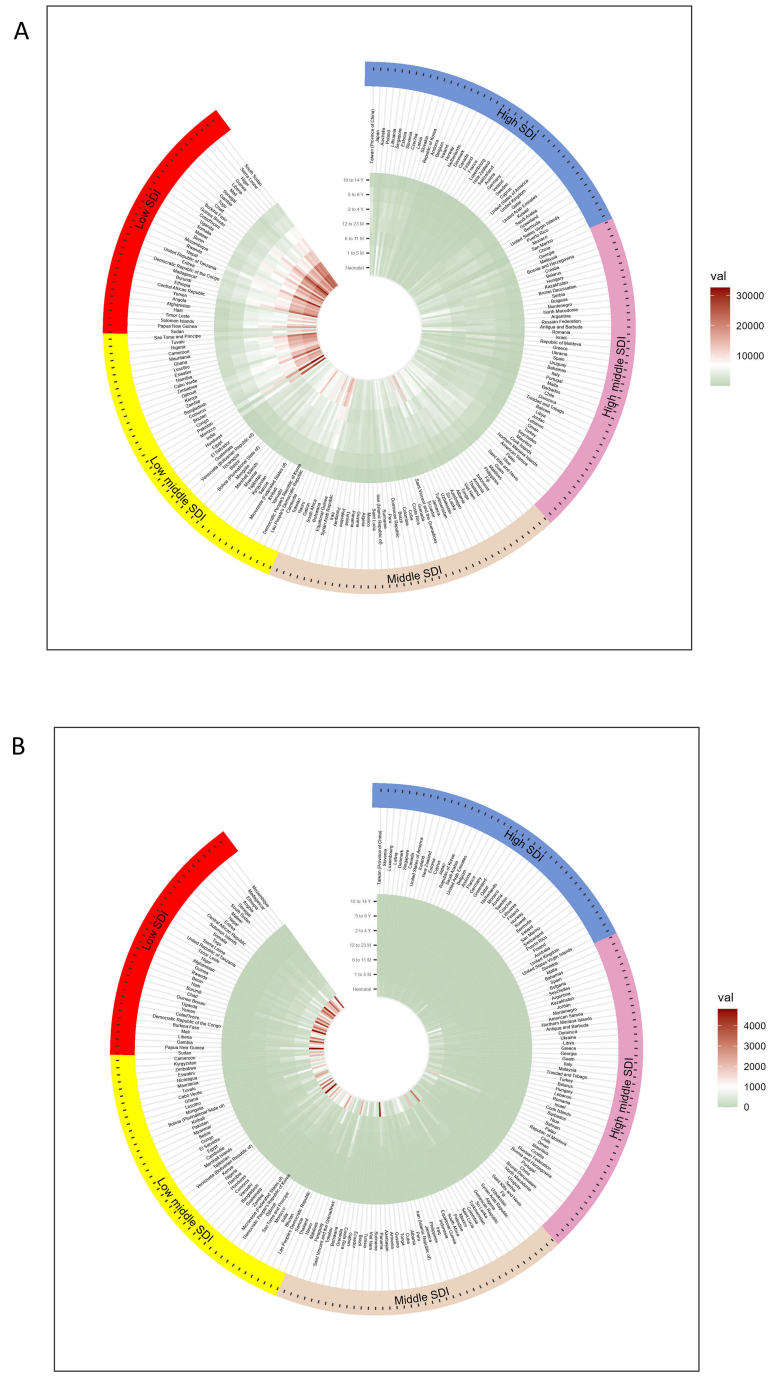

FIGURE 1
Circular heat map of the incidence and mortality of lower respiratory tract infections in children aged 0–14 years from countries with different SDI levels in 2021 **(A)** incidence and **(B)** mortality rates per 100,000 population, with colors representing global sextiles.

LRTI deaths in children aged 0-14 years, followed by influenza B (27.6%, 95% UI 22.4-33.1) and A/H1N1 (14.1%, 95% UI 10.3-18.7). The mortality burden was disproportionately concentrated in low-middle SDI regions, where influenza A/H3N2 caused 23.7 deaths per 100,000 (95% UI 19.2-28.9) - 3.2-fold higher than high-SDI regions. Vaccination coverage showed stark regional disparities: ≤15% in Sub-Saharan Africa vs. 63.2% in North America (WHO/UNICEF 2021 estimates). Notably, seasons with A/H3N2 dominance correlated with 42% higher mortality than H1N1-dominant years ($p<0.001$).

The top three pathogens contributing to LRTI-related DALYs among children aged 0–14 years globally were *S. pneumoniae* (135.877 DALYs per 100,000 population, 95% UI 108.004–163.224); *S. aureus* (47.620 DALYs per 100,000 population, 95% UI 38.402–57.603); and *K. pneumoniae* (436.123 million DALYs, 95% UI 347.301–532.681).

10.3389/fcimb.2025.1582159

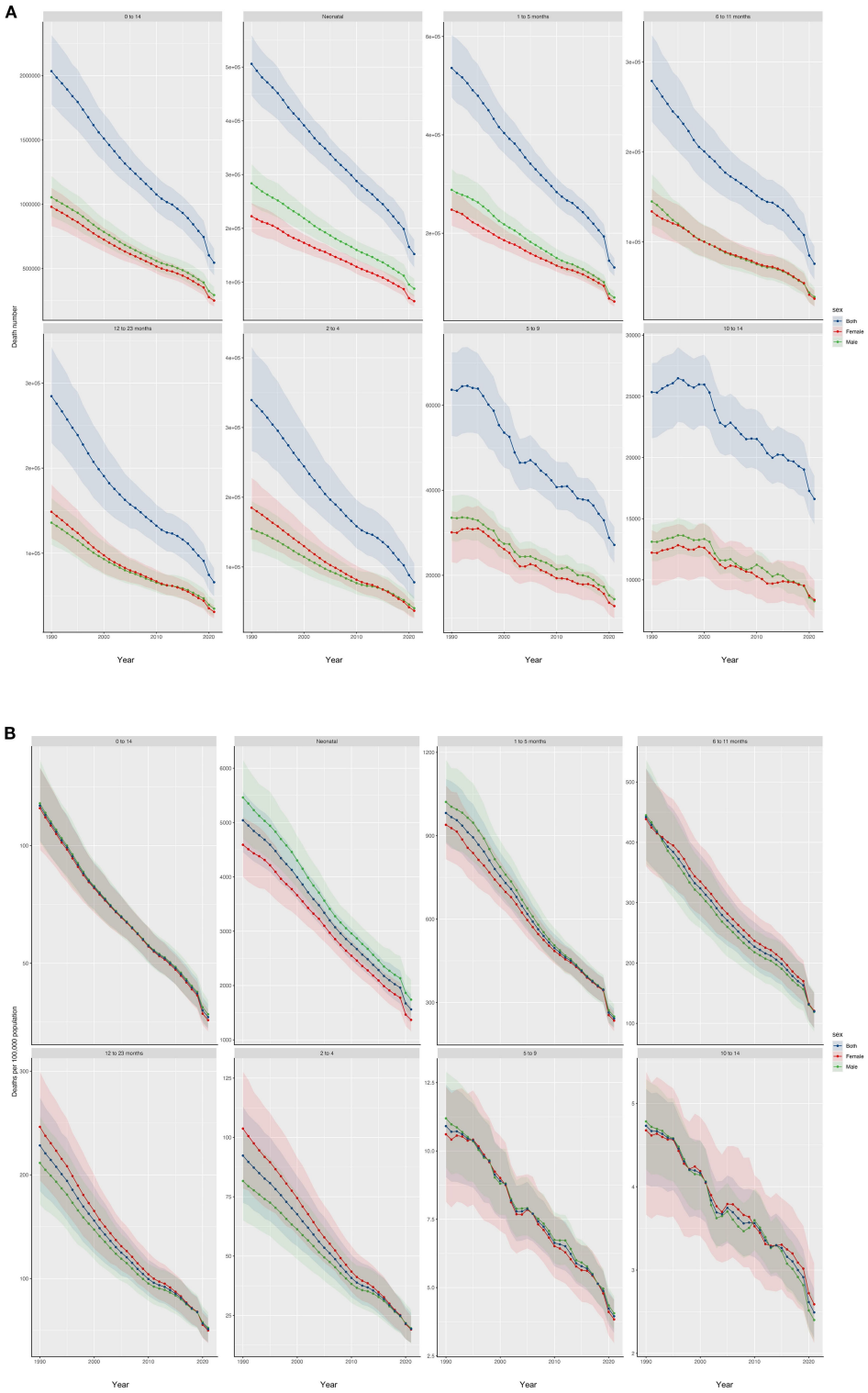

FIGURE 2
LRTI mortality rate and number of deaths from 1990 to 2021, stratified by age and sex The **(A)** number of deaths **(B)** mortality rate from 1990 to 2021, stratified by age and sex, are shown. The shaded areas represent 95% uncertainty intervals.

10.3389/fcimb.2025.1582159

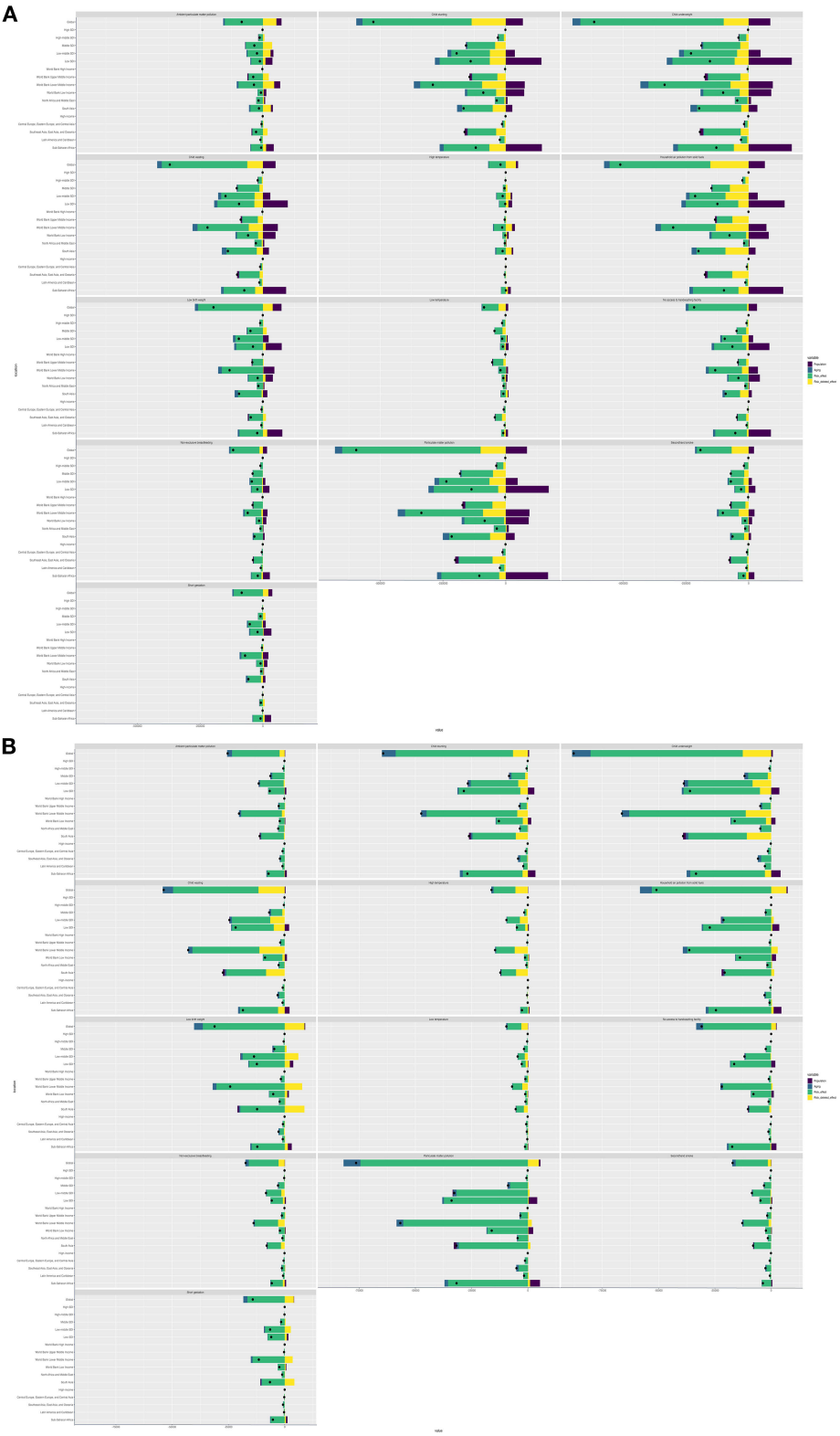

FIGURE 3
Risk factors for LRTIs in children aged 0–14 years in 1990–2019 and 2019–2021 analyses of risk factors for LRTIs in children aged 0–14 years **(A)** from 1990 to 2019 and **(B)** from 2019 to 2021.

Among the high-, high–middle-, and middle-SDI regions, the top three pathogens contributing to LRTI-related DALYs and deaths in this age group were *S. pneumoniae*, *S. aureus*, and other viruses. In low–middle-SDI regions, the top three pathogens were *S. pneumoniae*, *S. aureus*, and *K. pneumoniae*. In high-SDI regions, *S. pneumoniae* contributed 0.233 DALYs (95% UI 0.211–0.255) and 0.003 deaths (95% UI 0.002–0.003) per 100,000 population. In low-SDI regions, *S. pneumoniae* contributed 67.745 DALYs (95% UI 50.154–85.595) and 0.769 deaths (95% UI 0.569–0.072) per 100,000 population. *S. aureus* contributed 0.213 DALYs (95% UI 0.195–0.228) and 0.002 deaths (95% UI 0.002–0.003) per 100,000 population in high-SDI regions and 29.036 DALYs (95% UI 17.539–29.036) and 26.334 deaths (95% UI 19.929–32.064) per 100,000 population in low-SDI regions The pattern was similar among the countries stratified by income.

Among children aged 0–14 years across the 204 modeled countries and regions in 2021, *S. pneumoniae* was the leading cause of DALYs in 171 countries or regions, whereas *S. aureus* was the leading cause of LRTI deaths in the remaining 33 countries or regions. Across the seven age subgroups, *S. pneumoniae* was the most frequent pathogen causing LRTIs (Figure 4).

When stratified by age group, the top three pathogens contributing to LRTI-related DALYs and deaths among newborns aged 0–28 days globally were *K. pneumoniae*, Group B Streptococcus, and *Acinetobacter baumannii*. *K. pneumoniae* contributed 14.979 DALYs (95% UI 11.574–19.021) and 0.166 deaths (95% UI 0.129–0.211) per 100,000 population. Group B Streptococcus contributed 10.897 DALYs (95% UI 8.462–13.733) and 0.121 deaths (95% UI 0.094–0.153) per 100,000 population. *A. baumannii* contributed 10.397 DALYs (95% UI 5.507–17.695) and 0.116 deaths (95% UI 0.061–0.197) per 100,000 population. For children aged 1–5 months, 6–11 months, 2–4 years, 5–9 years, and 10–14 years, the top three pathogens contributing to LRTI-related DALYs and deaths were *S. pneumoniae*, *S. aureus*, and *K. pneumoniae* (Figure 4).

Changes in main pathogens and burden of lower respiratory tract infection in children from 2019 to 2021

In 2019, during the COVID-19 pandemic, the top three pathogens causing LRTI deaths in children aged 0–14 years were the same as those in 1990: *S. pneumoniae*, influenza, and RSV. *S. pneumoniae* was the most common cause of LRTI deaths globally, resulting in 188,090 deaths (95% UI 155,990 to 221,610). Influenza was the second leading pathogen, causing 82,190 deaths (95% UI 68,450 to 97,060), and RSV was the third leading pathogen, causing 79,110 deaths (95% UI 66,430 to 92,210) (Figure 5). In 2019, *S. pneumoniae* was the leading cause of LRTI deaths in all age groups, except in newborns. The leading pathogen causing LRTI deaths in newborns was RSV (29,180 deaths, 95% UI 24,510 to 34,620), followed by *K. pneumoniae* (18,810 deaths, 95% UI 14,980 to 23,370) and influenza (18,400 deaths, 95% UI 14,420 to 23,120).

In 2021, the top three pathogens causing LRTI deaths in children aged 0–14 years were *S. pneumoniae* (153,920 deaths, 95% UI 122,430 to 184,970), followed by *S. aureus* (53,990 deaths, 95% UI 43,530 to 65,330) and *K. pneumoniae* (49,130 deaths, 95% UI 39,120 to 60,030). In 2021, *S. pneumoniae* remained the leading cause of LRTI deaths in all age groups, except in newborns (Figure 4). Among newborns, the leading cause of LRTI deaths was *K. pneumoniae* (16,650 deaths, 95% UI 12,860 to 21,140), followed by Group B Streptococcus (12,110 deaths, 95% UI 9,400 to 15,260) and *A. baumannii* (11,560 deaths, 95% UI 6,120 to 19,670). Unlike the top three pathogens causing LRTI deaths among children aged 0–14 years in 2021, other viral etiologies of LRTIs

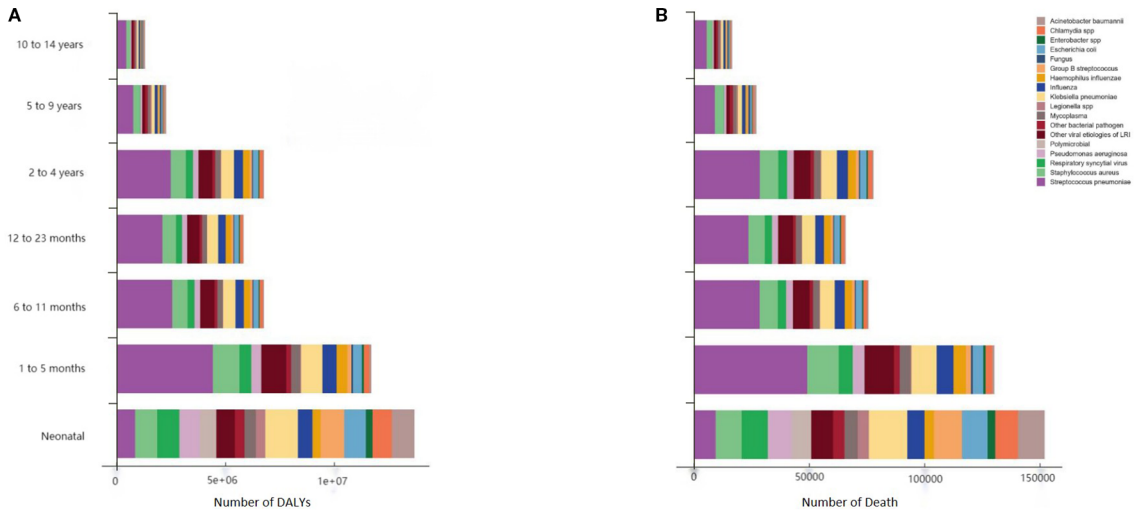

FIGURE 4
Etiological DALYs and number of deaths due to LRTIs among children globally in 2021, stratified by age group. The **(A)** DALYs and **(B)** number of deaths due to LRTIs; "Other viruses" included all studied viruses, except influenza and respiratory syncytial virus. DALYs, distribution of disability-adjusted life years; LRTI, lower respiratory tract infection.

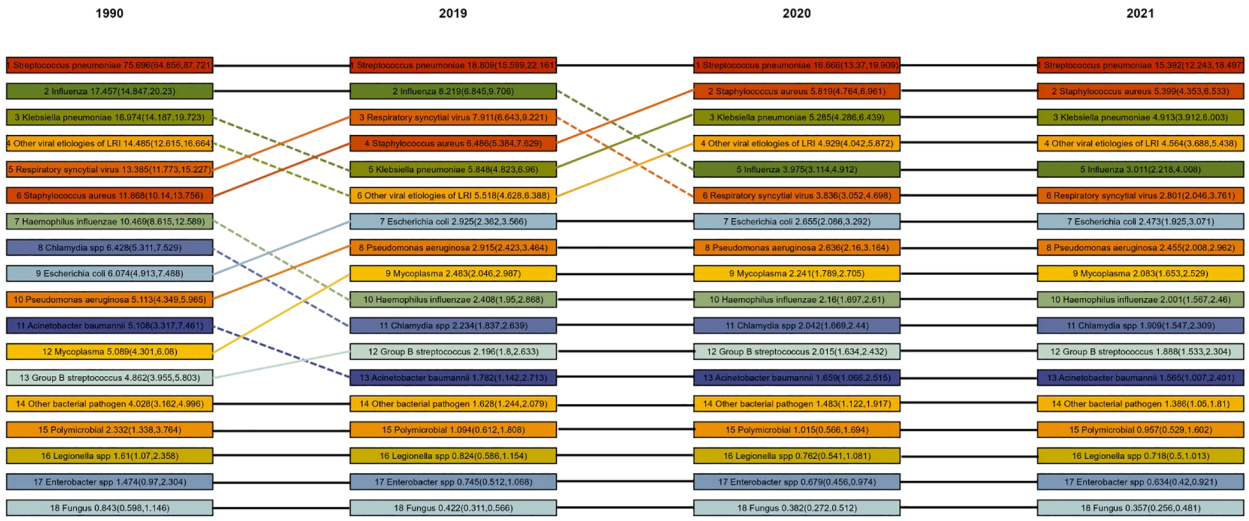

FIGURE 5
Global ranking of burden of death due to pathogens associated with lower respiratory tract infections among children aged 0–14 years in 1990, 2000, 2010, and 2021 Values represent the estimated number of deaths or DALYs per 100,000 population for each pathogen, with 95% uncertainty intervals shown in parentheses. Estimates are presented with three significant digits.

were the third leading cause of death among children under 5 years old, excluding newborns, causing 33,710 deaths (95% UI 26,330 to 41,440) (Figure 4). In 2021, the leading causes of LRTIS deaths across the 204 modeled countries and regions were *S. pneumoniae* in 172 countries and *S. aureus* in 31 countries. In Iceland, RSV was the leading cause of LRTI deaths in children aged 0–14 years.

From 1990 to 2019, the largest decrease in global mortality rate among children aged 0–14 years was from influenza (29.7% decrease, 95% UI 29.7–30.6), followed by Enterobacteriaceae (26.5% decrease, 95% UI 27.3–25.7). These improvements were most pronounced in children aged 2–4 years, with influenza-related deaths decreasing by 57.9% (95% UI 56.3–61.1), from 28,258.625 (95% UI 21,953.534–35,001.644) to 11,893.952 (95% UI 8,530.451–15,307.666), and Enterobacteriaceae-related deaths decreasing by 52.2% (95% UI 50.6–54.3), from 1,391.960 (95% UI 949.929–1,905.236) to 665.620 (95% UI 434.409–940.669).

After the start of the COVID-19 pandemic, we estimated that the number of influenza-related DALYs among children aged 0–14 years from 2019 to 2021 decreased by 63.4% (95% UI 52.1–73.0), from 7.279 million (95% UI 6.058–8.604) to 2.664 million (95% UI 1.962–3.547). A similar decrease of 63.4% (95% UI 52.0–72.9) was observed in the number of deaths, from 82,190 (95% UI 68,450–97,060) to 30,110 (95% UI 22,180–40,080). Among the 18 modeled pathogen categories, influenza decreased in rank from second in 2019 to fifth in 2021 as the leading cause of global LRTI DALYs and deaths among children aged 0–14 years (Figure 5). From 2019 to 2021, the mortality rate of influenza in this age group decreased the most in high-income regions (93.4%, 95% UI 89.6–96.0) and had the smallest decrease in Sub-Saharan Africa (57.3%, 95% UI 40.5–70.4).

Similarly, since 2019, the number of RSV-related DALYs globally has decreased by 64.6% (95% UI 53.8–74.2), from 7.069 million (95% UI 5.941–8.238) to 2.502 million (95% UI 1.828–3.358). Moreover, the number of RSV-related deaths decreased significantly by 64.6% (95% UI 53.7–74.2), from 79,110 (95% UI 66,430–92,210) in 2019 to 28,010 (95% UI 20,460–37,610) in 2021. Among the 18 modeled pathogen categories, RSV decreased in rank from third in 2019 to sixth in 2021 as the leading cause of global LRTI DALYs and deaths among children aged 0–14 years. Similar to influenza, the largest reduction in RSV mortality rates in this age group from 2019 to 2021 was observed in high-income regions (94.0%, 95% UI 90.7–96.3), whereas the smallest reduction was observed in Sub-Saharan Africa (57.6%, 95% UI 40.7–70.9).

Overall, for global non-COVID-19 LRTIs among children aged 0–14 years from 2019 to 2021, we estimated an 11.8% (95% UI 9.6–14.0) decrease in the overall incidence rate, from 790.176 (95% UI 706.289–897.168) to 699.005 (95% UI 621.350–797.806) per 100,000 population. The DALYs rate decreased by 27.1% (95% UI 22.3–31.2), from 483.630 (95% UI 396.663–580.345) to 661.162 (95% UI 554.592–773.710) per 100,000 population. The mortality rate decreased by 27.0% (95% UI 22.2–31.1), from 7.451 (95% UI 6.249–8.717) to 5.457 (95% UI 4.474–6.553) per 100,000 population.

Prediction of mortality rates for 18 pathogens of LRTIs in children Aged 0–14 years globally from 2021 to 2031

Between 2021 and 2031, the mortality rate of LRTI in children showed a significant downward trend. In 2021, the mortality rate for LRI in children was 27.124 per 100,000 population (95% UI 26.930–27.317), but by 2031, this figure had sharply decreased to 9.032 per 100,000 population (95% UI 4.244–13.819).

Among the 18 pathogens studied, the mortality rate caused by the influenza virus exhibited a unique trend, with an increase over

time, while the mortality rates associated with the other 17 pathogens declined to varying extents. Specifically, the mortality rate for children aged 0-14 years due to influenza virus in 2021 was 1.497 per 100,000 population (95% UI 1.993–1.102). This rate initially decreased to 1.071 per 100,000 population (95% UI 0–21.976) in 2029 but then gradually rose to 4.482 per 100,000 population (95% UI 0–302.115) in 2031. The male mortality rate was approximately 2.906 per 100,000 population (95% UI 0–162.567), while the female mortality rate was approximately 6.160 per 100,000 population (95% UI 0 –450.896), making influenza virus the leading cause of death from LRI in children.

In contrast, the mortality rate from pneumonia caused by Streptococcus pneumoniae for children aged 0-14 years declined from 7.651 per 100,000 population (95% UI 6.086–9.194) in 2021 to 3.129 per 100,000 population (95% UI 1.822–4.435) in 2031, with its ranking as the leading cause of death dropping to second place. Similarly, the mortality rate from Staphylococcus aureus also showed a notable decline, from 2.684 per 100,000 population (95% UI 2.163–3.247) in 2021 to 1.444 per 100,000 population (95% UI 0.720–2.167) in 2031, with its ranking as the second leading cause of death dropping to third place (Figure 6).

Discussion

This study analyzed the incidence and mortality rates of non-COVID-19 LRTI from 1990 to 2050 among children aged 0–14 years at the global, regional, and national levels using data from the 2021 GBD study. The results indicated significant differences in pediatric LRTI burden among geographic regions over time, and these were related to multiple factors, such as major pathogens, risk factors, and SDI. This study on pediatric LRTIs focused on trends of global incidence among different age groups and the main pathogenic characteristics. The results showed that although the global incidence and mortality rates of pediatric LRTIs significantly declined over the past three decades, notable differences among specific regions and age groups remain.

The significant downward trend in the global incidence of LRTIs among children aged 0–14 years from 1990 to 2021 can be mainly attributed to the promotion of vaccination, improved public health measures, and widespread availability of healthcare resources (Antimicrobial Resistance, 2022). This significantly reduced incidence was particularly observed in middle- and high-income countries, which have implemented vaccination and enhanced medical care (Raj et al., 2595 2023). However, in low-income and low–middle-income countries, the incidence remains high. For instance, the highest incidence rates were observed among children in South Asia and Sub-Saharan Africa, reflecting inadequate medical conditions and health infrastructure in these regions (Collaborators GBDAR, 2024). Moreover, public health measures and lockdown policies during the pandemic likely altered pathogen transmission patterns to some extent, with significant declines in the rates of influenza virus and RSV infection (Tang et al., 2021). Studies have shown that although LRTI has a gradually decreasing overall incidence, its epidemiology was significantly affected by COVID-19-related public health measures. Isolation and preventive measures during the pandemic led to a temporary decline in LRTI incidence, especially in high-income countries; however, after 2021, LRTI cases have rebounded in number and present with more severe clinical phenotypes— a phenomenon known as immunity debt (Nagelkerke et al., 2024).

Neonates had the highest incidence of LRTIs, reaching 14,740.851 cases per 100,000 population in 2021. The incidence gradually decreased with age, dropping to 1,840.776 cases per 100,000 population among children aged 10–14 years. The high incidence in neonates was mainly due to underdeveloped immune

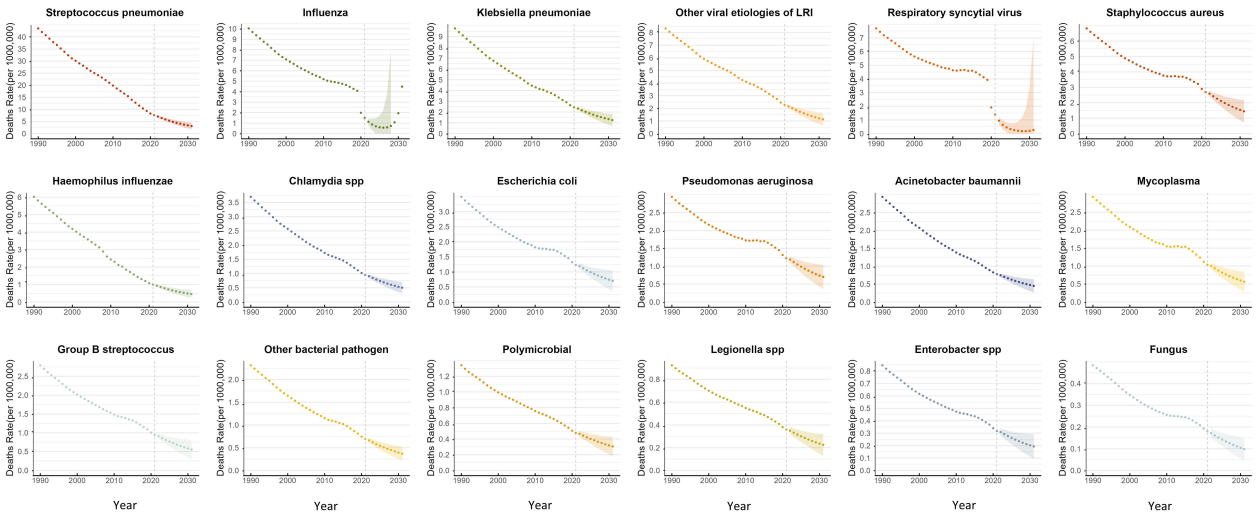

FIGURE 6
BAPC prediction of mortality rates for 18 pathogens of LRTIs in children aged 0-14 years globally from 2021 to 2031. The data from 1990 to 2021 are historical, while the BAPC predictions for 2021-2031 are presented with 95% UI.

systems, which likely increased the susceptibility to pathogen invasion (Feikin et al., 2024). Moreover, infants aged 1–5 months were found to be a high-risk group, reflecting the high susceptibility to respiratory infections among children in this age range.

Neonates and young children, especially those under 5 years old, were high-risk populations for LRTIs. During the COVID-19 pandemic, the significant decrease in LRTI incidence among infants under 1 year old was possibly related with social isolation measures and enhanced personal hygiene practices (Qiu et al., 2022). The varying incidence rates and LRTI pathogens among children of different age groups were likely due to differences in immune system development. Other studies have indicated that the COVID-19 pandemic not only altered the overall incidence trend of LRTIs but also changed the infection risk among children of different age groups, with younger children being more severely affected (Tang et al., 2021).

In 2021, *S. pneumoniae*, *S. aureus*, and *K. pneumoniae* were the main bacterial pathogens of pediatric LRTIs. Among them, *S. pneumoniae* was the leading cause of LRTI-related deaths globally, consistent with recent literature. Pneumococcal pneumonia caused 55.4% of all LRTI-related deaths across all age groups in high- and middle-income countries (Collaborators GL, 2017). Considering the relatively low vaccine coverage in low-income and low–middle-income countries, *S. pneumoniae* remains the primary pathogenic factor (Li et al., 2021).

Among older children, *S. pneumoniae*, *S. aureus*, and *K. pneumoniae* are relatively common pathogens (Raj et al., 2595 2023). Among older children (1 month to 9 years), *S. pneumoniae* and *S. aureus* were the bacterial pathogens significantly associated with severe pneumonia. These bacteria were reported to have relatively high prevalence rates in children with comorbidities (von Mollendorf et al., 2022), highlighting the need to implement targeted prevention and treatment strategies in this population. From 1990 to 2019, the significant decrease in *Haemophilus influenzae* and *S. pneumoniae* mortality rates by 77.4% and 76.1%, respectively, among children under 5 years old was mainly attributed to vaccination and improvements in medical conditions (Infections GBDLR and Antimicrobial Resistance C, 2024).

On the other hand, among neonates, this study found that the main pathogens were *K. pneumoniae*, Group B *Streptococcus*, and *A. baumannii*. *K. pneumoniae*, especially carbapenem-resistant and hypervirulent strains, poses a serious threat because of high mortality rates and treatment resistance. Group B *Streptococcus* is a leading cause of neonatal meningitis and sepsis and may have significant long-term impact on survivors. *A. baumannii* is a critical pathogen known for its antimicrobial resistance and association with severe infections (Broad et al., 2020; Furuta et al., 2022; Hu et al., 2023). These pathogens are relatively common in infants with weak immune systems. Eradicating these pathogens requires continuous surveillance, effective infection control measures, and development of new therapeutic strategies.

Despite widespread administration of pneumococcal conjugate and *H. influenzae* type b vaccines, bacterial pathogens remain important causes of moderate to severe disease in children with comorbidities (von Mollendorf et al., 2022). In addition, researchers have pointed out the urgent need to avoid overuse of antibiotics and reduce antimicrobial resistance in children with community-acquired pneumonia (Antimicrobial Resistance, 2022; Meyer Sauteur, 2024).

In 2019, the global leading cause of LRTI cases and deaths among children under 5 years old was *S. pneumoniae*, followed by RSV and influenza. In 2021, with the significant impact of the COVID-19 pandemic on influenza and RSV transmission, the incidence of influenza declined, but *S. pneumoniae* remained the most prevalent pathogen of LRTIs worldwide. Among children under 5 years old, RSV is the second most lethal pathogen after *S. pneumoniae (*Zdanowicz et al., 2023).

In this study, RSV was found to be the main virus causing neonatal death. In low-income and low–middle-income countries, RSV mainly affects younger children, highlighting the need for effective vaccines (Morgan et al., 2023). Over the past 30 years, the incidence rates of RSV and influenza have decreased; this trend was more pronounced in middle- and high-income countries, possibly because of better resources, management, and access to vaccines and monoclonal antibodies (Mezei et al., 2021). In low- and middle-income countries, prevention and management of RSV require improved diagnostics, education, timely access to new interventions, and engagement with policy makers (Carbonell-Estrany et al., 2022).

Our study have shown that the mortality rate from LRTIs has declined since the 1990s. However, despite a slight improvement in mortality rates from 18 LRTI pathogens over the next decade, influenza may cause an increase in childhood mortality starting in 2029, potentially becoming the leading cause of death among these pathogens, with higher mortality rates in females than in males. This trend is closely associated with the variability and immune escape properties of the influenza virus, as well as insufficient vaccination coverage, which result in some children's immune systems being unable to effectively respond to new viral strains and a reduction in the protective efficacy of vaccines (Smyk et al., 2022; Han et al., 2023). Influenza leads to higher mortality rates by triggering excessive immune responses, causing secondary bacterial infections (e.g., pneumococcal infections), and inducing complications such as acute respiratory distress syndrome (ARDS) (Jugulete et al., 2024). The mortality rate from influenza is particularly high among high-risk populations, such as immunocompromised children and pregnant women. Additionally, gender differences in influenza infection outcomes may be attributed to variations in immune responses, with female children potentially facing higher mortality risks (Li L. et al., 2023). Given these factors, future public health strategies should be tailored to address susceptibility factors, with specific measures to mitigate the pathogenicity of various respiratory pathogens, especially influenza.

Our study identified particulate matter pollution, child malnutrition, and household solid fuel pollution as the primary risk factors contributing to LRTI burden in children. Underweight

and malnutrition in children were also major risk factors leading to high LRTI incidence rates, similar with the research by Ruan et al (Ruan et al., 2021).

In China, the LRTI burden among children under 5 years old has significantly decreased, but it remains heavily influenced by particulate matter (PM) pollution, child malnutrition, and household solid fuel pollution (Li X. et al., 2023; Shi et al., 2023). The use of household solid fuels remains prevalent in low- and low–middle-income countries. Reducing exposure to environmental and household air pollutants and addressing child malnutrition are key strategies to mitigate the impact of LRTIs on global children's health.

Our research found that in 2020 and 2021, the burden of pediatric LRTIs increased in low-income countries. This underscored the need for global public health to focus on the impact of the COVID-19 pandemic on children's health. The COVID-19 pandemic disrupted routine childhood immunization programs, especially in low- and middle-income countries, leading to decreased vaccine coverage and making children more susceptible to LRTIs (Zar et al., 2020). The indirect pandemic effects, such as increased poverty and reduced access to healthcare, have further exacerbated this issue (Zar et al., 2020; Polasek et al., 2022). Despite these challenges, maintaining routine immunizations is crucial in order to prevent a large number of deaths and alleviate the burden of respiratory infections in children. Efforts should focus on sustaining and strengthening immunization programs to protect children's health during and after the pandemic. After contracting COVID-19, children with chronic lung diseases, such as cystic fibrosis and asthma, are prone to more severe respiratory complications, such as acute respiratory distress syndrome and respiratory failure. For these patients, COVID-19 not only worsens the underlying condition but also increases the need for oxygen therapy and other intensive care treatments (Feldstein et al., 2020; Pardasani, 2022; Bembea et al., 2023). Therefore, there is a relatively high incidence of coexisting pulmonary infections that require more intensive medical interventions and monitoring (Kim et al., 2022).

Our prediction of rising influenza mortality is primarily driven by A/H3N2's antigenic drift and low VE in pediatric populations. The 42% higher mortality in H3N2-dominant seasons underscores urgent needs for: (1) adjuvanted vaccines to improve cross-protection, (2) targeting ≥75% coverage in LMICs through GAVI partnerships, and (3) real-time strain surveillance in high-burden regions like South Asia where vaccine mismatch reached 68% in 2019-2021. The gender disparity in mortality (female:male RR=1.32 for A/H3N2) may reflect sex-dimorphic immune responses, warranting sex-stratified vaccine trials.

To reduce the future disease burden of pediatric LRTIs, our study recommends strengthening interventions in three areas. First, increase the coverage of pneumococcal vaccines, especially in low- and low–middle-income countries (Kim et al., 2022). Second, enhance control of air pollution, particularly particulate matter pollution and household solid fuel use. According to the research by Zubaidah Al-Janabi et al, improving household energy use and living conditions may effectively reduce the occurrence of pediatric LRTIs (Al-Janabi et al., 2021). Nevertheless, global public health interventions, including vaccination programs and policies that aim to improve air quality, have played a significant role in reducing the burden of LRTIs. In some countries, such as China, the incidence and mortality rates of pediatric LRTIs were significantly decreased by decreasing air pollution and promoting vaccination (Jin et al., 2021).Lastly, improve nutritional status, particularly by increasing aid to malnourished children, in order to significantly lower the incidence of LRTIs (Kirolos et al., 2021).

Limitations

This study has several limitations. It relied on data from specific medical institutions and countries, which may limit the generalizability, especially in low- and middle-income countries with varying healthcare resources. Additionally, the Global Burden of Disease (GBD) data lacks detailed pathogen information, restricting the ability to fully analyze the LRTI burden. The study also considered comorbidities but did not explore specific conditions like chronic lung disease, asthma, and obesity, which may impact the severity of LRTIs. Furthermore, seasonal and regional variations were not analyzed, which are crucial for understanding differences in incidence and predominant pathogens. Future research should expand the sample size, incorporate seasonal and regional analyses, and include more detailed data on comorbidities to improve the understanding of pediatric LRTIs.

Conclusions

This study analyzed the global trends and main pathogenic characteristics of pediatric LRTI. Although the incidence and mortality rates of LRTIs have declined globally, especially in high-income countries, the burden remains heavy in low- and middle-income countries. Moreover, younger children especially neonates were more susceptible to infections due to underdeveloped immune systems. *Streptococcus pneumoniae, Staphylococcus aureus, Klebsiella pneumoniae* were the most common causes of death in LRTIs. The burden of 18 common pathogens causing lower respiratory tract infections is expected to gradually decrease over the next decade, while the burden of influenza will steadily increase, becoming the leading cause of death, with higher mortality rates in females compared to males. The COVID-19 pandemic has reduced the transmission of respiratory viruses, but an ensuing immunity debt phenomenon led to more cases of severe infection, and the presence of COVID-19 is more likely to exacerbate underlying comorbidities among children. Particulate matter pollution and childhood underweight were the major risk factors contributing to the burden of LRTIs. Therefore, expanding vaccine coverage, improving sanitary conditions, and implementing early interventions for high-risk pediatric populations are crucial strategies to further reduce the burden of LRTIs.

Data availability statement

The original contributions presented in the study are included in the article/supplementary material. Further inquiries can be directed to the corresponding authors.

Ethics statement

The studies involving humans were approved by the Institutional Review Board (IRB) of the First Affiliated Hospital of Xinxiang Medical University. The studies were conducted in accordance with the local legislation and institutional requirements. Written informed consent for participation was not required from the participants or the participants' legal guardians/next of kin in accordance with the national legislation and institutional requirements.

Author contributions

WL: Conceptualization, Methodology, Writing – original draft, Writing – review & editing. XG: Data curation, Formal analysis, Writing – review & editing. YR: Data curation, Formal analysis, Writing – review & editing. LW: Data curation, Formal analysis, Writing – review & editing. TX: Data curation, Formal analysis, Writing – review & editing. YX: Data curation, Formal analysis, Writing – review & editing. DL: Data curation, Formal analysis, Writing – review & editing. NC: Data curation, Formal analysis, Writing – review & editing. SL: Data curation, Formal analysis, Writing – review & editing. XZ: Data curation, Formal analysis, Writing – review & editing. HL: Data curation, Formal analysis, Writing – review & editing. XW: Conceptualization, Methodology, Writing – original draft, Writing – review & editing.

Funding

The author(s) declare financial support was received for the research and/or publication of this article. Financial support was provided by the Youth Fund Project of the First Affiliated Hospital of Xinxiang Medical University (QN-2022-A05,QN-2022-A10), Henan Medical Science and Technology Joint Construction project(LHGJ20230509), Guangdong Basic and Applied Basic Research Foundation-Enterprise Joint Fund (2023A1515220134). Funding agencies did not play a role in study design, data collection, analysis and interpretation, and manuscript writing.

Acknowledgments

We sincerely thank the Institute for Health Metrics and Evaluation at the University of Washington and all the staff who provided data for this study.

Conflict of interest

The authors declare that the research was conducted in the absence of any commercial or financial relationships that could be construed as a potential conflict of interest.

Generative AI statement

The author(s) declare that no Generative AI was used in the creation of this manuscript.

Any alternative text (alt text) provided alongside figures in this article has been generated by Frontiers with the support of artificial intelligence and reasonable efforts have been made to ensure accuracy, including review by the authors wherever possible. If you identify any issues, please contact us.

Publisher's note

References

Al-Janabi, Z., Woolley, K. E., Thomas, G. N., and Bartington, S. E. (2021). A Cross-Sectional Analysis of the Association between Domestic Cooking Energy Source Type and Respiratory Infections among Children Aged under Five Years: Evidence from Demographic and Household Surveys in 37 Low-Middle Income Countries. *Int. J. Environ. Res. Public Health* 18, 8516. doi: 10.3390/ijerph18168516

Antimicrobial Resistance, C. (2022). Global burden of bacterial antimicrobial resistance in 2019: a systematic analysis. *Lancet.* 399, 629–655. doi: 10.1016/S0140-6736(21)02724-0

Bembea, M. M., Loftis, L. L., Thiagarajan, R. R., Young, C. C., McCadden, T. P., Newhams, M. M., et al. (2023). Extracorporeal membrane oxygenation characteristics and outcomes in children and adolescents with COVID-19 or multisystem inflammatory syndrome admitted to U.S. ICUs. *Pediatr. Crit. Care Med.* 24, 356–371. doi: 10.1097/PCC.0000000000003212

Broad, J., Le Doare, K., Heath, P. T., Hallchurch, P., Whelan, I., Boyd, H., et al. (2020). The current state of immunization against Gram-negative bacteria in children: a review of the literature. *Curr. Opin. Infect. Dis.* 33, 517–529. doi: 10.1097/QCO.0000000000000687

Carbonell-Estrany, X., Simoes, E. A. F., Bont, L. J., Gentile, A., Homaira, N., Scotta, M. C., et al. (2022). Identifying the research, advocacy, policy and implementation needs for the prevention and management of respiratory syncytial virus lower respiratory tract infection in low- and middle-income countries. *Front. Pediatr.* 10, 1033125. doi: 10.3389/fped.2022.1033125

Collaborators GBDAR (2024). Global burden of bacterial antimicrobial resistance 1990-2021: a systematic analysis with forecasts to 2050. *Lancet.* 404, 1199–1226. doi: 10.1016/S0140-6736(24)01867-1

Collaborators GL (2017). Estimates of the global, regional, and national morbidity, mortality, and aetiologies of lower respiratory tract infections in 195 countries: a systematic analysis for the Global Burden of Disease Study 2015. *Lancet Infect. Dis.* 17, 1133–1161. doi: 10.1016/S1473-3099(17)30396-1

Feikin, D. R., Karron, R. A., Saha, S. K., Sparrow, E., Srikantiah, P., Weinberger, D. M., et al. (2024). The full value of immunisation against respiratory syncytial virus for infants younger than 1 year: effects beyond prevention of acute respiratory illness. *Lancet Infect. Dis.* 24, e318–ee27. doi: 10.1016/S1473-3099(23)00568-6

Feldstein, L. R., Rose, E. B., Horwitz, S. M., Collins, J. P., Newhams, M. M., Son, M. B. F., et al. (2020). Multisystem inflammatory syndrome in U.S. Children and adolescents. *New Engl. J. Med.* 383, 334–346. doi: 10.1056/NEJMoa2021680

Furuta, A., Brokaw, A., Manuel, G., Dacanay, M., Marcell, L., Seepersaud, R., et al. (2022). Bacterial and host determinants of group B streptococcal infection of the neonate and infant. *Front. Microbiol.* 13, 820365. doi: 10.3389/fmicb.2022.820365

Han, A. X., de Jong, S. P. J., and Russell, C. A. (2023). Co-evolution of immunity and seasonal influenza viruses. *Nat. Rev. Microbiol.* 21, 805–817. doi: 10.1038/s41579-023-00945-8

Hu, Y., Yang, Y., Feng, Y., Fang, Q., Wang, C., Zhao, F., et al. (2023). Prevalence and clonal diversity of carbapenem-resistant Klebsiella pneumoniae causing neonatal infections: A systematic review of 128 articles across 30 countries. *PloS Med.* 20, e1004233. doi: 10.1371/journal.pmed.1004233

Infections GBDLR and Antimicrobial Resistance C (2024). Global, regional, and national incidence and mortality burden of non-COVID-19 lower respiratory infections and aetiologies, 1990-2021: a systematic analysis from the Global Burden of Disease Study 2021. *Lancet Infect. Dis.* 24, 974–1002. doi: 10.1016/S1473-3099(24)00176-2

Jia, R., Lu, L., Su, L., Lin, Z., Gao, D., Lv, H., et al. (2022). Resurgence of respiratory syncytial virus infection during COVID-19 pandemic among children in Shanghai, China. *Front. Microbiol.* 13, 938372. doi: 10.3389/fmicb.2022.938372

Jin, W., Huang, K., Ding, Z., Zhang, M., Li, C., Yuan, Z., et al. (2025). Global, regional, and national burden of esophageal cancer: a systematic analysis of the Global Burden of Disease Study 2021. *biomark. Res.* 13, 3. doi: 10.1186/s40364-024-00718-2

Jin, X., Ren, J., Li, R., Gao, Y., Zhang, H., Li, J., et al. (2021). Global burden of upper respiratory infections in 204 countries and territories, from 1990 to 2019. *EClinicalMedicine.* 37, 100986. doi: 10.1016/j.eclinm.2021.100986

Jugulete, G., Olariu, M. C., Stanescu, R., Luminos, M. L., Pacurar, D., Pavelescu, C., et al. (2024). The Clinical Effectiveness and Tolerability of Oseltamivir in Unvaccinated Pediatric Influenza Patients during Two Influenza Seasons after the COVID-19 Pandemic: The Impact of Comorbidities on Hospitalization for Influenza in Children. *Viruses* 16, 1576. doi: 10.3390/v16101576

Kim, S. H., Hong, J. Y., Bae, S., Lee, H., Wi, Y. M., Ko, J. H., et al. (2022). Risk factors for coronavirus disease 2019 (COVID-19)-associated pulmonary aspergillosis in critically ill patients: A nationwide, multicenter, retrospective cohort study. *J. Korean Med. Sci.* 37, e134. doi: 10.3346/jkms.2022.37.e134

Kirolos, A., Blacow, R. M., Parajuli, A., Welton, N. J., Khanna, A., Allen, S. J., et al. (2021). The impact of childhood malnutrition on mortality from pneumonia: a systematic review and network meta-analysis. *BMJ Glob Health* 6, e007411. doi: 10.1136/bmjgh-2021-007411

Li, L., Yan, Z. L., Luo, L., Liu, W., Yang, Z., Shi, C., et al. (2023). Influenza-associated excess mortality by age, sex, and subtype/lineage: population-based time-series study with a distributed-lag nonlinear model. *JMIR Public Health Surveill.* 9, e42530. doi: 10.2196/42530

Li, X., Li, Y., Yu, B., Nima, Q., Meng, H., Shen, M., et al. (2023). Urban-rural differences in the association between long-term exposure to ambient particulate matter (PM) and malnutrition status among children under five years old: A cross-sectional study in China. *J. Glob Health* 13, 04112. doi: 10.7189/jogh.13.04112

Li, X., Mukandavire, C., Cucunuba, Z. M., Echeverria Londono, S., Abbas, K., Clapham, H. E., et al. (2021). Estimating the health impact of vaccination against ten pathogens in 98 low-income and middle-income countries from 2000 to 2030: a modelling study. *Lancet.* 397, 398–408. doi: 10.1016/S0140-6736(20)32657-X

Meyer Sauteur, P. M. (2024). Childhood community-acquired pneumonia. *Eur. J. Pediatr.* 183, 1129–1136. doi: 10.1007/s00431-023-05366-6

Mezei, A., Cohen, J., Renwick, M. J., Atwell, J., and Portnoy, A. (2021). Mathematical modelling of respiratory syncytial virus (RSV) in low- and middle-income countries: A systematic review. *Epidemics.* 35, 100444. doi: 10.1016/j.epidem.2021.100444

Morgan, N., Buys, H., and Muloiwa, R. (2023). RSV infection in children hospitalised with severe lower respiratory tract infection in a low-middle-income setting: A cross-sectional observational study. *PloS One* 18, e0291433. doi: 10.1371/journal.pone.0291433

Mrcela, D., Markic, J., Zhao, C., Viskovic, D. V., Milic, P., Copac, R., et al. (2022). Changes following the Onset of the COVID-19 Pandemic in the Burden of Hospitalization for Respiratory Syncytial Virus Acute Lower Respiratory Infection in Children under Two Years: A Retrospective Study from Croatia. *Viruses* 14, 2746. doi: 10.3390/v14122746

Nagelkerke, M. C. M., Zagten, M. V., Sprij, A., Bekhof, J., Veen, M. V., and Kruizinga, M. D. (2024). Incidence, severity, and clinical characteristics of lower respiratory tract infections in children before and after the coronavirus disease 2019 lockdown: a Dutch single-center study. *Pediatr. Emerg. Med. J.* 11, 17–27. doi: 10.22470/pemj.2023.00836

Pardasani, S. A. (2022). 44 COVID-19 among pediatric patients with pre-existing pulmonary conditions: Preliminary results from the Pediatric COVID-19 U.S. Registry. *J. Pediatr. Infect. Dis. Soc.* 11, S7–SS. doi: 10.1093/jpids/piac041.026

Polasek, O., Wazny, K., Adeloye, D., Song, P., Chan, K. Y., Bojude, D. A., et al. (2022). Research priorities to reduce the impact of COVID-19 in low- and middle-income countries. *J. Glob Health* 12, 09003. doi: 10.7189/jogh.12.09003

Qiu, W., Zheng, C., Huang, S., Zhang, Y., and Chen, Z. (2022). Epidemiological trend of RSV infection before and during COVID-19 pandemic: A three-year consecutive study in China. *Infection Drug resistance.* 15, 6829–6837. doi: 10.2147/IDR.S388231

Raj, D., Rao Mallyala, S., Chirumamilla, A., Gajjar, J., Patel, S., Dekhne, A., et al. (2023). 2595. Burden of lower respiratory tract infection in United States of america and its trend from 1990-2019: A benchmarking analysis from the global burden of disease study. *Open Forum Infect. Dis.* 10, ofad500.2210. doi: 10.1093/ofid/ofad500.2210

Ruan, Z., Qi, J., Qian, Z. M., Zhou, M., Yang, Y., Zhang, S., et al. (2021). Disease burden and attributable risk factors of respiratory infections in China from 1990 to 2019. *Lancet Reg. Health West Pac.* 11, 100153. doi: 10.1016/j.lanwpc.2021.100153

Safiri, S., Mahmoodpoor, A., Kolahi, A. A., Nejadghaderi, S. A., Sullman, M. J. M., Mansournia, M. A., et al. (2022). Global burden of lower respiratory infections during the last three decades. *Front. Public Health* 10, 1028525. doi: 10.3389/fpubh.2022.1028525

Sah, R., Zaman, K., Mohanty, A., Al-Ahdal, T., Awad, H., Padhi, B. K., et al. (2023). Respiratory syncytial virus with ongoing COVID-19: is it an emerging threat? *Ann. Med. Surg. (Lond)* 85, 67–70. doi: 10.1097/MS9.0000000000000153

Shi, X., Wu, M., Jia, X., Bao, J., Wang, Y., Yang, C., et al. (2023). Trends of Incidence, Mortality, and Risk Factors for Lower Respiratory Infections among Children under 5 Years in China from 2000 to 2019. *Int. J. Environ. Res. Public Health* 20, 3547. doi: 10.3390/ijerph20043547

Shin, Y. H., Hwang, J., Kwon, R., Lee, S. W., Kim, M. S., Collaborators GBDAD, et al. (2023). Global, regional, and national burden of allergic disorders and their risk factors in 204 countries and territories, from 1990 to 2019: A systematic analysis for the Global Burden of Disease Study 2019. *Allergy.* 78, 2232–2254. doi: 10.1111/all.15807

Smyk, J. M., Szydlowska, N., Szulc, W., and Majewska, A. (2022). Evolution of influenza viruses-drug resistance, treatment options, and prospects. *Int. J. Mol. Sci.* 23, 12244. doi: 10.3390/ijms232012244

Tang, X., Dai, G., Jiang, X., Wang, T., Sun, H., Chen, Z., et al. (2021). Clinical characteristics of pediatric respiratory tract infection and respiratory pathogen isolation during the coronavirus disease 2019 pandemic. *Front. Pediatr.* 9, 759213. doi: 10.3389/fped.2021.759213

von Mollendorf, C., Berger, D., Gwee, A., Duke, T., Graham, S. M., Russell, F. M., et al. (2022). Aetiology of childhood pneumonia in low- and middle-income countries in the era of vaccination: a systematic review. *J. Glob Health* 12, 10009. doi: 10.7189/jogh.12.10009

Wang, X., Li, Y., Mei, X., Bushe, E., Campbell, H., and Nair, H. (2021). Global hospital admissions and in-hospital mortality associated with all-cause and virus-specific acute lower respiratory infections in children and adolescents aged 5-19 years between 1995 and 2019: a systematic review and modelling study. *BMJ Glob Health* 6, e006014. doi: 10.1136/bmjgh-2021-006014

Wu, X., Lu, W., Sang, X., Xu, Y., Wang, T., Zhan, X., et al. (2023). Timing of bronchoscopy and application of scoring tools in children with severe pneumonia. *Ital J. Pediatr.* 49, 44. doi: 10.1186/s13052-023-01446-3

Yigezu, A., Misganaw, A., Getnet, F., Berheto, T. M., Walker, A., Zergaw, A., et al. (2023). Burden of lower respiratory infections and associated risk factors across regions in Ethiopia: a subnational analysis of the Global Burden of Diseases 2019 study. *BMJ Open* 13, e068498. doi: 10.1136/bmjopen-2022-068498

Zar, H. J., Dawa, J., Fischer, G. B., and Castro-Rodriguez, J. A. (2020). Challenges of COVID-19 in children in low- and middle-income countries. *Paediatr. Respir. Rev.* 35, 70–74. doi: 10.1016/j.prrv.2020.06.016

Zdanowicz, K., Lewandowski, D., Majewski, P., Polkosnik, K., Liwoch-Nienartowicz, N., Reszec-Gielazyn, J., et al. (2023). Clinical presentation and co-detection of respiratory pathogens in children under 5 years with non-COVID-19 bacterial and viral respiratory tract infections: A prospective study in Bialystok, Poland (2021-2022). *Med. Sci. monitor: Int. Med. J. Exp. Clin. Res.* 29, e941785. doi: 10.12659/MSM.941785

Zhu, X., Ye, T., Zhong, H., Luo, Y., Xu, J., Zhang, Q., et al. (2022). Distribution and drug resistance of bacterial pathogens associated with lower respiratory tract infection in children and the effect of COVID-19 on the distribution of pathogens. *Can. J. Infect. Dis. Med. Microbiol.* 2022, 1181283. doi: 10.1155/2022/1181283

frontiers | Frontiers in Cellular and Infection Microbiology

TYPE Original Research
PUBLISHED 16 October 2025
DOI 10.3389/fcimb.2025.1532174

OPEN ACCESS

EDITED BY
Paraskevi C. Fragkou,
Evaggelismos General Hospital, Greece

REVIEWED BY
Zhang Yu Jing,
Huazhong University of Science and Technology, China
Ruth Lizzeth Madera Sandoval,
Mexican Social Security Institute, Mexico

*CORRESPONDENCE
Yao Wei
dr_betty@126.com
Jun Jin
jinjundoctor@163.com

†These authors have contributed equally to this work

RECEIVED 03 December 2024
ACCEPTED 23 September 2025
PUBLISHED 16 October 2025

CITATION
Tang Y, Yang J, Chen L, Liu X, Chen Z, Lin J, Jin J and Wei Y (2025) Evaluating lymphocyte change rate and lactate as predictors of prognosis in critical COVID-19 patients in the intensive care unit. *Front. Cell. Infect. Microbiol.* 15:1532174. doi: 10.3389/fcimb.2025.1532174

Evaluating lymphocyte change rate and lactate as predictors of prognosis in critical COVID-19 patients in the intensive care unit

Yuxiu Tang[1†], Jin Yang[2†], Liquan Chen[2], Xueke Liu[2], Zhen Chen[2], Jiaxi Lin[2], Jun Jin[2*] and Yao Wei[2*]

[1]Department of Intensive Care Unit, The Second Affiliated Hospital, Hengyang Medical School, University of South China, Hengyang, China, [2]Department of Intensive Care Unit, The First Affiliated Hospital of Soochow University, Suzhou, China

Background: Studies have shown that lymphocyte counts and lactate (LAC) levels have a certain relationship with the prognosis of COVID-19 patients. In the present study, we aimed to determine the predictive effects of new indicator lymphocyte change rate and LAC on the prognosis of COVID-19 patients.

Methods: In the present study, we retrospectively analyzed the clinical data of 137 adult patients (≥ 18 years old) diagnosed with the COVID-19 Omicron variant, who were admitted to the comprehensive, respiratory, or infection ICU of our hospital, between November 2022 and February 2023. Cox regression and causal mediation analyses were used to evaluate the relationship between the clinical test data and patient prognosis.

Results: A total of 137 patients with COVID-19 were included in the present study, 77.40% of whom were male, with an average age of 73 years and an overall mortality rate of 51.8%. Multifactorial logistic regression analysis showed that LAC (odds ratio [OR], 0.05; 95% confidence interval [CI], 0–0.1; P = 0.047] and the weekly rate of change in LYM (change in LMY over the course of a week/LYM on the day of admission) had a good predictive value for the prognosis of patients, while respiratory-related indicators had no significant relationship with prognosis ($P > 0.05$). The combined predictive value of LAC and the weekly rate of change in LYM was even greater, with an area under the curve of 0.7629. In terms of prognosis, 1.75 mmol/L was set as the cut-off value for LAC (sensitivity, 57.7%; specificity, 75.8%). The mortality rate of patients with LAC > 1.75 mmol/L was significantly higher than that those with LAC < 1.75 mmol/L, and NLR was found to have a mediating effect in lactate-mediated death.

Conclusion: In summary, lymphocyte change rate combined with LAC had the greatest predictive value for COVID-19 ICU patient prognosis, while respiratory-related indicators had no significant relationship with prognosis, so we suggest the increase of LAC in COVID-19 patients may be caused by microcirculatory disturbances.

KEYWORDS

coronavirus disease 2019, lactate, lymphocyte change rate, outcome, intensive care unit

1 Introduction

Coronavirus disease 2019 (COVID-19) was first encountered in Wuhan, China in December 2019, as a case of unexplained pneumonia caused by the novel severe acute respiratory syndrome coronavirus 2 (SARS-CoV-2), which was quickly followed by a global outbreak that was declared a pandemic by the World Health Organization (WHO) on March 11, 2020 (Guan et al., 2020; Zhu et al., 2020). According to the WHO, as of the time of the writing of this article, there have been 766,440,796 confirmed cases of COVID-19 worldwide, resulting in 6,932,591 deaths (WHO COVID-19 Dashboard, 2020). COVID-19, therefore, poses a serious threat to public health worldwide[3]. Viruses are highly diverse, due to their susceptibility to mutations and recombination (Huo et al., 2020), and during the last three years of the COVID-19 pandemic, numerous variants have been identified by the WHO, including Alpha, Beta, Gamma, Delta, and Omicron. The common mechanism by which COVID-19 invades the body is by targeting angiotensin-converting enzyme 2 (ACE2), exerting a pathogenic effect (Mathioudakis et al., 2022).

Lactate (LAC) is the final product of cellular glycolysis under anaerobic conditions, and is a metabolic waste product removed from the blood by the liver and kidneys (Rabinowitz and Enerbäck, 2020). Conventional wisdom has been that increased LAC levels are due to anaerobic metabolism caused by hypoxia in the body. Bakker et al (Bakker et al., 2013; Gupta, 2022) proposed that the cause of hyperlactatemia may be multifactorial, as it can also occur under completely aerobic conditions. It has been shown that the level of LAC can be significantly higher in patients hospitalized with COVID-19 compared to those that are not hospitalized, that the initial LAC level in deceased patients is higher than that in those that survive (Trebuian et al., 2024; Velavan et al., 2021), and that lactate dehydrogenase (LDH), a key enzyme in the conversion of pyruvate to LAC, can be used as a significant independent risk factor for predicting the occurrence respiratory failure in severe COVID-19 patients (Wang et al., 2024). Based on a multifactorial analysis of the increase in LAC levels, it is necessary to further explore whether the increase in LAC in patients with COVID-19 is due only to hypoxia from impaired ventilation and air exchange resulting from pulmonary changes, or if it is also due to a combination of local ischemia, which may result in an imbalance in the ventilation-to-blood flow ratio.

Significant changes can be observed in the immune systems of patients with COVID-19, which primarily manifest as a continuous and significant decrease in peripheral blood lymphocyte (LYM) count, the majority of which are CD4+T and CD8+T cells. These changes are significantly related to complications and poor prognoses (Zhou et al., 2020); therefore, changes in the LYM count should be dynamically observed in clinical practice. As such, we proposed using the rate of change in LYM over the course of one week (changes in LYM counts during the first week after admission)/(LYM counts on the day of admission) to determine the predictive value of LYM count for prognoses. LYM counts and its correlation with other test indicators, such as Neutrophil (NEU)-to- Lymphocyte ratio (NLR), Platelet-to-Lymphocyte ratio (PLR), and Lymphocyte-to-Monocyte ratio (LMR) have been studied extensively, of which NLR is considered an independent predictor of the risk of death in COVID-19 patients (Colaneri et al., 2024), with a higher ratio being associated with an increased risk of thrombosis (Pivina et al., 2024).

The present study, therefore, aimed to explore the predictive value of LAC and the weekly rate of change in LYM on the prognosis of patients, through a retrospective analysis of the clinical data of COVID-19 patients admitted to the intensive care unit (ICU), and whether there was any relationship with other clinical indicators.

2 Materials and methods

2.1 Study design

The following data were collected from 137 comprehensive, respiratory, and infection ICU patients with reverse transcription polymerase chain reaction (RT-PCR) assay-confirmed COVID-19: clinical demographic, vital signs (first and seventh day of ICU admission), related laboratory test results, clinical treatment and outcomes, and Acute Physiology and Chronic Health Evaluation II (APACHE II) and Sequential Organ Failure Assessment (SOFA) scores (first and seventh days of ICU admission). All data were obtained from the hospital's electronic medical record database during the initial implementation of the re-opening policy in China from November 2022 to February 2023.

2.2 Statistical analysis

The basic data from 168 ICU patients were processed, and after excluding patients with incomplete data, a total of 137 patients were included for analysis in the present study. The total number and proportions were used to represent categorical variables. For normally distributed variables, the data were expressed as mean and standard deviation (SD), while skewed data were expressed as median and interquartile range (Q1–Q3). The Chi-squared or Fisher's exact test was used to compare the categorical variables, the student's t-test was used to compare the normally distributed continuous variables, the Mann-Whitney U test was used to compare the skewed continuous variables, and multiple regression was selected to characterize the relationship between clinical indicators and primary outcomes. Baseline variables which were clinically relevant or had a univariate relationship with prognosis, such as age, fraction of inspired oxygen (FiO_2), LAC level, white blood cell (WBC) count, NEU count, NLR, LDH, D-dimer (DD) level, fibrinogen degradation product (FDP), and APACHE II and SOFA scores, were entered into the multivariate logistic regression model as covariates. The receiver operating characteristic (ROC) curve and the area under the curve (AUC) were calculated to evaluate and compare the diagnostic performance of each parameter. A restricted cubic spline (RCS) was used to predict the relationship between LAC level and event risk, and the inflection

point was set as the cut-off point. Stratified based on the LAC cut-off value in the ROC curve, the relationship of LAC level with associated factors, including APACHE II and SOFA scores on the seventh day as well as hospitalization time, was evaluated using the Cox proportional risk model, with covariates adjusted for sex and age for each model. We created a survival curve stratified based on LAC values, after which we conducted a causal mediation analysis (CMA) to determine whether other clinical indicators changed the relationship between LAC level and clinical outcomes. For this, we determined which indicators were simultaneously related to LAC level and clinical outcomes, and the shortlisted indicator, NLR, was subjected to CMA as described by previous studies (Huang and Yang, 2017; Choy et al., 2023), as an instrumental variable, with LAC level as the independent variable and clinical outcomes as the dependent variable. Statistical analyses were performed using R software version 4.2.0. (R Foundation for Statistical Computing) with statistical significance set at $P < 0.05$.

3 Results

3.1 Basic clinical characteristics of patients

A total of 137 patients were included in the present study, 77.40% of whom were male, with an average age of 72.7 years. The mortality rate was 51.8%, with the majority of deaths being men (84.5%), and the average length of stay in the ICU was 20 days. The age of the deceased patients, as well as their APACHE II and SOFA scores on the day of ICU admission were significantly higher than those of the surviving patients, although their hospitalization time was shorter. FIO_2, LAC level, WBC count, NEU count, NLR, blood urea nitrogen (BUN), aspartate aminotransferase (AST), alanine aminotransferase (ALT), LDH, FDP, and DD in the deceased patients were significantly higher ($P < 0.05$), while their albumin levels were significantly lower ($P = 0.047$) than those in the surviving patients (Table 1). The LYM count in the surviving patients showed a statistically significant upward trend within one week of ICU admission ($P < 0.001$). Multivariate regression analysis showed that age, LAC level, NLR, and SOFA score were significantly associated with the patients' prognoses ($P < 0.05$) (Table 2).

3.2 Relationship between LAC and prognosis

Multivariate analysis showed that, excluding the interference of other factors, LAC level was an independent outcome predictor for ICU patients with COVID-19 (odds ratio [OR], 0.05; 95% confidence interval [CI], 0–0.1; $P = 0.047$). For LAC level, the AUC was 0.70, and the cut-off value was 1.75 mmol/L. The sensitivity and specificity were 57.7% and 75.8%, respectively. Using a cut-off value of 1.75 mmol/L (Figure 1) to classify patients as having high or low LAC levels, it was found that the survival probability of patients with a LAC level >1.75 mmol/L was significantly decreased ($P = 0.00057$) (Figure 2). When the patient's LAC was > 1.75 mmol/L, their risk of death increased significantly (crude OR, 1.41; 95% CI, 1.2–1.65; $P < 0.001$), even after adjusting for age and gender (adjusted OR, 1.36; 95% CI, 1.15–1.58; $P < 0.001$) (Table 3). Additionally, we used the RCS function to flexibly model and visually predict the relationship between LAC level and all-cause mortality in patients hospitalized in the ICU with COVID-19, starting with a relatively stable risk of all-cause mortality until LAC concentrations reached 1.5–1.75 mmol/L, at which point all-cause mortality began to increase rapidly (non-linear $P < 0.001$) (Figure 3).

3.3 Predictive role of LAC combined with lymphocyte change rate on prognosis

The area under the ROC curve of the combination of lactate and lymphocyte change rate (AUC 0.7629) was significantly higher than that of lactate (AUC 0.70) and lymphocyte change rate (AUC 0.648) alone for prognosis ($P < 0.05$) (Figure 4).

3.4 Mediation analysis

Considering the complexity of the reasons behind an increase of LAC in the body, and the corresponding relationship of LAC with the body's immune and inflammatory responses, we evaluated in the present study whether or not there is a relationship between elevated LAC levels and other indicators, and whether that relationship has an enhancing or weakening effect on the relationship between LAC level and outcome. CMA is a method used to distinguish the total effect of something as the direct and indirect effect, where the indirect effect on an outcome is mediated by intermediate factors. CMA produces an average causal mediation effect (ACME), average direct effect (ADE), and total effect (Chen et al., 2020). Prior to the intermediate mediation analysis, the association between pre-specified mediators (including routine blood tests, biochemistry, coagulation, blood gas, and other related indicators) and prognosis was evaluated. Among the 15 clinical test indicators related to prognosis, only NLR showed a robust mediating effect after complete adjustment. The direct effect of LAC level and adverse outcomes (hazards ratio [HR], 0.306; 95% CI, 0.138–0.460; $P < 0.001$) was strengthened by the indirect effect of NLR (HR, 0.038; 95% CI, 0–0.090; $P < 0.05$), resulting in a greater total effect (HR, 0.344; 95% CI, 0.182–0.490; $P < 0.001$) (Figures 5, 6).

3.5 Correlation analysis between P/F and lactate and lymphocyte change rate

Correlation analysis of P/F with lactate and lymphocyte change rate revealed a negative correlation between P/F and lactate (R=-0.21, P = 0.013), which was statistically significant (Figure 7). And although there was a negative correlation between P/F and lymphocyte change rate, it was not statistically significant (R=-0.035, P = 0.69) (Figure 8).

10.3389/fcimb.2025.1532174

TABLE 1 Basic clinical characteristics of patients.

Variables	Total (n = 137)	Survival (n = 66)	Non-survival (n = 71)	*p*
Demographic and clinical characteristics				
Age (years), Median (Q1,Q3)	76 (66, 82)	72.5 (62.25, 80)	79 (70, 82.5)	0.003*
sex, n (%)				0.062
Female, n (%)	31 (23)	20 (30)	11 (15)	
Male, n (%)	106 (77)	46 (70)	60 (85)	
APACHII, Median (Q1,Q3)	15 (10, 19)	11 (8, 16)	17 (12.5, 21)	< 0.001*
SOFA, Median (Q1,Q3)	5 (3, 9)	4 (2, 6)	8 (4, 11)	< 0.001*
Time, Median (Q1,Q3)	16 (8, 28)	20.5 (12.25, 39.75)	11 (6, 18.5)	< 0.001*
Blood gas analysis				
RR, Median (Q1,Q3)	20 (16, 25)	18 (16, 23.75)	20 (17, 25.5)	0.15
FIO2(%), Median (Q1,Q3)	60 (43, 80)	55.5 (41, 70)	60 (50, 80)	0.022*
PO2(mmHg), Median (Q1,Q3)	78 (59.5, 125.8)	88.2 (61.65, 150.25)	74.3 (55.4, 110)	0.087
PCO2(mmHg), Median (Q1,Q3)	38.5 (33.5, 46.9)	37.15 (33.2, 42.35)	40 (35.25, 49.25)	0.098
SO2, Median (Q1,Q3)	95.6 (89.8, 98.8)	96.95 (92.03, 99.33)	94.2 (87.85, 97.85)	0.006*
LAC(mmol/L), Median (Q1,Q3)	1.5 (1.1, 2.5)	1.25 (1, 1.67)	2.1 (1.3, 3)	< 0.001*
<1.75	59 (43)	28 (42)	31 (44)	
>1.75	78 (57)	38 (58)	40 (56)	
PF(mmHg), Median (Q1,Q3)	149 (103, 254)	169 (117.25, 335.75)	131 (82.5, 184.5)	0.004*
Laboratory tests				
WBC(×109/L), Median (Q1,Q3)	9.22 (5.93, 12.66)	7.62 (5.4, 11.72)	10.7 (6.8, 14.62)	0.006*
NEU(×109/L), Median(Q1,Q3)	8.12 (5.04, 11.79)	6.62 (4.67, 10.25)	9.78 (5.64, 13.44)	0.004*
LYM(×109/L), Median (Q1,Q3)	0.53 (0.34, 0.85)	0.5 (0.31, 0.79)	0.56 (0.38, 0.93)	0.141
NLR(×109/L), Median (Q1,Q3)	7.9 (4.7, 11.5)	5.9 (4.05, 9.55)	9.6 (5.12, 13.2)	< 0.001*
LYMrate, Median (Q1,Q3)	0.24 (-0.44, 0.76)	0.46 (0.03, 1.24)	-0.3 (-0.62, 0.38)	< 0.001*
CRP(mg/L), Median (Q1,Q3)	93.5 (36.99, 154.24)	76.41 (28.49, 141.16)	109.74 (57.61, 167.55)	0.058
PLT(×109/L), Median (Q1,Q3)	169 (103, 219)	175 (132, 222.75)	142 (93, 214.5)	0.112
BUN(mmol/L), Median (Q1,Q3)	9.9 (6.98, 17.54)	9.16 (6.02, 12.52)	11.66 (8.09, 19.3)	0.001*
Cr(umol/L), Median (Q1,Q3)	76.2 (56.3, 114.3)	71 (54.65, 106.25)	83 (57.1, 126.65)	0.216
ALB(g/L), Median (Q1,Q3)	30.3 (26.9, 33.4)	30.85 (28.33, 34.38)	29.8 (25.65, 32.35)	0.047*
ALT(U/L), Median (Q1,Q3)	25 (16.8, 39.5)	22.5 (15, 32.75)	27.5 (19, 47)	0.035*
AST(U/L), Median (Q1,Q3)	34.1 (22, 54)	29.2 (20.32, 42.75)	41 (23.35, 68)	0.031*
TB(umol/L), Median (Q1,Q3)	12.6 (8.2, 17)	11.45 (8.03, 15.17)	12.9 (8.9, 22.3)	0.126
LDH(U/L), Median (Q1,Q3)	381.7 (232.4, 502.6)	283.8 (202.48, 432.7)	443.7 (320.05, 568.6)	< 0.001*
PT (sec), Median (Q1,Q3)	14.4 (13.5, 16.1)	14.2 (13.33, 15.95)	14.5 (13.6, 16.45)	0.272
APTT(sec), Median (Q1,Q3)	37.8 (33, 43.9)	37.35 (33.52, 42.77)	38.1 (32.6, 46.35)	0.613
INR, Median (Q1,Q3)	1.15 (1.07, 1.31)	1.14 (1.06, 1.29)	1.18 (1.08, 1.34)	0.253
FIB(g/L), Mean ± SD	4.55 ± 1.85	4.85 ± 1.69	4.27 ± 1.96	0.065

(Continued)

TABLE 1 Continued

Variables	Total (n = 137)	Survival (n = 66)	Non-survival (n = 71)	*p*
Laboratory tests				
FDP(mg/L), Median (Q1,Q3)	8.19 (4.13, 21.87)	7.37 (3.24, 14.48)	9.42 (5.36, 31.62)	0.011*
DD(ug/mL), Median (Q1,Q3)	2.86 (1.46, 7.3)	2.25 (1.15, 4.58)	4.69 (2.21, 10.26)	0.001*

*p-value < 0.05. Data are expressed as number of patients (n), percentages of total related variable (%) and mean ± SD for normally distributed variables and median (IQR) for skewed data. Patients were divided into 2 groups, depending on 28-day ICU mortality. APACHE, acute physiology and chronic health evaluation; SOFA, sequential organ failure assessment; RR, respiratory rate; FiO_2, fraction of inspired oxygen; PO_2, arterial partial pressure of oxygen; PCO_2, partial pressure of carbon dioxide; PF, PO2/FiO2; WBC, white blood cell; NEU, neutrophils; LYM, lymphocyte; NLR, neutrophil to lymphocyte ratio; LYM rate, the rate of change in lymphocyte within one week (Changes in lymphocyte during the week/lymphocyte counts on the first day); CRP, C-reactive protein; PLT, Platelet count; BUN, blood urea nitrogen; Cr, Creatinine; ALB, albumin; ALT, alanine aminotransferase; AST, aspartate aminotransferase; TB, total bilirubin; LDH, lactate dehydrogenase; PT, prothrombin time; APTT, activated partial thromboplastin time; INR, international normalized ratio; FDP, fibrin degradation product; FIB, fibrinogen; DD, D-Dimer.

4 Discussion

In a retrospective analysis of patients with COVID-19 admitted to our comprehensive, respiratory, and infection ICUs during the COVID-19 pandemic, the predictive value of LAC level combined with the weekly LYM change rate for determining prognoses was greater than that of either alone, which is of practical value for judging the prognosis of ICU patients with COVID-19. The risk of death in patients with a LAC level >1.75 mmol/L on the day of admission to the ICU was significantly higher than that in patients with lower LAC levels. The increase in LAC, however, was not found to be associated with respiratory-related indicators, which may, in turn, be related to microcirculation disorders due to SARS-CoV-2 infection.

TABLE 2 Results of multivariate regression analysis.

Variable	OR(95%CI)	*P*
Age	0.01(0~0.02)	0.003*
FIO2	0(-0.01~0)	0.093
SO2	-0.01(-0.02~0)	0.256
LAC	0.05(0~0.1)	0.047*
PF	0(0~0)	0.535
WBC	0(-0.06~0.05)	0.909
NEU	-0.02(-0.1~0.06)	0.638
NLR	0.03(0~0.06)	0.046*
LYMrate	-0.05(-0.01~0)	0.05
BUN	0(0~0.01)	0.29
ALB	0(-0.01~0.01)	0.88
ALT	0(0~0)	0.222
AST	0(0~0)	0.097
LDH	0(0~0)	0.265
DD	0(-0.01~0.02)	0.422
FDP	0(0~0)	0.522
APACHII	0.02(0~0.03)	0.05
SOFA	0.02(0~0.04)	0.025*

*p-value < 0.05.

Arterial blood LAC level is used as a routine parameter of clinical evaluation in ICU patients, as increased LAC levels are common in critically ill patients, and are often used to assess disease severity, monitor and guide treatment, and determine prognosis. For example, The Sepsis-3 guidelines include high LAC levels (> 2 mmol/L) as a diagnostic criterion for septic shock, and recommend normalizing LAC levels as a goal during early fluid resuscitation (Rhodes et al., 2017). Traditionally, it has been believed that an increase in blood LAC is the result of anaerobic metabolism due to tissue hypoxia; however, increased LAC concentrations can also be found in non-hypoxic states of the body, such as a decrease in clearance due to kidney or liver dysfunction (Kumar et al., 2025), an increase in aerobic glycolysis (Chen et al., 2025), and beta-adrenergic stimulation (Rimachi et al., 2012), as a result of the interaction of oxygen supply, tissue metabolism, and blood clearance. In the early stages of the COVID-19 epidemic in Wuhan, it was found that about 84% of elderly patients (≥ 60 years old) had elevated LAC levels (Li P. et al., 2020). A data analysis of 2,860 elderly patients admitted to the ICU with COVID-19 showed that the initial LAC levels of those that did not survive were significantly higher than in those that did survive, increased serum lactate on the first day was related to a significant increase in ICU mortality, as well as 30-day and 3-month mortality, and ICU mortality was negatively correlated with a decrease in the LAC level (Bruno et al., 2021). In a Greek single-center study, Alice et al (Vassiliou et al., 2020) proposed that a cut-off value of 1.85 mmol/L for LAC level could predict mortality in ICU patients with COVID-19. The statistical analysis performed in the present retrospective study found that 1.75 mmol/L could be used as a critical value to judge the prognosis of ICU patients with severe COVID-19, and found that lactate >1.75 mmol/L was significantly correlated with the patients' prognoses ($P < 0.001$). The difference in this cut-off value may be due to regional differences, different prevalent strains, or other factors.

Researchers have studied the pathogenic mechanism of SARS-CoV-2, the pathogen that causes COVID-19, and have found that the virus mainly exerts its toxic effect by binding to the host receptor membrane ACE2 through its spike S-glycoprotein (Gheblawi et al., 2020), while ACE2 is expressed in a variety of cells in the respiratory tract, so that the SARS-CoV-2 directly infects the bronchial and alveolar epithelial cells, causing lung tissue damage and affecting the ventilation and air exchange function of the body (Sungnak et al., 2020). In the present study, however, we found that partial pressure of oxygen (PO_2) and Oxygen saturation(SO_2)were lower, while

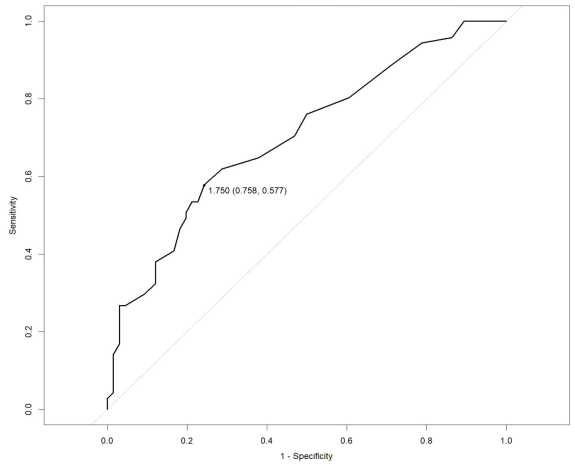

FIGURE 1
Receiver operating characteristic (ROC) curve for predicting the prognosis of severe COVID-19. LAC: cut-off 1.75 mmol/L, sensitivity 57.7%, specificity 75.8%.

partial pressure of carbon dioxide (PCO_2) and FIO_2 were higher, in patients who died of severe COVID-19 than in the surviving patients, although none of the differences were significant. Additionally, we observed no significant relationship between these values and prognosis, even after excluding interference from other factors through multifactorial regression analysis ($P > 0.05$), while LAC was found to be significantly associated with prognosis ($P = 0.047$). In regards to the source and clearance of LAC, an increase in LAC throughout the body may be caused by insufficient tissue perfusion. (Li H. et al., 2020) found that approximately 71.4% of patients who died of COVID-19 had disseminated intravascular coagulation, evidenced by the observation of a thrombus in the microvascular system upon autopsy (Wichmann et al., 2020). Tang et al (2020a; 2020b). reviewed coagulation parameters in COVID-19 patients, and proposed that FDP and DD levels were significantly higher in deceased than surviving patients, and that patients with DD levels exceeding six times the upper limit of normal had an increased mortality rate, suggesting that although other factors may contribute to the elevation of LAC in the body, reduced tissue perfusion due to thrombosis caused by microcirculatory thrombi may be the primary cause of increased LAC levels in patients with COVID-19.

Since ACE2 is highly expressed in arteriovenous endothelia, viruses cause damage and apoptosis to the vascular endothelia by binding to ACE2, triggering endothelial inflammation, and subsequently, thrombus formation (Varga et al., 2020). Simultaneously, ACE2, as a key link in the renin-angiotensin-aldosterone system (RASS), plays a role in vasodilation and anti-inflammatory actions; therefore, when ACE2 is blocked by the virus and its expression is downregulated, the microcirculatory blood flow decreases, resulting in inadequate circulatory perfusion of the tissue (Patel et al., 2016; Hanff et al., 2020), as oxygen exchange occurs in the microcirculatory system, and oxygen consumption is limited when systemic oxygen delivery is reduced (Wang et al., 2023). Moreover, SARS-CoV-2 infection can cause mitochondrial reactive oxygen species (ROS) production and dysfunction, inducing hypoxia-inducible factor-1 (HIF-1) activation, reduced oxidative phosphorylation, and increased aerobic glycolysis, resulting in an increase in LAC levels (Kumar et al., 2021; Tian et al., 2021; Yang et al., 2022). Additionally, a leftward shift in the oxygen dissociation curve can be observed in COVID-19 patients (Böning et al., 2021), indicating an increased affinity between

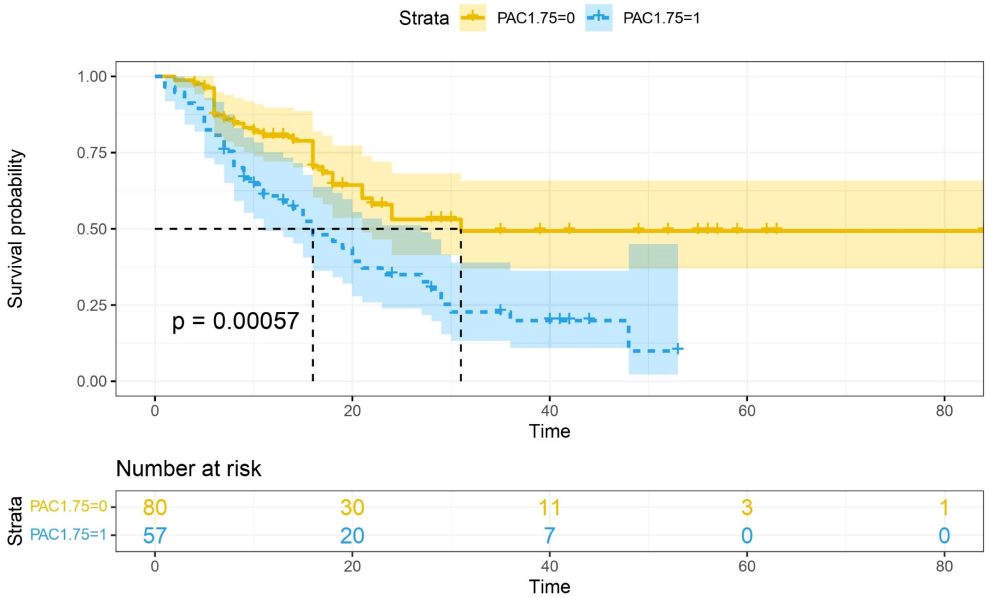

FIGURE 2
Survival curves stratified by lactate concentration. The blue curve represents the survival probability of patients with LAC > 1.75, and the yellow curve represents the survival probability of patients with LAC < 1.75. It was found that the survival probability of patients with LAC > 1.75 mmol/L was significantly reduced (p =0.00057).

TABLE 3 Associations between LAC>1.75mmol/L and outcomes.

	Crude			Adjusted**		
	OR	95% confidence interval	P	OR	95% confidence interval	*P*
SOFA-D7	8.1	0.89-73.1	0.06	7.81	0.83-73.13	0.07
APACHII-D7	1.18	0.07-19.9	0.9	0.99	0.05-17.08	0.99
Time	0.02	0.0001-4.47	0.16	0.02	0.0001-5.39	0.18
Outcome	1.41	1.2-1.65	0.00004*	1.36	1.15-1.58	0.0003*

*p-value < 0.05. **Adjusted for sex, age.

hemoglobin and oxygen. Even if the oxygen content in a patient's blood is guaranteed, the ability of the tissue to utilize oxygen decreases, which might explain the lack of significant difference in PO_2 between the deceased and surviving patients in the results of the present study, although there was a significant difference in LAC levels. In another retrospective study of COVID-19 patients, (Tang et al. 2020b) found that mortality in patients with COVID-19-associated coagulopathy who were treated with heparin was significantly lower than in those who did not receive anticoagulation. Li et al (Ma et al., 2022) demonstrated, for the first time, that low molecular weight heparin (LMWH) can reduce plasma LAC levels in patients with COVID-19, which may be associated with a reduction of microthrombus formation. Therefore, the authors of the present study suggest that even in patients with COVID-19 whose initial and most severely affected organ is the lungs, the elevation of LAC may not be entirely to ventilation and air exchange dysfunction caused by pulmonary thrombi, but may also be due to inflammation and immune response-induced alterations in the coagulation system of the body. These changes affect the microcirculatory blood flow, leading to insufficient tissue blood supply and reduced oxygen utilization, subsequently resulting in increased LAC production due to increased aerobic glycolysis.

The body's immune system is composed of an innate immune response, which is induced by neutrophils and is the body's first line of defense against invading pathogens, and an adaptive immune system, which is dominated by lymphocytes, including B-cells as well as T-cells, which provide specific antigenic responses to the

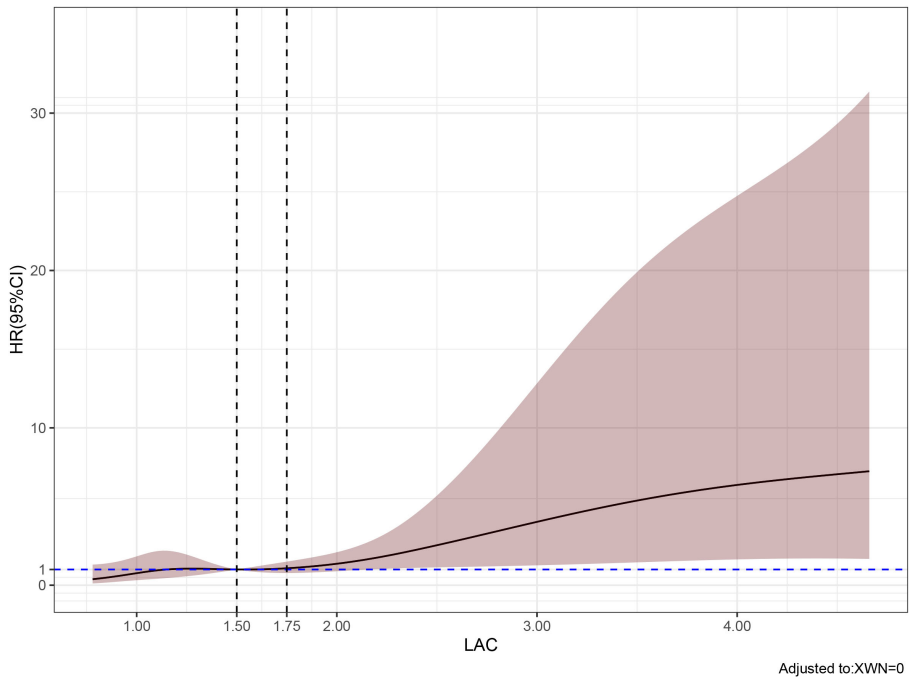

FIGURE 3
Predicted the correlation between LAC correlation and all-cause mortality in ICU patients with COVID-19. The risk ratio was expressed as a solid line, and 95% CI was shown as a shaded area. When the LAC concentration reaches and exceeds 1.5-1.75 mmol/L, the mortality rate of patients begins to increase rapidly.

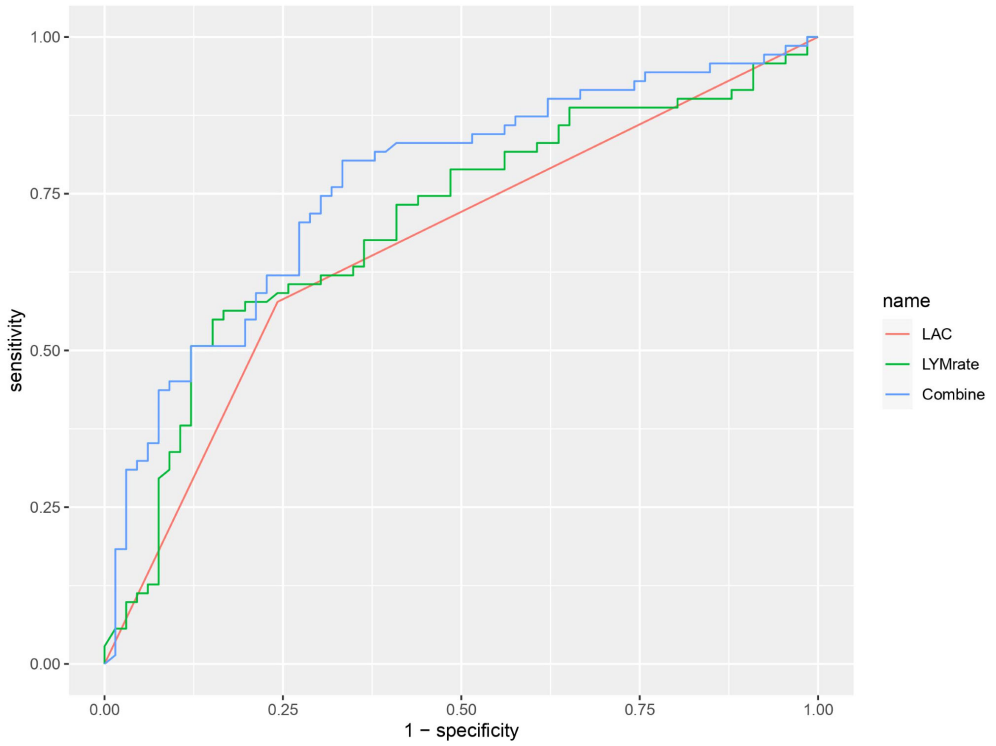

FIGURE 4
ROC curve graph showing the performance of three models: LAC (red), LYMrate (green), and Combine (blue). The x-axis represents 1-specificity and the y-axis represents sensitivity. The Combine model has the highest sensitivity across various thresholds.

body (Song et al., 2021; Buonacera et al., 2022). The two coordinate with each other and reflect the balance of the body 's immunity. Under normal conditions, T cells activated in response to inflammation, such as regulatory T cells (Treg), inhibit the production of the pro-inflammatory cytokine IL-6 by neutrophils, and transform into a large number of anti-inflammatory factors, such as IL-10, TGF-β, and indoleamine 2,3-dioxygenase (IDO)), which induce apoptosis in neutrophils and counteract the excessive inflammatory process mediated by neutrophils (Lewkowicz et al., 2013; Schönrich et al., 2020). In the early stage of SARS-CoV-2 infection, neutrophils are stimulated to activate and secrete large amounts of reactive oxygen species (ROS) (Jiang et al., 2025;

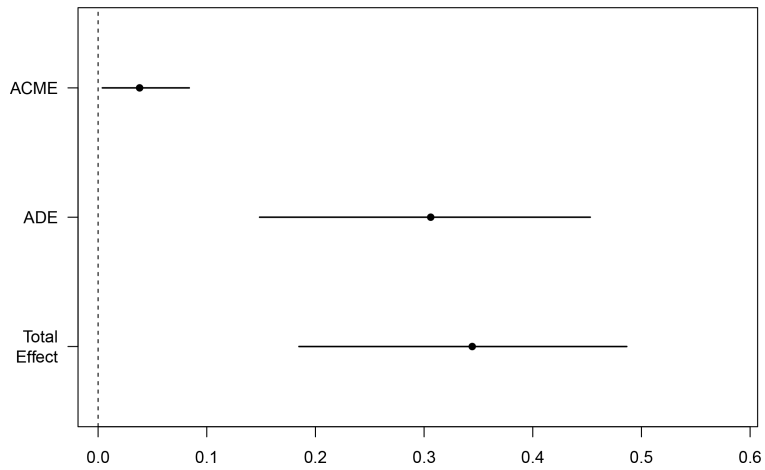

FIGURE 5
Mediating effect of NLR-mediated mediation of LAC on mortality in ICU COVID-19 patients; Total Effect, LAC combined with NLR mediated effect; ADE, LAC mediated effect; ACME, NLR mediated effect.

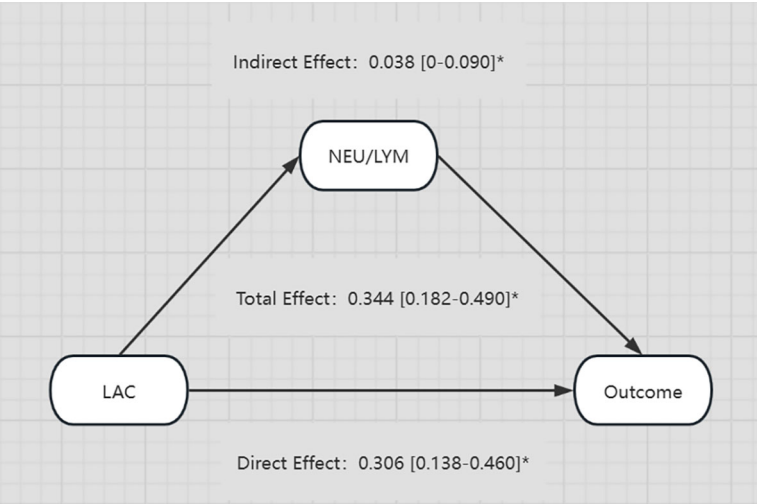

FIGURE 6
Diagram illustrating the relationships between LAC, NEU/LYM, and Outcome. LAC has a direct effect of 0.306 and an indirect effect through NEU/LYM of 0.038 on the Outcome. The total effect from LAC to Outcome is 0.344. All effects are provided with their respective confidence intervals and marked with an asterisk. *p-value < 0.05.

Schönrich et al., 2020), which induces oxidative stress and increases the formation of neutrophil extracellular traps (NET), thereby suppressing the activity of T lymphocytes (Tripathi et al., 2018). Moreover, SARS-CoV-2 can directly affect lymphoid organs and cells through ACE2, causing the destruction and apoptosis of lymphocyte (Gu et al., 2005). The virus can also cause an innate immune system overreaction and cytokine storm in the body, resulting in a substantial decrease in peripheral lymphocyte counts (Colantuoni et al., 2020). Similar to the results of previous studies, the results of the present study found that the majority of ICU patients diagnosed with COVID-19 had lymphopenia, and that there were significant differences in LYM counts between the deceased and surviving patients. To better determine the relationship between LYM counts and disease prognosis, we collected LYM counts on the first and seventh days of the ICU admission, and calculated the rate of over the course of one week (change in LYM count throughout the week/LYM count on day of admission) to define the immune dysregulation caused by COVID-19. Statistical analysis revealed that the LYM change rates were significantly correlated with patients' prognoses (P < 0.001), and

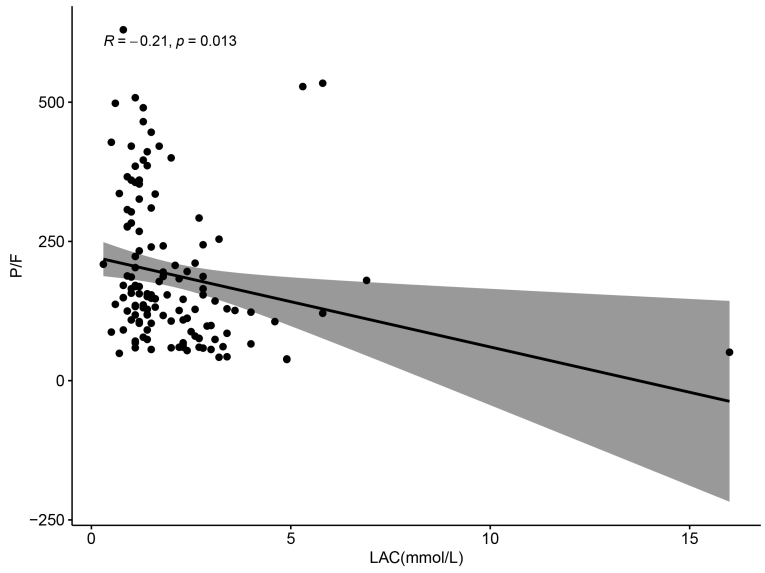

FIGURE 7
Scatter plot showing the relationship between LAC (mmol/L) and P/F ratio, with a negative correlation (R = -0.21, p = 0.013). Data points are scattered, and a trend line with a shaded confidence interval indicates a downward trend.

that the predictive value of this index combined with LAC for prognosis was greater than that of either index alone. Similar studies have been conducted on the impact of LAC and LYM counts on the prognosis of patients with COVID-19. For example, Wang et al. (2021) have pointed out that LYM counts were nonlinearly associated with the risk of death in patients hospitalized with COVID-19. With the decrease of LYM counts (< 0.95 × 109/L), the risk of death in hospitalized patients with COVID-19 will gradually increase. Vassiliou et al. (2020) found that initial blood lactate in COVID-19 patients admitted to the ICU served as an independent outcome predictor and that the time course of LAC reflected changes in organ dysfunction during hospitalization, which correlated with adverse clinical outcomes. Unlike previous studies, considering the continuous changes of lymphocytes in patients with severe COVID-19, the change rate of lymphocytes within one week was calculated, and the patient data collected in this study were from the pandemic period after the implementation of the COVID-19 open management policy in China. At this time, the popular strain was mainly Omicron, which had higher infection rate and immune evasion than other strains (Parsons and Acharya, 2023).

LAC is considered a functional chemical that can affect the body's immune response, which may also explain why NLR mediated the of LAC on the mortality of severe patients in the causal mediation analysis of this study; The study found that in severe COVID-19 patients, NK cells were strongly activated but their function was significantly reduced, mainly manifested as dim CD56dim phenotype cells, compared to bright phenotype CD56bright cells, and the former has a significant-inflammatory and cytotoxic effects (Maucourant et al., 2020; Osuchowski et al., 2021). While under low lactate levels, such as in the recovery period after exercise, the ratio of CD56bright to CD56dim cells increased significantly (Timmons and Cieslak, 2008; Gupta, 2022). In cancer patients, it was found that the acidosis induced by elevated LAC can significantly inhibit NK cell activity and reduce the level of interferon-γby it, while correcting acidosis can promote the degeneration of tumor cells (Greppi et al., 2024); T cells have specific transport proteins to sense lactate, inhibit its mobility, and increase the conversion of CD4+ T cells to an IL-17+ fraction, while reducing the cytolytic activity of CD8+ T cells (Pucino et al., 2019). In sepsis patients, increasing glycolysis, promoting ATP production, and relieving lactic acidosis can significantly offset the immunosuppressive effects of LAC and enhance the immune function of the body (Liu et al., 2024), so may be possible to explore the treatment of severe COVID-19 patients through corresponding LAC blocking strategies, so as to improve their prognosis.

Multivariate analysis revealed that the SOFA score also had a predictive value for the prognosis of patients with COVID-19; however, considering that the present study was retrospective in nature, the SOFA score included a subjective evaluation of the state of consciousness, and the SOFA score, as well as LAC, both indicated organ dysfunction in the body. Therefore, the present study did not include an evaluation of lactic acid combined with the SOFA score on the prognosis of patients with COVID-19; however, we did evaluate the predictive value of the combination of clinical detection indicators. In the present study, an increased NLR, when associated with increased LAC levels, mediated an increased risk of poor prognosis in ICU patients with COVID-19, which may be attributed to the body's systemic inflammatory and excessive immune response, with an increase in NEUs and a decrease in LYMs, while LAC regulates the immune and inflammatory responses of the body.

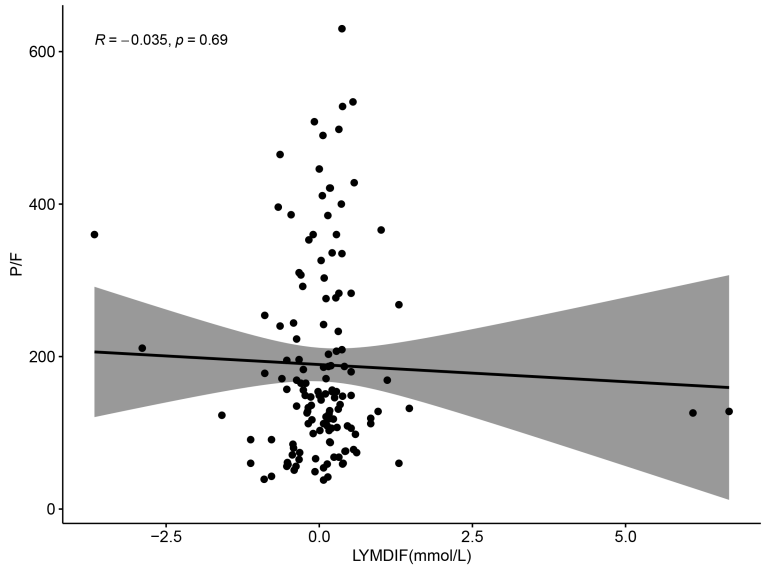

FIGURE 8
Scatter plot showing the relationship between LYMDIF (mmol/L) and P/F ratio. Data points are scattered with a best-fit line and shaded confidence interval. The correlation coefficient R is negative 0.035 with a p-value of 0.69, indicating no significant correlation.

5 Conclusions

The present study analyzed clinical indicators of patients admitted to the ICU during the Omicron variant phase of the COVID-19 pandemic, and found that clinical tests, such as LAC level, LYM change rate, and NLR, had predictive value for the prognosis of ICU patients with COVID-19. The cut-off value of LAC was found to be 1.75 mmol/L, and the prognosis of patients with a LAC level >1.75 mmol/L was significantly worse than that of patients with a LAC level <1.75 mmol/L. LAC level, combined with the weekly LYM change rate, had the greatest predictive value for the prognosis of patients in the ICU diagnosed with COVID-19. We suggest, therefore, that the elevated LAC levels may be caused by insufficient tissue blood supply due to microcirculatory thrombosis, rather than impaired pulmonary ventilation.

6 Limitations

The present study had a few limitations. First, the patient data collected in the present study came from different ICUs within the same hospital and all the patients included were from China; therefore, selection bias and variability in detection may be present. Secondly, the present study was retrospective in nature, encompassing a smaller sample size, which may limit the interpretation of the results. Moreover, because the subjects were ICU patients who may have been treated in the general ward prior to being admitted to the ICU, not all patients were admitted directly from the emergency department, which may have affected the results of the present study. Finally, the patients' viral loads were not measured or statistically analyzed. Additionally, whether or not patients received the vaccine before the onset of the disease was not included in the present study. These factors, therefore, may have impacted our results.

Data availability statement

The datasets presented in this study can be found in online repositories. The names of the repository/repositories and accession number(s) can be found in the article/Supplementary Material.

Ethics statement

The studies involving humans were approved by Ethics Approval The research was approved by the ethics committee of the First Affiliated Hospital of Soochow University (2024-620). The studies were conducted in accordance with the local legislation and institutional requirements. Written informed consent for participation was not required from the participants or the participants' legal guardians/next of kin in accordance with the national legislation and institutional requirements.

Author contributions

YT: Conceptualization, Data curation, Formal analysis, Investigation, Visualization, Writing – original draft, Writing – review & editing. JY: Conceptualization, Data curation, Formal analysis, Investigation, Writing – original draft. LC: Conceptualization, Data curation, Formal analysis, Investigation, Methodology, Writing – review & editing. XL: Conceptualization, Data curation, Formal analysis, Resources, Supervision, Visualization, Writing – review & editing. ZC: Conceptualization, Data curation, Formal analysis, Resources, Supervision, Visualization, Writing – review & editing. JL: Data curation, Formal analysis, Software, Writing – review & editing. JJ: Conceptualization, Project administration, Supervision, Validation, Writing – original draft, Writing – review & editing. YW: Conceptualization, Funding acquisition, Investigation, Resources, Supervision, Validation, Visualization, Writing – original draft, Writing – review & editing.

Funding

The author(s) declare financial support was received for the research and/or publication of this article. This work was supported by the National Natural Science Foundation of China [grant number 81801886] and Graduate Research and Innovation Projects of Jiangsu Province [grant number M2020013].

Conflict of interest

The authors declare that the research was conducted in the absence of any commercial or financial relationships that could be construed as a potential conflict of interest.

Generative AI statement

The author(s) declare that no Generative AI was used in the creation of this manuscript.

Any alternative text (alt text) provided alongside figures in this article has been generated by Frontiers with the support of artificial intelligence and reasonable efforts have been made to ensure accuracy, including review by the authors wherever possible. If you identify any issues, please contact us.

Publisher's note

References

Bakker, J., Nijsten, M. W., and Jansen, T. C. (2013). Clinical use of lactate monitoring in critically ill patients. *Ann. Intensive Care* 3, 12. doi: 10.1186/2110-5820-3-12

Böning, D., Kuebler, W. M., and Bloch, W. (2021). The oxygen dissociation curve of blood in COVID-19. *Am. J. Physiol. Lung Cell Mol. Physiol.* 321, L349–l357. doi: 10.1152/ajplung.00079.2021

Bruno, R. R., Wernly, B., Flaatten, H., Fjølner, J., Artigas, A., Bollen Pinto, B., et al. (2021). Lactate is associated with mortality in very old intensive care patients suffering from COVID-19: results from an international observational study of 2860 patients. *Ann. Intensive Care* 11, 128. doi: 10.1186/s13613-021-00911-8

Buonacera, A., Stancanelli, B., Colaci, M., and Malatino, L. (2022). Neutrophil to lymphocyte ratio: an emerging marker of the relationships between the immune system and diseases. *Int. J. Mol. Sci.* 23 (7). doi: 10.3390/ijms23073636

Chen, Y., Zhu, H., Luo, Y., Xie, T., Hu, Y., Yan, Z., et al. (2025). ALDOC promotes neuroblastoma progression and modulates sensitivity to chemotherapy drugs by enhancing aerobic glycolysis. *Front. Immunol.* 16. doi: 10.3389/fimmu.2025.1573815

Chen, H., Zhu, Z., Zhao, C., Guo, Y., Chen, D., Wei, Y., et al. (2020). Central venous pressure measurement is associated with improved outcomes in septic patients: an analysis of the MIMIC-III database. *Crit. Care* 24, 433. doi: 10.1186/s13054-020-03109-9

Choy, M., Huang, Y., Peng, Y., Liang, W., He, X., Chen, C., et al. (2023). Association between epicardial adipose tissue and incident heart failure mediating by alteration of natriuretic peptide and myocardial strain. *BMC Med.* 21, 117. doi: 10.1186/s12916-023-02836-4

Colaneri, M., Genovese, C., Fassio, F., Canuti, M., Giacomelli, A., Ridolfo, A. L., et al. (2024). Prognostic significance of NLR and PLR in COVID-19: A multi-cohort validation study. *Infect. Dis. Ther.* 13, 1147–1157. doi: 10.1007/s40121-024-00967-6

Colantuoni, A., Martini, R., Caprari, P., Ballestri, M., Capecchi, P. L., Gnasso, A., et al. (2020). COVID-19 sepsis and microcirculation dysfunction. *Front. Physiol.* 11. doi: 10.3389/fphys.2020.00747

Gheblawi, M., Wang, K., Viveiros, A., Nguyen, Q., Zhong, J. C., Turner, A. J., et al. (2020). Angiotensin-converting enzyme 2: SARS-CoV-2 receptor and regulator of the renin-angiotensin system: celebrating the 20th anniversary of the discovery of ACE2. *Circ. Res.* 126, 1456–1474. doi: 10.1161/circresaha.120.317015

Greppi, M., De Franco, F., Obino, V., Rebaudi, F., Goda, R., Frumento, D., et al. (2024). NK cell receptors in anti-tumor and healthy tissue protection: Mechanisms and therapeutic advances. *Immunol. Lett.* 270, 106932. doi: 10.1016/j.imlet.2024.106932

Gu, J., Gong, E., Zhang, B., Zheng, J., Gao, Z., Zhong, Y., et al. (2005). Multiple organ infection and the pathogenesis of SARS. *J. Exp. Med.* 202, 415–424. doi: 10.1084/jem.20050828

Guan, W. J., Ni, Z. Y., Hu, Y., Liang, W. H., Ou, C. Q., He, J. X., et al. (2020). Clinical characteristics of coronavirus disease 2019 in China. *N Engl. J. Med.* 382, 1708–1720. doi: 10.1056/NEJMoa2002032

Gupta, G. S. (2022). The lactate and the lactate dehydrogenase in inflammatory diseases and major risk factors in COVID-19 patients. *Inflammation* 45, 2091–2123. doi: 10.1007/s10753-022-01680-7

Hanff, T. C., Mohareb, A. M., Giri, J., Cohen, J. B., and Chirinos, J. A. (2020). Thrombosis in COVID-19. *Am. J. Hematol.* 95, 1578–1589. doi: 10.1002/ajh.25982

Huang, Y. T., and Yang, H. I. (2017). Causal mediation analysis of survival outcome with multiple mediators. *Epidemiology* 28, 370–378. doi: 10.1097/ede.0000000000000651

Huo, J., Le Bas, A., Ruza, R. R., Duyvesteyn, H. M. E., Mikolajek, H., Malinauskas, T., et al. (2020). Neutralizing nanobodies bind SARS-CoV-2 spike RBD and block interaction with ACE2. *Nat. Struct. Mol. Biol.* 27, 846–854. doi: 10.1038/s41594-020-0469-6

Jiang, L., Su, Z., Zhang, Y., Liu, H., and Wang, H. (2025). LPS promotes the production of ROS in neutrophils to regulate their killing activity against Mycobacterium tuberculosis. *Sci. Rep.* 15, 26785. doi: 10.1038/s41598-025-12232-y

Kumar, S., Sahu, N., Jawaid, T., Jayasingh Chellammal, H. S., and Upadhyay, P. (2025). Dual role of lactate in human health and disease. *Front. Physiol.* 16. doi: 10.3389/fphys.2025.1621358

Kumar, A., Vaish, M., Karuppagounder, S. S., Gazaryan, I., Cave, J. W., Starkov, A. A., et al. (2021). HIF1α stabilization in hypoxia is not oxidant-initiated. *Elife* 10. doi: 10.7554/eLife.72873

Lewkowicz, N., Klink, M., Mycko, M. P., and Lewkowicz, P. (2013). Neutrophil–CD4+CD25+ T regulatory cell interactions: a possible new mechanism of infectious tolerance. *Immunobiology* 218, 455–464. doi: 10.1016/j.imbio.2012.05.029

Li, P., Chen, L., Liu, Z., Pan, J., Zhou, D., Wang, H., et al. (2020). Clinical features and short-term outcomes of elderly patients with COVID-19. *Int. J. Infect. Dis.* 97, 245–250. doi: 10.1016/j.ijid.2020.05.107

Li, H., Liu, L., Zhang, D., Xu, J., Dai, H., Tang, N., et al. (2020). SARS-CoV-2 and viral sepsis: observations and hypotheses. *Lancet* 395, 1517–1520. doi: 10.1016/s0140-6736(20)30920-x

Liu, H., Pan, M., Liu, M., Zeng, L., Li, Y., Huang, Z., et al. (2024). Lactate: a rising star in tumors and inflammation. *Front. Immunol.* 15. doi: 10.3389/fimmu.2024.1496390

Ma, L., Zeng, Y., Zhao, B., Xu, L., Li, J., Zhu, T., et al. (2022). Low molecular weight heparin reduces arterial blood lactic acid content and increases estimated glomerular filtration rate in patients with moderate Covid-19 pneumonia. *Chin. Med. J. (Engl)* 135, 691–696. doi: 10.1097/cm9.0000000000001923

Mathioudakis, N., Zachiotis, M., Papadakos, S., Triantafyllou, M., Karapanou, A., Samara, S., et al. (2022). Onodera's prognostic nutritional index: Comparison of its role in the severity and outcomes of patients with COVID–19 during the periods of alpha, delta and omicron variant predominance. *Exp. Ther. Med.* 24, 675. doi: 10.3892/etm.2022.11611

Maucourant, C., Filipovic, I., Ponzetta, A., Aleman, S., Cornillet, M., Hertwig, L., et al. (2020). Natural killer cell immunotypes related to COVID-19 disease severity. *Sci. Immunol.* 5 (50). doi: 10.1126/sciimmunol.abd6832

Osuchowski, M. F., Winkler, M. S., Skirecki, T., Cajander, S., Shankar-Hari, M., Lachmann, G., et al. (2021). The COVID-19 puzzle: deciphering pathophysiology and phenotypes of a new disease entity. *Lancet Respir. Med.* 9, 622–642. doi: 10.1016/s2213-2600(21)00218-6

Parsons, R. J., and Acharya, P. (2023). Evolution of the SARS-CoV-2 omicron spike. *Cell Rep.* 42, 113444. doi: 10.1016/j.celrep.2023.113444

Patel, V. B., Zhong, J. C., Grant, M. B., and Oudit, G. Y. (2016). Role of the ACE2/angiotensin 1–7 axis of the renin-angiotensin system in heart failure. *Circ. Res.* 118, 1313–1326. doi: 10.1161/circresaha.116.307708

Pivina, L., Batenova, G., Ygiyeva, D., Orekhov, A., Pivin, M., and Dyussupov, A. (2024). Assessment of the predictive ability of the neutrophil-to-lymphocyte ratio in patients with in-stent restenosis after COVID-19. *Diagnost. (Basel)* 14 (20). doi: 10.3390/diagnostics14202262

Pucino, V., Certo, M., Bulusu, V., Cucchi, D., Goldmann, K., Pontarini, E., et al. (2019). Lactate buildup at the site of chronic inflammation promotes disease by inducing CD4(+) T cell metabolic rewiring. *Cell Metab.* 30, 1055–1074.e1058. doi: 10.1016/j.cmet.2019.10.004

Rabinowitz, J. D., and Enerbäck, S. (2020). Lactate: the ugly duckling of energy metabolism. *Nat. Metab.* 2, 566–571. doi: 10.1038/s42255-020-0243-4

Rhodes, A., Evans, L. E., Alhazzani, W., Levy, M. M., Antonelli, M., Ferrer, R., et al. (2017). Surviving sepsis campaign: international guidelines for management of sepsis and septic shock: 2016. *Intensive Care Med.* 43, 304–377. doi: 10.1007/s00134-017-4683-6

Rimachi, R., Bruzzi de Carvahlo, F., Orellano-Jimenez, C., Cotton, F., Vincent, J. L., and De Backer, D. (2012). Lactate/pyruvate ratio as a marker of tissue hypoxia in circulatory and septic shock. *Anaesth. Intensive Care* 40, 427–432. doi: 10.1177/0310057x1204000307

Schönrich, G., Raftery, M. J., and Samstag, Y. (2020). Devilishly radical NETwork in COVID-19: Oxidative stress, neutrophil extracellular traps (NETs), and T cell suppression. *Adv. Biol. Regul.* 77, 100741. doi: 10.1016/j.jbior.2020.100741

Song, M., Graubard, B. I., Rabkin, C. S., and Engels, E. A. (2021). Neutrophil-to-lymphocyte ratio and mortality in the United States general population. *Sci. Rep.* 11, 464. doi: 10.1038/s41598-020-79431-7

Sungnak, W., Huang, N., Bécavin, C., Berg, M., Queen, R., Litvinukova, M., et al. (2020). SARS-CoV-2 entry factors are highly expressed in nasal epithelial cells together with innate immune genes. *Nat. Med.* 26, 681–687. doi: 10.1038/s41591-020-0868-6

Tang, N., Bai, H., Chen, X., Gong, J., Li, D., and Sun, Z. (2020a). Anticoagulant treatment is associated with decreased mortality in severe coronavirus disease 2019 patients with coagulopathy. *J. Thromb. Haemost.* 18, 1094–1099. doi: 10.1111/jth.14817

Tang, N., Li, D., Wang, X., and Sun, Z. (2020b). Abnormal coagulation parameters are associated with poor prognosis in patients with novel coronavirus pneumonia. *J. Thromb. Haemost.* 18, 844–847. doi: 10.1111/jth.14768

Tian, M., Liu, W., Li, X., Zhao, P., Shereen, M. A., Zhu, C., et al. (2021). HIF-1α promotes SARS-CoV-2 infection and aggravates inflammatory responses to COVID-19. *Signal Transduct. Target Ther.* 6, 308. doi: 10.1038/s41392-021-00726-w

Timmons, B. W., and Cieslak, T. (2008). Human natural killer cell subsets and acute exercise: a brief review. *Exerc. Immunol. Rev.* 14, 8–23.

Trebuian, C. I., Brici, O. M., Sutoi, D., Popa, D. I., Chioibas, D. R., and Mederle, O. A. (2024). Lactate levels and clearance: key predictors of prognosis for COVID-19 and non-COVID-19 septic shock patients in the emergency department. *Clin. Pract.* 14, 834–845. doi: 10.3390/clinpract14030065

Tripathi, J. K., Sharma, A., Sukumaran, P., Sun, Y., Mishra, B. B., Singh, B. B., et al. (2018). Oxidant sensor cation channel TRPM2 regulates neutrophil extracellular trap formation and protects against pneumoseptic bacterial infection. *FASEB J.* 32, fj201800605. doi: 10.1096/fj.201800605

Varga, Z., Flammer, A. J., Steiger, P., Haberecker, M., Andermatt, R., Zinkernagel, A. S., et al. (2020). Endothelial cell infection and endotheliitis in COVID-19. *Lancet* 395, 1417–1418. doi: 10.1016/s0140-6736(20)30937-5

Vassiliou, A. G., Jahaj, E., Ilias, I., Markaki, V., Malachias, S., Vrettou, C., et al. (2020). Lactate kinetics reflect organ dysfunction and are associated with adverse outcomes in intensive care unit patients with COVID-19 pneumonia: preliminary results from a GREEK single-centre study. *Metabolites* 10 (12). doi: 10.3390/metabo10100386

Velavan, T. P., Kieu Linh, L. T., Kreidenweiss, A., Gabor, J., Krishna, S., and Kremsner, P. G. (2021). Longitudinal monitoring of lactate in hospitalized and ambulatory COVID-19 patients. *Am. J. Trop. Med. Hyg.* 104, 1041–1044. doi: 10.4269/ajtmh.20-1282

Wang, S., Liu, J., Hu, S., and Mao, Y. (2024). LDH and NLR, as inflammatory markers, the independent risk factors for COVID-19 complicated with respiratory failure in elderly patients. *Pak J. Med. Sci.* 40, 2112–2117. doi: 10.12669/pjms.40.9.8728

Wang, S., Sheng, Y., Tu, J., and Zhang, L. (2021). Association between peripheral lymphocyte count and the mortality risk of COVID-19 inpatients. *BMC Pulm. Med.* 21, 55. doi: 10.1186/s12890-021-01422-9

Wang, J., Weng, L., Xu, J., and Du, B. (2023). Blood gas analysis as a surrogate for microhemodynamic monitoring in sepsis. *World J. Emerg. Med.* 14, 421–427. doi: 10.5847/wjem.j.1920-8642.2023.093

WHO COVID-19 Dashboard. (2020). (Geneva: World Health Organization). Available online at: https://covid19.who.int/ (Accessed May 15, 2023).

Wichmann, D., Sperhake, J. P., Lütgehetmann, M., Steurer, S., Edler, C., Heinemann, A., et al. (2020). Autopsy findings and venous thromboembolism in patients with COVID-19: A prospective cohort study. *Ann. Intern. Med.* 173, 268–277. doi: 10.7326/m20-2003

Yang, K., Holt, M., Fan, M., Lam, V., Yang, Y., Ha, T., et al. (2022). Cardiovascular dysfunction in COVID-19: association between endothelial cell injury and lactate. *Front. Immunol.* 13. doi: 10.3389/fimmu.2022.868679

Zhou, F., Yu, T., Du, R., Fan, G., Liu, Y., Liu, Z., et al. (2020). Clinical course and risk factors for mortality of adult inpatients with COVID-19 in Wuhan, China: a retrospective cohort study. *Lancet* 395, 1054–1062. doi: 10.1016/s0140-6736(20)30566-3

Zhu, N., Zhang, D., Wang, W., Li, X., Yang, B., Song, J., et al. (2020). A novel coronavirus from patients with pneumonia in China 2019. *N Engl. J. Med.* 382, 727–733. doi: 10.1056/NEJMoa2001017

Frontiers in
Cellular and Infection Microbiology

Investigates how microorganisms interact with their hosts

Explores bacteria, fungi, parasites, viruses, endosymbionts, prions and all microbial pathogens as well as the microbiota and its effect on health and disease in various hosts.

Discover the latest Research Topics

See more →

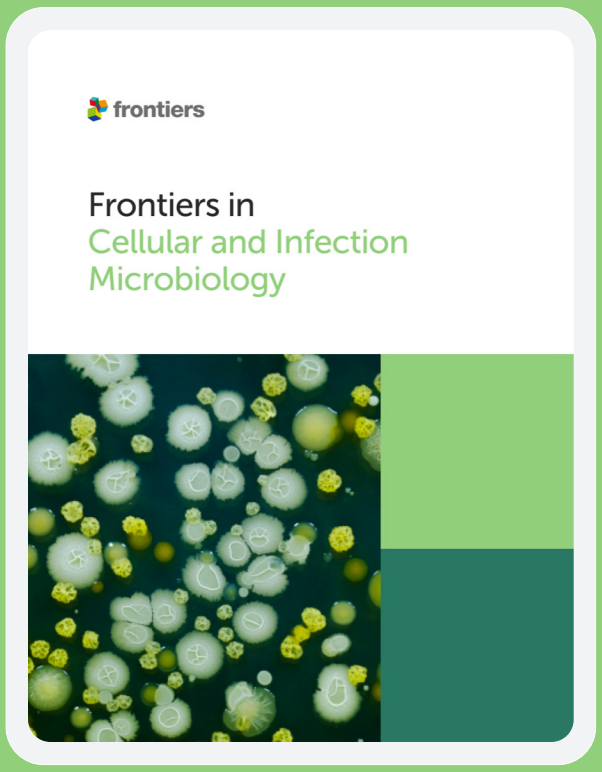

Frontiers

Avenue du Tribunal-Fédéral 34
1005 Lausanne, Switzerland
frontiersin.org

Contact us

+41 (0)21 510 17 00
frontiersin.org/about/contact